



**COMPARISON OF TWO METHODS USED TO MEASURE  
AERODYNAMIC LOADS ACTING ON CAPTIVE STORE  
MODELS IN WIND TUNNEL TESTS**

**PROPULSION WIND TUNNEL FACILITY  
ARNOLD ENGINEERING DEVELOPMENT CENTER  
AIR FORCE SYSTEMS COMMAND  
ARNOLD AIR FORCE STATION, TENNESSEE 37389**

**September 1976**

**Final Report for Period April 1973 - May 1976**

Approved for public release; distribution unlimited.

**Prepared for**

**AIR FORCE ARMAMENT LABORATORY (DLJC)  
EGLIN AIR FORCE BASE, FLORIDA 32542**

## NOTICES

When U. S. Government drawings specifications, or other data are used for any purpose other than a definitely related Government procurement operation, the Government thereby incurs no responsibility nor any obligation whatsoever, and the fact that the Government may have formulated, furnished, or in any way supplied the said drawings, specifications, or other data, is not to be regarded by implication or otherwise, or in any manner licensing the holder or any other person or corporation, or conveying any rights or permission to manufacture, use, or sell any patented invention that may in any way be related thereto.

Qualified users may obtain copies of this report from the Defense Documentation Center.

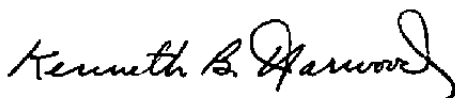
References to named commercial products in this report are not to be considered in any sense as an endorsement of the product by the United States Air Force or the Government.

This report has been reviewed by the Information Office (OI) and is releasable to the National Technical Information Service (NTIS). At NTIS, it will be available to the general public, including foreign nations.

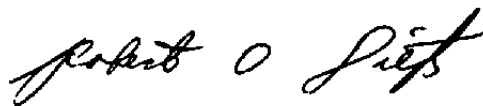
## APPROVAL STATEMENT

This technical report has been reviewed and is approved for publication.

FOR THE COMMANDER



KENNETH B. HARWOOD  
Major, CF  
Research & Development  
Division  
Directorate of Technology



ROBERT O. DIETZ  
Director of Technology

# UNCLASSIFIED

REPORT DOCUMENTATION PAGE		READ INSTRUCTIONS BEFORE COMPLETING FORM
1 REPORT NUMBER <b>AEDC-TR-76-122</b>	2 GOVT ACCESSION NO.	3 RECIPIENT'S CATALOG NUMBER
4 TITLE (and Subtitle) <b>COMPARISON OF TWO METHODS USED TO MEASURE AERODYNAMIC LOADS ACTING ON CAPTIVE STORE MODELS IN WIND TUNNEL TESTS</b>		5 TYPE OF REPORT & PERIOD COVERED <b>Final Report - April 1973 - May 1976</b>
7 AUTHOR(s)  <b>R. E. Dix, ARO, Inc.</b>		6 PERFORMING ORG REPORT NUMBER
9 PERFORMING ORGANIZATION NAME AND ADDRESS <b>Arnold Engineering Development Center (DY) Air Force Systems Command Arnold Air Force Station, Tennessee 37389</b>		8. CONTRACT OR GRANT NUMBER(s)
11 CONTROLLING OFFICE NAME AND ADDRESS <b>Arnold Engineering Development Center(DYFS) Air Force Systems Command Arnold Air Force Station, Tennessee 37389</b>		10 PROGRAM ELEMENT, PROJECT, TASK AREA & WORK UNIT NUMBERS <b>Program Element 62602F Project 2567</b>
14 MONITORING AGENCY NAME & ADDRESS (if different from Controlling Office)		12 REPORT DATE <b>September 1976</b>
		13 NUMBER OF PAGES <b>261</b>
		15 SECURITY CLASS (of this report)  <b>UNCLASSIFIED</b>
		15a DECLASSIFICATION/DOWNGRADING SCHEDULE <b>N/A</b>
16 DISTRIBUTION STATEMENT (of this Report)  <b>Approved for public release; distribution unlimited.</b>		
17 DISTRIBUTION STATEMENT (of the abstract entered in Block 20, if different from Report)		
18 SUPPLEMENTARY NOTES  <b>Available in DDC</b>		
19 KEY WORDS (Continue on reverse side if necessary and identify by block number)  <div style="display: flex; justify-content: space-between;"> <div style="width: 45%;"> wind tunnel model tests support (sting) aerodynamic </div> <div style="width: 45%;"> loads store (captive) F-4C aircraft (parent) </div> </div>		
20 ABSTRACT (Continue on reverse side if necessary and identify by block number)  <p>In a series of wind tunnel tests, measurements were made of the aerodynamic loads acting on eight different store configurations supported in and near the external captive position on a 1/20-scale model of the F-4C aircraft. Store models included blunt and contoured afterbody shapes, stable and unstable configurations, and large (pylon-mounted) and small (rack-mounted) configurations. Six components of forces and moments were measured</p>		

# UNCLASSIFIED

# UNCLASSIFIED

## 20. ABSTRACT (Continued)

using two methods of supporting the store models: an internal bracket support technique (IBS), and a dual sting support technique. Using the captive trajectory system (CTS) as a dual-support technique, it was possible to evaluate both the effects of the "touchwire" gap necessary to prevent fouling between the store and aircraft models, and the effectiveness of using the CTS for measuring captive loads. Some characteristics of the interference flow field of the aircraft were also inferred. During the tests, which were conducted over a range of Mach number from 0.6 to 1.2, it was determined that under many conditions, captive loads can be measured with equal success using either IBS or CTS techniques. However, severe gradients were observed in normal force and pitching moment and in some cases side force and yawing moment, acting on the store within 0.2 store diameter of the captive position (especially for rack-mounted stores). These gradients, together with the inherent difficulty of positioning a store in the captive position when both store and parent aircraft are supported with separate stings, indicated a preference for bracket-support techniques. Influences of the aircraft flow field were observed to extend, in most cases, to more than five store diameters from the captive position. Beyond 0.2 store diameter from the captive position, and at subsonic conditions, store loading decayed exponentially to free-stream values.

UNCLASSIFIED



## PREFACE

The work reported herein was conducted by the Arnold Engineering Development Center (AEDC), Air Force Systems Command (AFSC), at the request of the Air Force Armament Laboratory (AFATL), under Program Element 62602F, Project 2567. The monitor of the project was Capt. Visi Arajs, AFATL (DLJC). The results were obtained by ARO, Inc. (a subsidiary of Sverdrup & Parcel and Associates, Inc.), contract operator of AEDC (AFSC), Arnold Air Force Station, Tennessee. The work was done under ARO Projects No. PF419, P32A-35A, and P34A-C4A. The author of this report was R. E. Dix, ARO, Inc. Analysis of the data was completed in March 1976, and the manuscript (ARO Control No. ARO-PWT-TR-76-55) was submitted for publication on May 21, 1976.

## CONTENTS

	<u>Page</u>
1.0 INTRODUCTION . . . . .	11
2.0 EXPERIMENTAL APPARATUS	
2.1 Test Facility . . . . .	12
2.2 Models . . . . .	13
2.3 Instrumentation . . . . .	15
3.0 DESCRIPTION OF TESTS	
3.1 Flow Conditions and Test Procedures . . . . .	15
3.2 Corrections . . . . .	16
3.3 Precision of Measurements . . . . .	17
4.0 DISCUSSION OF RESULTS	
4.1 Pylon-Mounted Stores . . . . .	19
4.2 Rack-Mounted Stores . . . . .	21
5.0 CONCLUSIONS . . . . .	26
REFERENCES . . . . .	28

## ILLUSTRATIONS

### Figure

1. Two Methods of Supporting a Store in the Captive Position in Wind Tunnel Tests . . . . .	29
2. Schematic Illustration of the Captive Trajectory System (CTS) . . . . .	30
3. Schematic Illustration of a Typical Model Installation in Tunnel 4T . . . . .	31
4. 1/20-Scale Model of the F-4C Aircraft . . . . .	32
5. Details of the Models of the Multiple and Triple Ejector Racks . . . . .	33
6. Nomenclature of Ejector Rack Stations . . . . .	34
7. Details of the Models of the F-4C Pylons . . . . .	35
8. Dimensions of Pylon-Mounted Store Models . . . . .	36
9. Dimensions of Rack-Mounted Store Models . . . . .	39
10. Typical Installation of an Internal Balance-Supporting Bracket . . . . .	42
11. Details of the Stings . . . . .	43
12. Comparison of Dummy Sting and Functional Sting Installations . . . . .	44

<u>Figure</u>		<u>Page</u>
13.	Illustration of Axes Used for Translating Store to Obtain Store Loads as a Function of Separation Distance from the Captive Position . . . . .	15
14.	Coefficient of Normal Force Acting on the Black Crow Store as a Function of Normal Distance between the Store and the Captive Position . . . . .	46
15.	Coefficient of Side Force Acting on the Black Crow Store as a Function of Normal Distance between the Store and the Captive Position . . . . .	50
16.	Coefficient of Axial Force Acting on the Black Crow Store as a Function of Normal Distance between the Store and the Captive Position . . . . .	54
17.	Coefficient of Rolling Moment Acting on the Black Crow Store as a Function of Normal Distance between the Store and the Captive Position . . . . .	58
18.	Coefficient of Pitching Moment Acting on the Black Crow Store as a Function of Normal Distance between the Store and the Captive Position . . . . .	62
19.	Coefficient of Yawing Moment Acting on the Black Crow Store as a Function of Normal Distance between the Store and the Captive Position . . . . .	66
20.	Coefficients of Forces and Moments Acting on the BLU-1 Store as a Function of Normal Distance between the Store and the Captive Position on the LIB Pylon . . . . .	70
21.	Coefficient of Normal Force Acting on the HSM Store as a Function of Normal Distance between the Store and the Captive Position . . . . .	76
22.	Coefficient of Side Force Acting on the HSM Store as a Function of Normal Distance between the Store and the Captive Position . . . . .	80
23.	Coefficient of Axial Force Acting on the HSM Store as a Function of Normal Distance between the Store and the Captive Position . . . . .	84
24.	Coefficient of Rolling Moment Acting on the HSM Store as a Function of Normal Distance between the Store and the Captive Position . . . . .	88
25.	Coefficient of Pitching Moment Acting on the HSM Store as a Function of Normal Distance between the Store and the Captive Position . . . . .	92

<u>Figure</u>		<u>Page</u>
26.	Coefficient of Yawing Moment Acting on the HSM Store as a Function of Normal Distance between the Store and the Captive Position . . . . .	96
27.	Coefficients of Forces and Moments Acting on the M-118 Store as a Function of Normal Distance between the Store and the Captive Position on the LIB Pylon . . . . .	100
28.	Coefficient of Normal Force Acting on the ASP Store as a Function of Normal Distance between the Store and Four Captive Positions on the MER Mounted on the C-L Pylon . . . . .	106
29.	Coefficient of Side Force Acting on the ASP Store as a Function of Normal Distance between the Store and Four Captive Positions on the MER Mounted on the C-L Pylon . . . . .	110
30.	Coefficient of Axial Force Acting on the ASP Store as a Function of Normal Distance between the Store and Four Captive Positions on the MER Mounted on the C-L Pylon . . . . .	114
31.	Coefficient of Rolling Moment Acting on the ASP Store as a Function of Normal Distance between the Store and Four Captive Positions on the MER Mounted on the C-L Pylon . . . . .	118
32.	Coefficient of Pitching Moment Acting on the ASP Store as a Function of Normal Distance between the Store and Four Captive Positions on the MER Mounted on the C-L Pylon . . . . .	122
33.	Coefficient of Yawing Moment Acting on the ASP Store as a Function of Normal Distance between the Store and Four Captive Positions on the MER Mounted on the C-L Pylon . . . . .	126
34.	Coefficient of Normal Force Acting on the ASP Store as a Function of Normal Distance between the Store and Four Captive Positions on the MER Mounted on the LOB Pylon . . . . .	130
35.	Coefficient of Side Force Acting on the ASP Store as a Function of Normal Distance between the Store and Four Captive Positions on the MER Mounted on the LOB Pylon . . . . .	134

<u>Figure</u>		<u>Page</u>
36.	Coefficient of Axial Force Acting on the ASP Store as a Function of Normal Distance between the Store and Four Captive Positions on the MER Mounted on the LOB Pylon . . . . .	138
37.	Coefficient of Rolling Moment Acting on the ASP Store as a Function of Normal Distance between the Store and Four Captive Positions on the MER Mounted on the LOB Pylon . . . . .	142
38.	Coefficient of Pitching Moment Acting on the ASP Store as a Function of Normal Distance between the Store and Four Captive Positions on the MER Mounted on the LOB Pylon . . . . .	146
39.	Coefficient of Yawing Moment Acting on the ASP Store as a Function of Normal Distance between the Store and Four Captive Positions on the MER Mounted on the LOB Pylon . . . . .	150
40.	Local Flow Velocity in the Vicinity of the TER Mounted on the LIB Pylon and Loaded with M-117 Store Models, $FS = 16.0$ , $M_\infty = 0.85$ . . . . .	154
41.	Coefficient of Normal Force Acting on the CBU-46 (SUU-7) Store as a Function of Normal Distance between the Store and Two Captive Positions on the TER Mounted on the LIB Pylon . . . . .	155
42.	Coefficient of Side Force Acting on the CBU-46 (SUU-7) Store as a Function of Normal Distance between the Store and Two Captive Positions on the TER Mounted on the LIB Pylon . . . . .	159
43.	Coefficient of Axial Force Acting on the CBU-46 (SUU-7) Store as a Function of Normal Distance between the Store and Two Captive Positions on the TER Mounted on the LIB Pylon . . . . .	163
44.	Coefficient of Rolling Moment Acting on the CBU-46 (SUU-7) Store as a Function of Normal Distance between the Store and Two Captive Positions on the TER Mounted on the LIB Pylon . . . . .	167
45.	Coefficient of Pitching Moment Acting on the CBU-46 (SUU-7) Store as a Function of Normal Distance between the Store and Two Captive Positions on the TER Mounted on the LIB Pylon . . . . .	171

<u>Figure</u>		<u>Page</u>
46.	Coefficient of Yawing Moment Acting on the CBU-46 (SUU-7) Store as a Function of Normal Distance between the Store and Two Captive Positions on the TER Mounted on the LIB Pylon . . . . .	175
47.	Coefficient of Normal Force Acting on the CBU-24 (SUU-30) Store as a Function of Normal Distance between the Store and Four Captive Positions on the MER Mounted on the C-L Pylon . . . . .	179
48.	Coefficient of Side Force Acting on the CBU-24 (SUU-30) Store as a Function of Normal Distance between the Store and Four Captive Positions on the MER Mounted on the C-L Pylon . . . . .	183
49.	Coefficient of Axial Force Acting on the CBU-24 (SUU-30) Store as a Function of Normal Distance between the Store and Four Captive Positions on the MER Mounted on the C-L Pylon . . . . .	187
50.	Coefficient of Rolling Moment Acting on the CBU-24 (SUU-30) Store as a Function of Normal Distance between the Store and Four Captive Positions on the MER Mounted on the C-L Pylon . . . . .	191
51.	Coefficient of Pitching Moment Acting on the CBU-24 (SUU-30) Store as a Function of Normal Distance between the Store and Four Captive Positions on the MER Mounted on the C-L Pylon . . . . .	195
52.	Coefficient of Yawing Moment Acting on the CBU-24 (SUU-30) Store as a Function of Normal Distance between the Store and Four Captive Positions on the MER Mounted on the C-L Pylon . . . . .	199
53.	Coefficient of Normal Force Acting on the CBU-24 (SUU-30) Store as a Function of Normal Distance between the Store and Four Captive Positions on the MER Mounted on the LOB Pylon . . . . .	203
54.	Coefficient of Side Force Acting on the CBU-24 (SUU-30) Store as a Function of Normal Distance between the Store and Four Captive Positions on the MER Mounted on the LOB Pylon . . . . .	207
55.	Coefficient of Axial Force Acting on the CBU-24 (SUU-30) Store as a Function of Normal Distance between the Store and Four Captive Positions on the MER Mounted on the LOB Pylon . . . . .	211

<u>Figure</u>		<u>Page</u>
56.	Coefficient of Rolling Moment Acting on the CBU-24 (SUU-30) Store as a Function of Normal Distance between the Store and Four Captive Positions on the MER Mounted on the LOB Pylon . . . . .	215
57.	Coefficient of Pitching Moment Acting on the CBU-24 (SUU-30) Store as a Function of Normal Distance between the Store and Four Captive Positions on the MER Mounted on the LOB Pylon . . . . .	219
58.	Coefficient of Yawing Moment Acting on the CBU-24 (SUU-30) Store as a Function of Normal Distance between the Store and Four Captive Positions on the MER Mounted on the LOB Pylon . . . . .	223
59.	Coefficient of Normal Force Acting on the MK 83 Store as a Function of Normal Distance between the Store and Three Captive Positions on the TER Mounted on the LIB Pylon . . . . .	227
60.	Coefficient of Side Force Acting on the MK 83 Store as a Function of Normal Distance between the Store and Three Captive Positions on the TER Mounted on the LIB Pylon . . . . .	232
61.	Coefficient of Axial Force Acting on the MK 83 Store as a Function of Normal Distance between the Store and Three Captive Positions on the TER Mounted on the LIB Pylon . . . . .	237
62.	Coefficient of Rolling Moment Acting on the MK 83 Store as a Function of Normal Distance between the Store and Three Captive Positions on the TER Mounted on the LIB Pylon . . . . .	242
63.	Coefficient of Pitching Moment Acting on the MK 83 Store as a Function of Normal Distance between the Store and Three Captive Positions on the TER Mounted on the LIB Pylon . . . . .	247
64.	Coefficient of Yawing Moment Acting on the MK 83 Store as a Function of Normal Distance between the Store and Three Captive Positions on the TER Mounted on the LIB Pylon . . . . .	252

## TABLES

	<u>Page</u>
1. Miscellaneous Dimensions of Store Models . . . . .	257
2. Uncertainty Intervals in Force and Moment Coefficients for Store Models . . . . .	258
NOMENCLATURE . . . . .	259



## 1.0 INTRODUCTION

A large and varied assortment of engines, fuel tanks, mission-assistance pods, and weapons can be stored aboard contemporary aircraft, especially military versions. In many cases, these stores are attached to the exterior of the carrier, or parent, aircraft. Therefore, prior to routine flight operations, it is necessary to evaluate the aerodynamic and functional compatibility of a specified aircraft-store configuration. Two questions of compatibility that must be answered are (1) can the aircraft be flown safely with the captive store, and (2) can the store be separated safely from the aircraft during flight? Answers to these questions are customarily based on data acquired during tests of appropriate models in wind tunnels. As part of the answer to the first question, aerodynamic loads acting on the store in the captive position must be measured over an appropriate range of parameters describing both the physical configuration and the flight regime. In the majority of wind tunnel tests, captive loads are measured using conventional "force" test techniques. The reactions of a strain-gage balance mounted within the store to the actions of the store under the influence of the flow field are monitored as a measure of the aerodynamic forces acting on the store. Several "techniques" of supporting a store in the captive position have been used, but all of these techniques may be classified as applications of one of two "methods," either the internal balance support method, or the dual-support method, as illustrated in Fig. 1 and discussed in Ref. 1.

To aid in answering the second question, the captive trajectory system (CTS), a dual-support technique, has been developed. By using the CTS, a store can be moved with respect to the aircraft in six degrees of freedom. Electrical signals commanding movements of the store result from calculations performed by a digital computer. Input information for the computer consists of measurements of parameters describing the flow and the output signals from the strain-gage balance mounted within the store. A schematic illustration of the CTS is provided in Fig. 2. A more detailed discussion of the CTS is available in Ref. 2.

An interest in identifying and evaluating the effects on loads acting on a store of using either of the above methods to support the store in the captive position led to the study described herein. Since inertial forces acting on a store in captive flight are generally greater than aerodynamic forces, the impact of test technique on structural design loads is secondary. However, as a store is released, the contribution of captive aerodynamic loads to the subsequent trajectory becomes significant, and the influence of the technique used to measure the aerodynamic loads acting on the store, especially in the interference flow field of the aircraft, should be identified. It was recognized that when a store was supported in the captive position using the internal-support method, the resulting configuration would be firmly

held at the correct distance from the aircraft, and with no alteration of the afterbody. The sole distortion of the correct configuration would be the bracket protruding through the upper surface of the store body. It was also clear that, when using the dual-support method, alteration of the afterbody of many stores was required to accommodate the sting, and an unrealistic gap was maintained between the two sting-supported bodies to prevent physical contact during testing.

A series of wind tunnel tests has been conducted in an effort to evaluate all of the above effects for eight stores carried by a typical contemporary fighter aircraft. Of the large quantity of data that has been collected, only the effects of supporting the store in a location near to, but not coincident with, the captive position along the Z axis of the pylon or ejector rack are presented herein. The effects of the presence of a sting, and the effects of altering the afterbody of a store are presented in an earlier report (Ref. 3).

## 2.0 EXPERIMENTAL APPARATUS

### 2.1 TEST FACILITY

Tests were conducted in the Aerodynamic Wind Tunnel (4T) of the Propulsion Wind Tunnel Facility, a closed-circuit design in which continuous flow can be maintained at various density settings. Mach number in the free stream can be set at any value from 0.2 to 1.3. Nozzle blocks can be installed to provide discrete Mach numbers of 1.6 and 2.0. Stagnation pressure can be established at values from 300 to 3,700 psfa. The test section is 4 ft square, 12.5 ft long, and is equipped with perforated walls that can be adjusted by remote control to provide a porosity in the nominal range of from zero to 10 percent open area. A desired fraction of the flow through the test section can be evacuated through the porous walls into a plenum chamber in which the test section is completely enclosed.

Models are supported in the test section with a conventional strut-sting system. A model can be pitched from approximately -12 to 28 deg with respect to the centerline of the tunnel. A capability of rolling a model from -180 to 180 deg about the centerline of the sting is also available. An illustration of a typical model installed for testing using the CTS is presented in Fig. 3.

## 2.2 MODELS

### 2.2.1 Aircraft

It was considered desirable by the sponsor of the research to obtain data for realistic aircraft and store configurations rather than for highly simplified and idealized wing-body shapes. After consideration of several contemporary aircraft configurations, the F-4C was selected (Fig. 4). A primary reason for the selection was the capability of the F-4C to carry both pylon-mounted and rack-mounted stores. ("Pylon-mounted" stores include rather large stores. In flight, only one of these stores is normally mounted on a pylon. "Rack-mounted" stores include rather small stores, several of which can be carried on a pylon through the use of either a triple ejector rack (TER) or a multiple ejector rack (MER), Fig. 5.) Several other specific factors also influenced the selection: (1) the F-4C is a low-wing configuration, and as such, the flow field in the vicinity of the stores is not complicated by sidewash from the fuselage, (2) an extensive collection of data was available from previous flow field and store separation tests using the F-4C, and (3) a model of suitable scale was available.

For the tests involving pylon-mounted store configurations, the right-wing pylons were omitted, but the centerline (C-L), left inboard (LIB), and left outboard (LOB) pylons were always installed. During the tests involving rack-mounted stores, the right inboard and right outboard pylons were also installed. Pylon-mounted store models were tested on only one pylon at a time, with other pylons empty. Rack-mounted store models were tested on only one specified rack, mounted on only one specified pylon at a time, and with other pylons empty. On the rack, however, the store model with the internal balance was moved from station to station in a realistic release sequence. All other appropriate rack stations were fitted with dummy (empty) models of the store configuration. An example of MER loading would be as follows: with the balance-mounted store model on MER station 4 (see Fig. 6 for rack station numbering), stations 1, 2, and 3 would be empty, and dummy models would be mounted on stations 5 and 6.

Additional details of the pylons are presented in Fig. 7. Throughout all tests, the tail surfaces of the F-4C model were omitted. Airflow was allowed through the simulated engine ducts, with cruise configuration exhaust ports installed. For convenience, testing was accomplished with the F-4C installed inverted in the test section.

## 2.2.2 Stores

During the process of selecting store configurations for the investigation, stores were classified first as either pylon-mounted or rack-mounted, as defined in Section 2.2.1. Within these two categories, stores were further classified as either stable or unstable. Further, two stores were selected from each of these four sub-categories, one with a blunted-base design that would accommodate a sting without alteration of the afterbody, and one with an afterbody shape that would require significant alteration to allow insertion of a sting. Hence, eight stores were tested during the investigation.

Pylon-mounted stores included the unstable Black Crow gun pod, the stable Hard Structure Munition (HSM), the unstable BLU-1 bomb, and the stable M-118 bomb, all depicted in Fig. 8. Rack-mounted stores included the unstable All-Altitude Spin-Projected dispenser (ASP), the stable CBU-24 bomb, the unstable CBU-46 (SUU-7) launcher pod, and the stable MK 83 bomb, all depicted in Fig. 9. Miscellaneous dimensions of the store models are presented in Table 1.

## 2.2.3 Internal Balance Support Brackets

To obtain measurements of aerodynamic loads acting on store models in the captive position, the internal bracket support (IBS) technique was used. Store models on which aerodynamic loads were being measured were securely fastened to one end of a six-component strain-gage balance. The other end of the balance was firmly supported through use of a rigid bracket protruding through the upper surface of the store model and tightly attached to the appropriate pylon or rack. To allow unrestricted reaction of the store model (hence the balance) to aerodynamic loading, the opening in the upper surface of the store model through which the bracket protruded was made large enough to ensure a clearance of at least 0.050 in. around the bracket. A drawing of a typical installation is presented in Fig. 10. The base of each bracket-mounted store model was either fabricated as solid, or later filled in with a plug to prevent flow through the interior of the store model and past the balance.

## 2.2.4 Stings

To obtain measurements of aerodynamic loads acting on store models as a function of normal separation distance from the captive position, the dual-support technique was used. The parent aircraft was supported on one sting attached to the conventional tunnel pitch sector, while the store models were supported on a separate sting attached to the CTS. Two store stings were used, one for each of the fundamental categories of stores identified, i.e., pylon-mounted and rack-mounted. For the larger, pylon-mounted store models, the sting was of 0.4-in. diameter. For the smaller, rack-mounted store models, the sting was of 0.25-in. diameter. These stings represented typical sizes used with similar models in routine tests. Dimensions of the stings are presented in Fig. 11.

To ensure matching of the captive store configurations tested using the IBS and dual-support techniques, a dummy sting was supported downstream of the store model when using the IBS technique. The dummy sting configurations matched the functional stings, and a dummy sting holder, attached to the parent aircraft sting, simulated the CTS equipment. A schematic comparison of an actual sting-mounted configuration with the corresponding dummy sting installation is presented in Fig. 12. A complete description of the dummy sting installation is contained in Ref. 3.

## 2.3 INSTRUMENTATION

Conventional strain-gage balances were used to sense the aerodynamic forces acting on the store models. Six components of forces and moments were resolved, as described in Section 3.3.

The gravimetric angle of attack of the parent aircraft model was sensed with an oil-damped pendulum fitted with strain gages and mounted in the aircraft model. Using the internal sensor for setting and recording the angle of attack of the parent aircraft model rather than the purely mechanical indication associated with the standard tunnel pitch sector, it was unnecessary to separately account for deflections of the aircraft model-sting combination. The gravimetric angle of attack of the store model was matched to that of the aircraft model using the CTS technique of computer-commanded servomechanisms. Sting and balance deflections for the store were included in the computations carried out by the computer in commanding the servomechanisms.

## 3.0 DESCRIPTION OF TESTS

### 3.1 FLOW CONDITIONS AND TEST PROCEDURES

Aerodynamic forces and moments acting on the store models were measured, with some exemptions, at nominal free-stream Mach numbers of 0.6, 0.8, 0.9, 1.1, and 1.2. Reynolds number was maintained at approximately  $3.5 \times 10^6$  per foot throughout the tests. Porosity of the test section walls was varied in a manner determined through previous calibration studies in the tunnel to minimize wall interference and buoyancy effects (Refs. 4 and 5).

As discussed in Section 1.0, a store model was supported in the captive position in one of two ways: with an internal bracket attached directly to the pylon or rack (IBS method), or with a conventional rear-entry sting separate from the aircraft sting (CTS method). The procedure used in setting aircraft attitude was the same for both methods, i.e., flow conditions were established before attitude was set. For IBS

tests, the aircraft was simply pitched through a sequence of angles of attack, pausing for about three sec at each value to record data. Only the data recorded at an aircraft angle of attack (gravimetric) of one deg (with respect to the waterline of the aircraft) are presented herein. At this attitude, the gravimetric angle of attack of the store was zero deg. In runs made using the dual-sting support method (CTS), loads acting on the store were acquired not only at the captive position, but also in the flow field along a path of approach to the captive position. For pylon-mounted stores, after the attitude of the aircraft was set, and using the gravimetric angle of attack of the parent aircraft model (Section 2.3) as a reference value, the CTS was used to position the store model in an appropriate corresponding attitude, aligned in pitch, yaw, roll, axial, and lateral degrees of freedom (according to pretest calibrations), but separated from the captive position in the Z direction, as illustrated in Fig. 13. Upon signal from the operator, the store model was translated in an approach to the captive position along the Z direction only, and at fixed gravimetric attitude. The approach motion was terminated upon contact of the store model with the touch-wire, a 0.030-in.-diam wire protruding from the pylon or rack, lightly spring-loaded to avoid damage to the balance, and electrically insulated from the parent aircraft so as to function as a switch. Data points were recorded at finite intervals along the approach path. After completing an approach sequence, motion along the approach path was reversed, and additional data points were recorded as the store model receded to a location well away from the aircraft model, usually about five or six store diameters. After all data were recorded, the store model was positioned approximately one store diameter from the aircraft model while the attitude was changed. The approach sequence was then repeated. Gravimetric angle of attack of the aircraft model was set at nominal values of -4 to 10 deg in 2-deg increments. For rack-mounted stores, a similar procedure was followed, but the approach path was either a simple Z-axis movement parallel to the  $Z_T$  axis for the bottom stations of a rack or an oblique path in the  $Y_T$ - $Z_T$  plane for the shoulder stations. Diagrams of the approach axes used for the various pylon and rack combinations are presented in Fig. 13. The roll angle of the store model was monitored by the computer for automatic selection of the appropriate approach motion.

## 3.2 CORRECTIONS

As discussed in Section 2.3, the attitude of the aircraft model was set using a gravity-sensing device mounted in the model. Therefore, no correction was necessary for deflections of the aircraft model with respect to the sting, or for deflections of the sting with respect to the pitching sector. For the balances used inside the store models, calibrations of the deflections of the mounting point of the store as a function of impressed load were used to identify contributions of balance and sting flexibility to the attitude of the store model. The

calibration data were used in the data reduction equations to derive the correct gravimetric attitude of the store model. (It is appropriate to recall here that all store models were supported with longitudinal axis parallel to the lower surface of the pylons, i.e., with a one-deg nose-down attitude with respect to the waterline of the aircraft model, Fig. 7.) No corrections were made in either aircraft or store model attitude to account for flow angularity in the free stream.

### 3.3 PRECISION OF MEASUREMENTS

Uncertainty intervals (including 95 percent of the calibration data) for the basic flow parameters, i.e.,  $p_{t\infty}$  and  $M_\infty$ , were estimated from both repeated calibrations of the instrumentation and the repeatability and uniformity of the free-stream flow in the test section during tunnel calibration. Uncertainty intervals for the instrumentation systems were estimated from repeated calibrations of the systems using secondary standards with accuracies traceable to the National Bureau of Standards. Uncertainty intervals for values of forces and moments derived from the output of the balance gages were determined from a root-mean-square analysis of the calibration data for the balance. Values of the above uncertainties were combined using the Taylor series method of error propagation to determine the precision of the force and moment coefficients. Values of the uncertainty intervals for the force and moment coefficients for all models tested are presented in Table 2.

For all flow conditions, the uncertainty interval for gravimetric angle of attack was  $\pm 0.1$  deg. However, two uncertainty intervals must be cited for Mach number. First, the uncertainty in setting Mach number was  $\pm 0.002$ , reflecting instrumentation capabilities. Second, there was the uncertainty in Mach number in the free stream, attributable to nonuniform flow effects such as angularity. A table of values of the uncertainty interval for Mach number is presented below:

Nominal $M_\infty$	Uncertainty in $M_\infty$
0.6	$\pm 0.005$
0.8	$\pm 0.005$
0.9	$\pm 0.003$
1.1	$\pm 0.006$
1.2	$\pm 0.010$

The precision with which the store model could be positioned in the tunnel was determined primarily by minor imperfections in the hardware of the CTS, and inexact corrections for the effects of system flexibility in response to static and dynamic loading during tunnel operation. Translational movements could be completed to within  $\pm 0.050$  in., and rotational movements to within  $\pm 0.150$  deg.

## 4.0 DISCUSSION OF RESULTS

When considering the results of the tests, it should be noted that the aircraft-store combinations investigated were not necessarily practical. Specifically, even though the size, shape, and salient features of both aircraft and store models were correctly scaled, the store models were mounted on the aircraft model in positions that did not necessarily correspond to accepted operational practice. For instance, when the TER was installed on the left wing inboard pylon, the other pylons were empty, thereby loading the aircraft asymmetrically. Further, during tests of pylon-mounted stores, an excessive gap was maintained between stores and pylons (approximately 2.5 in. full scale), while throughout the tests of rack-mounted stores, the gap was varied slightly from store to store. Equivalent full-scale gaps maintained throughout the tests were approximately 0.8 in. for the ASP and CBU-24 (SUU-30) stores, 1.0 in. for the CBU-46 (SUU-7) store, and 1.8 in. for the MK 83 store.

As discussed in Section 3.1, loads acting on the store models were acquired in two ways: with the balance supported by a bracket attached to the pylon or rack, and with the balance supported by a sting mounted in the CTS rig. Since a dummy sting was mounted downstream of the bracket-mounted store model, the physical appearances of the two separate installations of a given store were quite similar. Hence, data acquired with the store model supported by a bracket could be compared with sting-mounted data. One difference in the configurations did exist, however, that in retrospect was apparently significant: in the sting-mounted mode, data were recorded with the store model merely near, but not necessarily coincident with, the captive position because of the termination of CTS movement brought about by contact between store model and touchwire. As discussed in subsequent sections, strong gradients and inflections in the trends of loads acting on a store near the captive position were often observed or indicated, making it extremely desirable to obtain data within the range of the length of the touchwire. At the other extreme, however, as the store model was separated from the captive position by significant distance (over five or six store diameters), it was observed that the loads acting on the store model approached free-stream values, i.e., essentially zero (for all components except axial force) for the symmetrical store configurations investigated, and at zero angle of attack.

Attention should also be given to the bracket used to support the balance in the IBS mode of testing. To allow firm attachment to the aircraft model, the bracket in each case protruded through the upper surface of the store model. Since the appearance of the bracket was that of a solid blade, or fin bridging the gap between store model and pylon (or rack), it is plausible that the essential effect of the bracket on the flow was the same as an extension of the pylon or rack. (An investigation of such an effect is underway.) It can be estimated that



the effect of the bracket was to disturb the pressure distribution over the upper surface of the store model, resulting in a decrease in normal force and a forward shift in the location of the center of pressure.

## 4.1 PYLON-MOUNTED STORES

### 4.1.1 Unstable Configurations

Aerodynamic loads acting on two unstable pylon-mounted store configurations, the Black Crow and the BLU-1, are presented in Figs. 14 through 19; and 20, respectively. Data were acquired for the Black Crow mounted, successively, on three different pylons at four Mach numbers, but for the BLU-1 mounted on just the LIB pylon at the same four Mach numbers. Hence, in presenting the data, two different formats were adopted: for the Black Crow, values of one coefficient at one Mach number for all three pylons are presented on a given page; for the BLU-1, values of one coefficient for all four Mach numbers and the one pylon are presented on a page.

Throughout Figs. 15 through 19, it is clear that good agreement exists between bracket-supported and dual sting-supported loads. Only fragmentary data are available for some cases; however, it appears that for  $M_\infty < 1$ , the variation of all load components with separation from the captive position is apparently a simple exponential decay to free-stream values.

Comparing separate graphs, a variation is noted in the Z/D coordinate of the data point closest to the bracket-supported captive position. Spatial location of the captive position could not be precisely repeated because of the use of the touchwire system to ensure the absence of fouling between aircraft and store models. Since the CTS was used to move the store model about in the test section, as described in Section 3.1, reference coordinates for contact with the touchwire (captive position) were required. These coordinates were recorded during wind-off installation procedures. However, during wind-on testing, deflections of both aircraft and store models occurred, compromising the validity of the recorded coordinates. Compensation for deflections of the store model was accomplished using information available from the balance outputs, but since there was no balance in the aircraft model, it was not possible to compensate for deflections of the aircraft model.

Within the smooth portion of the load-decay curves, generally for  $Z/D > 0.4$ , an occasional data point not conforming to the curve may be ignored as extraneous. However, at Mach numbers exceeding 1.0, and for  $Z/D < 0.4$ , there is ample evidence to indicate that the variation of store loads with separation distance is not necessarily a simple exponential decay (cf. any of the data of Figs. 14 through 27 that correspond to  $M_\infty = 1.1$  and 1.2). The existence of many data points that appear to

be spurious, yet were accumulated for a variety of store configurations, pylon positions, flow conditions, and instants in time, should be an indication of consistency in flow phenomena rather than of random or transient events. It is, therefore, concluded that there are strong gradients in normal and side forces, and pitching and yawing moments acting on a pylon-mounted store in locations very near the captive position, say  $Z/D < 0.2$ .

Throughout Figs. 16, 17, and 20c and d, it is clear that axial force and rolling moment are almost constant for all Mach numbers and pylon positions, with very small gradients in the flow field. For an unstable store, of course, the behavior of the rolling moment, i.e., vanishingly small value showing no change, is predictable. The near-constant value of axial force is likewise not astonishing, and could justify omitting the axial-force element in the design of a balance to meet size or shape limitations.

#### 4.1.2 Stable Configurations

In Figs. 21 through 26, and 27, respectively, are presented aerodynamic loads acting on the Hard Structure Munition (HSM), and the M-118, both stable pylon-mounted store configurations. Data were acquired for the HSM mounted, successively, on three different pylons at four Mach numbers, but the M-118 was tested on just the LIB pylon at the same four Mach numbers. As in the case of unstable configurations, the format in which the data are presented is changed, as appropriate, to include either all pylons or all Mach numbers on a page for a given load component.

Agreement between approach data and captive data is generally good for the HSM (Figs. 21 through 26), excellent for the M-118 (Fig. 27). Complete approach data were not acquired in every case with the HSM, precluding a firm conclusion concerning the nature of the variation of load components through the flow field. Only the approach data to the LIB pylon at  $M_\infty = 0.9$  were acquired over a substantial range of values of  $Z/D$ . Considering the axial-force data, it appears that even the limited data of Figs. 23b and c indicate a simple exponential decay similar to the unstable stores (Section 4.1.1). However, these data are strictly valid for only Mach numbers 0.9 and 1.1, and the danger of generalization is demonstrated by the axial-force data for the M-118, Fig. 27c. An exponential decay adequately describes the data except for Mach number 1.2, at which a slight increase in axial force is noted as separation distance increases. The increase, not evident in the case of the HSM at a subsonic condition (Fig. 23b, the only complete axial-force "trajectory" available for comparison), can probably be attributed to increasing interference from shock structures developing in the flow field as the store model is separated from the aircraft.

No conclusive explanation is offered for the discrepancies between approach data and bracket-supported data for side force and pitching moment (Figs. 22 and 25). As discussed in Section 4.1.1, there is a tendency for inflections and relatively strong gradients in both forces and moments to develop for  $0 < Z/D < 0.2$  (cf. Figs. 21a and c, and 25a and c).

An interesting trend is observed in yawing moment for both stable store configurations (Figs. 26b and 27f): as the store model is separated from the captive position on the LIB pylon, yawing moment increases from an initial negative value (nose left, or outboard) to a positive value (nose right, or inboard) before decreasing to the expected free-stream value of zero. In the absence of complete "trajectories" from other pylons, no statement can be made concerning the existence of the trend at other locations. However, at the LIB pylon, because of the Mach numbers at which the trajectories are noted (0.9, 1.1, and 1.2), the trend apparently exists throughout the transonic range, when the interference flow field to which the store model is exposed contains regions of critical flow. It is possible to attribute the changes in sense of the yawing moment to changing pressure distributions, perhaps because of shocks impinging on the store, since the side force is essentially constant in both cases (Figs. 22b and 27b).

## 4.2 RACK-MOUNTED STORES

### 4.2.1 Unstable Configurations

Two unstable rack-mounted store configurations were investigated, the ASP and the CBU-46 (SUU-7) launcher pod. The ASP was tested on the MER, mounted on the C-L and LOB pylons (Figs. 28 through 33 and 34 through 39), and the CBU-46 was tested on the TER, mounted on just the LIB pylon (Figs. 41 through 46). Aerodynamic loads acting on the ASP and CBU-46 were acquired with the store models approaching (and/or receding from) MER stations 1, 2, 3, and 4, and TER stations 2 and 3, respectively. Data corresponding to trajectories from either all four MER stations or both TER stations, as appropriate, and on one pylon station are presented on each page for one Mach number.

Upon inspection of the normal force data for the ASP on the C-L pylon at Mach number 0.6, Fig. 28a, it would appear that the bracket-support (captive) and dual-support (approach) data are in good agreement for all stations except MER station 2. For MER-2, the discrepancy between the measurements made with the two techniques appears to be irreconcilable. However, upon examination of normal-force data for MER-2 at Mach numbers 0.9, 1.1, and 1.2, Figs. 28b, c, and d, respectively, it appears certain that the discrepancy is not real, but rather that there are inflections and severe gradients in the normal force acting on the store model when  $0 < Z/D < 0.2$ , just as noted for the large pylon-

mounted configurations (Section 4.1). Allowing for slight errors in locating the store with respect to the captive position as described in Section 4.1.1, it appears, in fact, that the two test techniques yield data that are in very good agreement. Equally good results are evident for both side force and axial force (Figs. 29 and 30) except that the most severe inflection and gradient occurs for MER station 3. For the unstable ASP, rolling moment is, of course, negligible throughout the flow field (Fig. 31). Pitching-moment and yawing-moment data (Figs. 32 and 33, respectively) also indicate excellent agreement between captive and approach techniques.

In all cases, data points are connected not by faired curves, but by straight-line segments. Despite the discontinuous fairing of the data, it is interesting to note that for all MER stations and Mach numbers, the decay of loads to free-stream values cannot be described by a simple exponential function, except for axial force.

Figures 34 through 39 include data for the ASP/MER combination on the LOB pylon. Again, as for the C-L pylon data, very good agreement between captive and approach data is observed for normal force (Fig. 34). The most severe gradients occur for MER station 2, and the decidedly non-exponential decay to free-stream values is evident, just as for the C-L pylon. Rolling moment is predictably negligible throughout the flow field (Fig. 37). Axial force generally decays exponentially through the flow field, except for MER station 3 at Mach number 0.6, for which the inflection and strong gradient phenomenon appears (not previously observed for axial force) (Fig. 36a). Equally surprising is the exponential increase in axial force for Mach numbers of 0.9 and above for the store model separating from MER stations 1 and 3 (Figs. 36b, c, and d). Side force is somewhat erratic near MER stations 3 and 4 (Fig. 35), varying from nose-inboard to nose-outboard values over very small ranges of values for  $Z/D$ . At subsonic conditions, yawing moment corresponds to side force consistently, i.e., positive side force-positive yaw, and negative side force-negative yaw, except for MER station 4 at Mach number 0.9 (cf. Figs. 35b and 39b). Even more inconsistent results are noted for Mach numbers 1.1 and 1.2 (Figs. 35c and d and 39c and d). Particular attention is drawn to MER stations 3 and 4, for which yawing moment is of opposite sign to side force for  $Z/D < 0.5$ , but of the same sign for  $Z/D > 1.0$ . Normal-force and pitching-moment variations are equally disturbing (Figs. 34 and 38). It is apparent that the pressure distribution over the store changes as a function of  $Z/D$ , specifically in the flow field near the captive position.

In 1971, Smith (Ref. 6) hypothesized rapid changes in pitching and yawing moments as a store leaves a "sheltered" position such as MER station 3. He was inspired to do so by serious discrepancies between flight-test trajectories and analytically predicted trajectories. In his analytical approach, Smith used tables of free-stream loads acting on the store as a function of Mach number and angle of attack, with

contributions of the interference flow field of the aircraft included through use of a table of influence coefficients. However, the influence coefficients were assumed to decrease linearly with  $Z/D$ , and inflections and severe gradients of the type noted above were not anticipated. The probable existence of strong gradients was indicated by store attitudes determined from in-flight data which disagreed with predicted first maximum pitch and yaw attitudes by as much as 12 deg. Smith's conjecture is apparently substantiated by the wind tunnel data described herein. Both Smith's in-flight data and the wind tunnel data clearly illustrate the complexity of the flow field through which MER-mounted stores must pass during separation, especially from outboard pylon stations. That equally complex flow fields exist around TER installations can be seen in Fig. 40 (taken from Ref. 7). Local flow velocities were measured with a tiny probe over a grid of locations near the LIB pylon of an F-4C at Mach number 0.85. Differences exist between the configuration of Fig. 40 and the configurations tested for the study discussed herein, such as the presence of the fuel tank and the fact that the store was the M-117 bomb, but the data of Fig. 40, acquired at a fuselage station near the aft end of the TER (consequently near the fins of a stable store), surely indicate clearly the severe flow gradients to which a rack-mounted store could be exposed.

Presented in Figs. 41 through 46 are loads acting on the unstable CBU-46 store configuration both in the captive position and approaching the shoulder stations of the TER-9A on the LIB pylon. During the tests, only the two shoulder stations of the TER were occupied; when the instrumented model was mounted on one station, a dummy model was mounted on the other.

At first glance, the approach data appear to be discontinuous at approximately  $Z/D = 0.4$ . The discontinuous appearance is false, though, because of the manner in which data were acquired. Data were actually acquired both approaching and receding from the captive position, as described in Section 3.1, resulting in redundant coverage of approximately the range  $0 < Z/D < 0.4$ . Since the redundant approaching and receding data are in slight disagreement, there is apparently some hysteresis from an unidentified source.

Agreement between approach data and captive data is excellent for all load components at TER station 2, but only fair for normal-force coefficient at TER station 3. Since the agreement is so good for all other components, including pitching and yawing moments, it is considered that the captive data are substantially correct. Hence, there probably are inflections and strong gradients in the normal force approach data in the range  $0 < Z/D < 0.1$  that would, if measurable, establish better agreement with the captive data.

By using the data acquired for both MER and TER installations, it is not possible to describe the mode of decay of the load components to free-stream values along a Z axis that the stores would more nearly follow in a conventional separation. The axes along which data were acquired were perpendicular to the faces of the shoulder stations on the rack and, therefore, in the y-z plane (cf. Section 3.1 and Fig. 13). Discontinuities in the approach data (other than those attributable to fairing of the data as discussed above) can probably be ascribed to the canted approach axes, which subjected the store models to stronger interference from adjacent features on the aircraft than would a vertical approach.

#### 4.2.2 Stable Configurations

Two stable rack-mounted store configurations were investigated, the CBU-24 (SUU-30) and MK 83 bombs. The CBU-24 was tested on the MER, mounted on the C-L and LOB pylons (Figs. 47 through 52 and 53 through 58), and the MK 83 was tested on the TER, mounted on the LIB pylon (Figs. 59 through 64). Aerodynamic loads acting on the CBU-24 and MK 83 were acquired with the store models approaching and/or receding from MER stations 1, 2, 3, and 4, and TER stations 1, 2, and 3, respectively. Data corresponding to trajectories from either all four MER stations or all three TER stations, as appropriate, and on one pylon station are presented on each page for one Mach number.

Just as in the case of the unstable ASP configuration on the C-L pylon (Section 4.2.1), the approach data for normal force acting on the CBU-24 appear to be in poor agreement with the bracket-support (captive) data for MER station 2 at Mach number 0.6 (Fig. 47a). However, again just as for the ASP, the normal-force data at MER-2 for Mach numbers 0.9, 1.1, and 1.2 indicate that there are inflections and severe gradients in the range  $0 < Z/D < 0.2$  (Figs. 47b, c, and d). Strong reversals appear at MER station 1, as well.

Excellent agreement between the two test techniques is evident for side force (Fig. 48), axial force (Fig. 49), and rolling moment (Fig. 50). It is noted that for the CBU-24, even though stabilized with fins, the values of rolling moment are negligible everywhere except in and very close to ( $Z/D < 0.1$ ) the captive position. Corresponding data for the CBU-24 and ASP configurations are remarkably similar (cf. corresponding sub-titles of Figs. 28 through 33 and 47 through 52), a consistency that tends to certify the validity of the test results.

After allowances for deflection-induced mislocations of the touch point (see Section 4.1.1) and inflections in the range  $0 < Z/D < 0.2$ , pitching and yawing moments determined by the two techniques appear to be in excellent agreement (Figs. 51 and 52). Values of pitching moment cover a much wider range of values, especially in the negative direction, than for the ASP, but that is understandable for a finned configuration.

The contorted decay modes evident for MER stations 1 and 3 are further indication of the complexity of the flow field to which a rack-mounted store is exposed during separation (Section 4.2.1). Very little yawing moment develops, since the rack is located on the C-L pylon, with significant values noted only at Mach numbers 1.1 and 1.2, during the oblique approaches to MER stations 3 and 4 (Figs. 52c and d). Shocks emanating from adjacent physical features of the aircraft likely cause these moments.

Figures 53 through 58 are comprised of data for the CBU-24/MER combination on the LOB pylon. As for the C-L data, very good agreement between captive and approach data is evident. For normal force (Fig. 53), the most severe gradients occur for MER stations 1 and 2 at subsonic conditions, and for these plus MER station 3 at Mach numbers 1.1 and 1.2. Very clear evidence for the inflection-gradient phenomenon exists for all Mach numbers, and for all MER stations investigated except MER-4. With adjacent stations empty (as described in Section 2.2.1, appropriate dummy store models were removed as the instrumented store was moved from stations 1 to 4), the flow field in the vicinity of MER station 4 is apparently less complex than when the rack is loaded with a full complement of stores.

Side force (Fig. 54), axial force (Fig. 55), rolling moment (Fig. 56), and yawing moment (Fig. 58) all represent very good-to-excellent agreement between approach and captive data. Even pitching moment (Fig. 57), with many discontinuities attributable to the various reasons discussed above and in Section 4.2.1, reflects good agreement between techniques. The reader is again cautioned to recall that approaches to MER stations 3 and 4 are along oblique axes in the Y-Z plane instead of along a simple Z axis, probably explaining many of the apparent discontinuities in not only pitching moment, but also in the other load components.

Results for the MK 83 store configuration are presented in Figs. 59 through 64. Both bracket-supported captive loads and sting-supported loads were acquired with the instrumented store model at all three TER stations. When the instrumented store model was on or approaching or receding from TER station 1, dummy models of the store were mounted on TER stations 2 and 3, but when the instrumented store model was on or approaching or receding from either TER station 2 or 3, TER station 1 was empty, and a dummy store model was on the opposite station. No captive data were acquired for TER station 2, and none at Mach number 1.2 for TER station 1, or Mach number 0.8 for TER station 3. (The MK 83 was the only configuration for which data were acquired at Mach number 0.8.)

In Fig. 59, the existence of inflections and strong gradients in normal force in the range  $Z/D < 0.2$  can be surmised from the data presented for TER station 3. Although the data for TER station 2 appear to decay toward free-stream values in a purely exponential manner, the existence of data points for  $Z/D < 0$  simply indicates a shift in captive position between wind-off and wind-on conditions, so that the correct captive position may have been at  $Z/D = -0.2$  or so. (A discussion of the reasons for this position error is presented in Section 4.1.1.) For  $Z/D > 0.2$ , the decay of normal force to free-stream values for all TER stations and subsonic Mach numbers is exponential. At supersonic Mach numbers, the decay is not simply exponential, but is complicated by the complex flow field through which the store model passes in moving along the oblique approach axis for the shoulder stations of the rack.

Agreement between dual-support and bracket-support data is very good for side force (Fig. 60) and axial force (Fig. 61). Rolling moment correlates well (Fig. 64), with an exponential decay to free-stream indicated at all rack stations and Mach numbers. For subsonic Mach numbers, pitching moment (Figs. 63a, b, and c) indicates excellent agreement between support techniques, with an exponential decay rate to free-stream values. For supersonic Mach numbers, pitching moment decays in a complicated manner, not only from the shoulder stations, but also from TER station 1, probably because of shock-induced interference (Figs. 63d and e). It is notable that even at five or six store diameters from the captive position at TER-1, free-stream values have not been reached, indicating the extent of the interference flow field of the aircraft. Trends in yawing moment (Fig. 64) are similar to pitching moment, with good agreement between bracket-support and sting-support data. The reader is cautioned to recall that throughout all of the above tests, the store model was constrained to a fixed attitude of zero deg, and that the loads acting on the store under this condition would not necessarily be the loads acting during a free fall.

## 5.0 CONCLUSIONS

In a series of wind tunnel tests conducted over a range of Mach number from 0.6 to 1.2, measurements were made of the aerodynamic loads acting on models of eight store configurations supported in and near the captive position on a model of a contemporary fighter aircraft. Loads were measured using two methods of supporting the store models: internal bracket support and dual sting support. Using the CTS as a dual-support technique, it was possible to evaluate both the effects of the "touchwire" gap necessary to prevent fouling between store and aircraft models, and the effectiveness of using the CTS for measuring captive loads. Characteristics of the interference flow field of the aircraft were determined as secondary observations. Conclusions that have been drawn from an analysis of the data include the following:

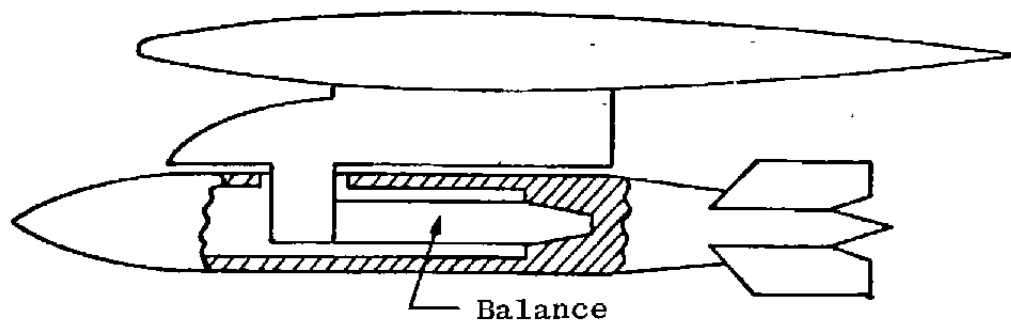


1. Under many conditions, aerodynamic loads acting on a store model in the captive position on an aircraft model can be measured with equal success in a wind tunnel using either internal bracket-support techniques or dual sting-support techniques. However, inflections and severe gradients in normal force, side force, pitching moment, and yawing moment can occur close to the captive position, principally in the range of  $0 < Z/D < 0.2$ . Therefore, extrapolation of closest-approach data (acquired using dual sting-support techniques) to the captive position can lead to large errors in estimates of captive loads, both in magnitude and sense. In the design of store carriage hardware, critical loading arises from consideration of the total flight envelope for an aircraft, especially maneuvering flight. In other words, inertial loading of a structural component usually is more significant than the aerodynamic loading. Hence, for structural design purposes, the aerodynamic loads determined using either technique discussed herein can be adequately valid. However, discretion is indicated in the application of aerodynamic captive loads acquired using dual-support techniques in analytical predictions of store separation trajectories.
2. Particularly strong gradients exist in the region defined by  $0 < Z/D < 0.2$  for MER-mounted stores, especially on MER stations 1 and 3. For these stations, extrapolation of nearest-approach data obtained using dual sting-support techniques can lead to large errors in estimates of captive loads.
3. Influences attributable to the touchwire gap are least evident for axial force and rolling moment. Axial force decays within two diameters of the store to free-stream values in a simple exponential fashion for all pylon/rack/store combinations tested, except for any store mounted on MER stations 1 and 3, for which the store is in the wake of the forward store until separation begins. Rolling moment is either negligible or decays within two diameters of the store to free-stream values in an exponential fashion for all pylon/rack/store combinations tested.
4. At subsonic conditions, effects of the interference flow field of the aircraft on aerodynamic loads acting on both stable and unstable stores decrease in a simple exponential manner in the range of  $Z/D > 0.2$ . However, when  $M_\infty > 0.9$ , the development of shock structures in the flow field leads to discontinuities in the decay of interference effects.
5. The influence of the interference flow field of an aircraft on normal force and pitching moment acting on a store can extend beyond five store diameters from the captive position for the configurations tested.

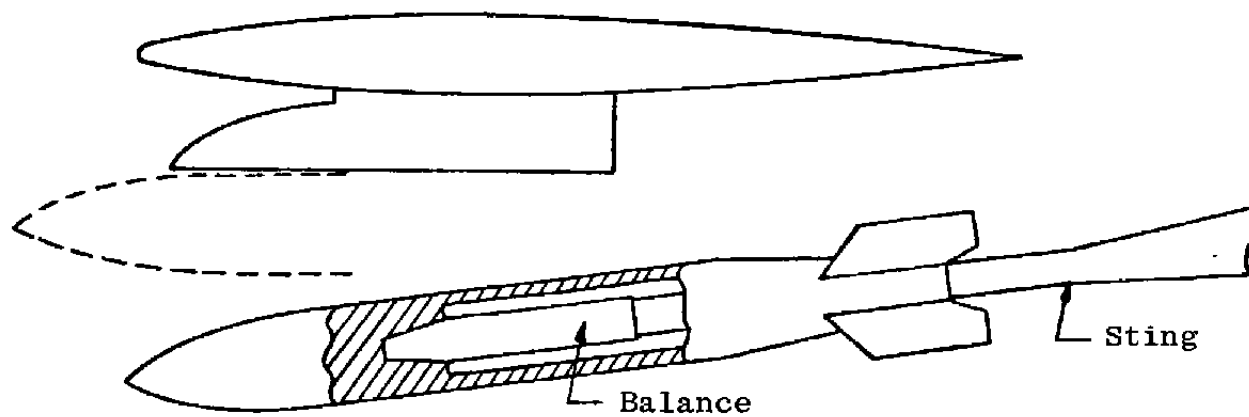
6. Difficulty in accurately positioning a store in the captive position limits the precision with which captive loads can be measured using dual sting-support techniques. Sources of error include: deflections of both store and aircraft models and associated support equipment; design tolerances and wear in positioning mechanisms, and aeroelastic vibration of both models. If extreme precision in captive loads is required, either bracket-support techniques should be used, or the above inadequacies must be overcome to allow closer approach of the store to the captive position.

## REFERENCES

1. Dix, R. E. "A Review of Methods of Measuring Aerodynamic Forces and Moments Acting on Captive Stores in Wind Tunnel Tests." AEDC-TR-72-108 (AD902816L), August 1972.
2. Christopher, J. P. and Carleton, W. E. "Captive-Trajectory Store-Separation System of the AEDC-PWT 4-Foot Transonic Tunnel." AEDC-TR-68-200 (AD839743), September 1968.
3. Dix, R. E. "Influences of Sting Support on Aerodynamic Loads Acting on Captive Store Models." AEDC-TR-76-1, AFATL-TR-76-25 (ADA022257), March 1976.
4. Jacocks, J. L. and Hartley, M. S. "Calibration of the AEDC-PWT 4-Foot Transonic Tunnel with Modified Walls." AEDC-TR-69-134 (AD853841), June 1969.
5. Gunn, J. A. "Calibration of the AEDC-PWT Aerodynamic Wind Tunnel (4T) Using Diffuser Flap Plenum Suction." AEDC-TR-70-74 (AD867975), April 1970.
6. Smith, R. E. "Prediction of Store-Separation Motion Using Initial Captive Loads." NWC TP5261 (AD890671L), October 1971.
7. Davis, Ronald E. "Flow Field Characteristics Beneath the F-4C Aircraft at Mach Numbers 0.5 and 0.85." AEDC-TR-70-8 (AD864702), February 1970.



Internal Support



Dual Support

Figure 1. Two methods of supporting a store in the captive position in wind tunnel tests.

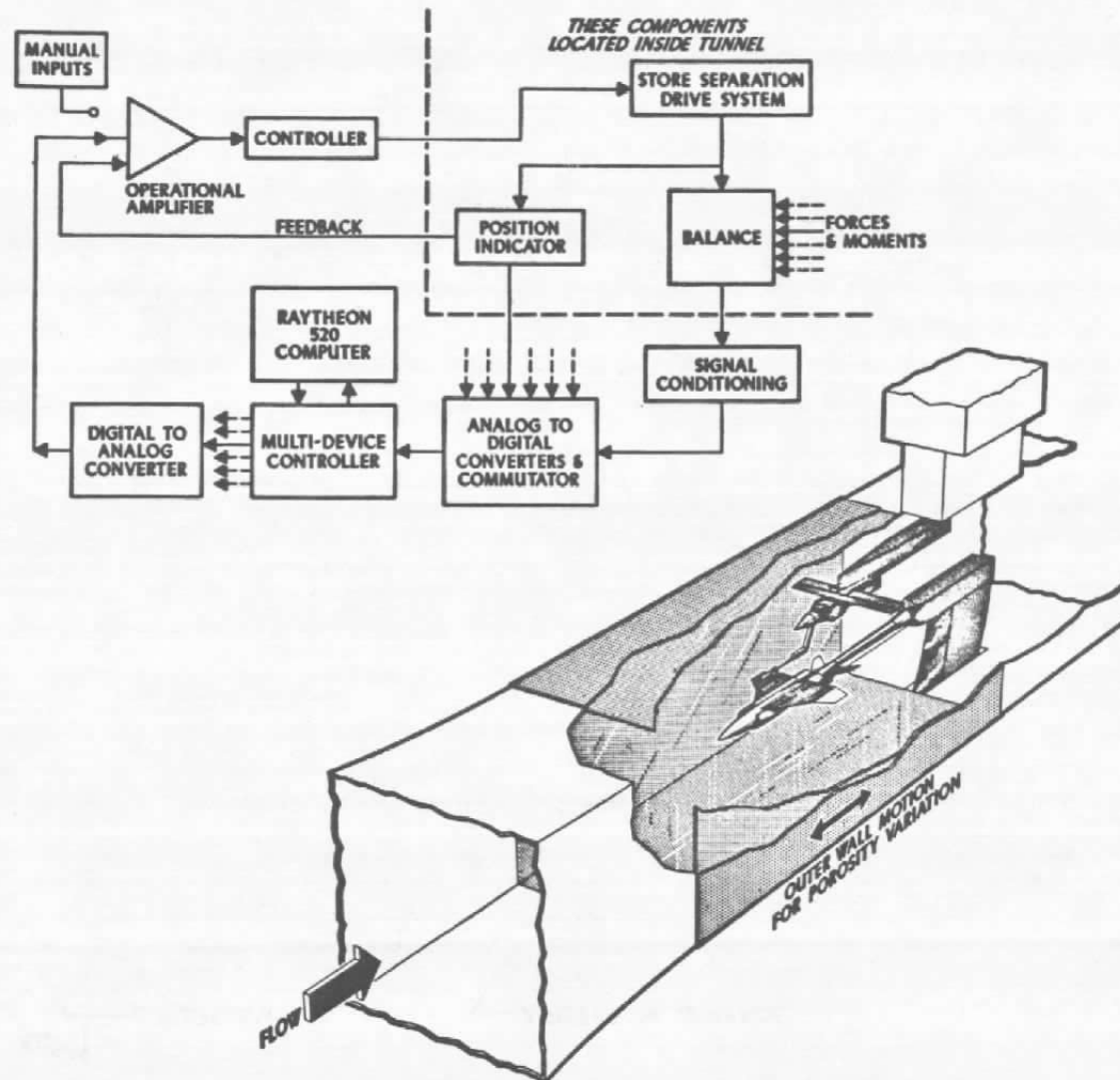
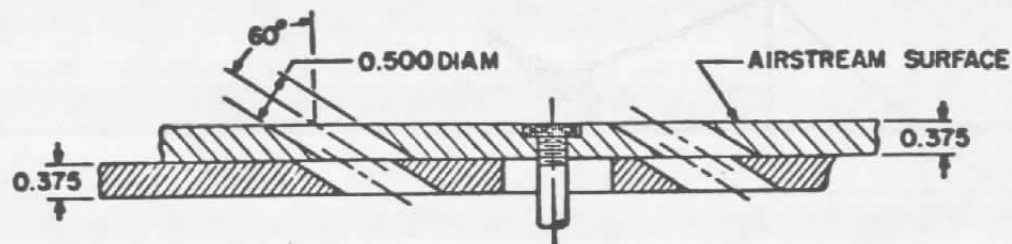


Figure 2. Schematic illustration of the captive trajectory system (CTS).



TYPICAL PERFORATED WALL CROSS SECTION

TUNNEL STATIONS AND DIMENSIONS  
ARE IN INCHES

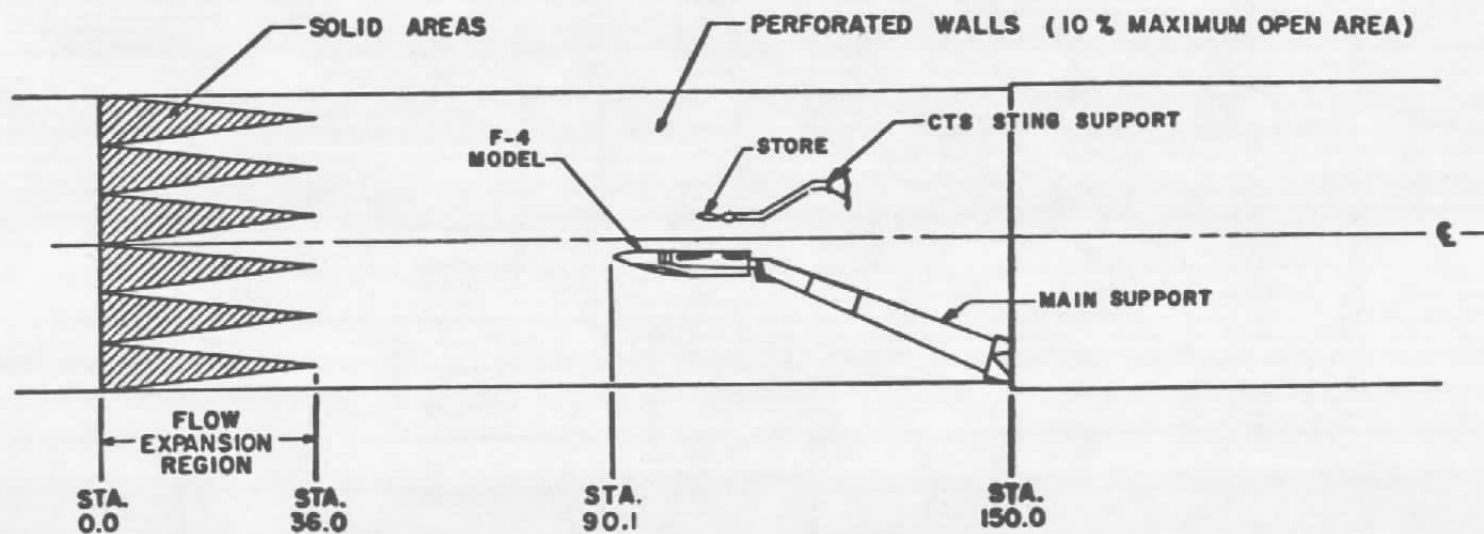


Figure 3. Schematic illustration of a typical model installation in Tunnel 4T.

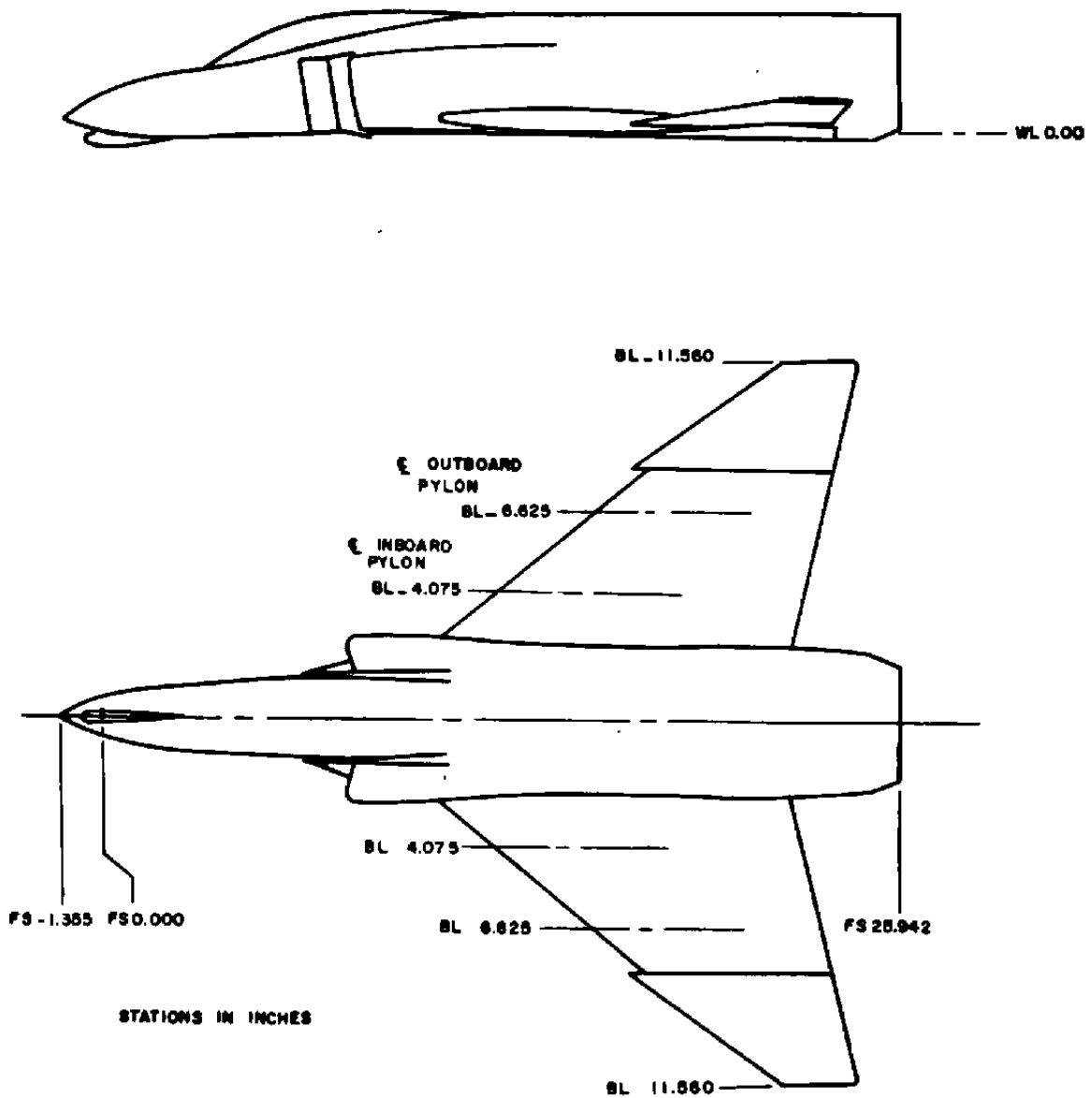
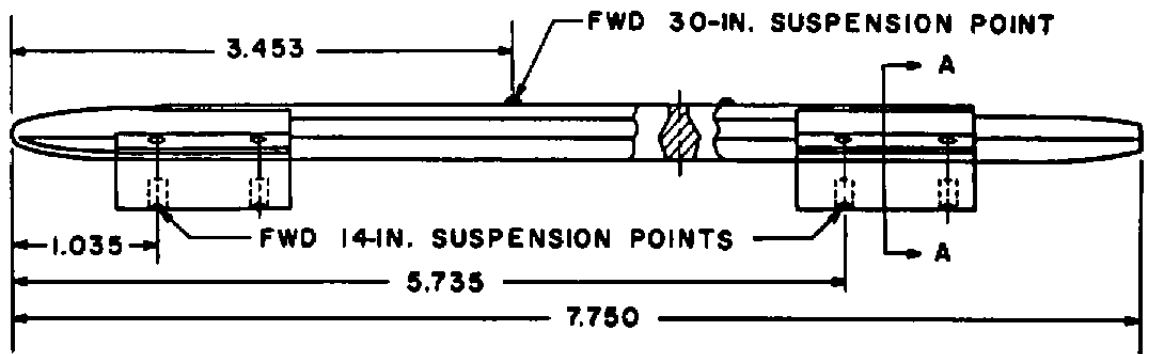
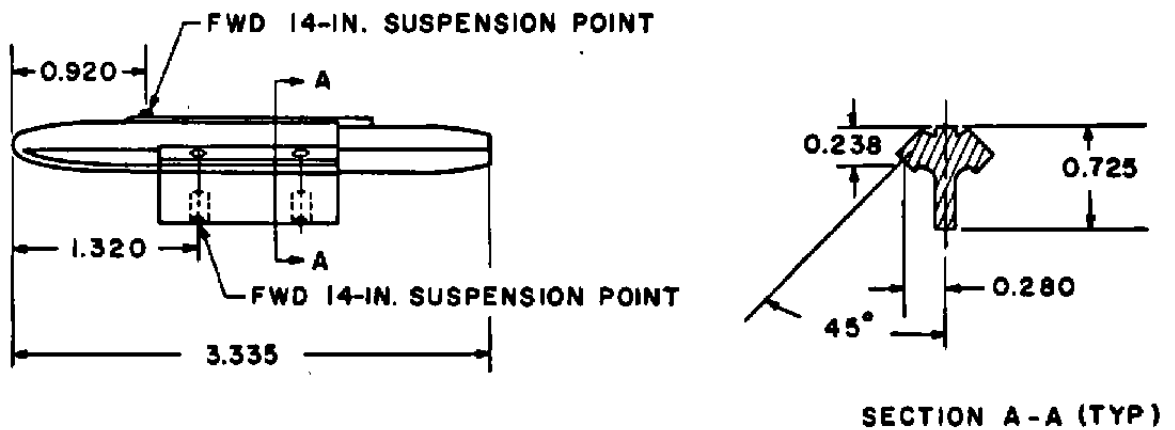


Figure 4. 1/20-scale model of the F-4C aircraft.



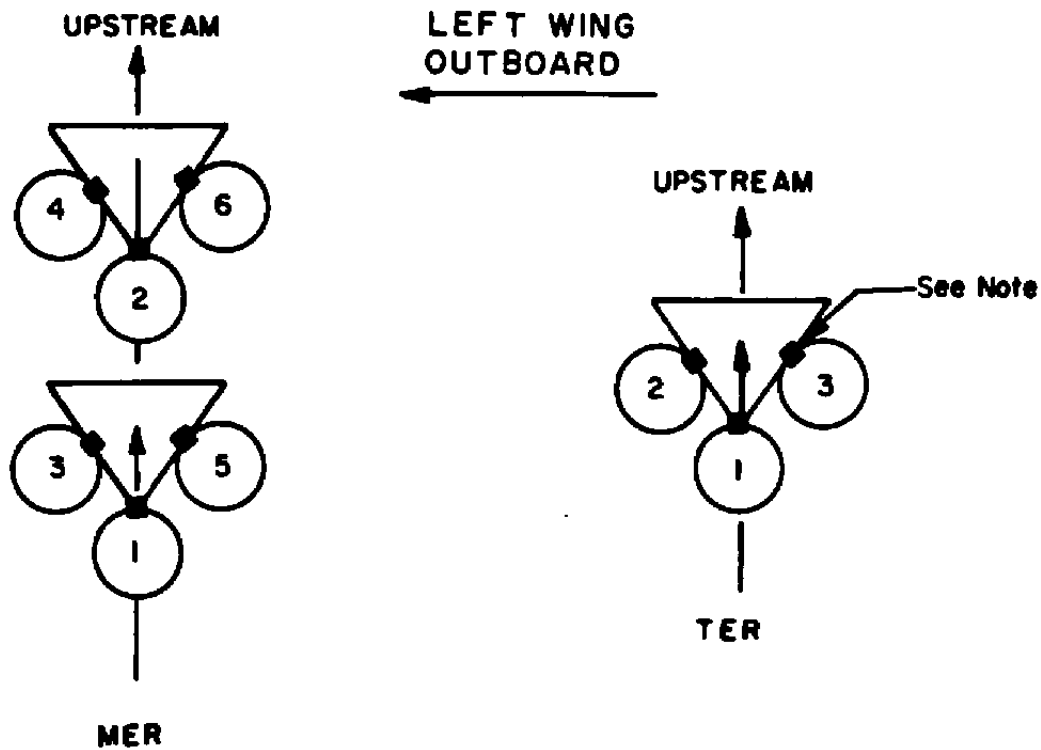
a. Multiple ejection rack, model MER-10A



DIMENSIONS IN INCHES

b. Triple ejection rack, model TER-9A

Figure 5. Details of the models of the multiple and triple ejector racks.



NOTE: The square indicates the orientation of the suspension lugs

TYPE RACK	STATION	ROLL ORIENTATION, deg
MER ↓	1	0
	2	0
	3	45
	4	45
	5	-45
	6	-45
TER ↓	1	0
	2	45
	3	-45

Figure 6. Nomenclature of ejector rack stations.



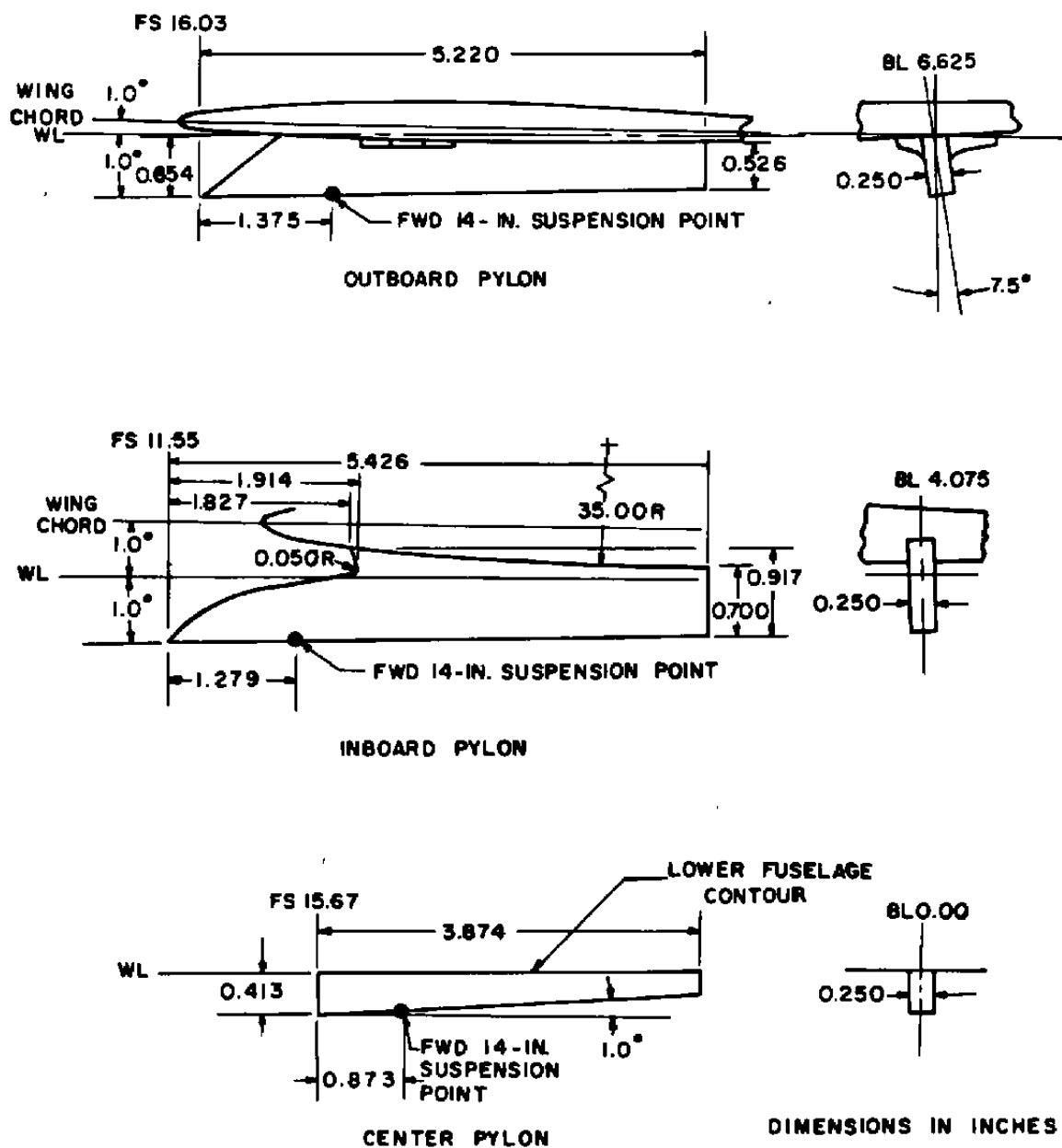
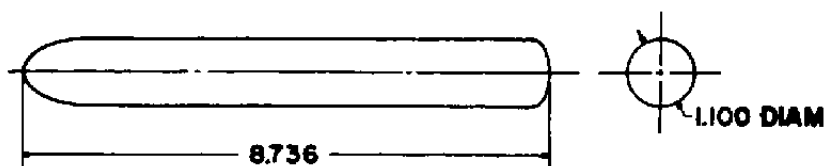
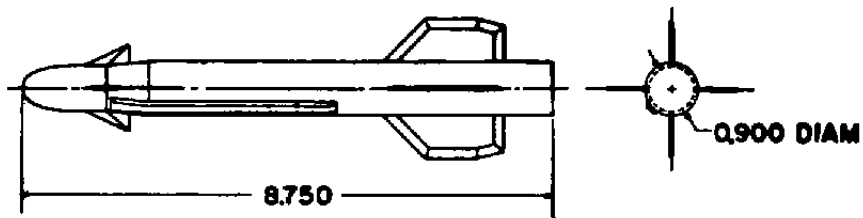


Figure 7. Details of the models of the F-4C pylons.



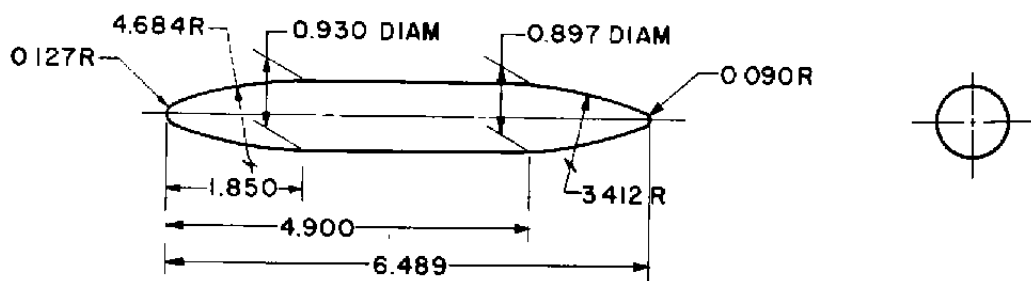
a. Black Crow (modified SUU-16/23)



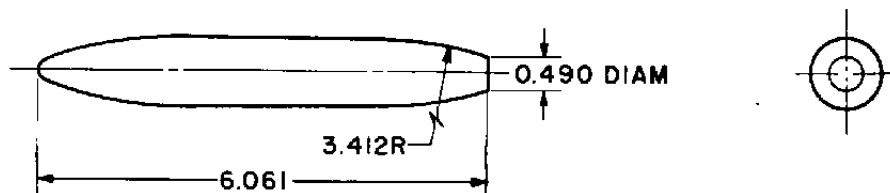
DIMENSIONS IN INCHES

b. Hard Structure Munition

Figure 8. Dimensions of pylon-mounted store models.



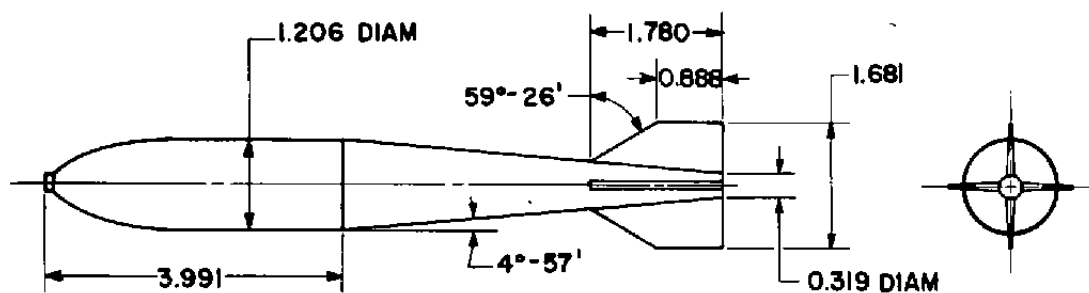
ACTUAL CONFIGURATION



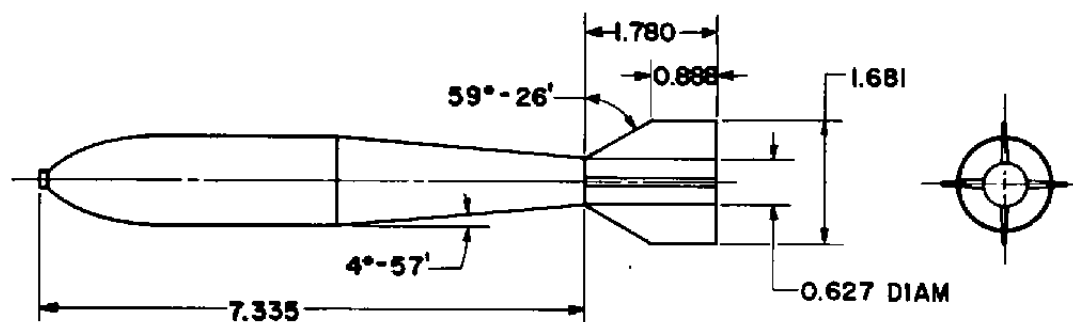
CONFIGURATION MODIFIED FOR STING SUPPORT

DIMENSIONS IN INCHES

c. BLU-1 bomb  
Figure 8. Continued.



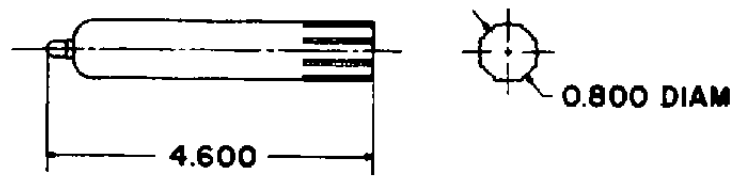
ACTUAL CONFIGURATION



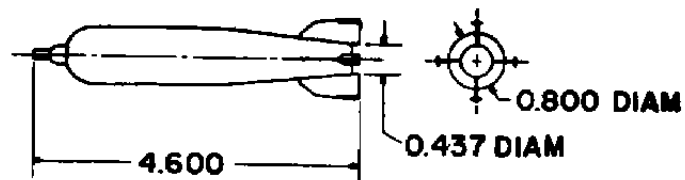
CONFIGURATION MODIFIED FOR STING SUPPORT

DIMENSIONS IN INCHES

d. M-118 bomb  
Figure 8. Concluded.



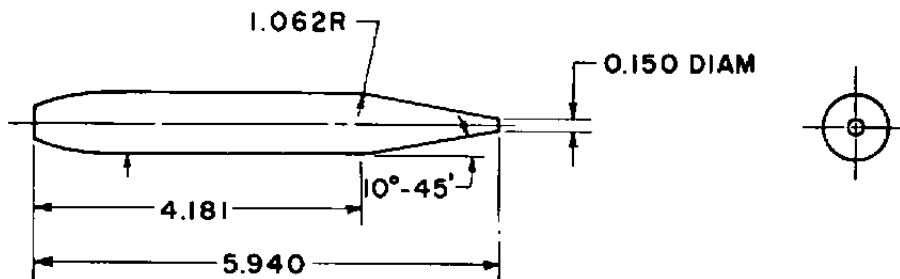
a. ASP



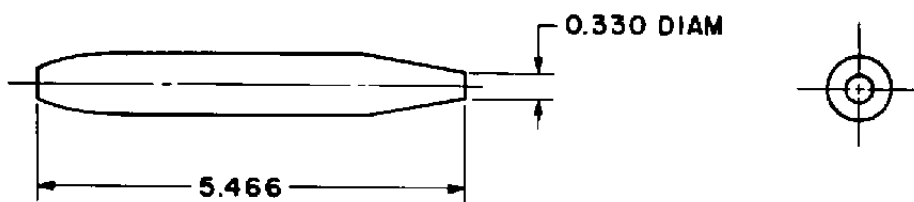
DIMENSIONS IN INCHES

b. SUU-30B/B (CBU-24)

Figure 9. Dimensions of rack-mounted store models.



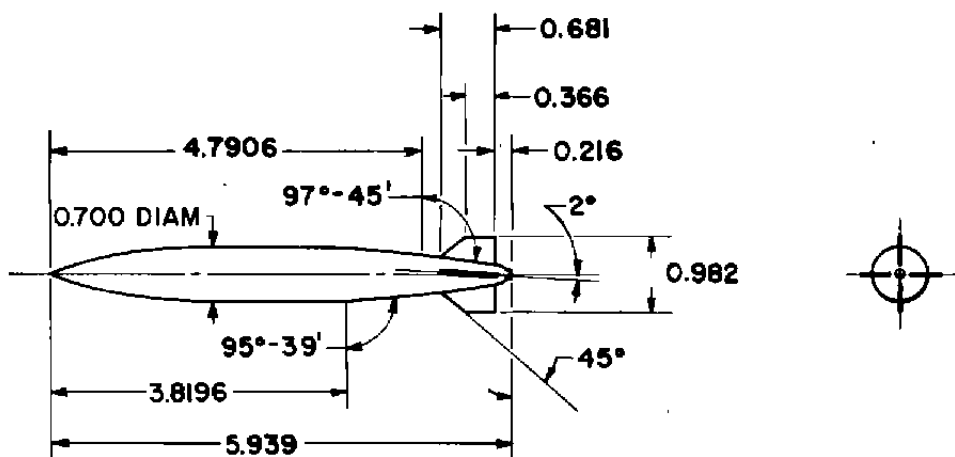
ACTUAL CONFIGURATION



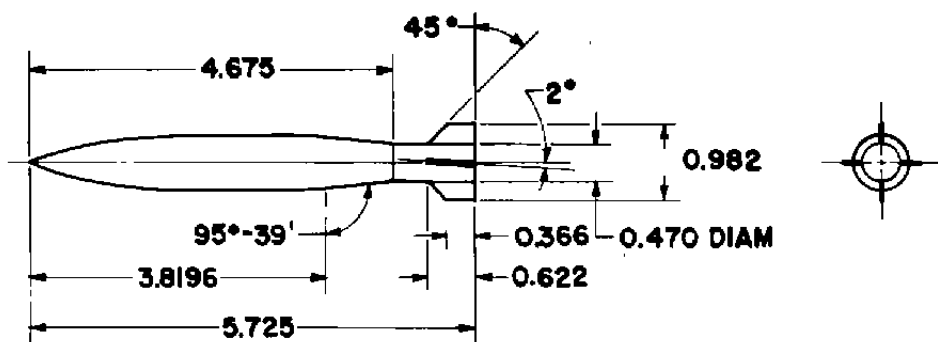
CONFIGURATION MODIFIED FOR STING SUPPORT

DIMENSIONS IN INCHES

c. CBU-46 (SUU-7) launcher pod  
Figure 9. Continued.



ACTUAL CONFIGURATION



CONFIGURATION MODIFIED FOR STING SUPPORT

DIMENSIONS IN INCHES

d. MK-83 bomb  
Figure 9. Concluded.

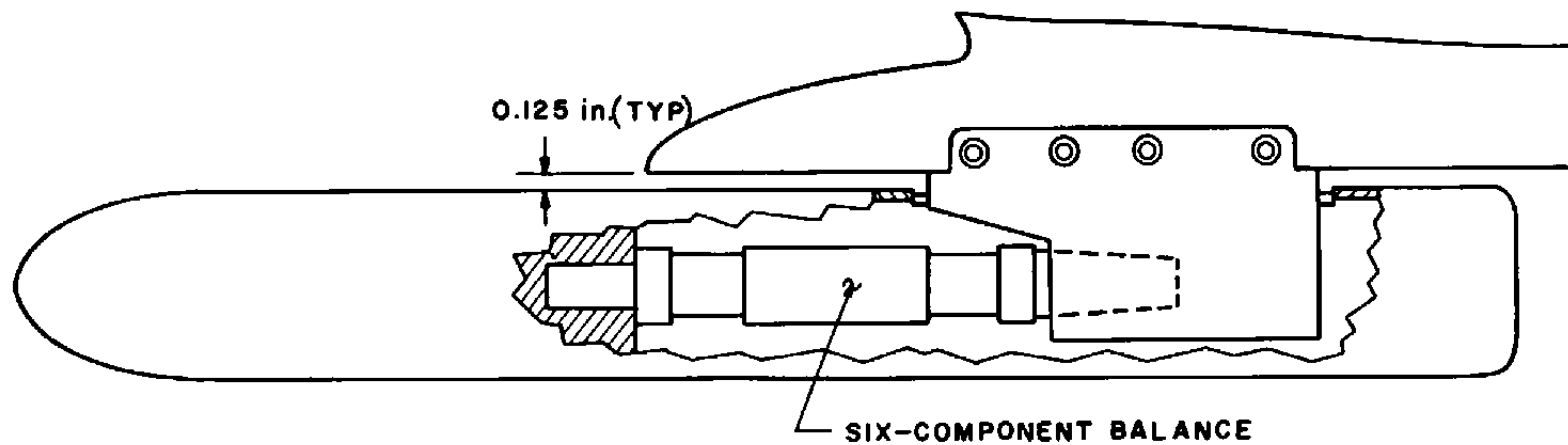
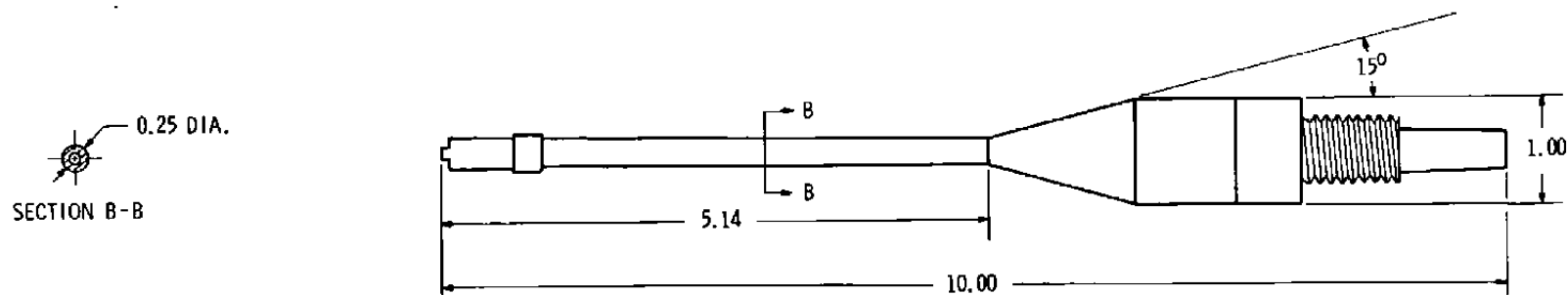
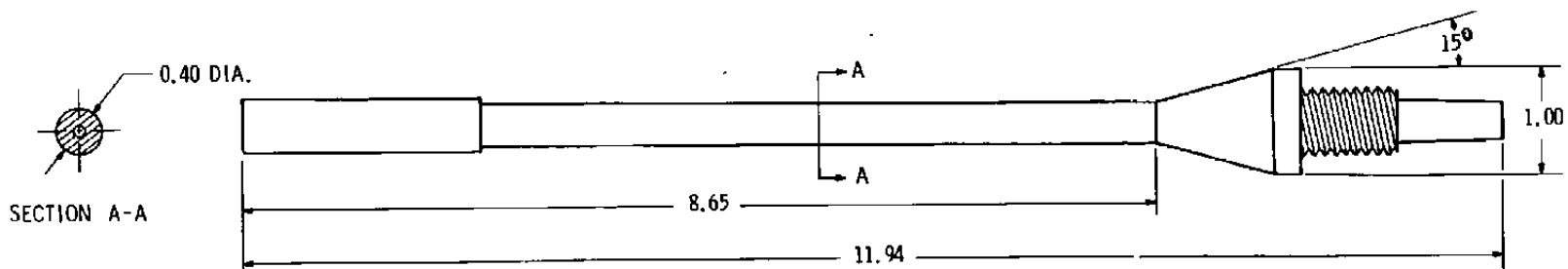


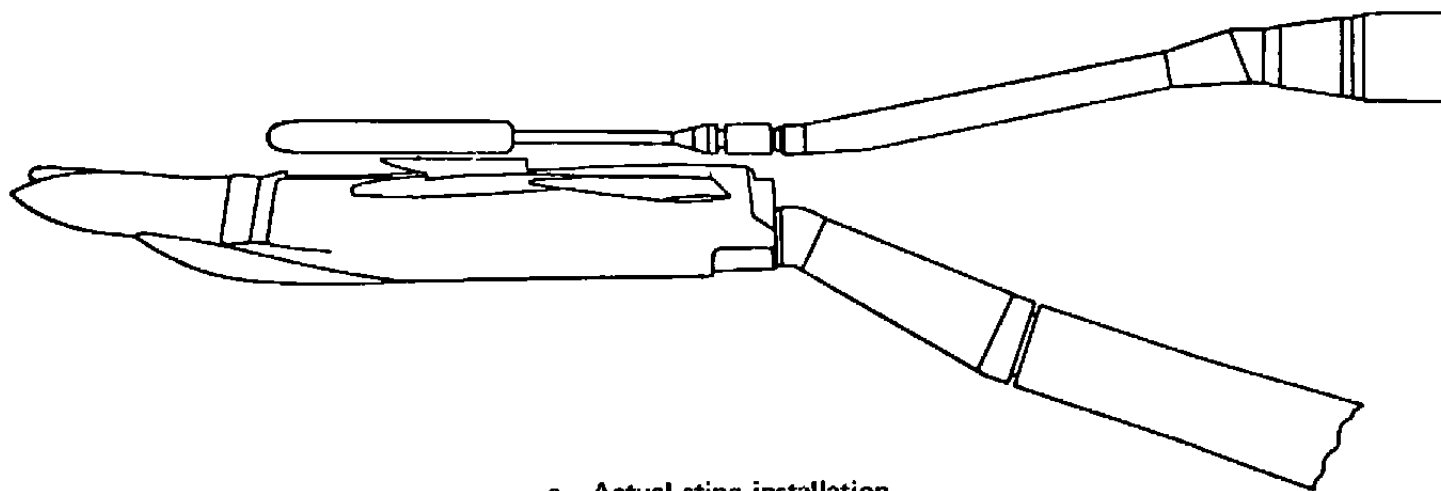
Figure 10. Typical installation of an internal balance-supporting bracket.



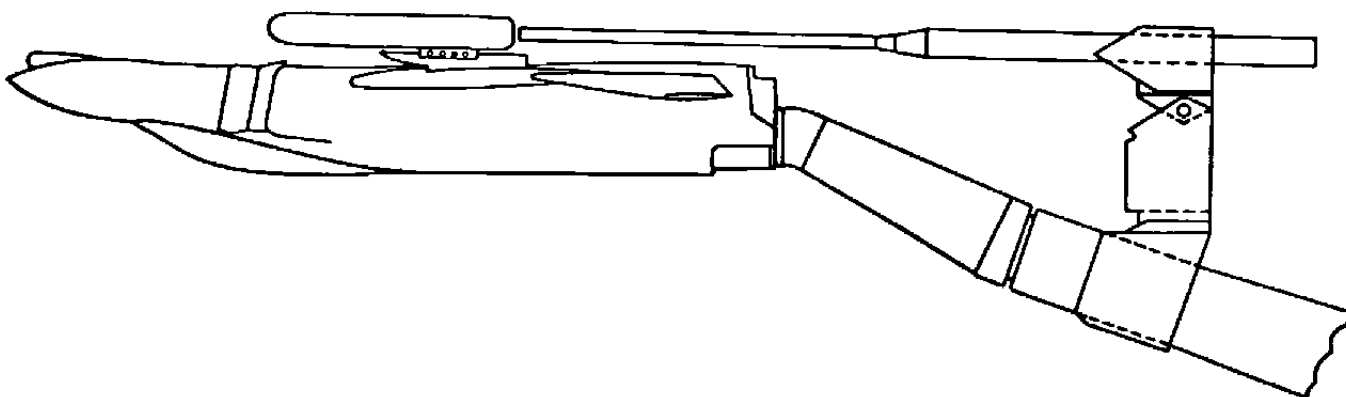


DIMENSIONS IN INCHES

Figure 11. Details of the stings.

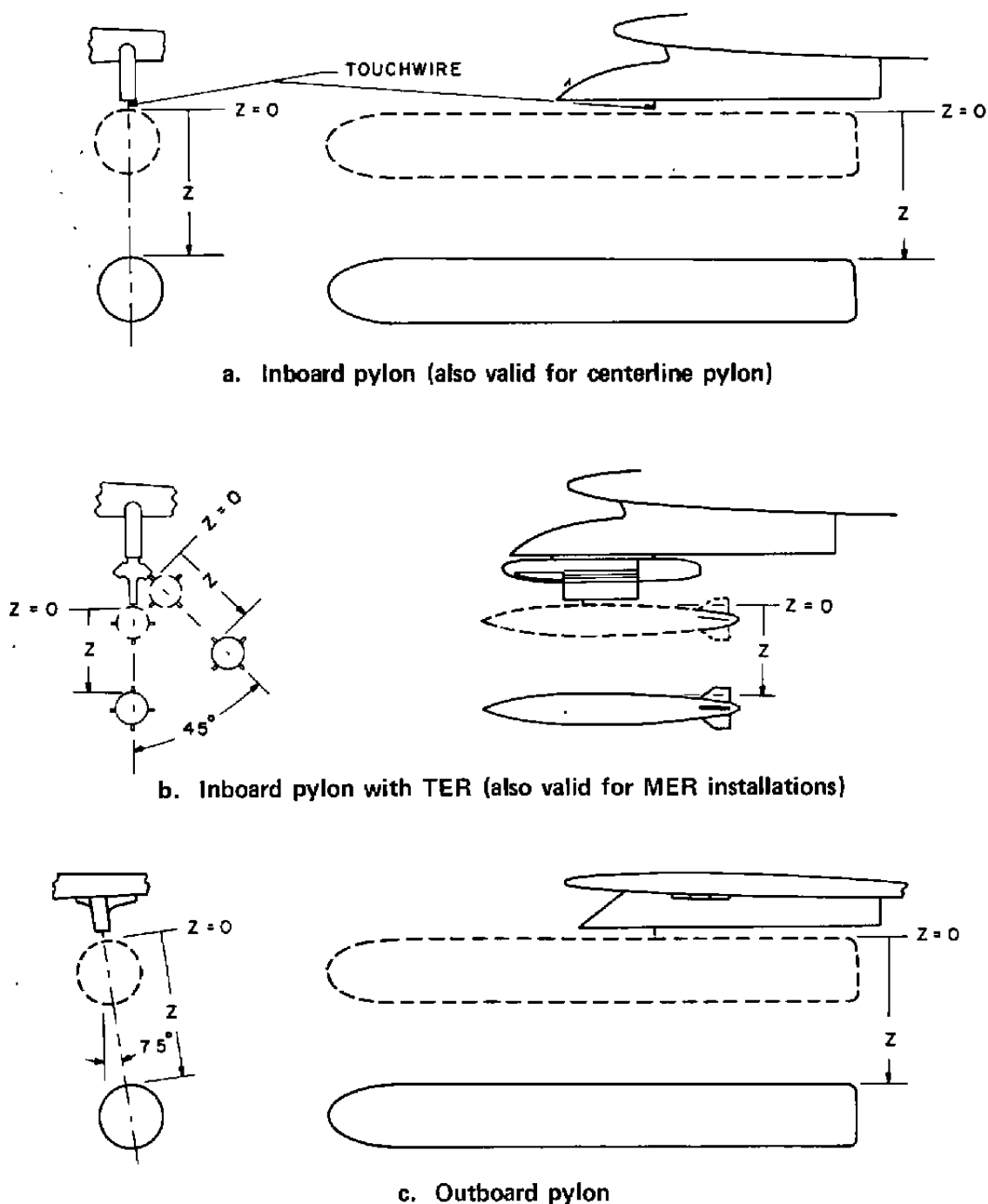


a. Actual sting installation



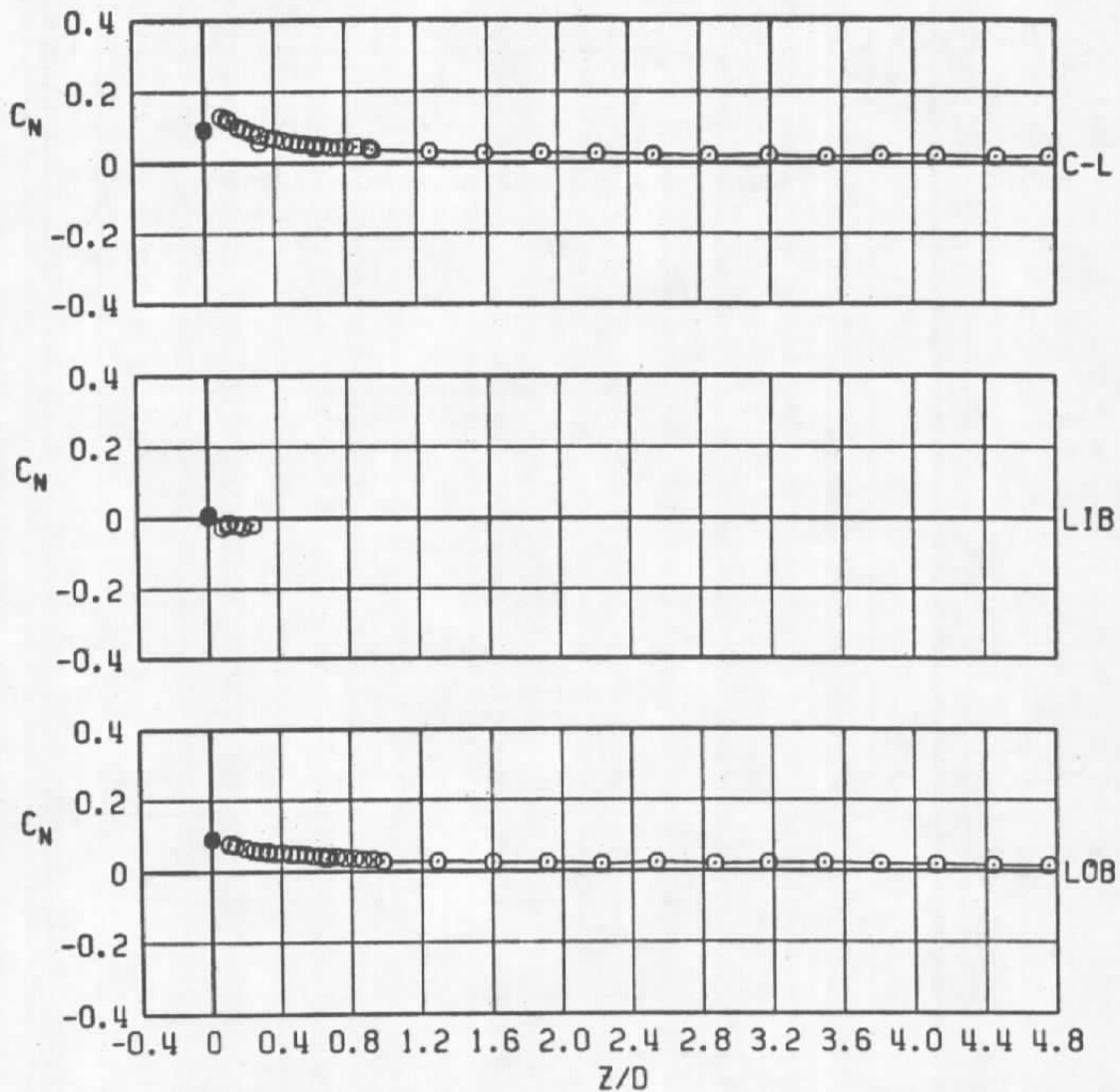
b. Dummy sting installation

Figure 12. Comparison of dummy sting and functional sting installations.



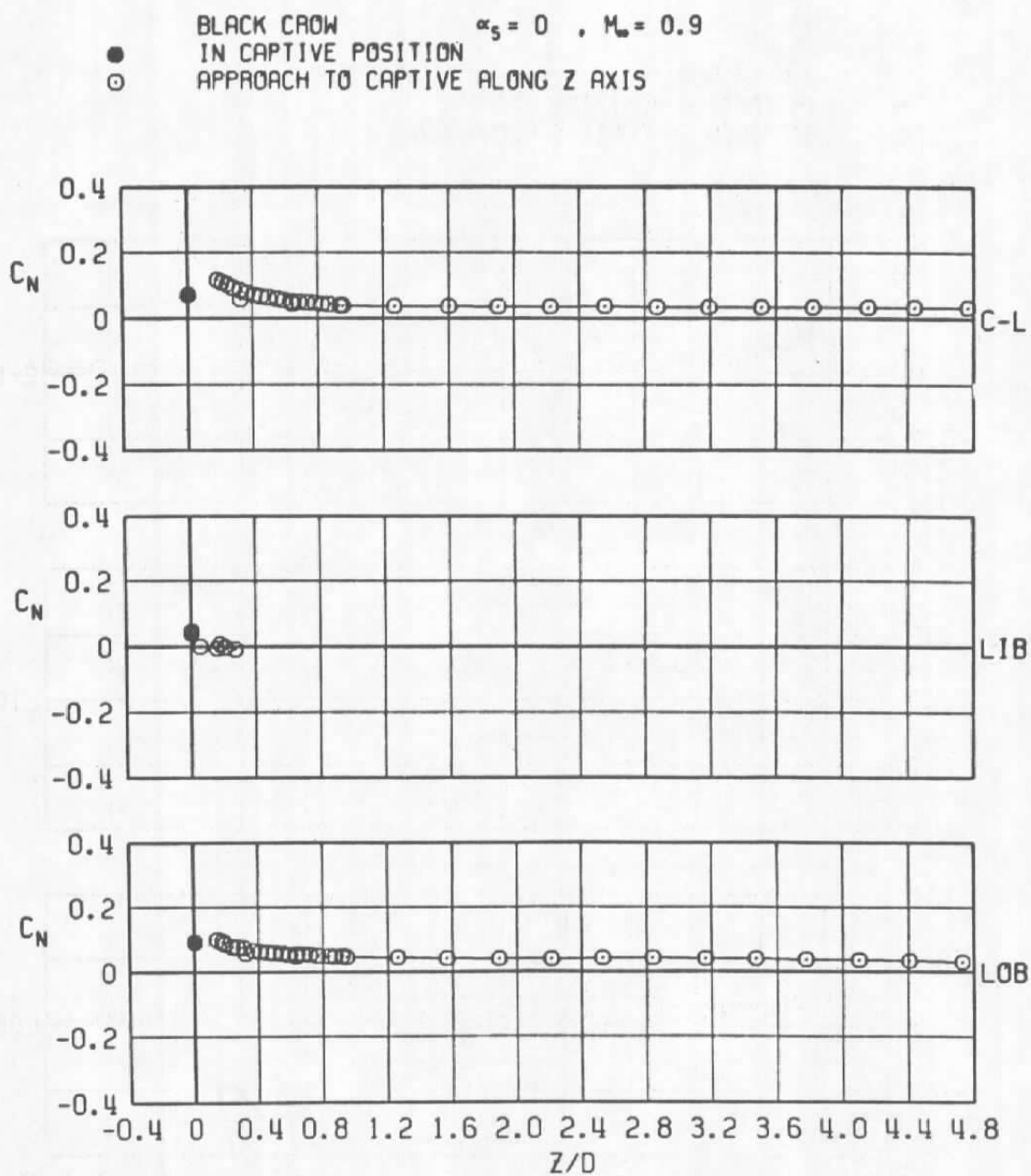
**Figure 13.** Illustration of axes used for translating store to obtain store loads as a function of separation distance from the captive position.

BLACK CROW  $\alpha_s = 0$  .  $M_\infty = 0.6$   
 IN CAPTIVE POSITION  
 APPROACH TO CAPTIVE ALONG Z AXIS



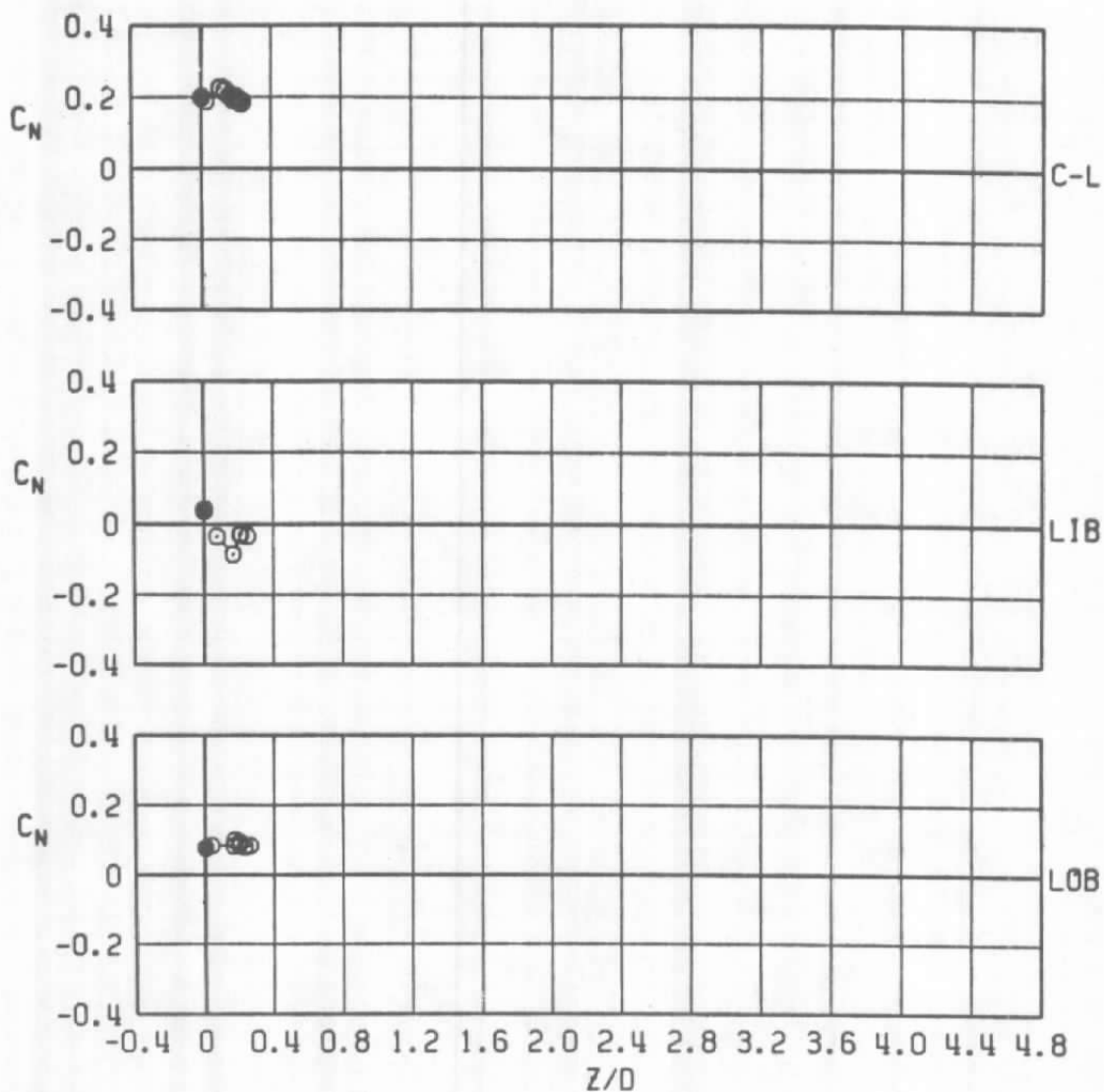
a.  $M_\infty = 0.6$

Figure 14. Coefficient of normal force acting on the Black Crow store as a function of normal distance between the store and the captive position.



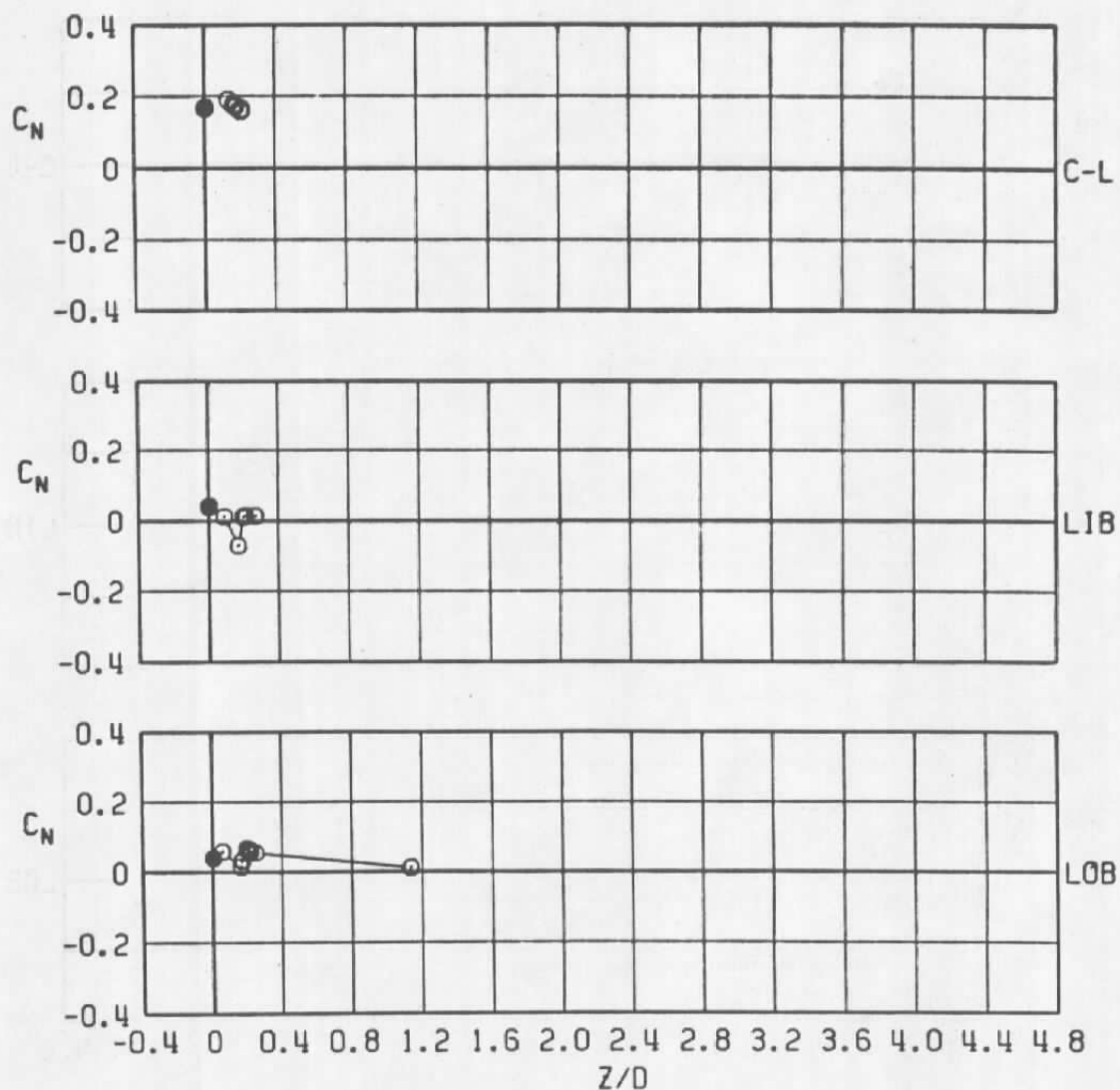
b.  $M_\infty = 0.9$   
 Figure 14. Continued.

● BLACK CROW  
 IN CAPTIVE POSITION  
 ○ APPROACH TO CAPTIVE ALONG Z AXIS  
 $\alpha_s = 0$  ,  $M_\infty = 1.1$



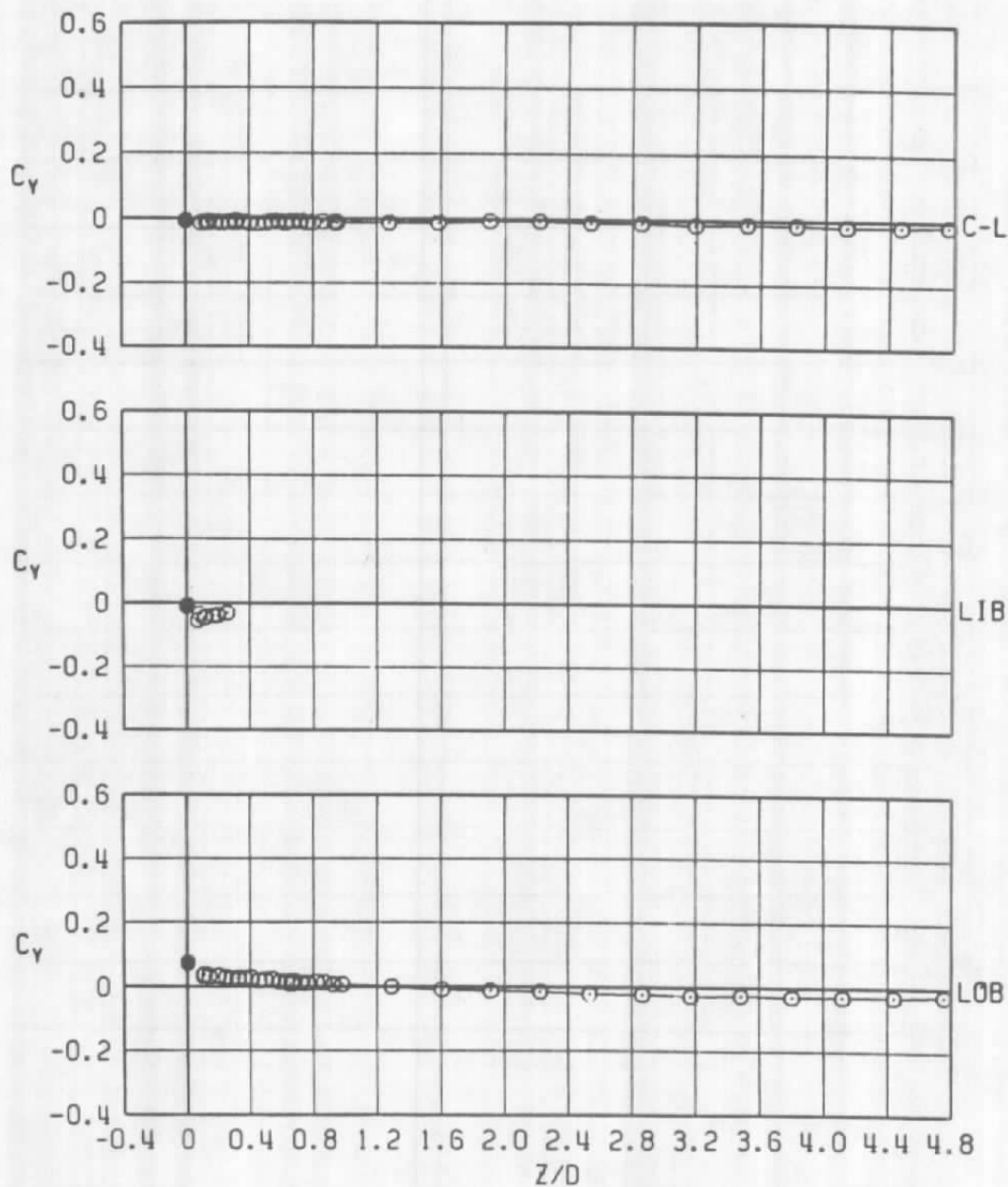
c.  $M_\infty = 1.1$   
 Figure 14. Continued.

● BLACK CROW  
 IN CAPTIVE POSITION  
 ○ APPROACH TO CAPTIVE ALONG Z AXIS



d.  $M_\infty = 1.2$   
 Figure 14. Concluded.

● BLACK CROW  
 IN CAPTIVE POSITION  
 ○ APPROACH TO CAPTIVE ALONG Z AXIS

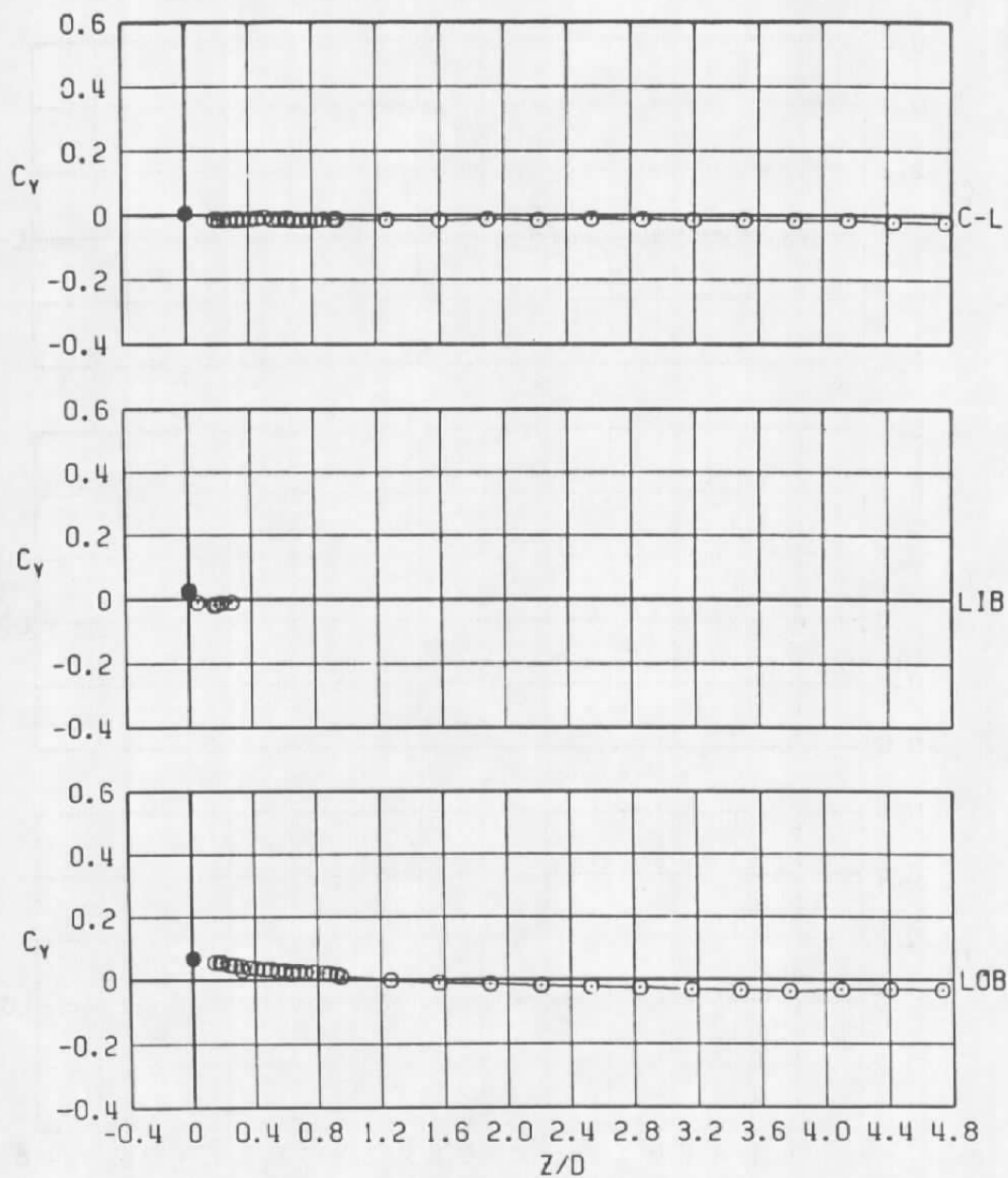


a.  $M_\infty = 0.6$

Figure 15. Coefficient of side force acting on the Black Crow store as a function of normal distance between the store and the captive position.

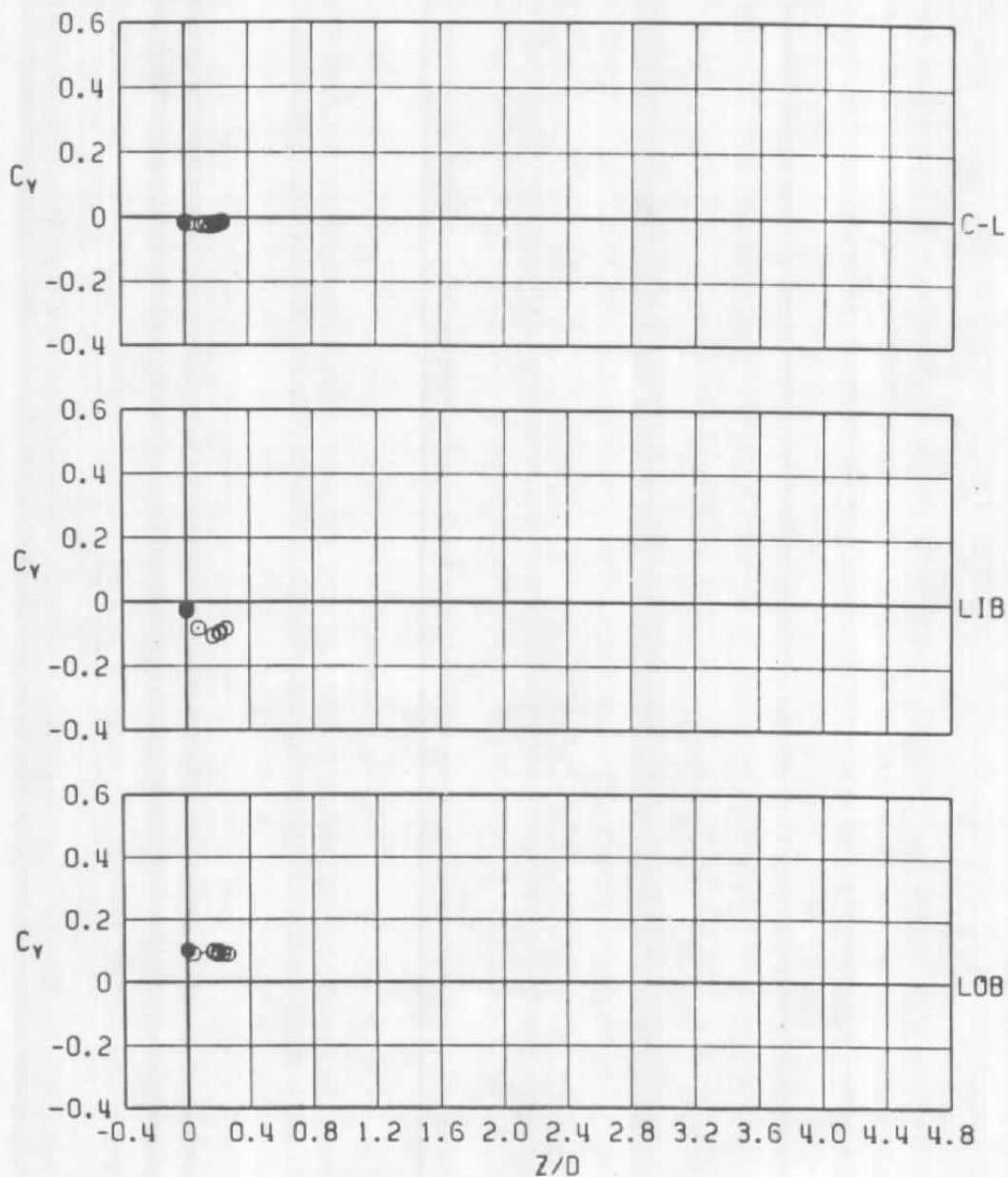


● BLACK CROW  
 IN CAPTIVE POSITION  
 ○ APPROACH TO CAPTIVE ALONG Z AXIS



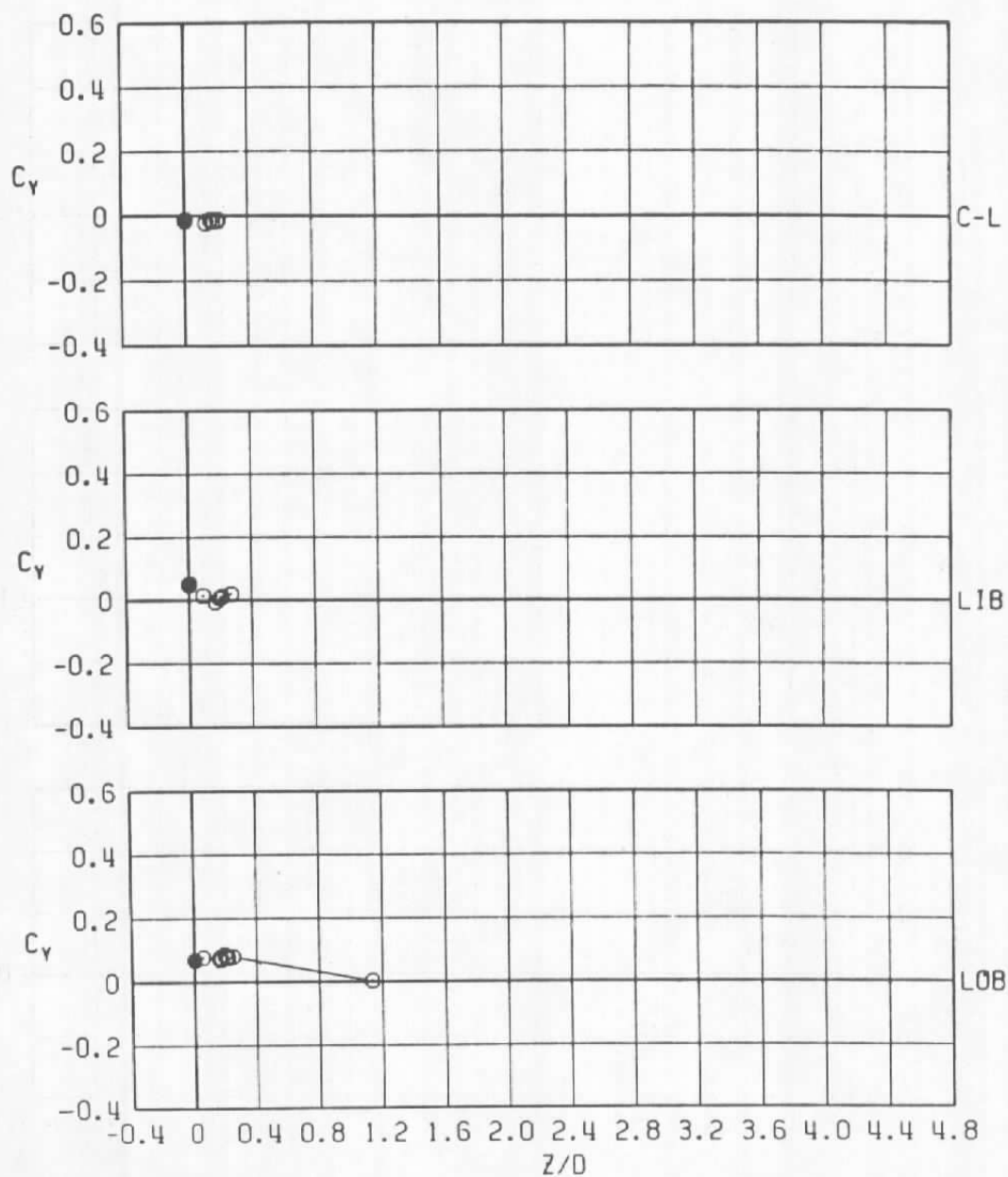
b.  $M_\infty = 0.9$   
 Figure 15. Continued.

- BLACK CROW  
 IN CAPTIVE POSITION  
 ○ APPROACH TO CAPTIVE ALONG Z AXIS



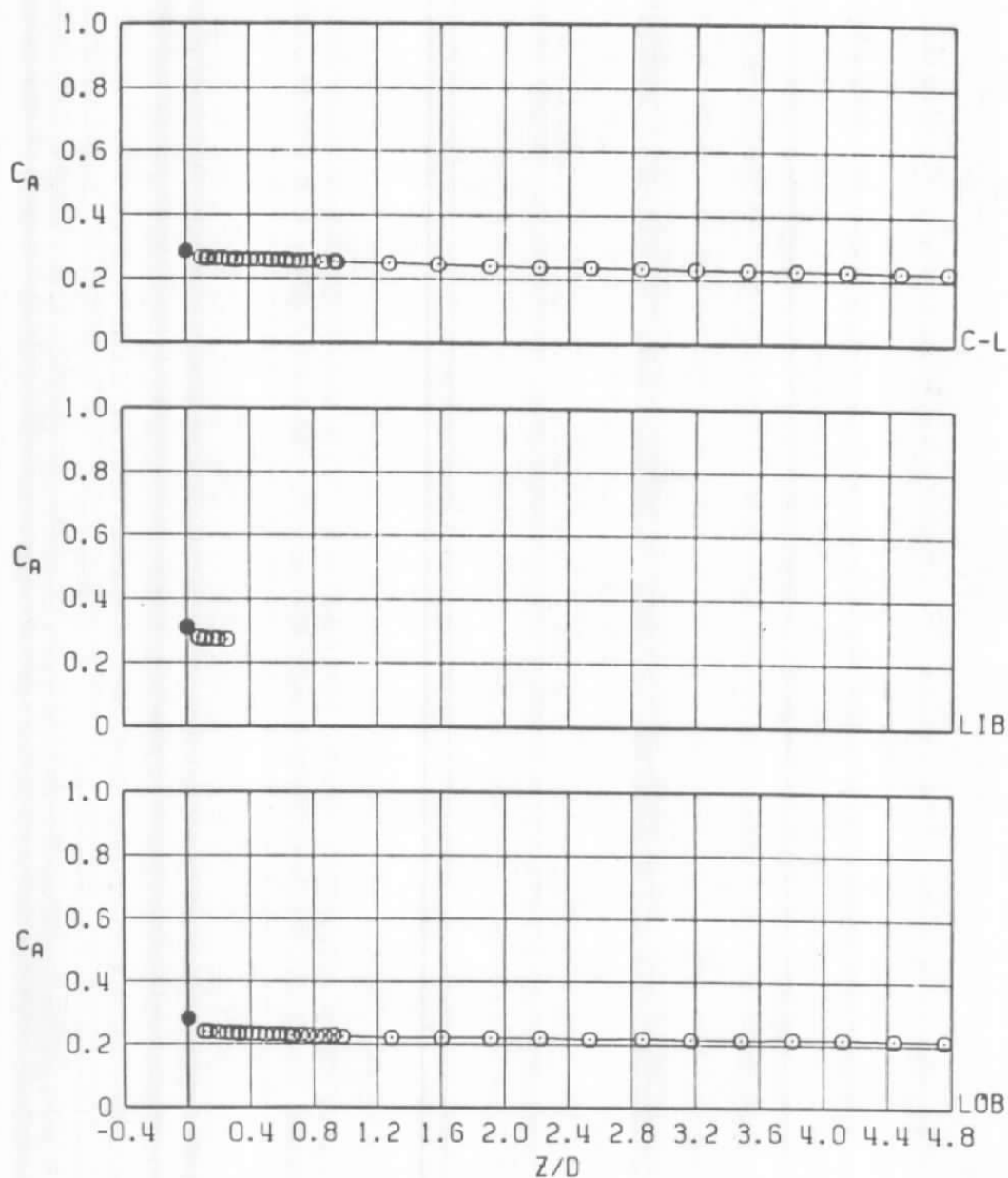
c.  $M_\infty = 1.1$   
 Figure 15. Continued.

● BLACK CROW  
 IN CAPTIVE POSITION  
 ○ APPROACH TO CAPTIVE ALONG Z AXIS



d.  $M_\infty = 1.2$   
 Figure 15. Concluded.

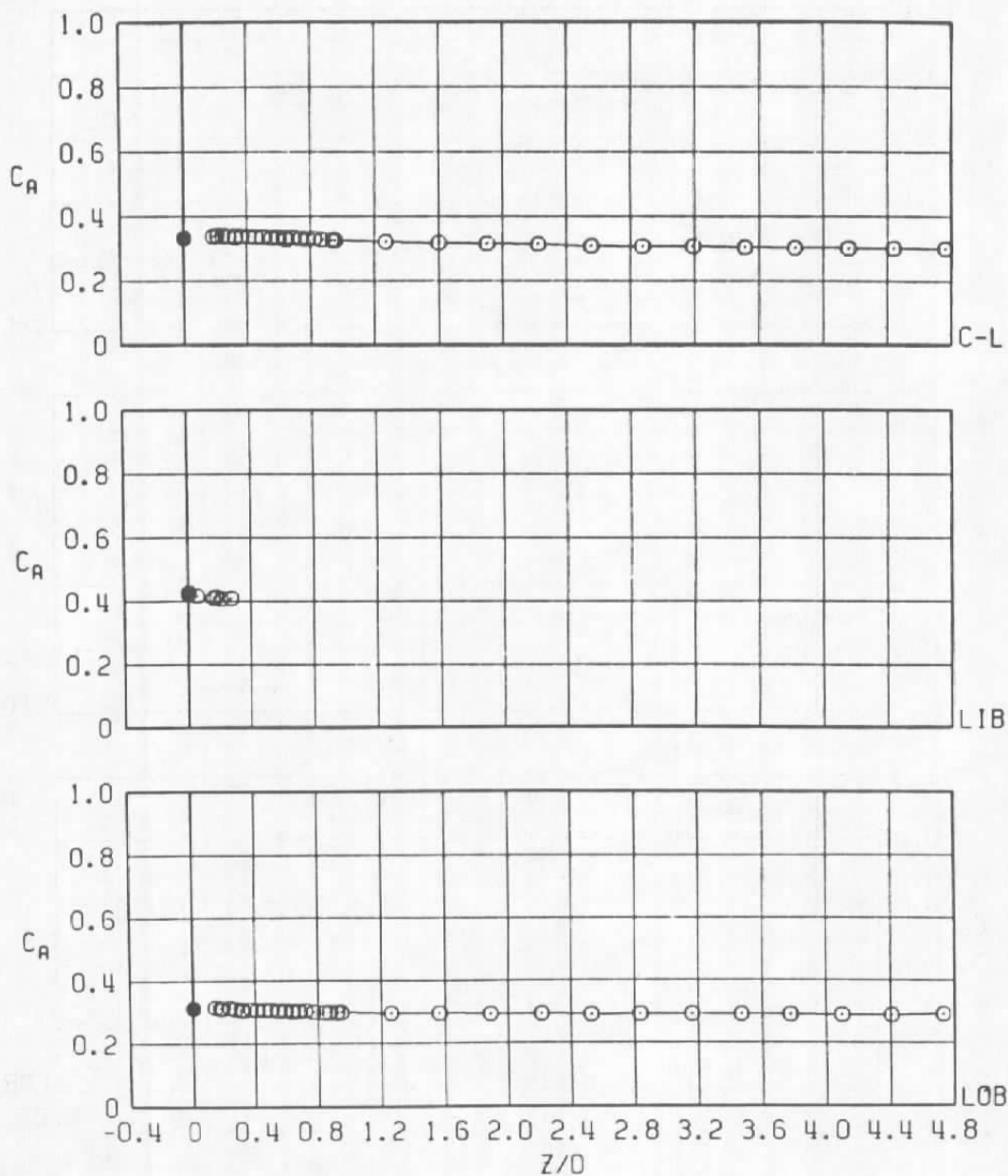
● BLACK CROW  
 IN CAPTIVE POSITION  
 ○ APPROACH TO CAPTIVE ALONG Z AXIS



a.  $M_\infty = 0.6$

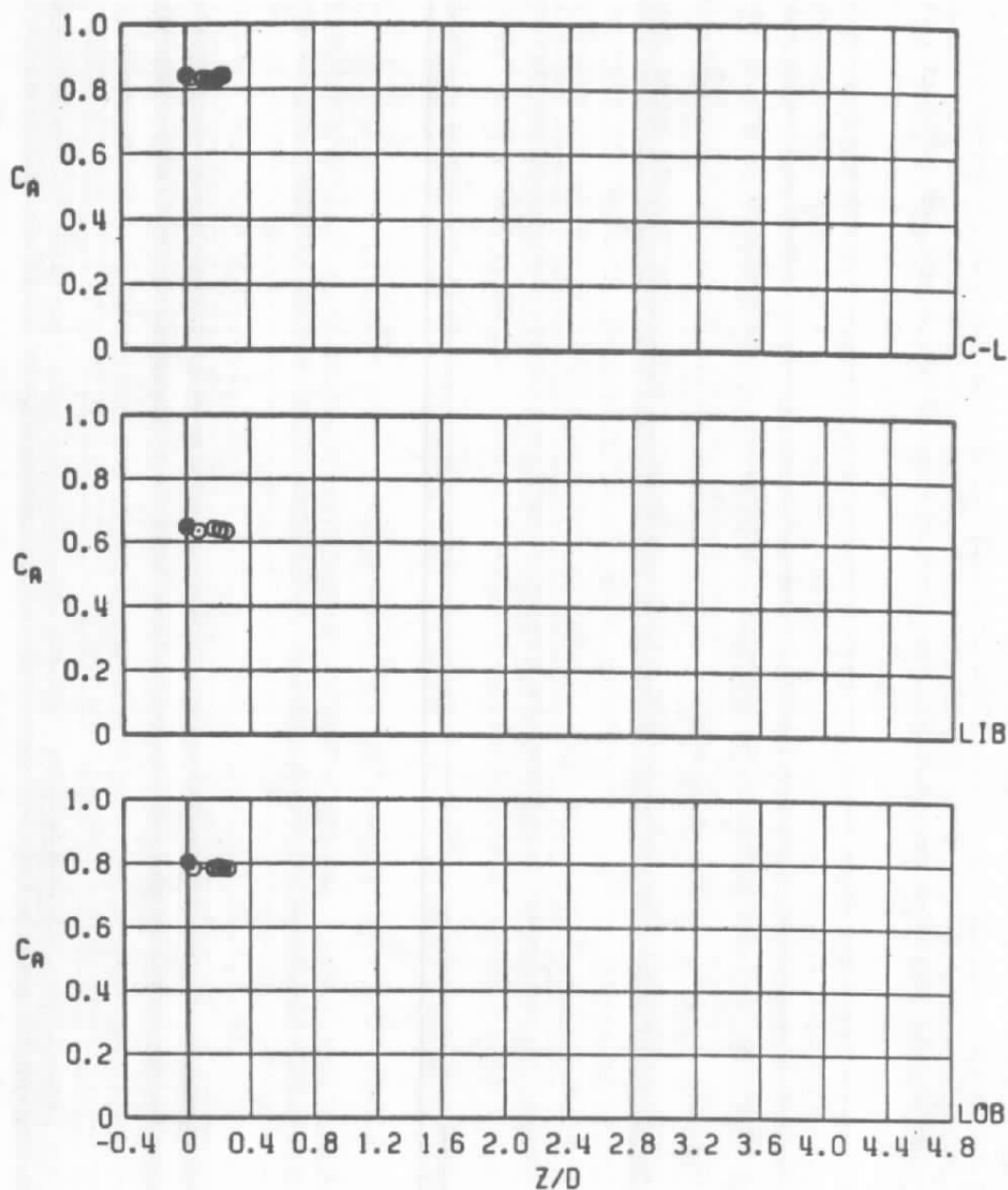
Figure 16. Coefficient of axial force acting on the Black Crow store as a function of normal distance between the store and the captive position.

● BLACK CROW  
 IN CAPTIVE POSITION  
 ○ APPROACH TO CAPTIVE ALONG Z AXIS

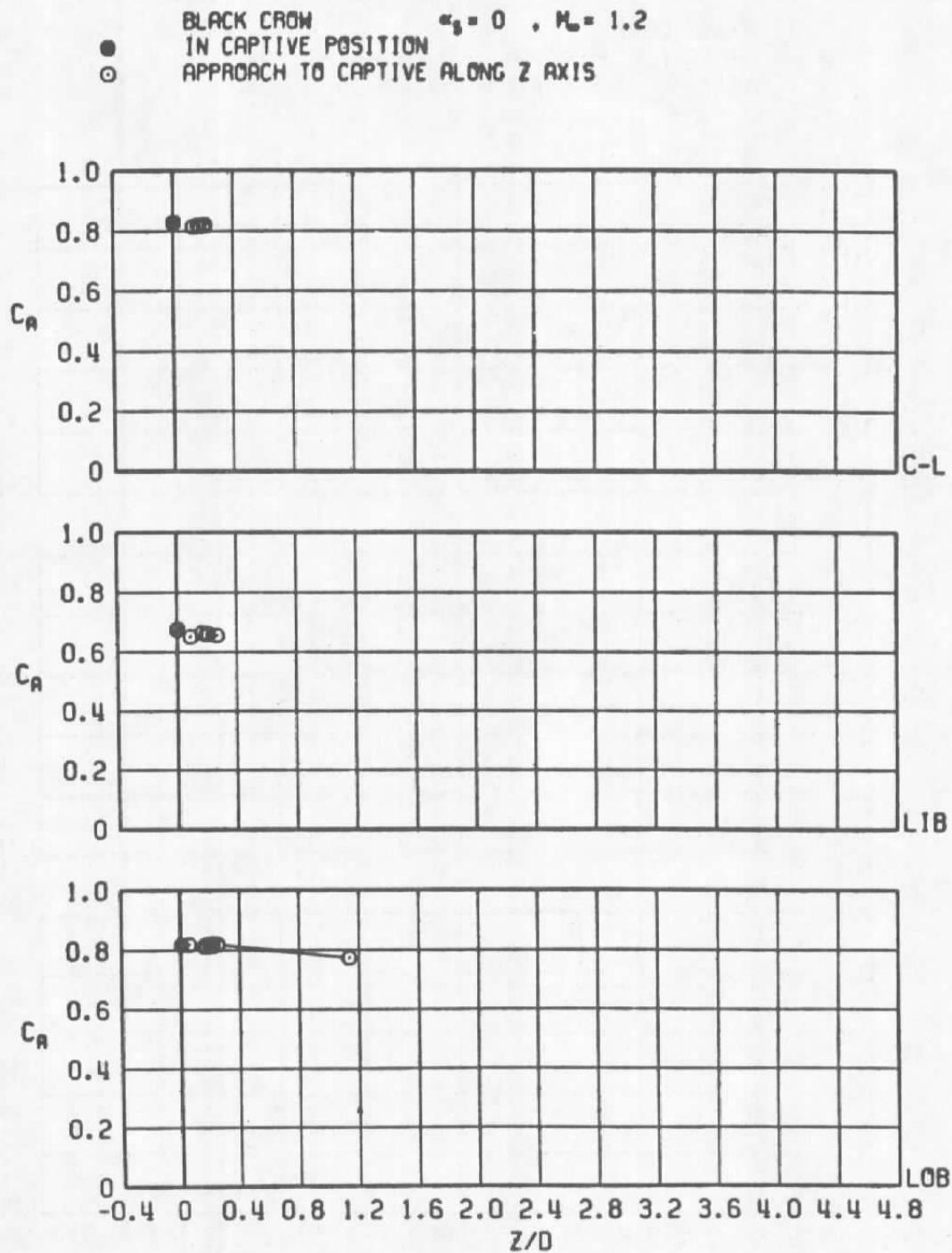


b.  $M_\infty = 0.9$   
 Figure 16. Continued.

● BLACK CROW  
 IN CAPTIVE POSITION  
 ○ APPROACH TO CAPTIVE ALONG Z AXIS

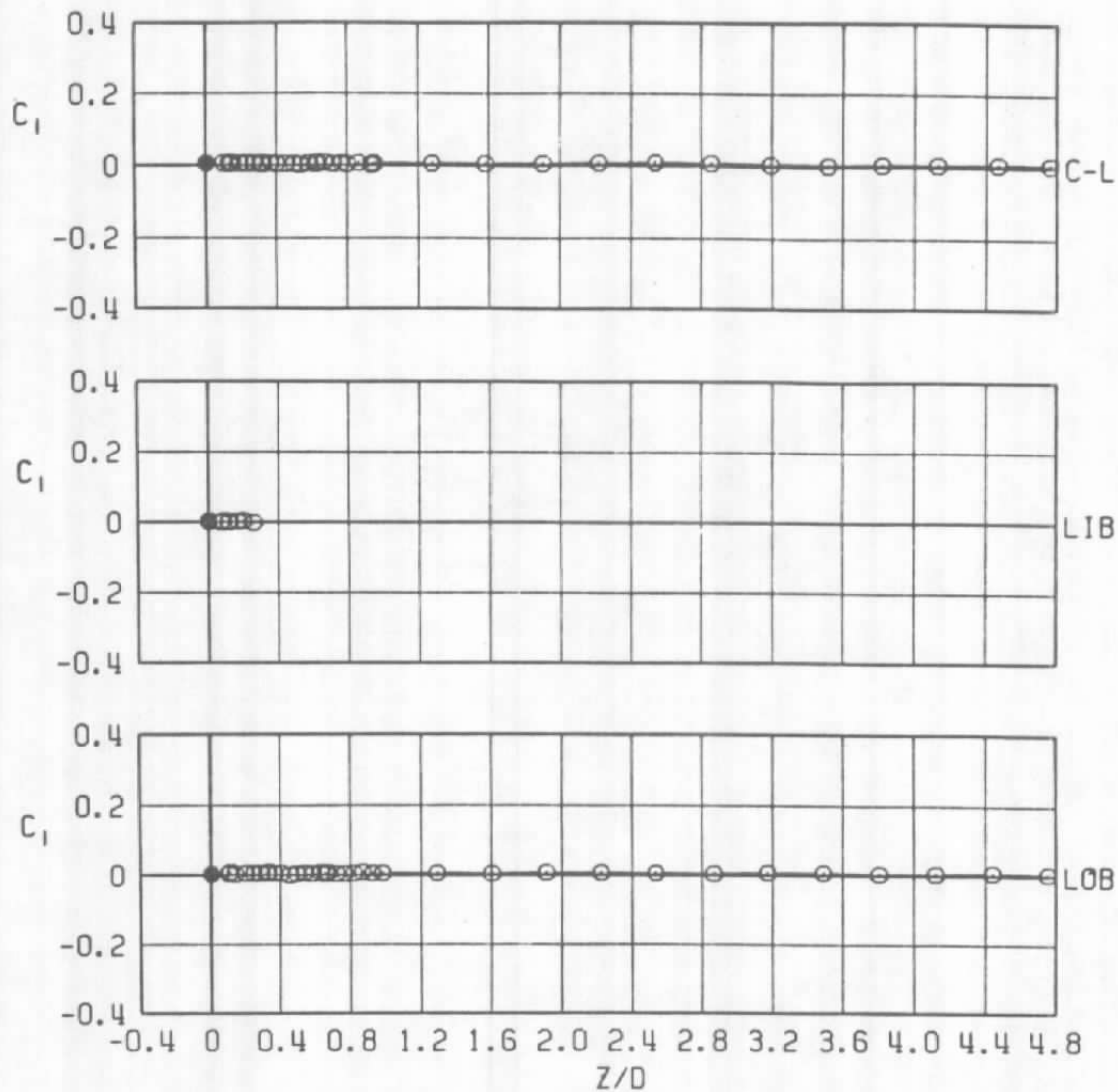


c.  $M_\infty = 1.1$   
 Figure 16. Continued.



d.  $M_\infty = 1.2$   
 Figure 16. Concluded.

● BLACK CROW  
 IN CAPTIVE POSITION  
 ○ APPROACH TO CAPTIVE ALONG Z AXIS

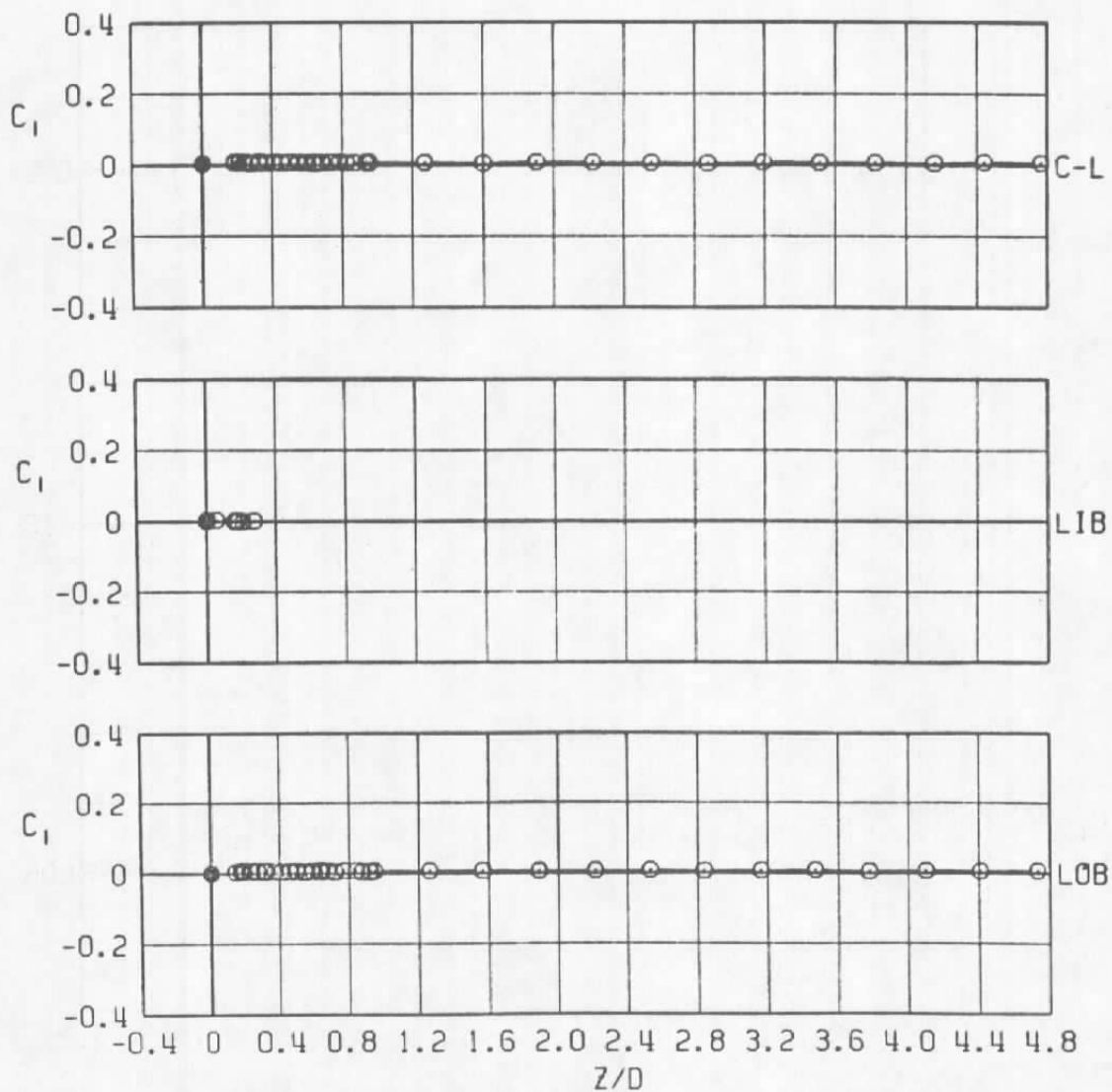


a.  $M_\infty = 0.6$

Figure 17. Coefficient of rolling moment acting on the Black Crow store as a function of normal distance between the store and the captive position.

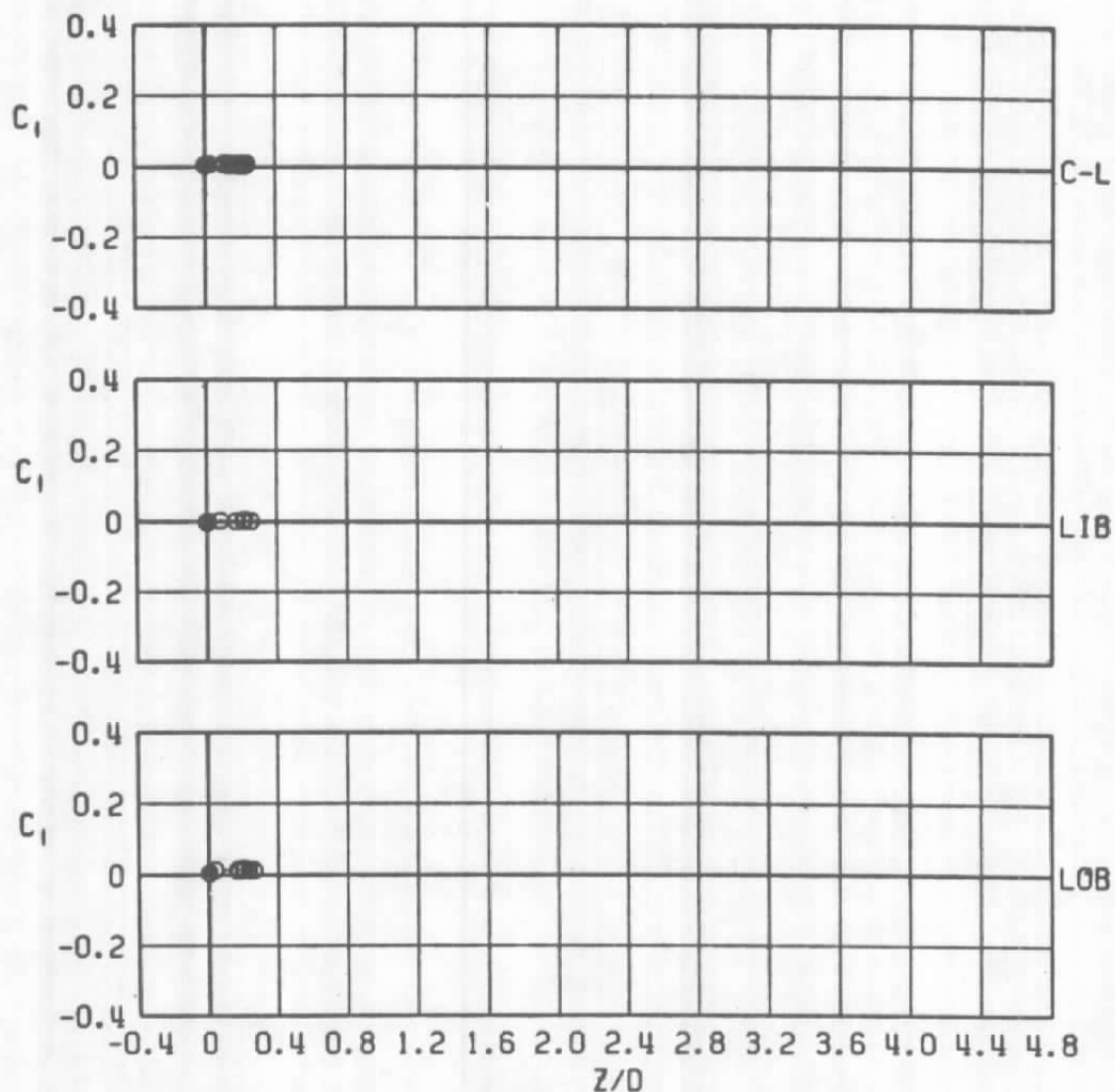


● BLACK CROW  $\alpha_s = 0$  ,  $M_\infty = 0.9$   
 ○ IN CAPTIVE POSITION  
 ○ APPROACH TO CAPTIVE ALONG Z AXIS



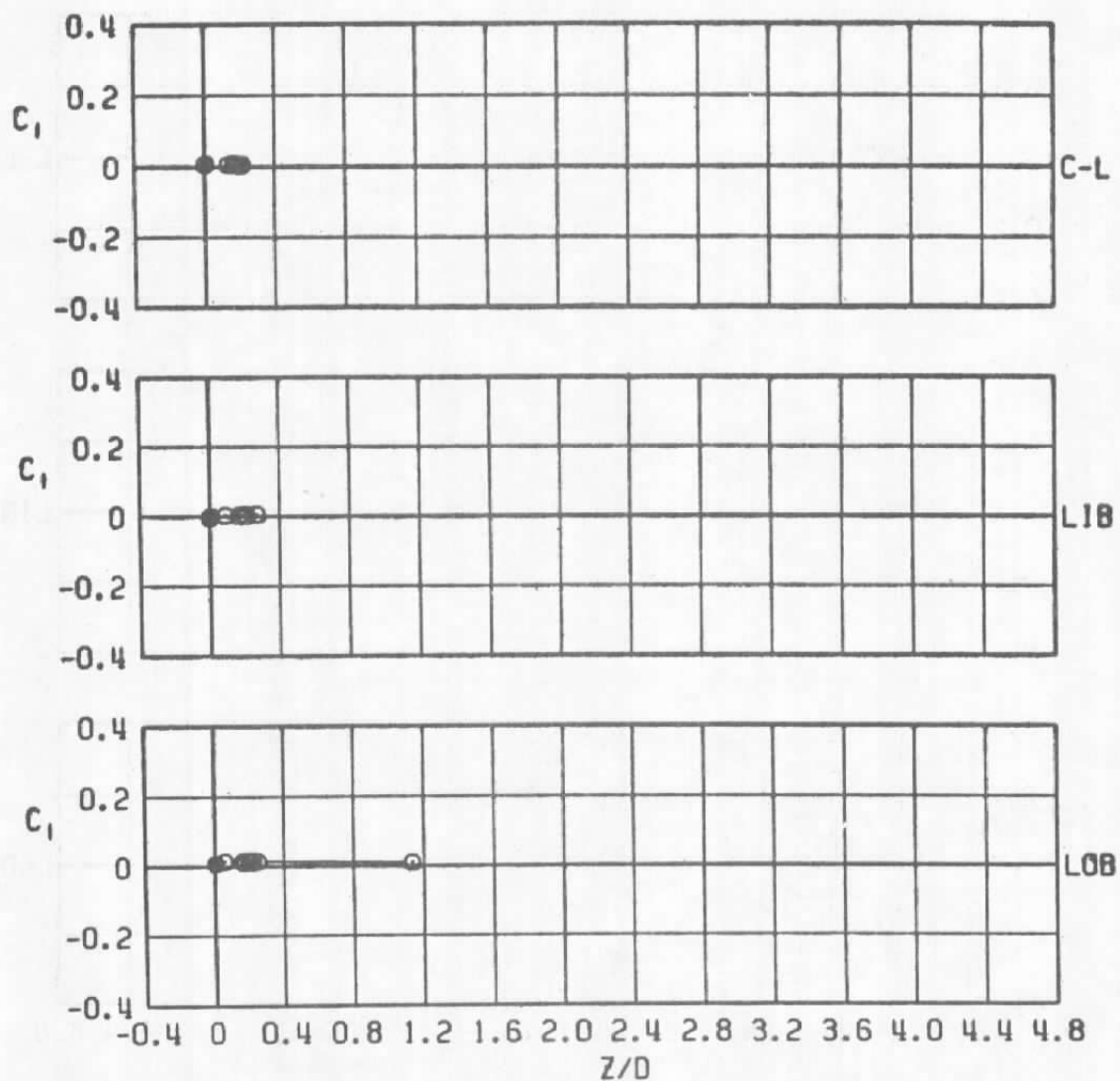
b.  $M_\infty = 0.9$   
 Figure 17. Continued.

● BLACK CROW  
 IN CAPTIVE POSITION  
 ○ APPROACH TO CAPTIVE ALONG Z AXIS



c.  $M_\infty = 1.1$   
 Figure 17. Continued.

● BLACK CROW  
 IN CAPTIVE POSITION  
 ○ APPROACH TO CAPTIVE ALONG Z AXIS



d.  $M_\infty = 1.2$   
 Figure 17. Concluded.

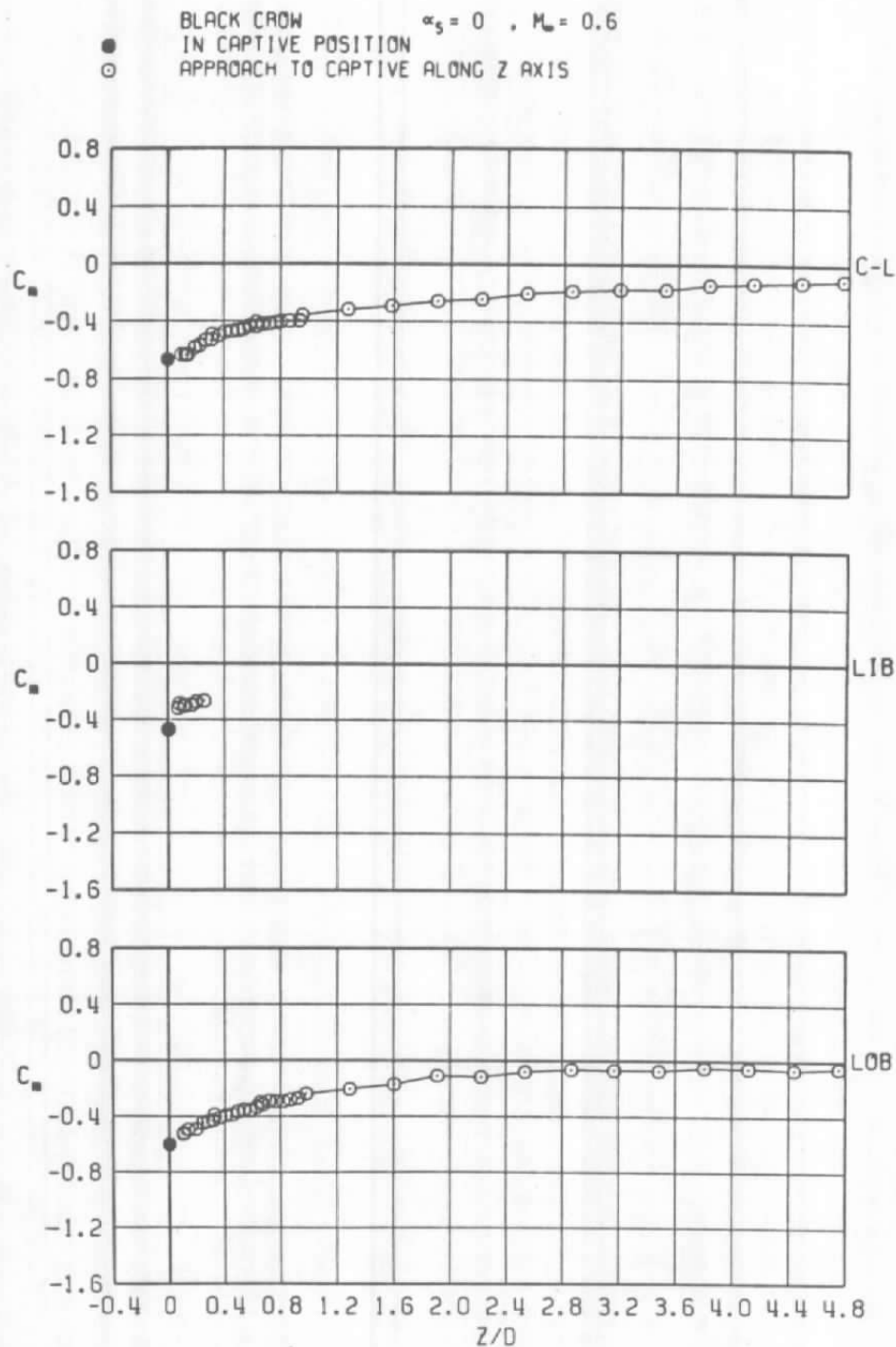
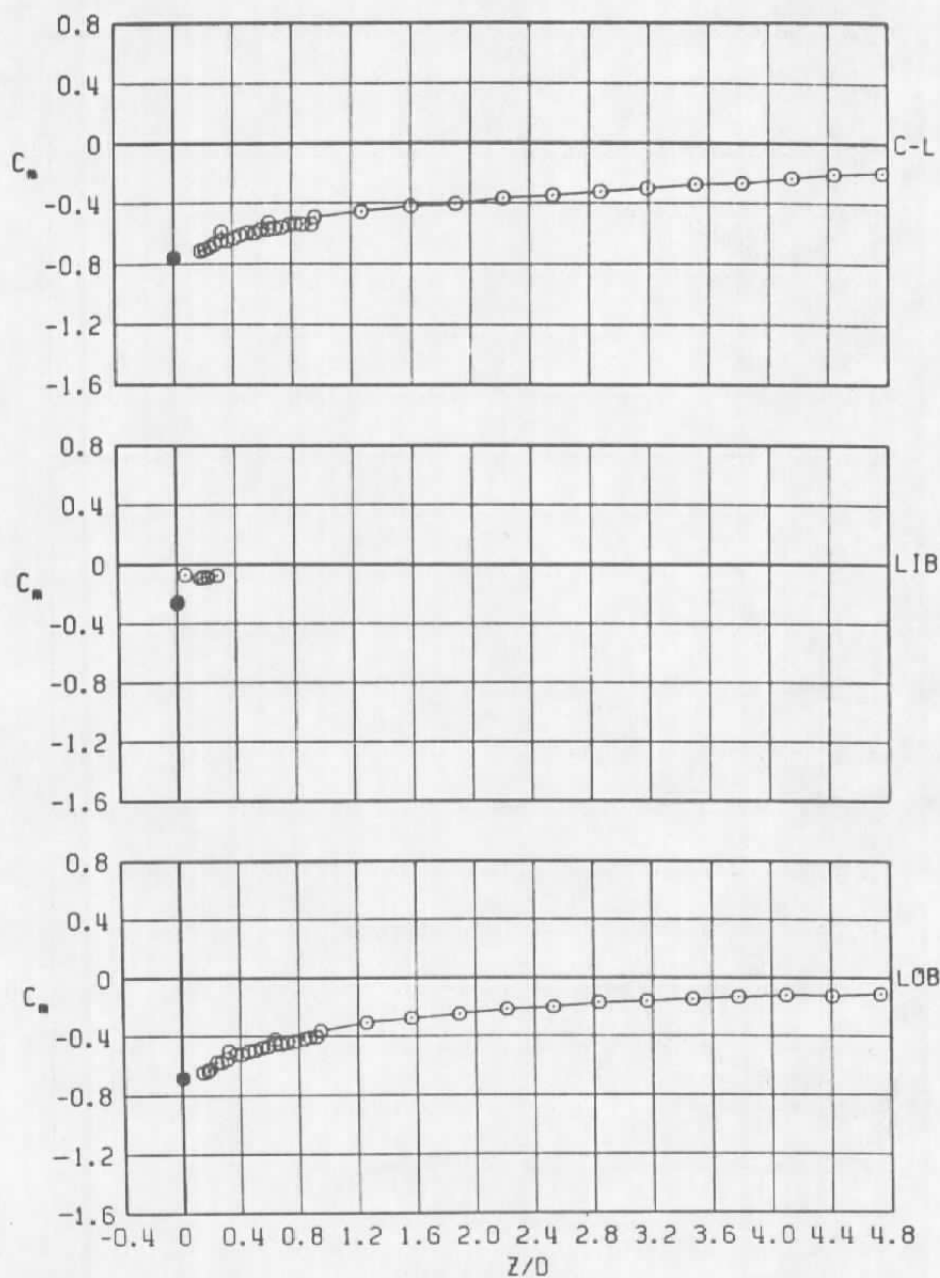
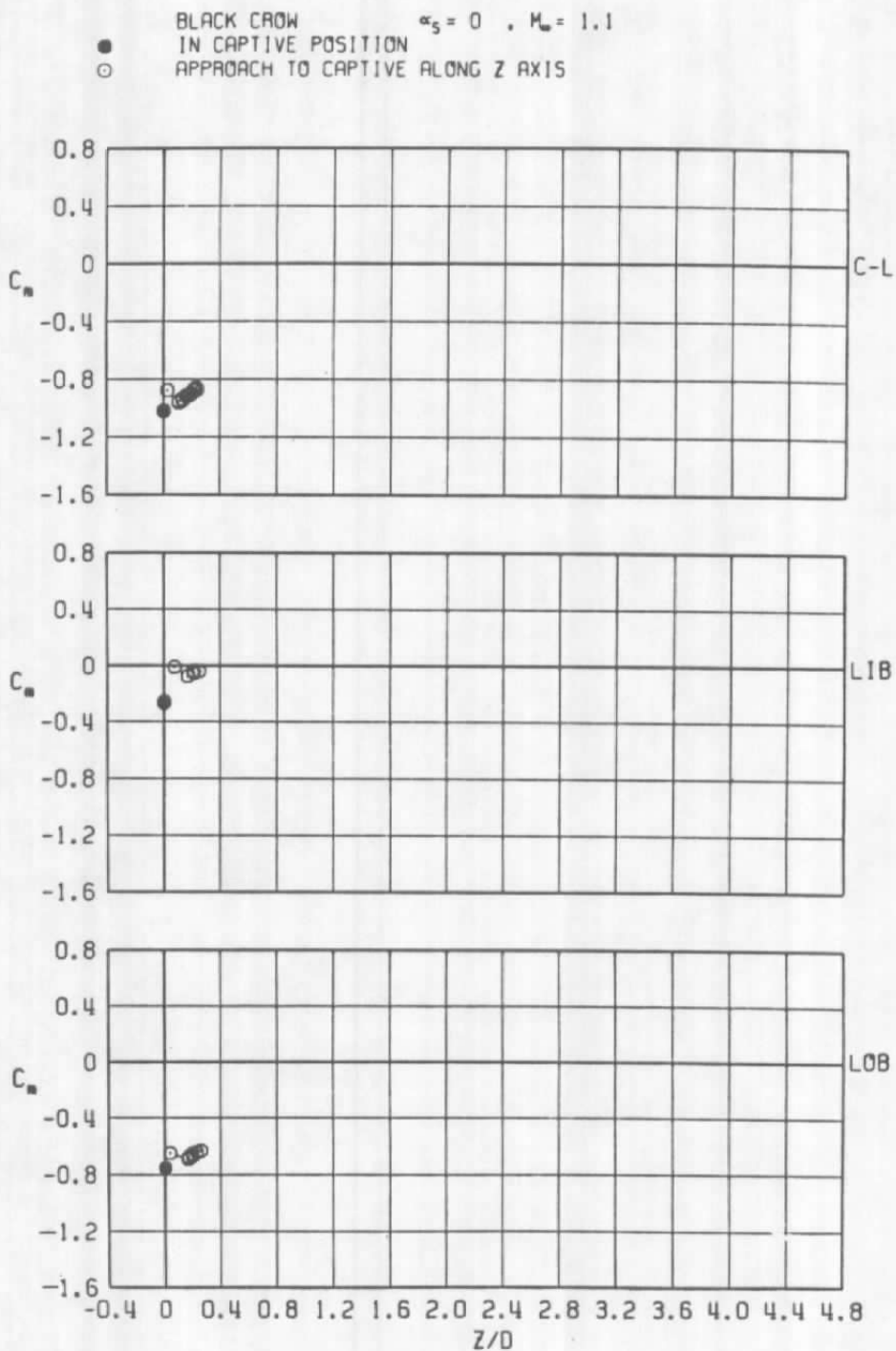
a.  $M_\infty = 0.6$ 

Figure 18. Coefficient of pitching moment acting on the Black Crow store as a function of normal distance between the store and the captive position.

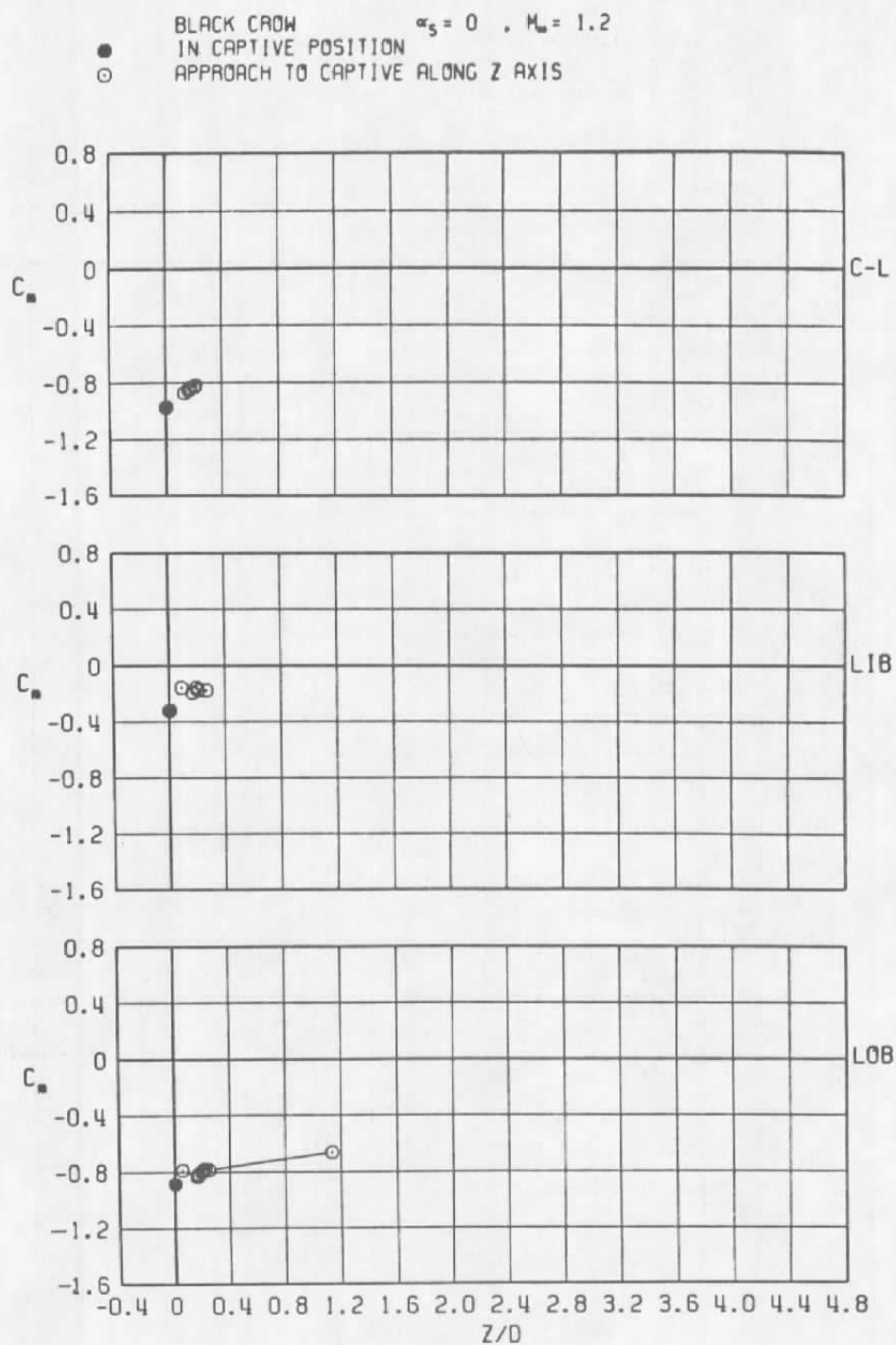
● BLACK CROW  $\alpha_s = 0$  ,  $M_\infty = 0.9$   
 IN CAPTIVE POSITION  
 ○ APPROACH TO CAPTIVE ALONG Z AXIS



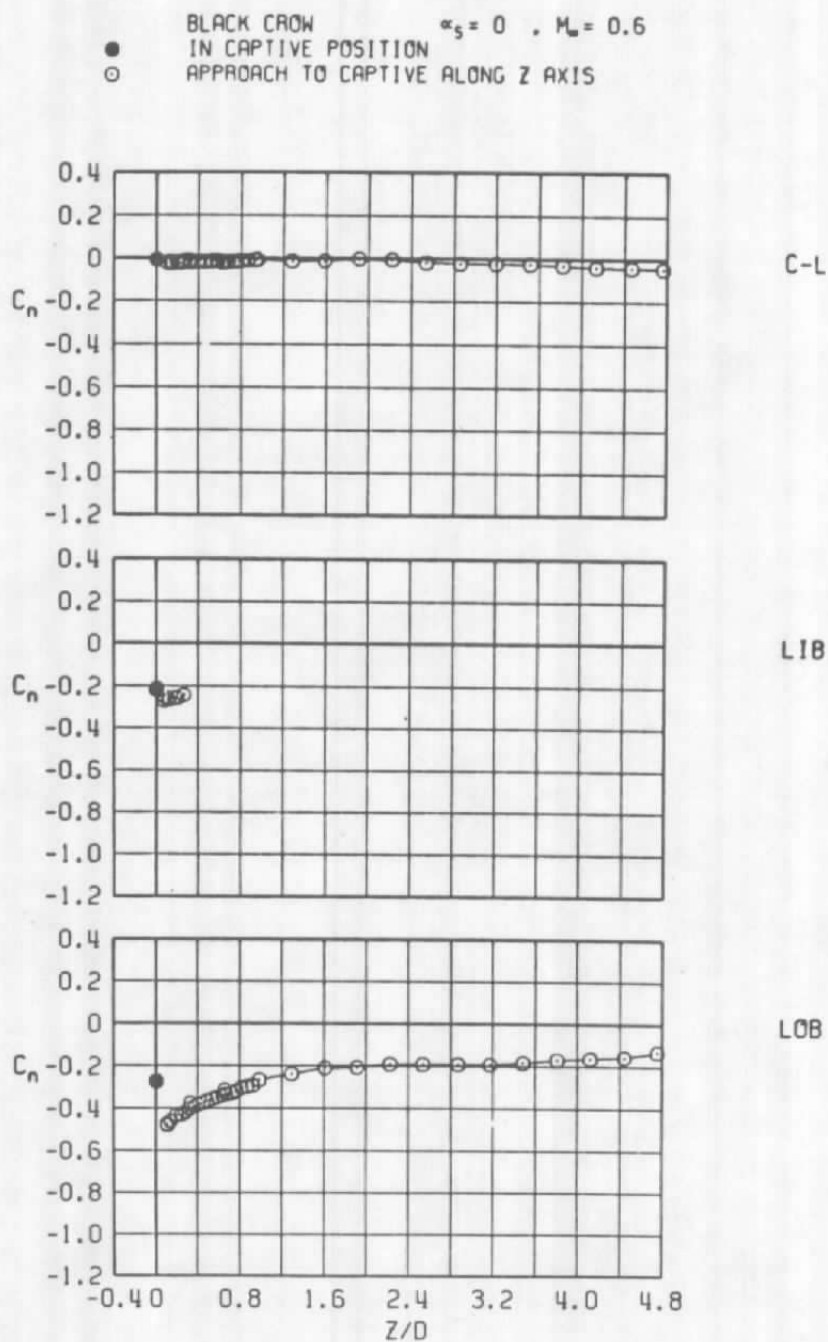
b.  $M_\infty = 0.9$   
 Figure 18. Continued.



c.  $M_\infty = 1.1$   
 Figure 18. Continued.



d.  $M_\infty = 1.2$   
 Figure 18. Concluded.

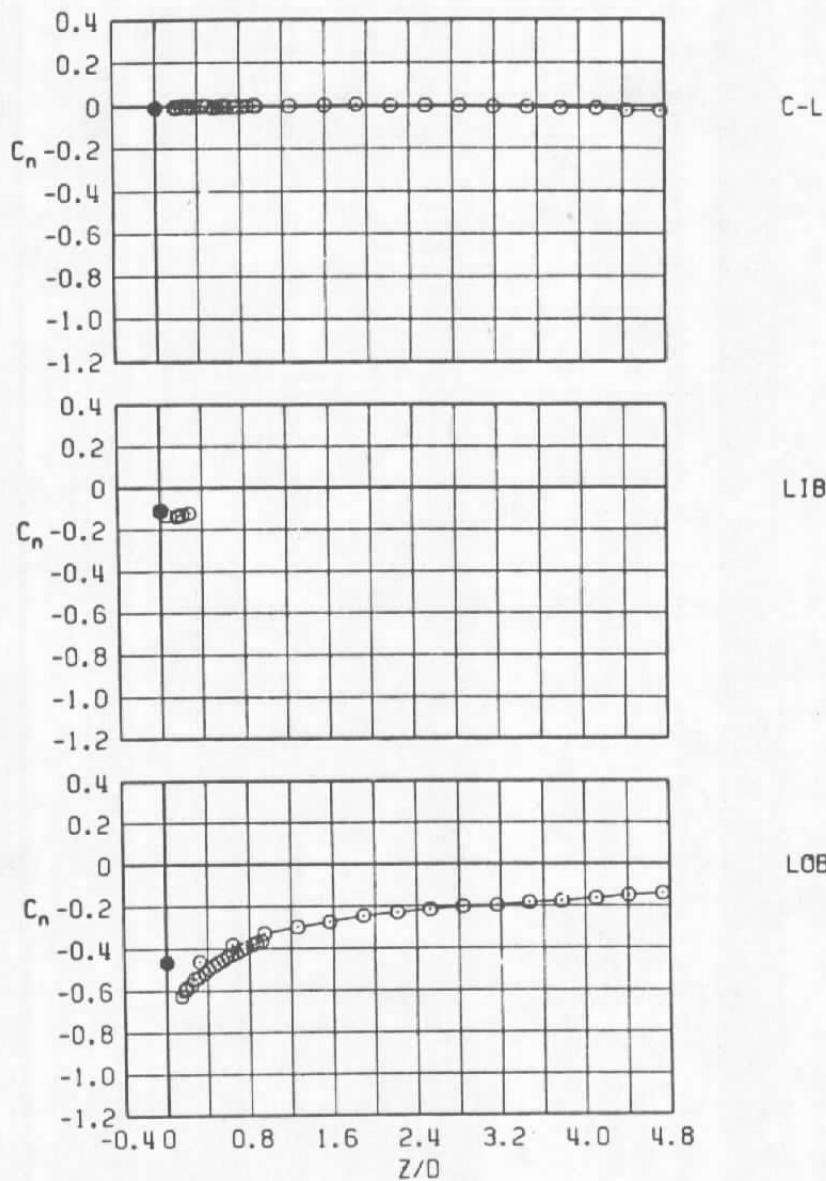


a.  $M_\infty = 0.6$

Figure 19. Coefficient of yawing moment acting on the Black Crow store as a function of normal distance between the store and the captive position.

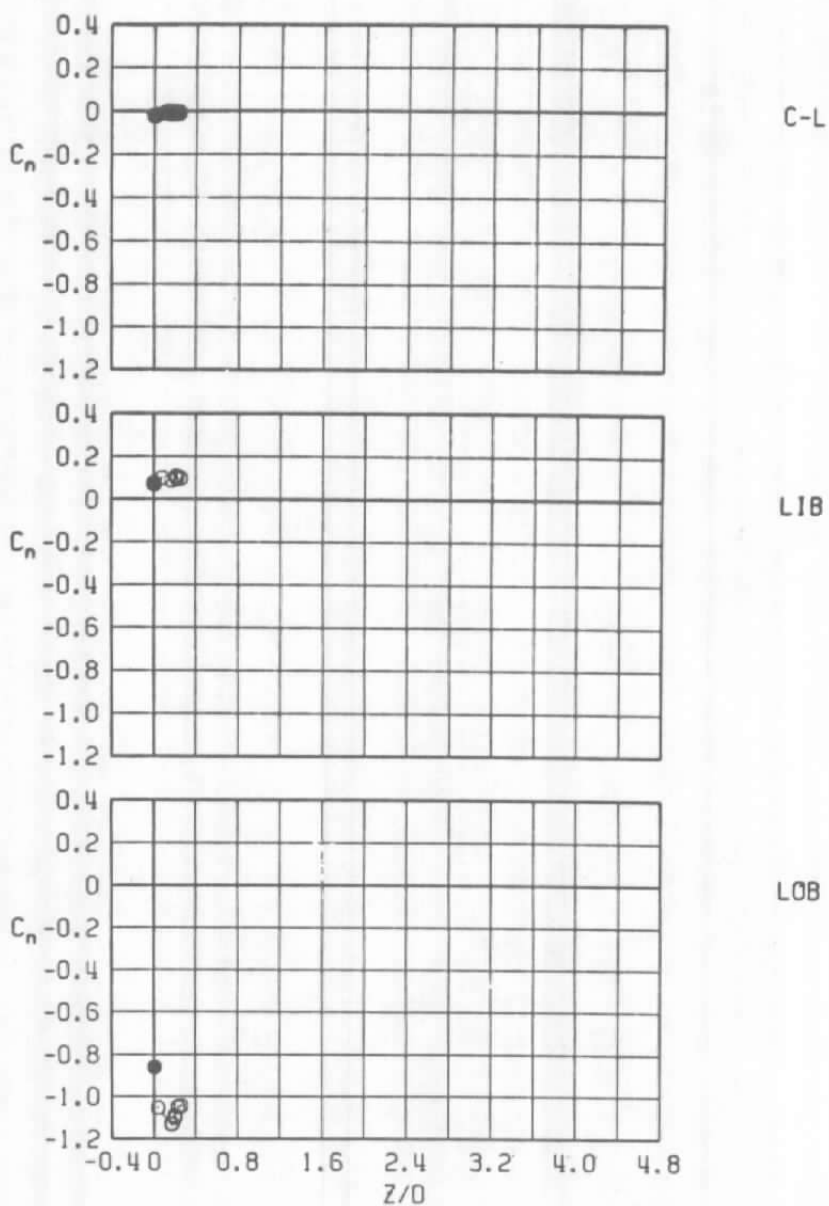


● BLACK CROW  $\alpha_s = 0$  ,  $M_\infty = 0.9$   
 ○ IN CAPTIVE POSITION  
 ○ APPROACH TO CAPTIVE ALONG Z AXIS



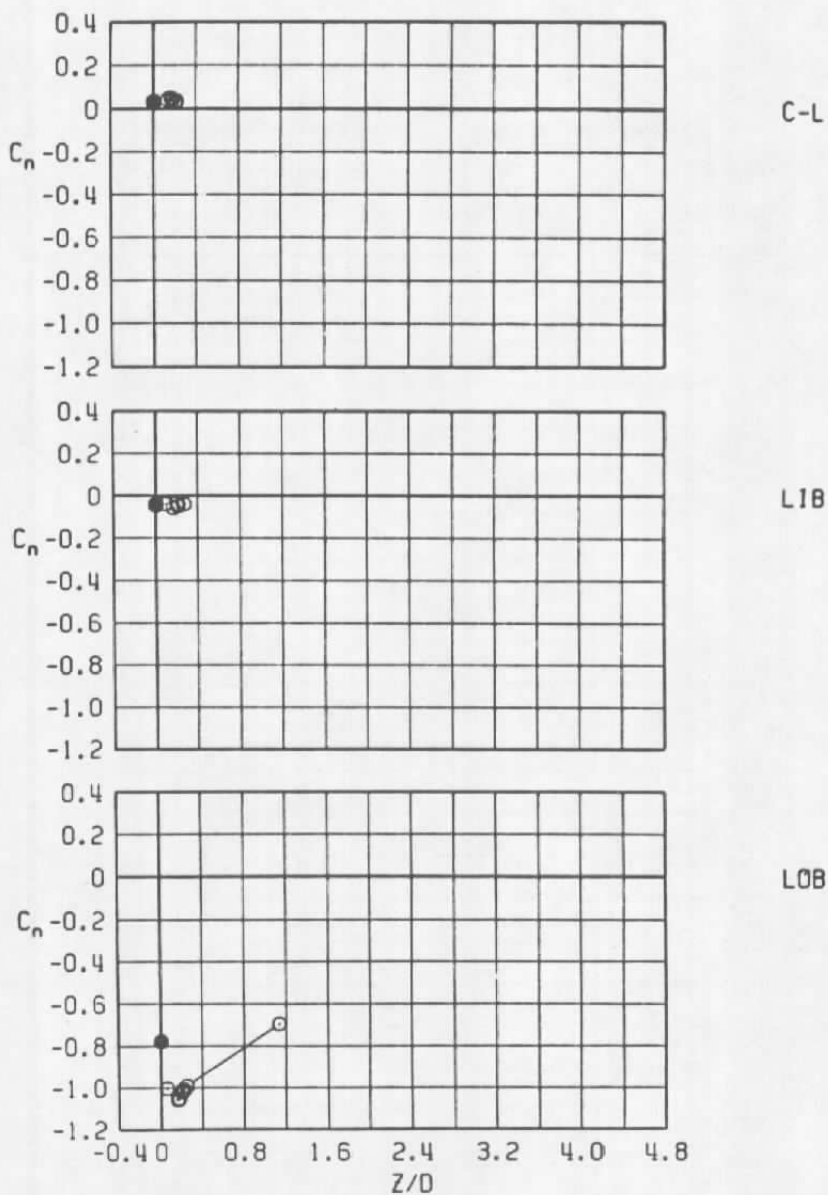
b.  $M_\infty = 0.9$   
 Figure 19. Continued.

● BLACK CROW  $\alpha_s = 0$  ,  $M_\infty = 1.1$   
 IN CAPTIVE POSITION  
 ○ APPROACH TO CAPTIVE ALONG Z AXIS

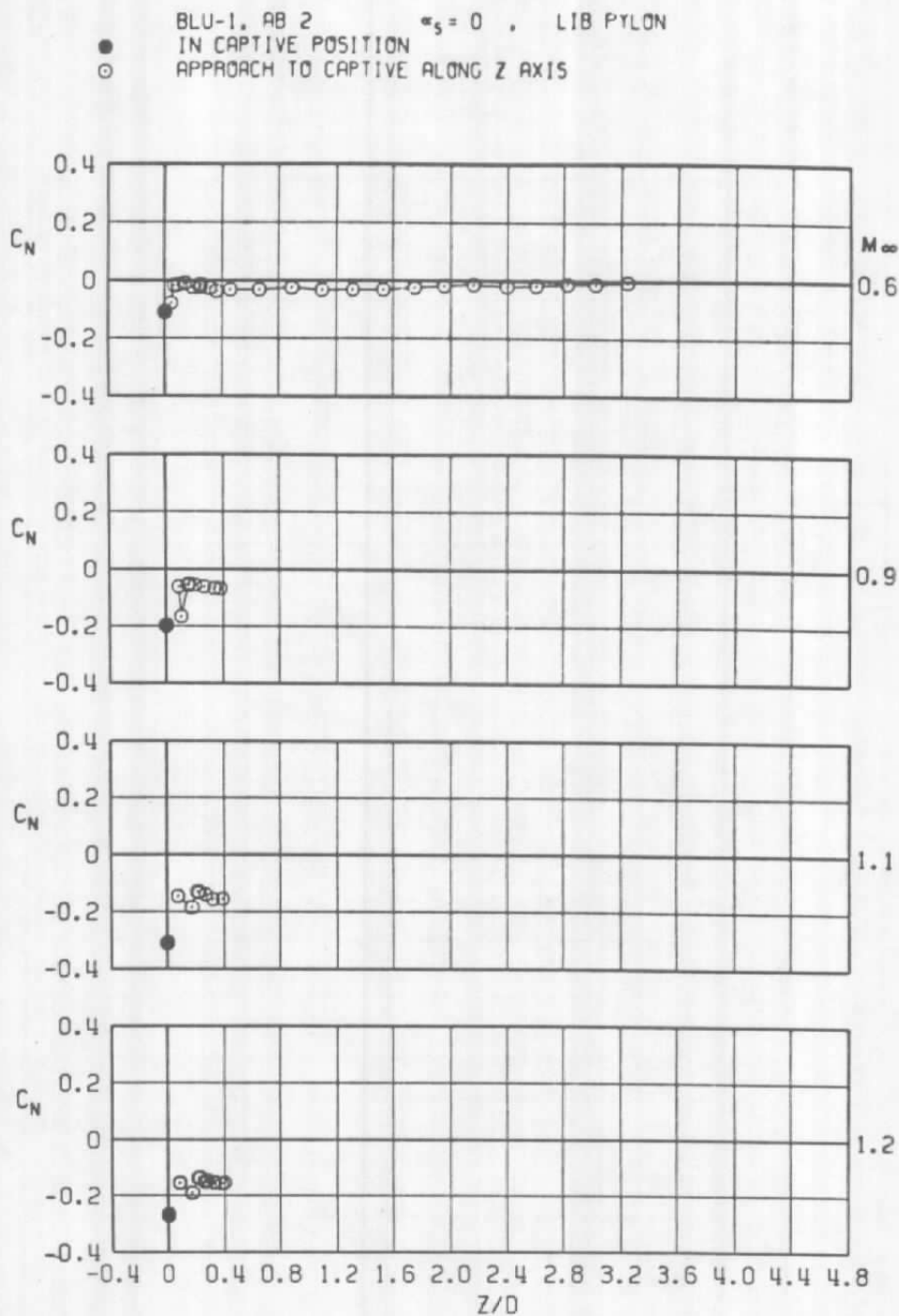


c.  $M_\infty = 1.1$   
 Figure 19. Continued.

● BLACK CROW  $\alpha_s = 0$  ,  $M_\infty = 1.2$   
 IN CAPTIVE POSITION  
 ○ APPROACH TO CAPTIVE ALONG Z AXIS



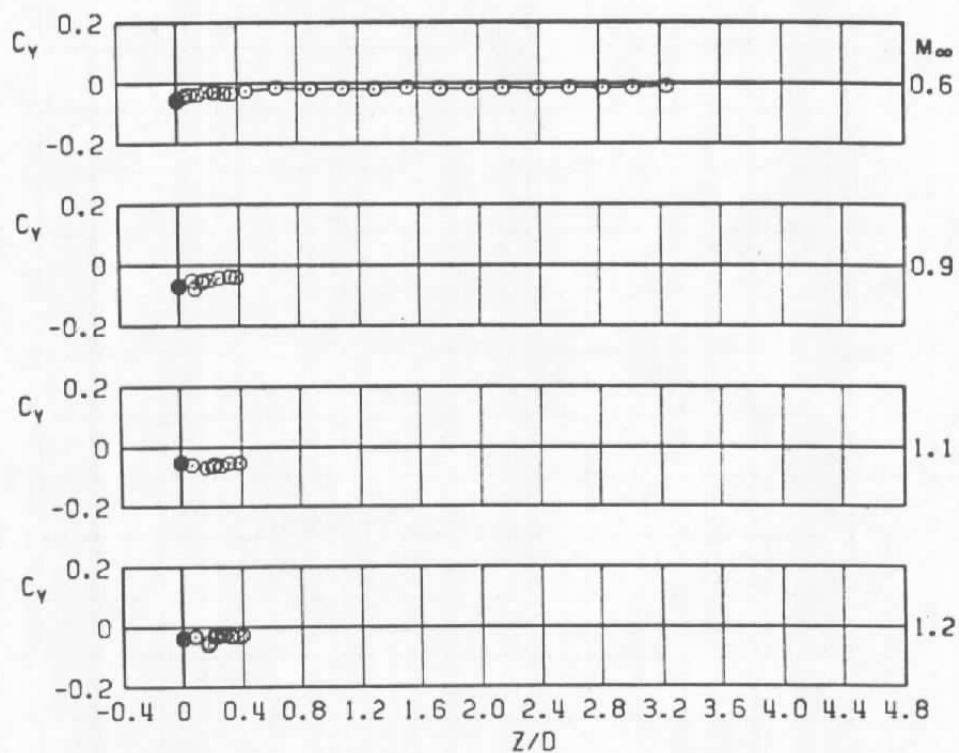
d.  $M_\infty = 1.2$   
 Figure 19. Concluded.



a. Normal force

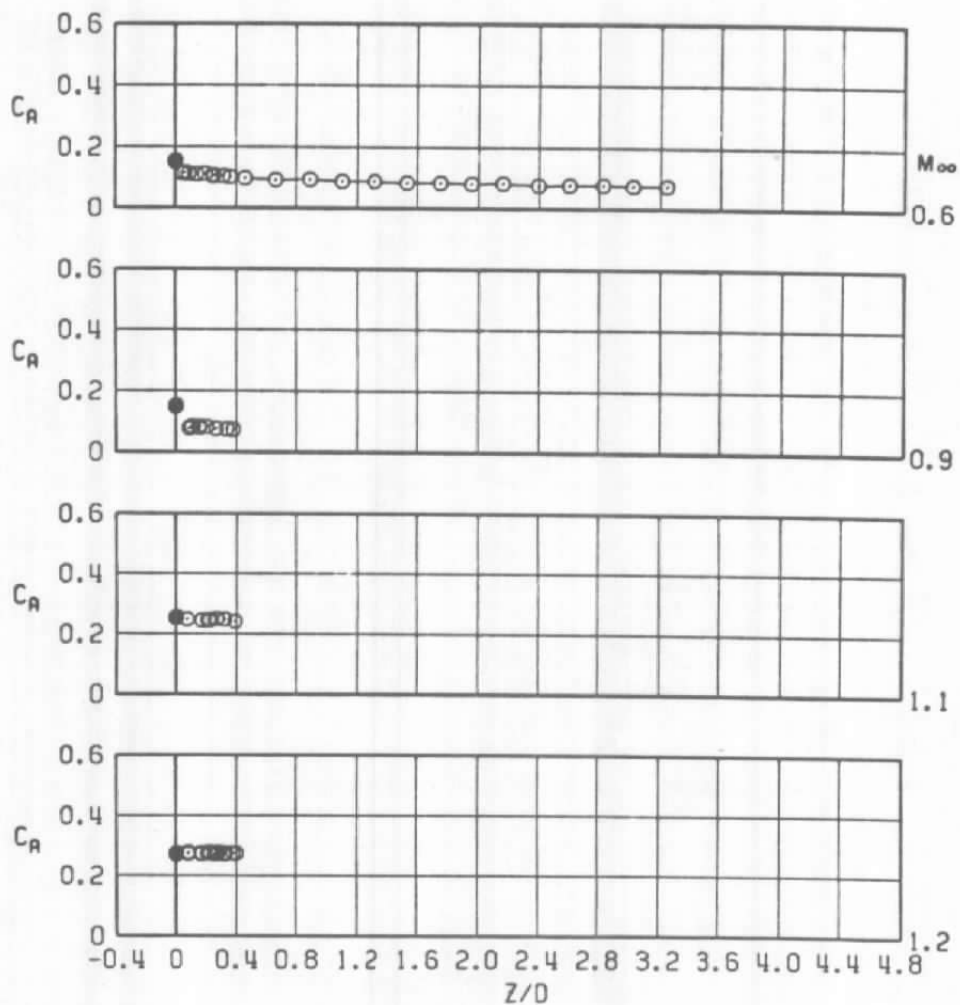
Figure 20. Coefficients of forces and moments acting on the BLU-1 store as a function of normal distance between the store and the captive position on the LIB pylon.

● BLU-1, AB 2       $\alpha_s = 0$       LIB PYLON  
 ○ IN CAPTIVE POSITION  
 ○ APPROACH TO CAPTIVE ALONG Z AXIS

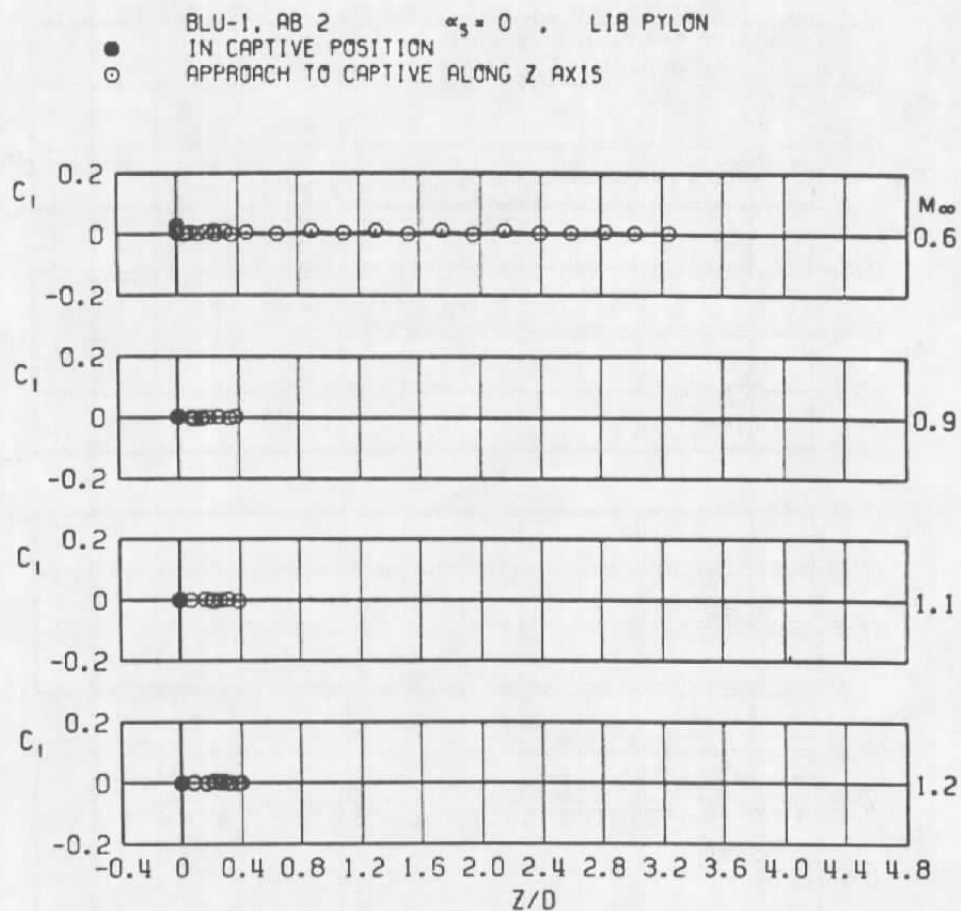


b. Side force  
 Figure 20. Continued.

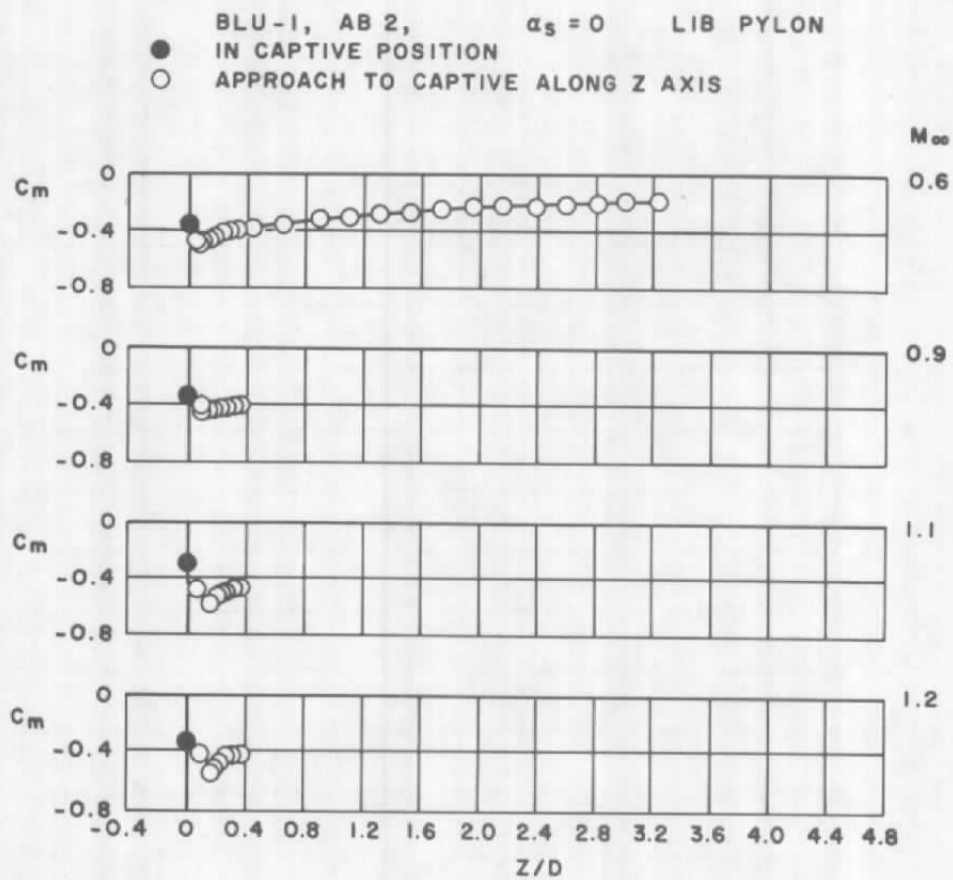
- BLU-1, AB 2  $\alpha_s = 0$  LIB PYLON  
 ○ IN CAPTIVE POSITION  
 ○ APPROACH TO CAPTIVE ALONG Z AXIS



c. Axial force  
Figure 20. Continued.



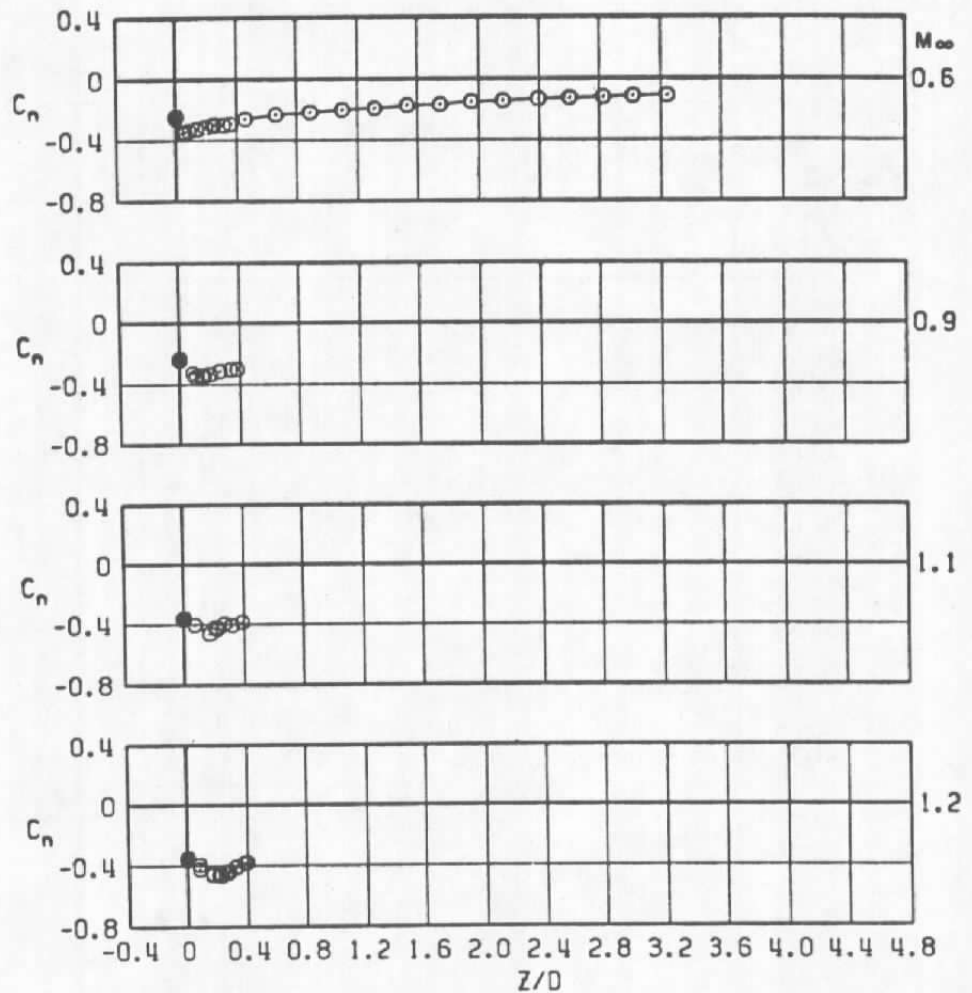
d. Rolling moment  
 Figure 20. Continued.



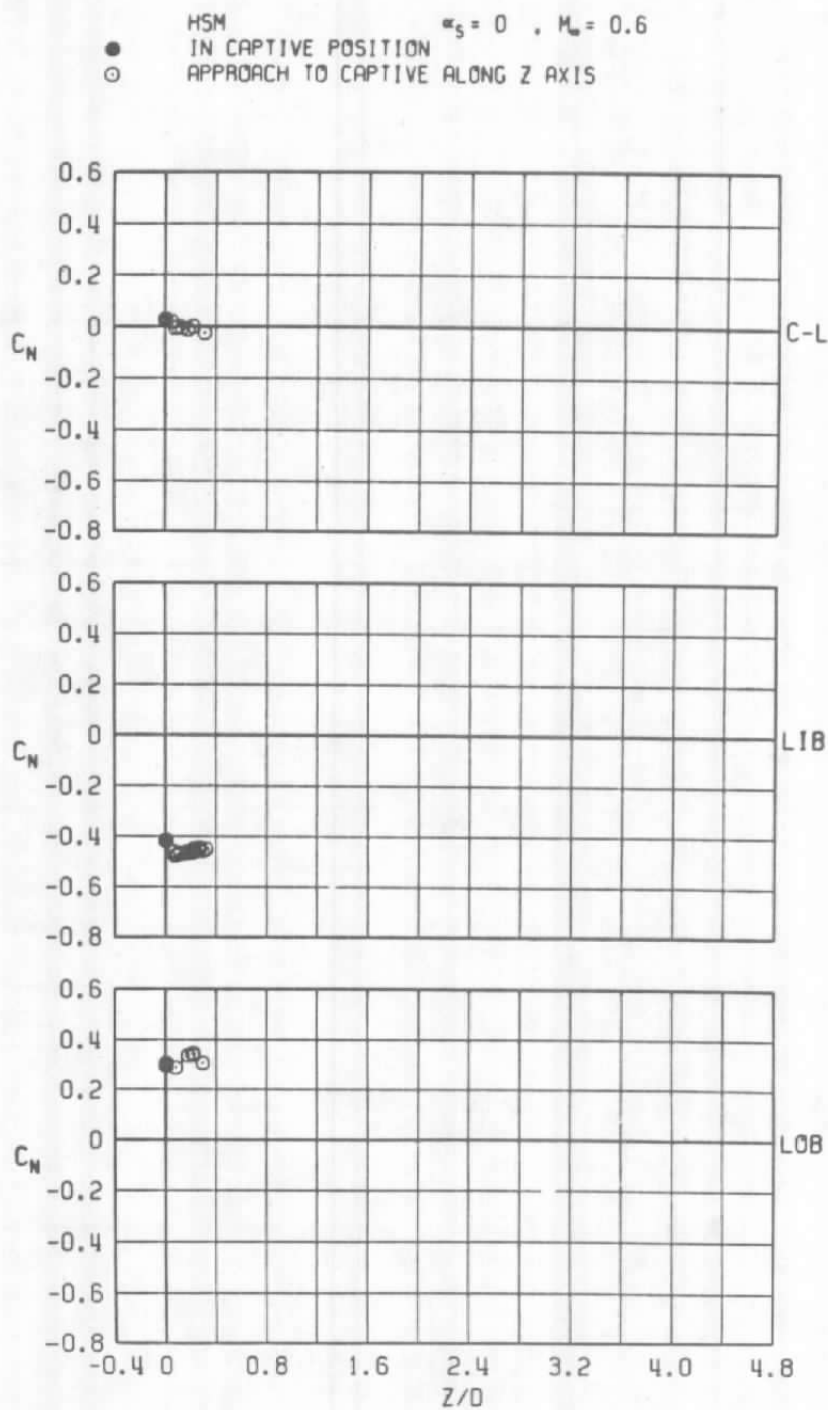
e. Pitching moment  
Figure 20. Continued.



● BLU-1, AB 2       $\alpha_3 = 0$  . LIB PYLON  
 ○ IN CAPTIVE POSITION  
 ○ APPROACH TO CAPTIVE ALONG Z AXIS



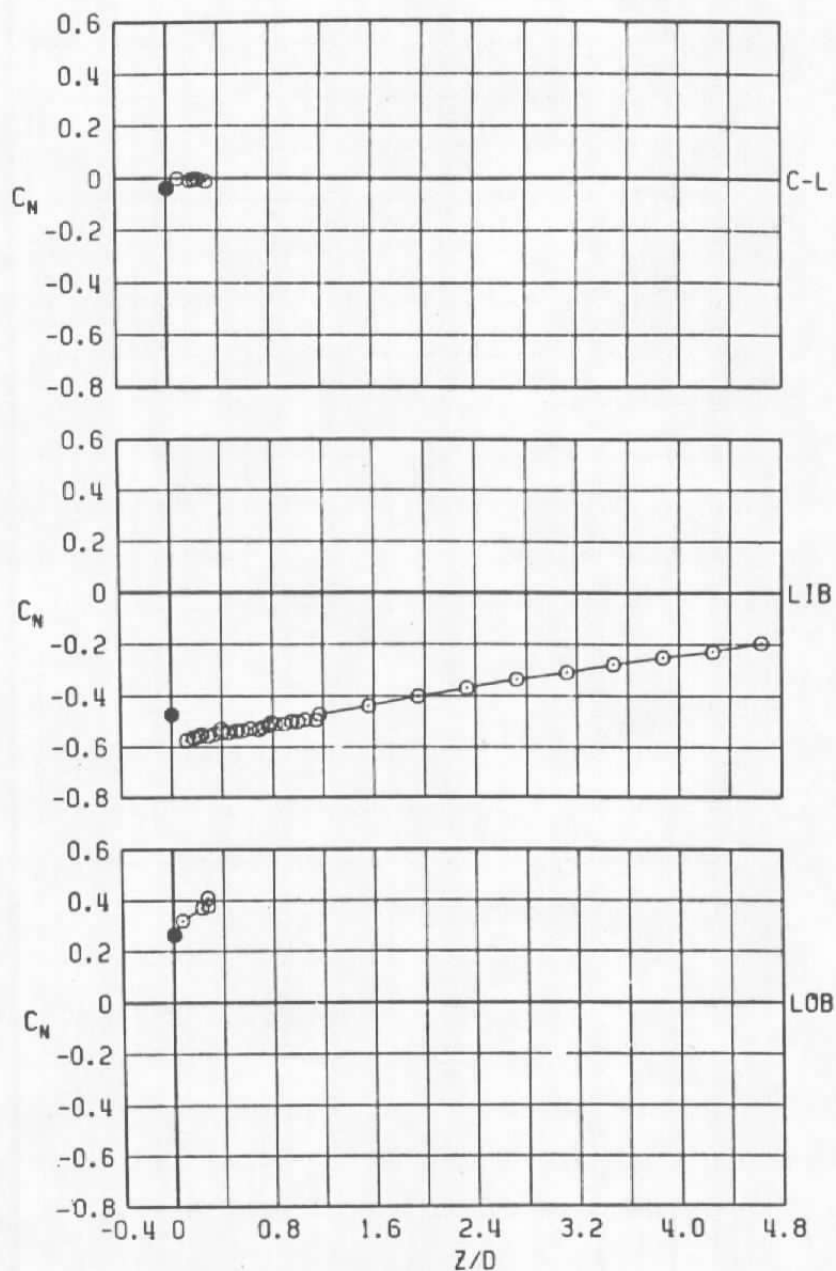
f. Yawing moment  
Figure 20. Concluded.



a.  $M_\infty = 0.6$

Figure 21. Coefficient of normal force acting on the HSM store as a function of normal distance between the store and the captive position.

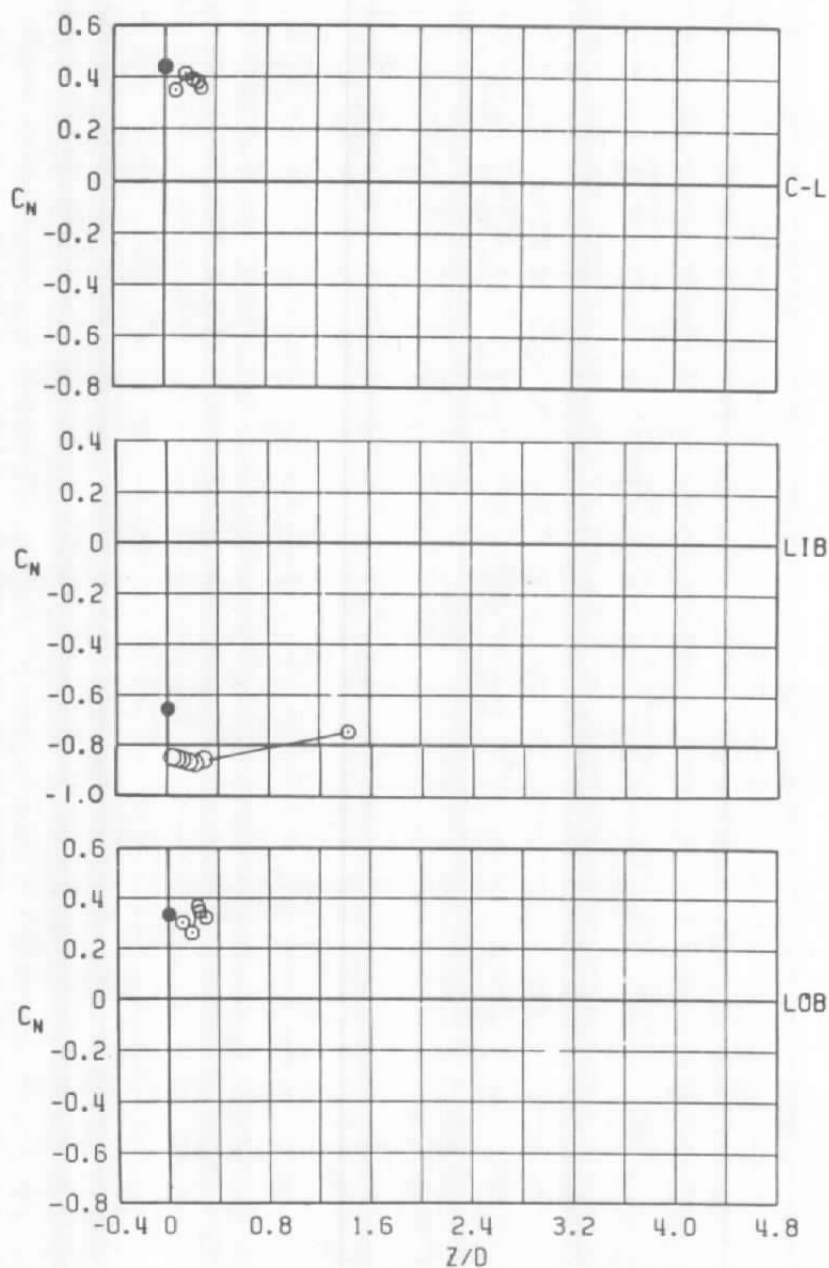
HSM  $\alpha_s = 0$  ,  $M_\infty = 0.9$   
 ● IN CAPTIVE POSITION  
 ○ APPROACH TO CAPTIVE ALONG Z AXIS



b.  $M_\infty = 0.9$

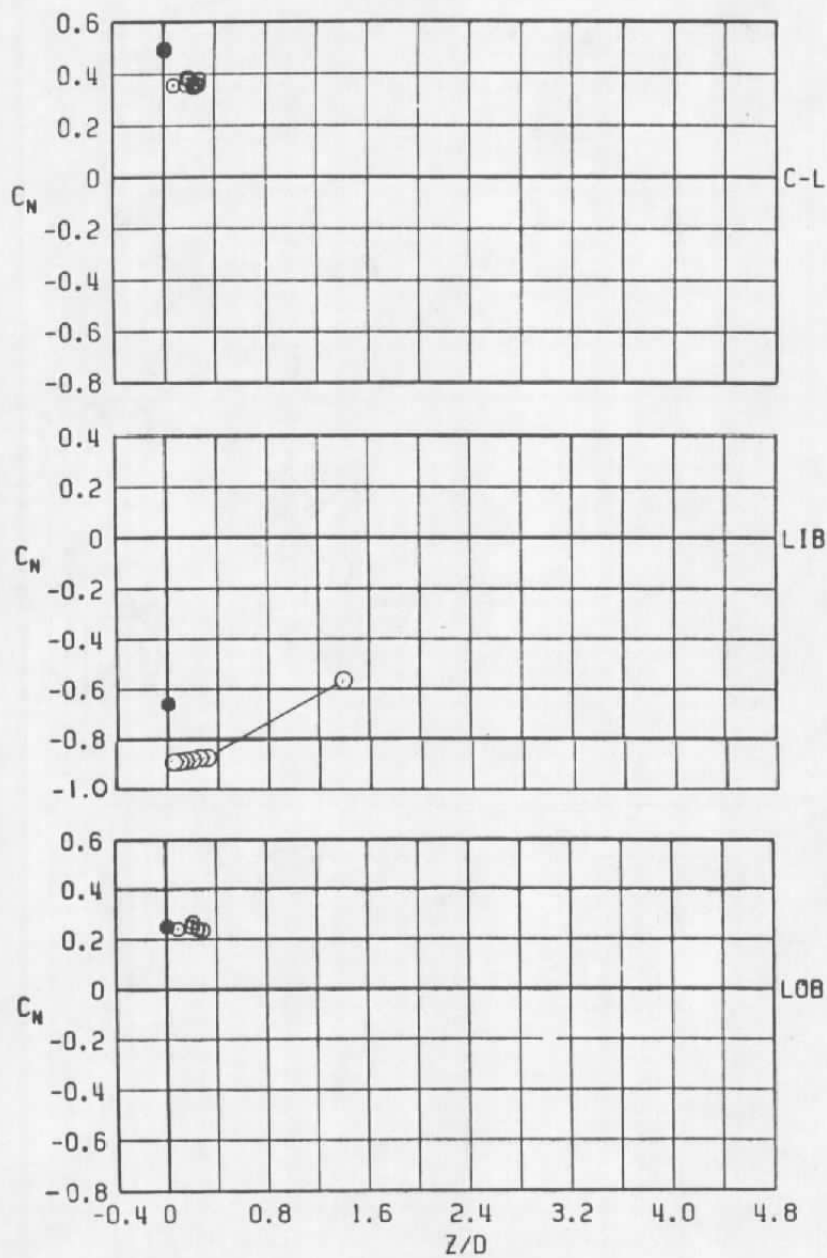
Figure 21. Continued.

HSM  $\alpha_s = 0$ ,  $M_\infty = 1.1$   
 ● IN CAPTIVE POSITION  
 ○ APPROACH TO CAPTIVE ALONG Z AXIS



c.  $M_\infty = 1.1$   
 Figure 21. Continued.

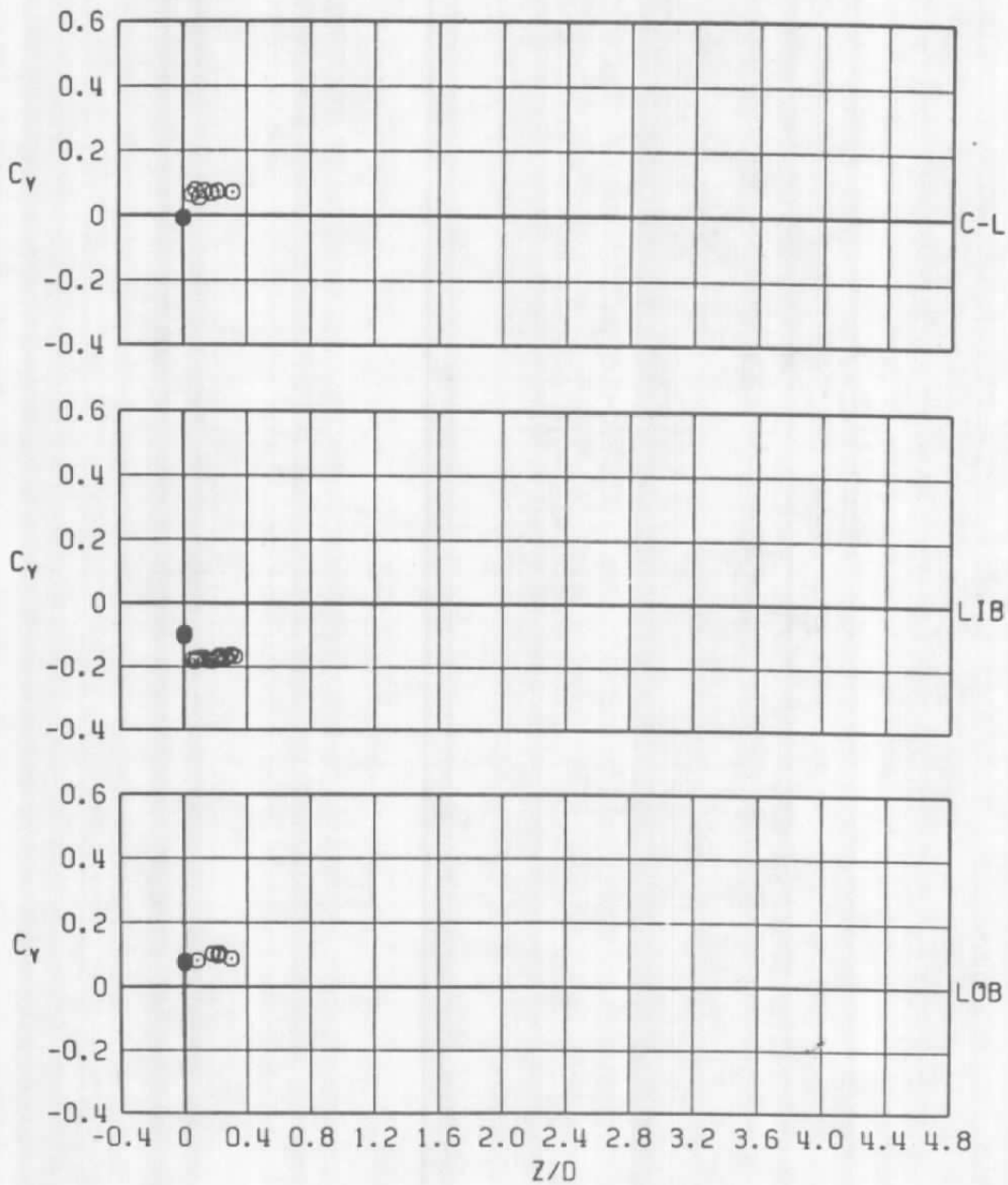
- HSM  $\alpha_s = 0$ ,  $M_\infty = 1.2$   
 ○ IN CAPTIVE POSITION  
 ○ APPROACH TO CAPTIVE ALONG Z AXIS



d.  $M_\infty = 1.2$

Figure 21. Concluded.

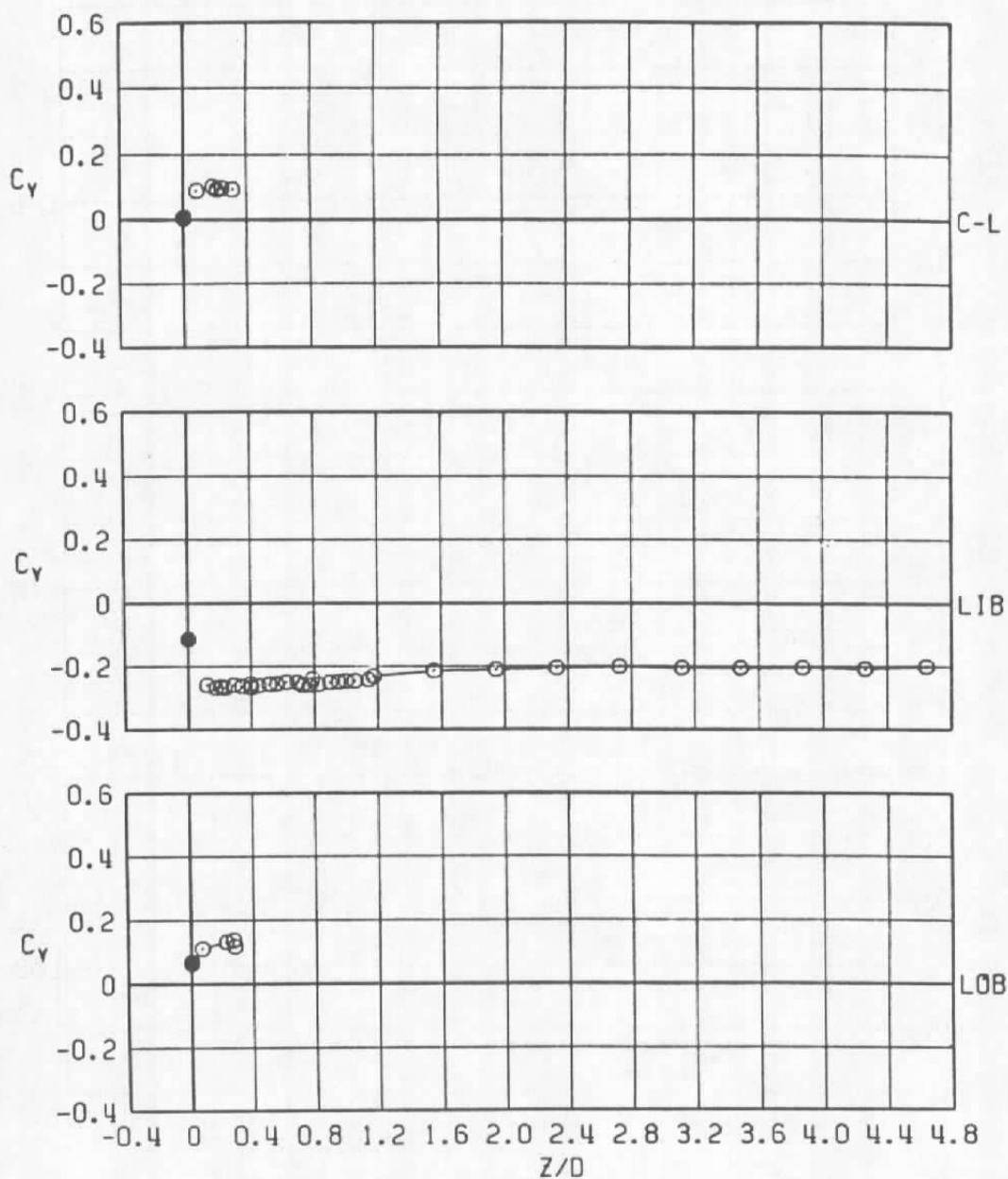
- HSM  $\alpha_s = 0$  ,  $M_\infty = 0.6$   
 IN CAPTIVE POSITION  
 ○ APPROACH TO CAPTIVE ALONG Z AXIS



a.  $M_\infty = 0.6$

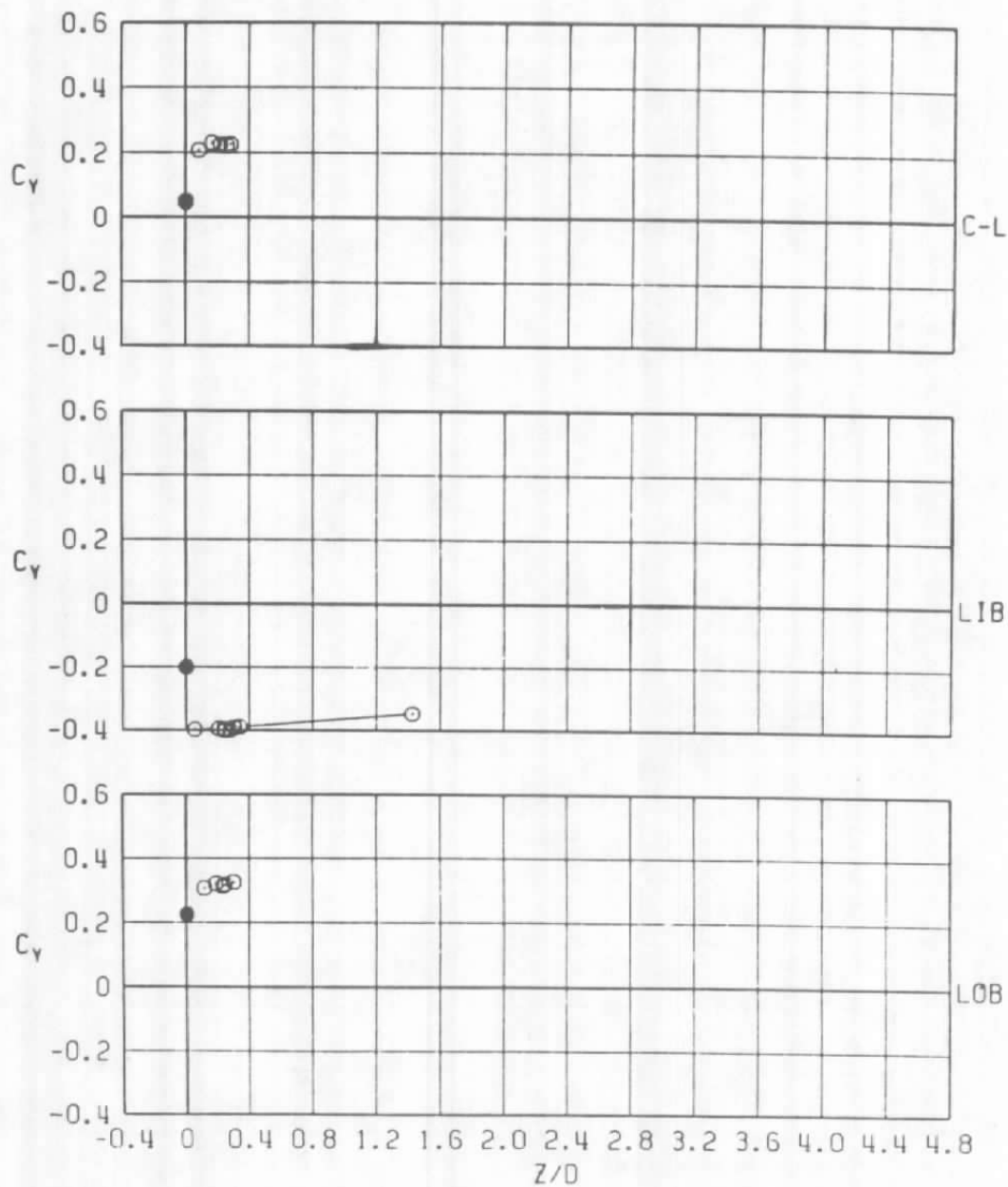
Figure 22. Coefficient of side force acting on the HSM store as a function of normal distance between the store and the captive position.

● HSM  $\alpha_s = 0$  ,  $M_\infty = 0.9$   
 ○ IN CAPTIVE POSITION  
 ○ APPROACH TO CAPTIVE ALONG Z AXIS



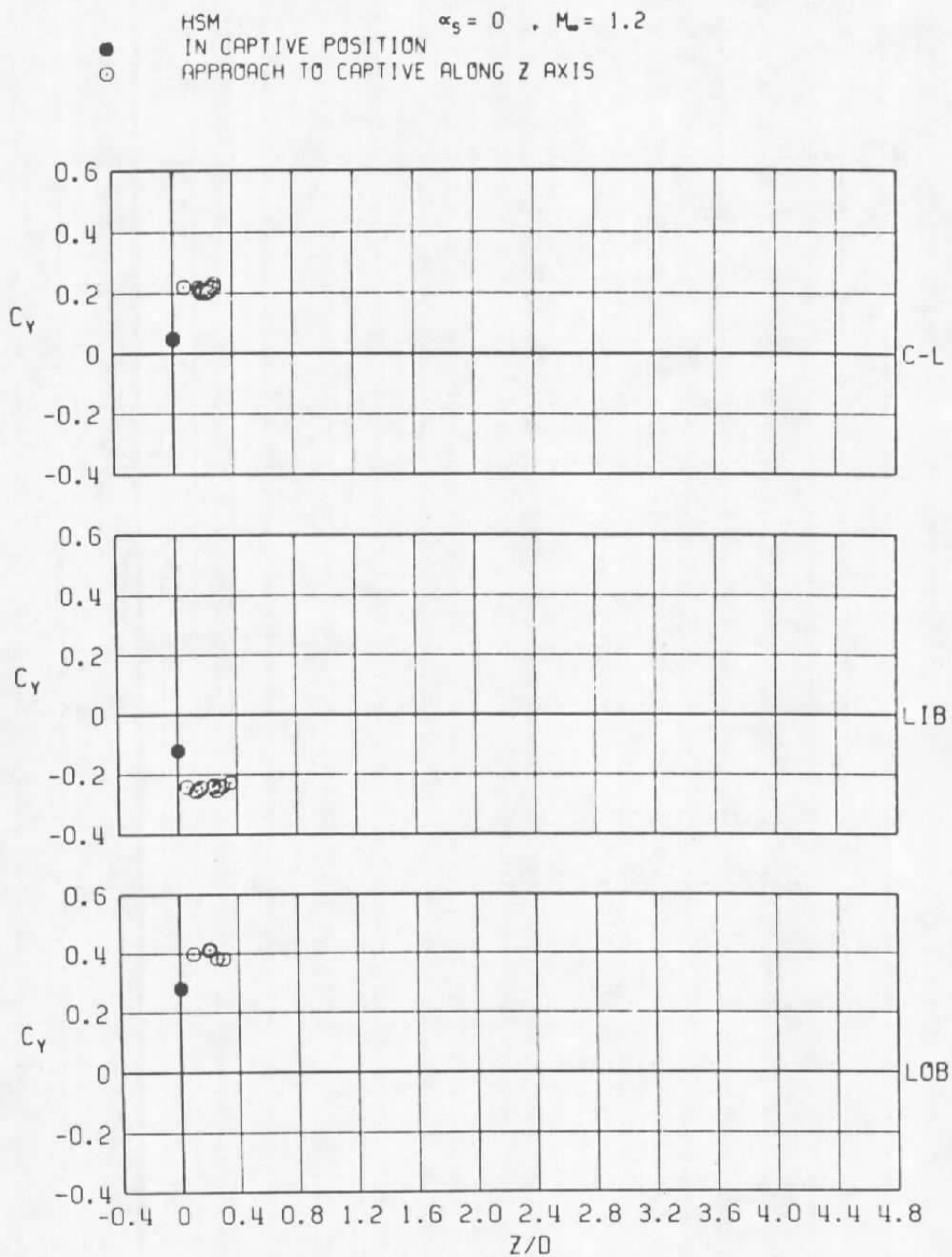
b.  $M_\infty = 0.9$   
 Figure 22. Continued.

- HSM  $\alpha_5 = 0$  ,  $M_\infty = 1.1$   
 ○ IN CAPTIVE POSITION  
 ○ APPROACH TO CAPTIVE ALONG Z AXIS



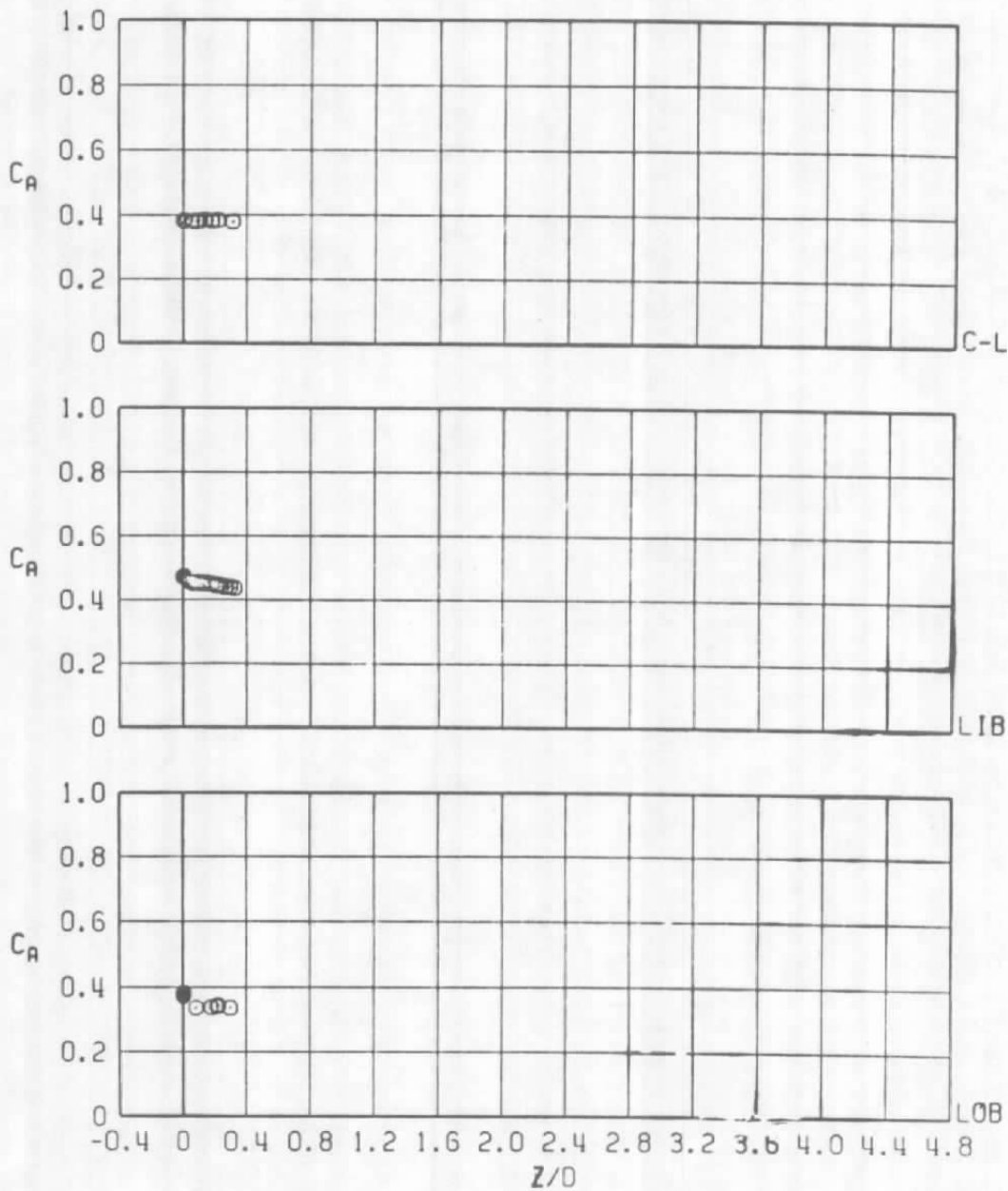
c.  $M_\infty = 1.1$   
 Figure 22. Continued.





d.  $M_\infty = 1.2$   
 Figure 22. Concluded.

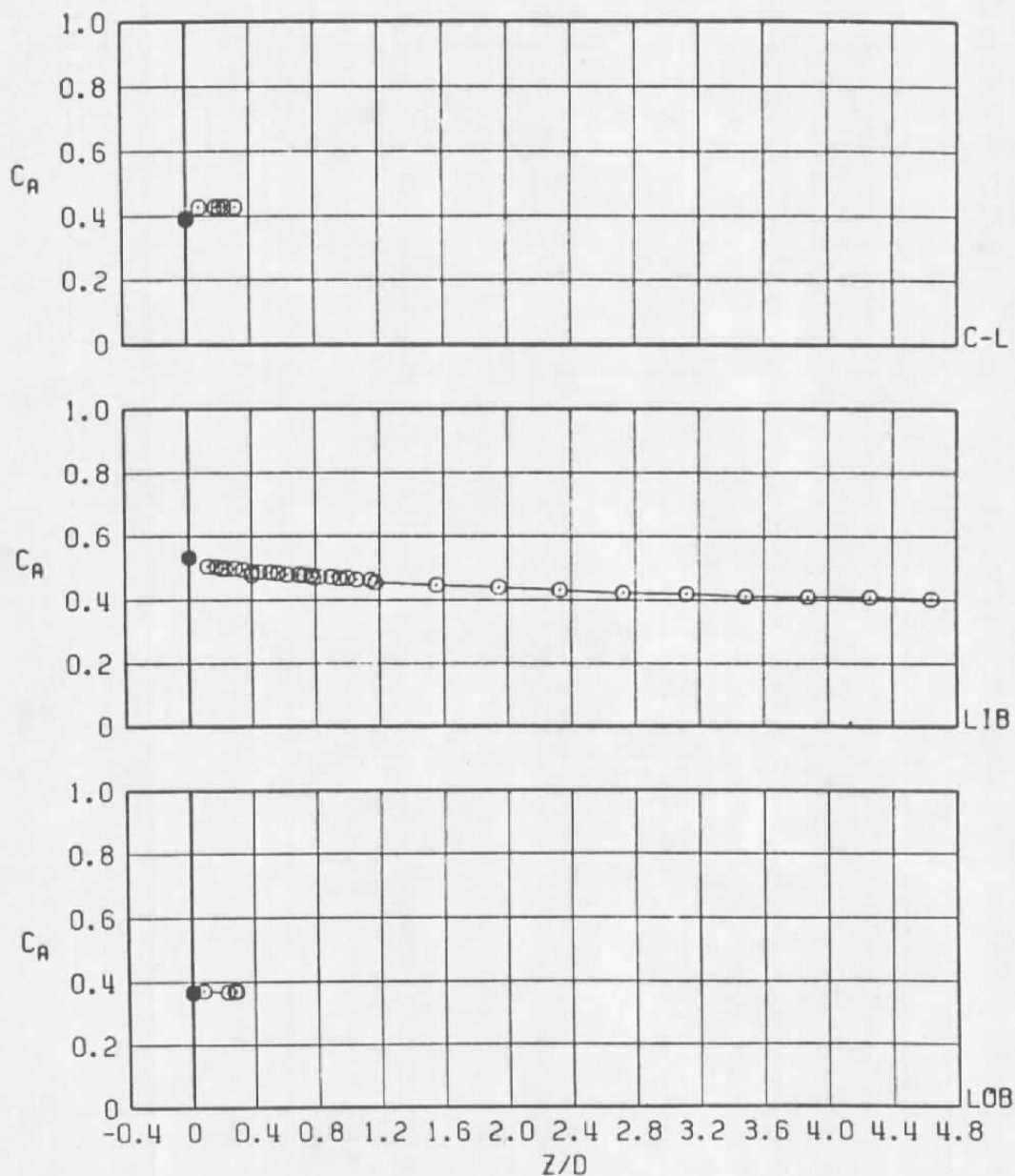
● HSM  $\alpha_s = 0$  ,  $M_\infty = 0.6$   
 ○ IN CAPTIVE POSITION  
 ○ APPROACH TO CAPTIVE ALONG Z AXIS



a.  $M_\infty = 0.6$

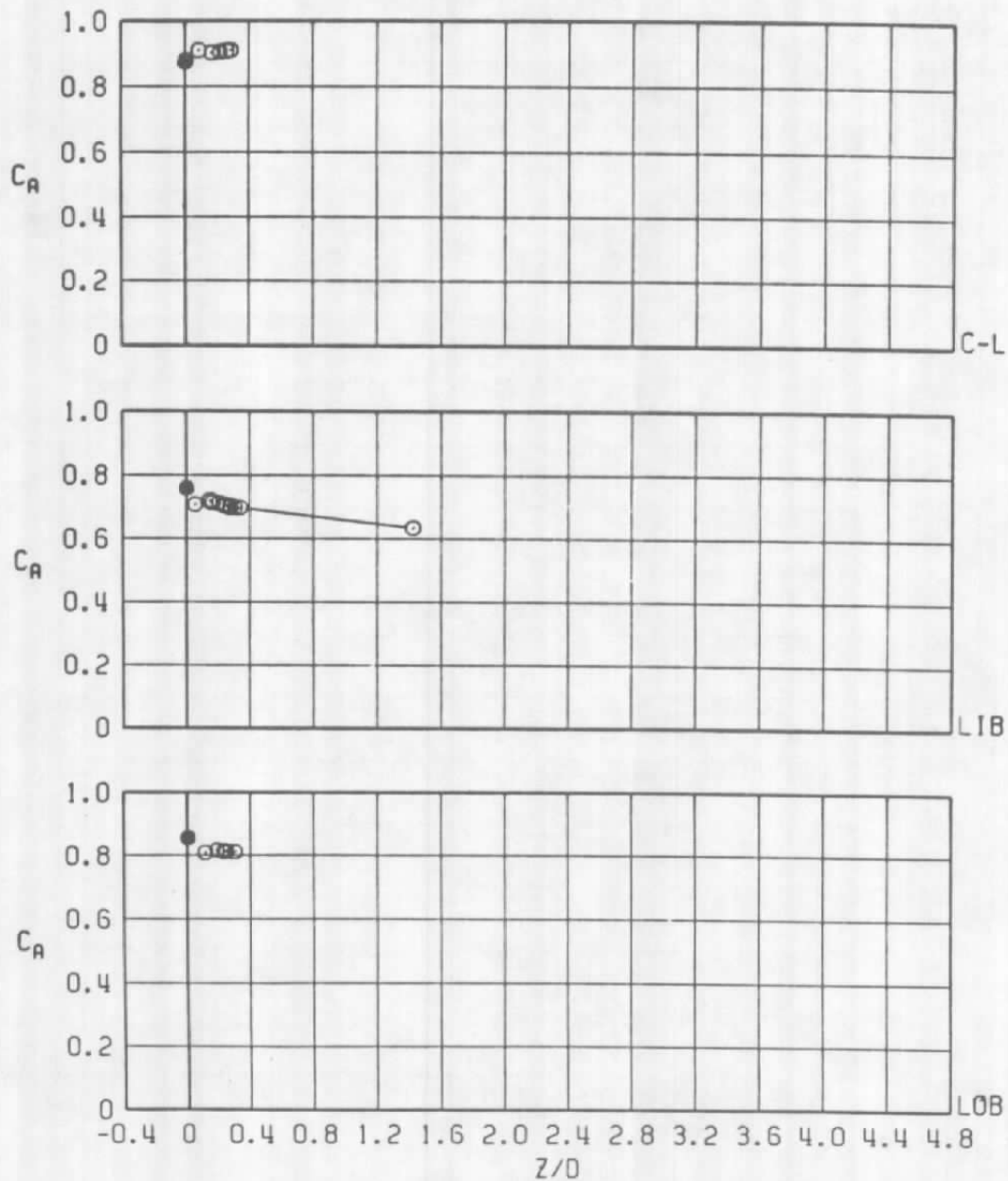
Figure 23. Coefficient of axial force acting on the HSM store as a function of normal distance between the store and the captive position.

- HSM  $\alpha_s = 0$  ,  $M_\infty = 0.9$   
 ○ IN CAPTIVE POSITION  
 ○ APPROACH TO CAPTIVE ALONG Z AXIS



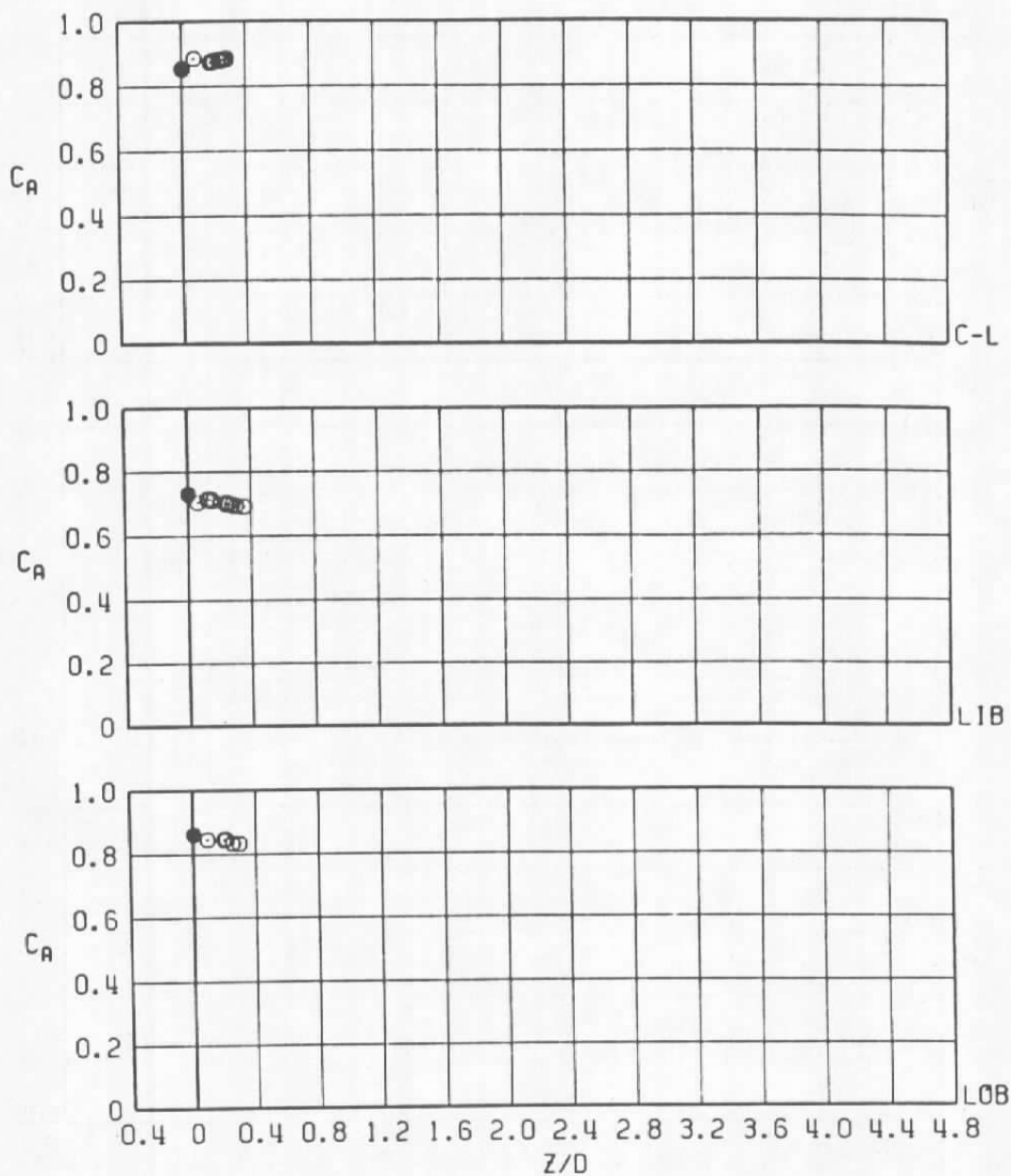
b.  $M_\infty = 0.9$   
 Figure 23. Continued.

- HSM  $\alpha_s = 0$  ,  $M_\infty = 1.1$   
 IN CAPTIVE POSITION  
 ○ APPROACH TO CAPTIVE ALONG Z AXIS

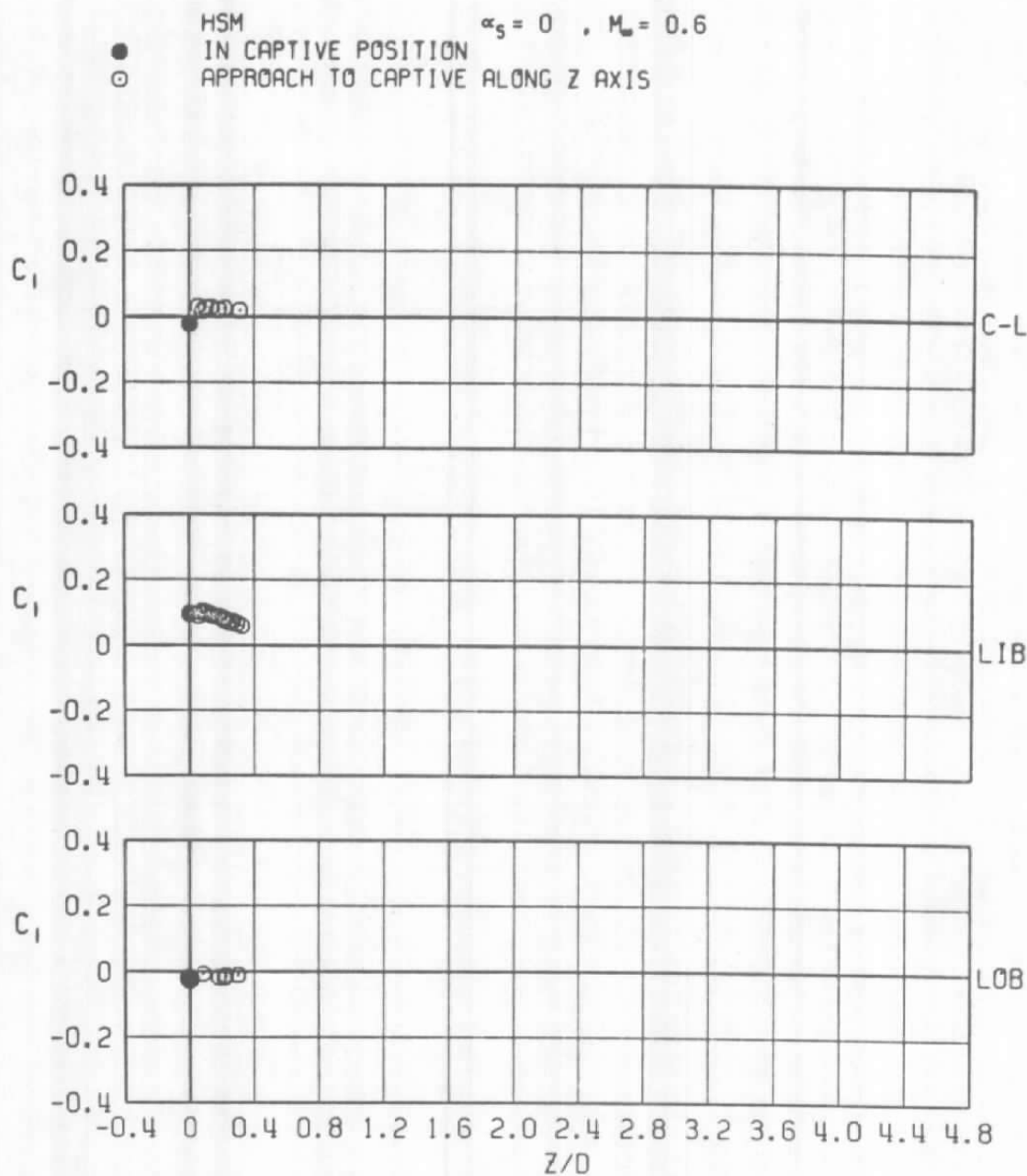


c.  $M_\infty = 1.1$   
Figure 23. Continued.

● HSM  $\alpha_5 = 0$  ,  $M_\infty = 1.2$   
 ○ IN CAPTIVE POSITION  
 ○ APPROACH TO CAPTIVE ALONG Z AXIS



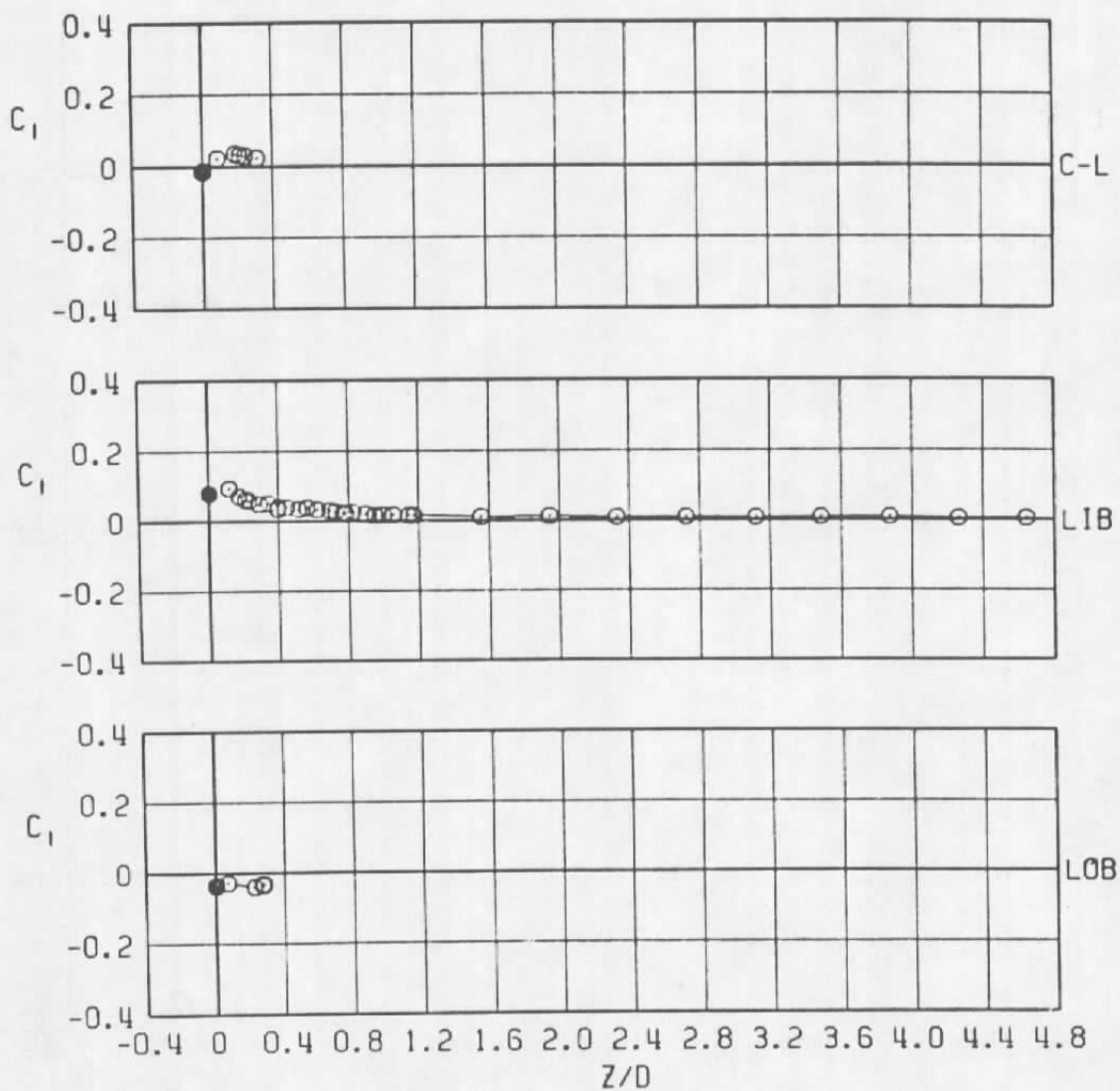
d.  $M_\infty = 1.2$   
 Figure 23. Concluded.



a.  $M_\infty = 0.6$

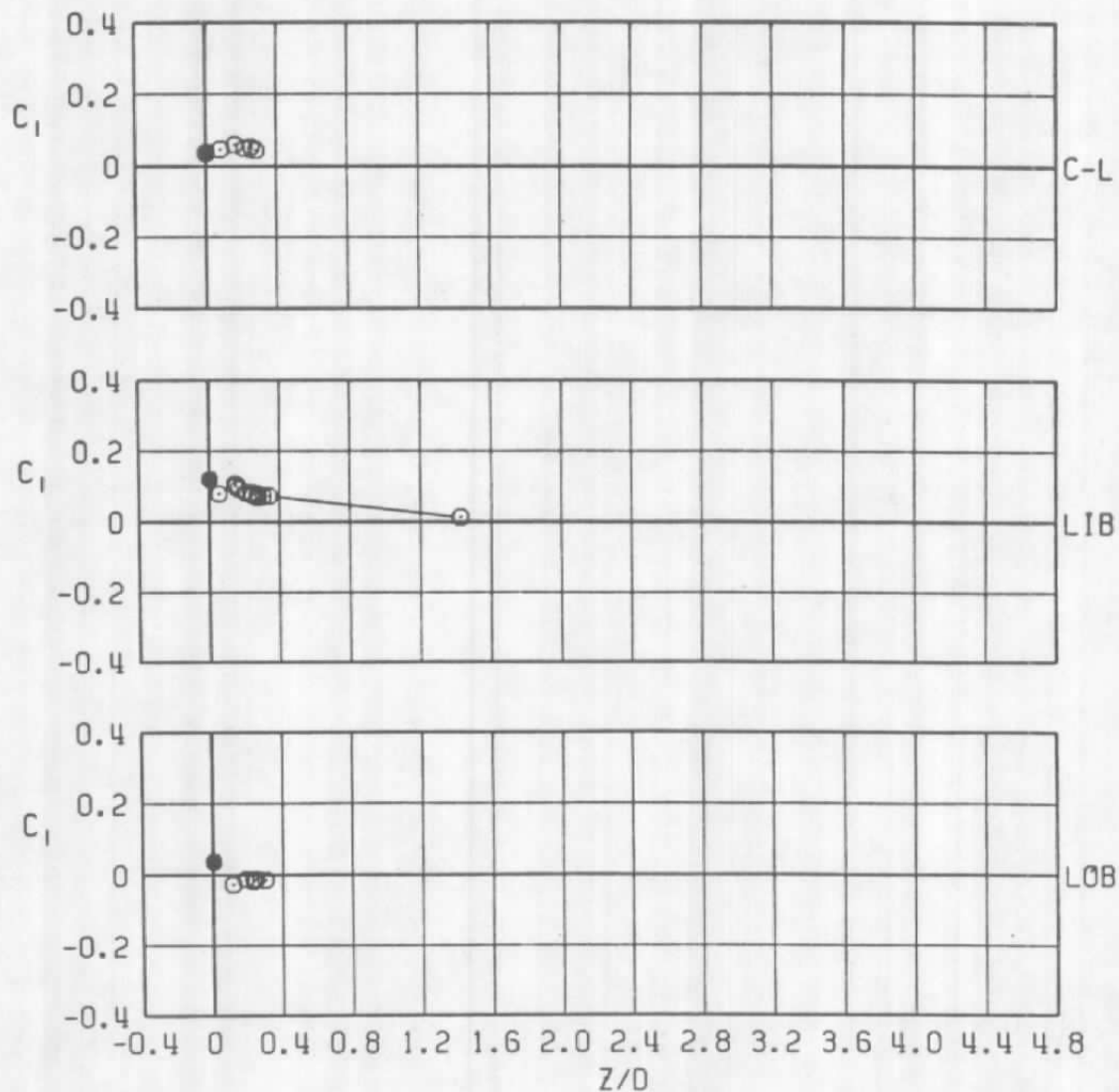
Figure 24. Coefficient of rolling moment acting on the HSM store as a function of normal distance between the store and the captive position.

● HSM  $\alpha_s = 0$  ,  $M_\infty = 0.9$   
 ○ IN CAPTIVE POSITION  
 ○ APPROACH TO CAPTIVE ALONG Z AXIS



b.  $M_\infty = 0.9$   
 Figure 24. Continued.

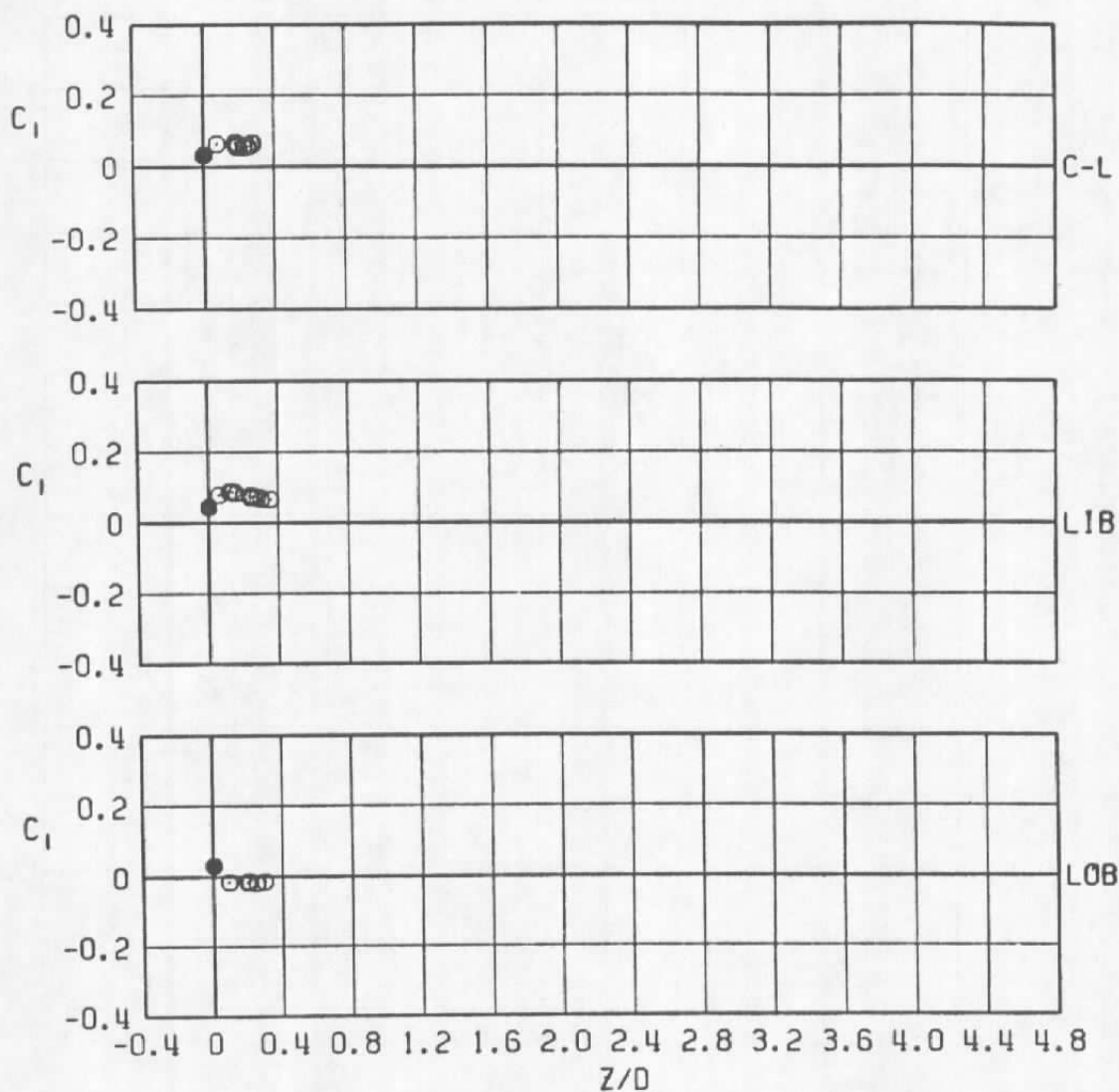
● HSM  $\alpha_s = 0$  ,  $M_\infty = 1.1$   
 ○ IN CAPTIVE POSITION  
 ○ APPROACH TO CAPTIVE ALONG Z AXIS



c.  $M_\infty = 1.1$   
 Figure 24. Continued.



● HSM  $\alpha_s = 0$  ,  $M_\infty = 1.2$   
 ○ IN CAPTIVE POSITION  
 ○ APPROACH TO CAPTIVE ALONG Z AXIS



d.  $M_\infty = 1.2$   
 Figure 24. Concluded.

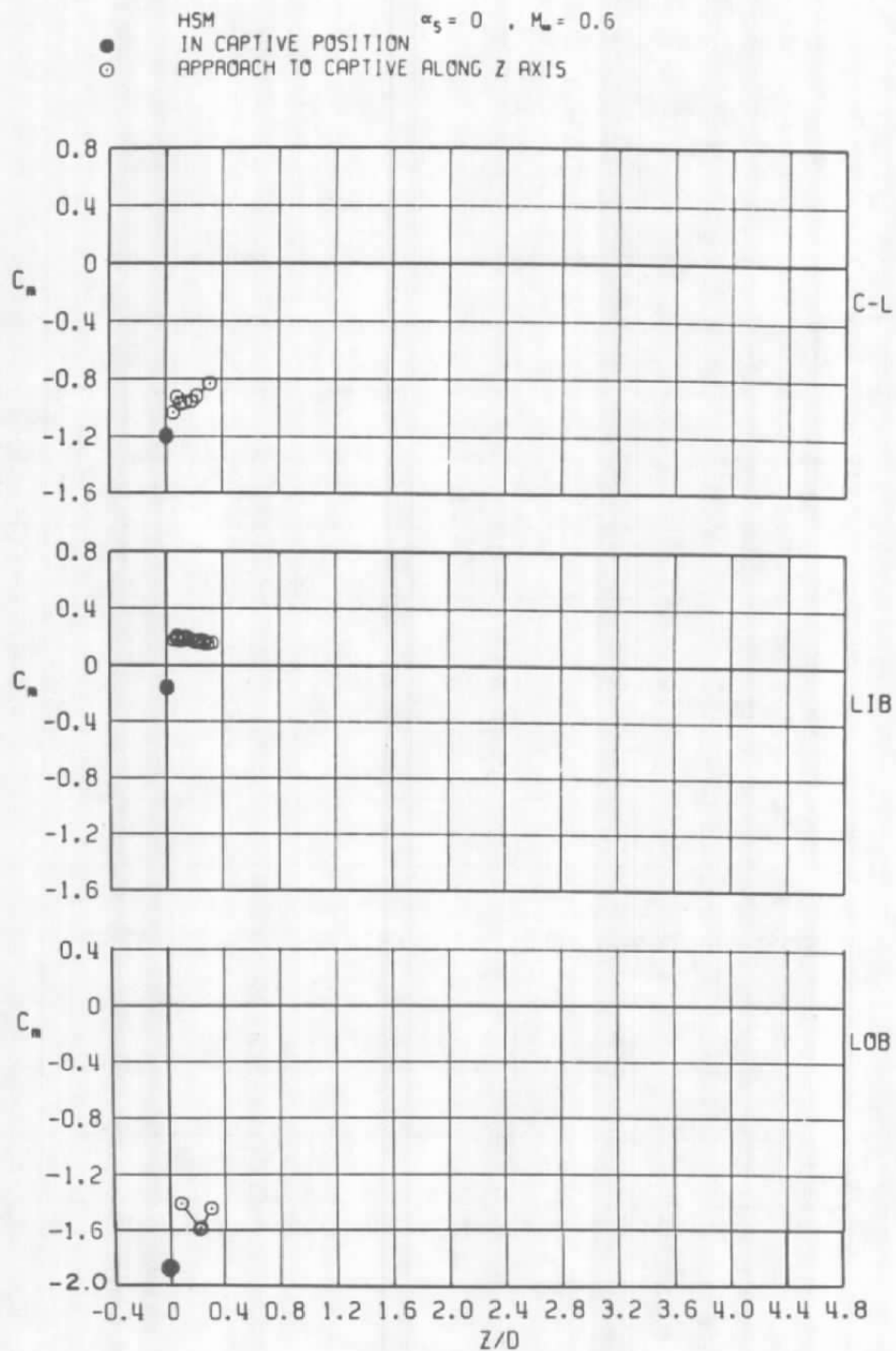
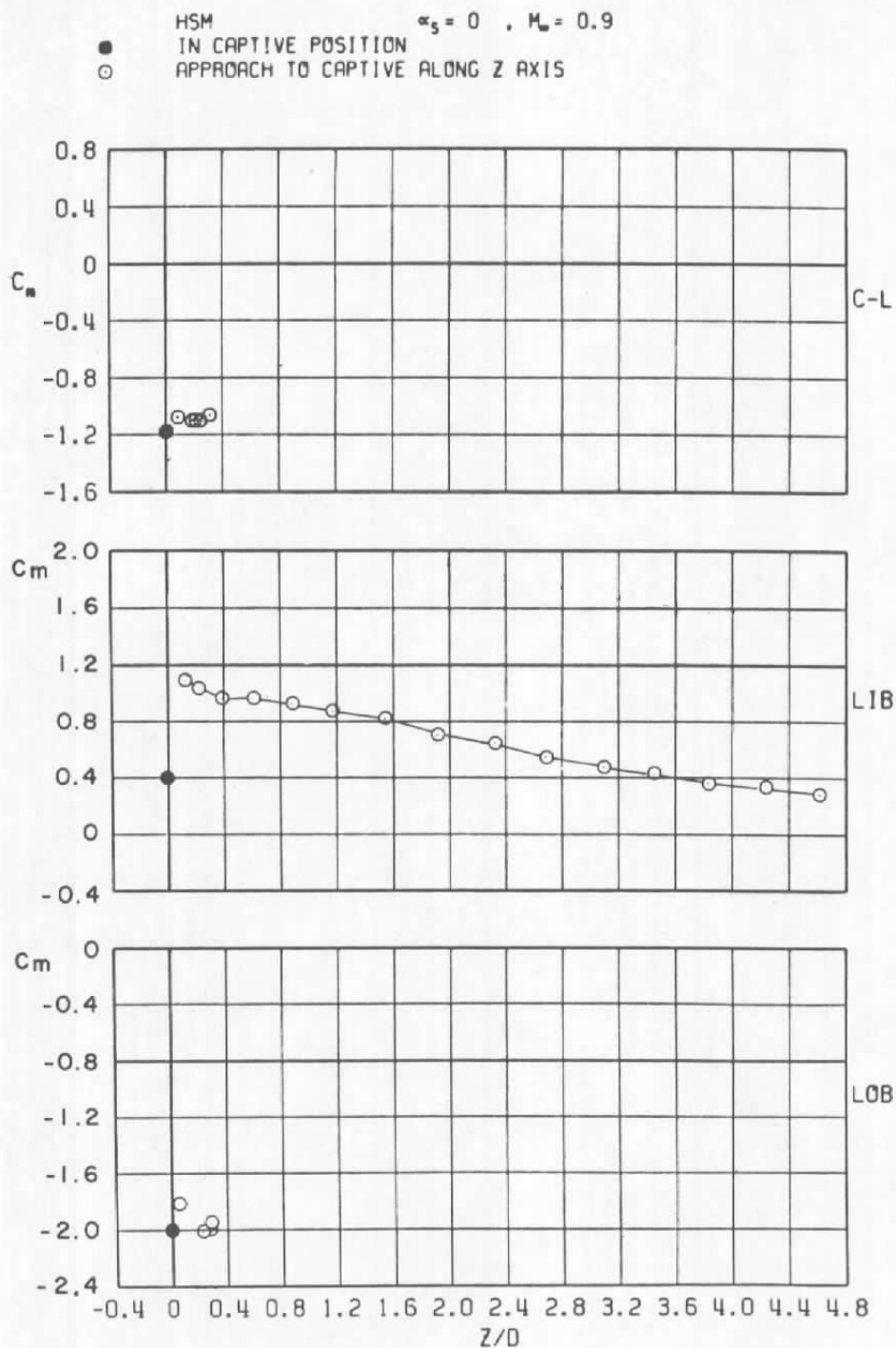
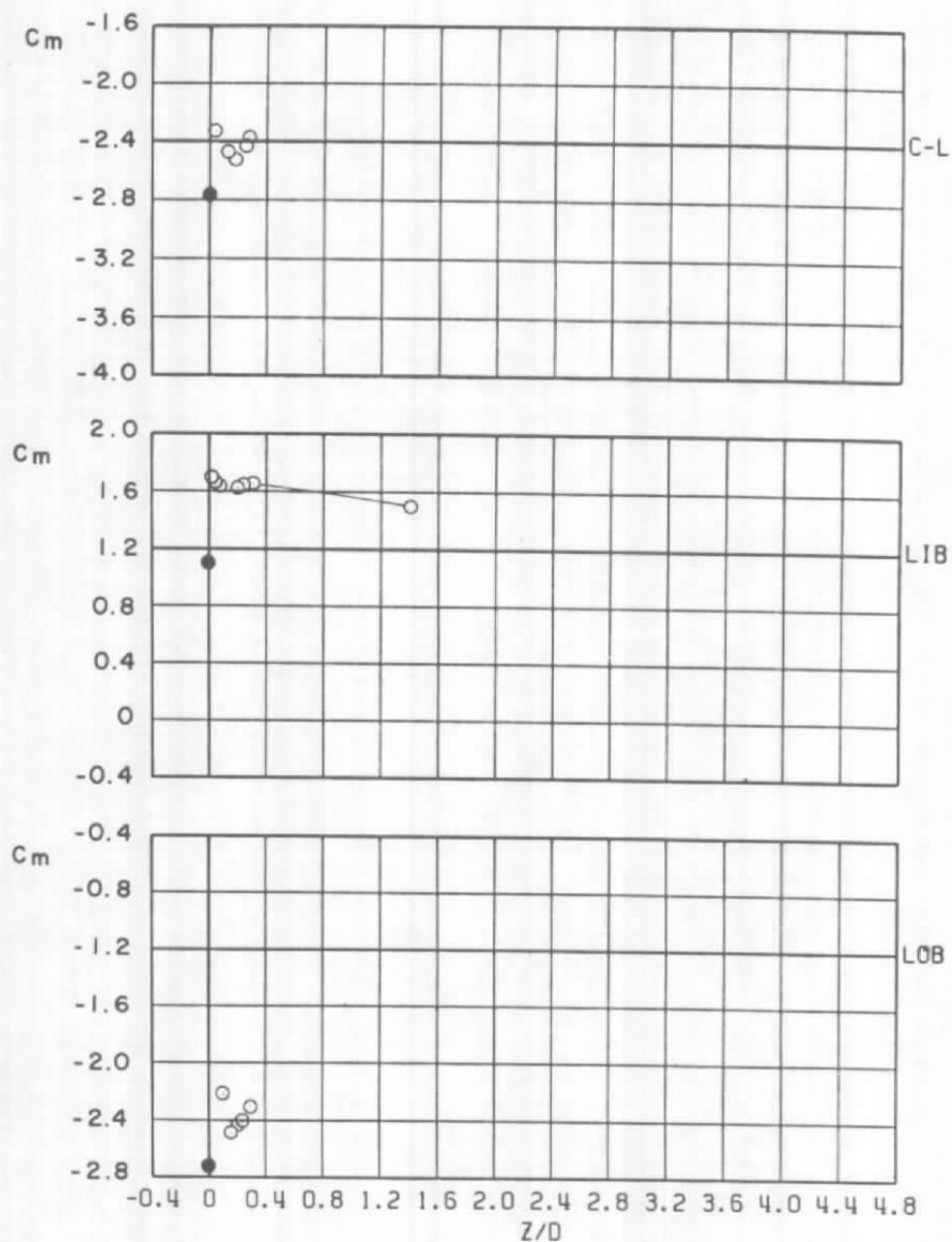
a.  $M_\infty = 0.6$ 

Figure 25. Coefficient of pitching moment acting on the HSM store as a function of normal distance between the store and the captive position.



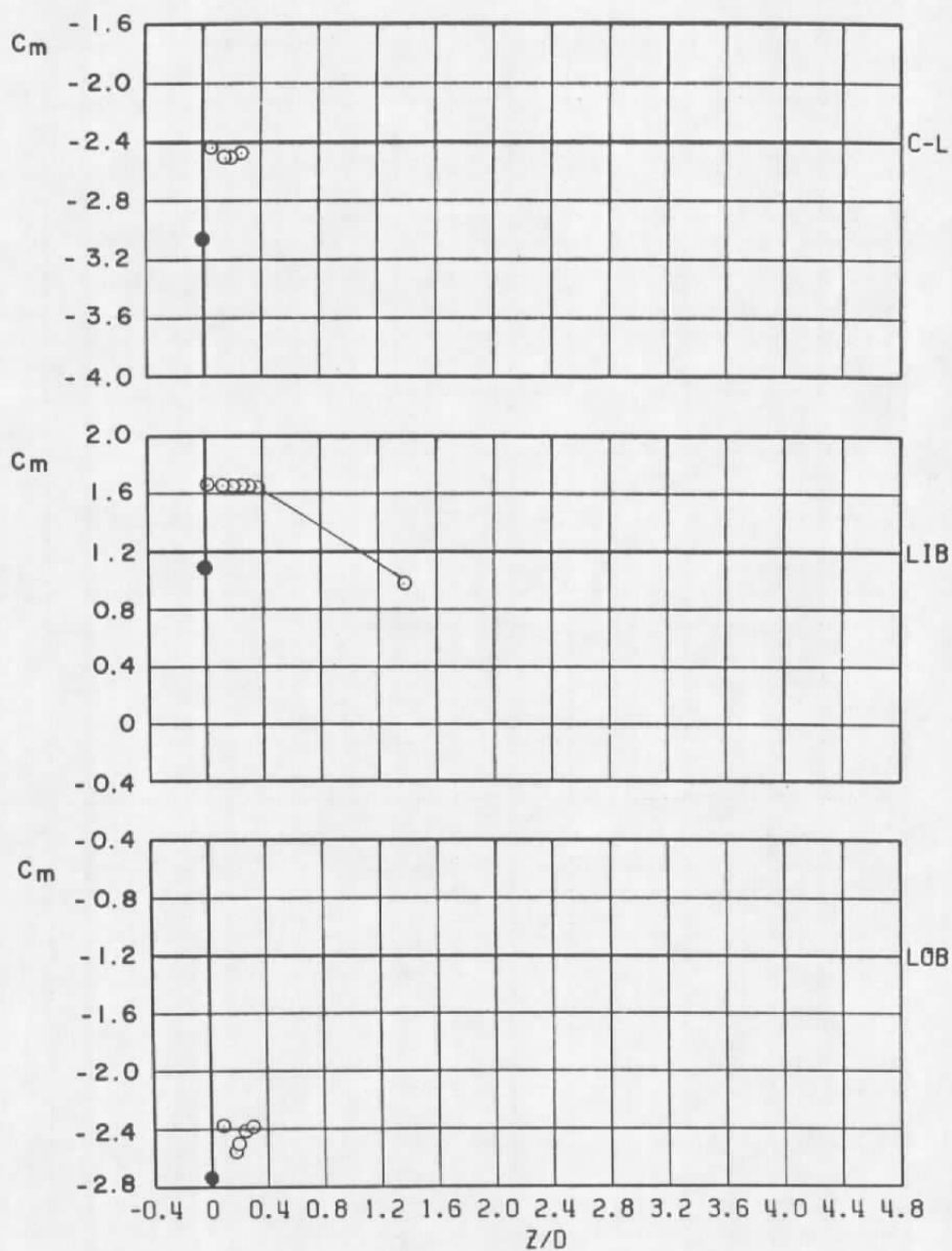
b.  $M_\infty = 0.9$   
 Figure 25. Continued.

HSM  $\alpha_s = 0$ ,  $M_\infty = 1.1$   
 ● IN CAPTIVE POSITION  
 ○ APPROACH TO CAPTIVE ALONG Z AXIS



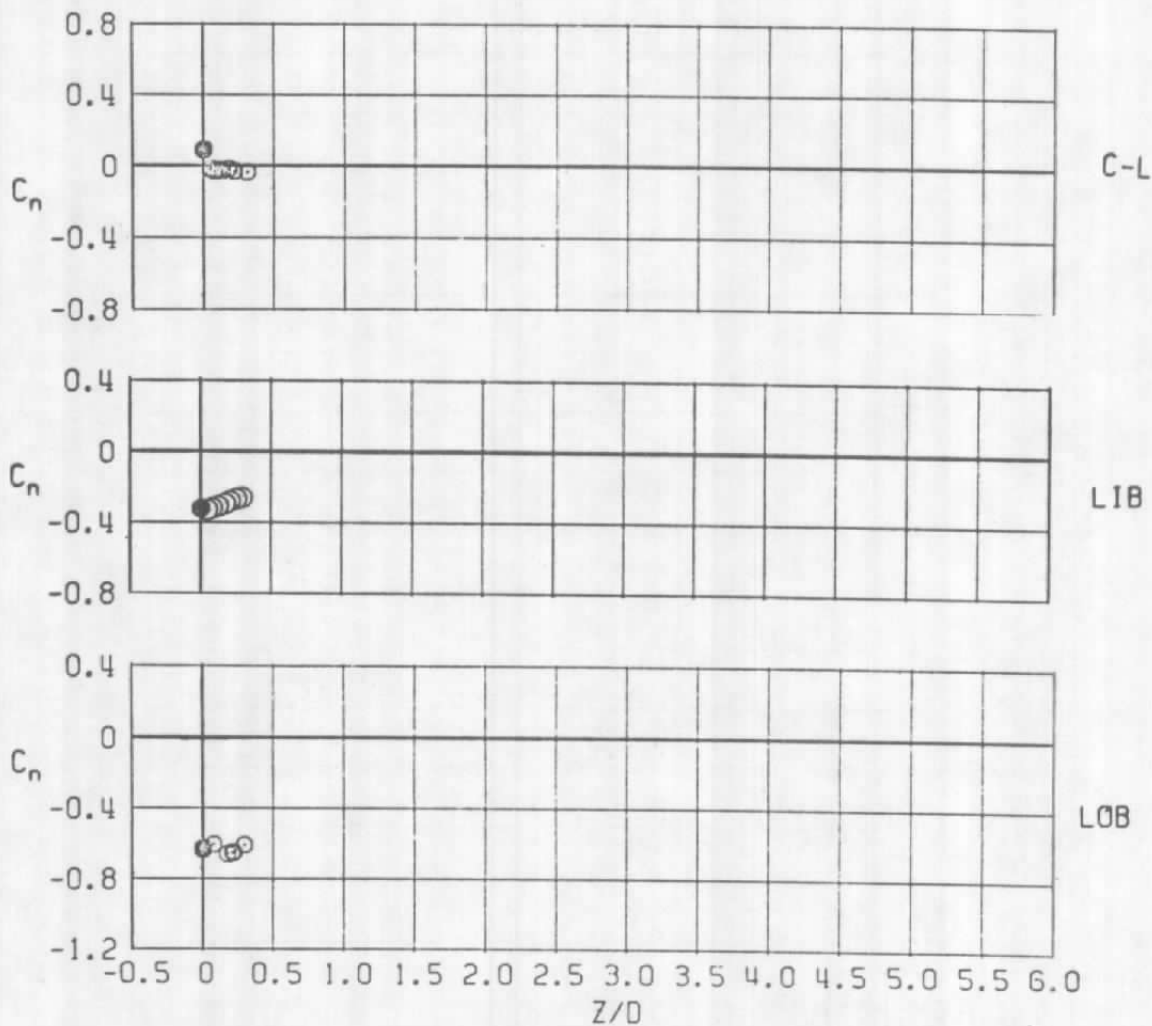
c.  $M_\infty = 1.1$   
 Figure 25. Continued.

● HSM  $\alpha_s = 0$ ,  $M_\infty = 1.2$   
 ○ IN CAPTIVE POSITION  
 ○ APPROACH TO CAPTIVE ALONG Z AXIS



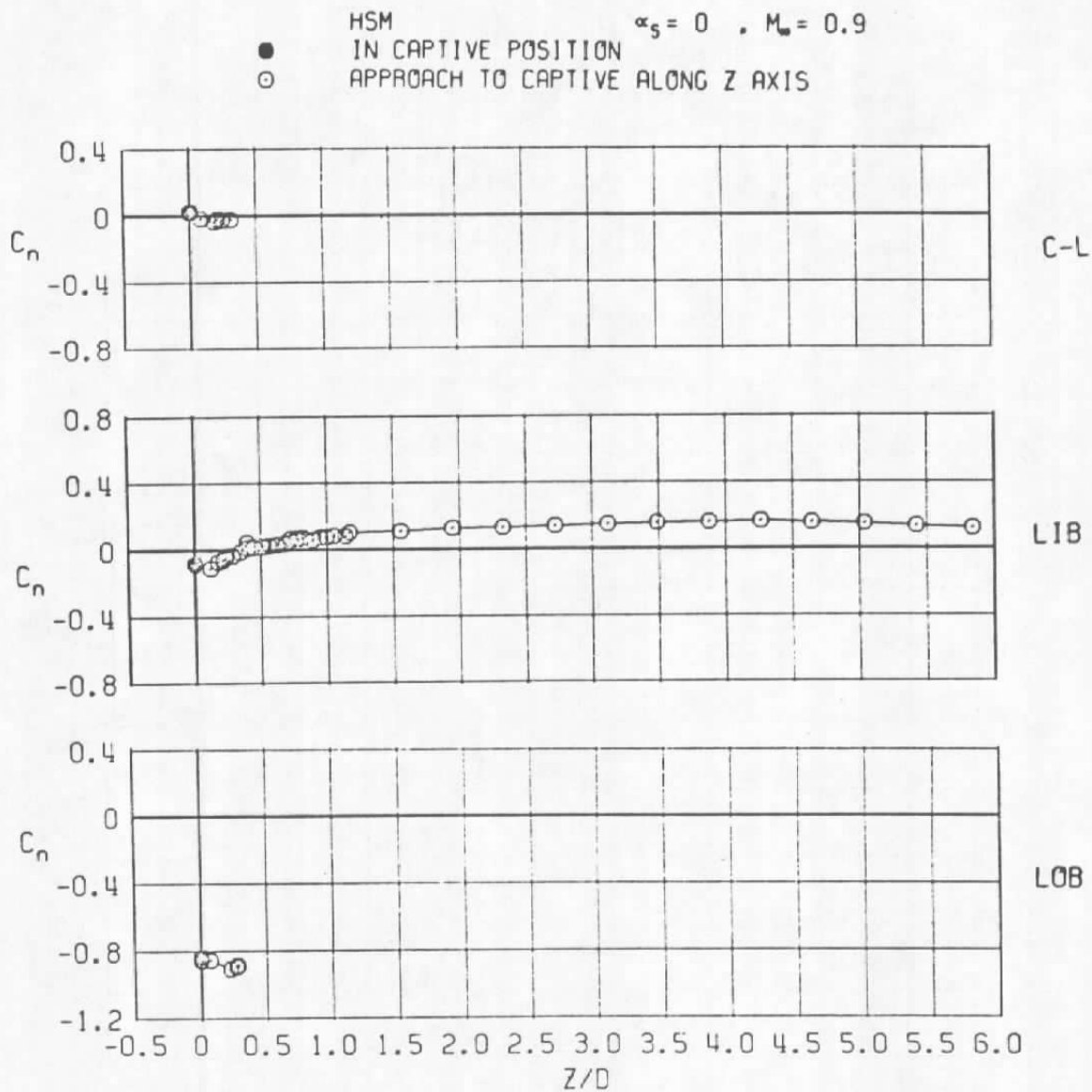
d.  $M_\infty = 1.2$   
 Figure 25. Concluded.

● HSM  $\alpha_s = 0$  ,  $M_\infty = 0.6$   
 ○ IN CAPTIVE POSITION  
 ○ APPROACH TO CAPTIVE ALONG Z AXIS

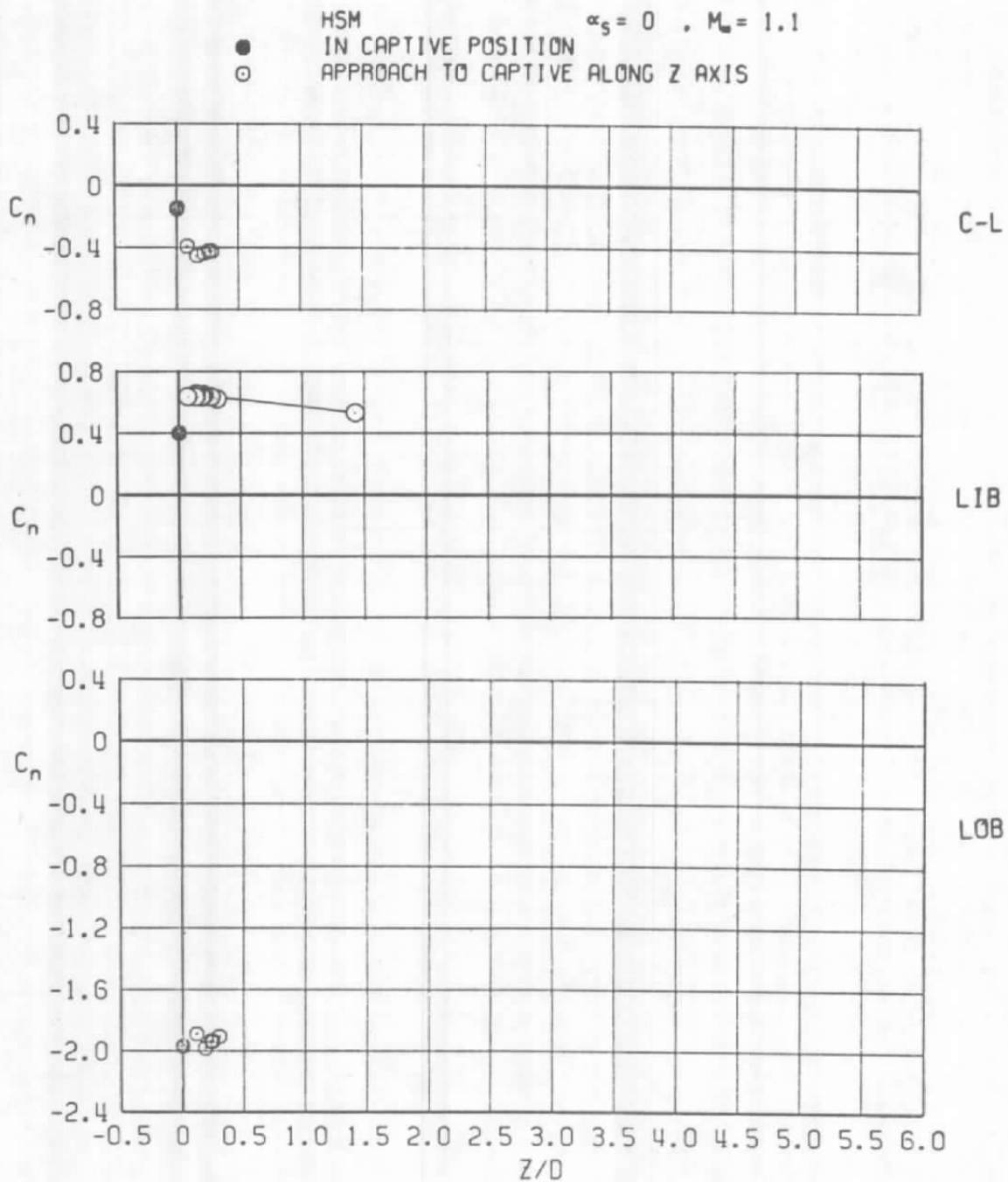


a.  $M_\infty = 0.6$

Figure 26. Coefficient of yawing moment acting on the HSM store as a function of normal distance between the store and the captive position.

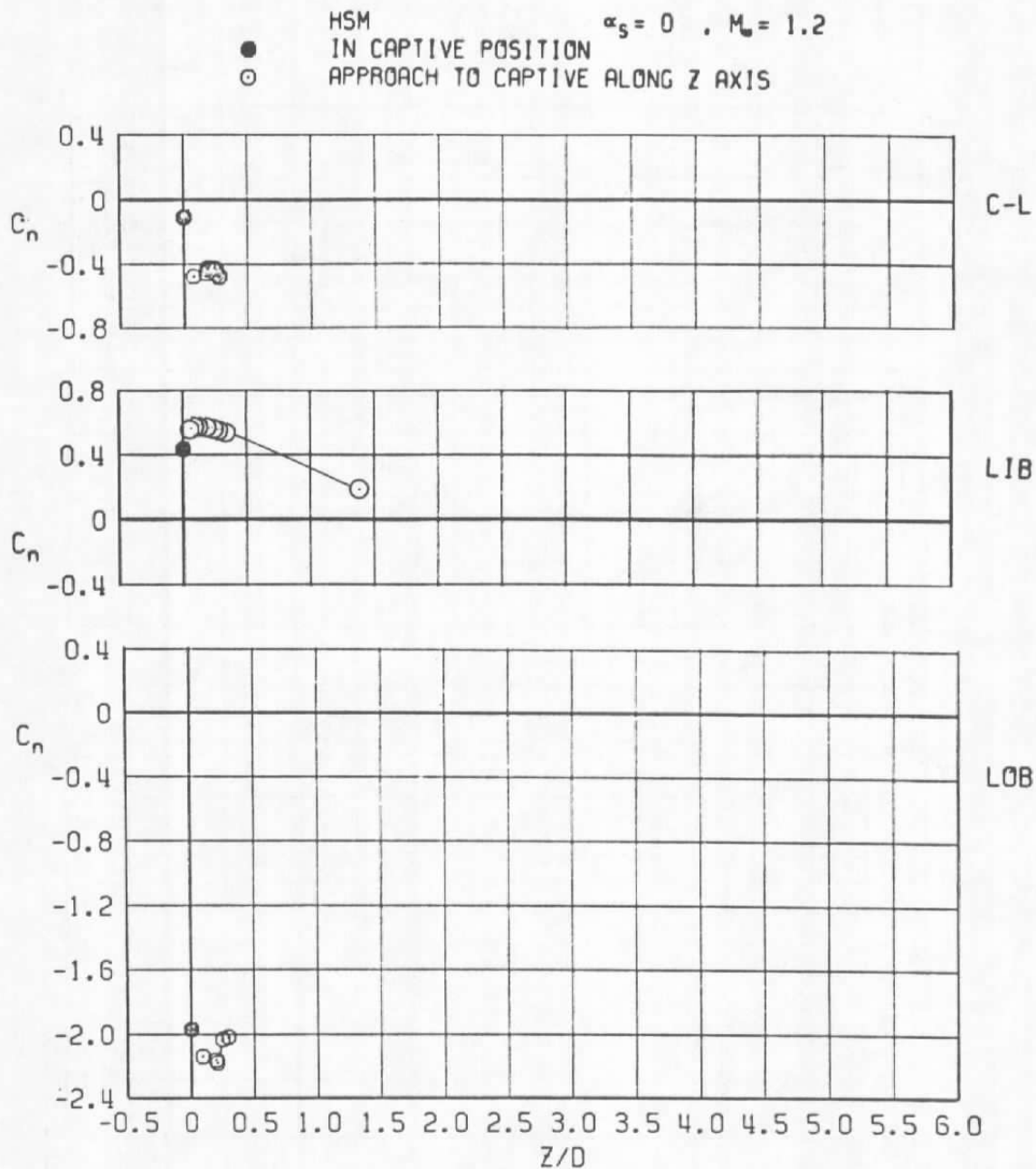


b.  $M_\infty = 0.9$   
Figure 26. Continued.

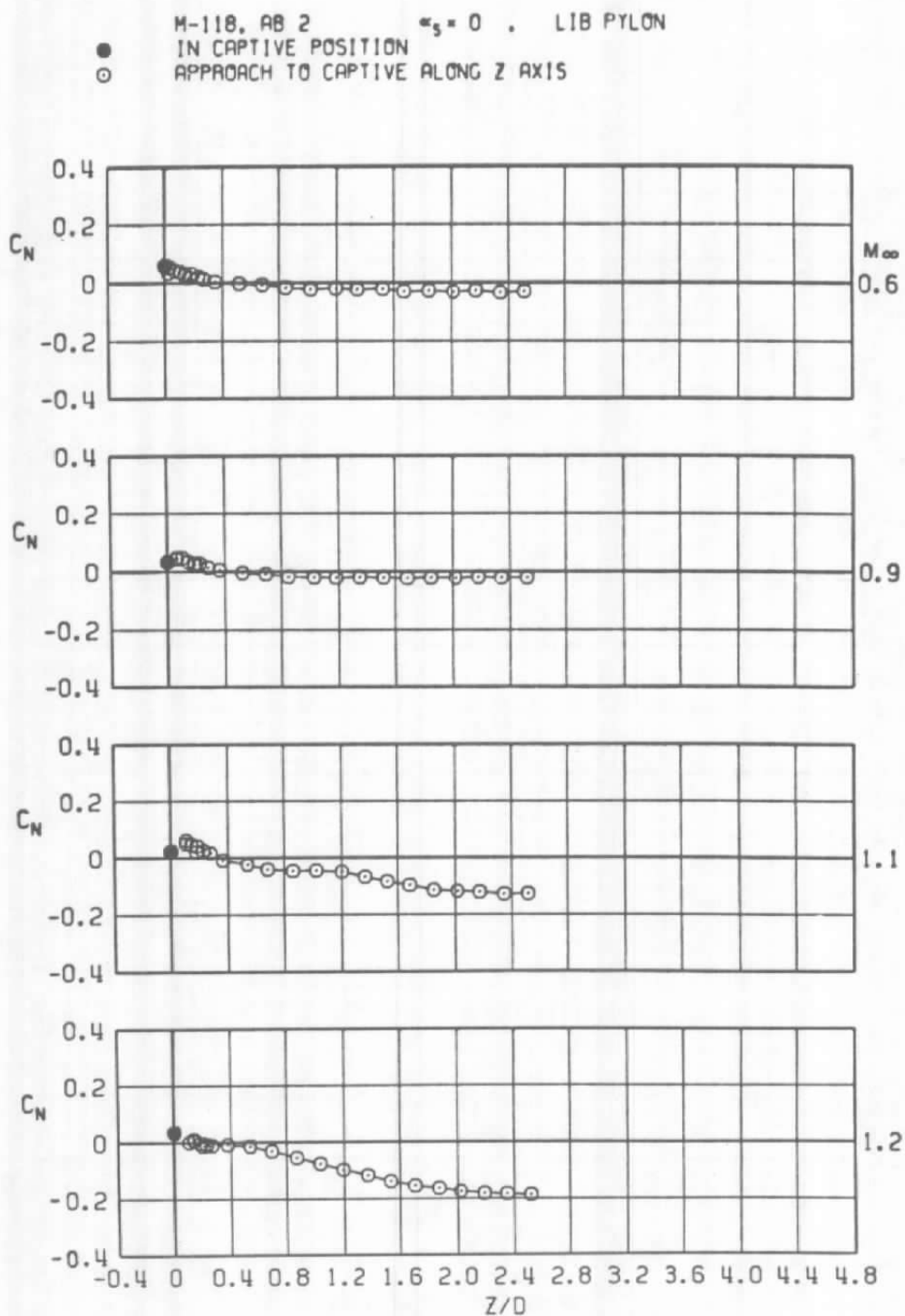


c.  $M_\infty = 1.1$   
 Figure 26. Continued.





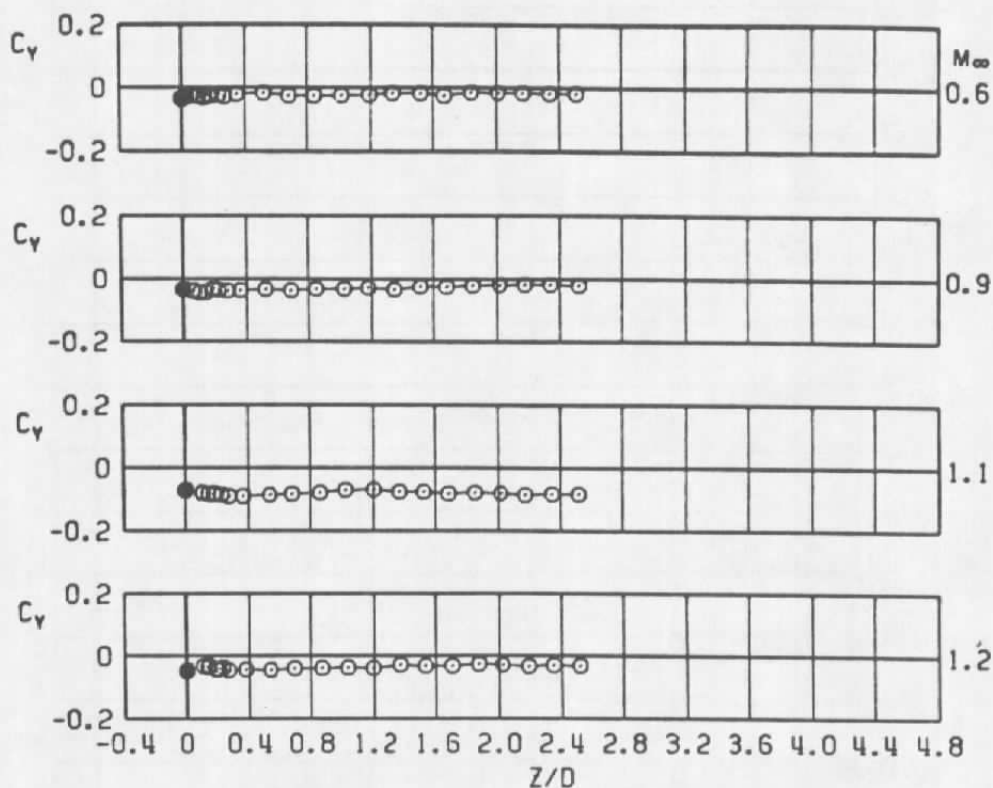
d.  $M_\infty = 1.2$   
 Figure 26. Concluded.



a. Normal force

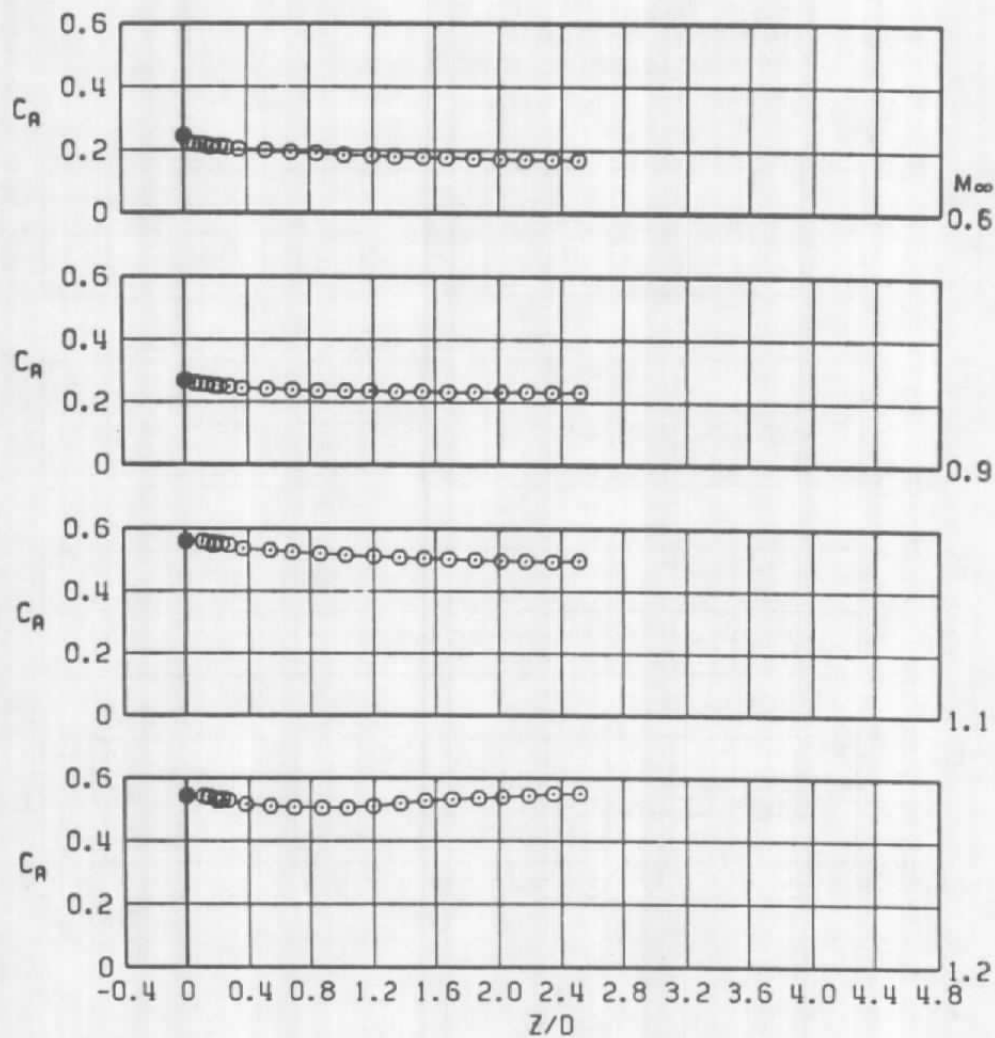
Figure 27. Coefficients of forces and moments acting on the M-118 store as a function of normal distance between the store and the captive position on the LIB pylon.

● M-118, AB 2  $\alpha_s = 0$  , LIB PYLON  
 IN CAPTIVE POSITION  
 ○ APPROACH TO CAPTIVE ALONG Z AXIS



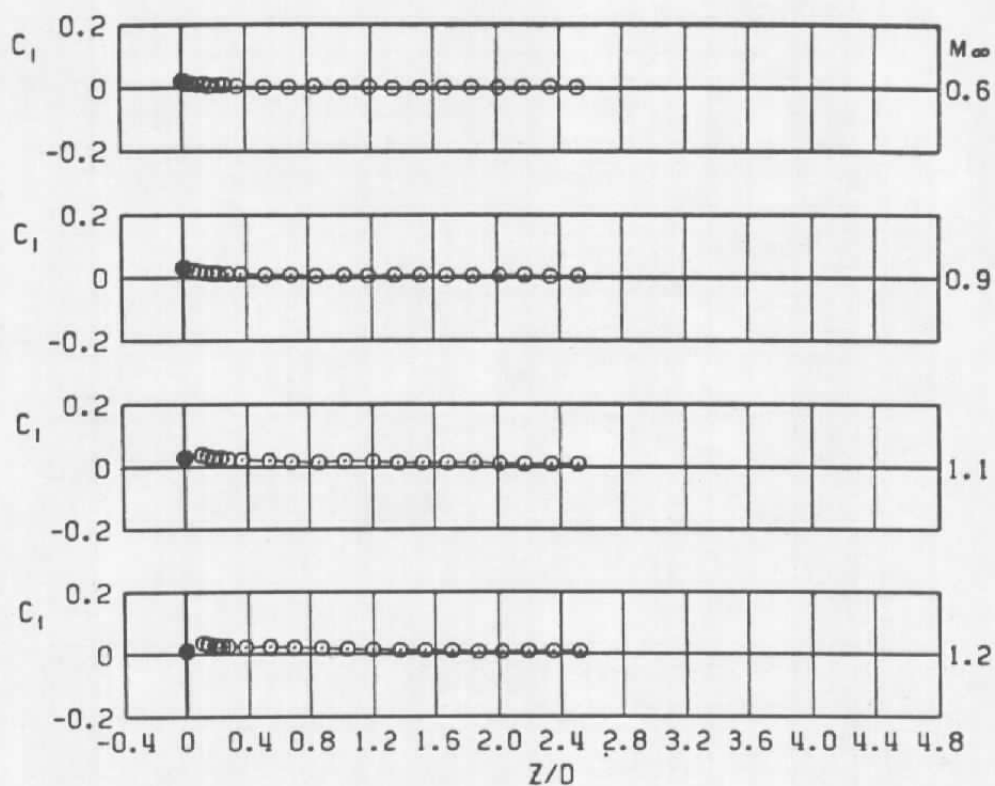
b. Side force  
 Figure 27. Continued.

M-118, AB 2       $\alpha_s = 0$       LIB PYLON  
 ● IN CAPTIVE POSITION  
 ○ APPROACH TO CAPTIVE ALONG Z AXIS

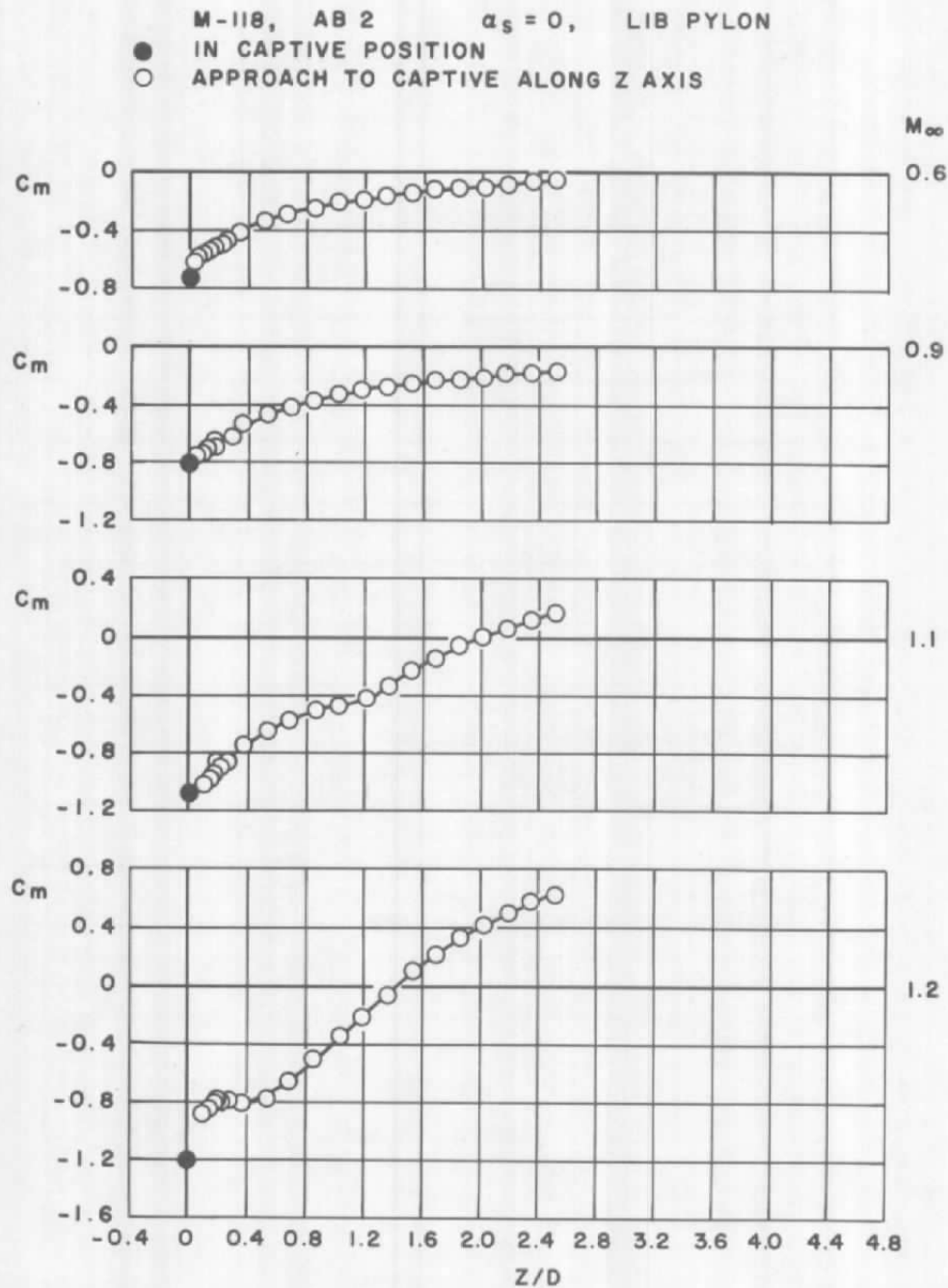


c. Axial force  
 Figure 27. Continued.

M-118, AB 2       $\alpha_s = 0$  , LIB PYLON  
 ● IN CAPTIVE POSITION  
 ○ APPROACH TO CAPTIVE ALONG Z AXIS

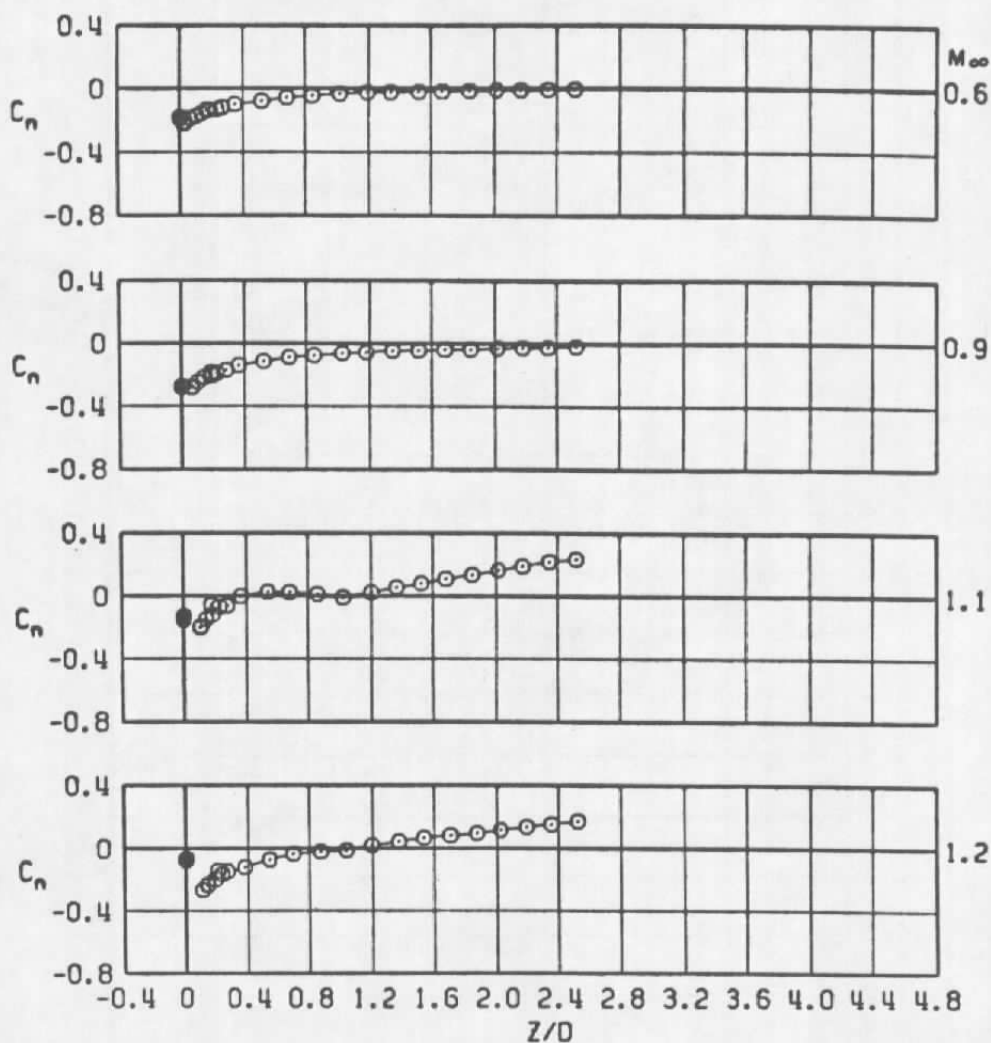


d. Rolling moment  
 Figure 27. Continued.

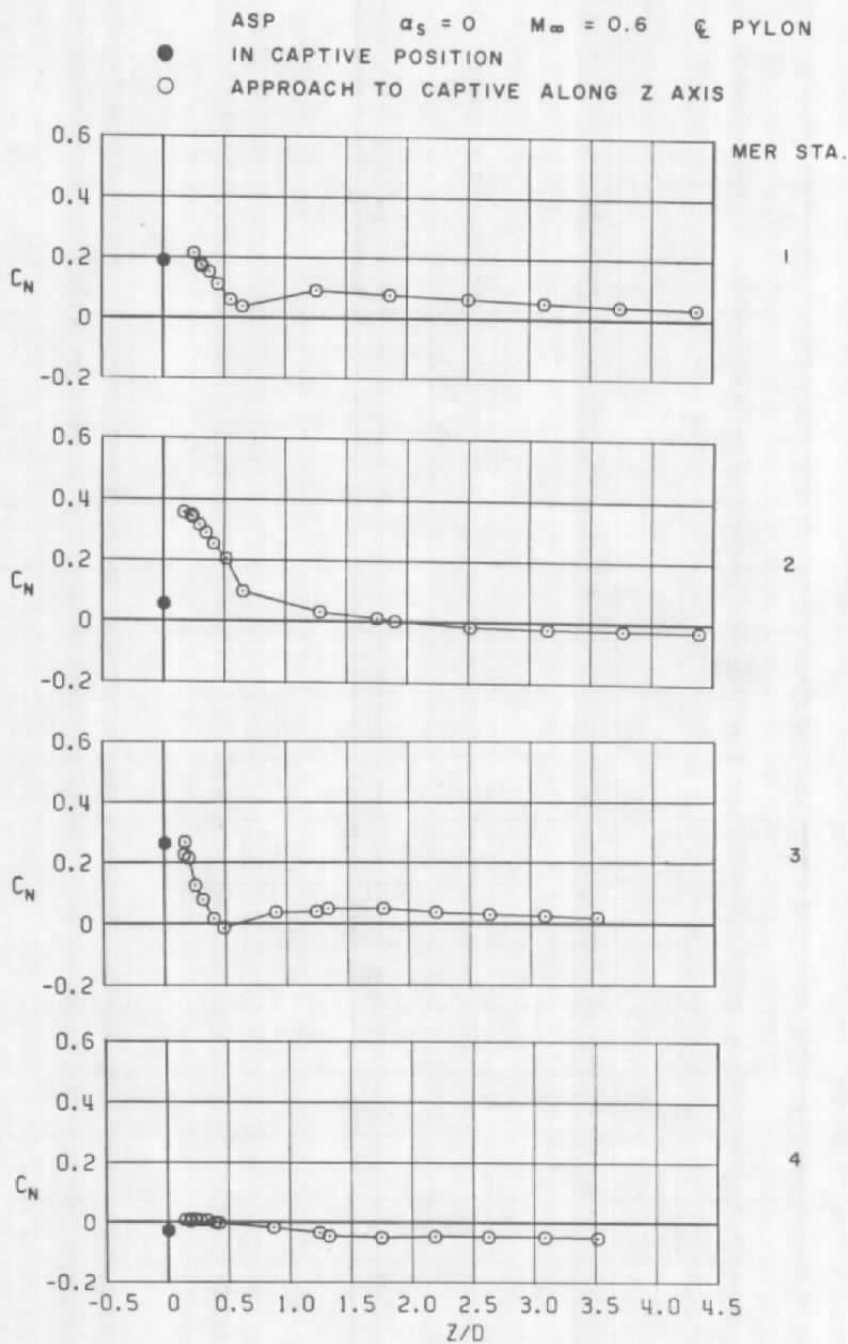


e. Pitching moment  
Figure 27. Continued.

M-118, AB 2       $\alpha_3 = 0$       LIB PYLON  
 ● IN CAPTIVE POSITION  
 ○ APPROACH TO CAPTIVE ALONG Z AXIS



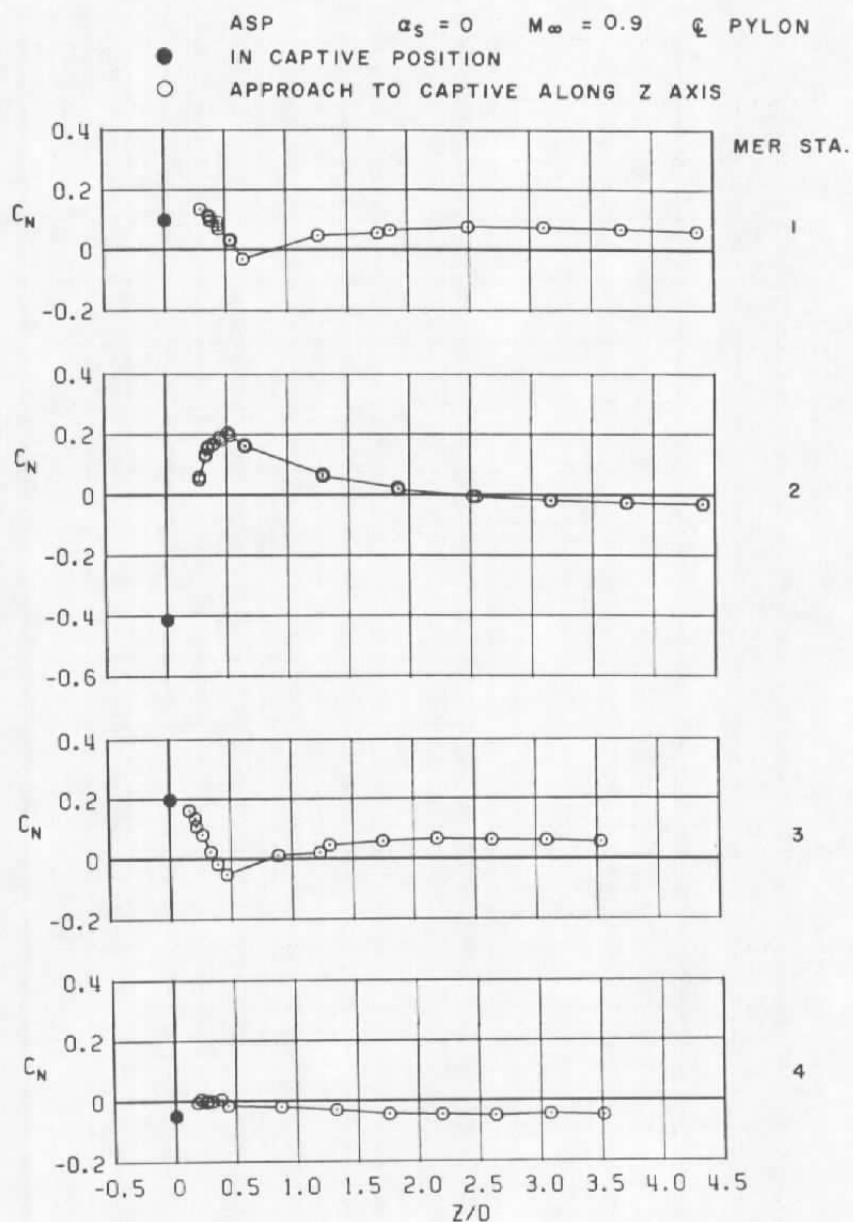
f. Yawing moment  
 Figure 27. Concluded.



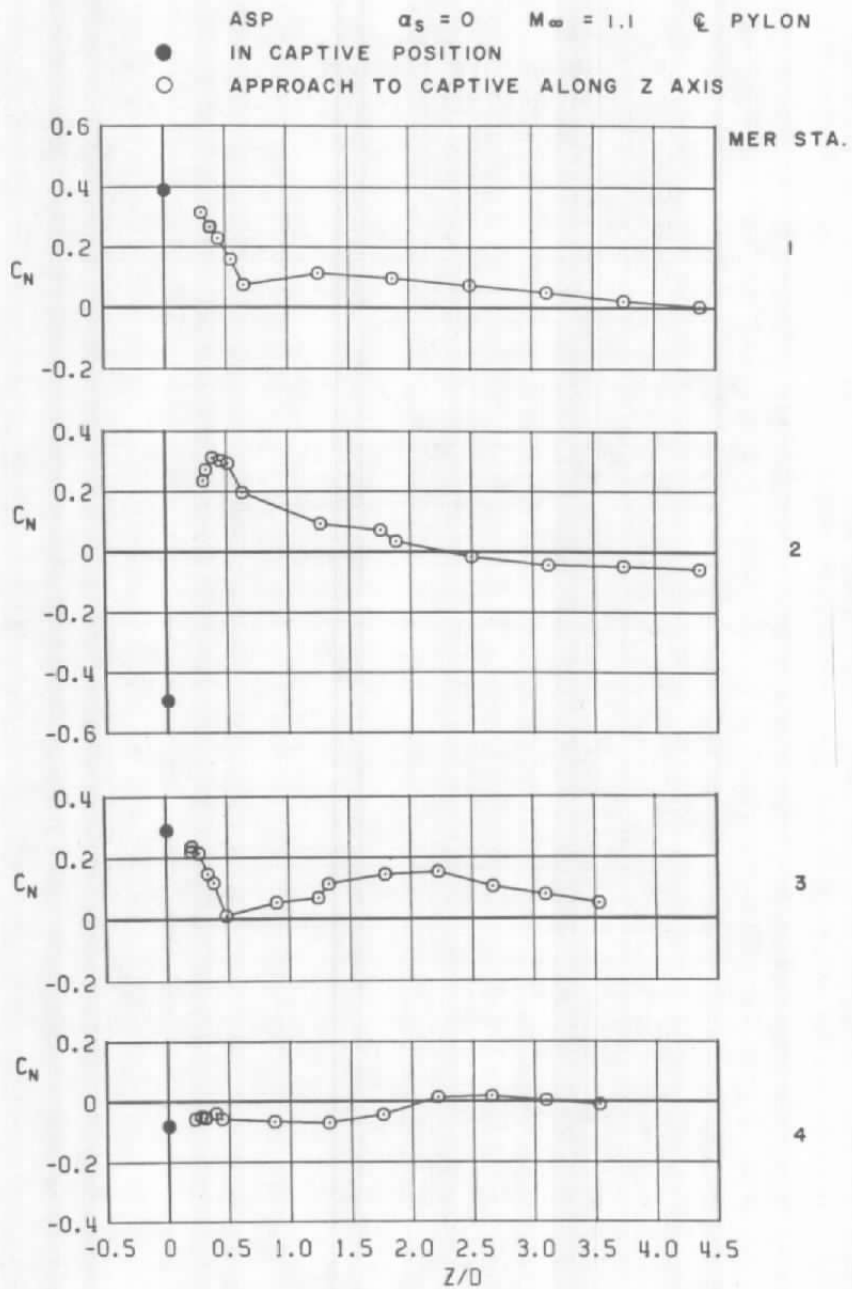
a.  $M_\infty = 0.6$

Figure 28. Coefficient of normal force acting on the ASP store as a function of normal distance between the store and four captive positions on the MER mounted on the C-L pylon.

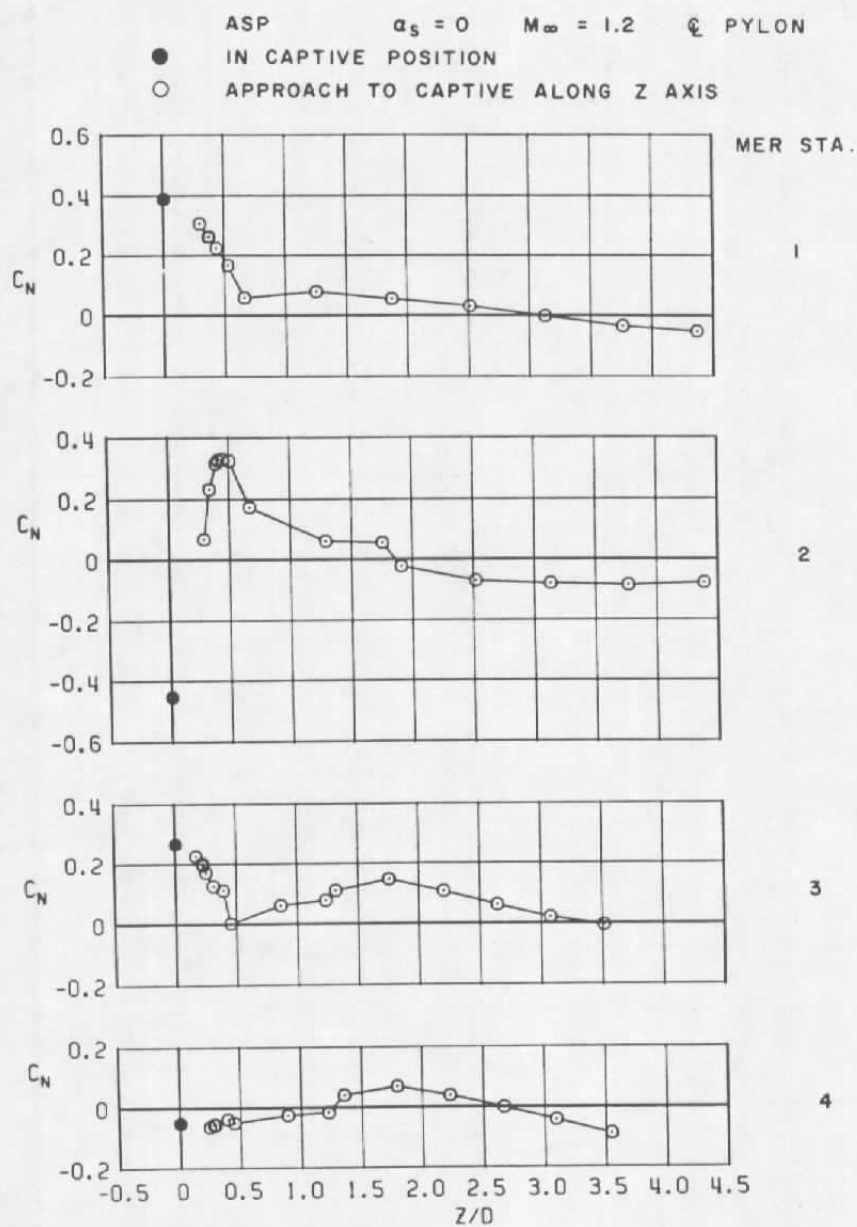




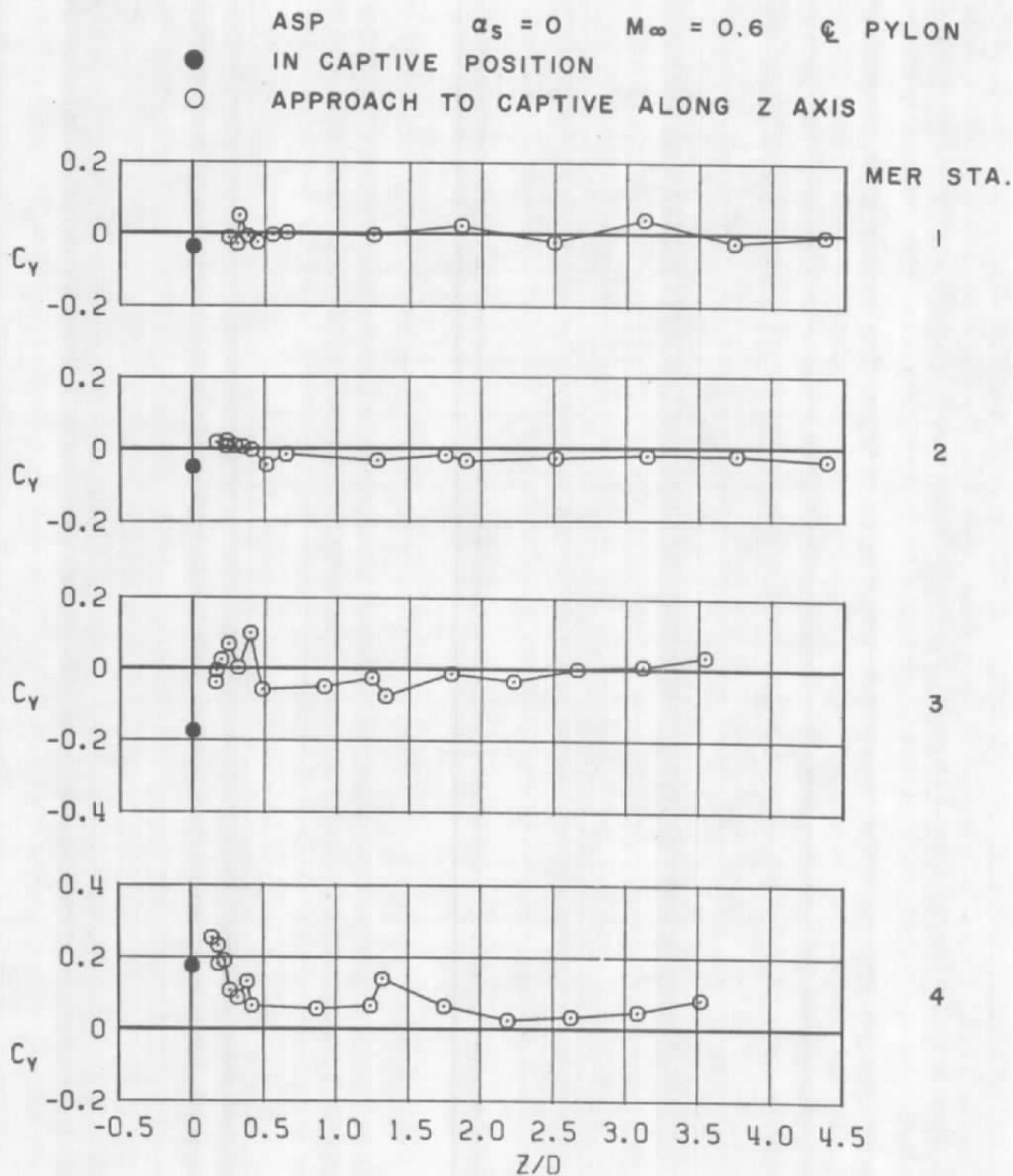
b.  $M_\infty = 0.9$   
Figure 28. Continued.



c.  $M_\infty = 1.1$   
Figure 28. Continued.

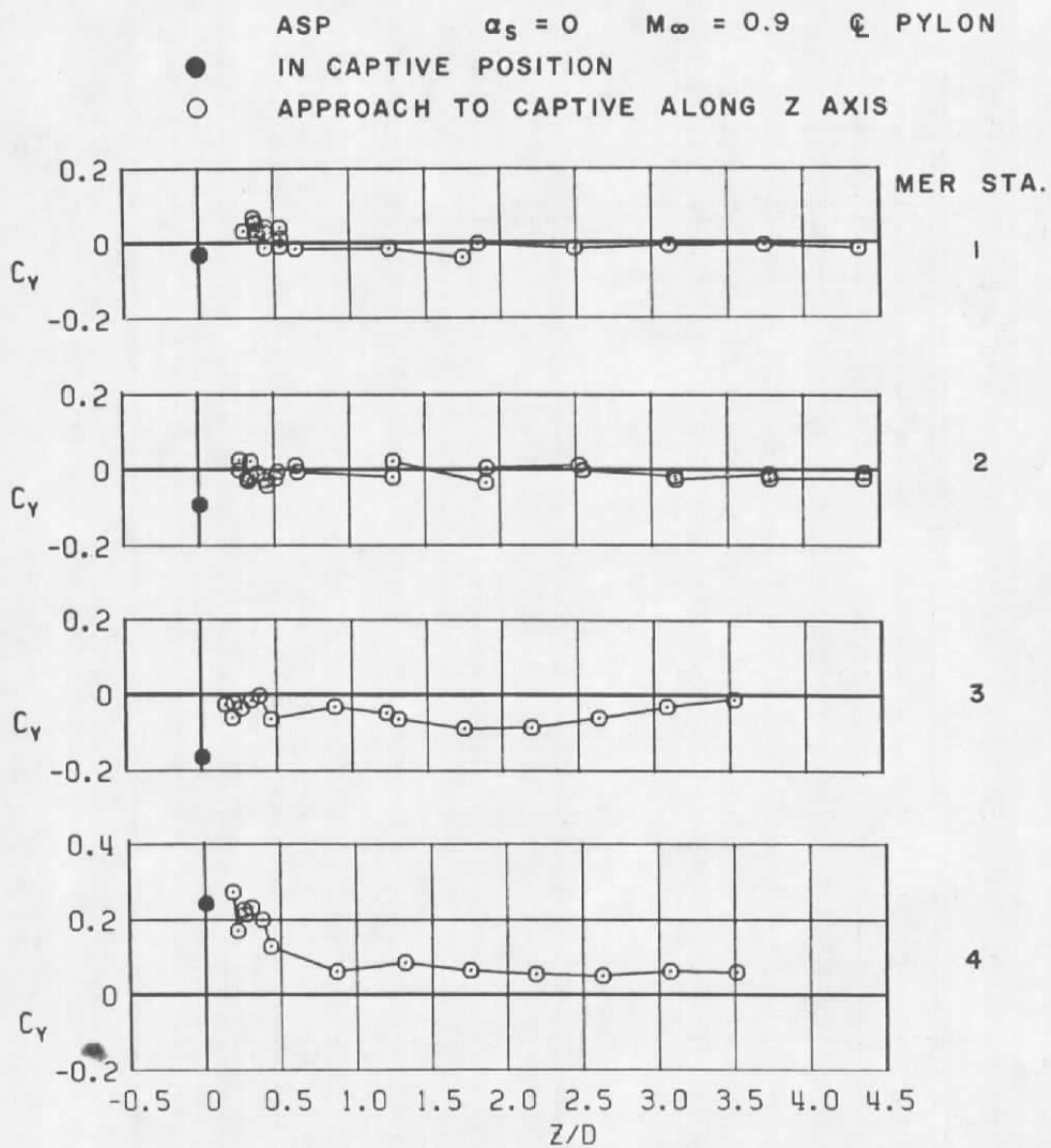


d.  $M_\infty = 1.2$   
Figure 28. Concluded.



a.  $M_\infty = 0.6$

Figure 29. Coefficient of side force acting on the ASP store as a function of normal distance between the store and four captive positions on the MER mounted on the C-L pylon.

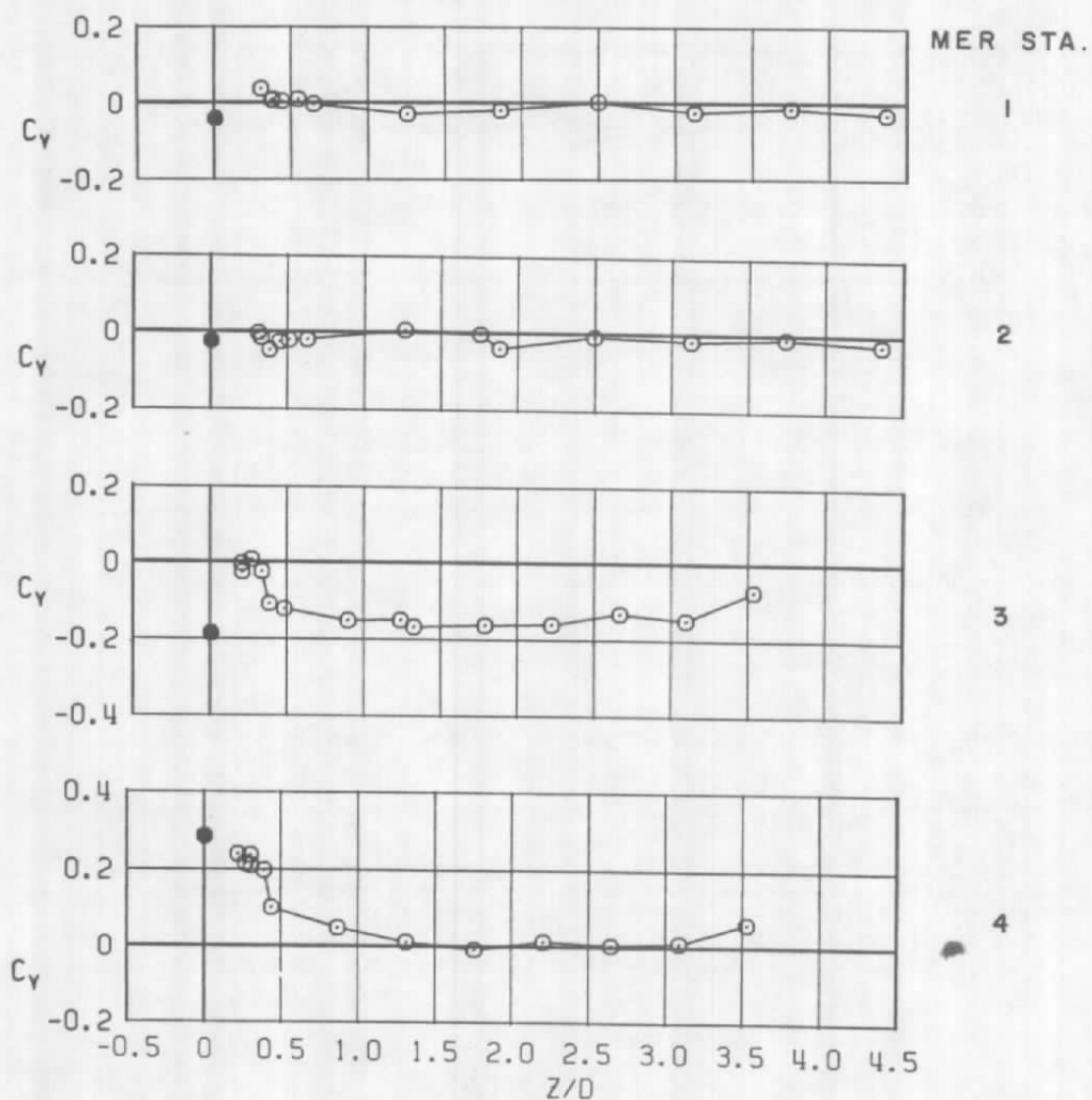


b.  $M_\infty = 0.9$   
Figure 29. Continued.

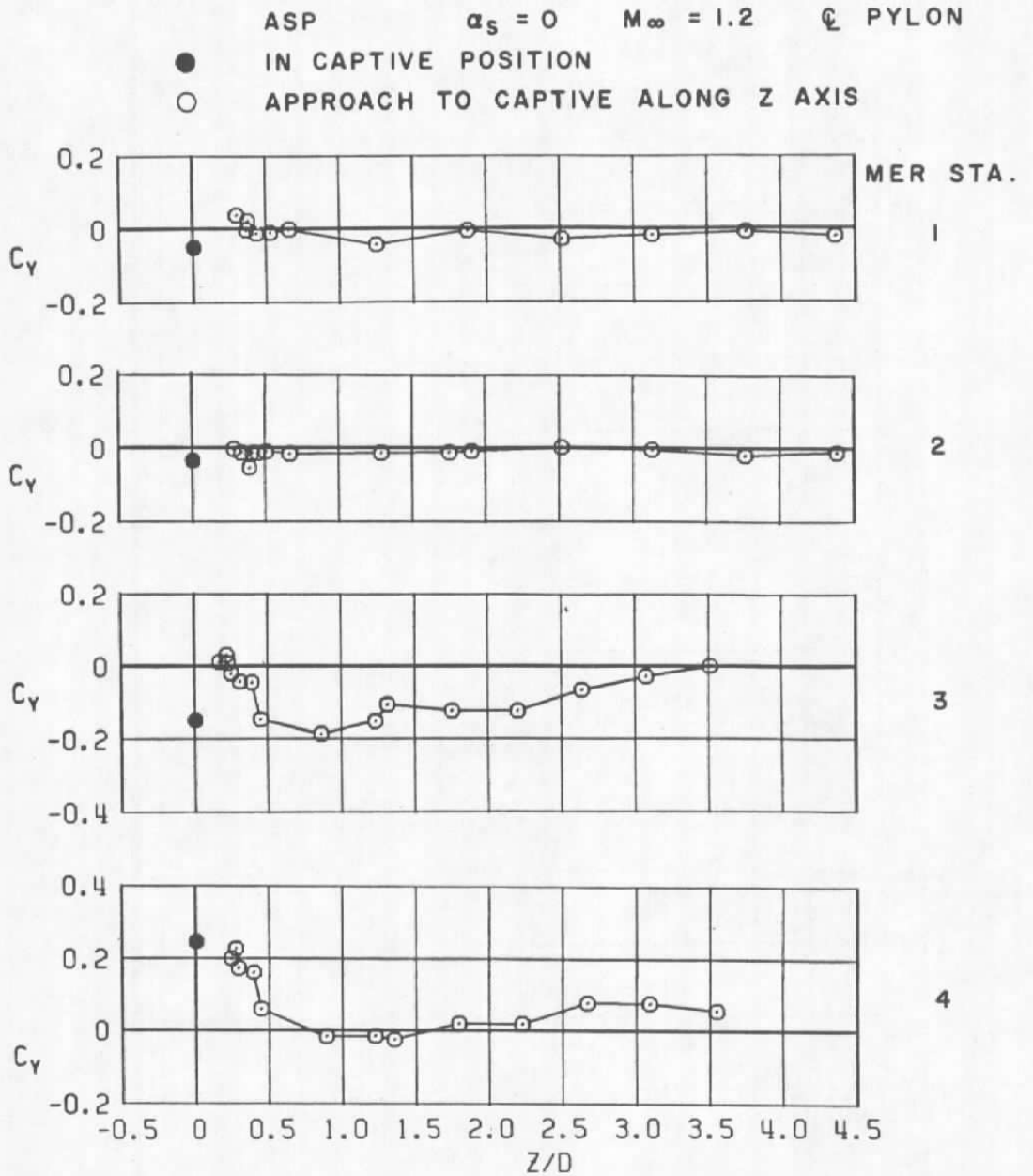
ASP  $\alpha_s = 0$   $M_\infty = 1.1$   $\zeta$  PYLON

● IN CAPTIVE POSITION

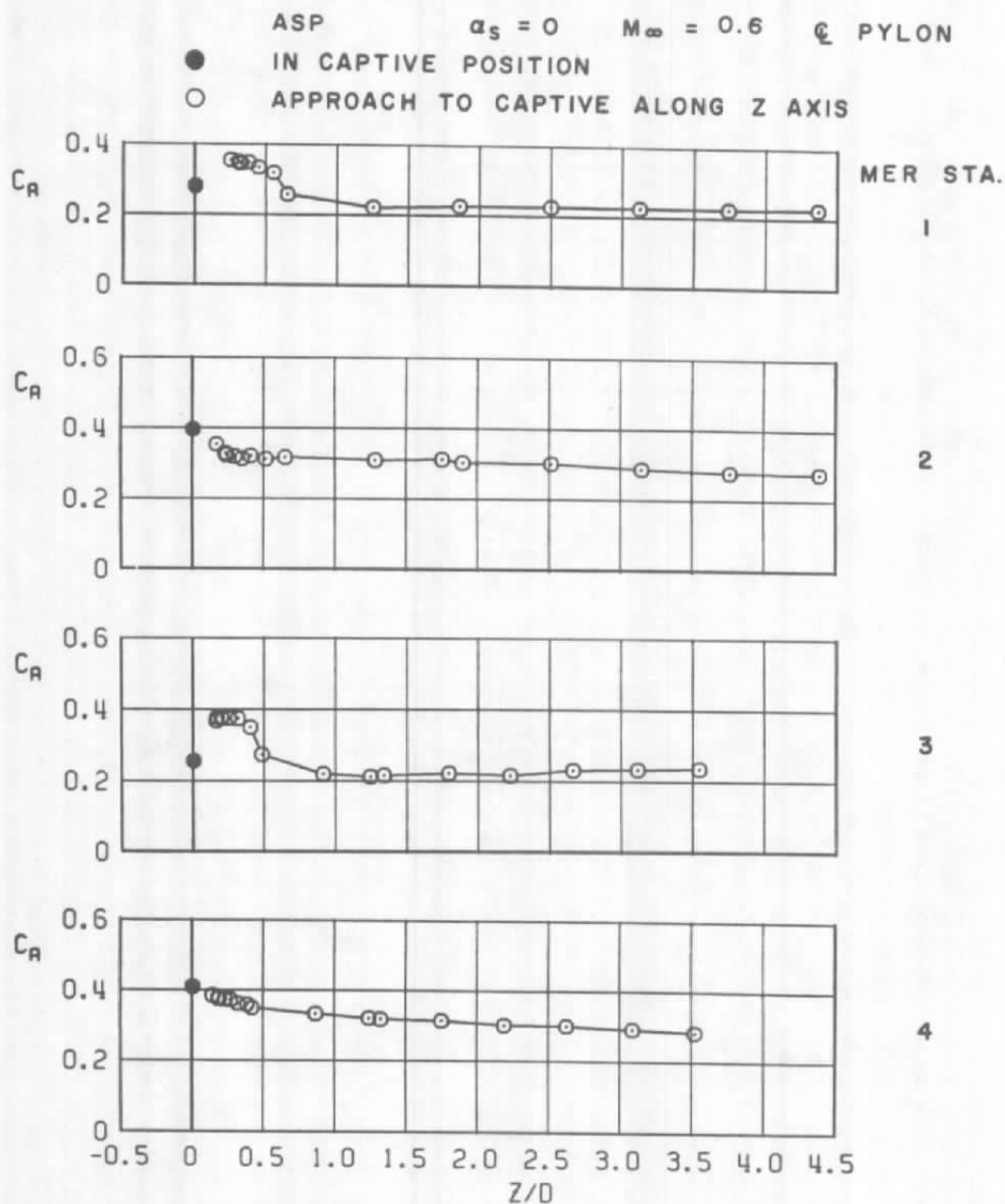
○ APPROACH TO CAPTIVE ALONG Z AXIS



c.  $M_\infty = 1.1$   
Figure 29. Continued.



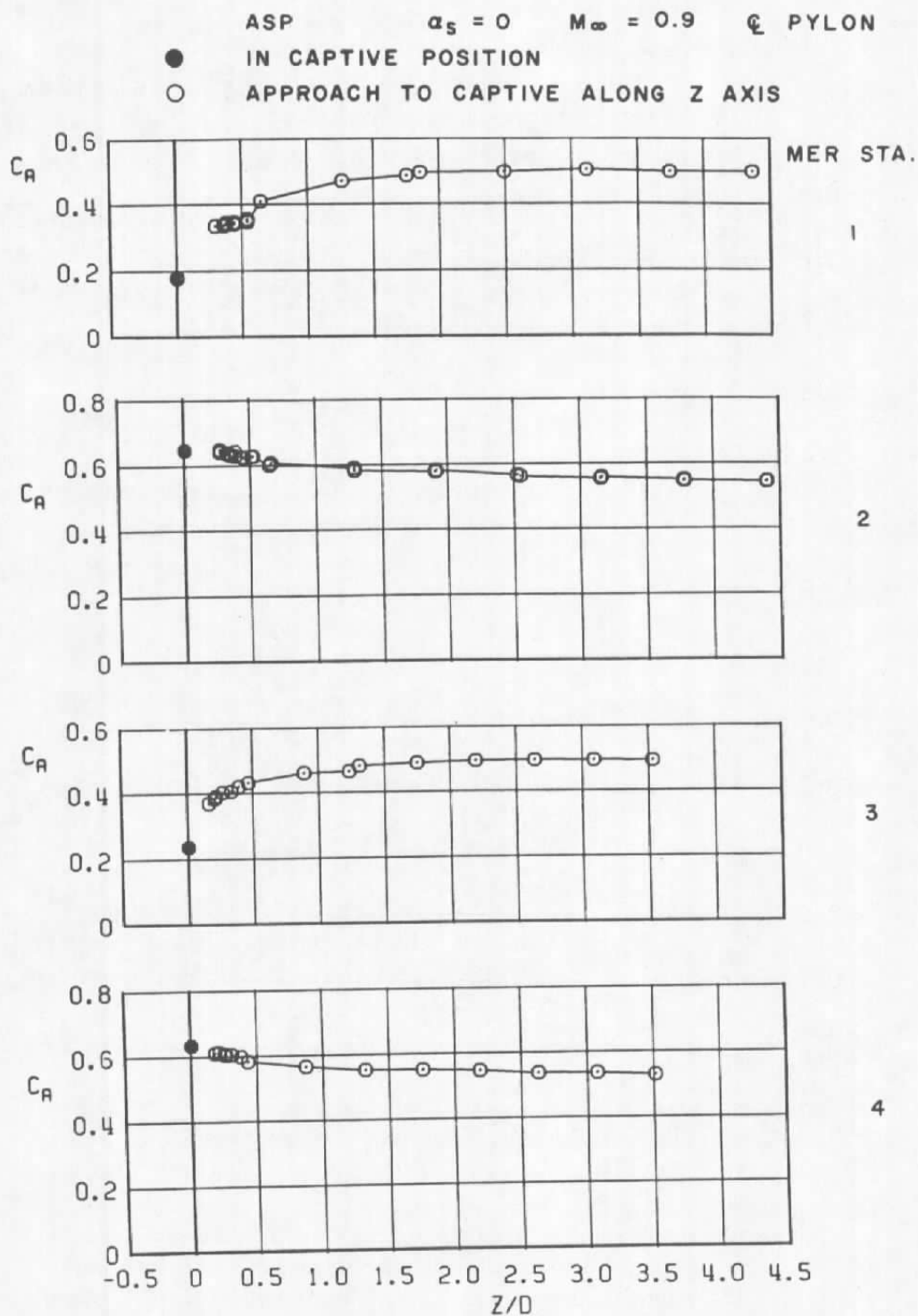
d.  $M_\infty = 1.2$   
Figure 29. Concluded.



a.  $M_\infty = 0.6$

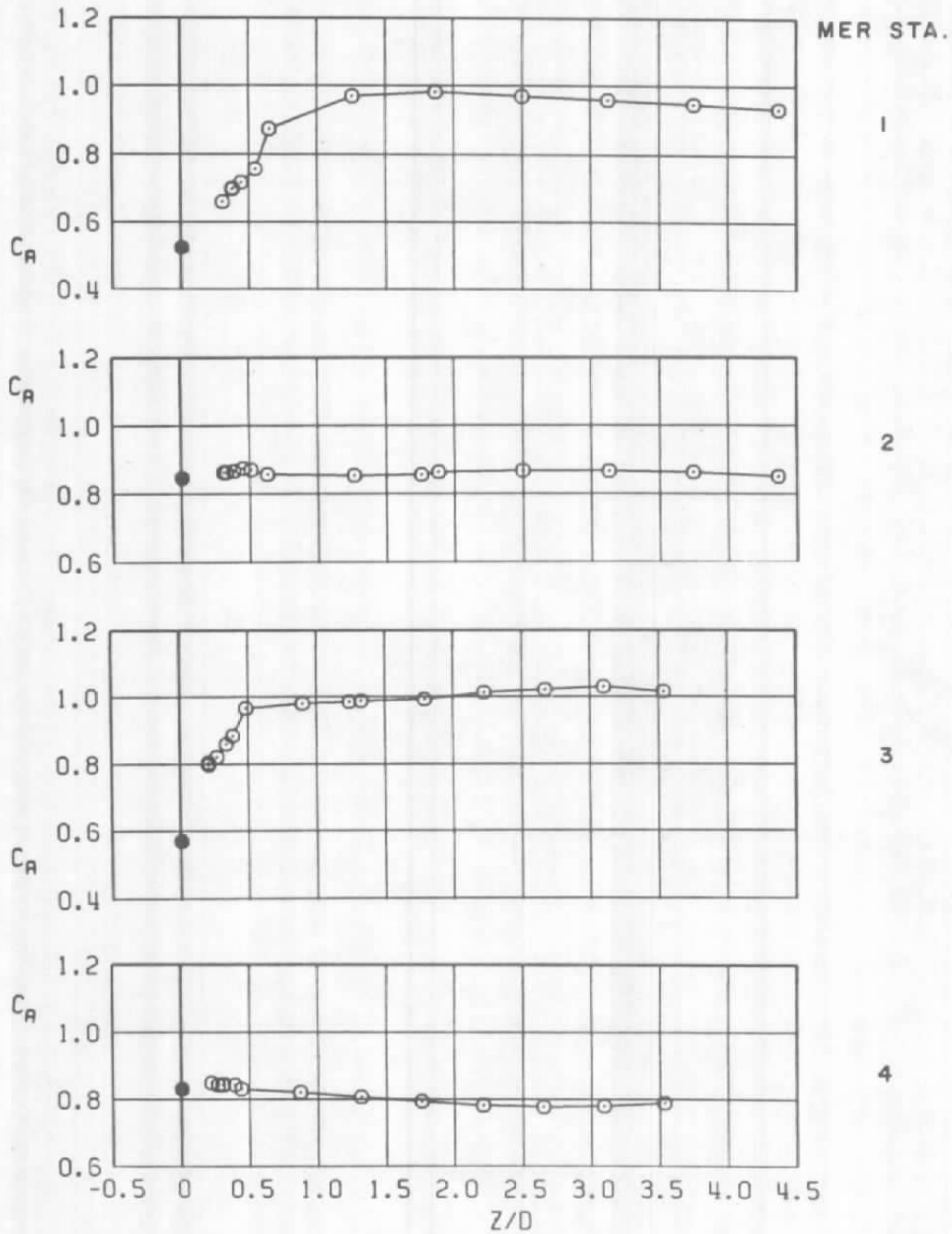
Figure 30. Coefficient of axial force acting on the ASP store as a function of normal distance between the store and four captive positions on the MER mounted on the C-L pylon.



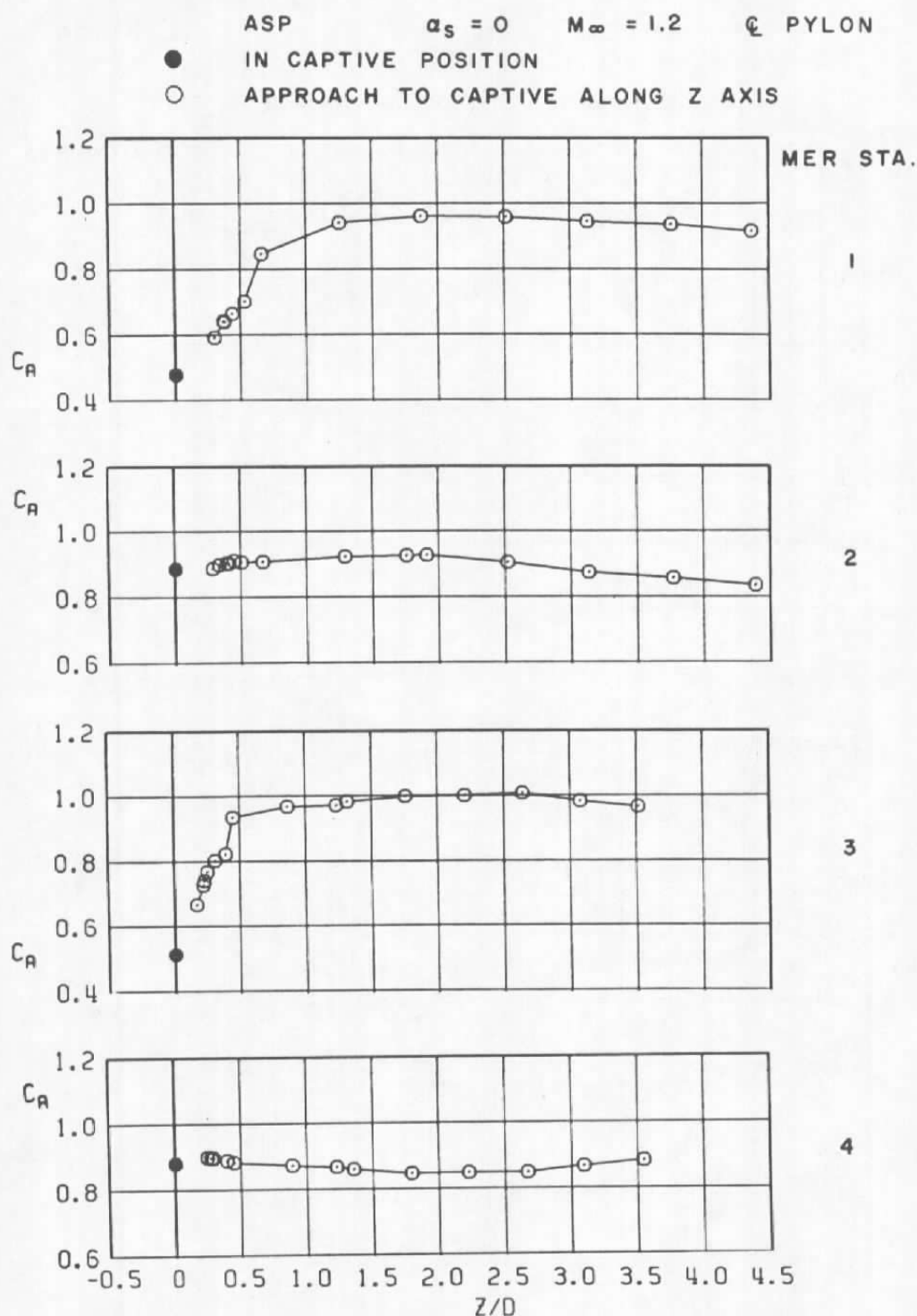


b.  $M_\infty = 0.9$   
Figure 30. Continued.

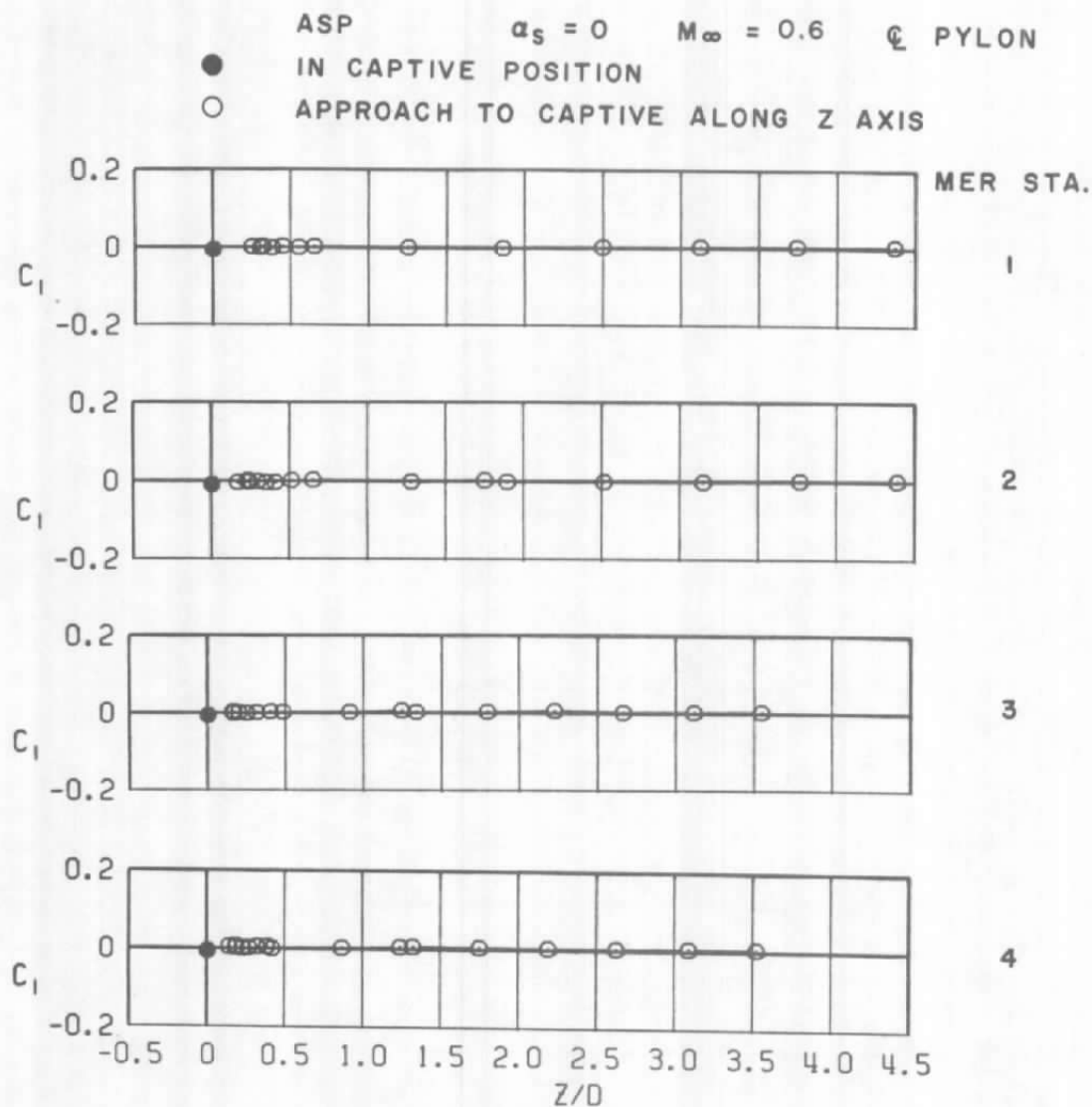
ASP       $\alpha_s = 0$        $M_\infty = 1.1$       @ PYLON  
 ● IN CAPTIVE POSITION  
 ○ APPROACH TO CAPTIVE ALONG Z AXIS



c.  $M_\infty = 1.1$   
 Figure 30. Continued.

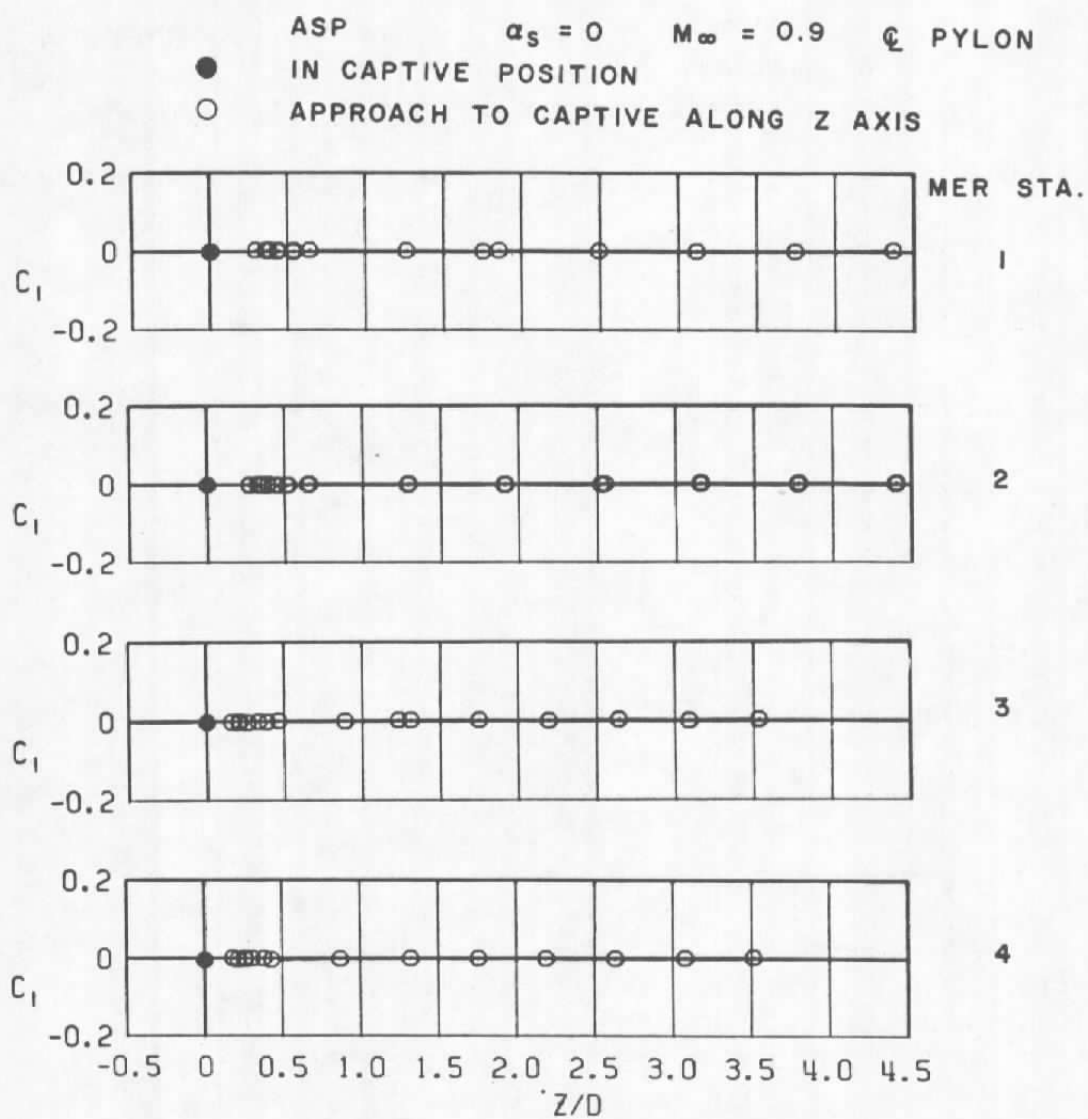


d.  $M_\infty = 1.2$   
Figure 30. Concluded.

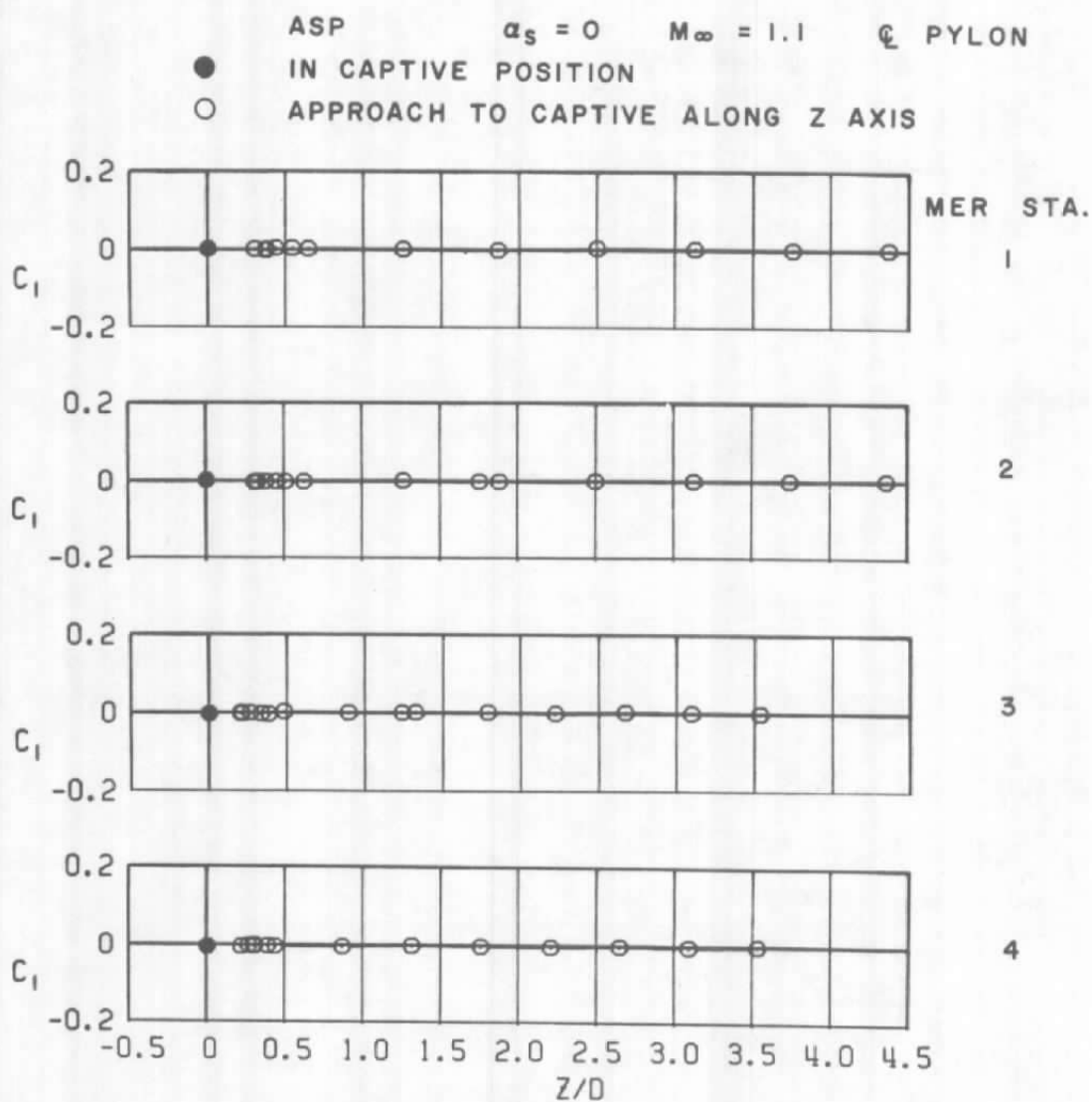


a.  $M_\infty = 0.6$

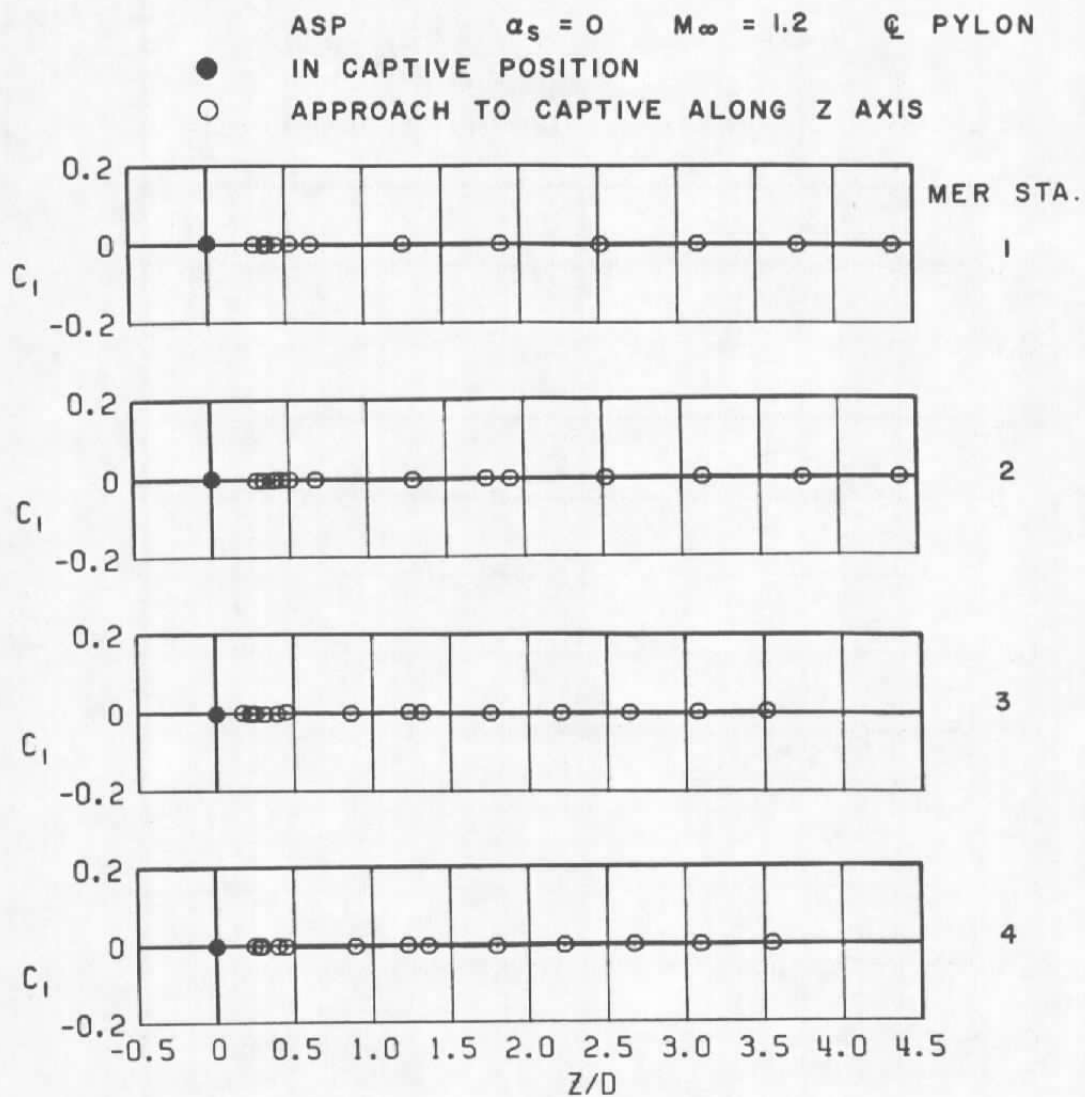
Figure 31. Coefficient of rolling moment acting on the ASP store as a function of normal distance between the store and four captive positions on the MER mounted on the C-L pylon.



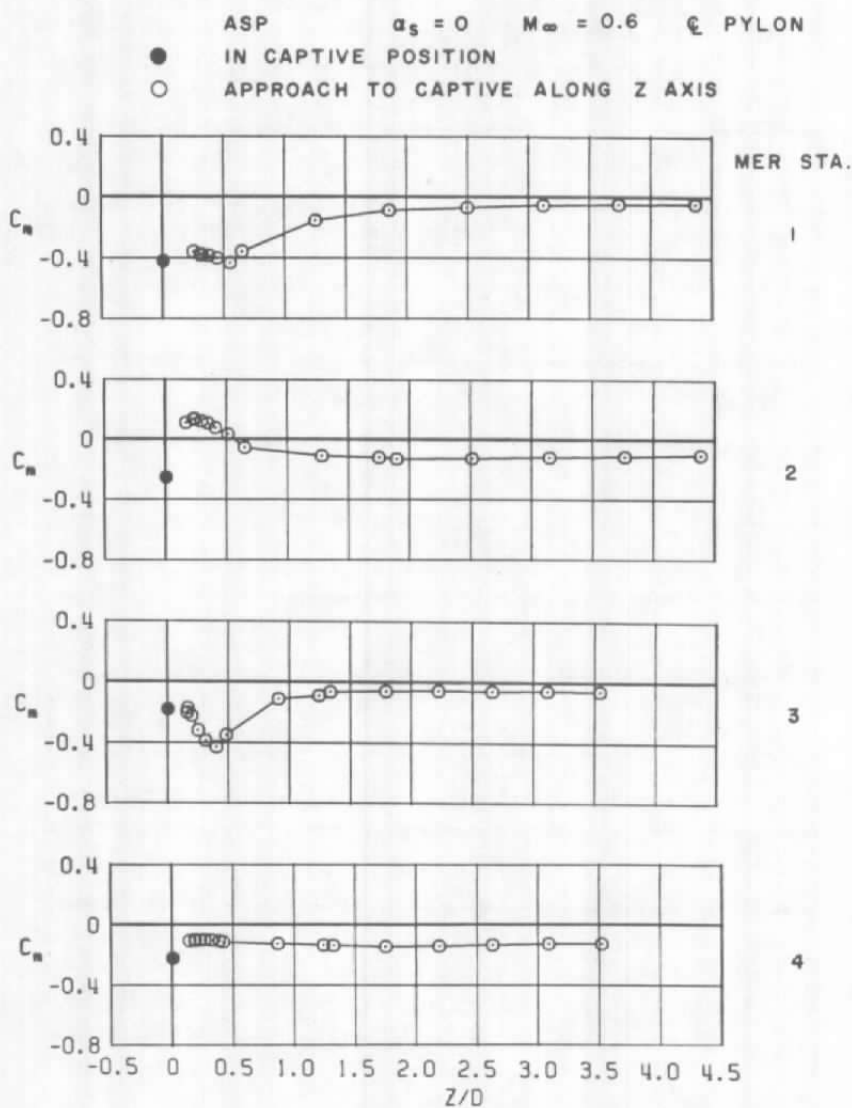
b.  $M_\infty = 0.9$   
Figure 31. Continued.



c.  $M_\infty = 1.1$   
Figure 31. Continued.



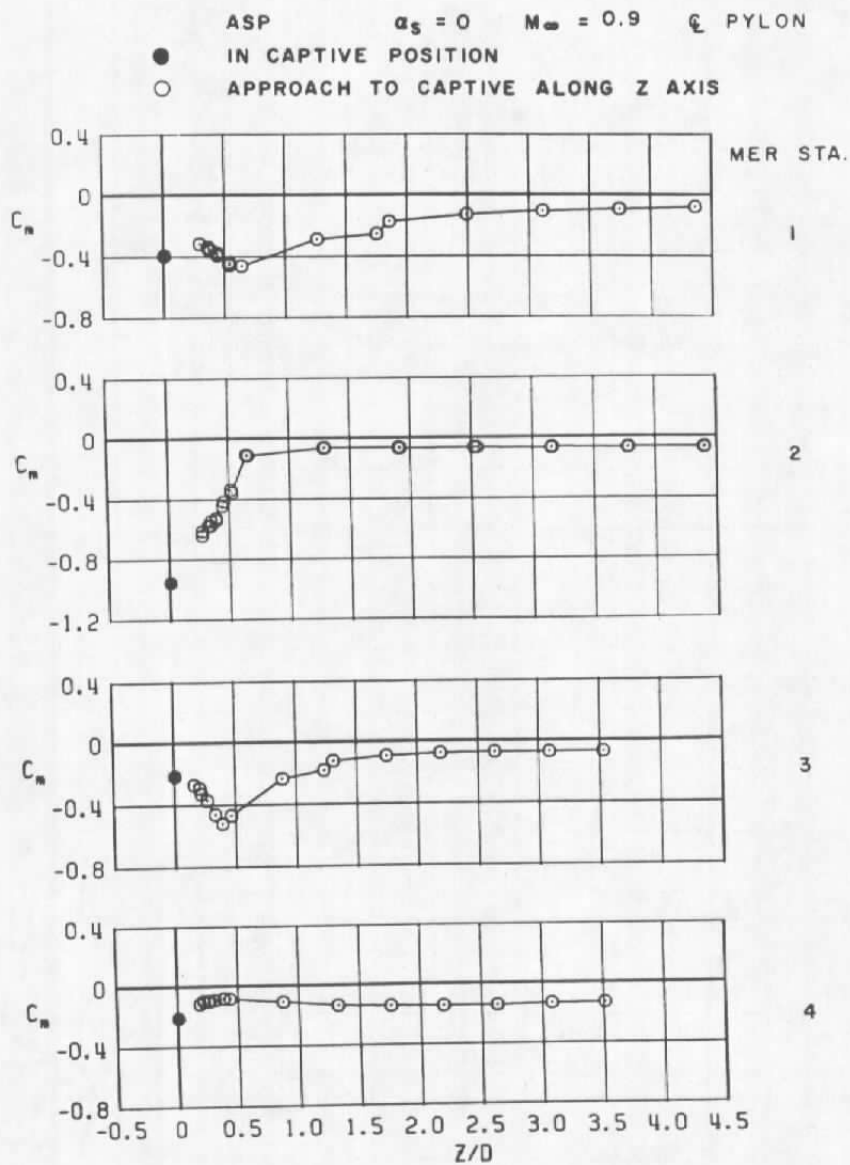
d.  $M_\infty = 1.2$   
Figure 31. Concluded.



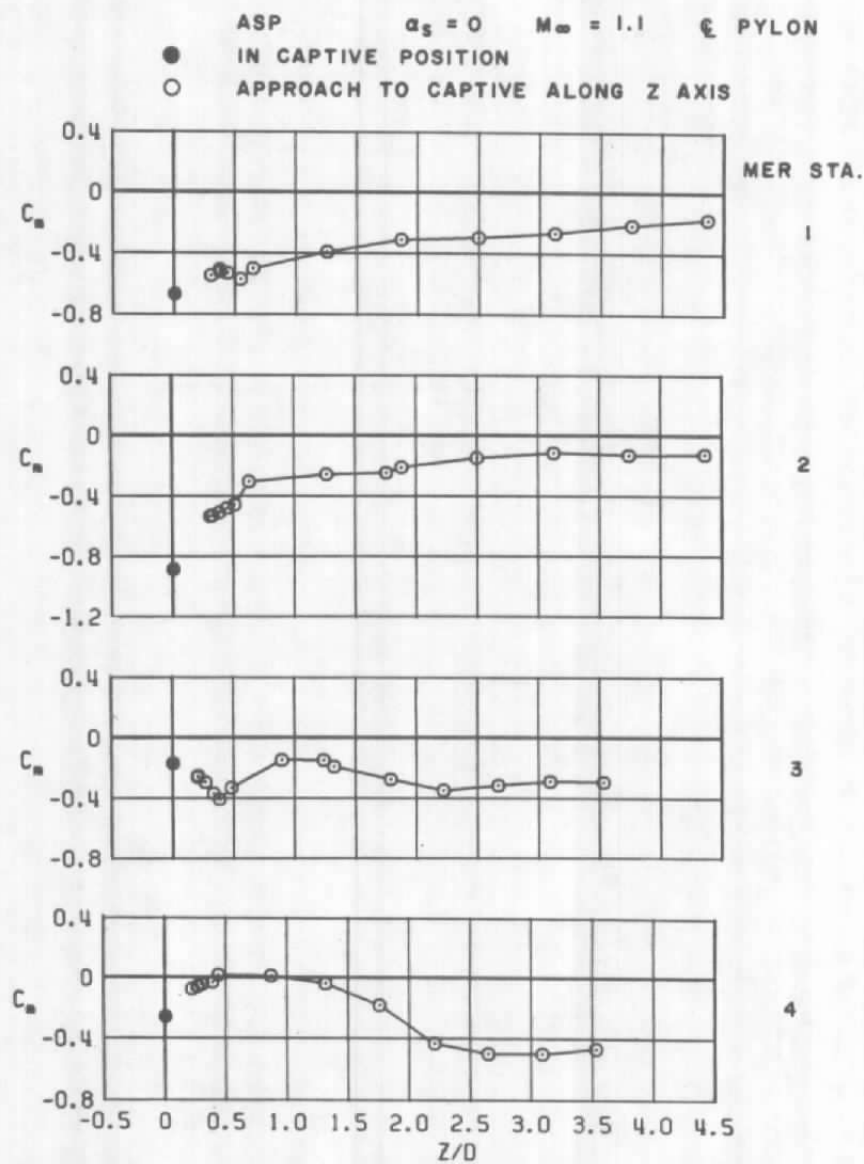
a.  $M_\infty = 0.6$

Figure 32. Coefficient of pitching moment acting on the ASP store as a function of normal distance between the store and four captive positions on the MER mounted on the C-L pylon.

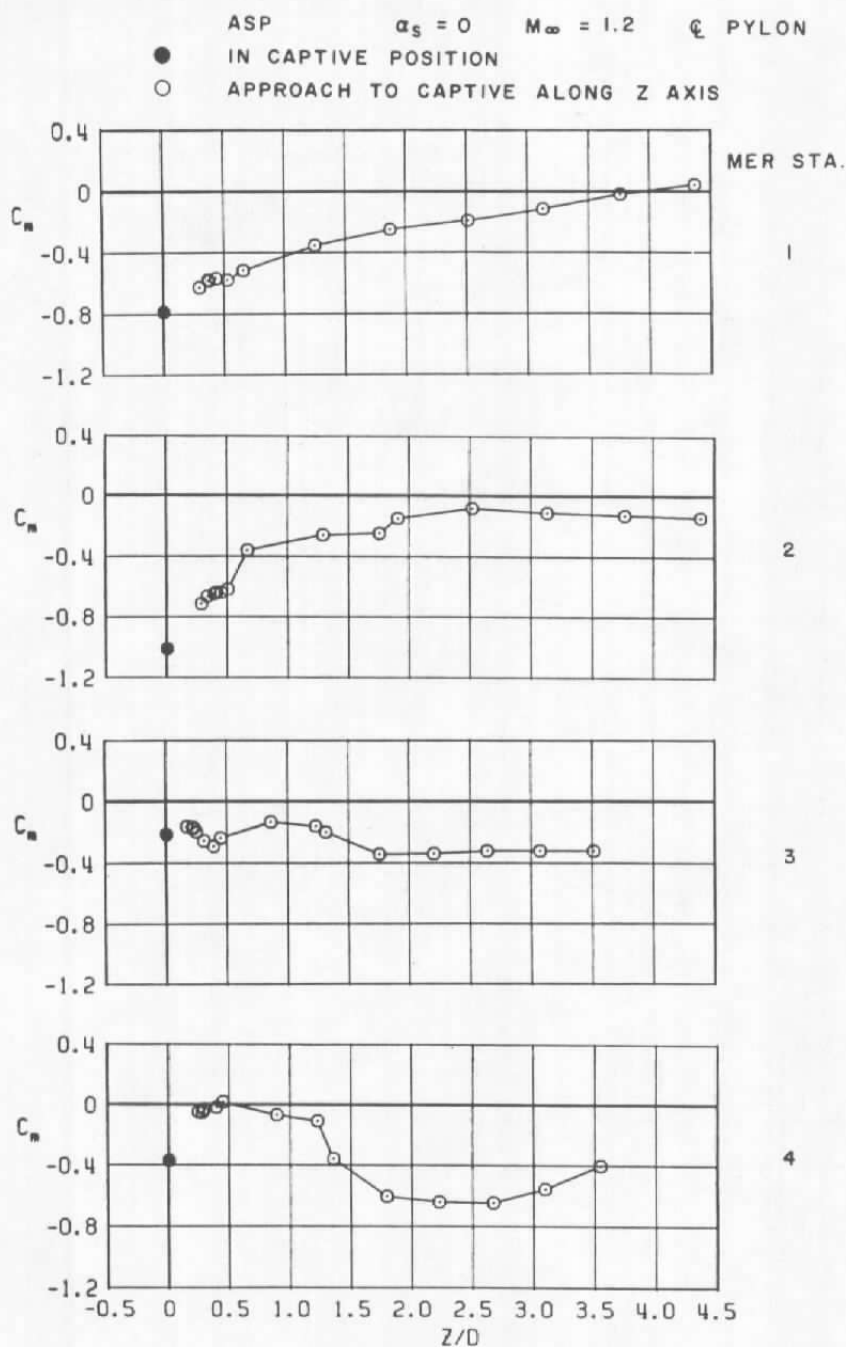




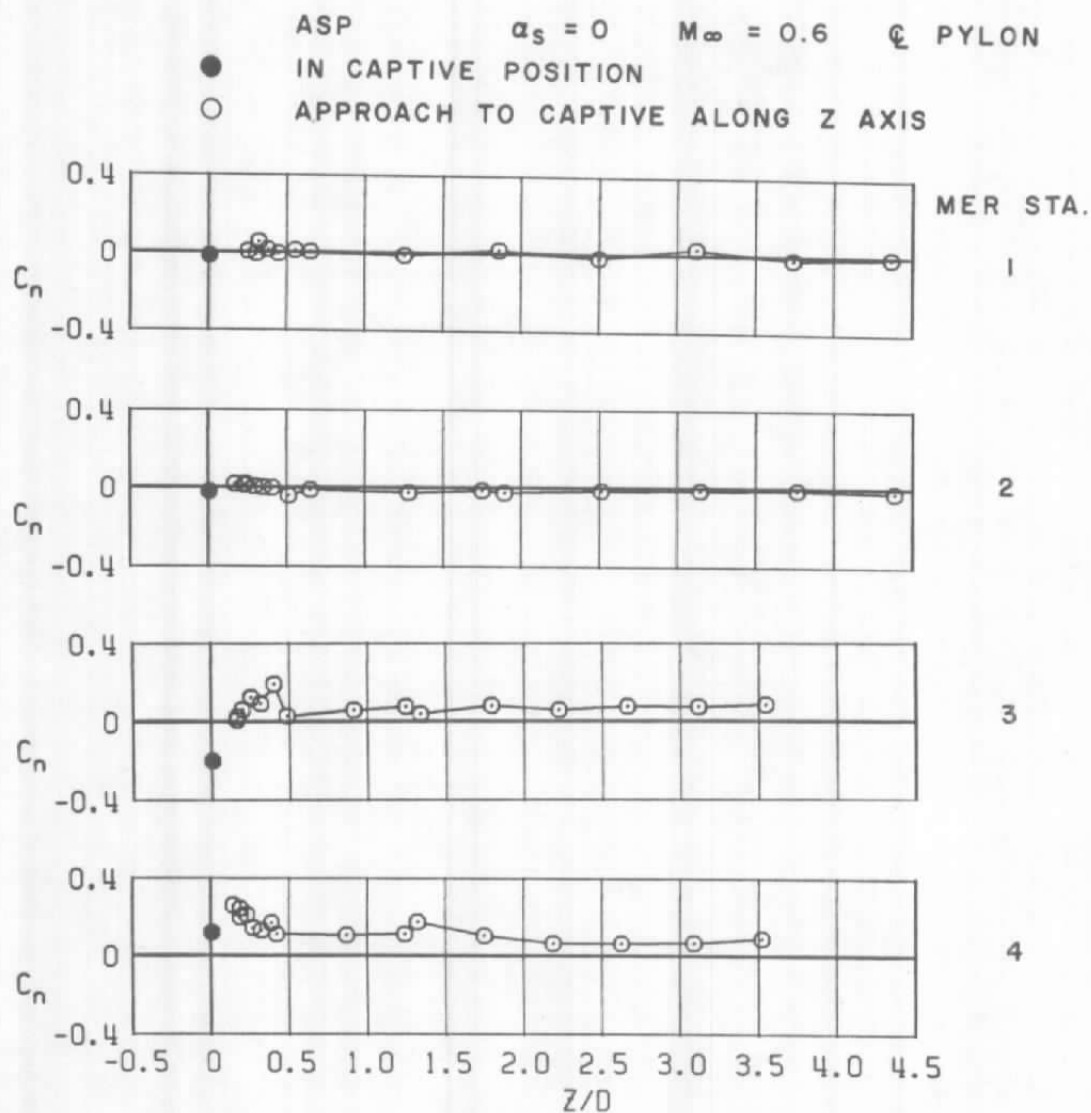
b.  $M_\infty = 0.9$   
Figure 32. Continued.



c.  $M_\infty = 1.1$   
Figure 32. Continued.

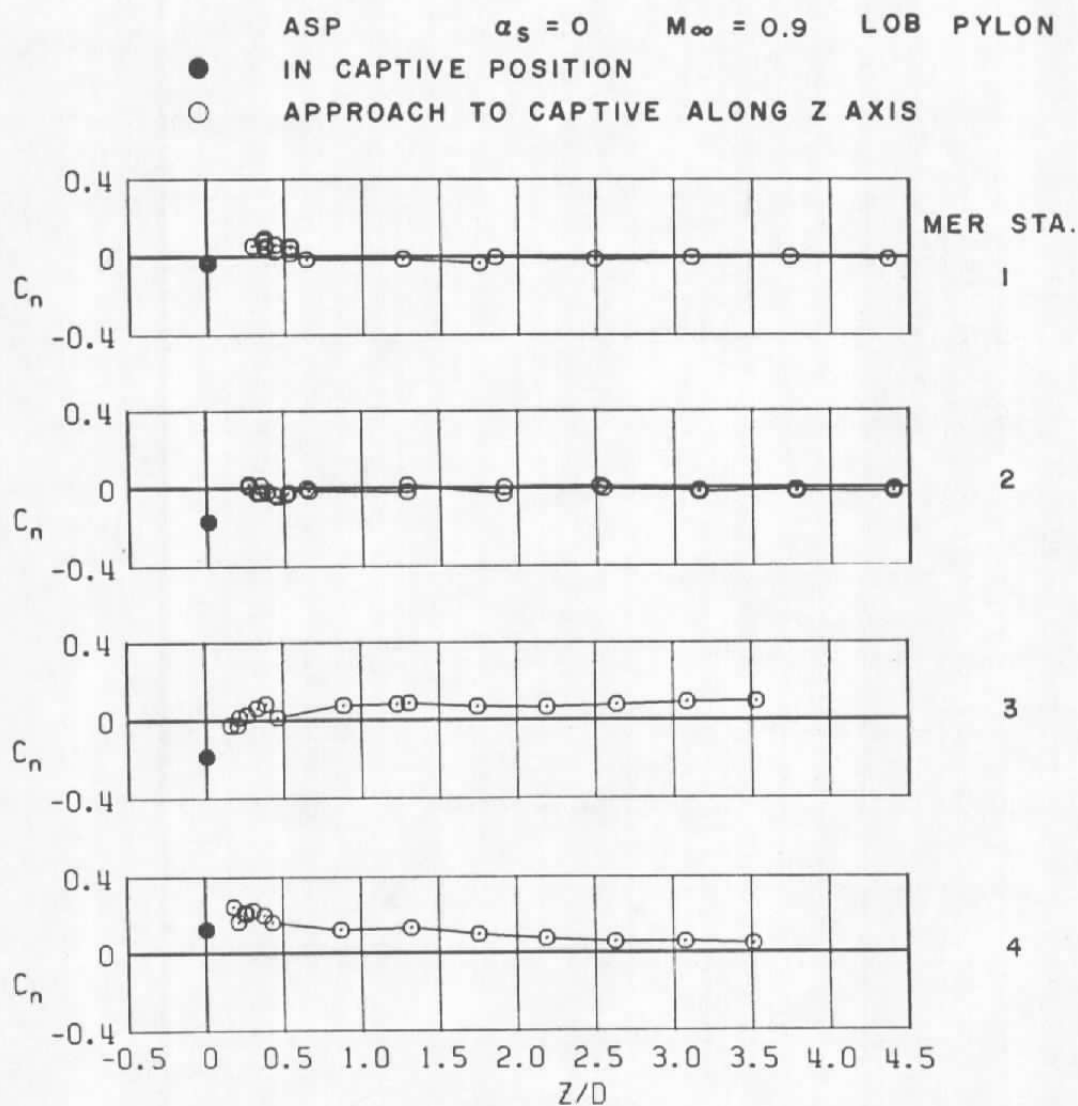


d.  $M_\infty = 1.2$   
Figure 32. Concluded.

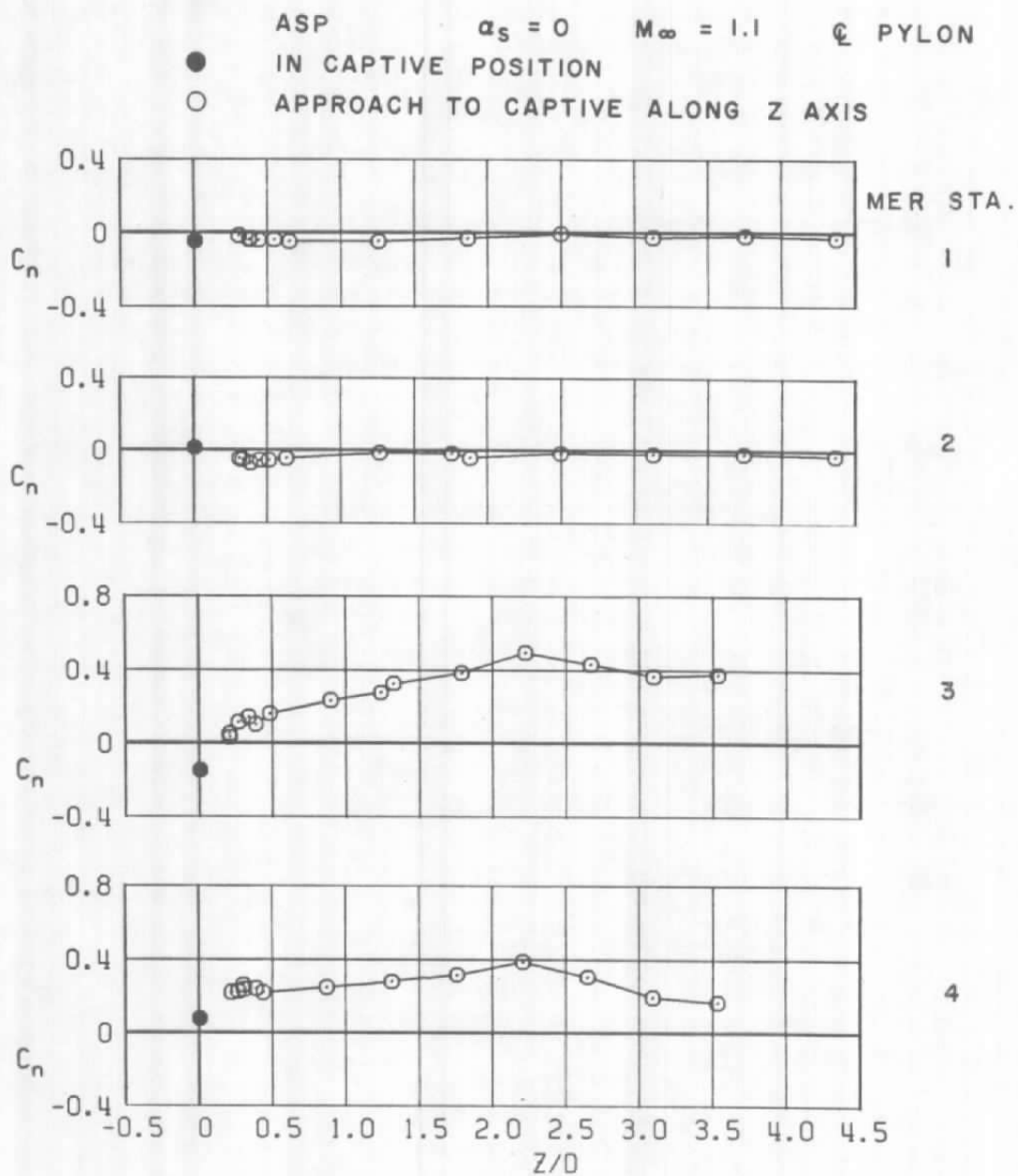


a.  $M_\infty = 0.6$

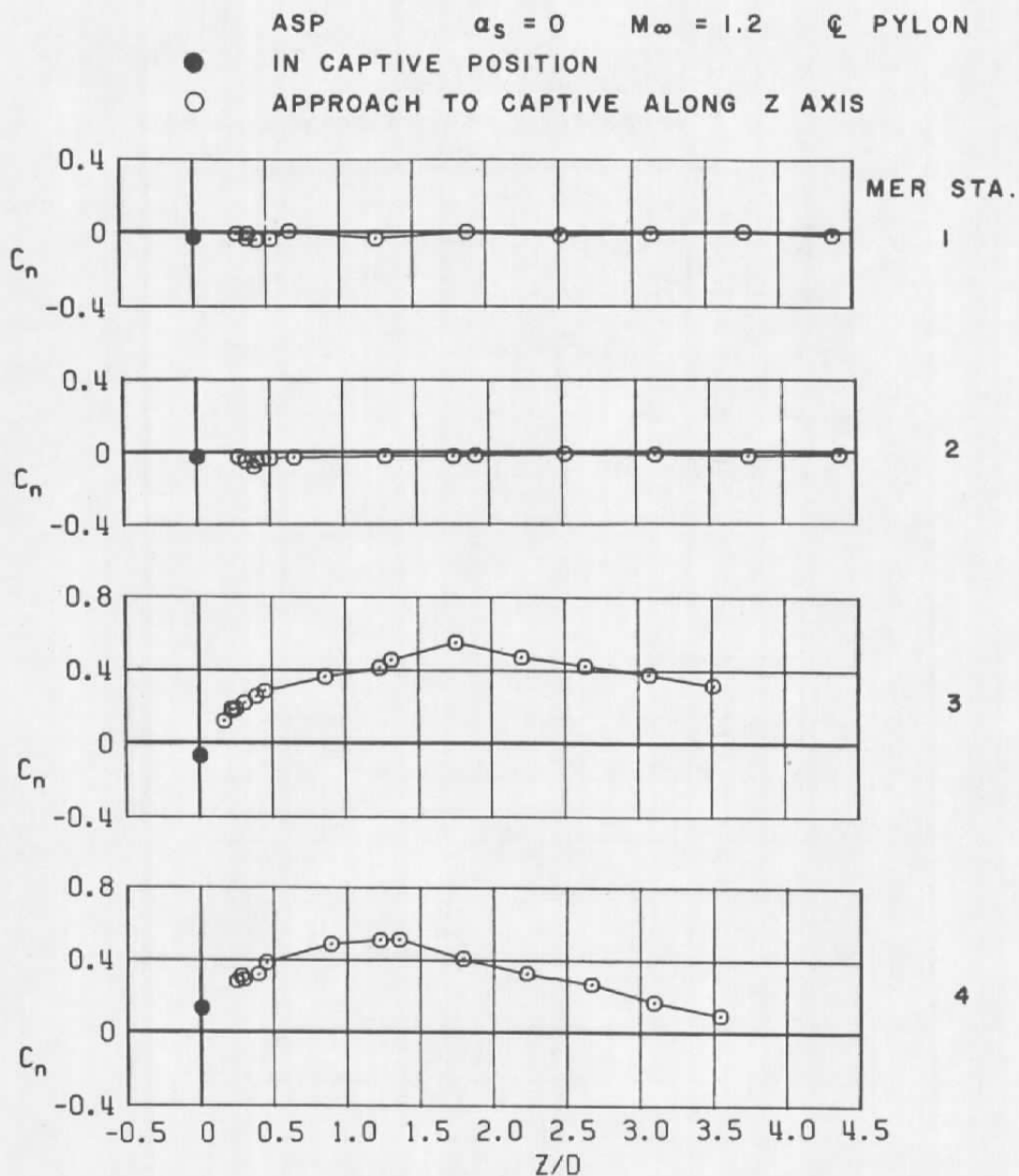
Figure 33. Coefficient of yawing moment acting on the ASP store as a function of normal distance between the store and four captive positions on the MER mounted on the C-L pylon.



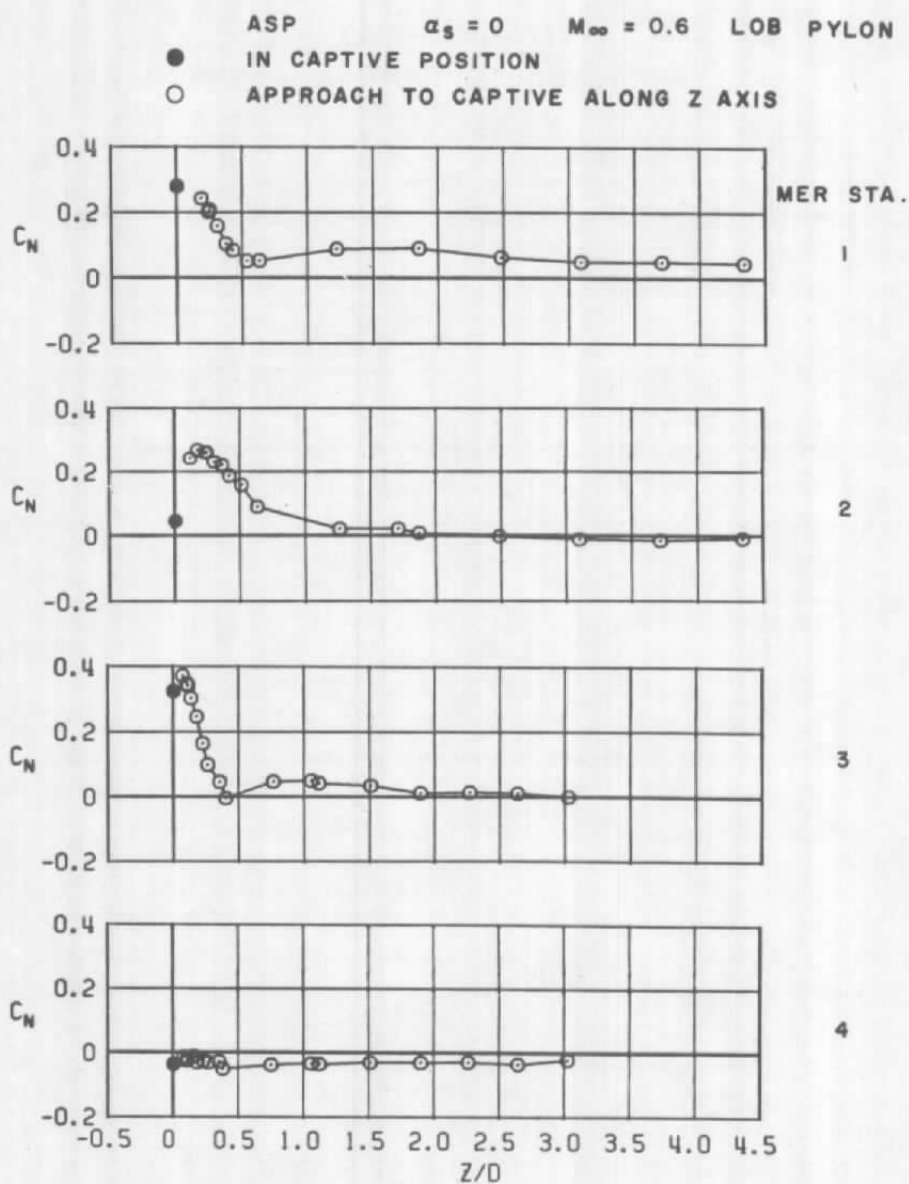
b.  $M_\infty = 0.9$   
Figure 33. Continued.



c.  $M_\infty = 1.1$   
Figure 33. Continued.



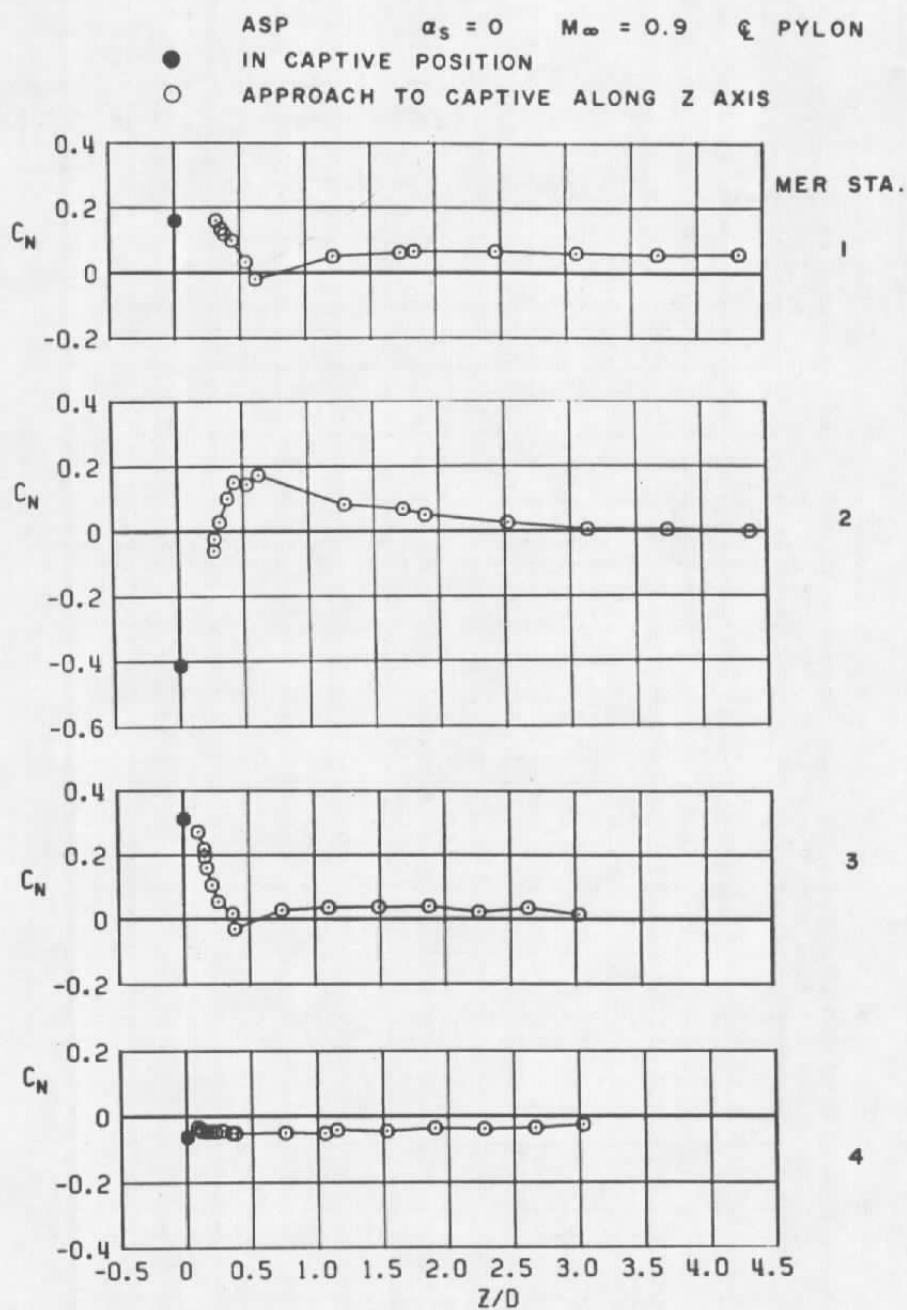
d.  $M_\infty = 1.2$   
Figure 33. Concluded.



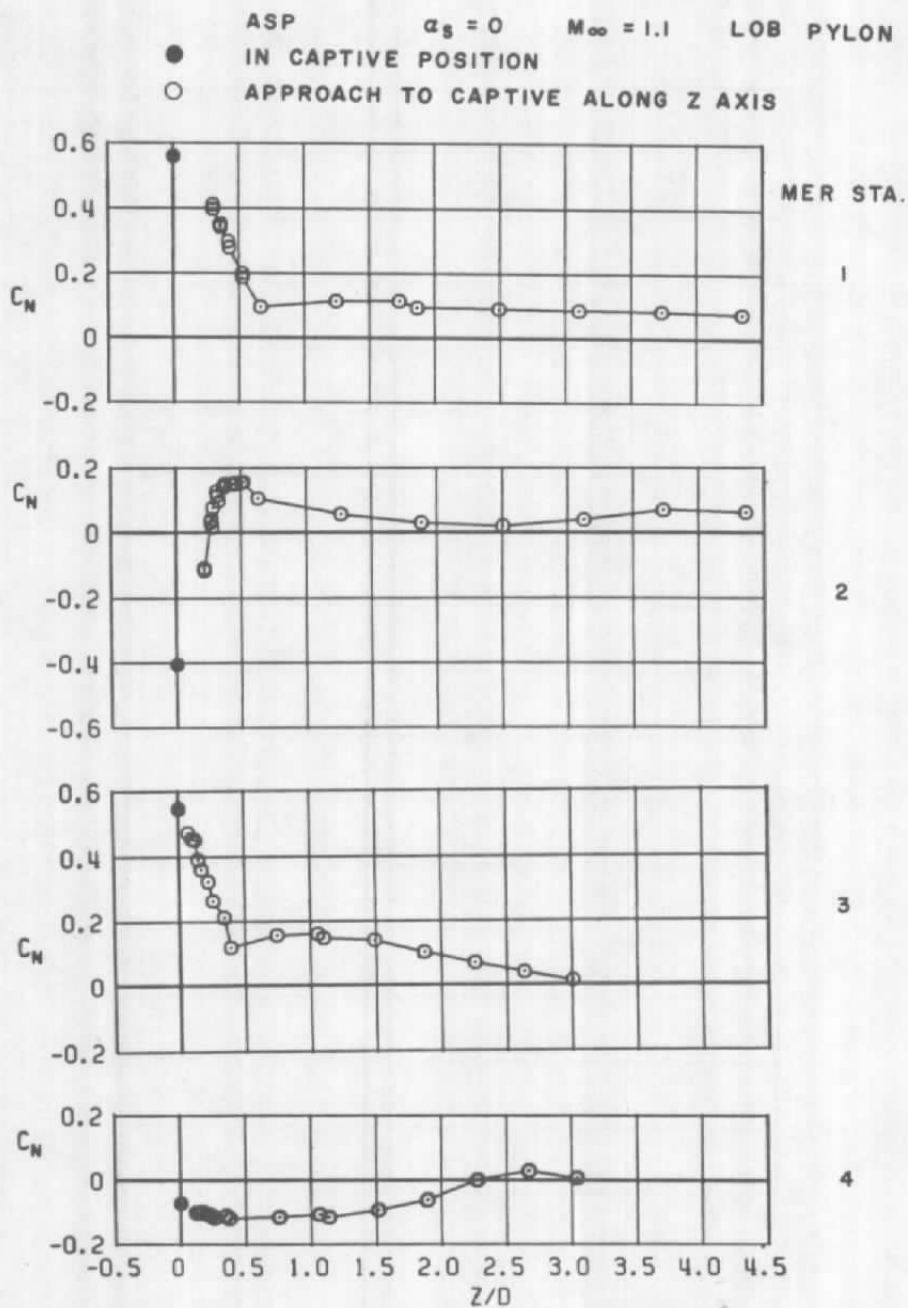
a.  $M_\infty = 0.6$

Figure 34. Coefficient of normal force acting on the ASP store as a function of normal distance between the store and four captive positions on the MER mounted on the LOB pylon.

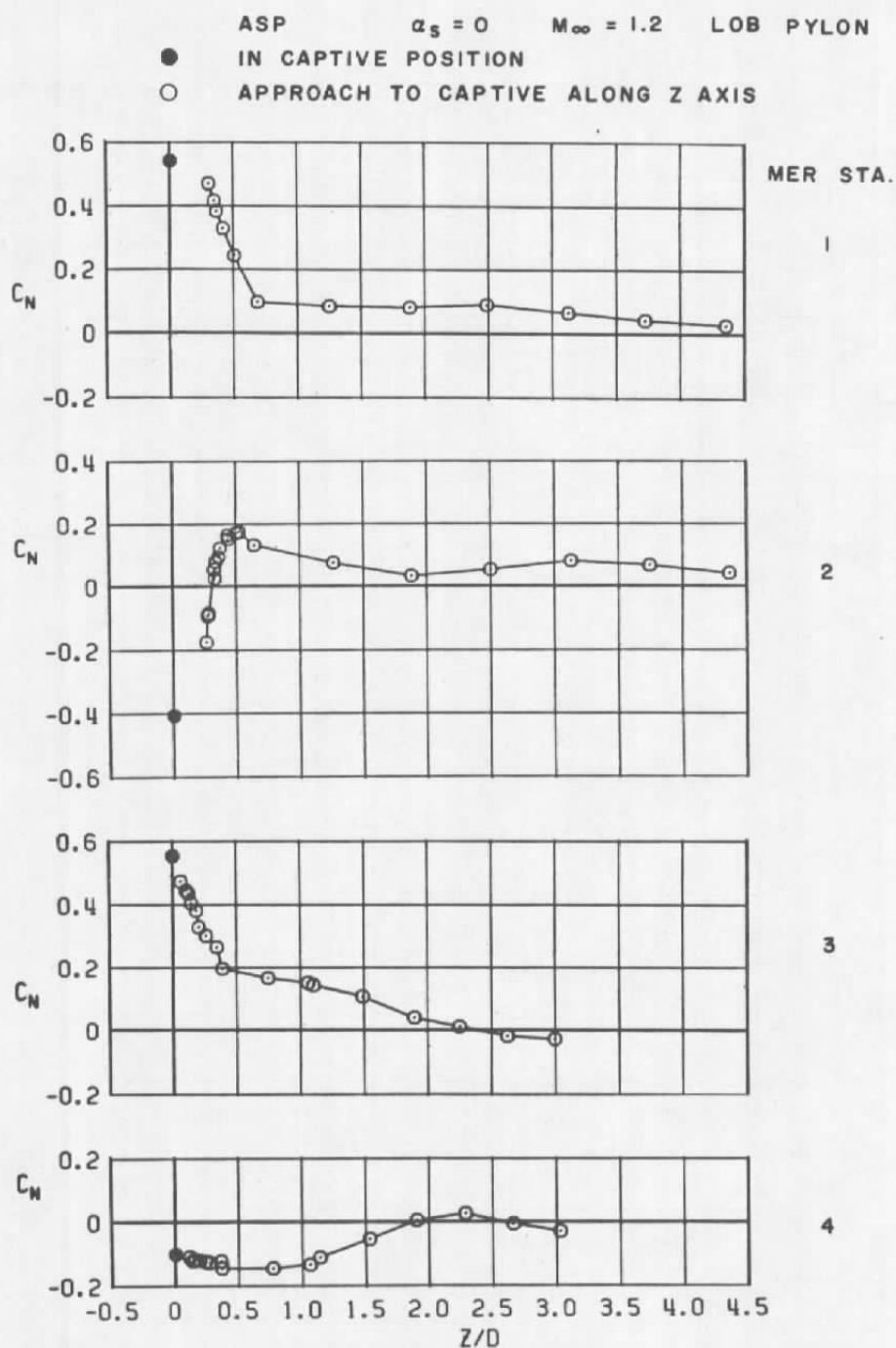




b.  $M_\infty = 0.9$   
Figure 34. Continued.



c.  $M_\infty = 1.1$   
Figure 34. Continued.



d.  $M_\infty = 1.2$   
Figure 34. Concluded.

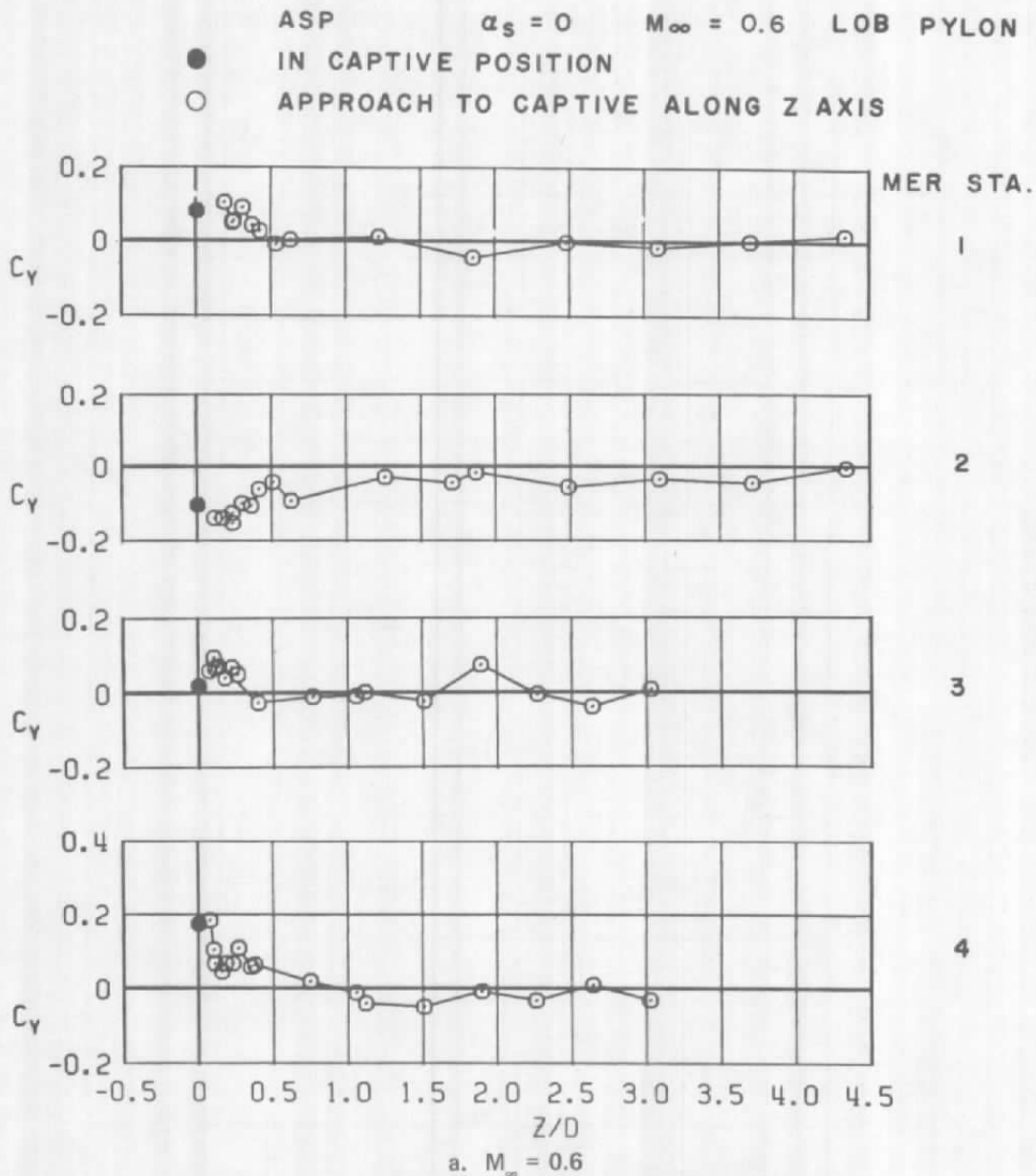
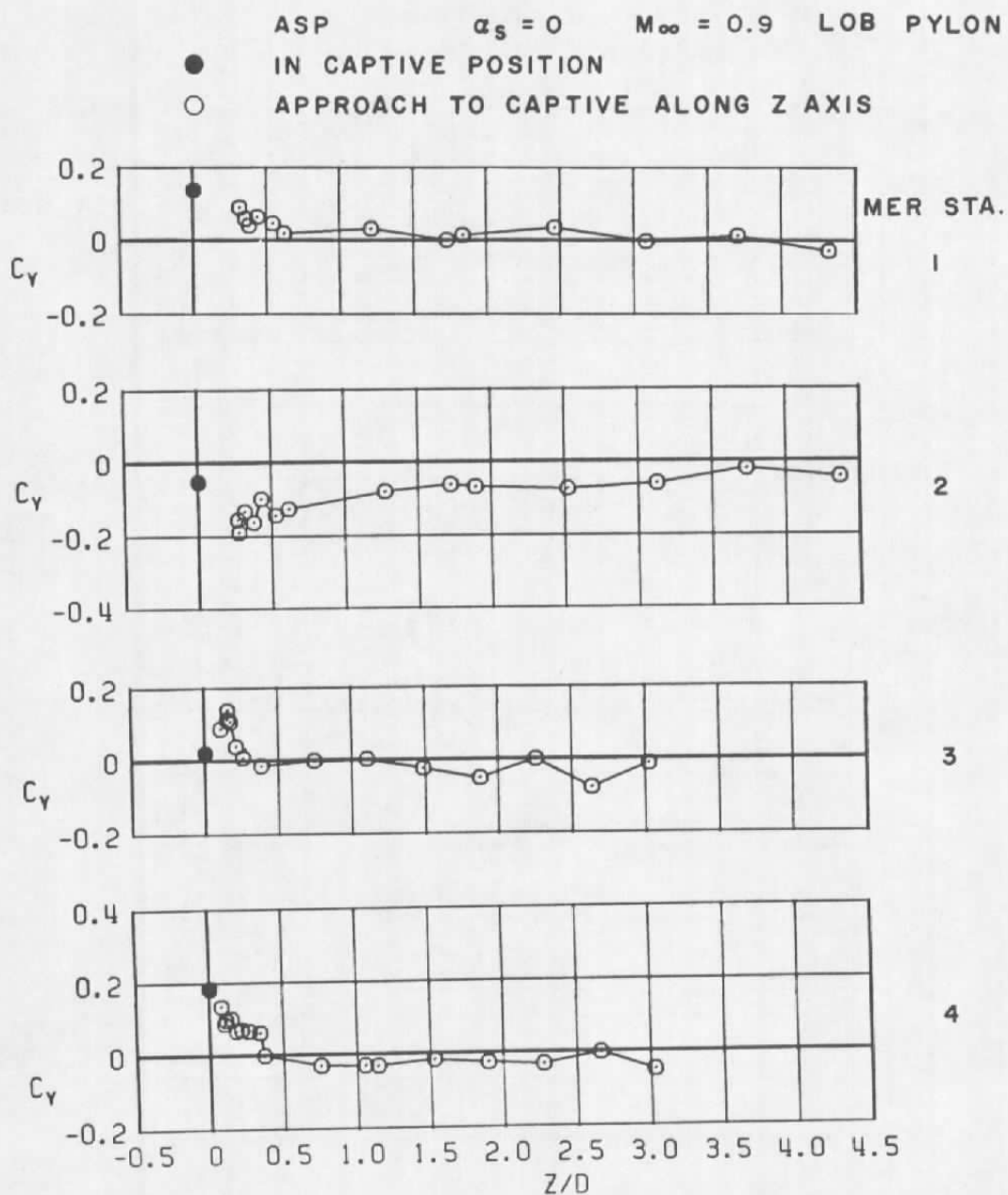


Figure 35. Coefficient of side force acting on the ASP store as a function of normal distance between the store and four captive positions on the MER mounted on the LOB pylon.

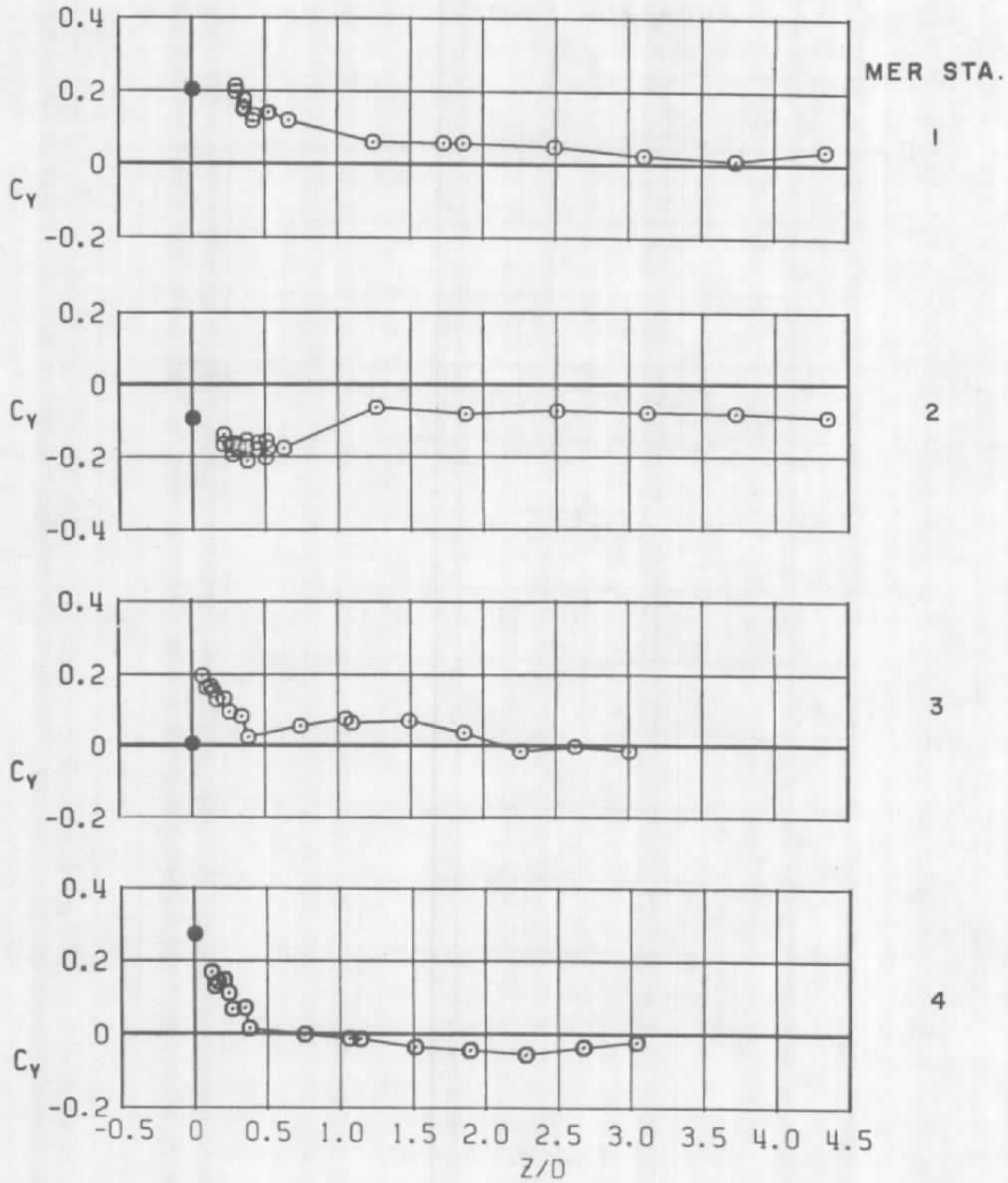


b.  $M_\infty = 0.9$   
Figure 35. Continued.

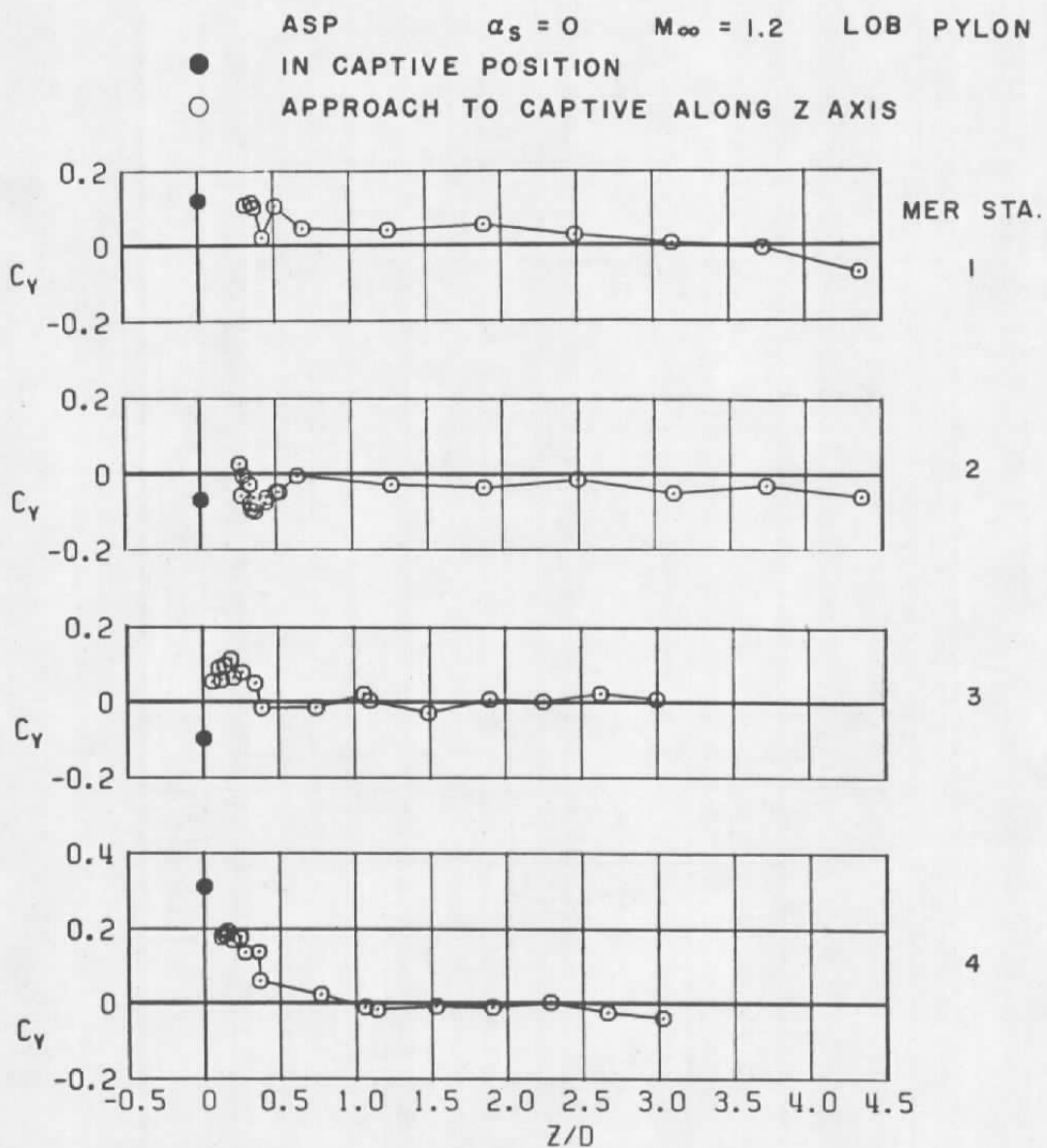
ASP  $\alpha_s = 0$   $M_\infty = 1.1$  LOB PYLON

● IN CAPTIVE POSITION

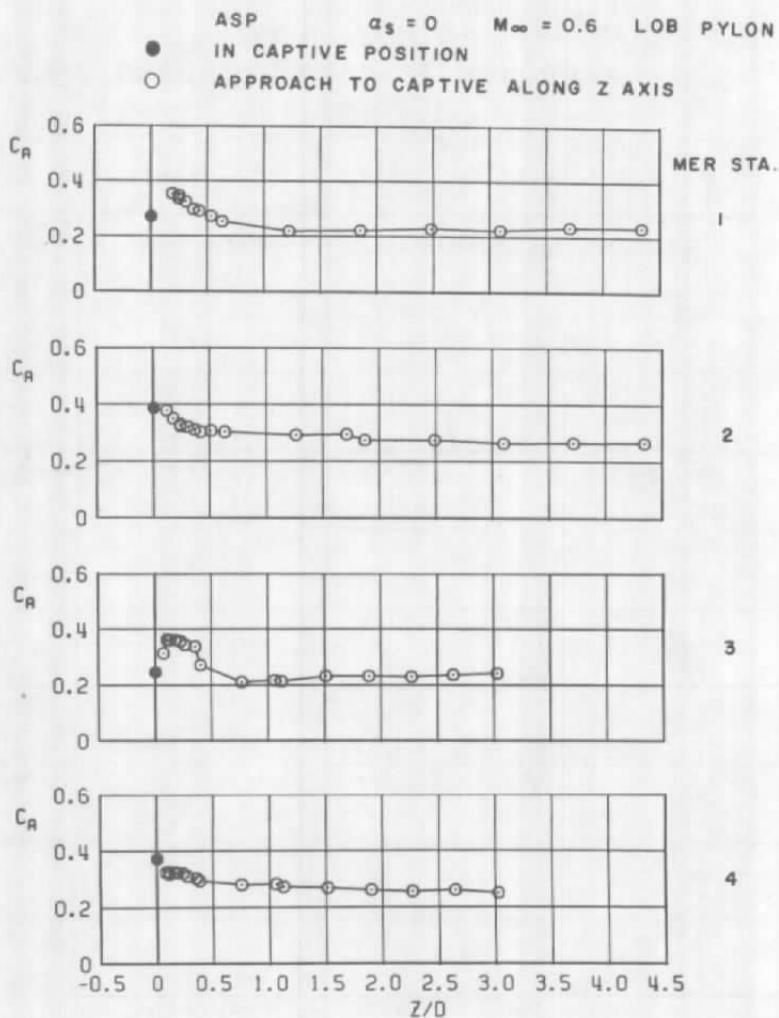
○ APPROACH TO CAPTIVE ALONG Z AXIS



c.  $M_\infty = 1.1$   
Figure 35. Continued.



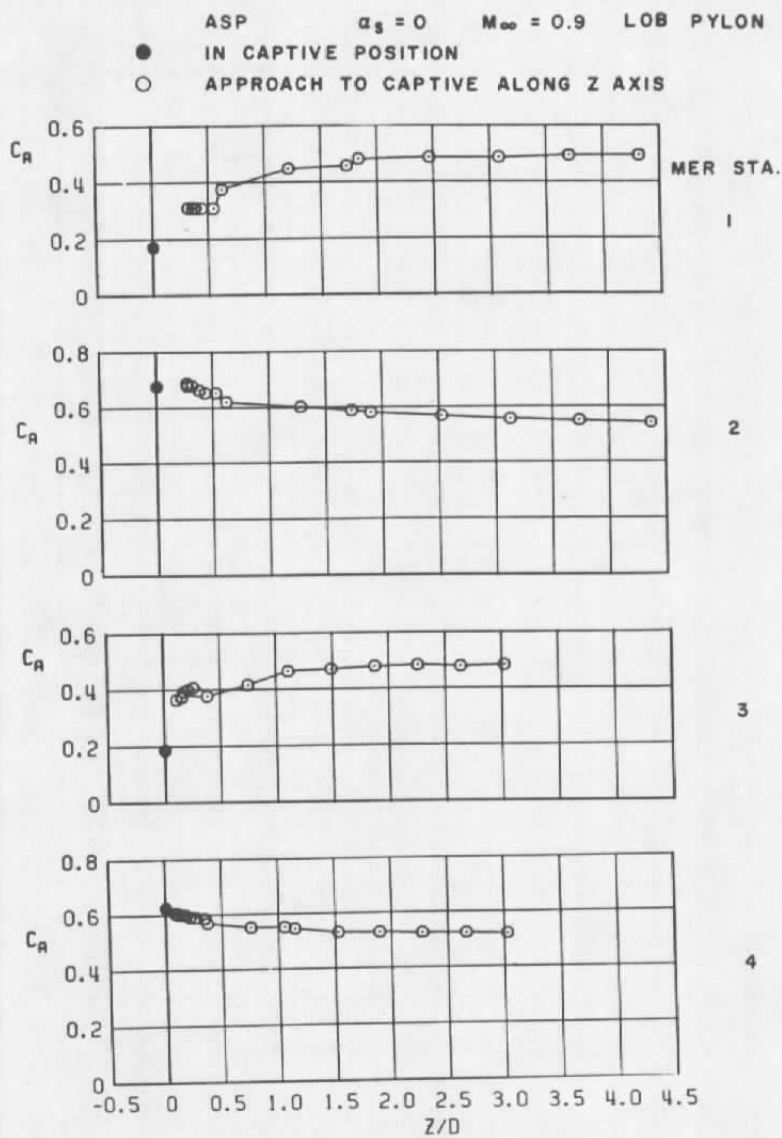
d.  $M_\infty = 1.2$   
Figure 35. Concluded.



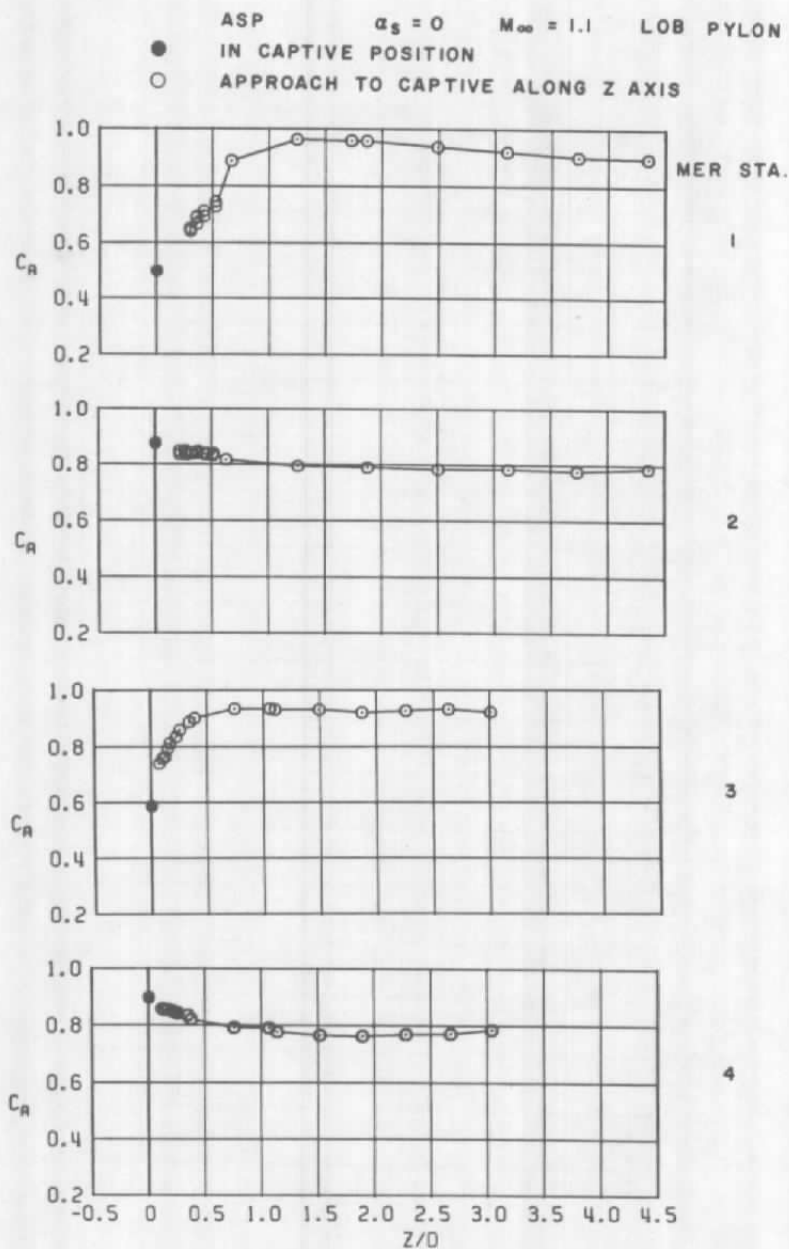
a.  $M_\infty = 0.6$

Figure 36. Coefficient of axial force acting on the ASP store as a function of normal distance between the store and four captive positions on the MER mounted on the LOB pylon.

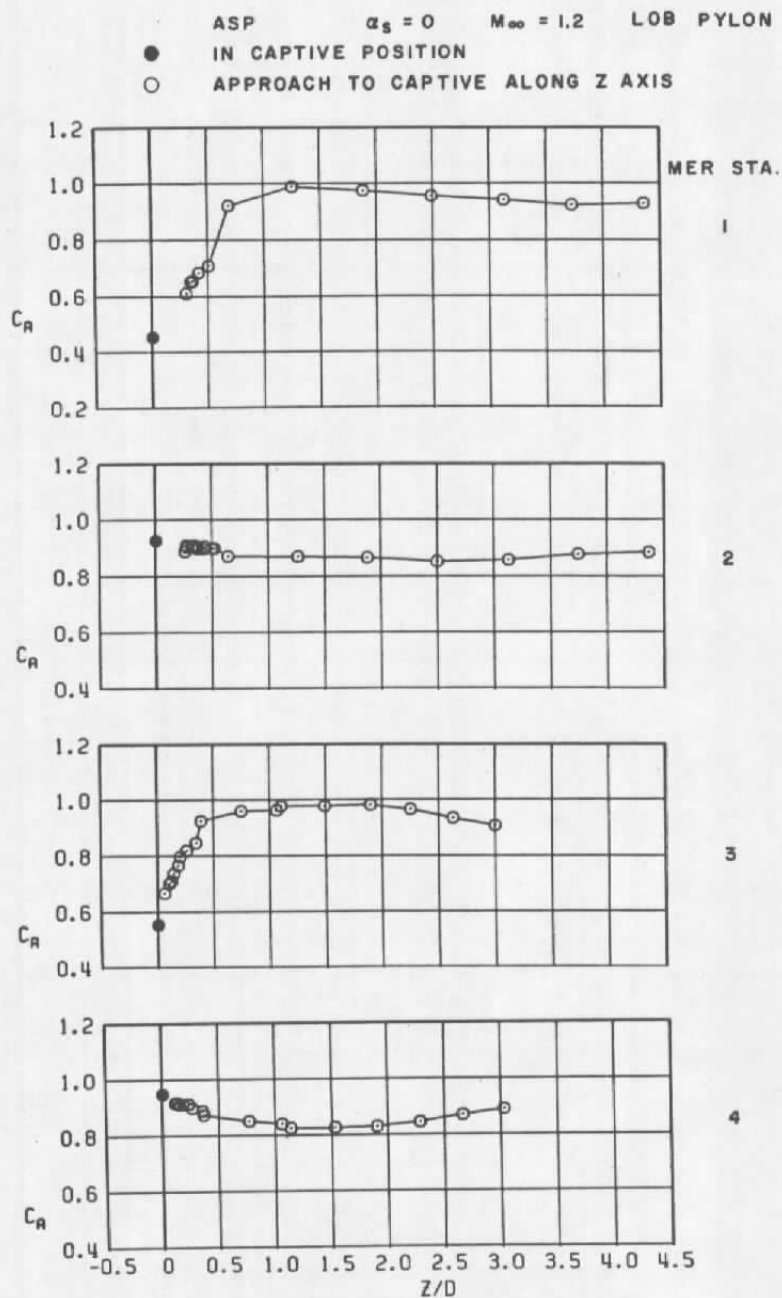




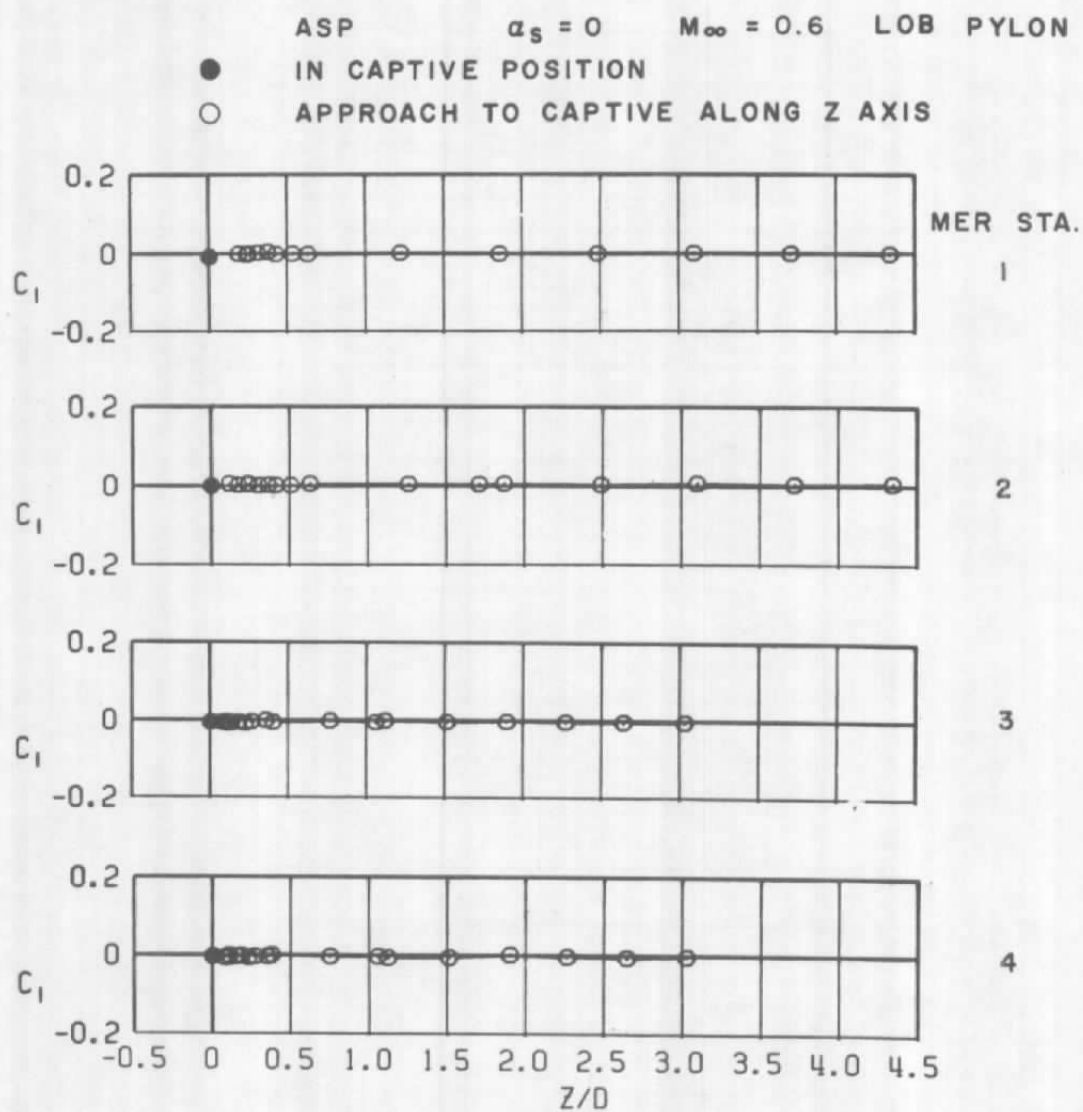
b.  $M_\infty = 0.9$   
Figure 36. Continued.



c.  $M_{\infty} = 1.1$   
Figure 36. Continued.

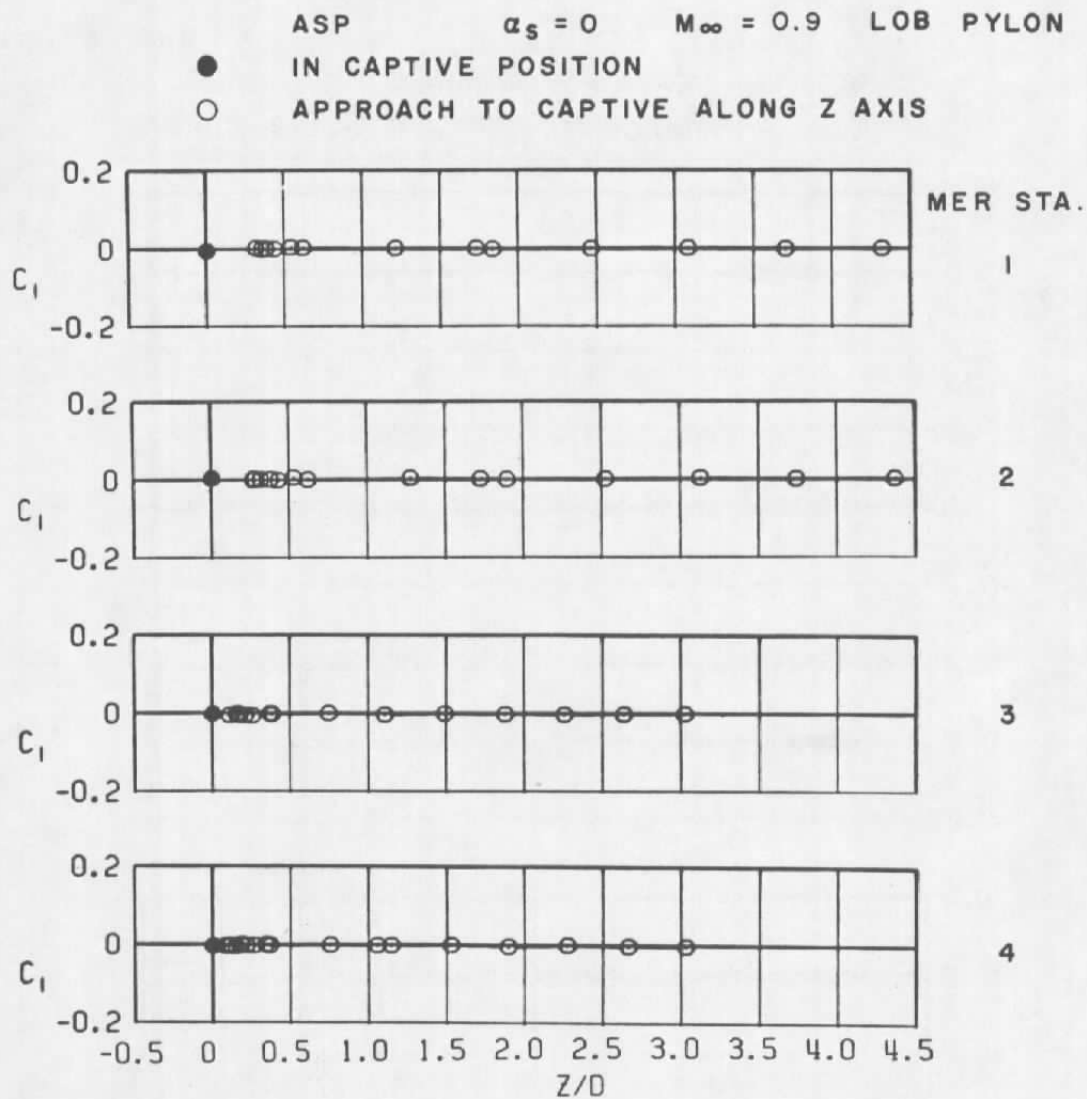


d.  $M_\infty = 1.2$   
Figure 36. Concluded.

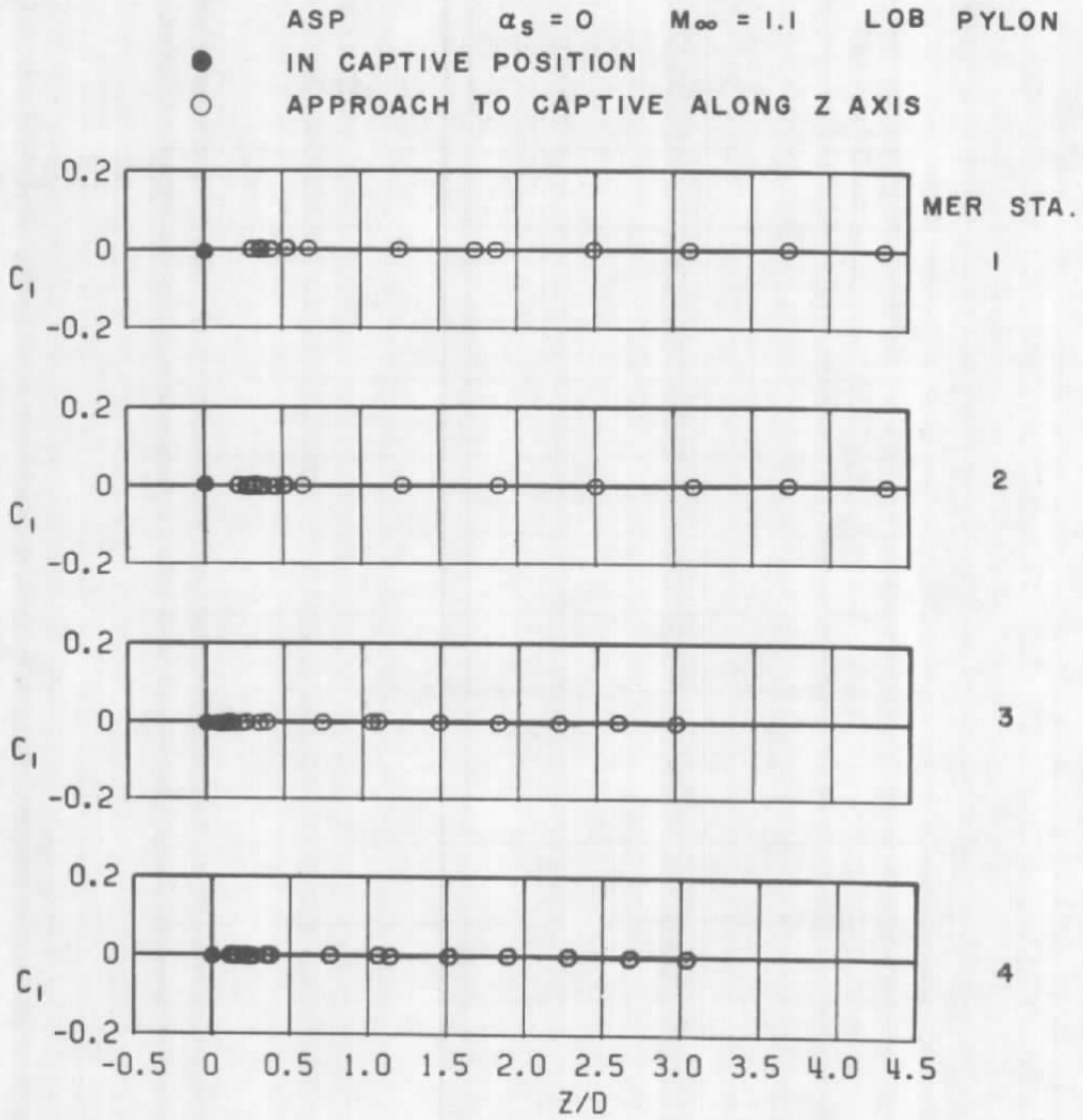


a.  $M_\infty = 0.6$

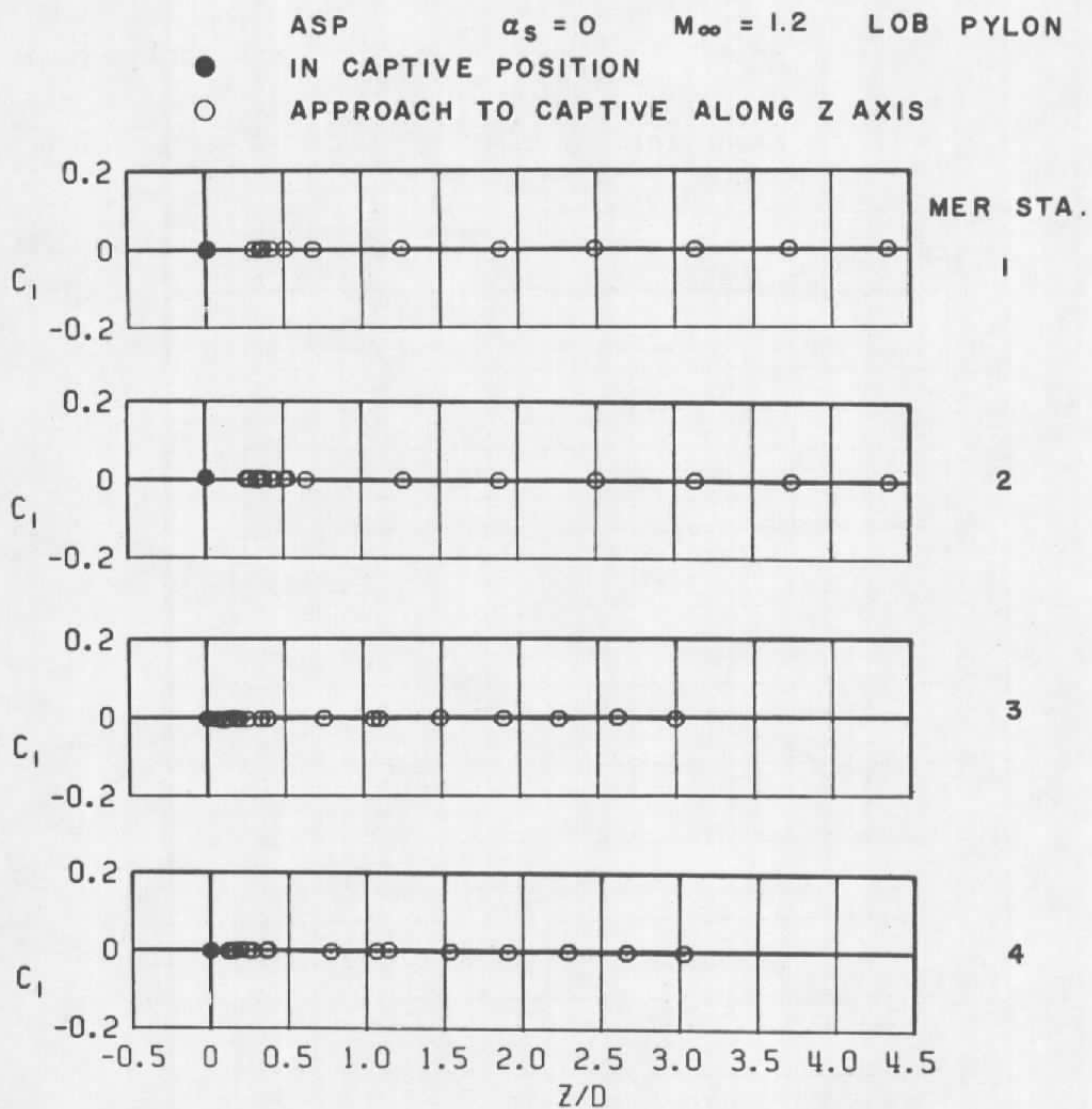
Figure 37. Coefficient of rolling moment acting on the ASP store as a function of normal distance between the store and four captive positions on the MER mounted on the LOB pylon.



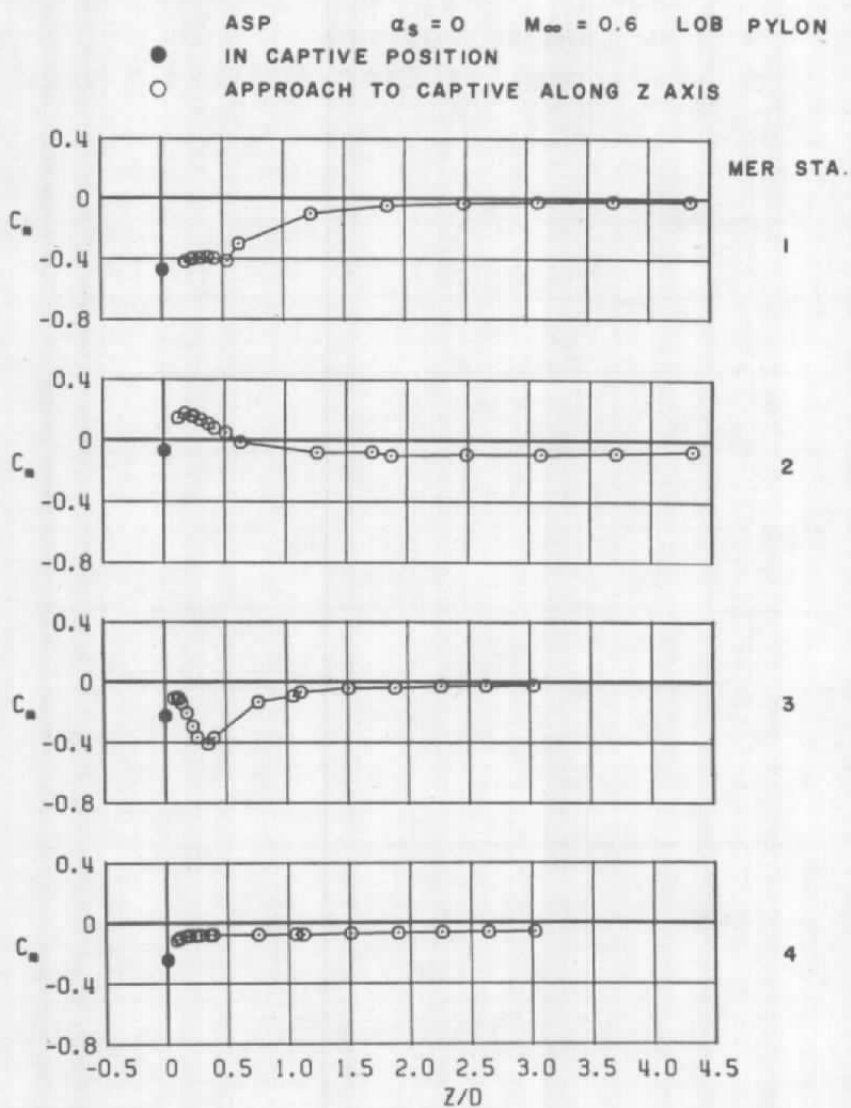
b.  $M_\infty = 0.9$   
Figure 37. Continued.



c.  $M_\infty = 1.1$   
Figure 37. Continued.



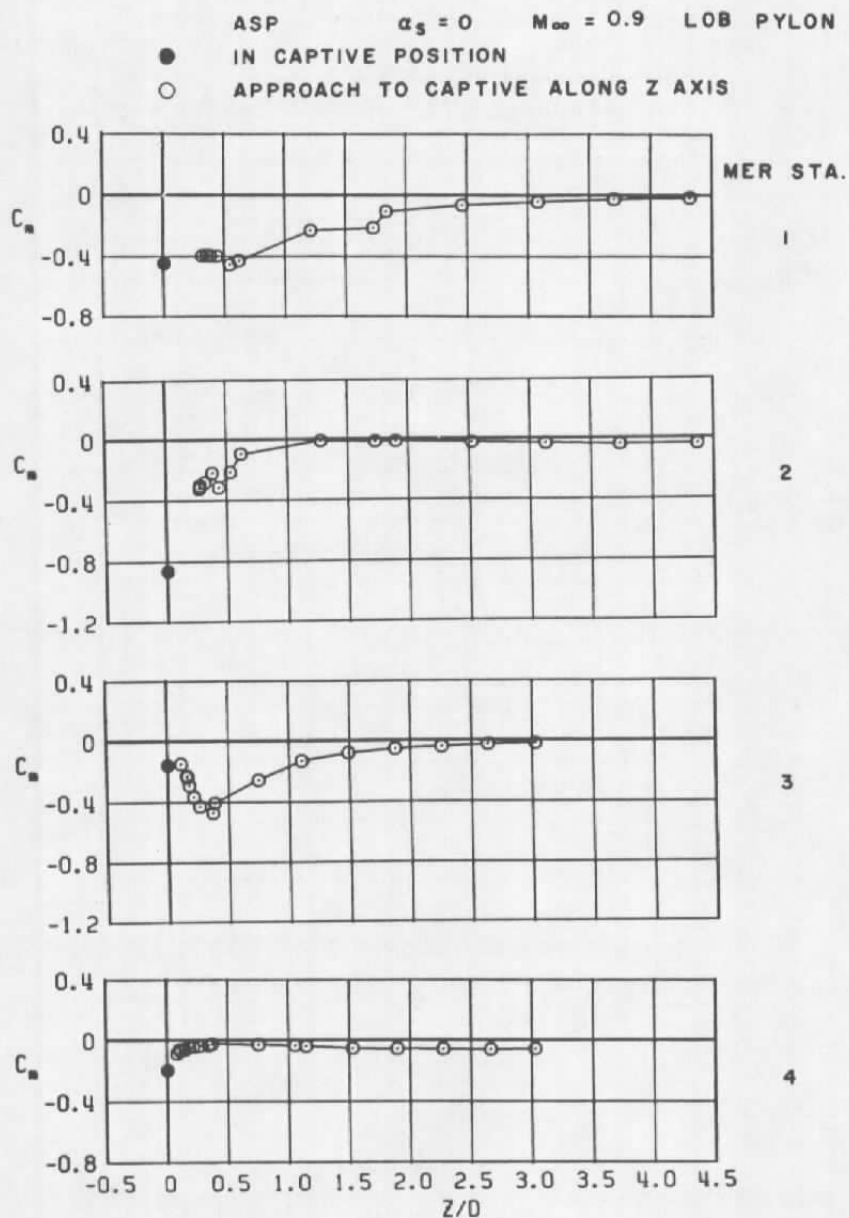
d.  $M_\infty = 1.2$   
Figure 37. Concluded.



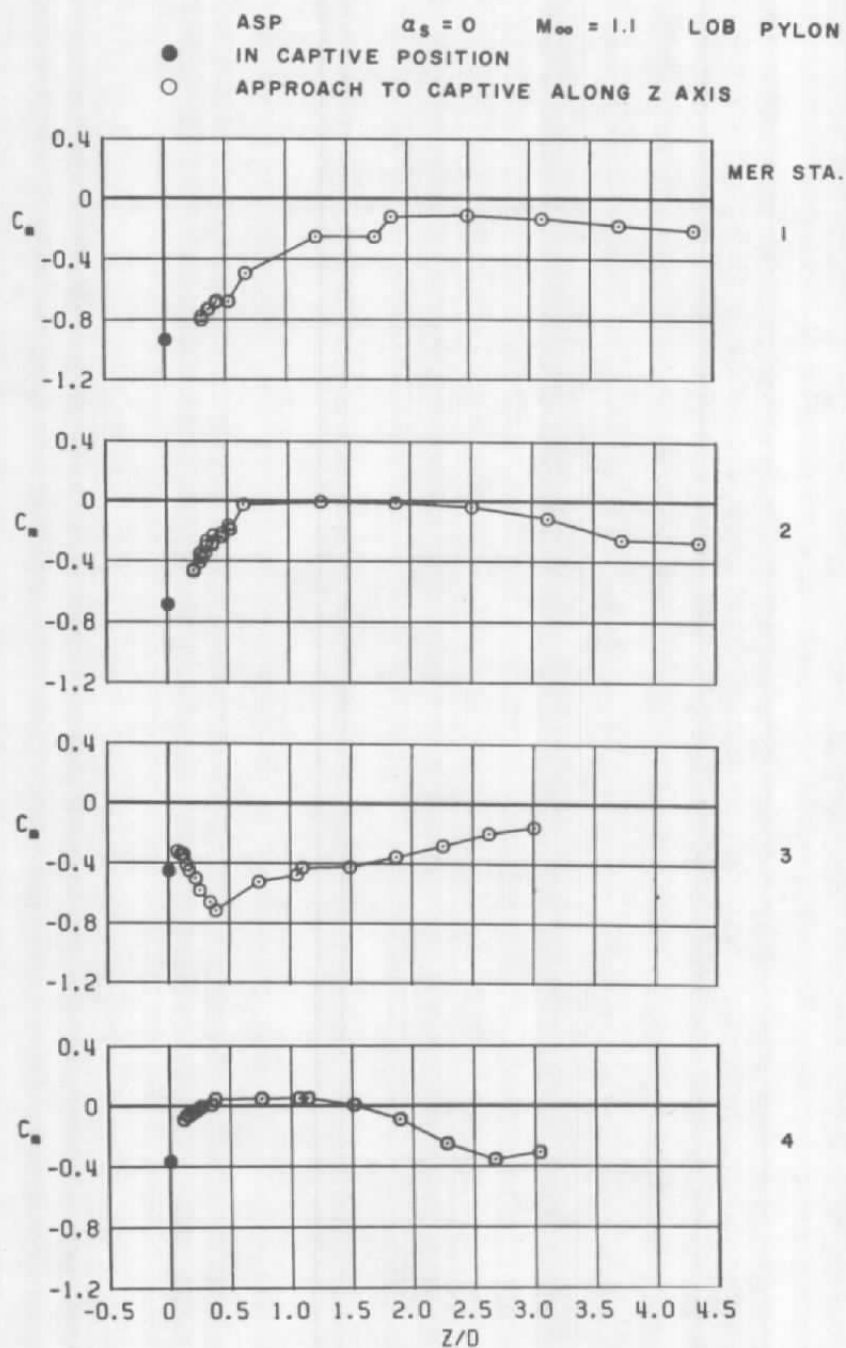
a.  $M_\infty = 0.6$

Figure 38. Coefficient of pitching moment acting on the ASP store as a function of normal distance between the store and four captive positions on the MER mounted on the LOB pylon.

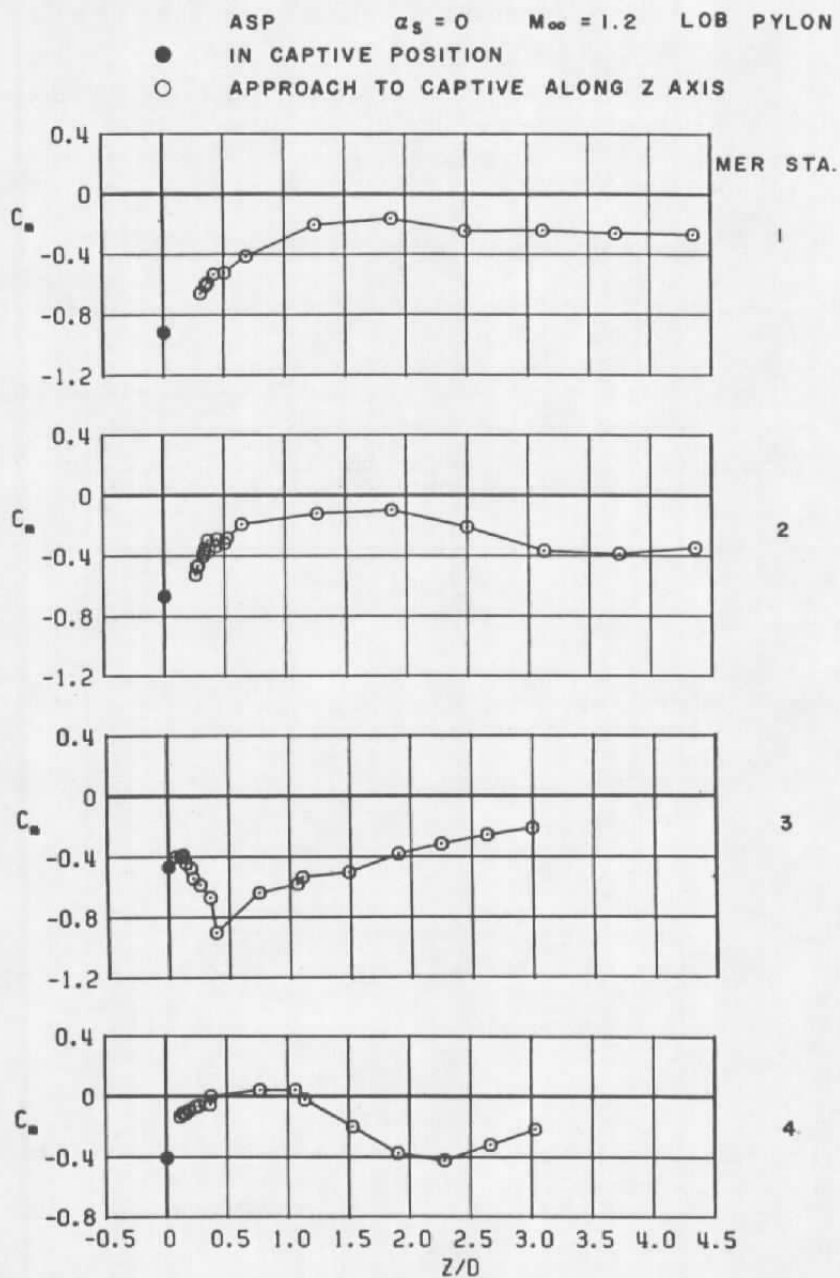




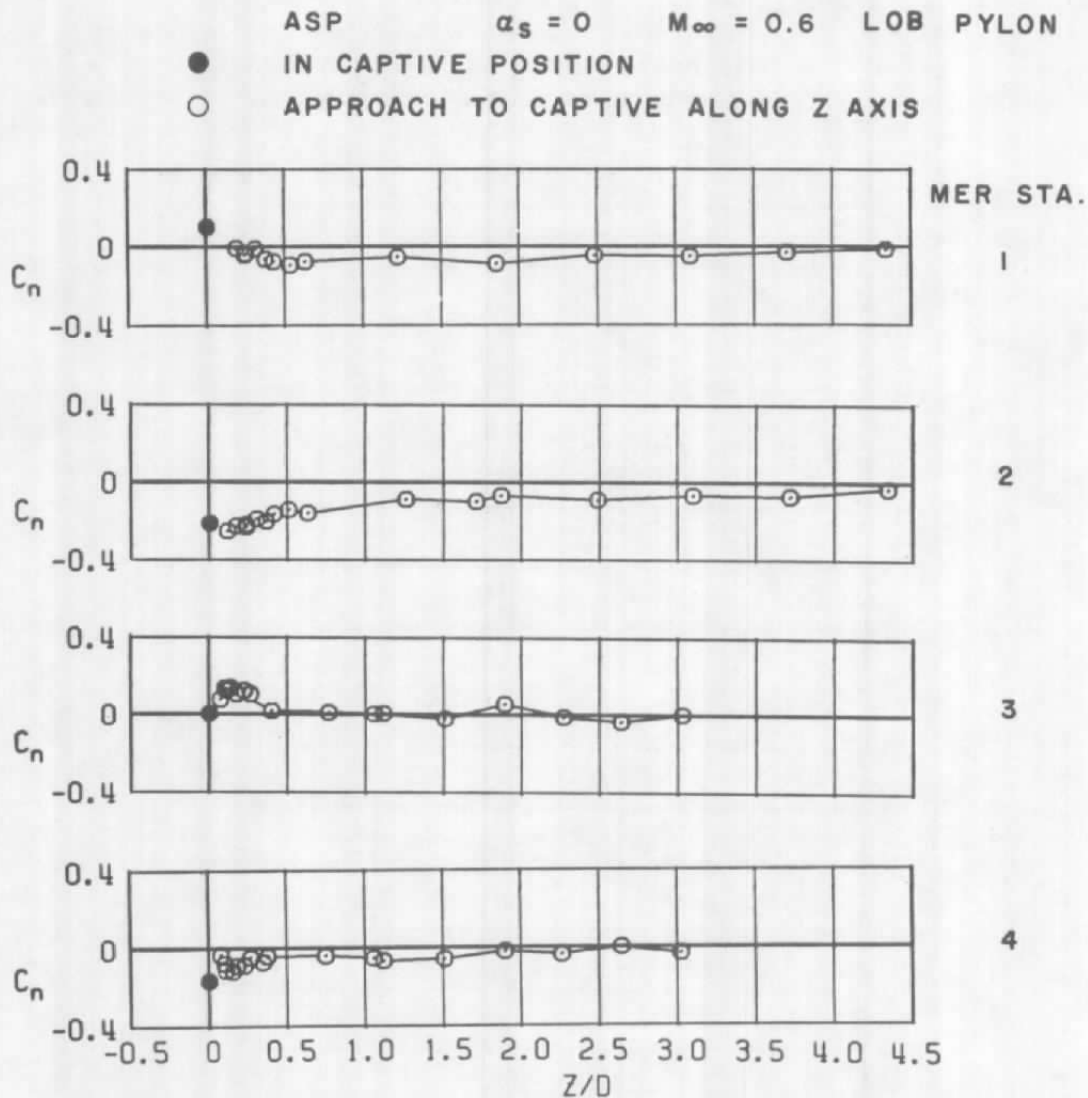
b.  $M_\infty = 0.9$   
Figure 38. Continued.



c.  $M_{\infty} = 1.1$   
Figure 38. Continued.

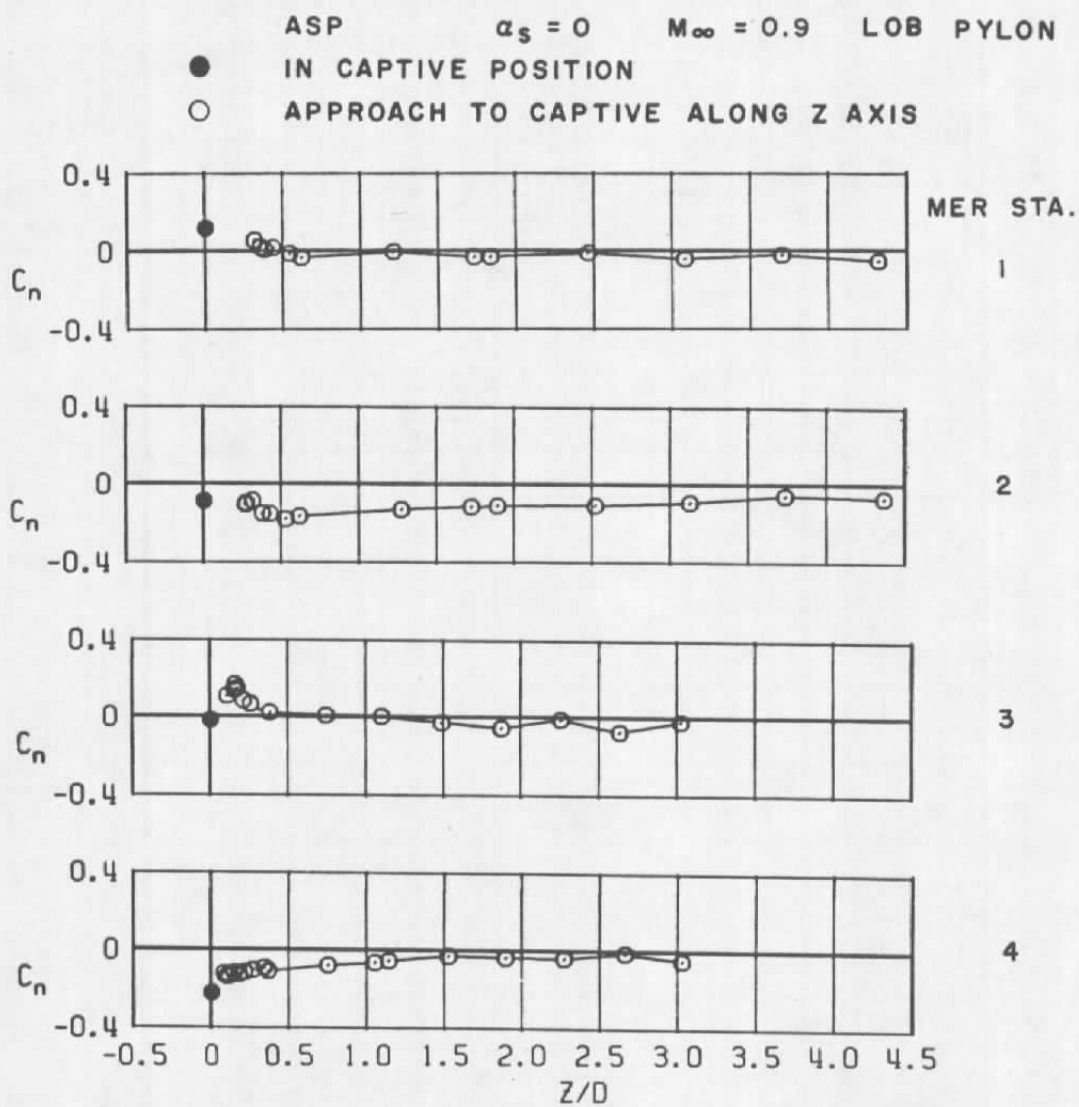


d.  $M_\infty = 1.2$   
Figure 38. Concluded.



a.  $M_\infty = 0.6$

Figure 39. Coefficient of yawing moment acting on the ASP store as a function of normal distance between the store and four captive positions on the MER mounted on the LOB pylon.

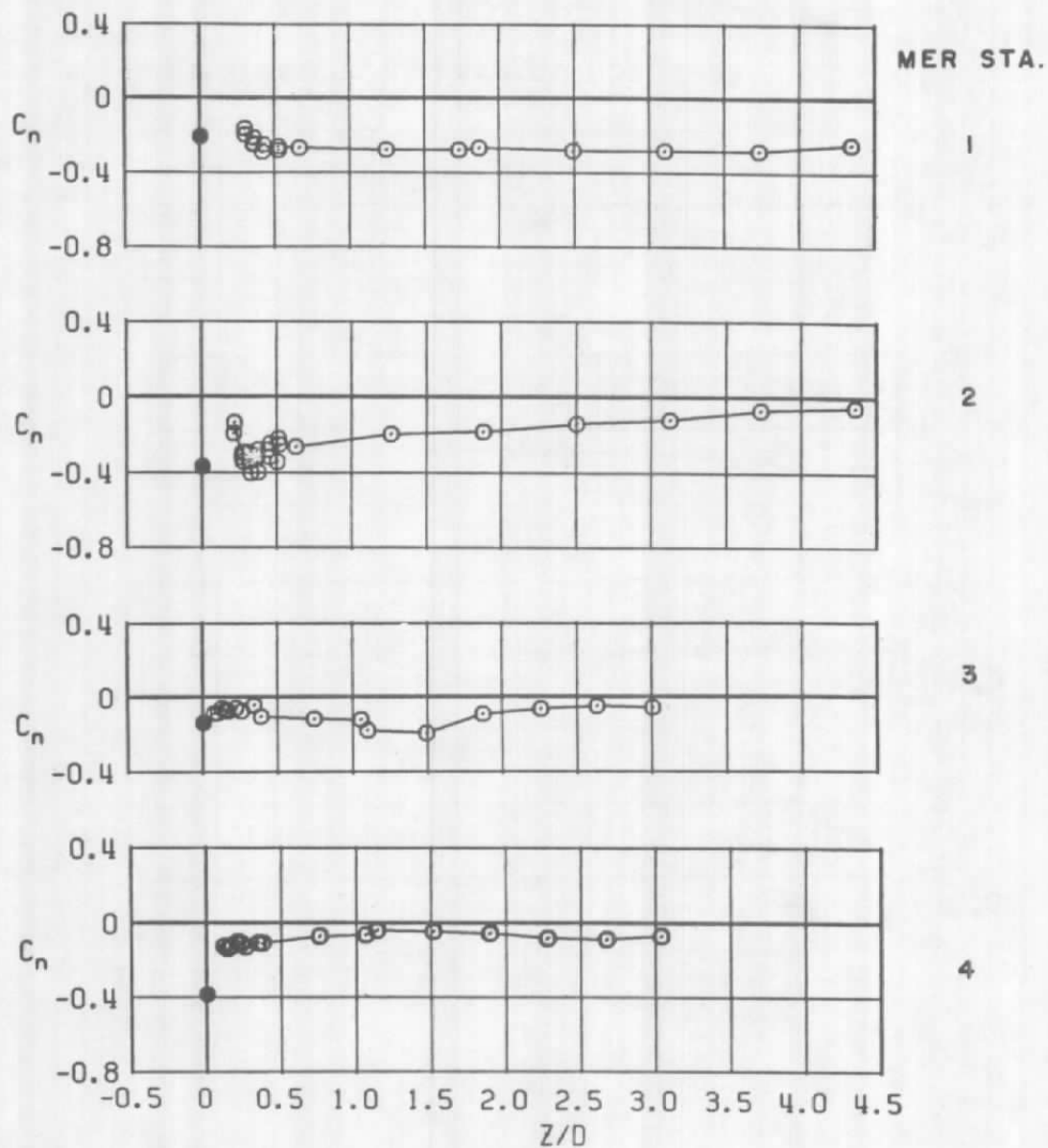


b.  $M_\infty = 0.9$   
Figure 39. Continued.

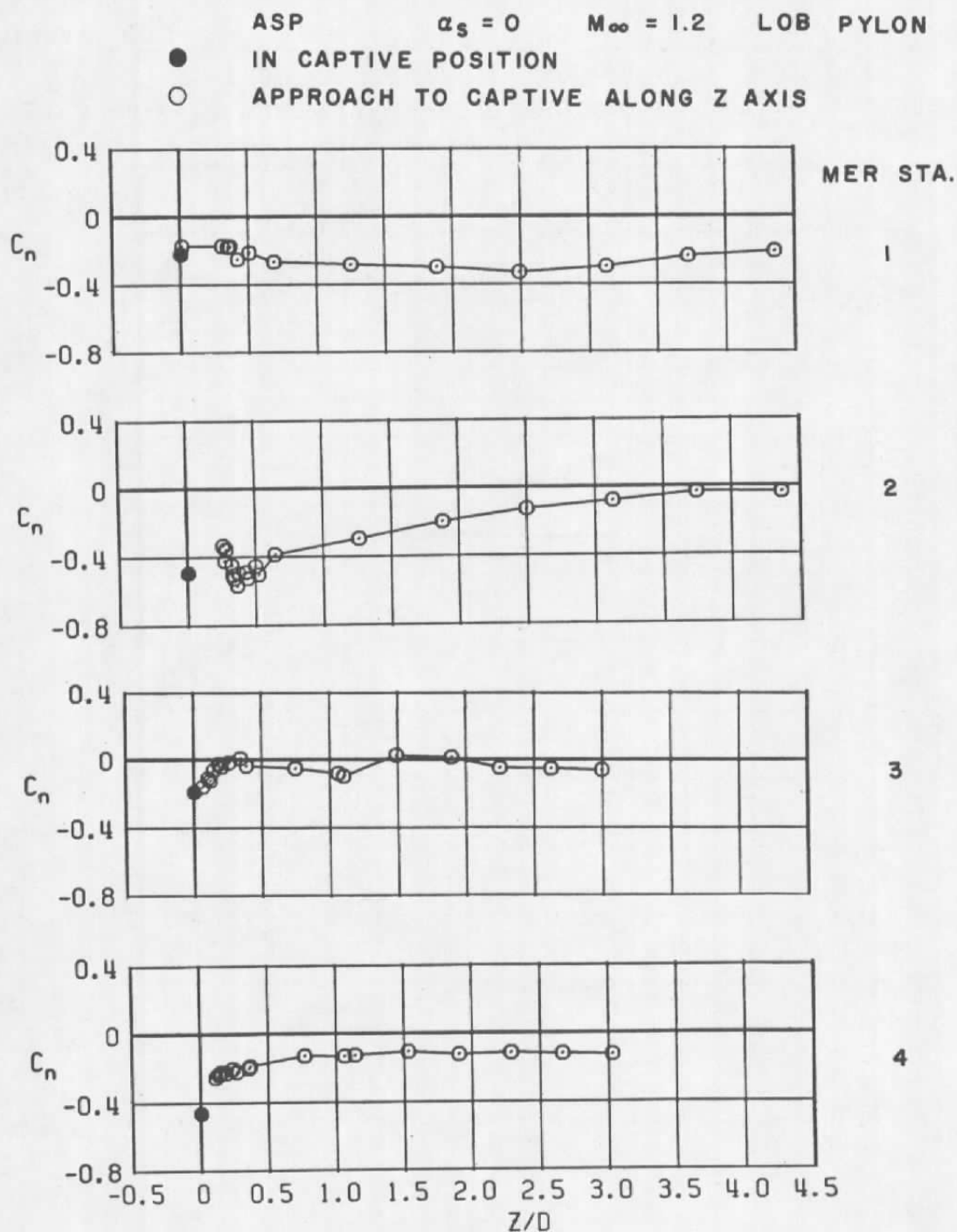
ASP  $\alpha_s = 0$   $M_\infty = 1.1$  LOB PYLON

● IN CAPTIVE POSITION

○ APPROACH TO CAPTIVE ALONG Z AXIS



c.  $M_\infty = 1.1$   
Figure 39. Continued.



d.  $M_\infty = 1.2$   
Figure 39. Concluded.

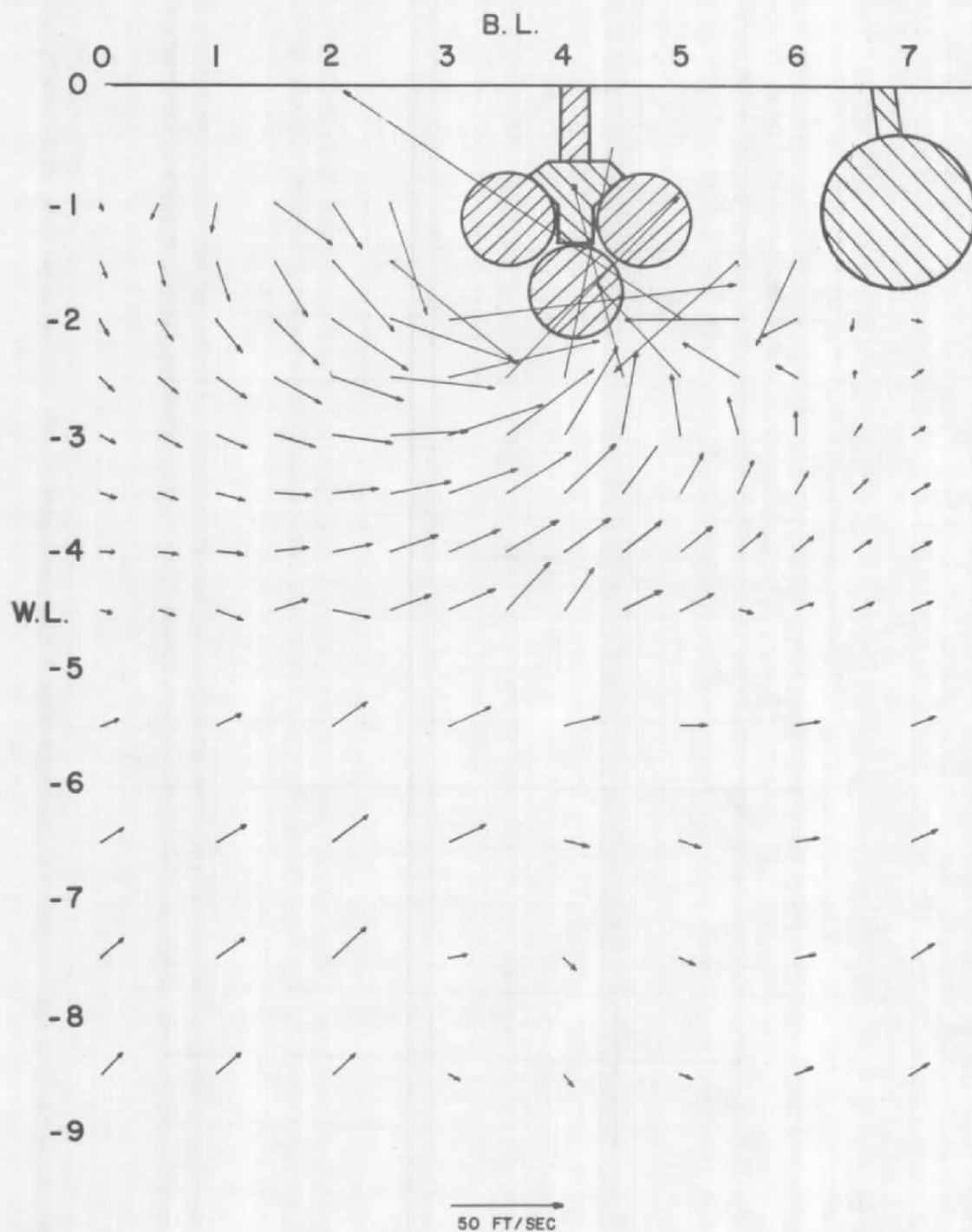
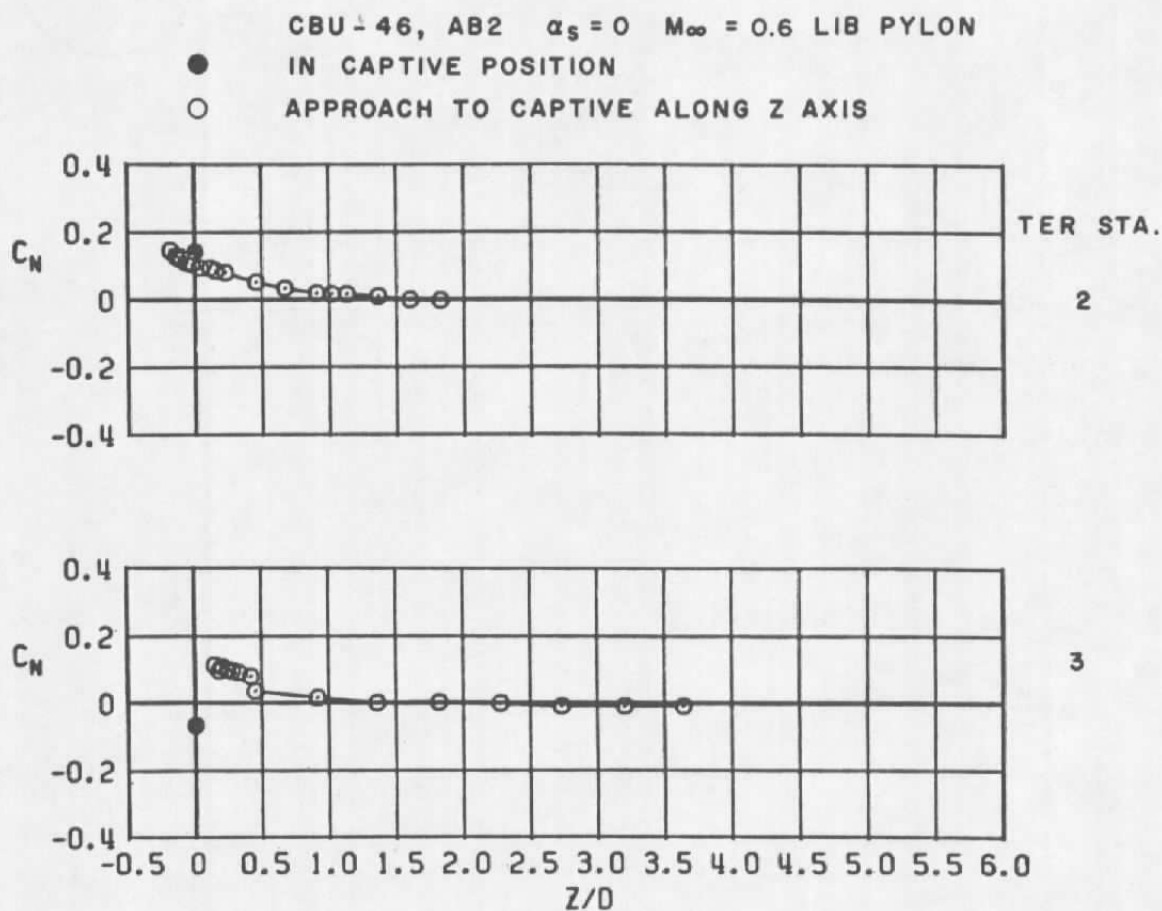


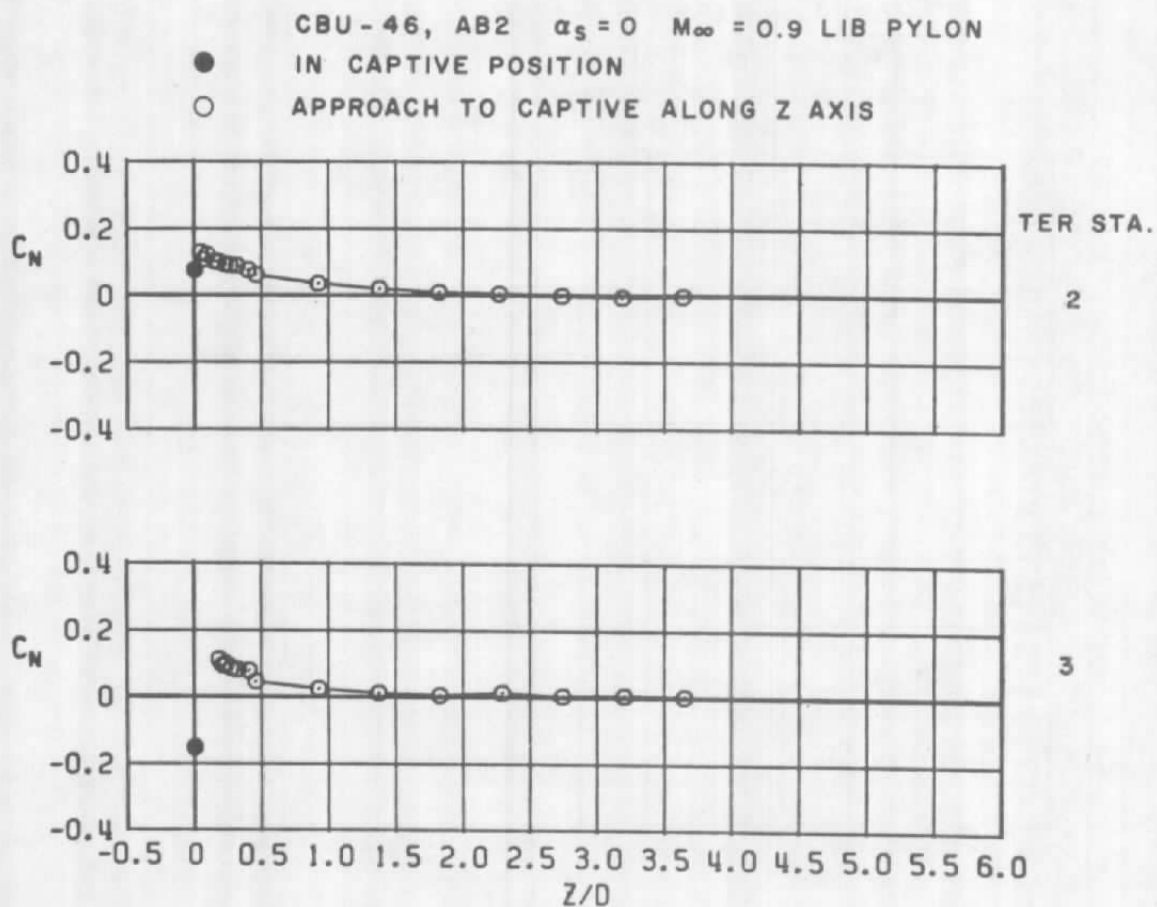
Figure 40. Local flow velocity in the vicinity of the TER mounted on the LIB pylon and loaded with M-117 store models,  $FS = 16.0$ ,  $M_\infty = 0.85$ .



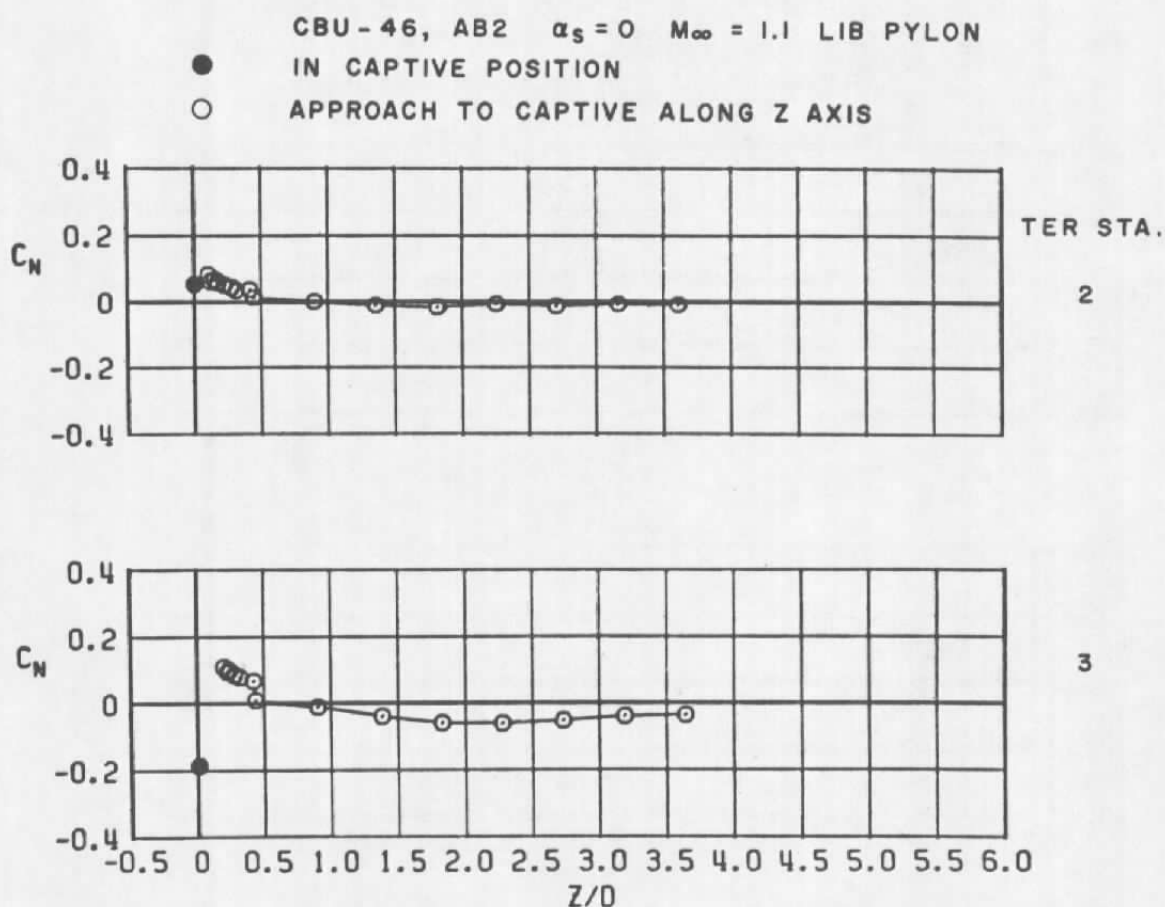


a.  $M_\infty = 0.6$

Figure 41. Coefficient of normal force acting on the CBU-46 (SUU-7) store as a function of normal distance between the store and two captive positions on the TER mounted on the LIB pylon.



b.  $M_\infty = 0.9$   
 Figure 41. Continued.



c.  $M_\infty = 1.1$   
 Figure 41. Continued.

CBU-46, AB2  $\alpha_s = 0$   $M_\infty = 1.2$  LIB PYLON

● IN CAPTIVE POSITION

○ APPROACH TO CAPTIVE ALONG Z AXIS

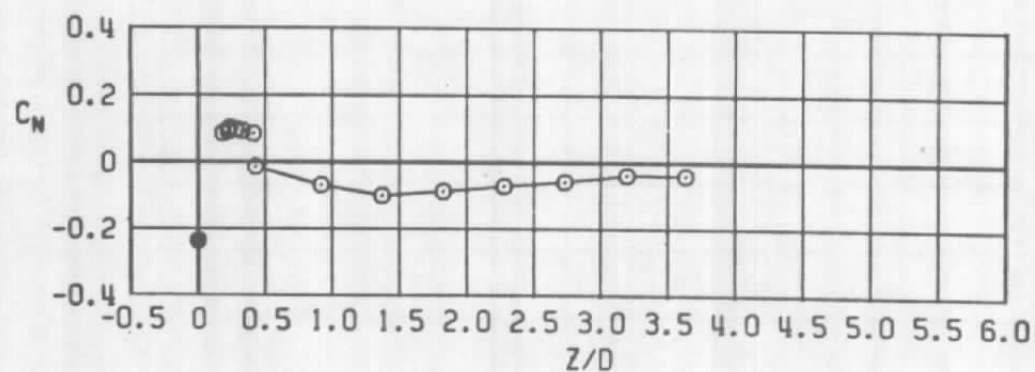
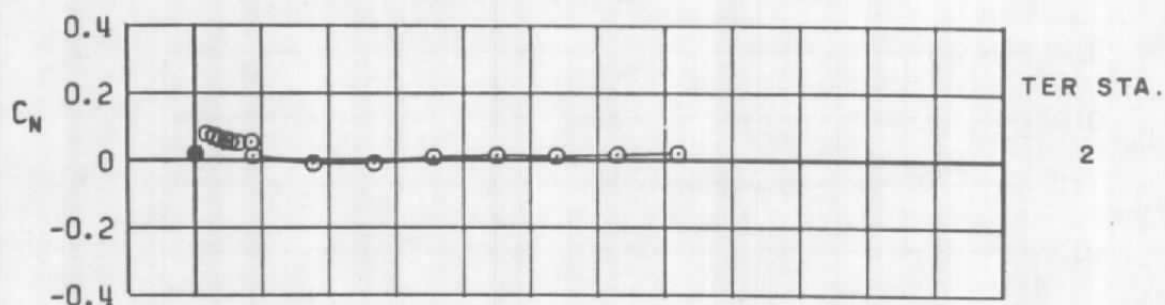
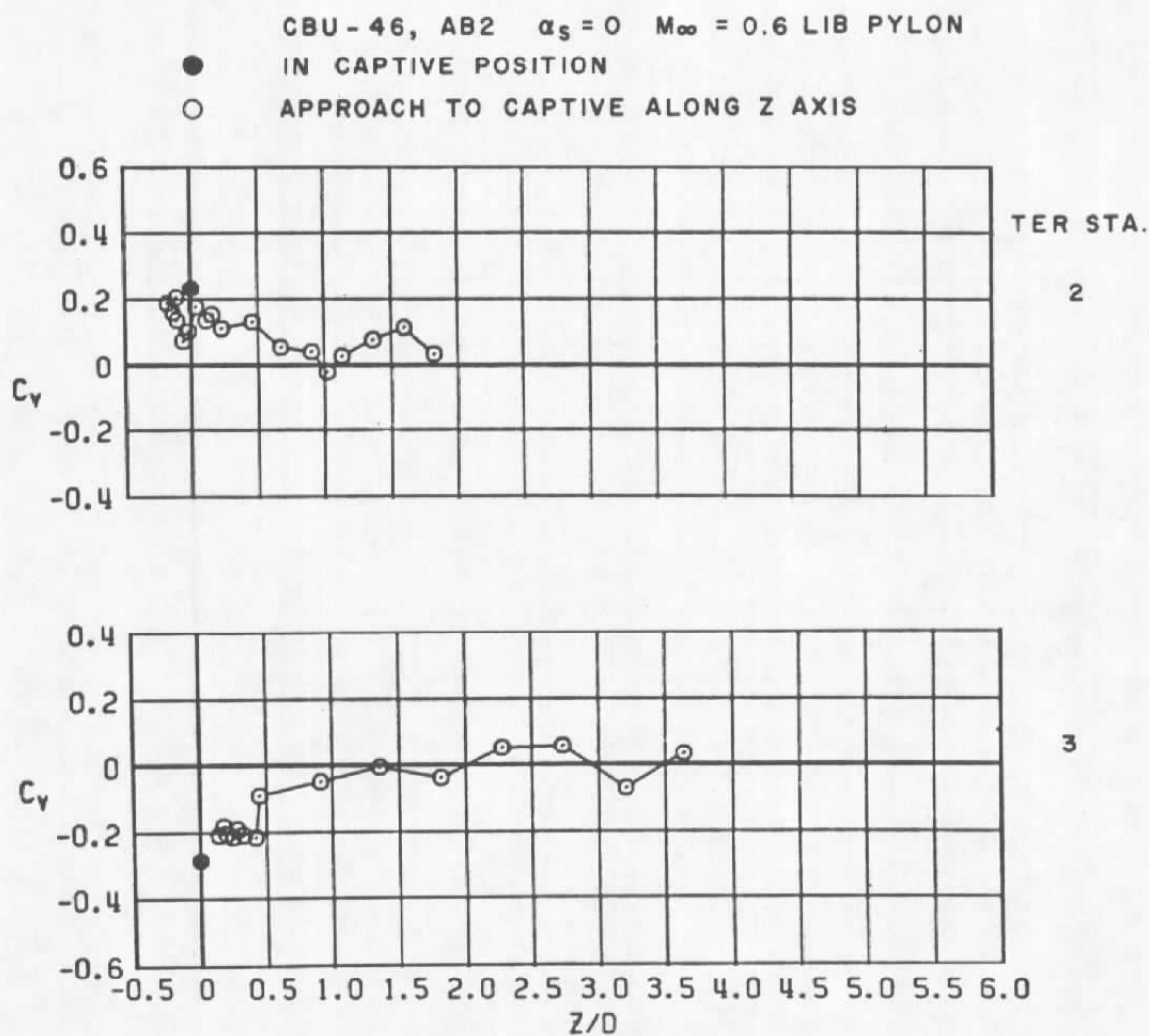
d.  $M_\infty = 1.2$ 

Figure 41. Concluded.



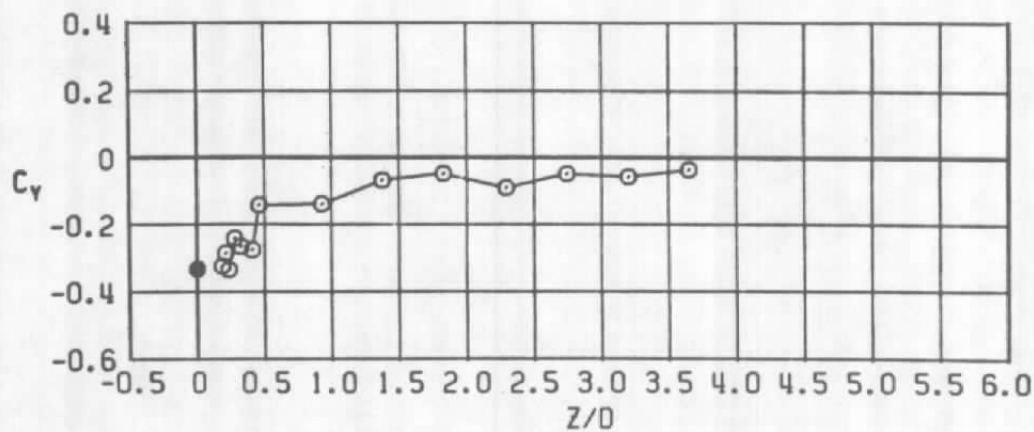
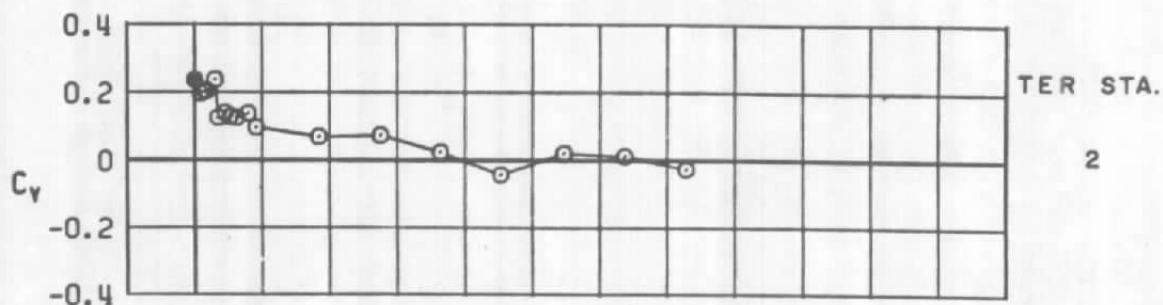
a.  $M_\infty = 0.6$

Figure 42. Coefficient of side force acting on the CBU-46 (SUU-7) store as a function of normal distance between the store and two captive positions on the TER mounted on the LIB pylon.

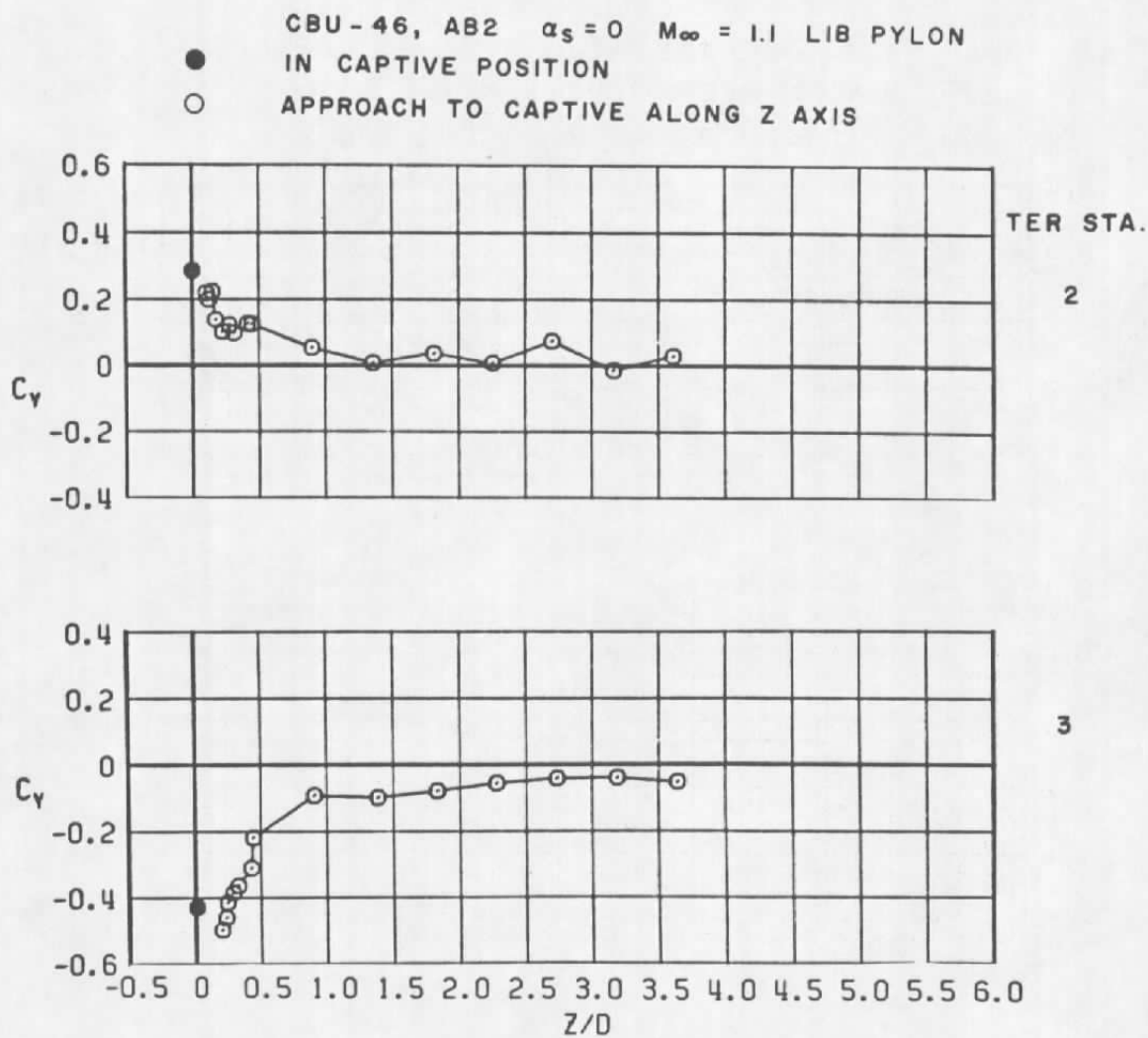
CBU - 46, AB2  $\alpha_s = 0$   $M_\infty = 0.9$  LIB PYLON

● IN CAPTIVE POSITION

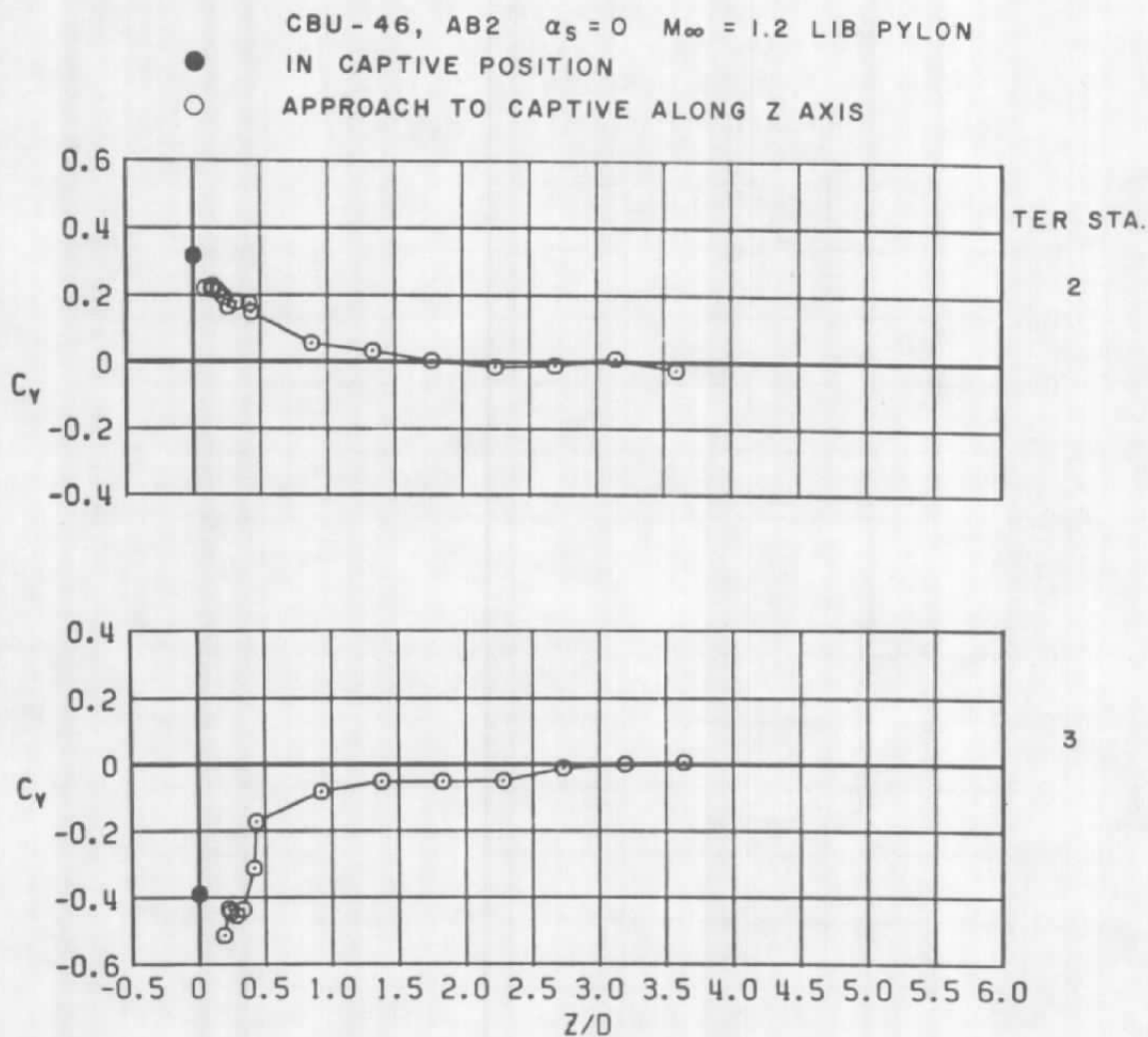
○ APPROACH TO CAPTIVE ALONG Z AXIS



b.  $M_\infty = 0.9$   
Figure 42. Continued.

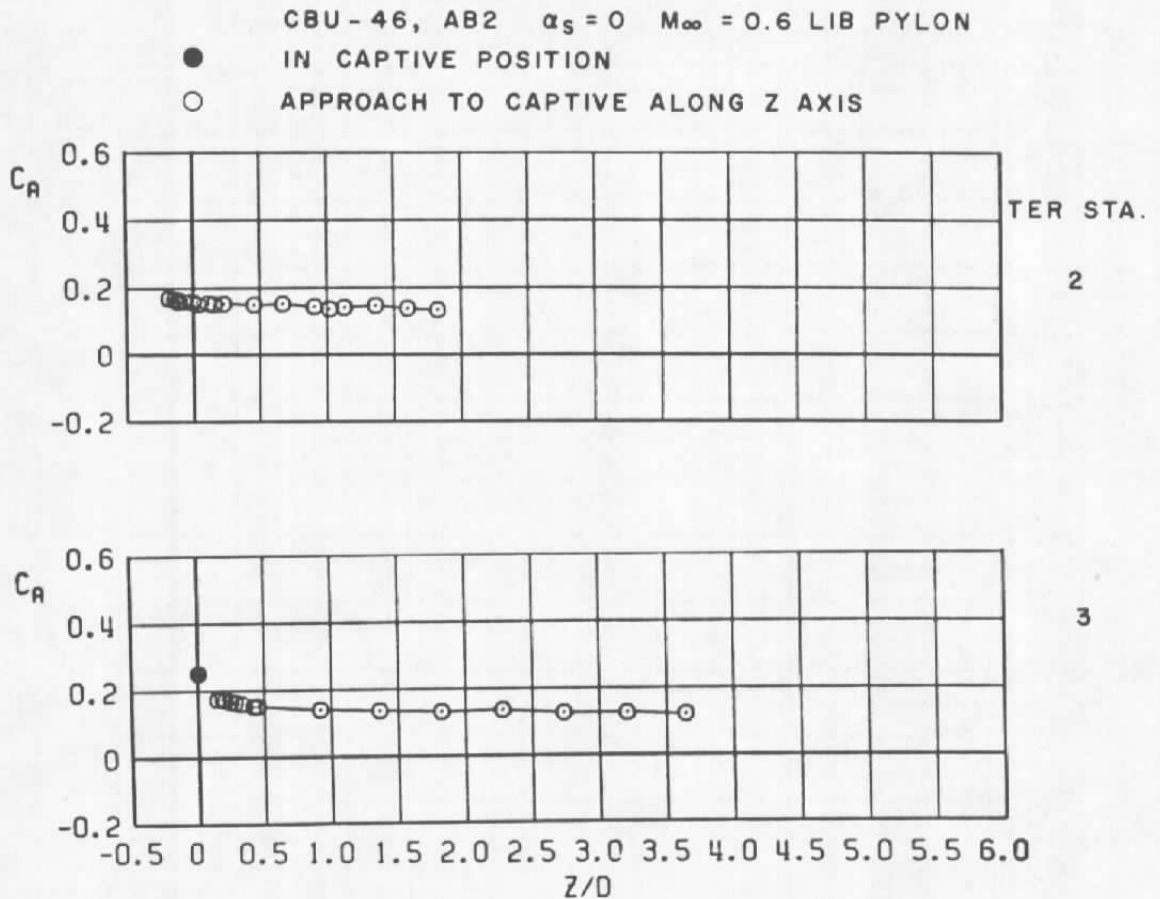


c.  $M_\infty = 1.1$   
 Figure 42. Continued.



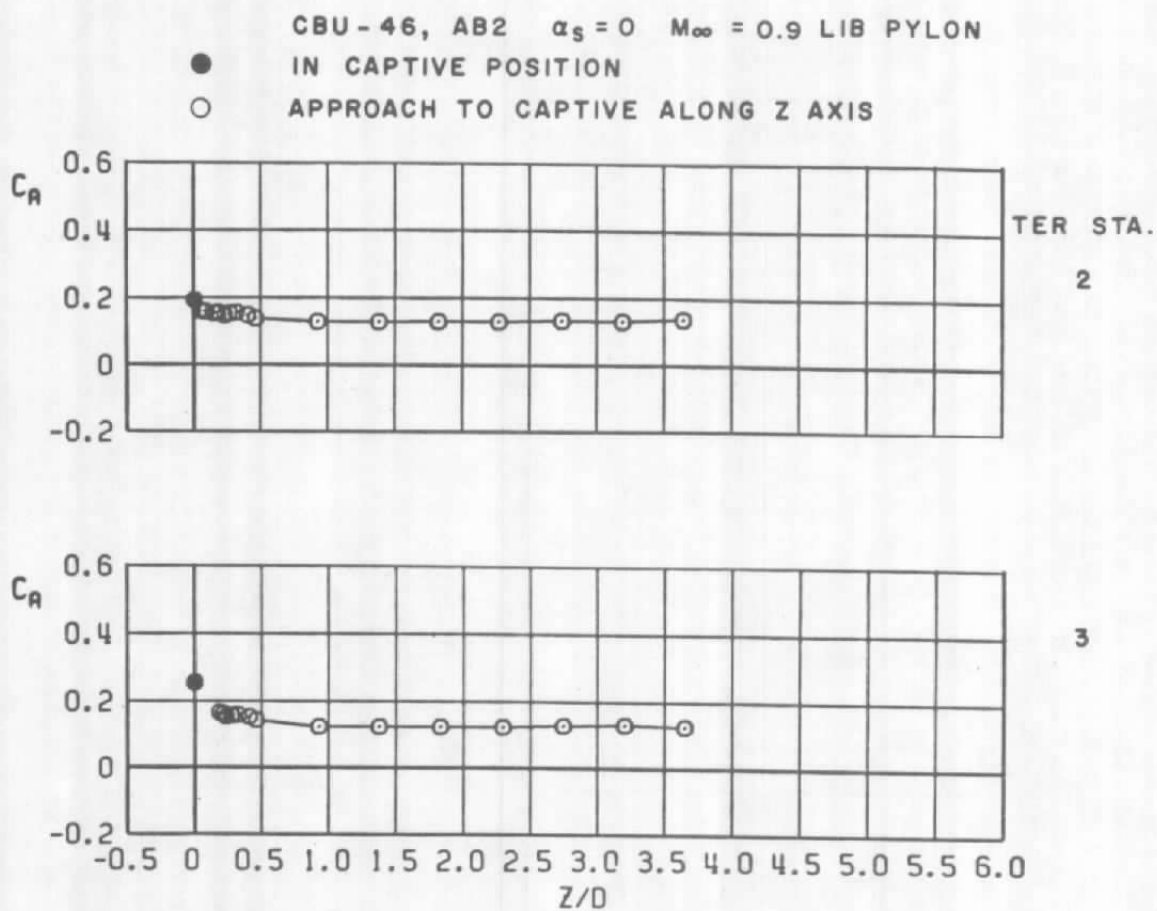
d.  $M_\infty = 1.2$   
 Figure 42. Concluded.



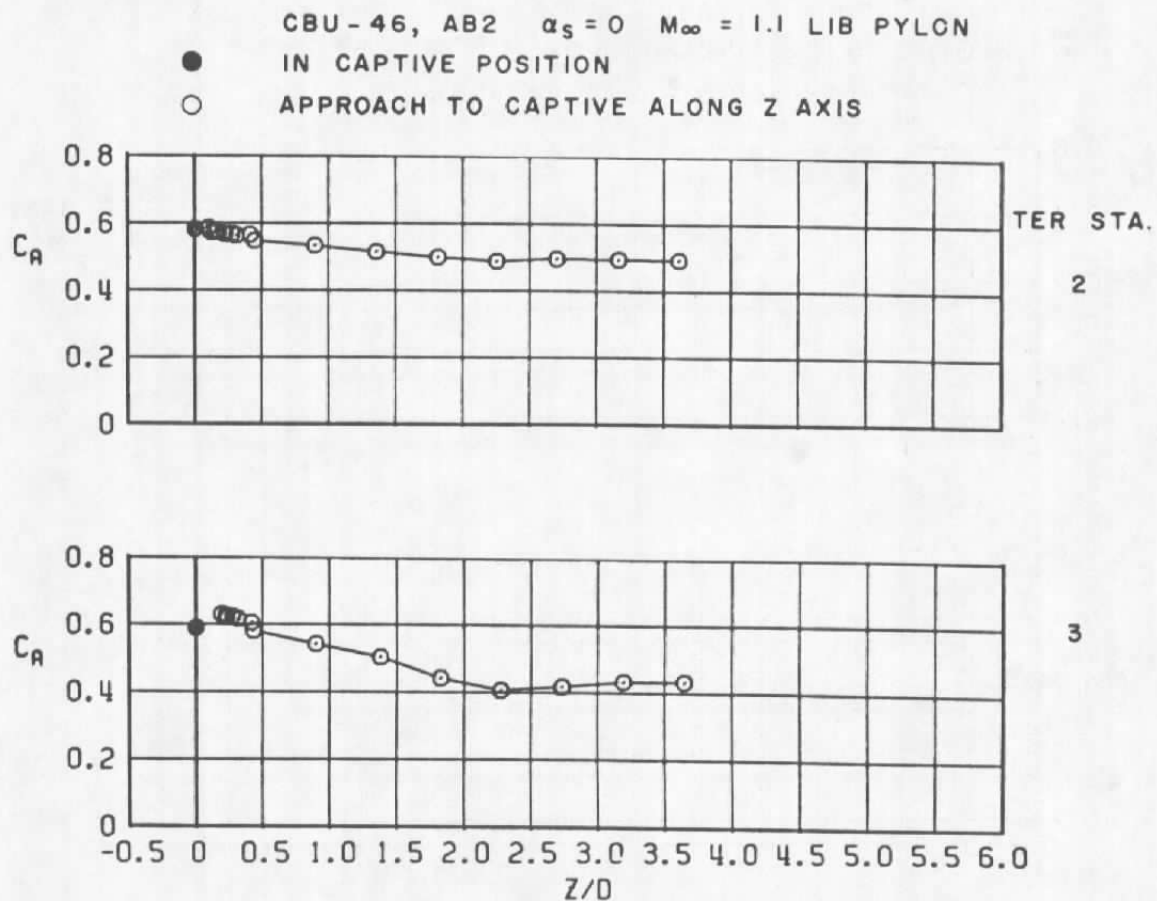


a.  $M_\infty = 0.6$

Figure 43. Coefficient of axial force acting on the CBU-46 (SUU-7) store as a function of normal distance between the store and two captive positions on the TER mounted on the LIB pylon.



b.  $M_\infty = 0.9$   
 Figure 43. Continued.

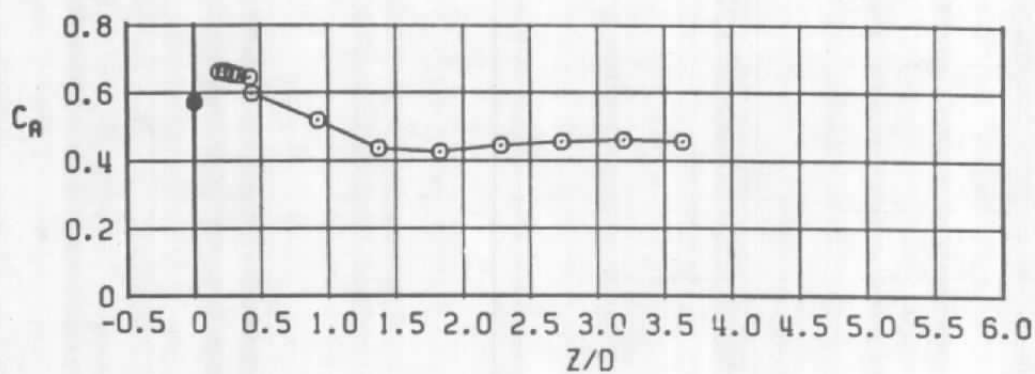
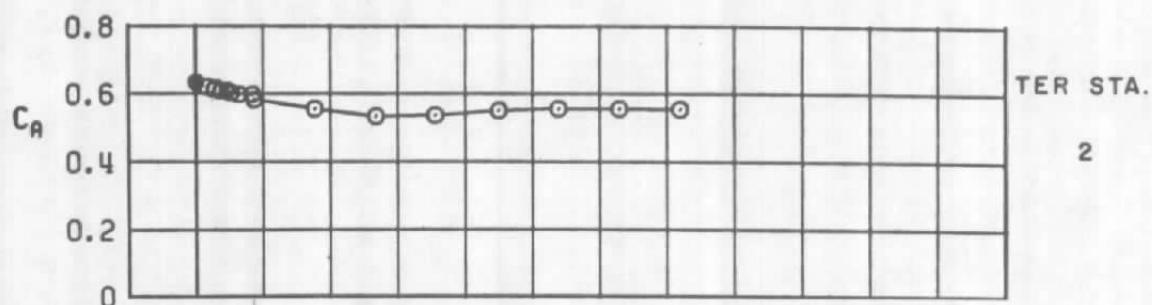


c.  $M_\infty = 1.1$   
Figure 43. Continued.

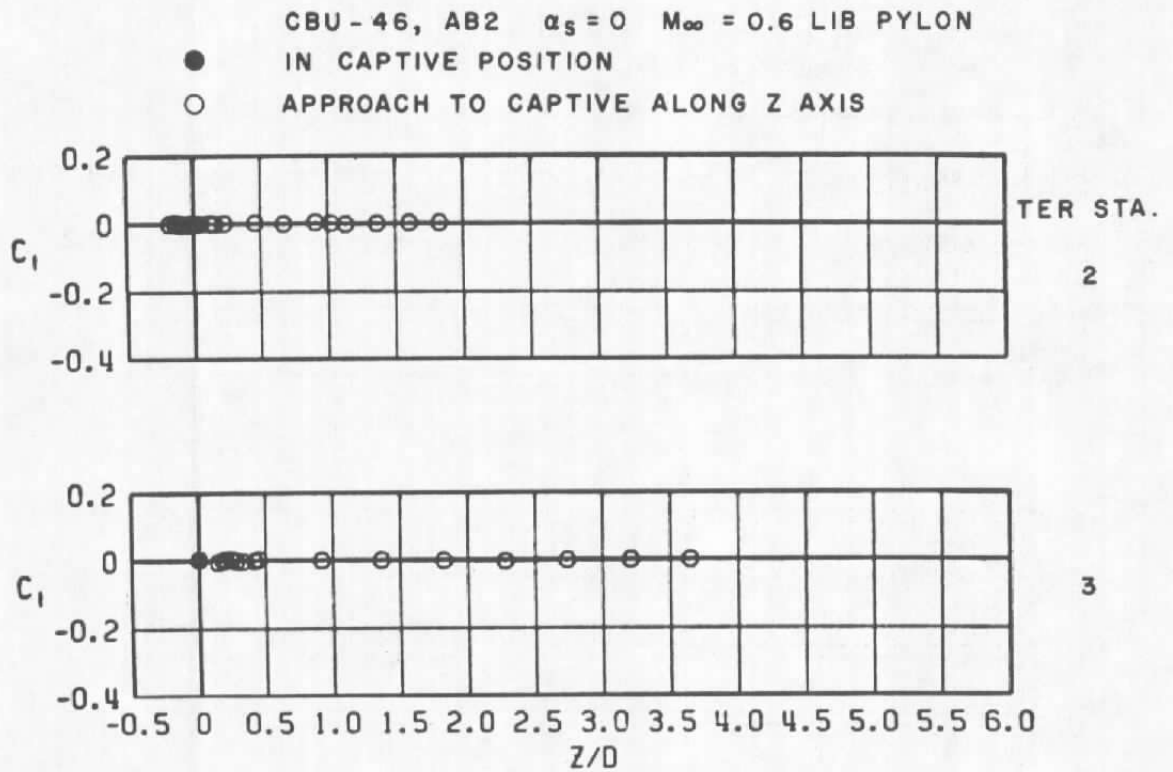
CBU-46, AB2  $\alpha_s = 0$   $M_\infty = 1.2$  LIB PYLON

● IN CAPTIVE POSITION

○ APPROACH TO CAPTIVE ALONG Z AXIS

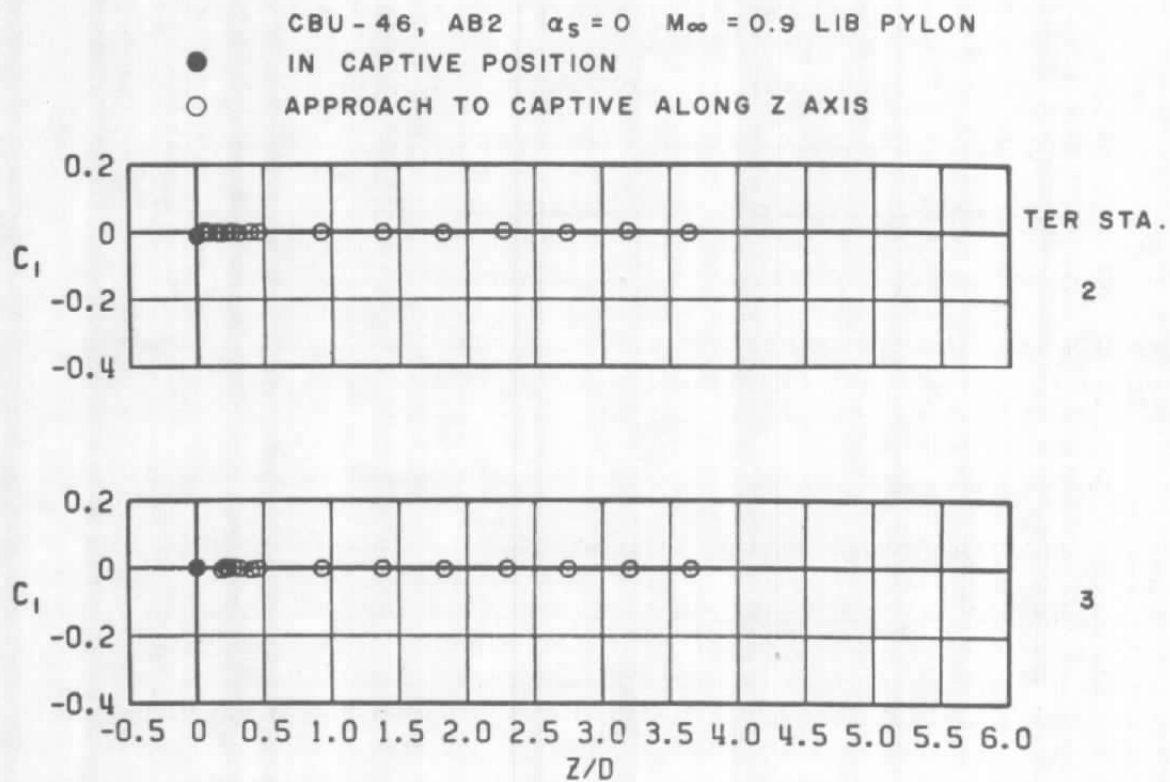


d.  $M_\infty = 1.2$   
Figure 43. Concluded.

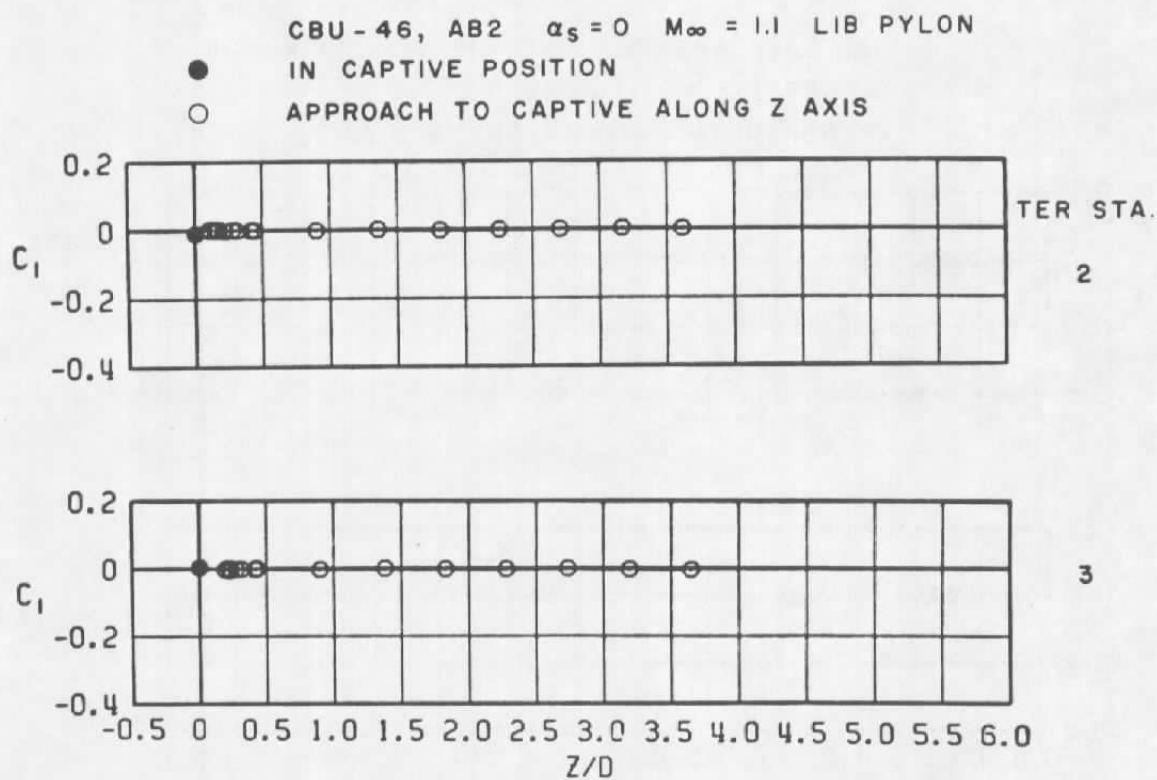


a.  $M_\infty = 0.6$

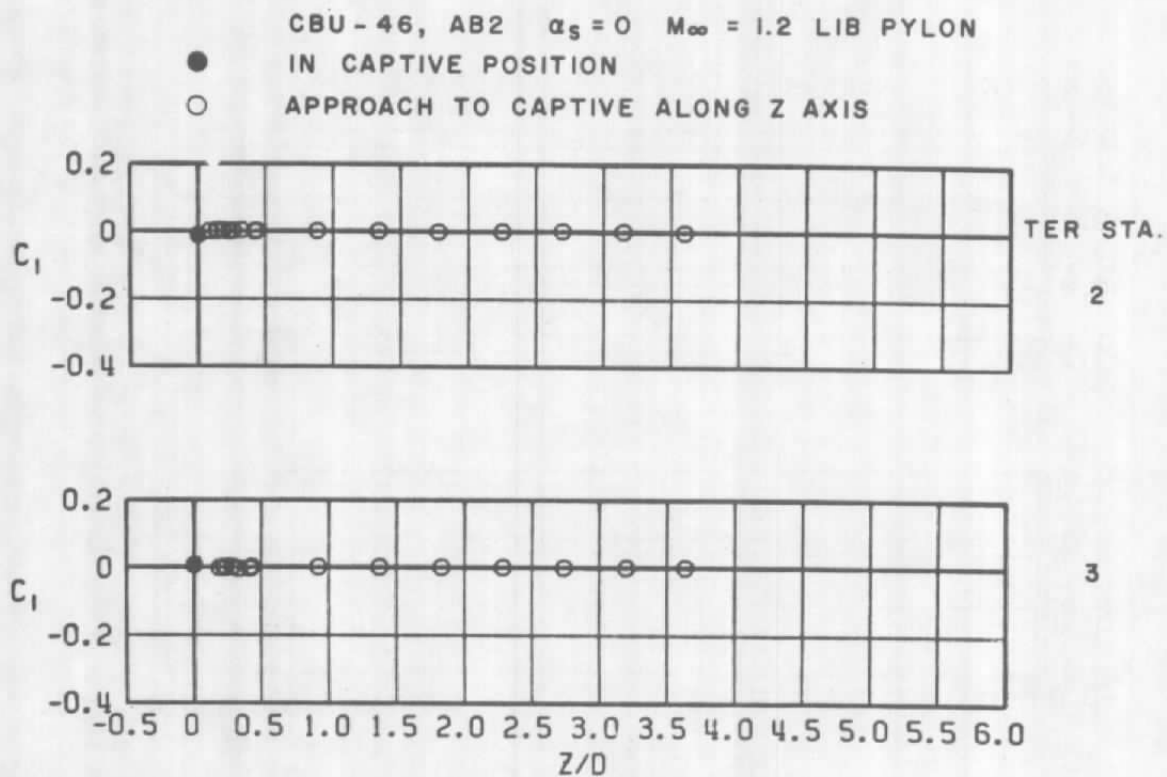
Figure 44. Coefficient of rolling moment acting on the CBU-46 (SUU-7) store as a function of normal distance between the store and two captive positions on the TER mounted on the LIB pylon.



b.  $M_\infty = 0.9$   
 Figure 44. Continued.

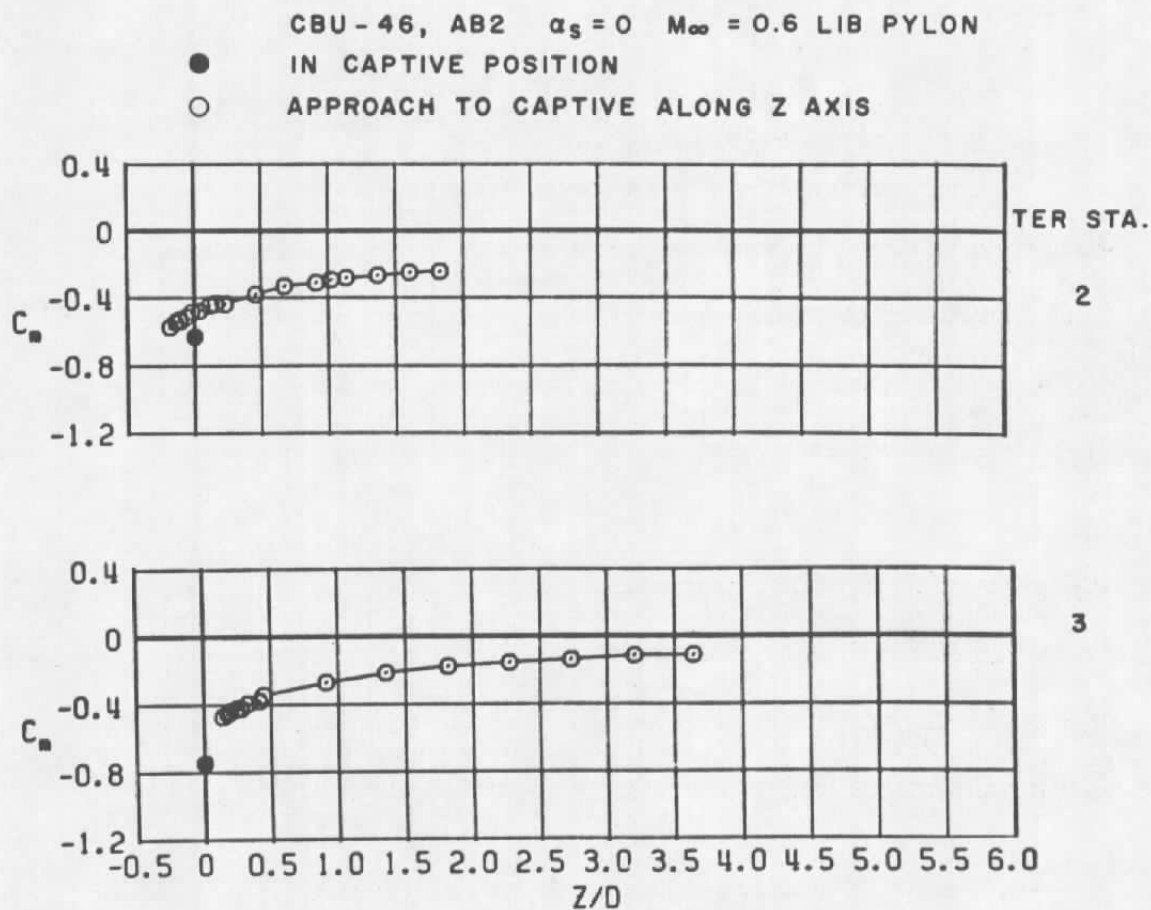


c.  $M_\infty = 1.1$   
 Figure 44. Continued.



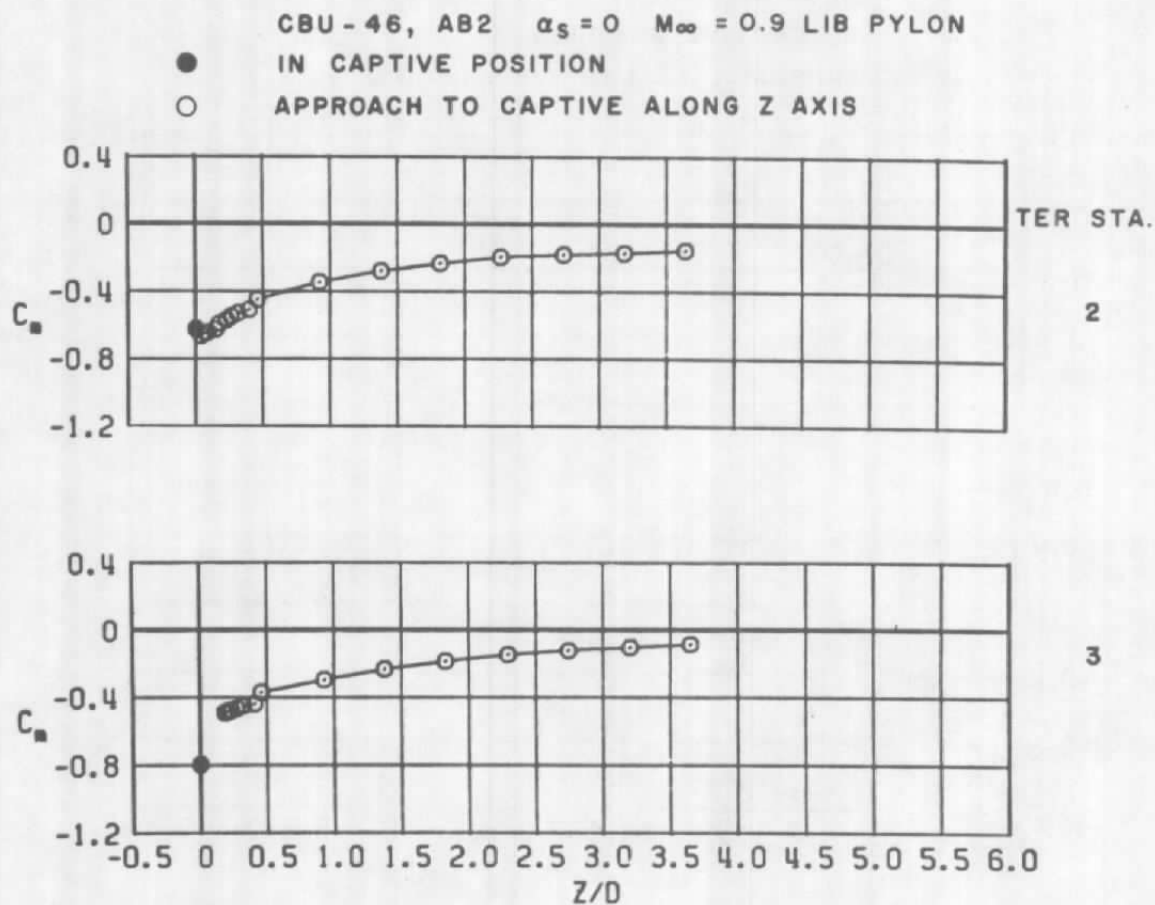
d.  $M_\infty = 1.2$   
 Figure 44. Concluded.



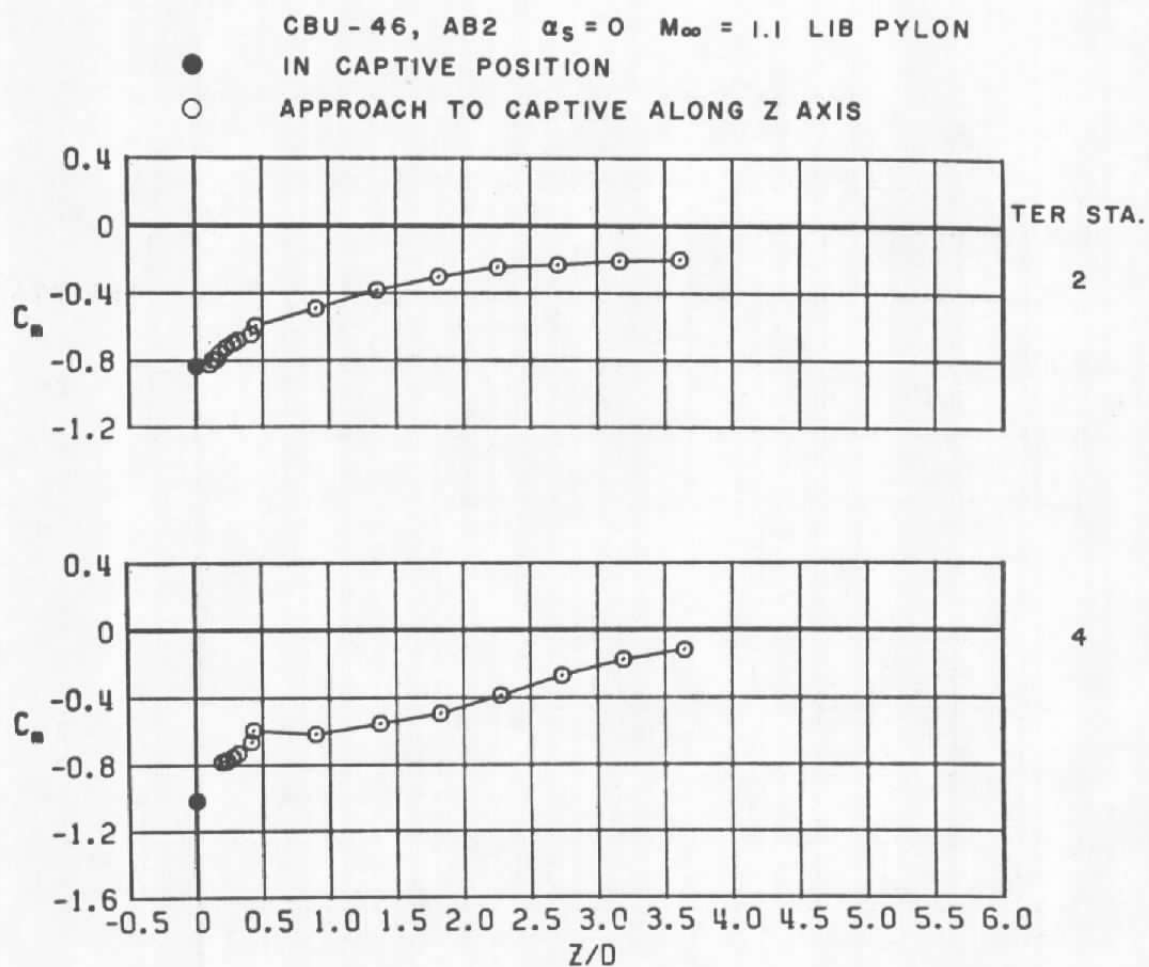


a.  $M_\infty = 0.6$

Figure 45. Coefficient of pitching moment acting on the CBU-46 (SUU-7) store as a function of normal distance between the store and two captive positions on the TER mounted on the LIB pylon.



b.  $M_\infty = 0.9$   
Figure 45. Continued.



c.  $M_\infty = 1.1$   
 Figure 45. Continued.

CBU-46, AB2  $\alpha_s = 0$   $M_\infty = 1.2$  LIB PYLON

● IN CAPTIVE POSITION

○ APPROACH TO CAPTIVE ALONG Z AXIS

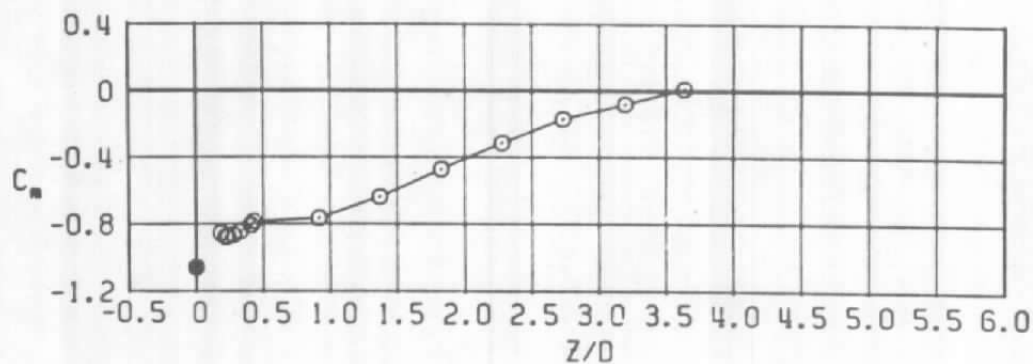
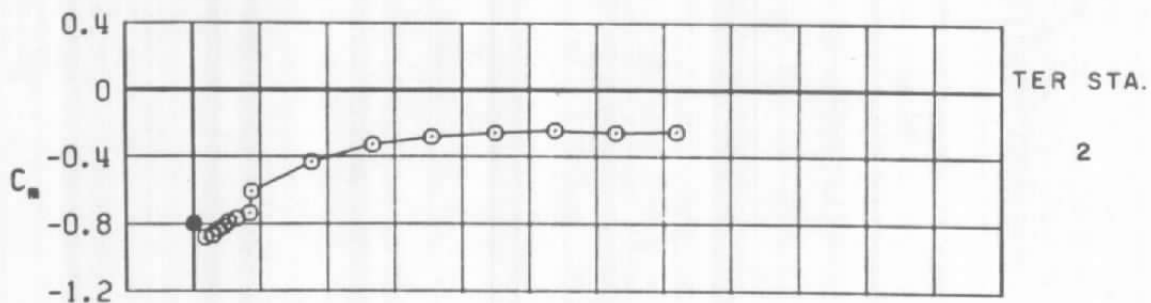
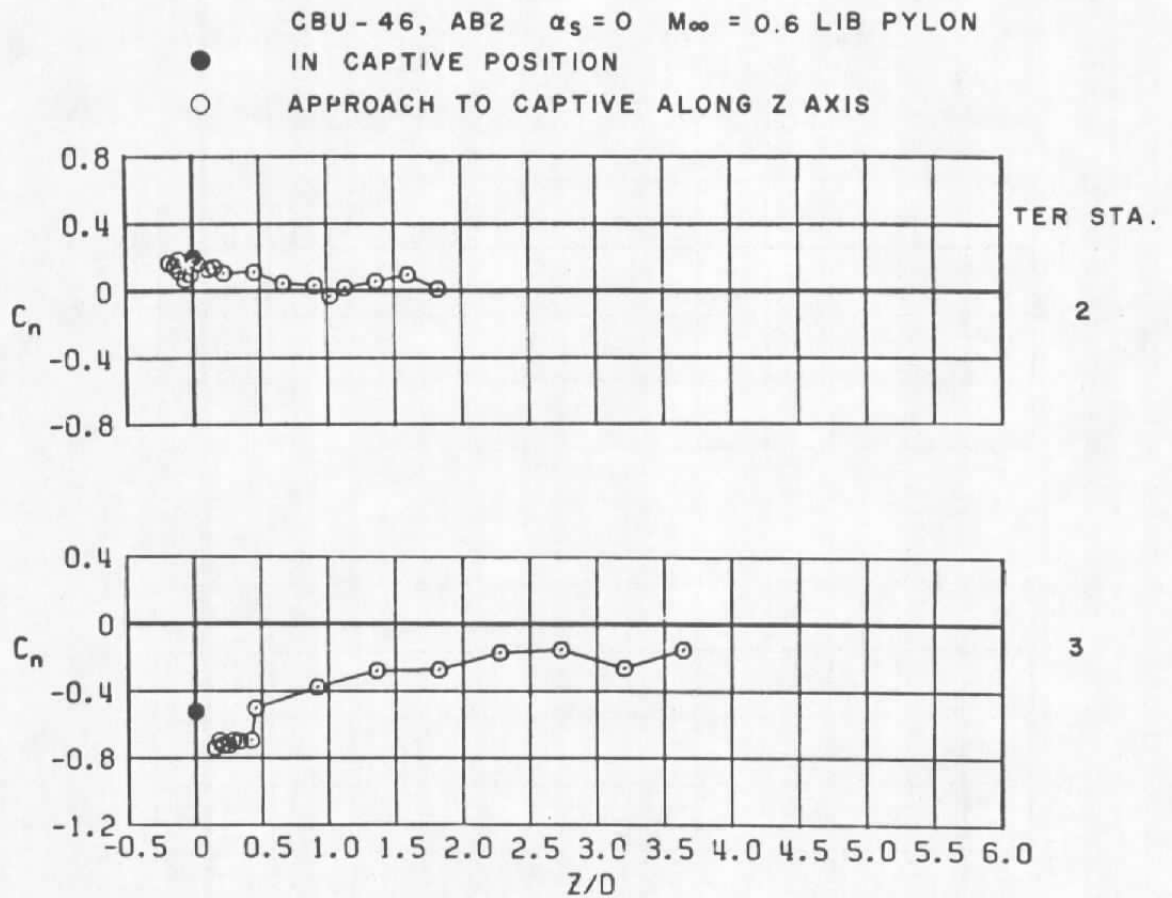
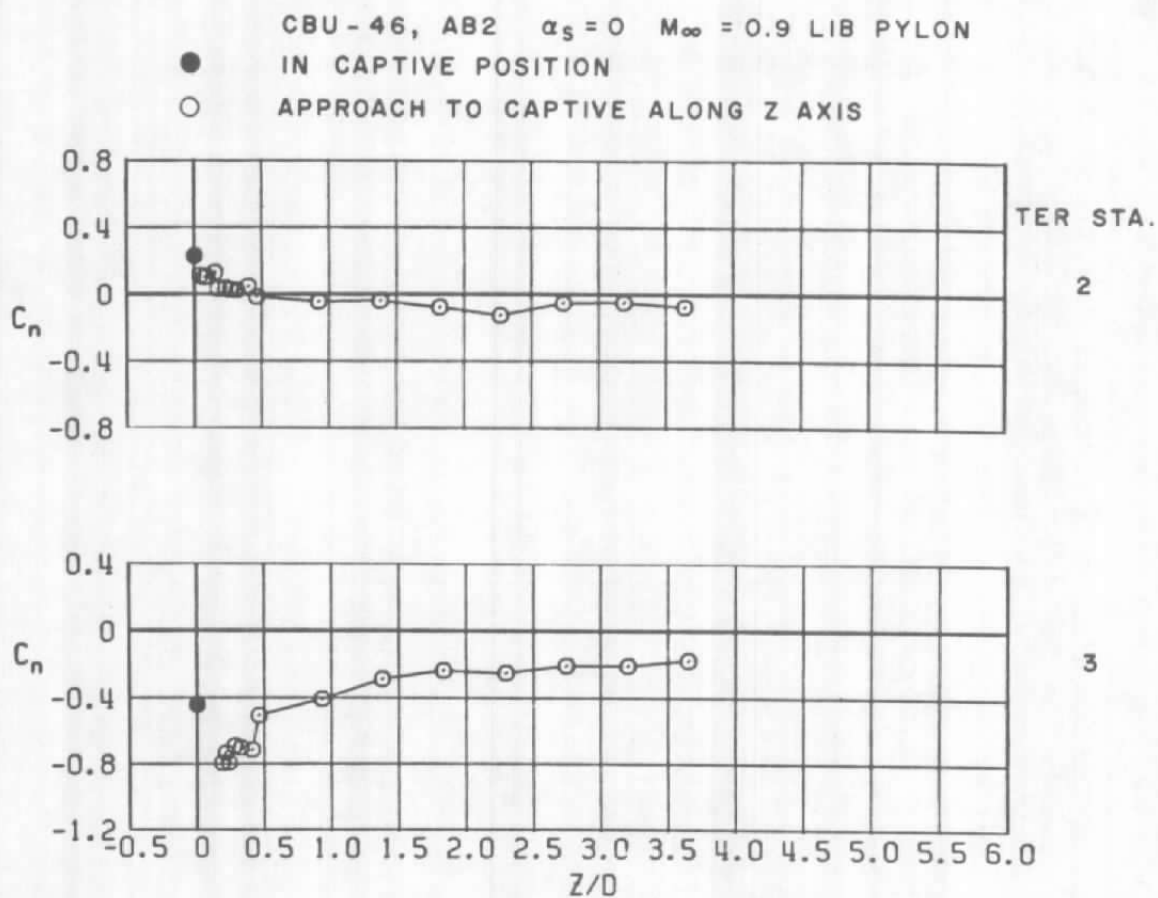
d.  $M_\infty = 1.2$ 

Figure 45. Concluded.

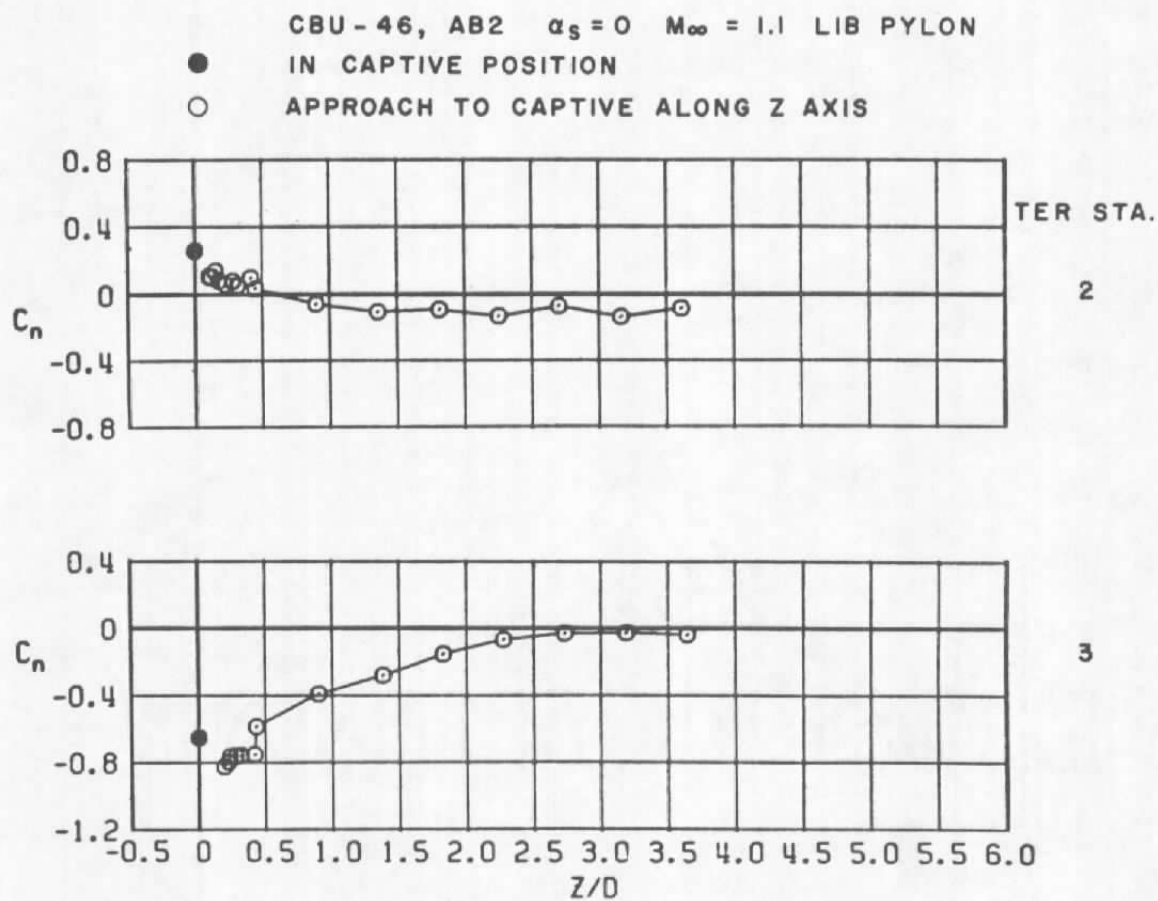


a.  $M_\infty = 0.6$

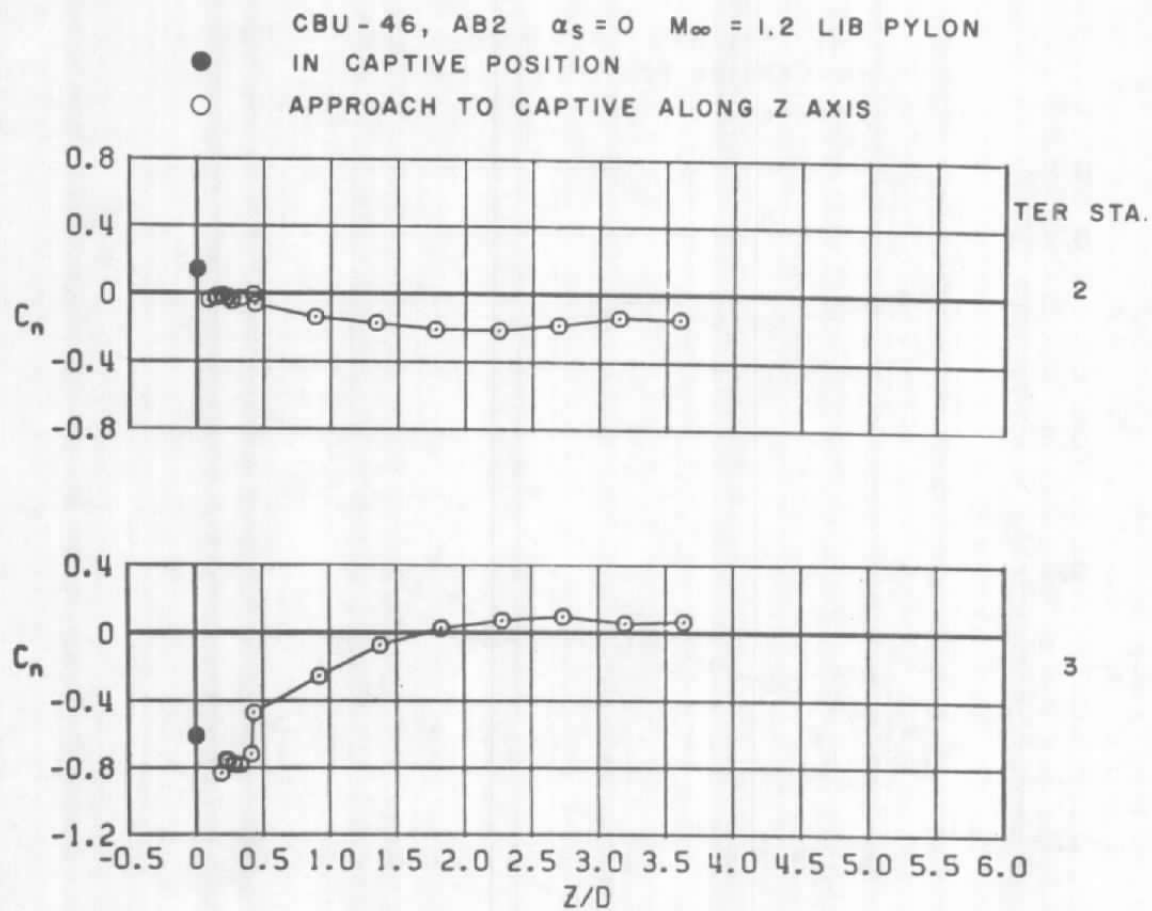
Figure 46. Coefficient of yawing moment acting on the CBU-46 (SUU-7) store as a function of normal distance between the store and two captive positions on the TER mounted on the LIB pylon.



b.  $M_\infty = 0.9$   
 Figure 46. Continued.

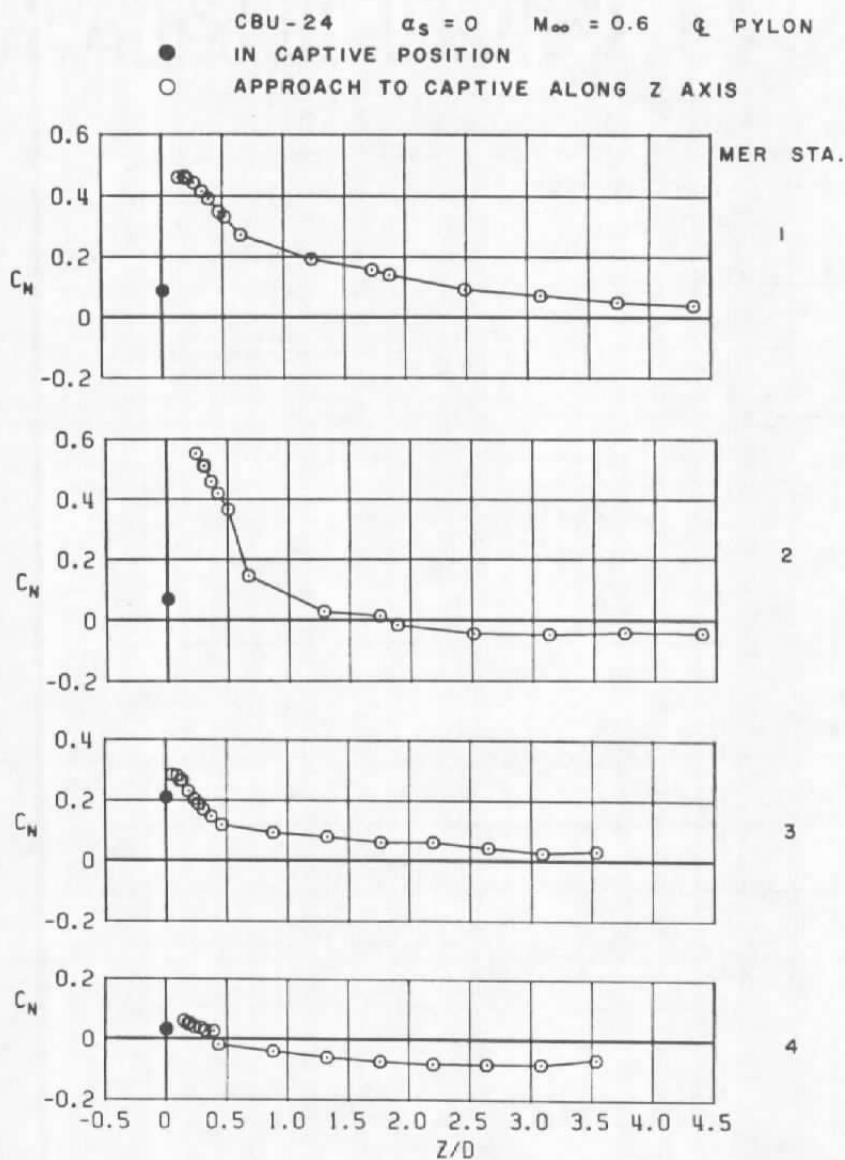


c.  $M_\infty = 1.1$   
 Figure 46. Continued.



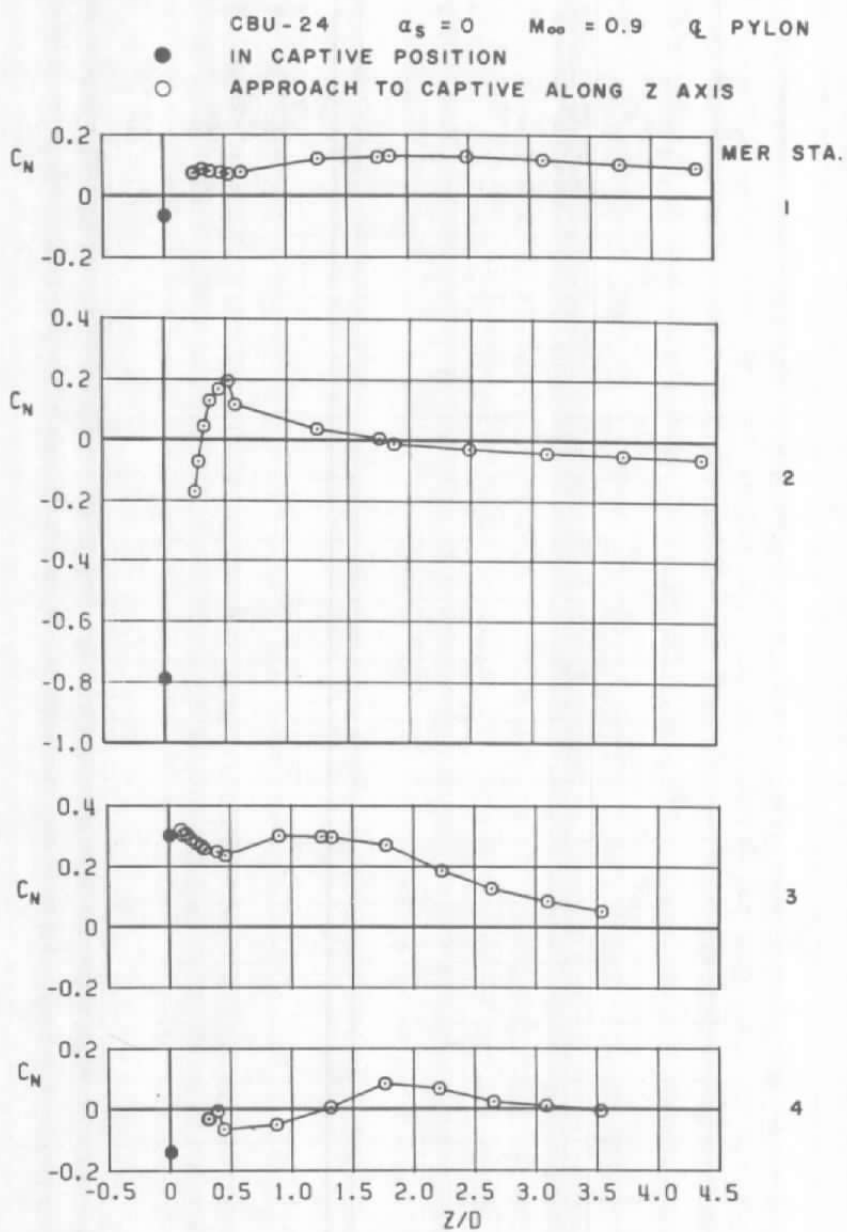
d.  $M_\infty = 1.2$   
 Figure 46. Concluded.



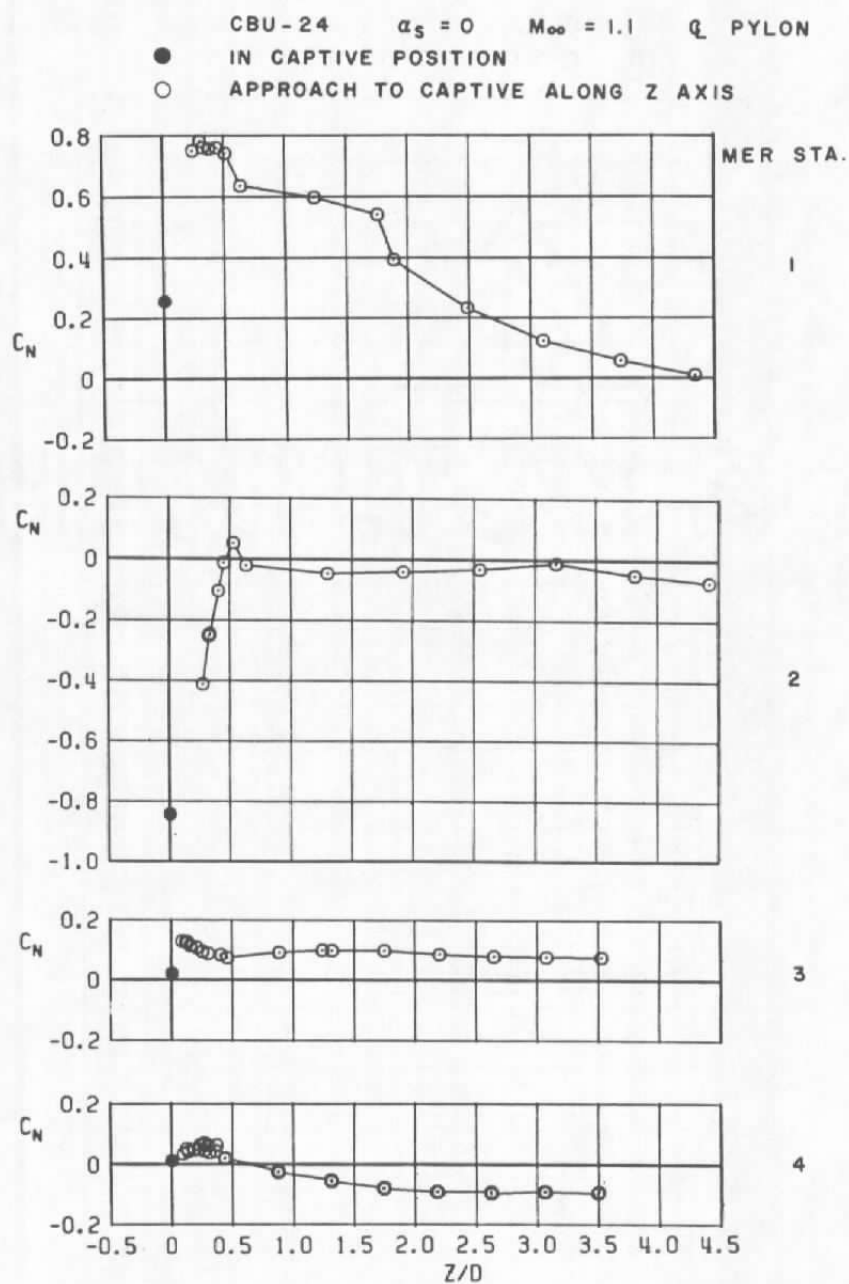


a.  $M_{\infty} = 0.6$

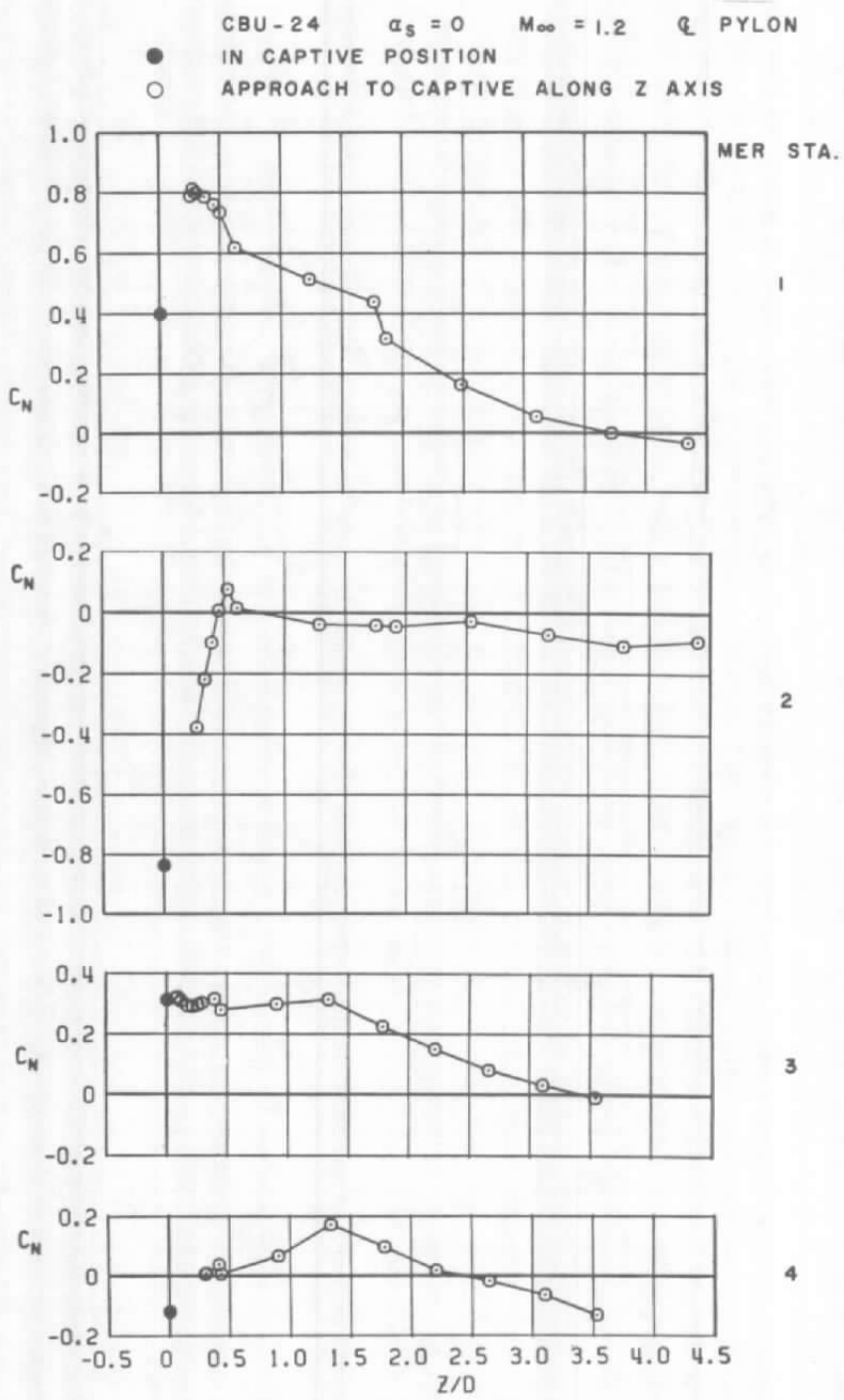
Figure 47. Coefficient of normal force acting on the CBU-24 (SUU-30) store as a function of normal distance between the store and four captive positions on the MER mounted on the C-L pylon.



b.  $M_{\infty} = 0.9$   
 Figure 47. Continued.



c.  $M_\infty = 1.1$   
Figure 47. Continued.



d.  $M_\infty = 1.2$   
 Figure 47. Concluded.

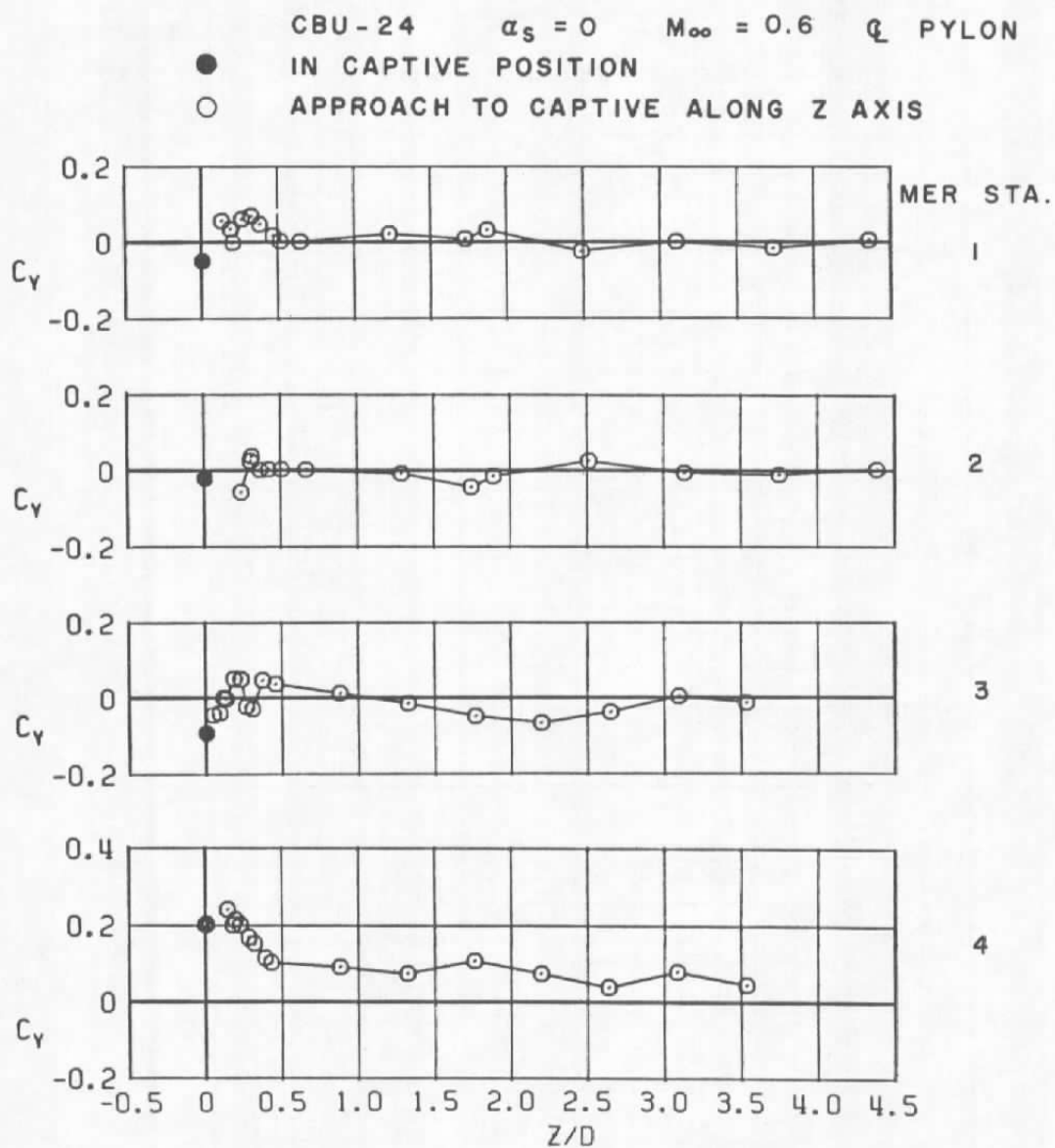
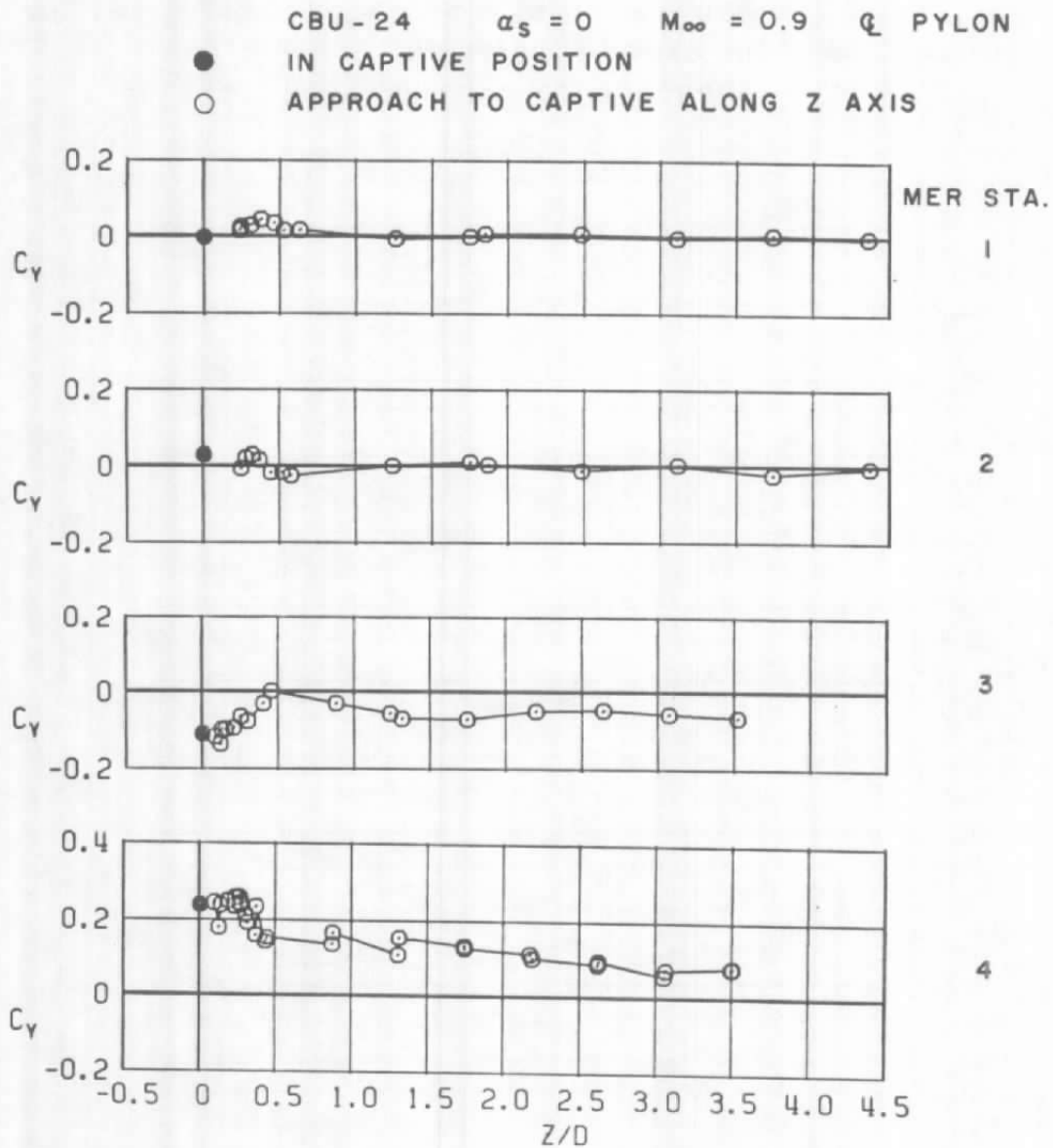
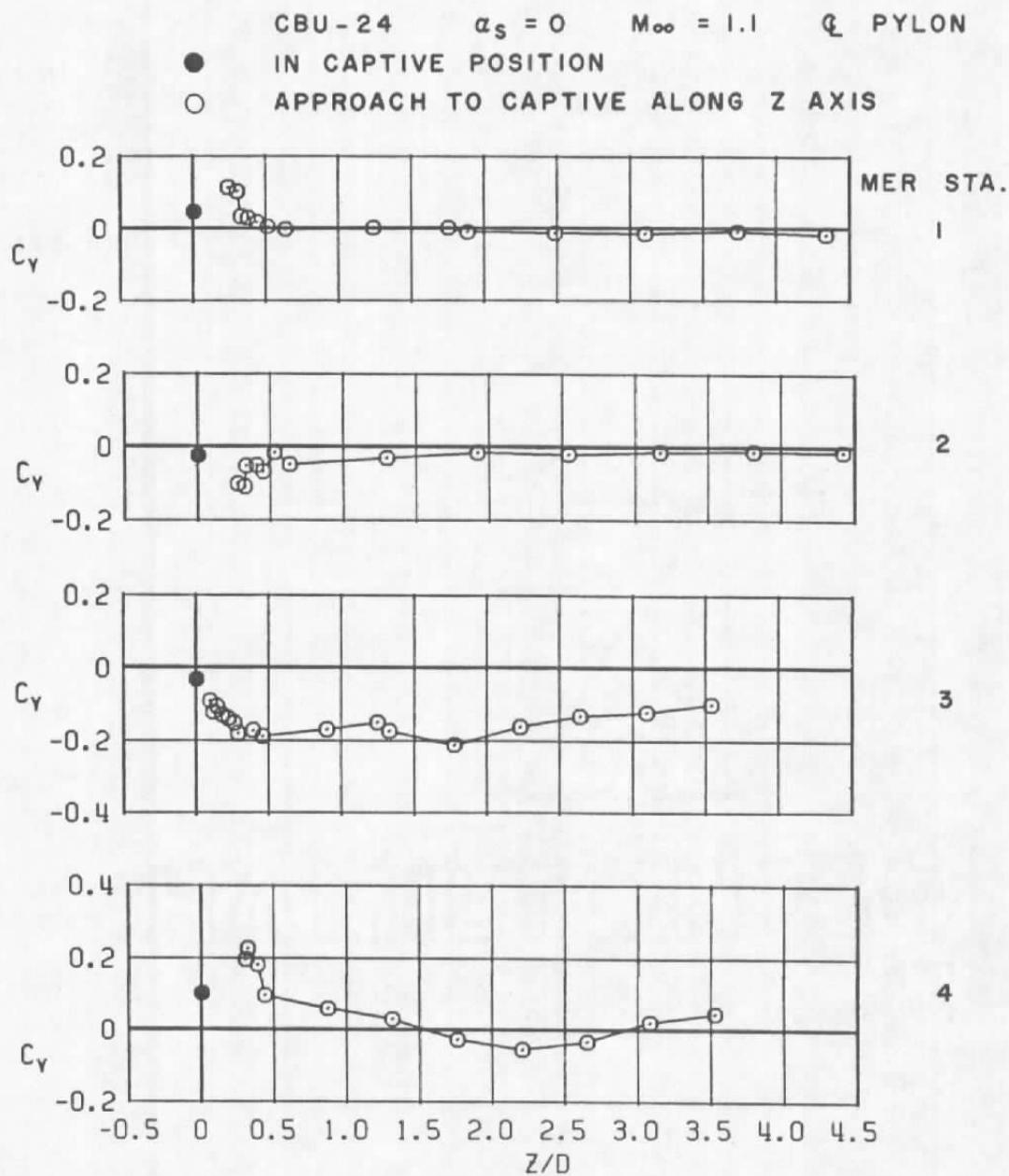
a.  $M_\infty = 0.6$ 

Figure 48. Coefficient of side force acting on the CBU-24 (SUU-30) store as a function of normal distance between the store and four captive positions on the MER mounted on the C-L pylon.-



b.  $M_{\infty} = 0.9$   
Figure 48. Continued.

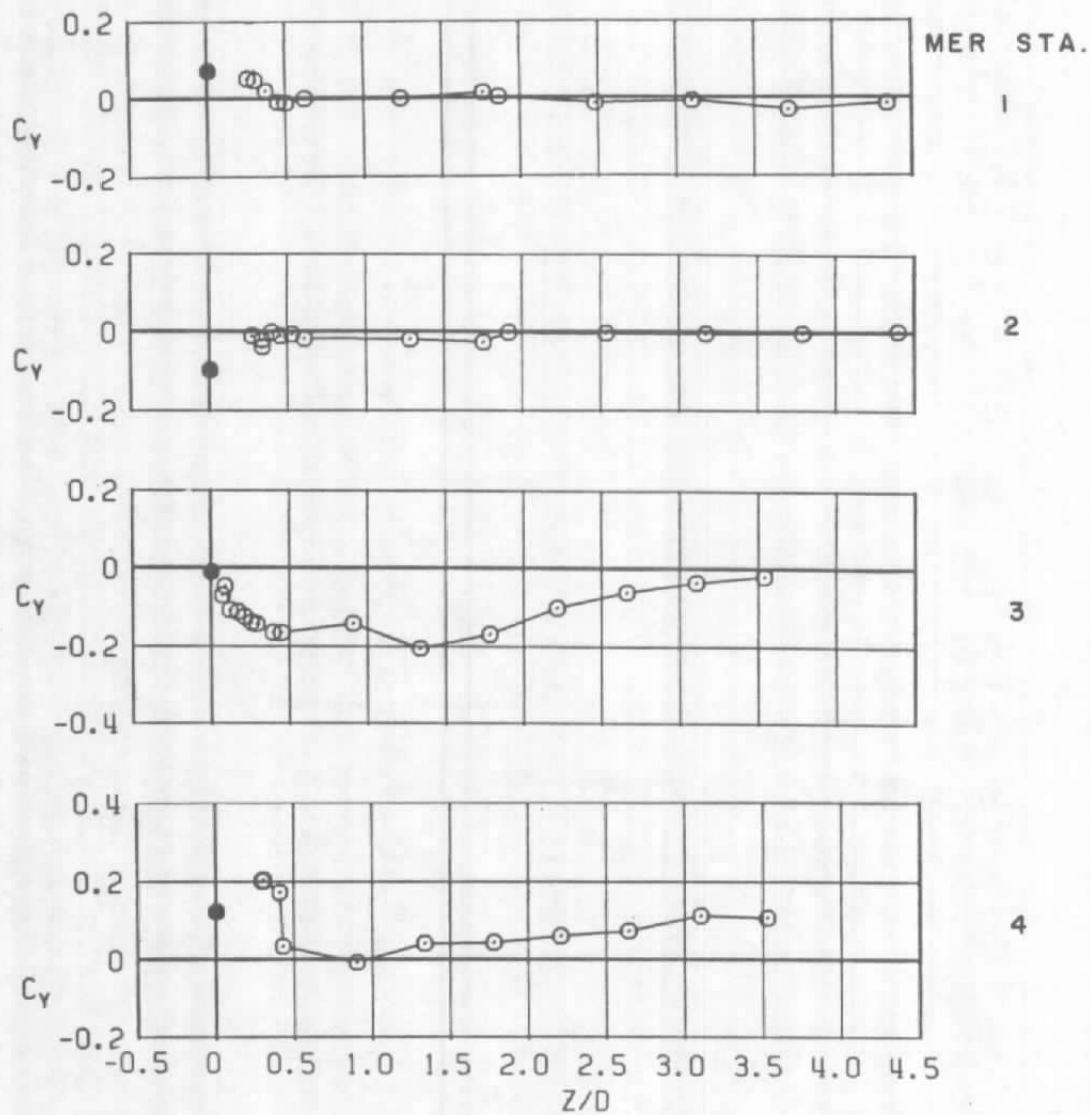


c.  $M_\infty = 1.1$   
Figure 48. Continued.

CUB-24  $\alpha_s = 0$   $M_\infty = 1.2$   $\zeta$  PYLON

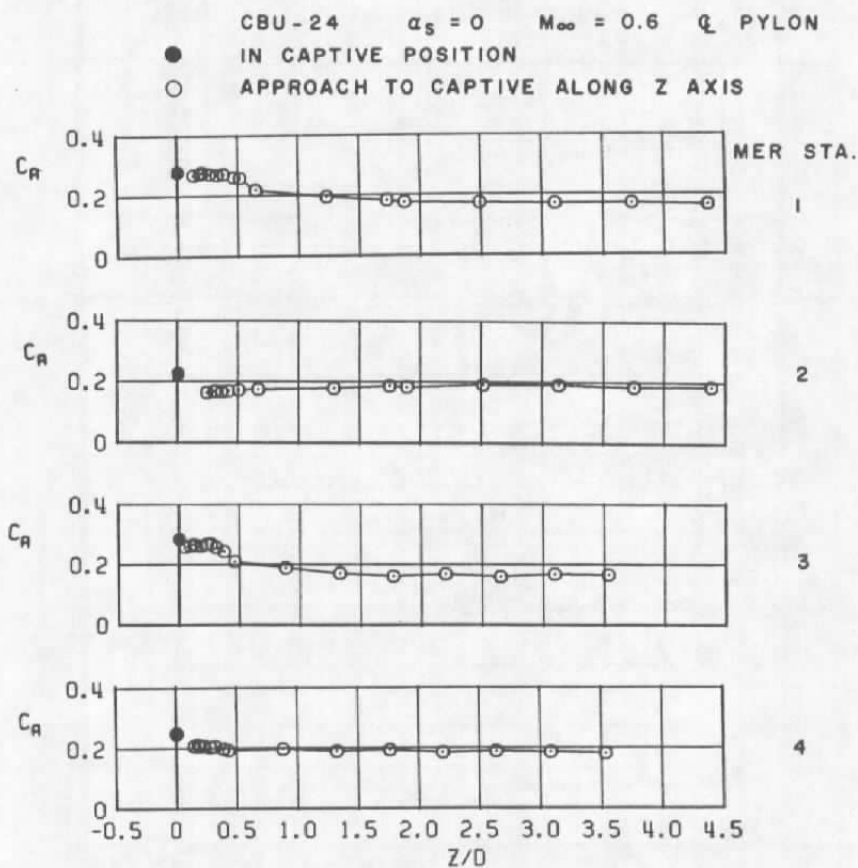
● IN CAPTIVE POSITION

○ APPROACH TO CAPTIVE ALONG Z AXIS



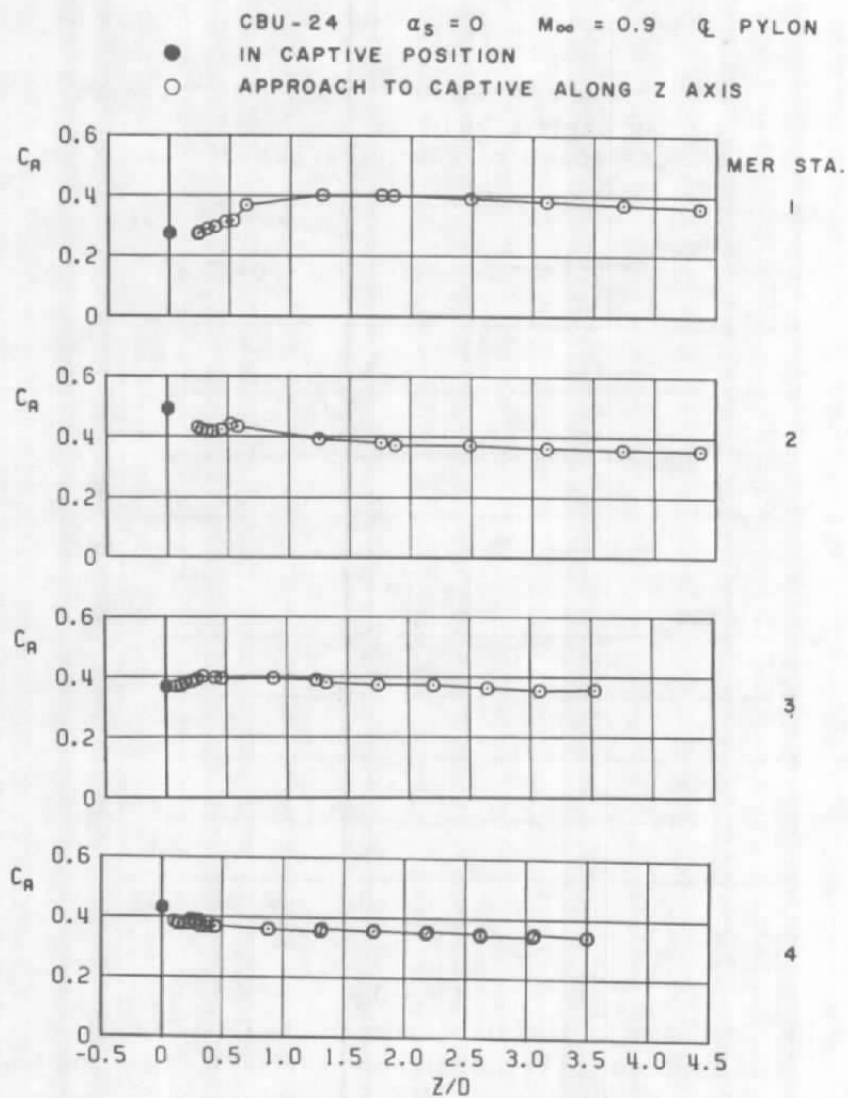
d.  $M_\infty = 1.2$   
Figure 48. Concluded.



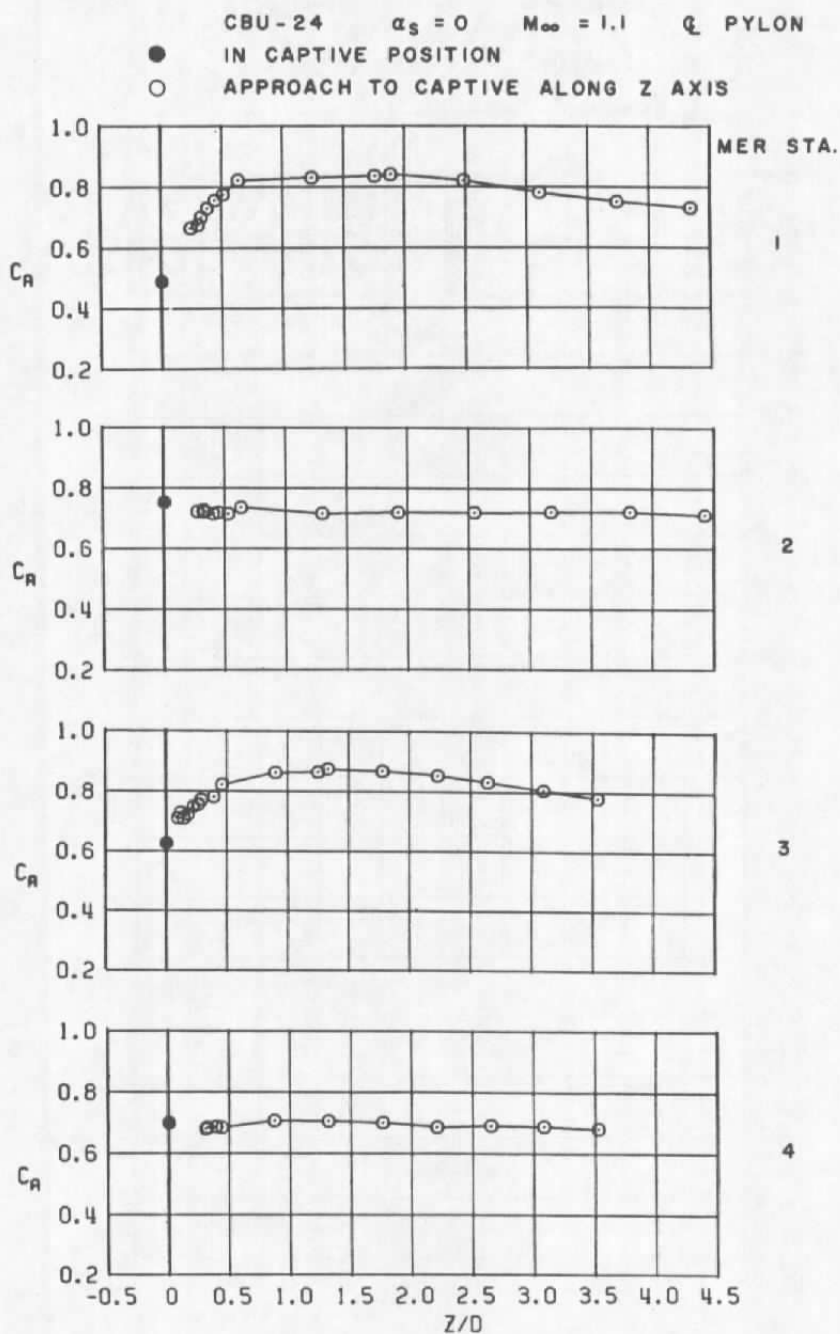


a.  $M_\infty = 0.6$

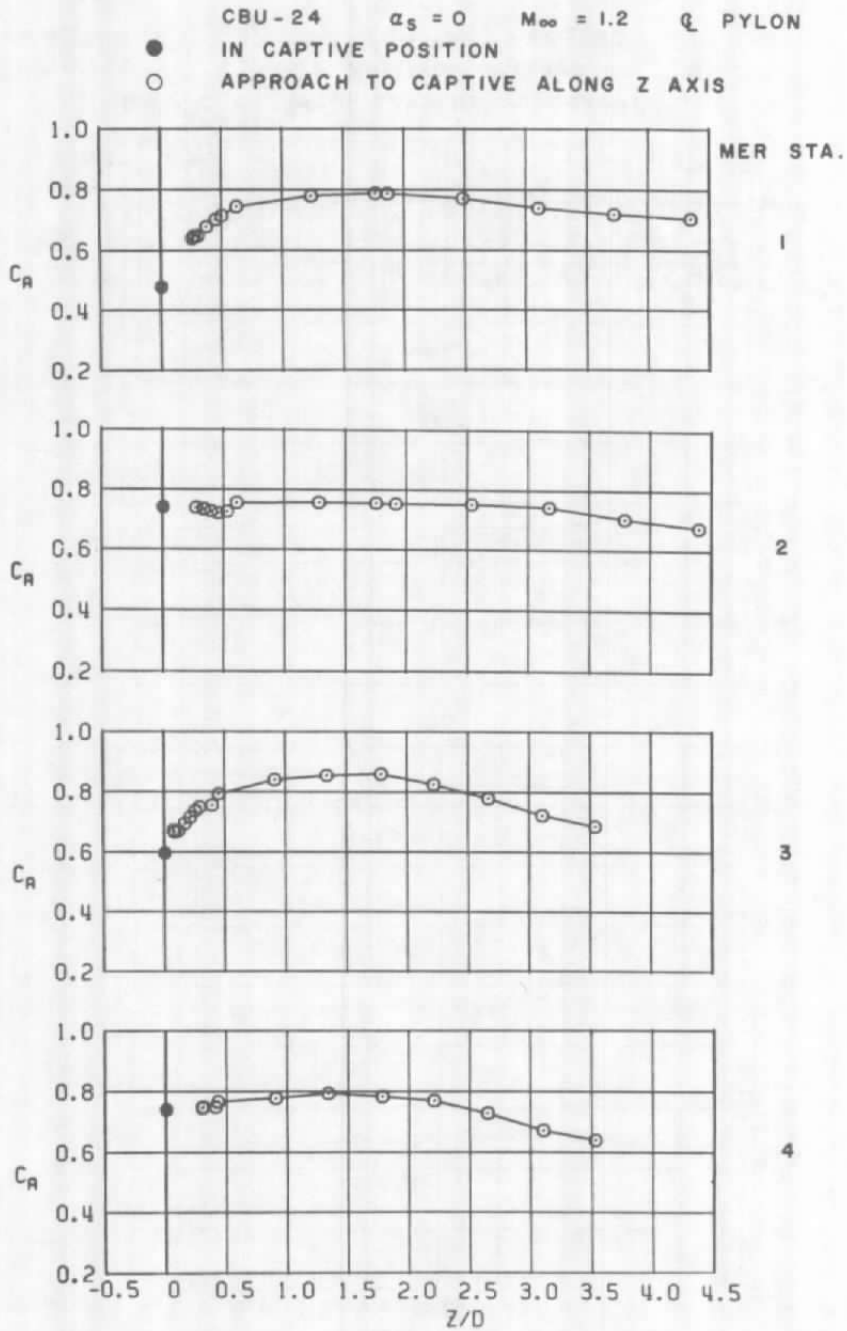
Figure 49. Coefficient of axial force acting on the CBU-24 (SUU-30) store as a function of normal distance between the store and four captive positions on the MER mounted on the C-L pylon.



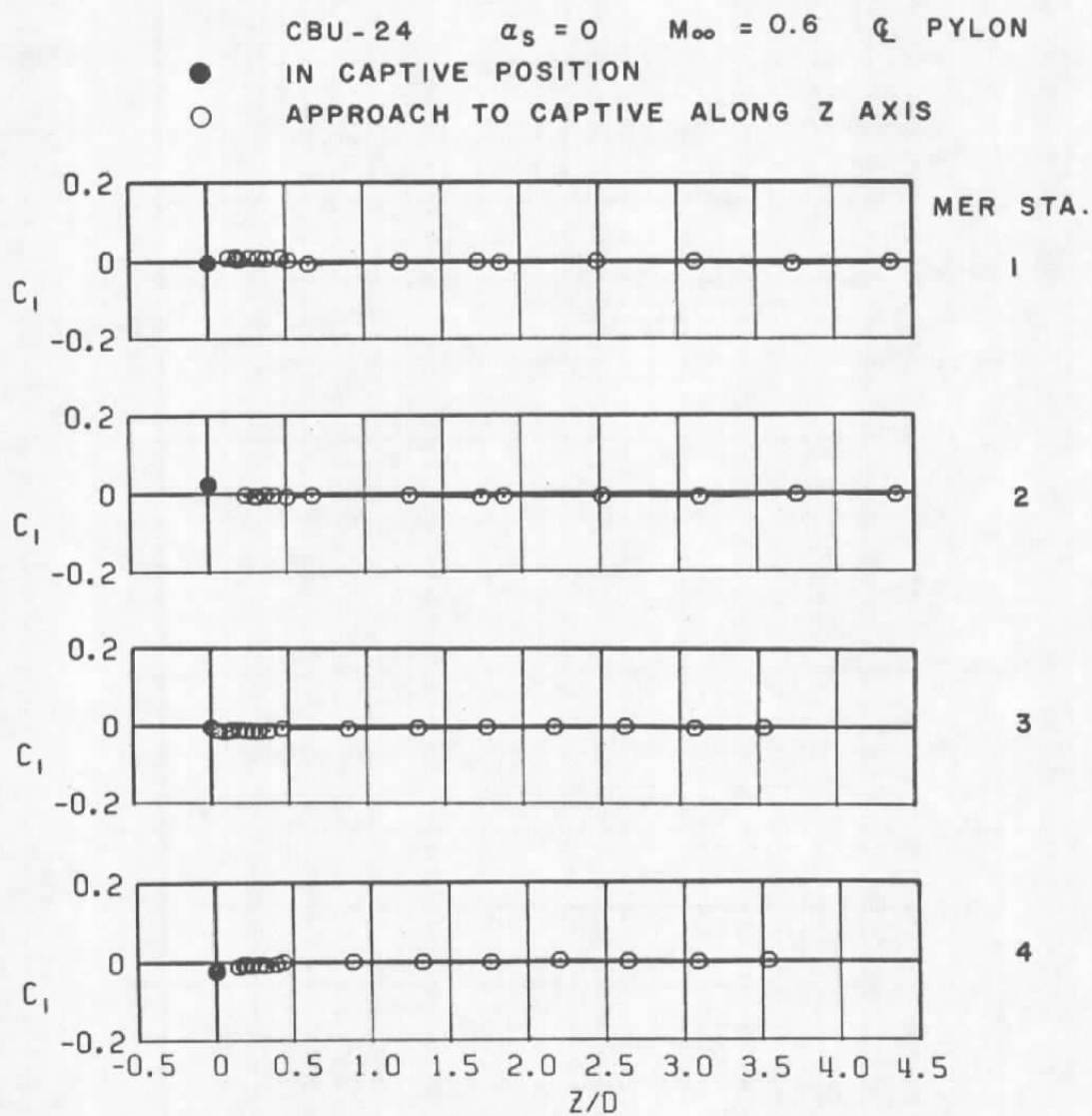
b.  $M_\infty = 0.9$   
 Figure 49. Continued.



c.  $M_\infty = 1.1$   
 Figure 49. Continued.



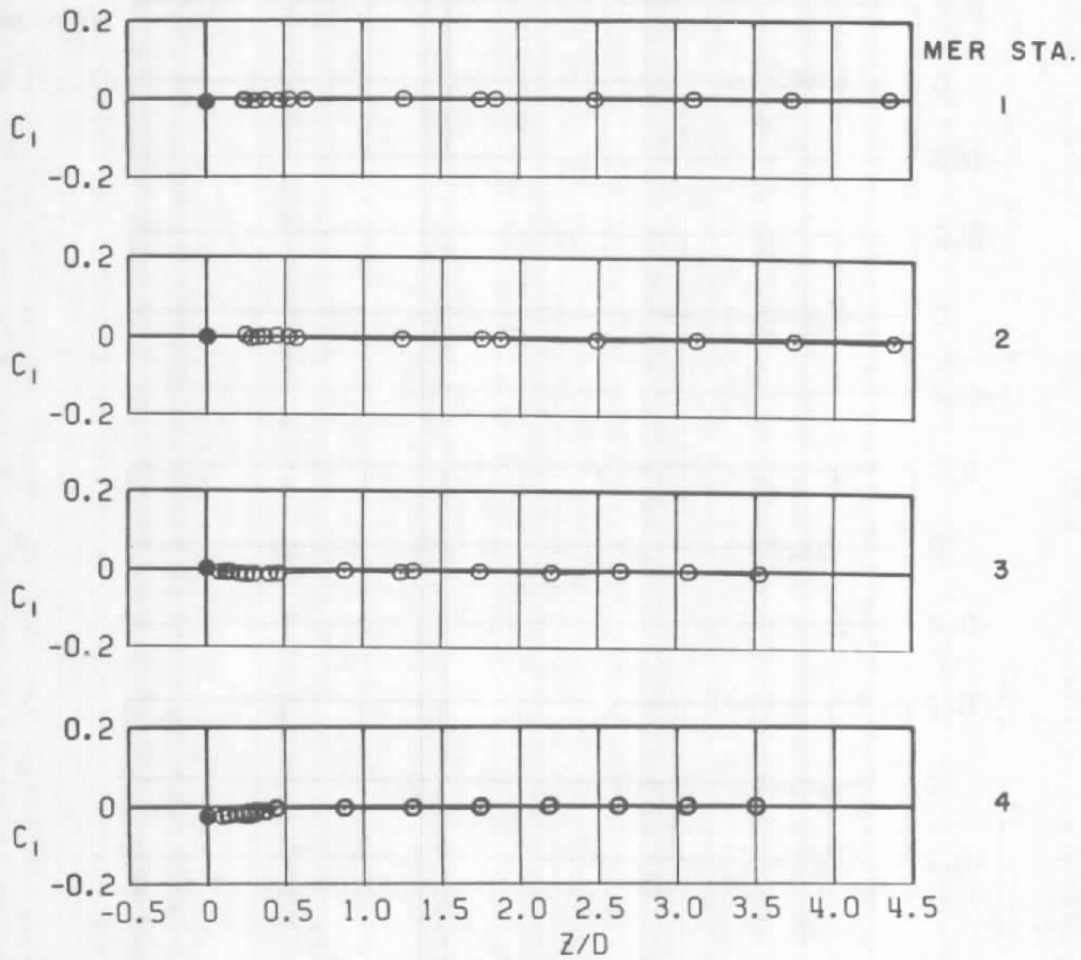
d.  $M_{\infty} = 1.2$   
 Figure 49. Concluded.



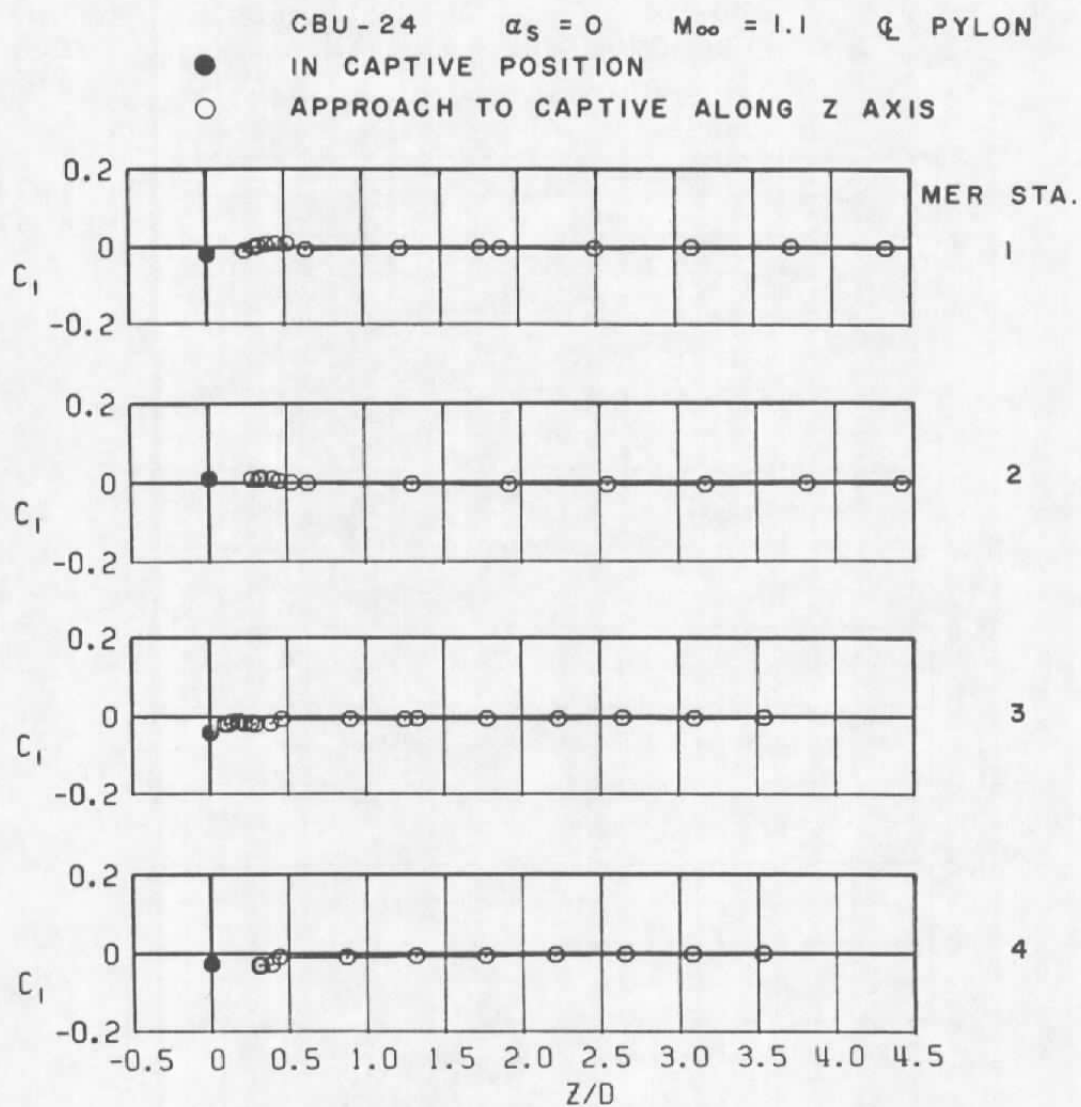
a.  $M_\infty = 0.6$

Figure 50. Coefficient of rolling moment acting on the CBU-24 (SUU-30) store as a function of normal distance between the store and four captive positions on the MER mounted on the C-L pylon.

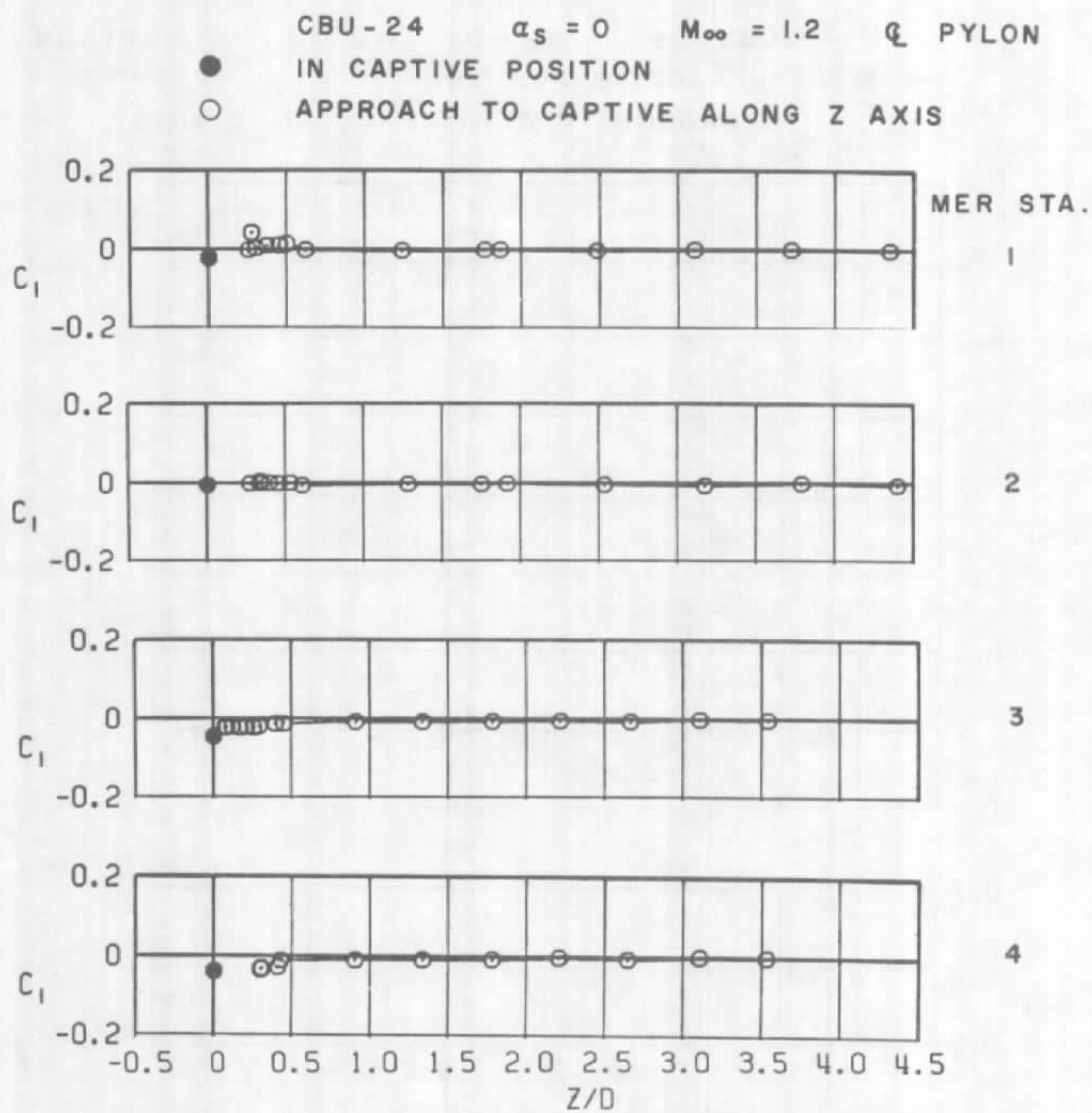
CBU-24       $\alpha_s = 0$        $M_\infty = 0.9$        $Q_L$  PYLON  
 ● IN CAPTIVE POSITION  
 ○ APPROACH TO CAPTIVE ALONG Z AXIS



b.  $M_\infty = 0.9$   
 Figure 50. Continued.

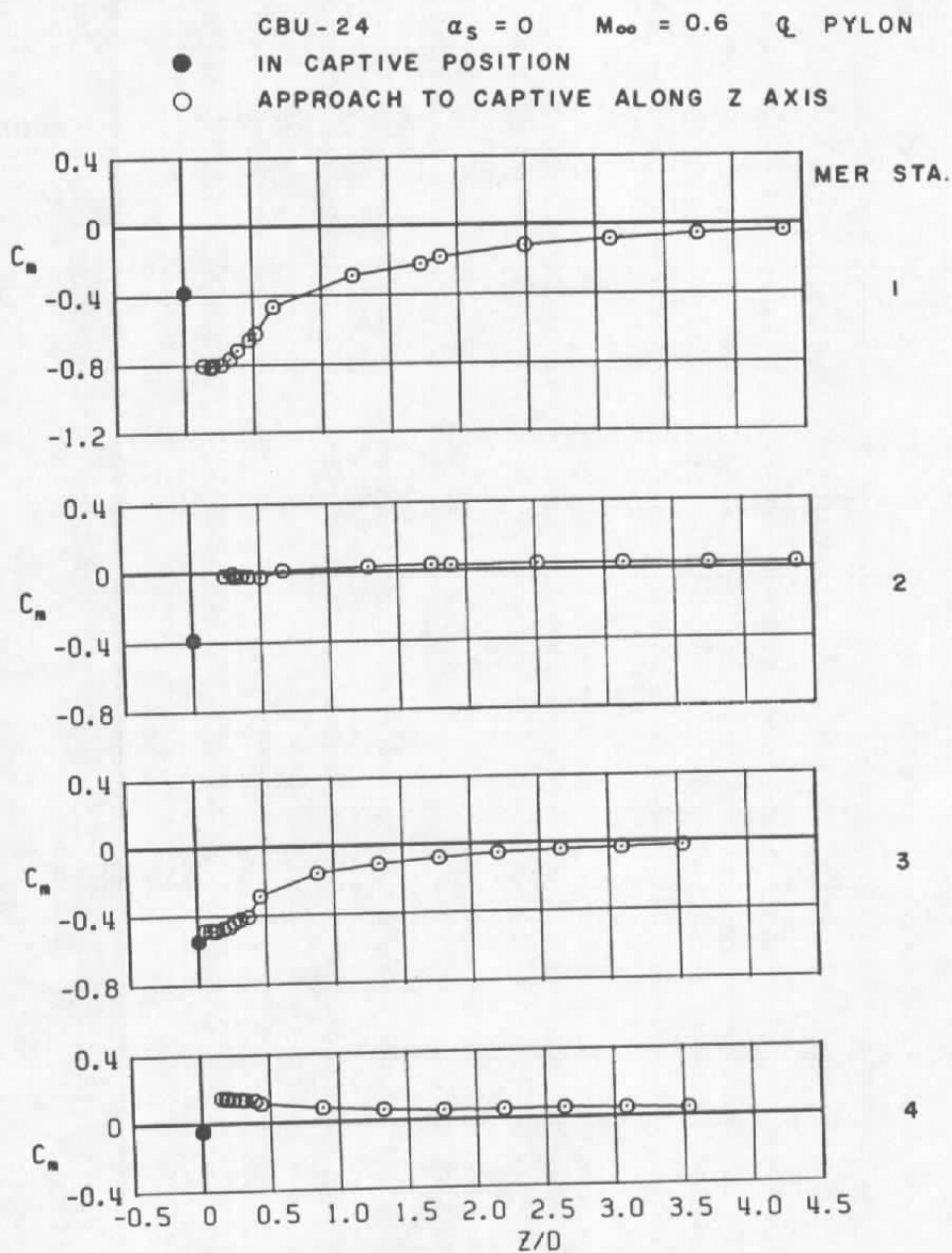


c.  $M_{\infty} = 1.1$   
 Figure 50. Continued.



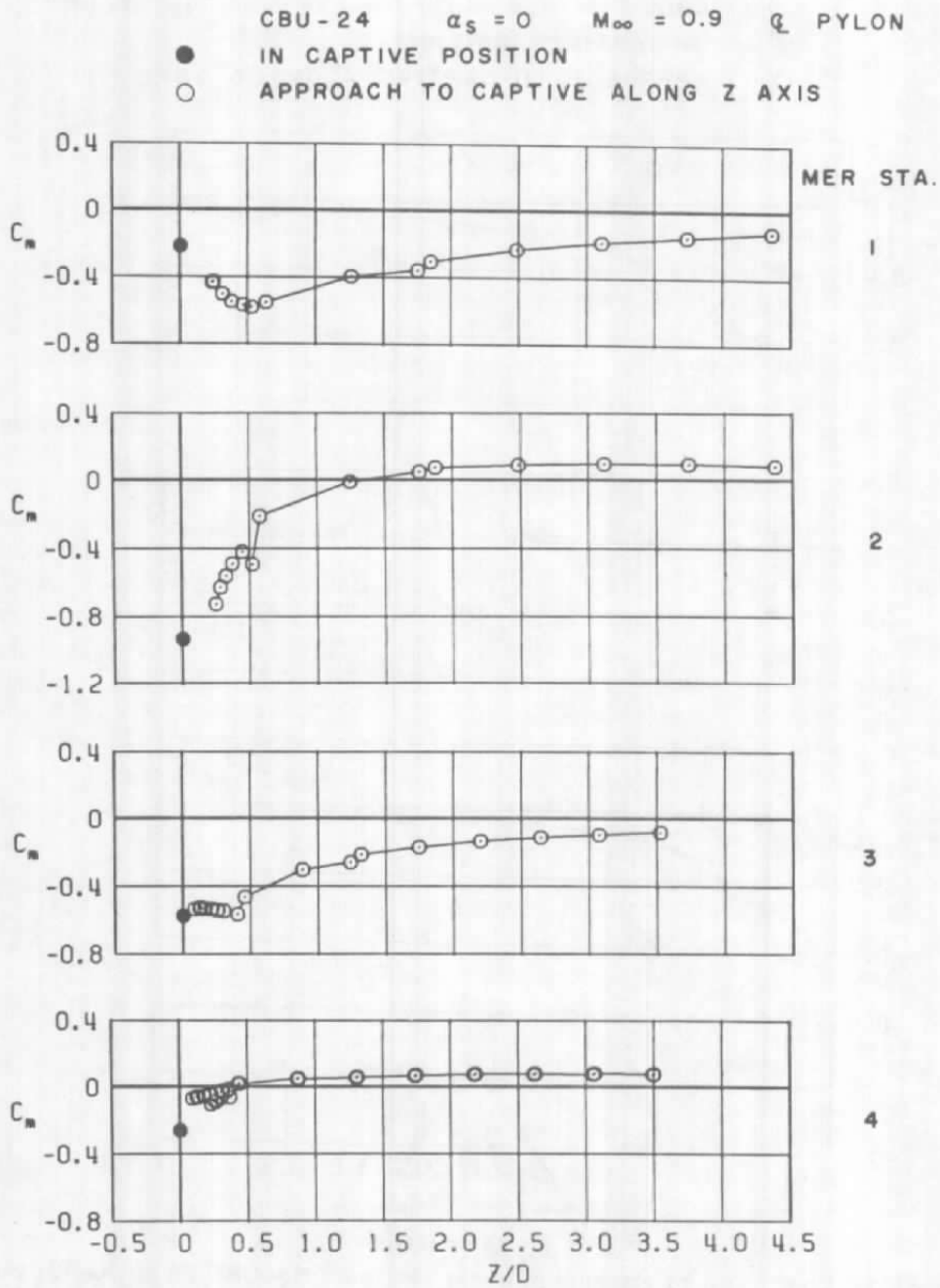
d.  $M_\infty = 1.2$   
 Figure 50. Concluded.





a.  $M_\infty = 0.6$

Figure 51. Coefficient of pitching moment acting on the CBU-24 (SUU-30) store as a function of normal distance between the store and four captive positions on the MER mounted on the C-L pylon.

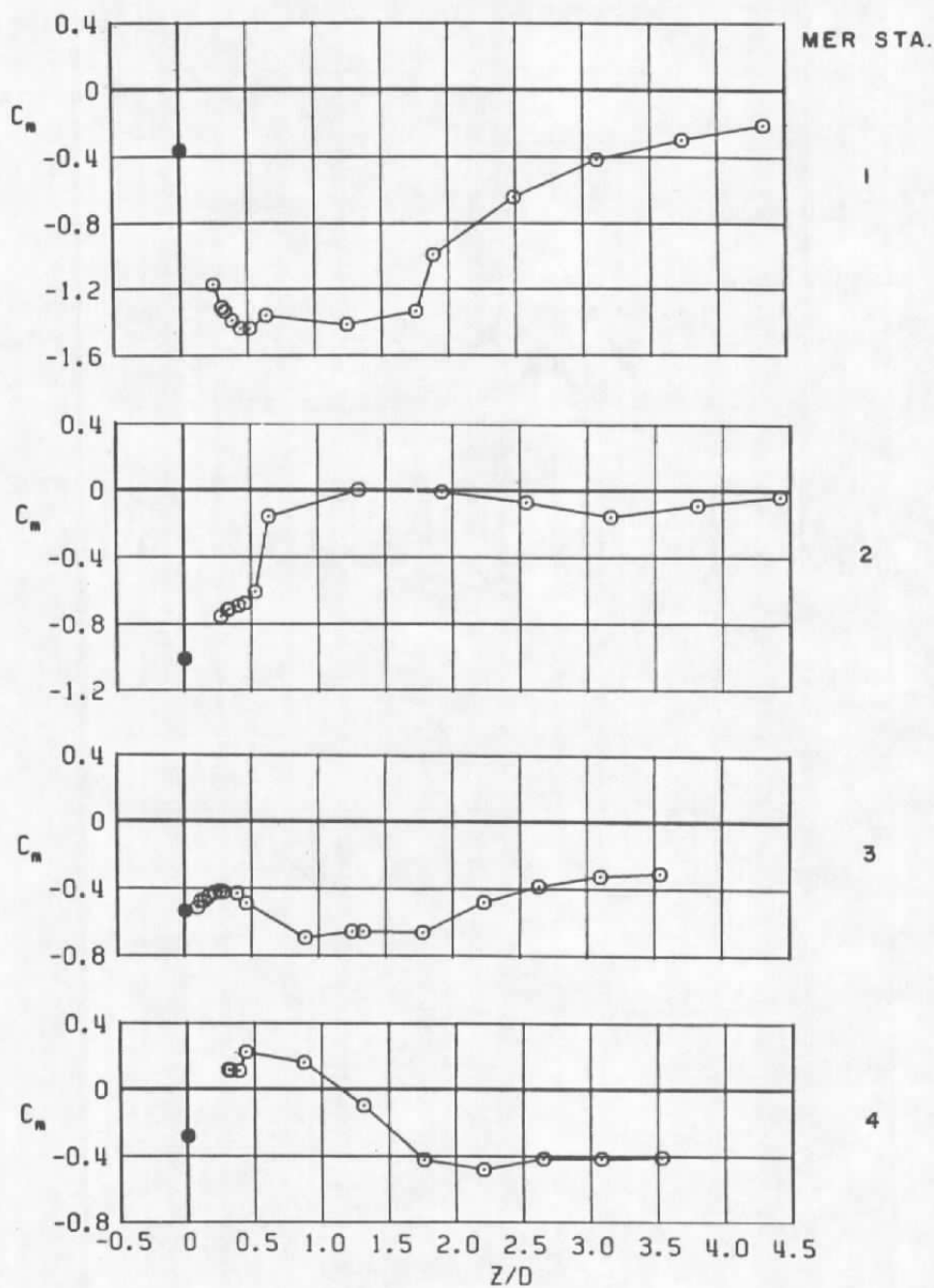


b.  $M_\infty = 0.9$   
 Figure 51. Continued.

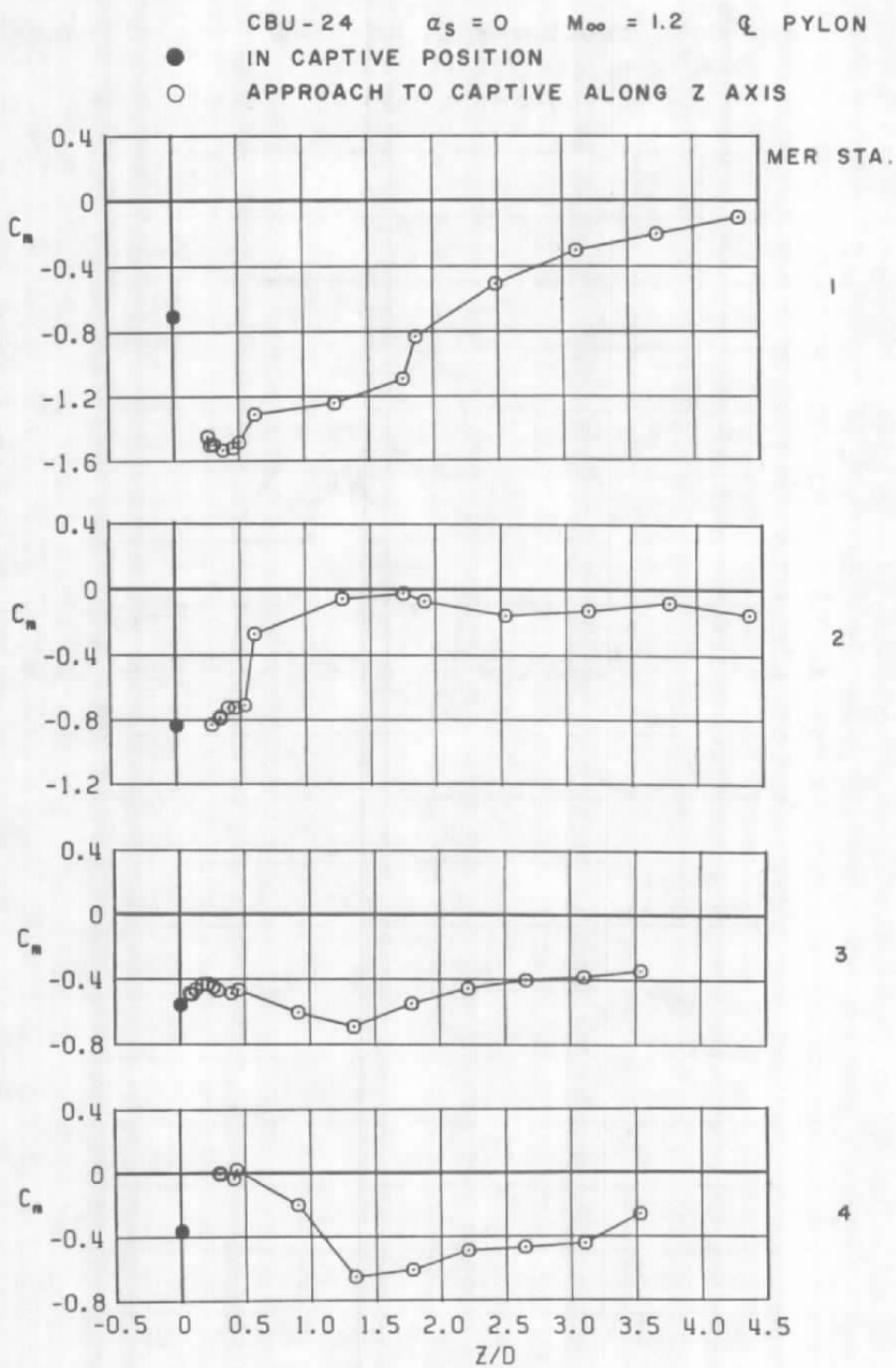
CBU-24  $\alpha_s = 0$   $M_{\infty} = 1.1$   $Q$  PYLON

● IN CAPTIVE POSITION

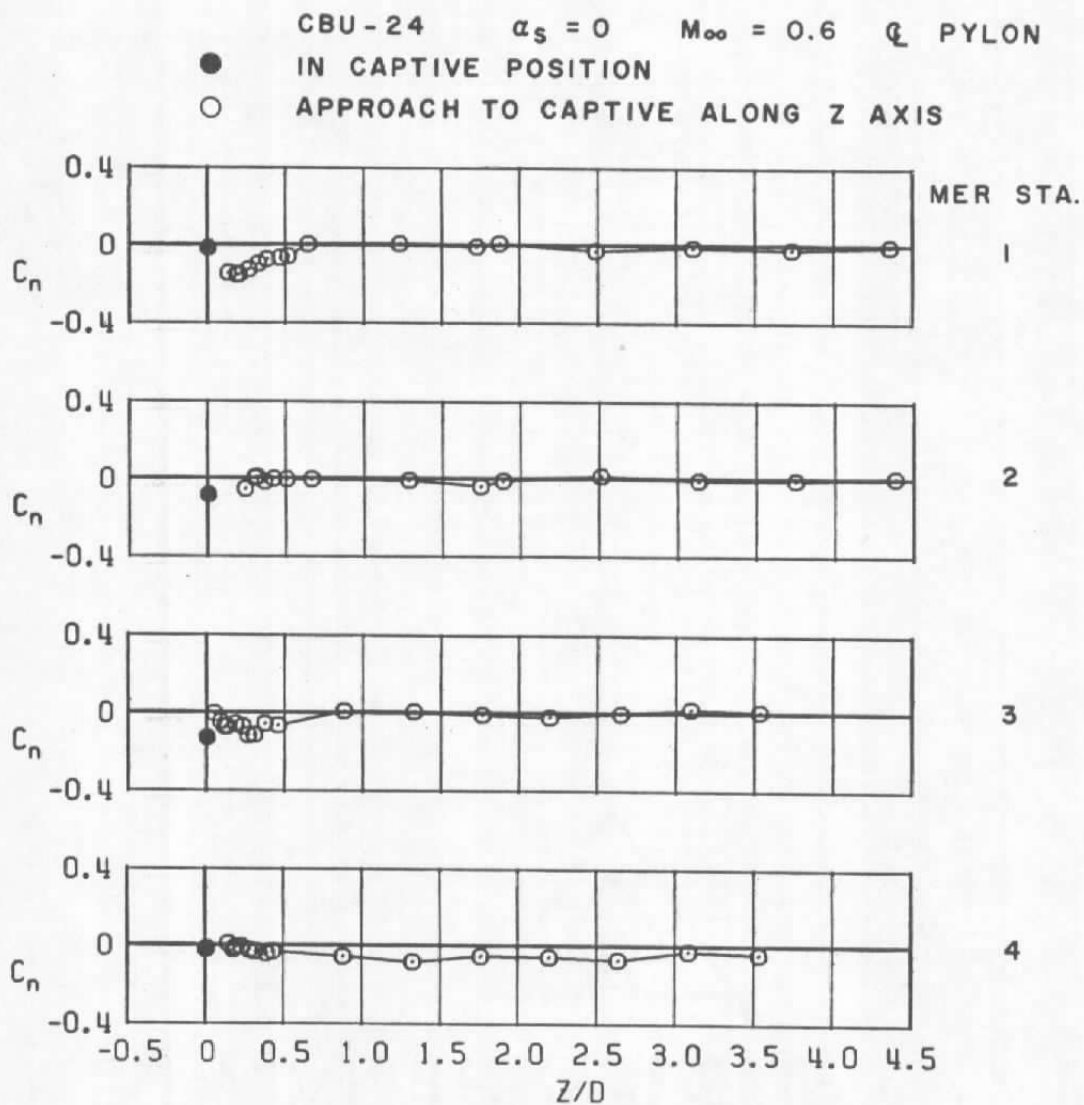
○ APPROACH TO CAPTIVE ALONG Z AXIS



c.  $M_{\infty} = 1.1$   
Figure 51. Continued.



d.  $M_\infty = 1.2$   
 Figure 51. Concluded.



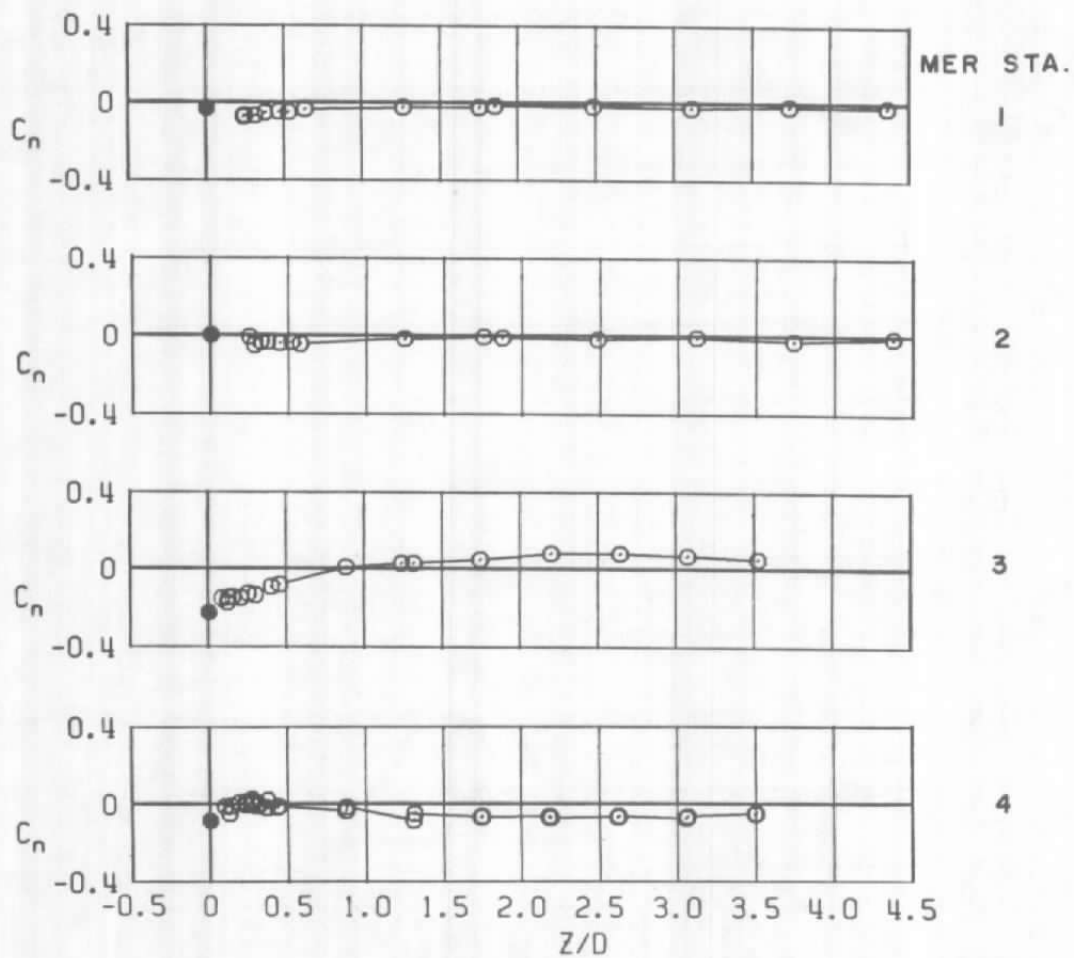
a.  $M_\infty = 0.6$

Figure 52. Coefficient of yawing moment acting on the CBU-24 (SUU-30) store as a function of normal distance between the store and four captive positions on the MER mounted on the C-L pylon.

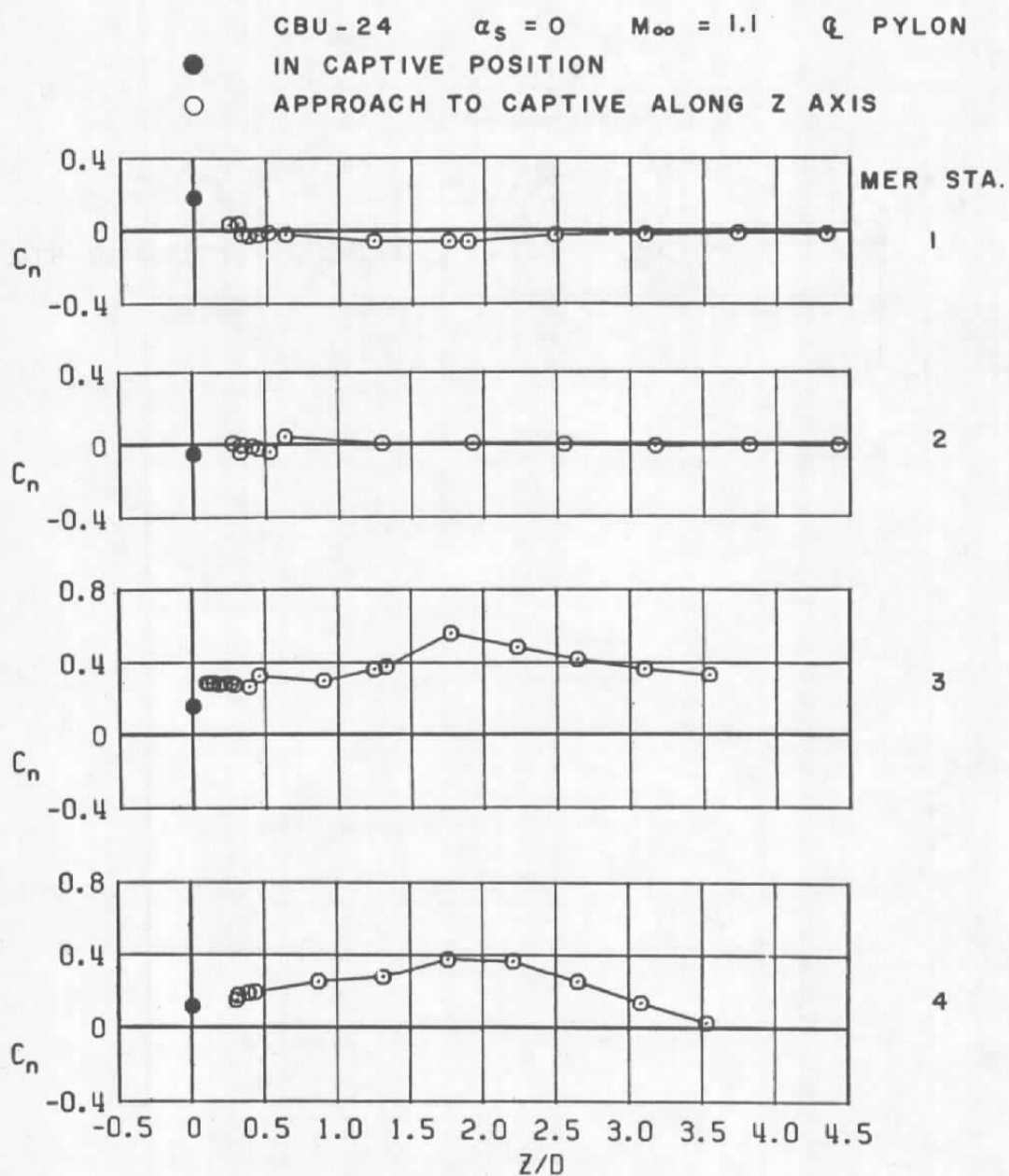
CBU-24  $\alpha_s = 0$   $M_\infty = 0.9$   $\phi$  PYLON

● IN CAPTIVE POSITION

○ APPROACH TO CAPTIVE ALONG Z AXIS



b.  $M_\infty = 0.9$   
Figure 52. Continued.

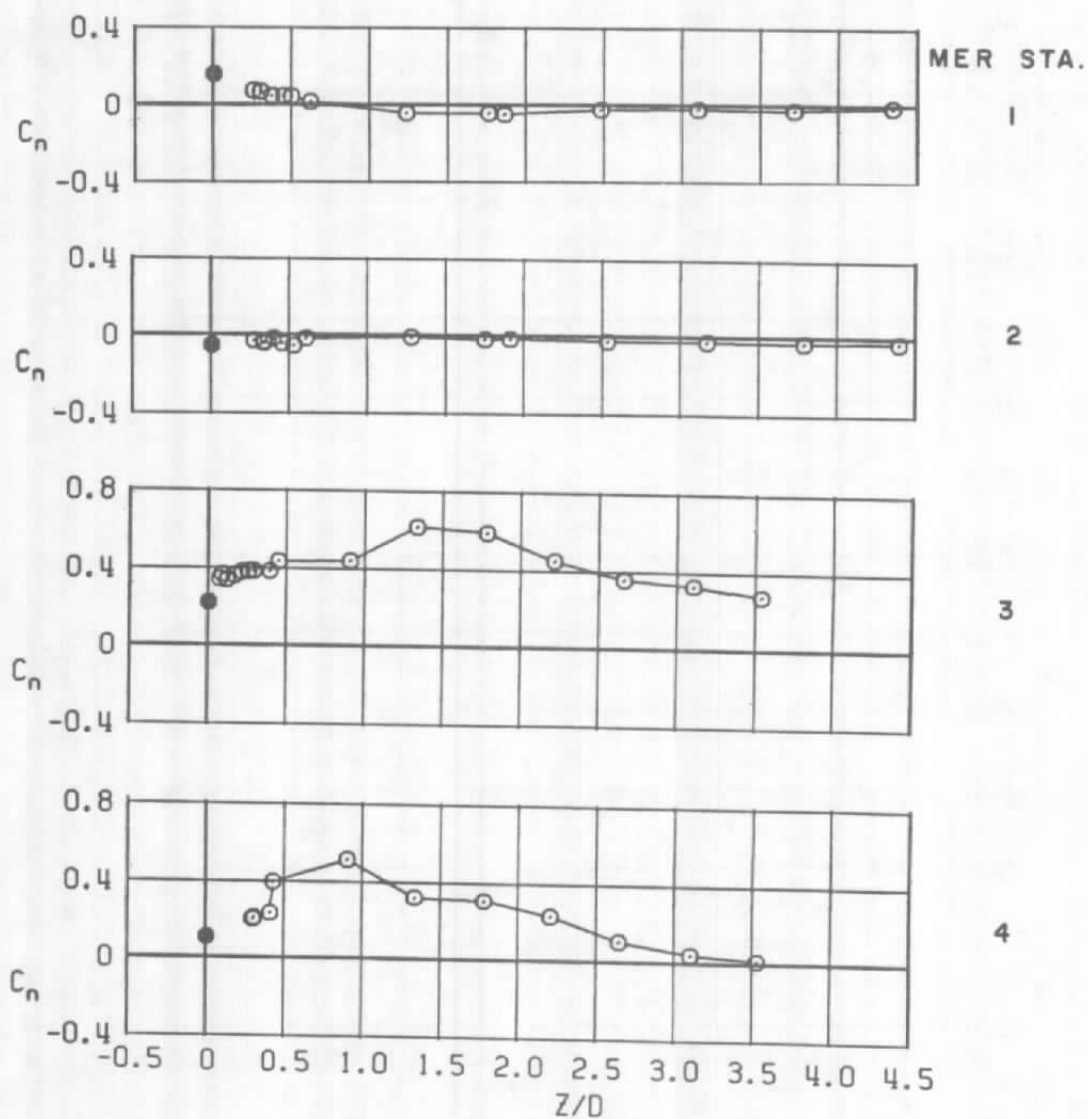


c.  $M_\infty = 1.1$   
 Figure 52. Continued.

CUB-24  $\alpha_s = 0$   $M_\infty = 1.2$  Q PYLON

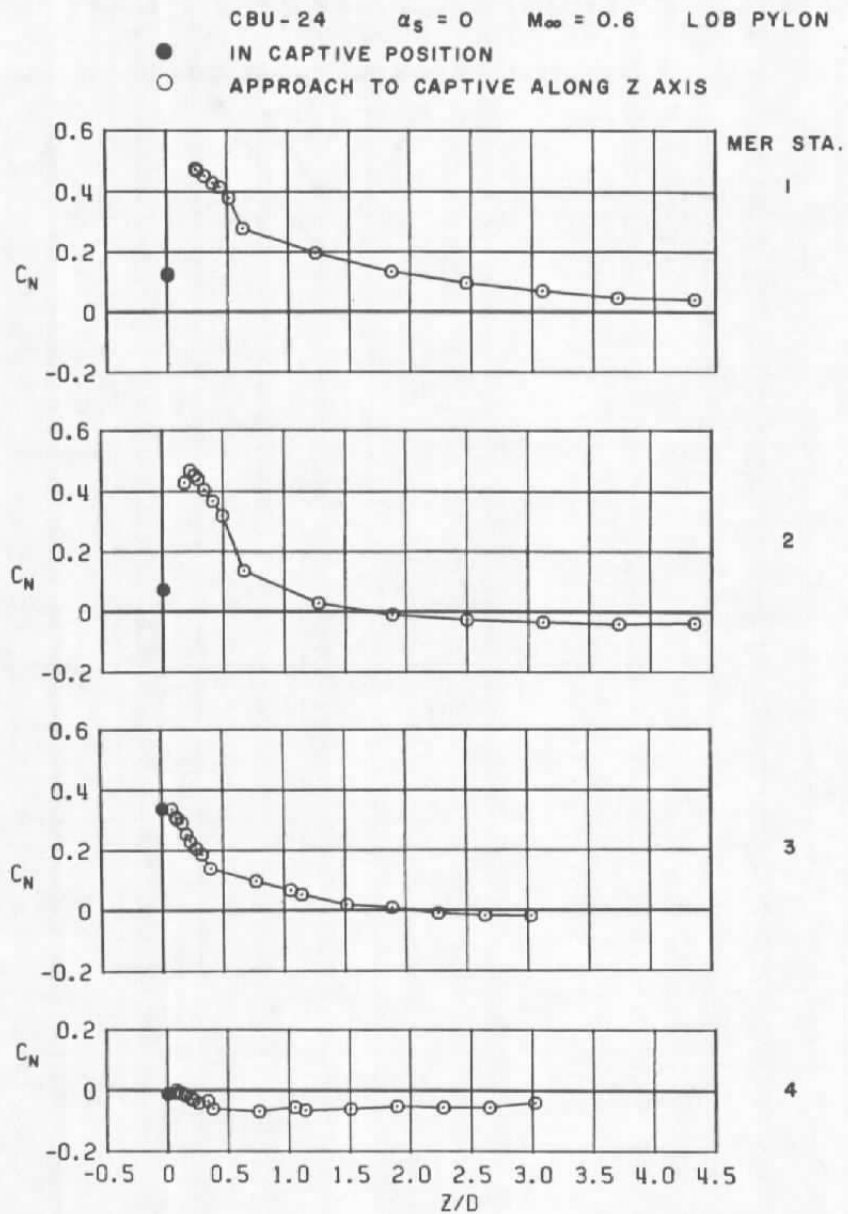
● IN CAPTIVE POSITION

○ APPROACH TO CAPTIVE ALONG Z AXIS



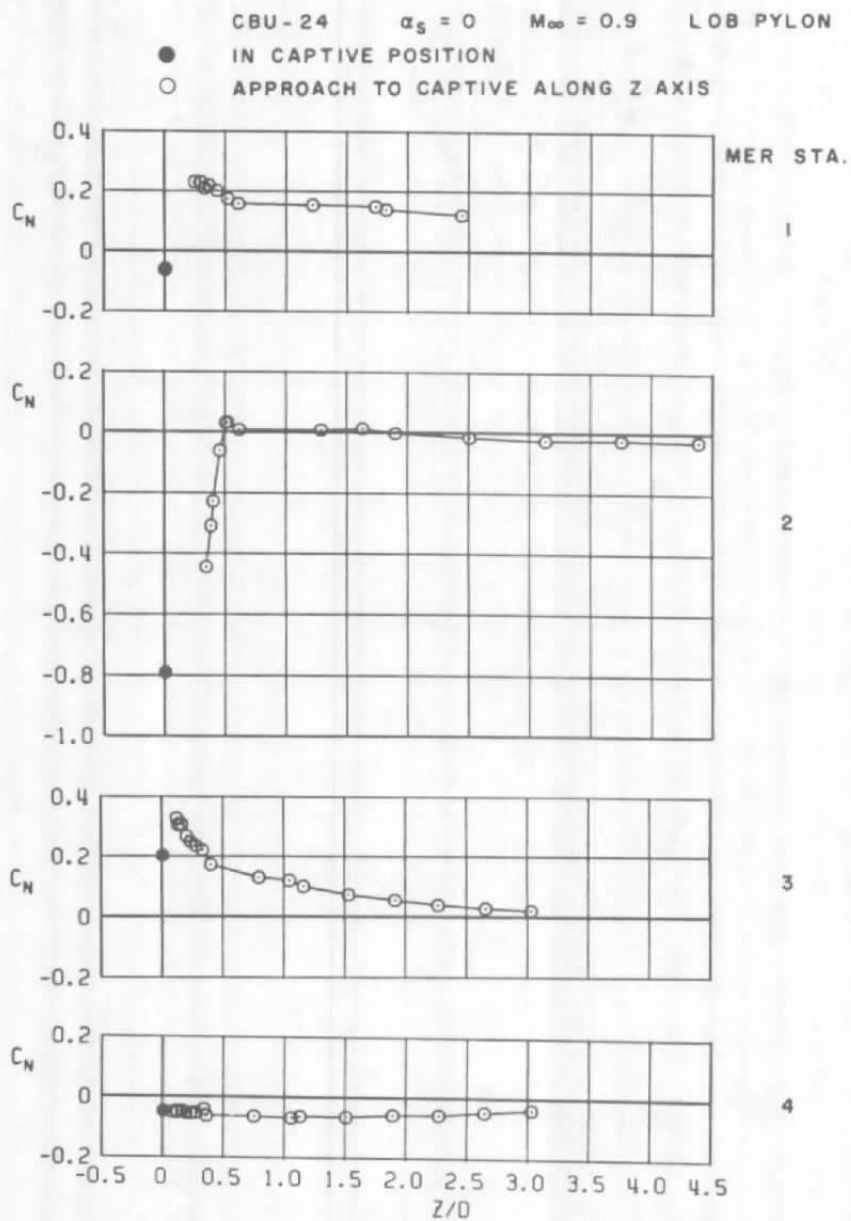
d.  $M_\infty = 1.2$   
Figure 52. Concluded.



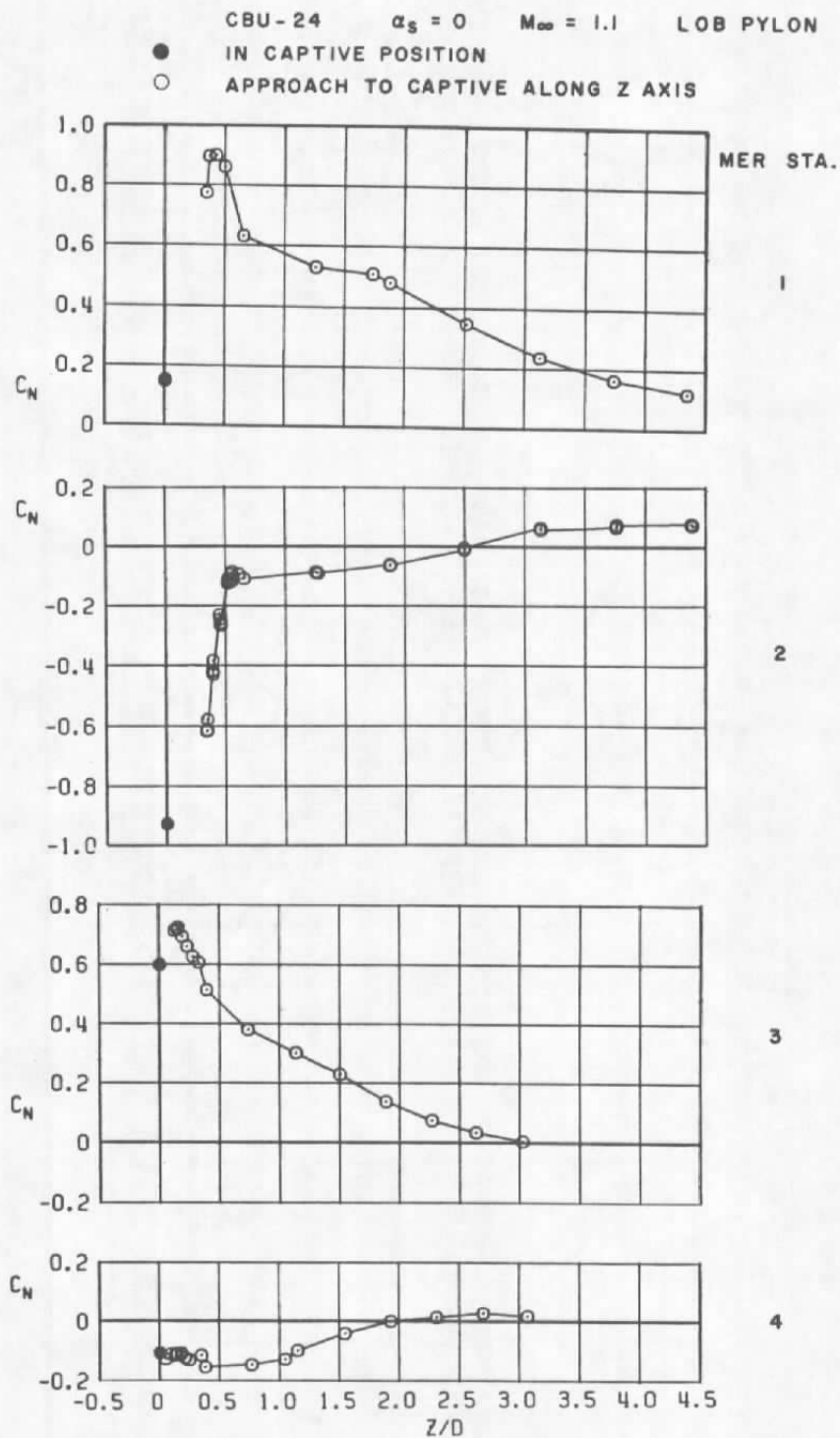


a.  $M_\infty = 0.6$

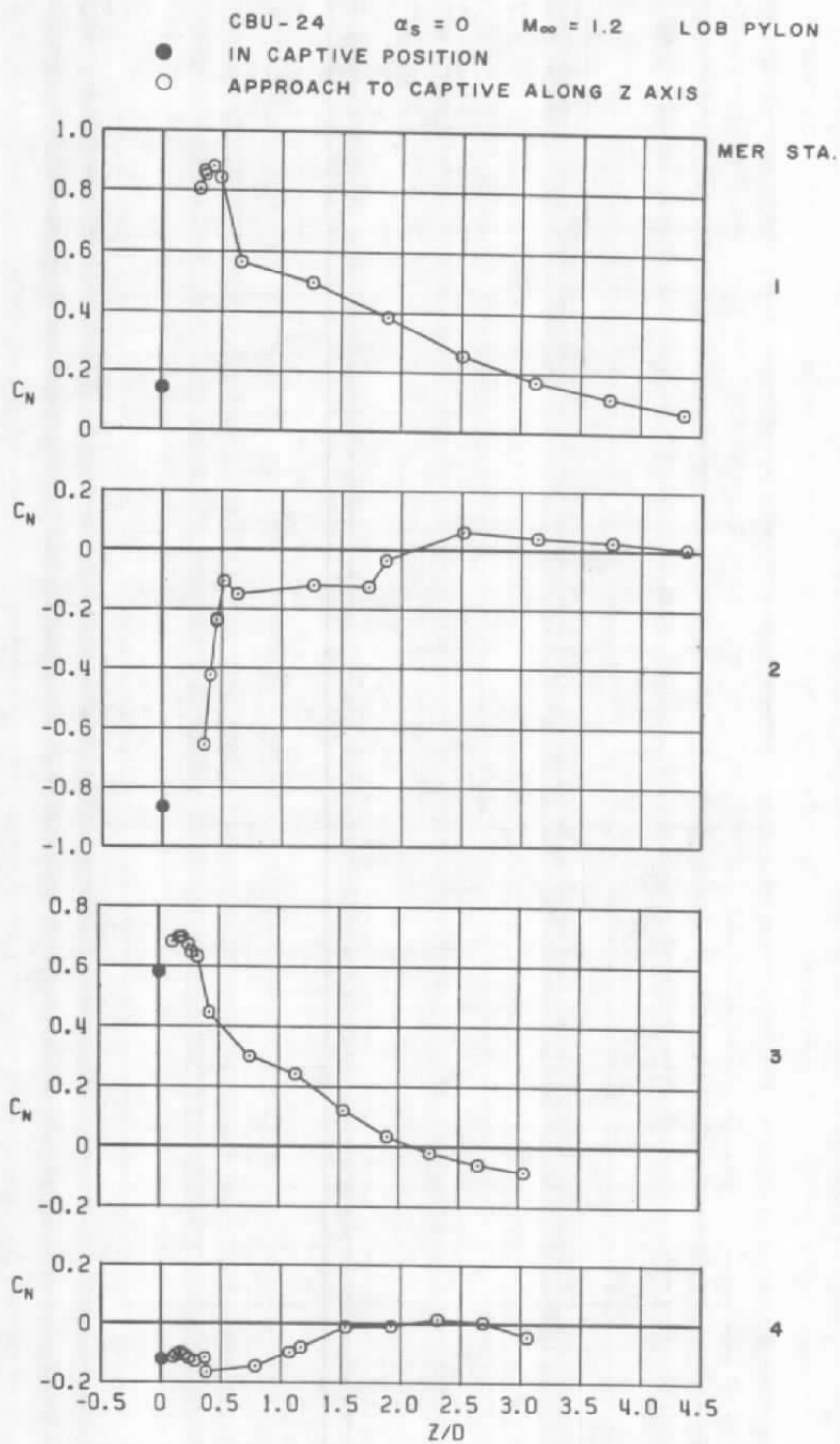
Figure 53. Coefficient of normal force acting on the CBU-24 (SUU-30) store as a function of normal distance between the store and four captive positions on the MER mounted on the LOB pylon.



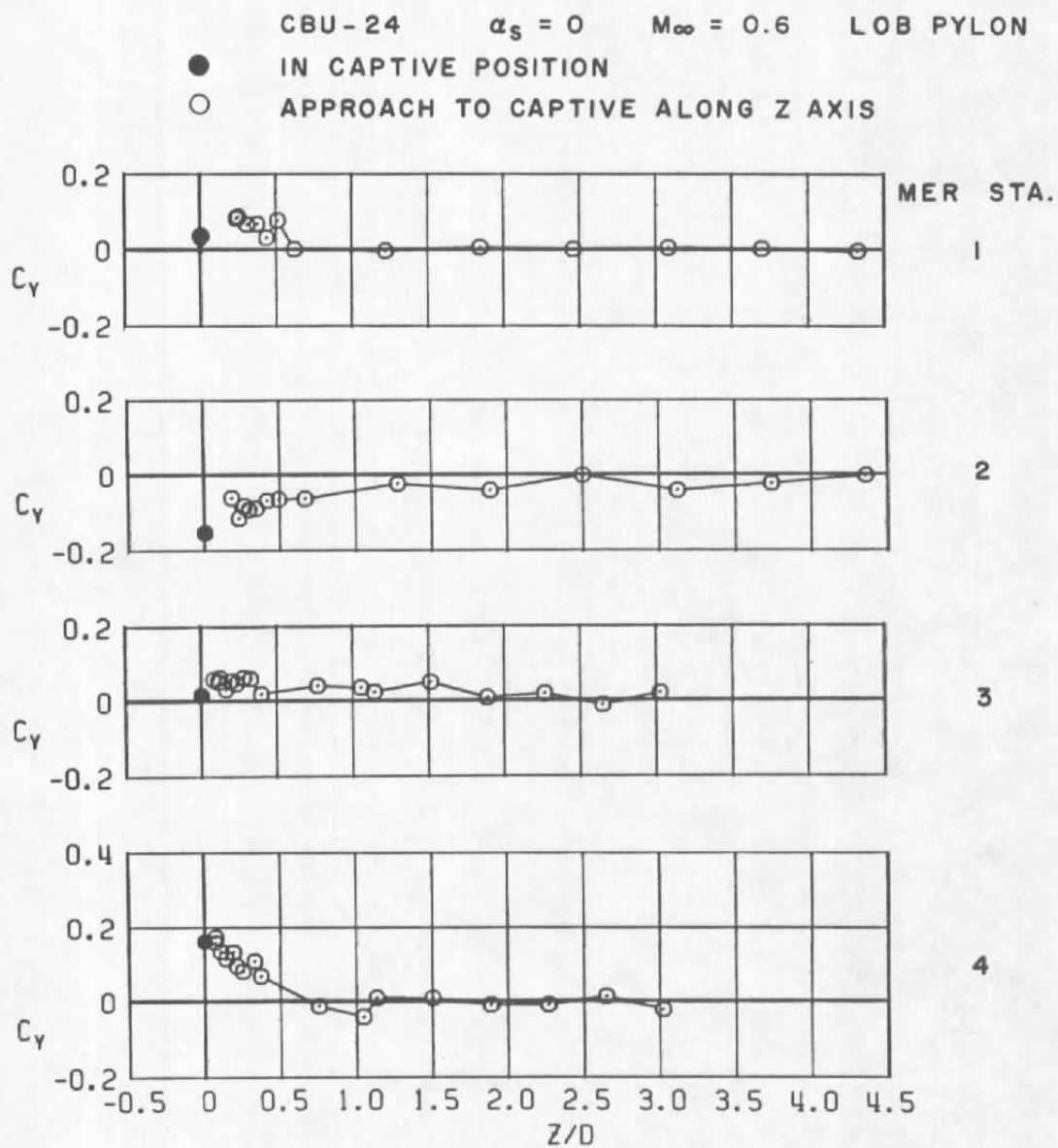
b.  $M_\infty = 0.9$   
Figure 53. Continued.



c.  $M_\infty = 1.1$   
 Figure 53. Continued.



d.  $M_\infty = 1.2$   
 Figure 53. Concluded.



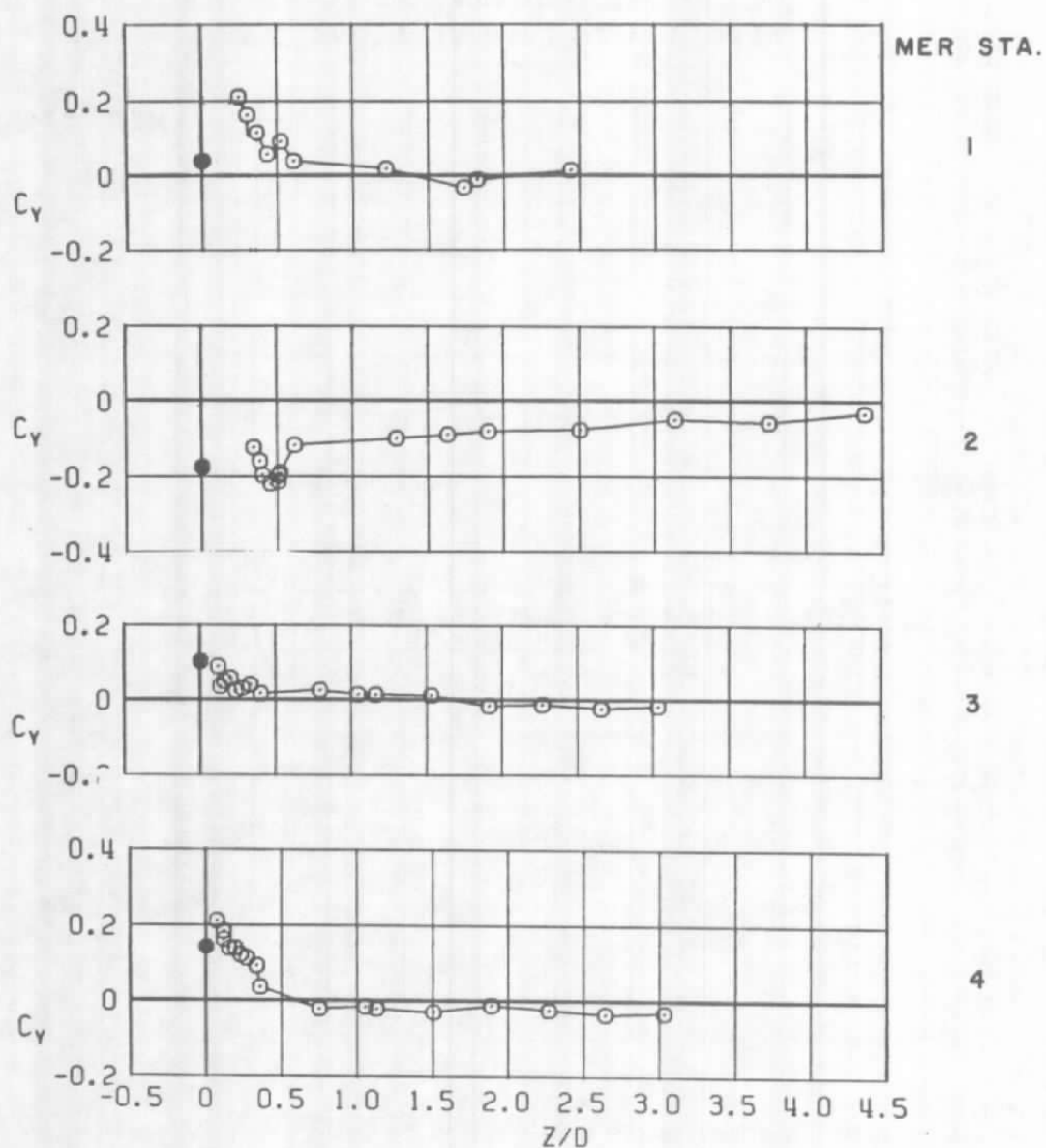
a.  $M_\infty = 0.6$

Figure 54. Coefficient of side force acting on the CBU-24 (SUU-30) store as a function of normal distance between the store and four captive positions on the MER mounted on the LOB pylon.

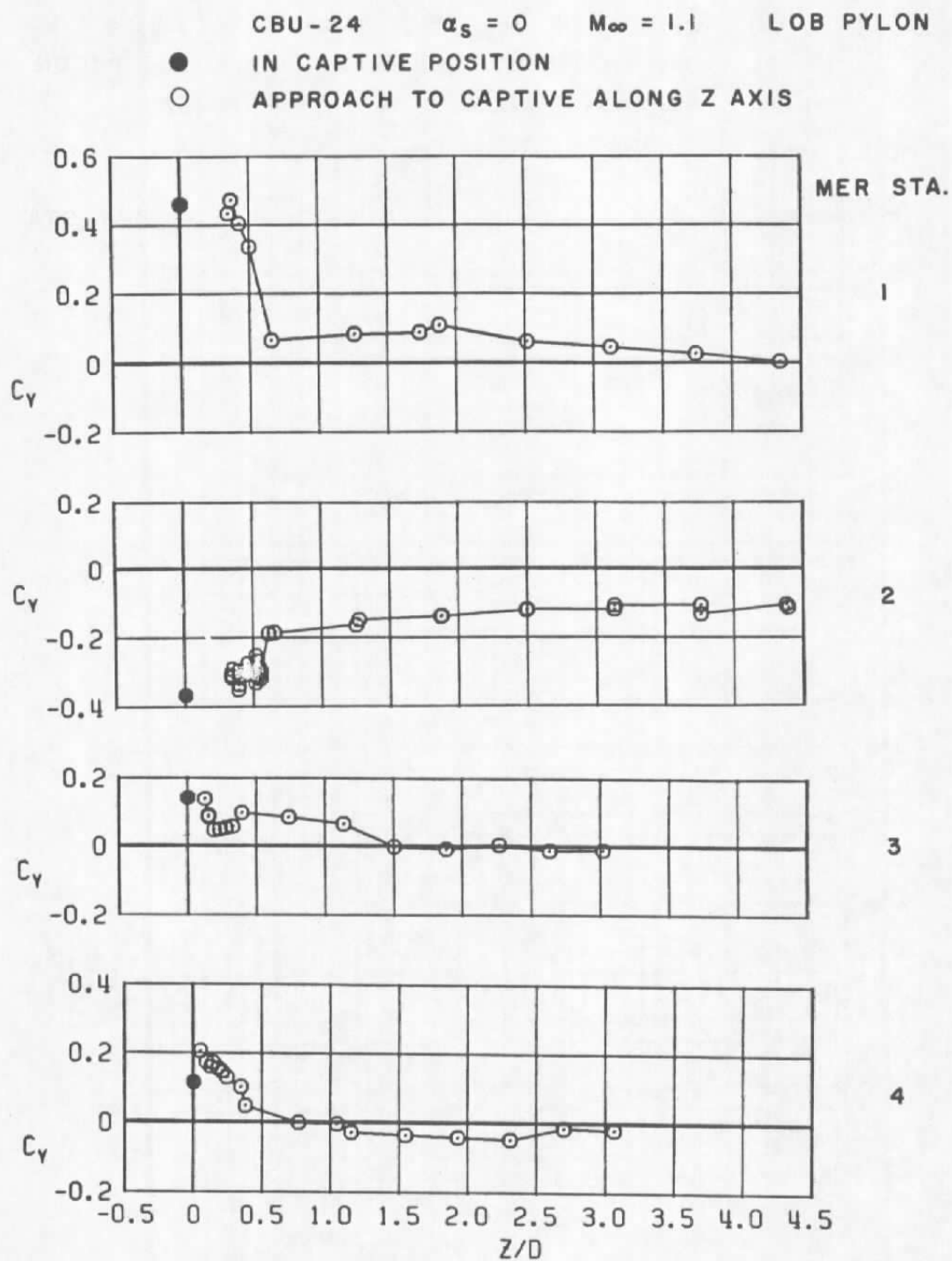
CUB-24  $\alpha_s = 0$   $M_\infty = 0.9$  LOB PYLON

● IN CAPTIVE POSITION

○ APPROACH TO CAPTIVE ALONG Z AXIS



b.  $M_\infty = 0.9$   
Figure 54. Continued.



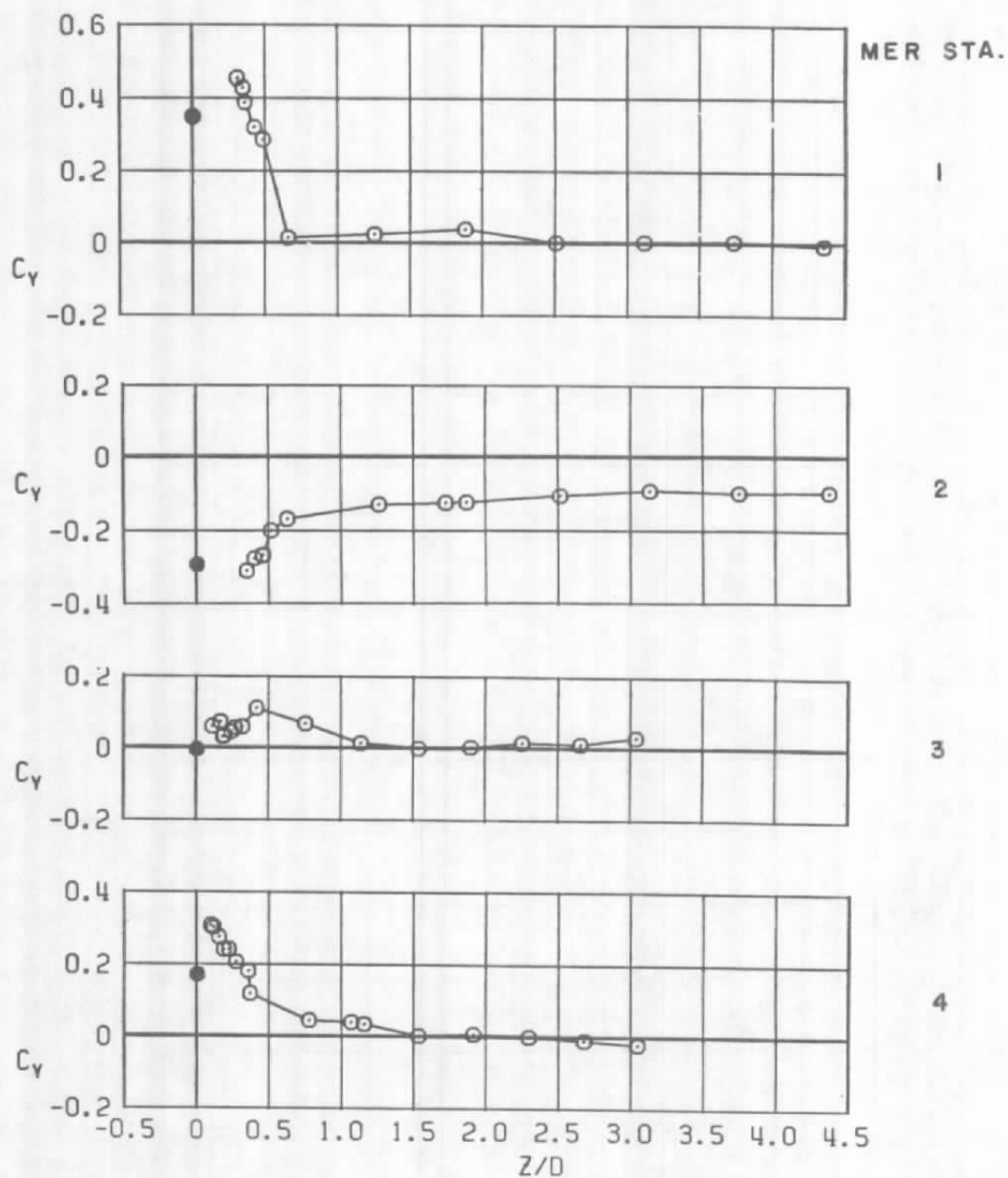
c.  $M_\infty = 1.1$   
Figure 54. Continued.

CBU-24  $\alpha_s = 0$   $M_\infty = 1.2$  LOB PYLON

IN CAPTIVE POSITION

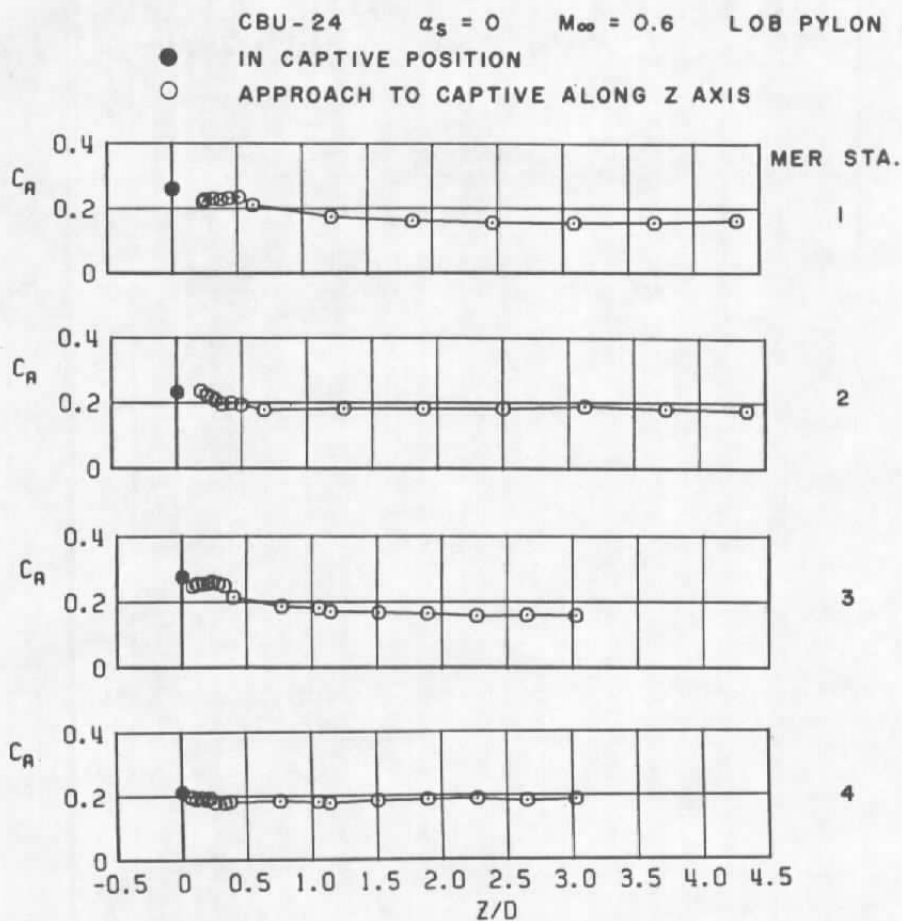


APPROACH TO CAPTIVE ALONG Z AXIS



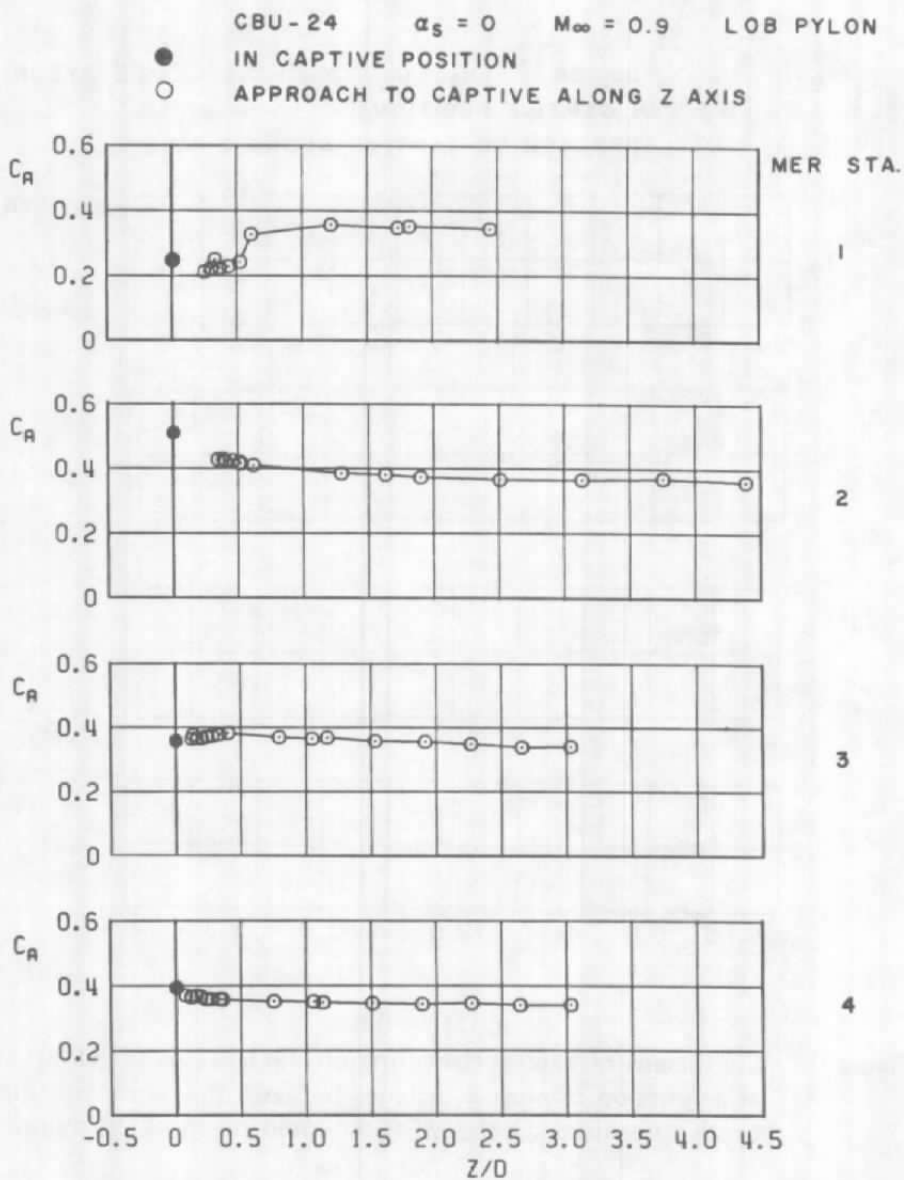
d.  $M_\infty = 1.2$   
Figure 54. Concluded.





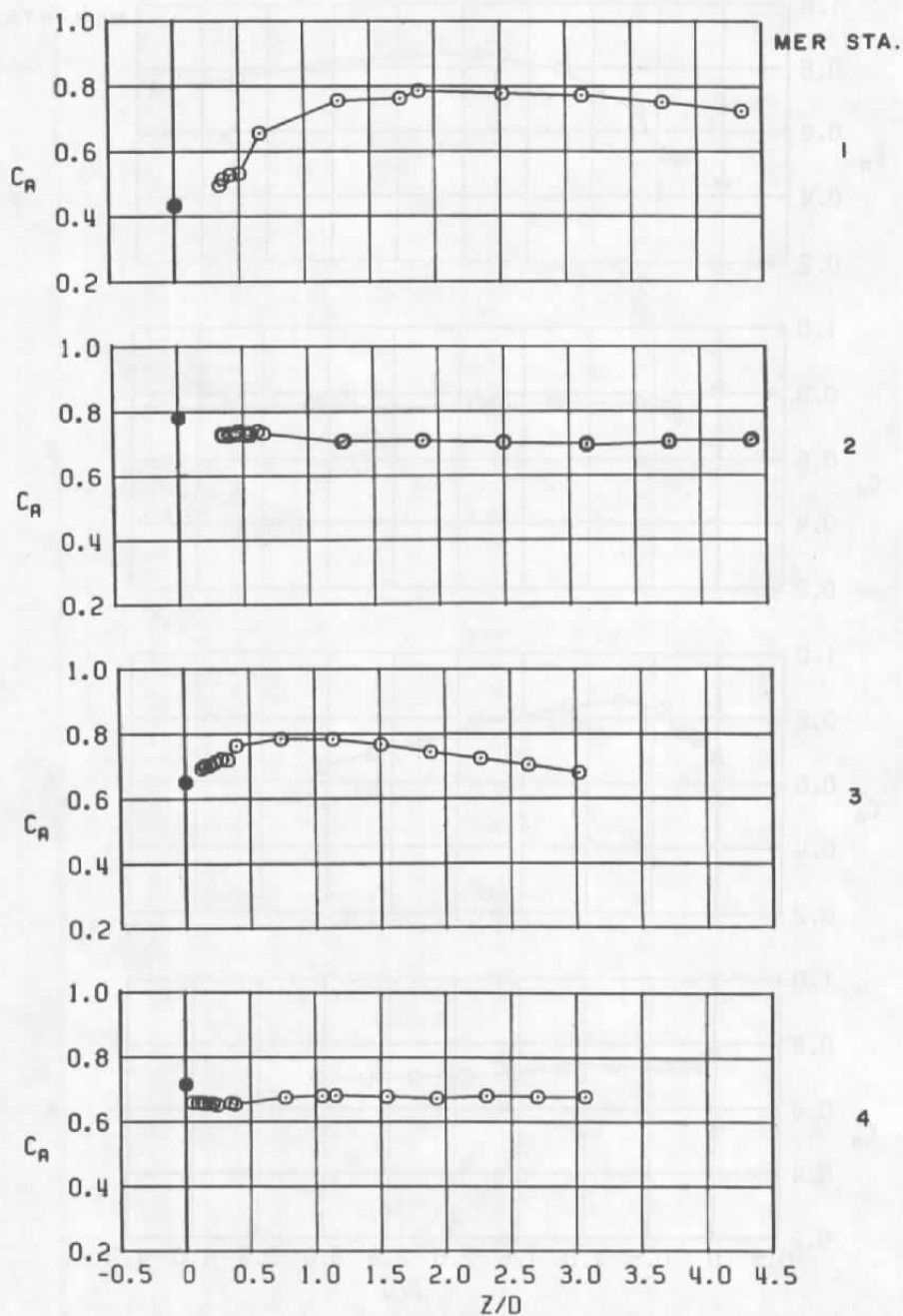
a.  $M_\infty = 0.6$

**Figure 55.** Coefficient of axial force acting on the CBU-24 (SUU-30) store as a function of normal distance between the store and four captive positions on the MER mounted on the LOB pylon.

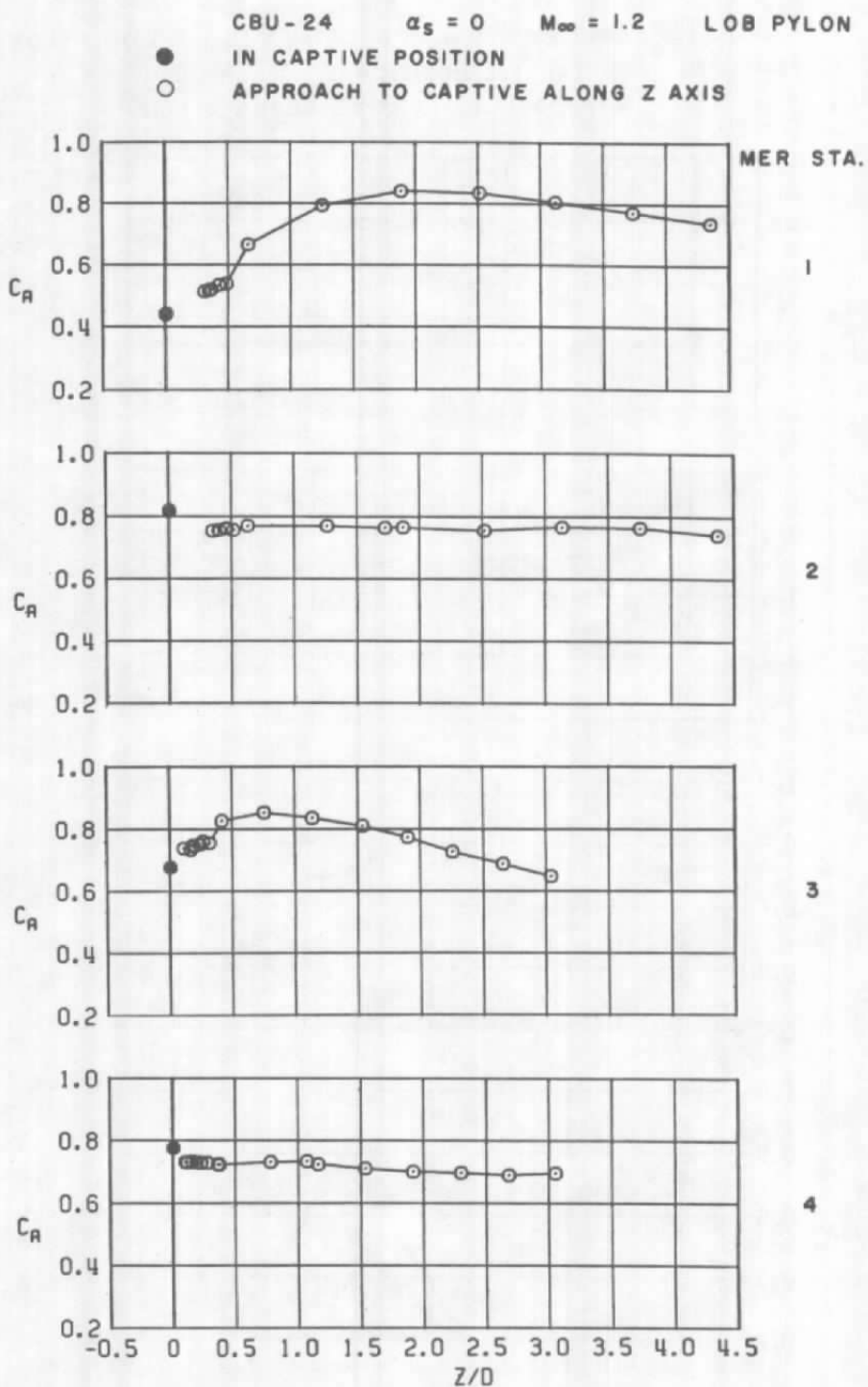


b.  $M_\infty = 0.9$   
 Figure 55. Continued.

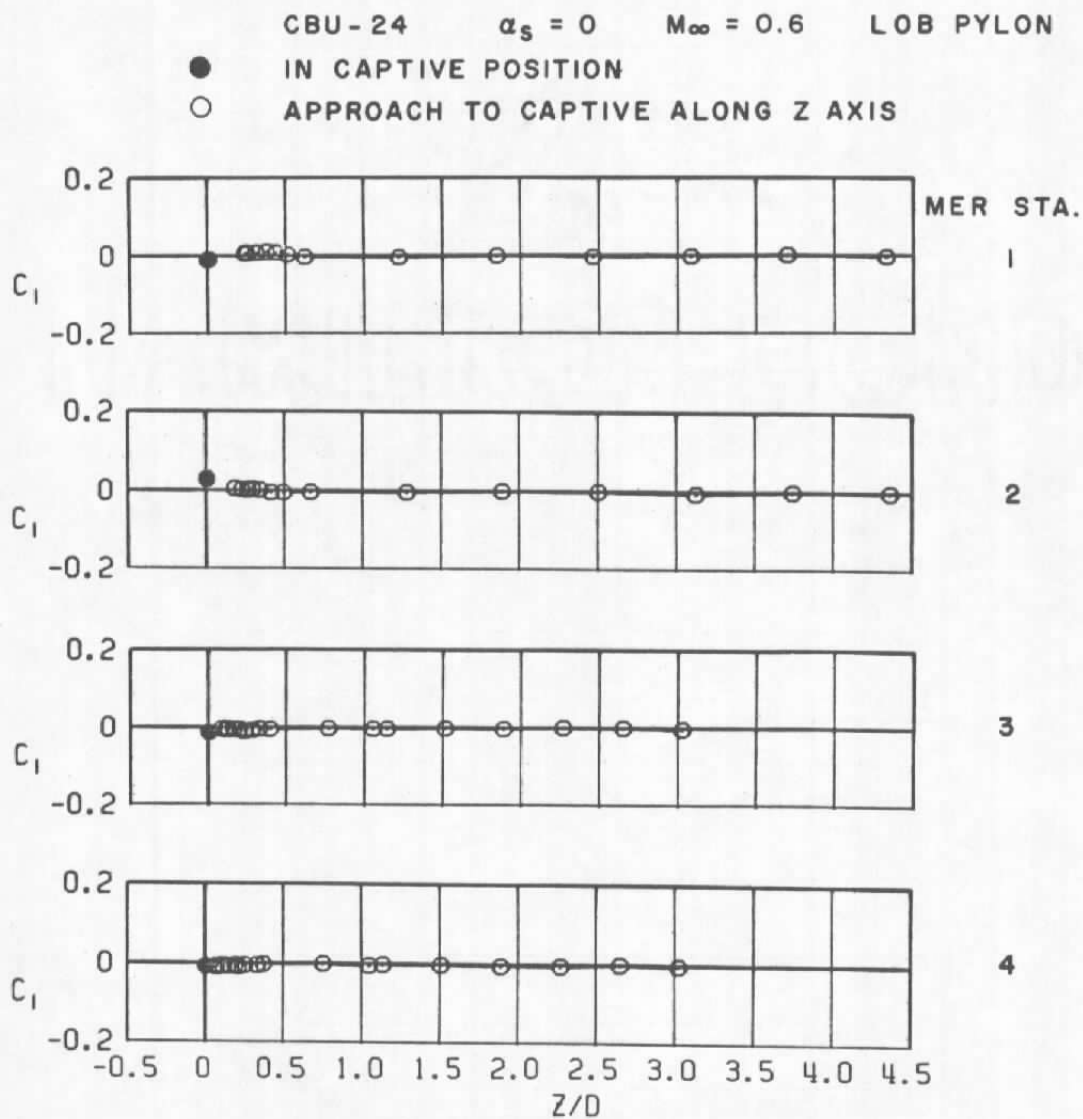
CBU-24  $\alpha_s = 0$   $M_\infty = 1.1$  LOB PYLON  
 ● IN CAPTIVE POSITION  
 ○ APPROACH TO CAPTIVE ALONG Z AXIS



c.  $M_\infty = 1.1$   
 Figure 55. Continued.

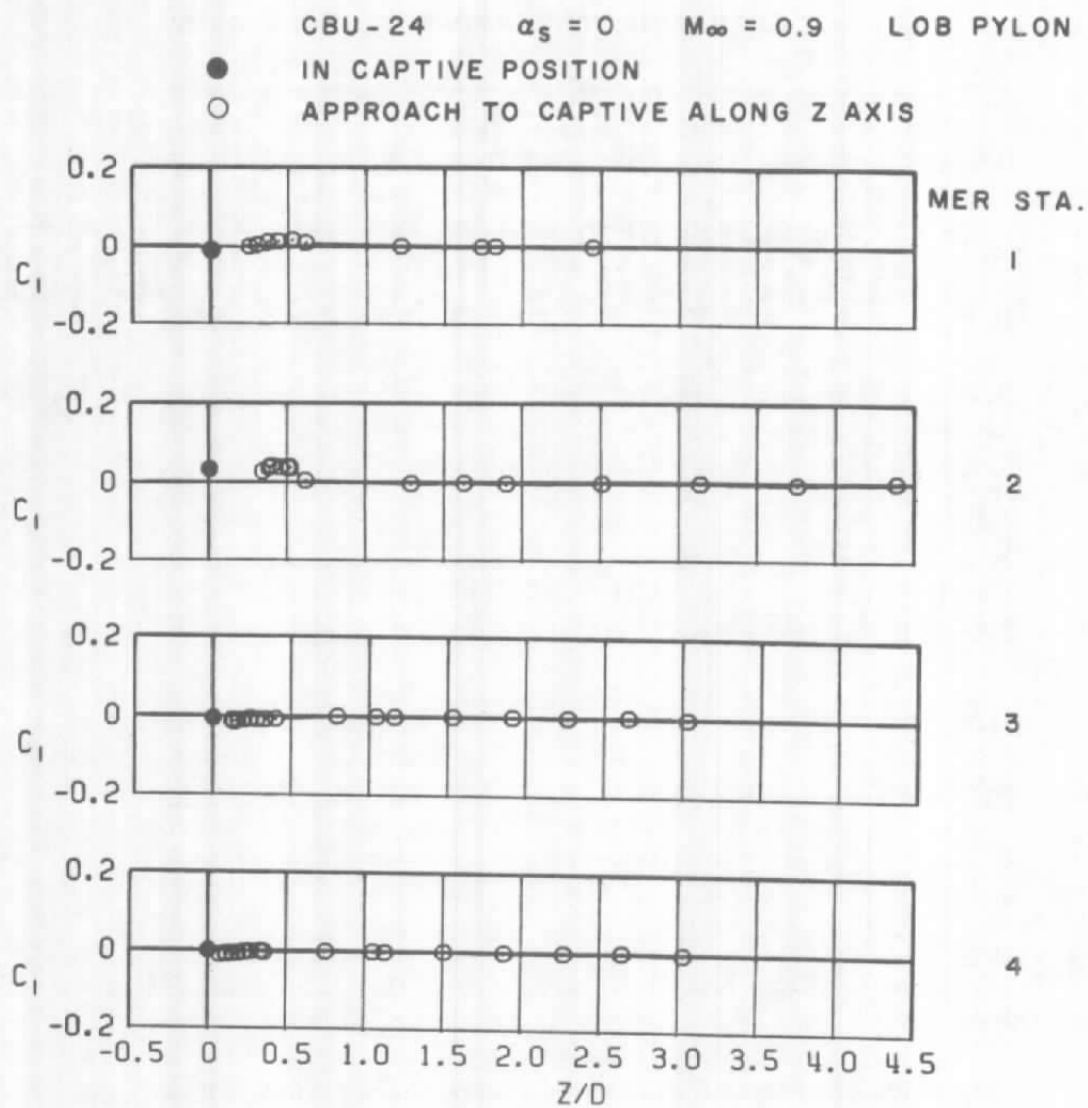


d.  $M_\infty = 1.2$   
 Figure 55. Concluded.

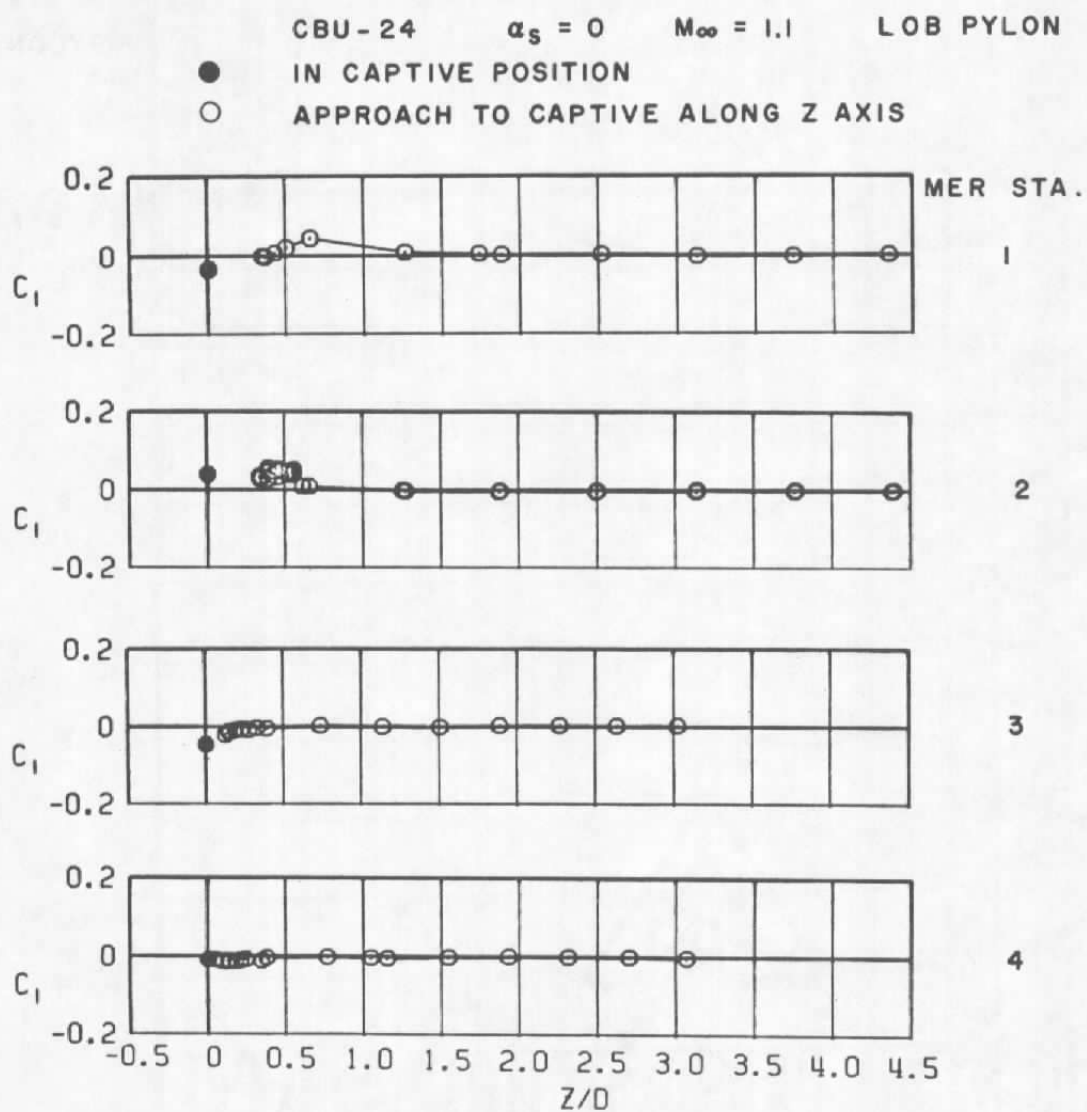


a.  $M_\infty = 0.6$

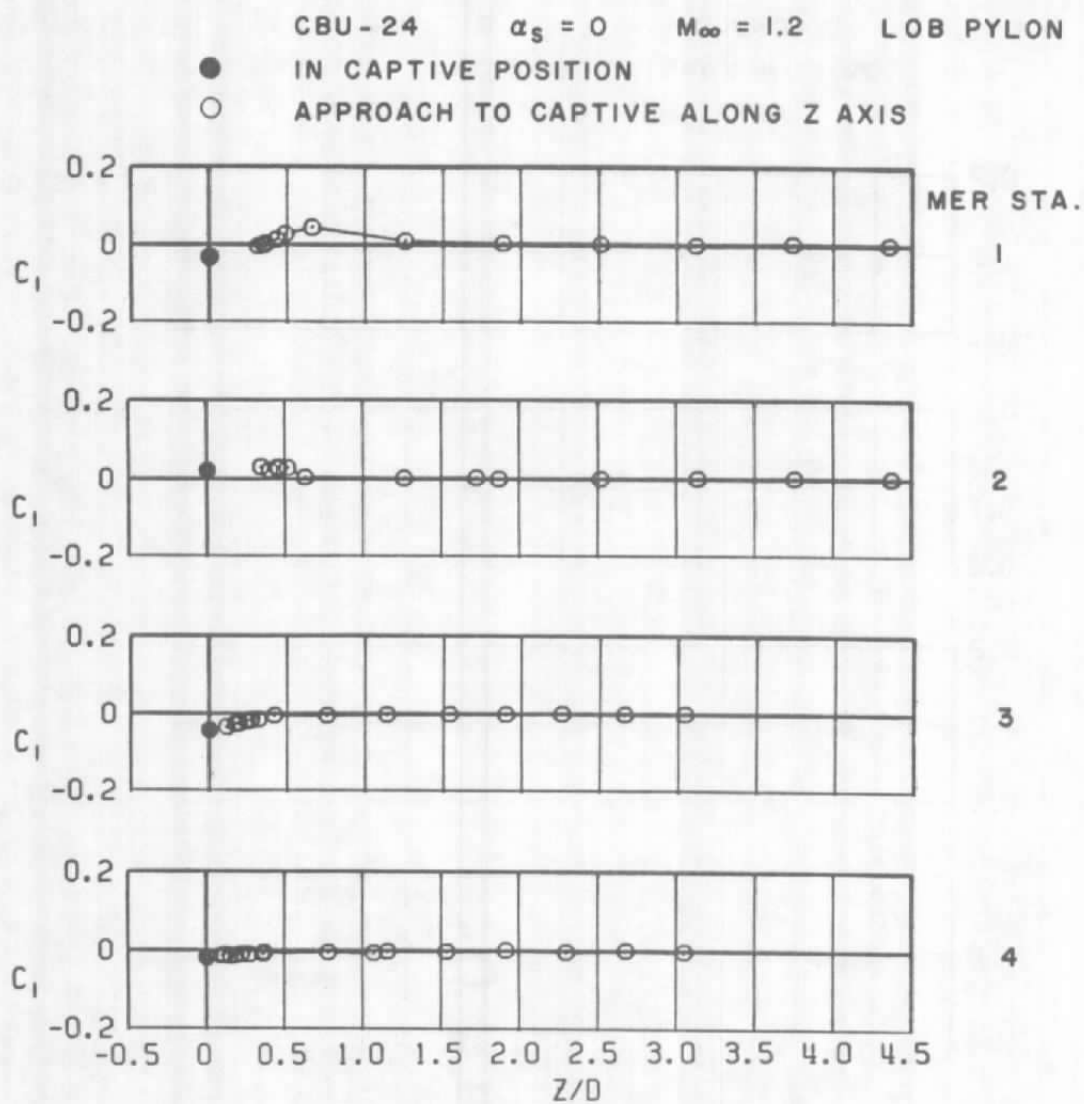
Figure 56. Coefficient of rolling moment acting on the CBU-24 (SUU-30) store as a function of normal distance between the store and four captive positions on the MER mounted on the LOB pylon.



b.  $M_\infty = 0.9$   
 Figure 56. Continued.

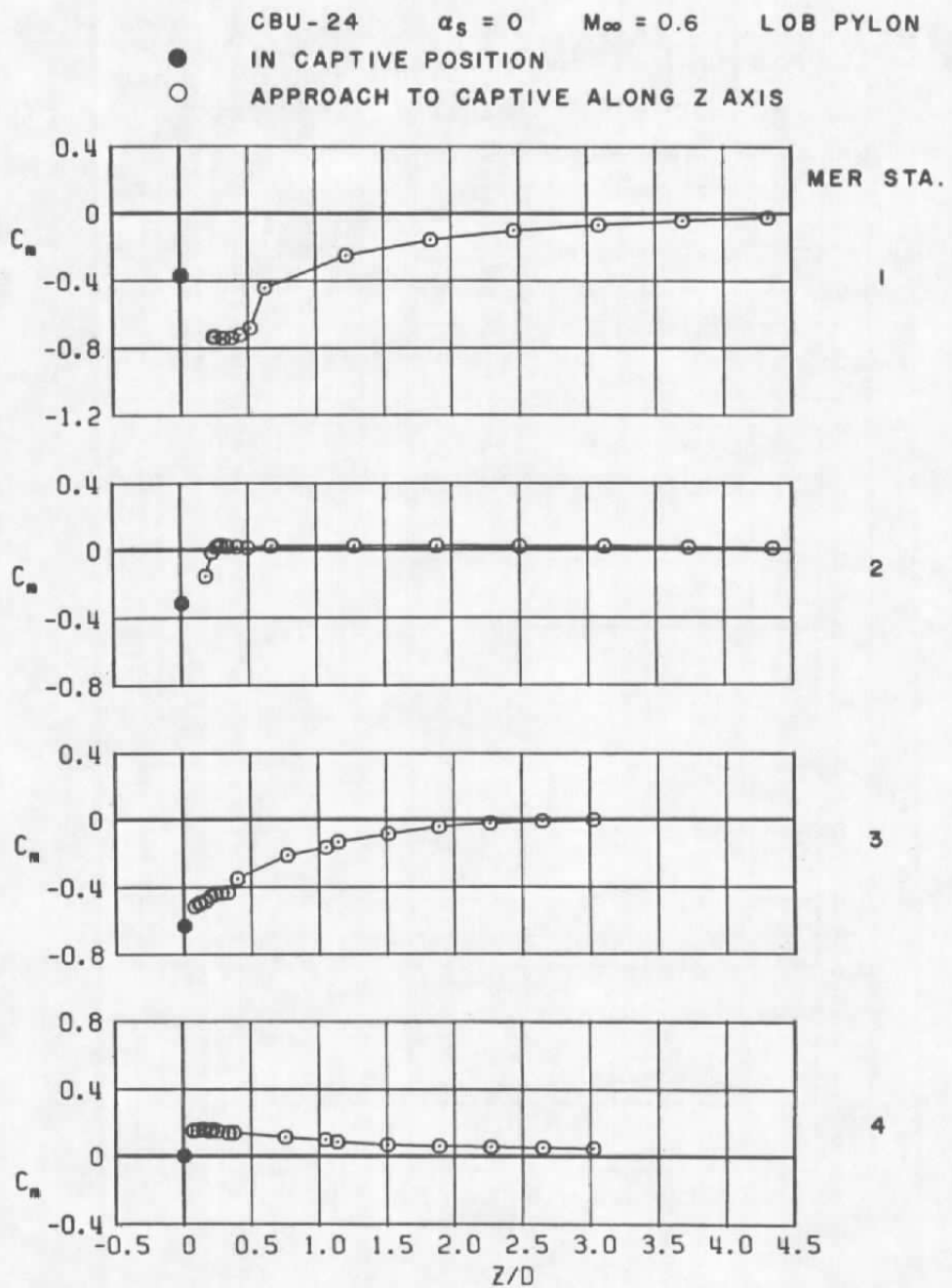


c.  $M_\infty = 1.1$   
 Figure 56. Continued.



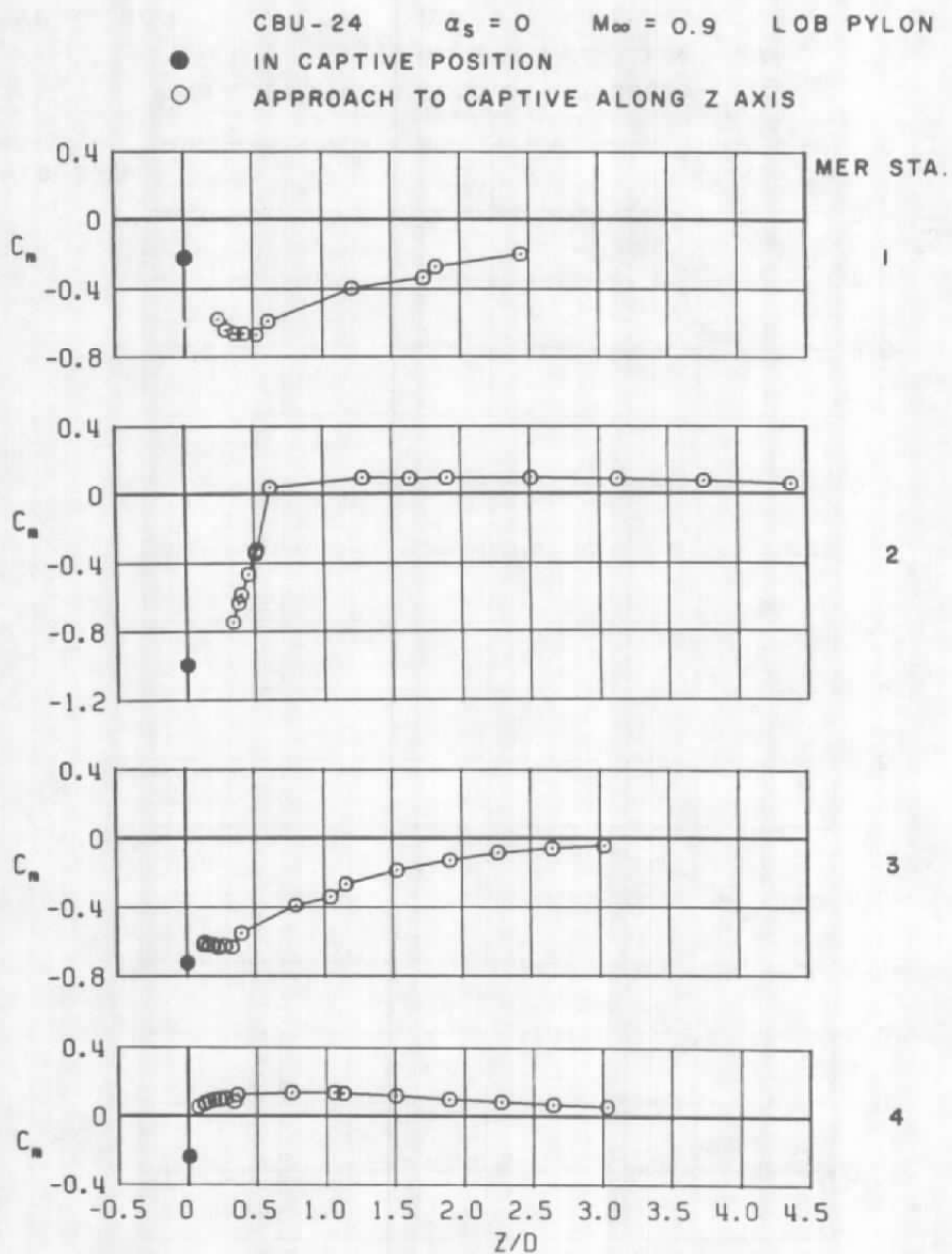
d.  $M_\infty = 1.2$   
 Figure 56. Concluded.





a.  $M_\infty = 0.6$

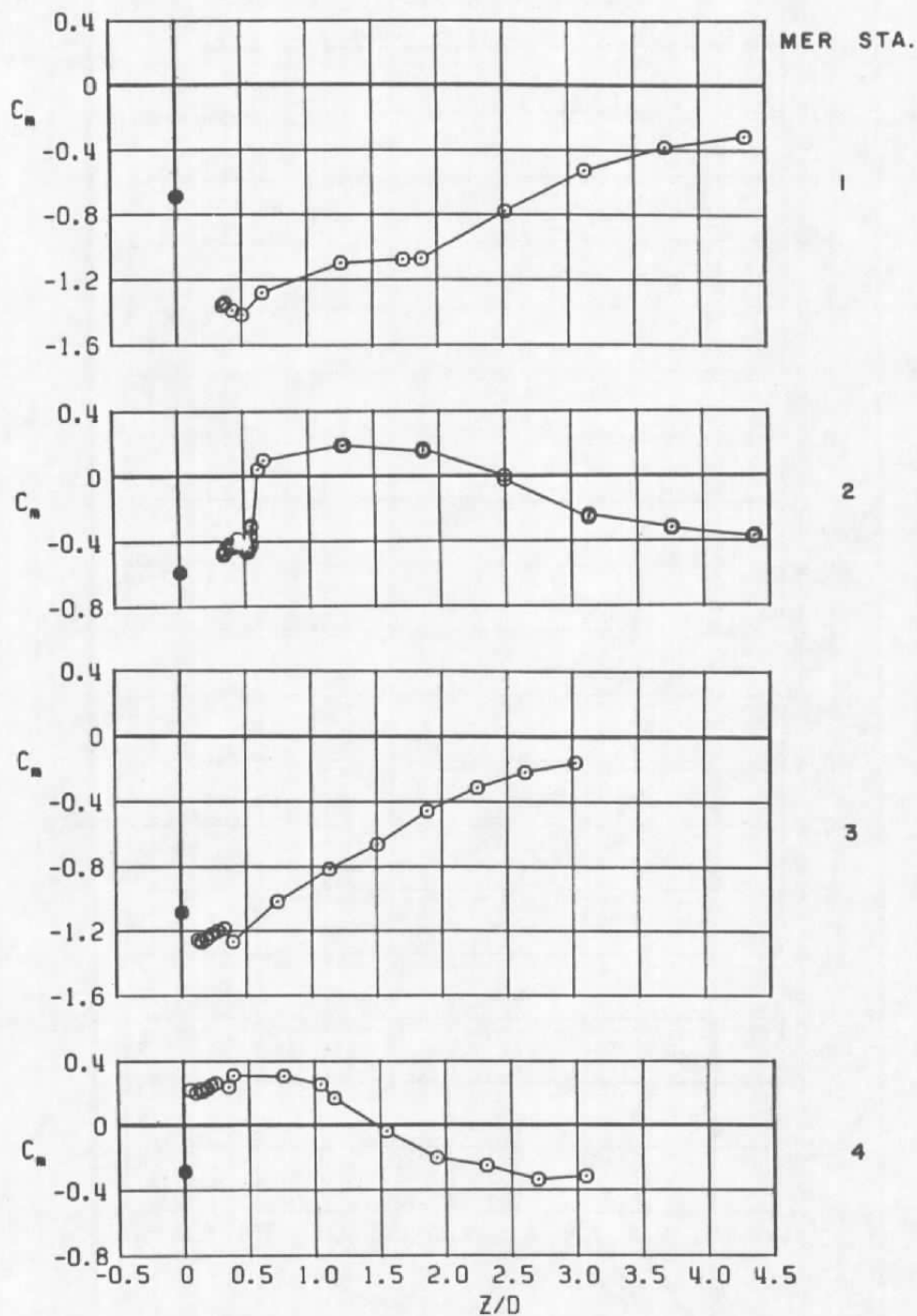
Figure 57. Coefficient of pitching moment acting on the CBU-24 (SUU-30) store as a function of normal distance between the store and four captive positions on the MER mounted on the LOB pylon.



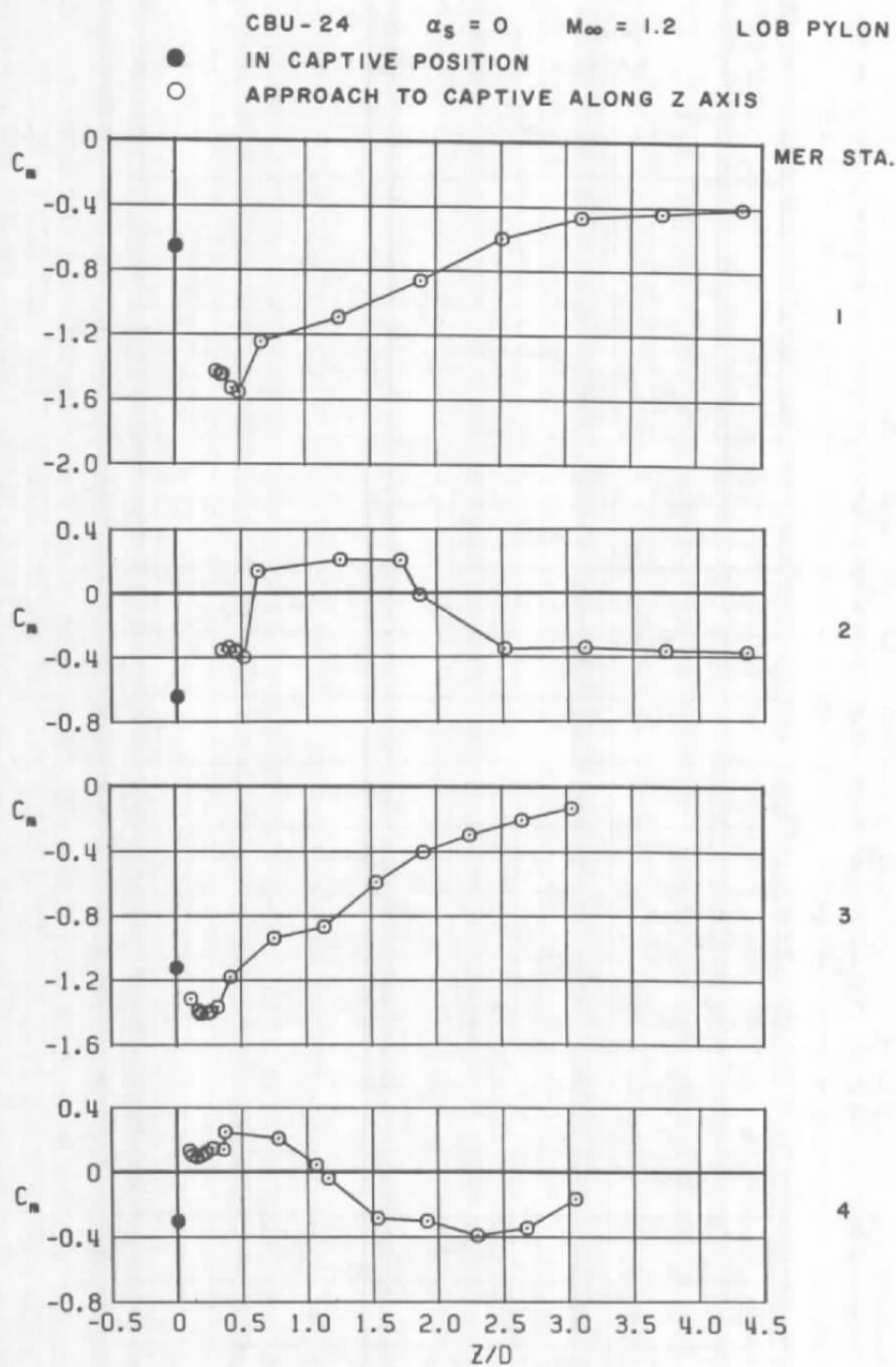
b.  $M_\infty = 0.9$   
 Figure 57. Continued.

CBU-24  $\alpha_s = 0$   $M_\infty = 1.1$  LOB PYLON

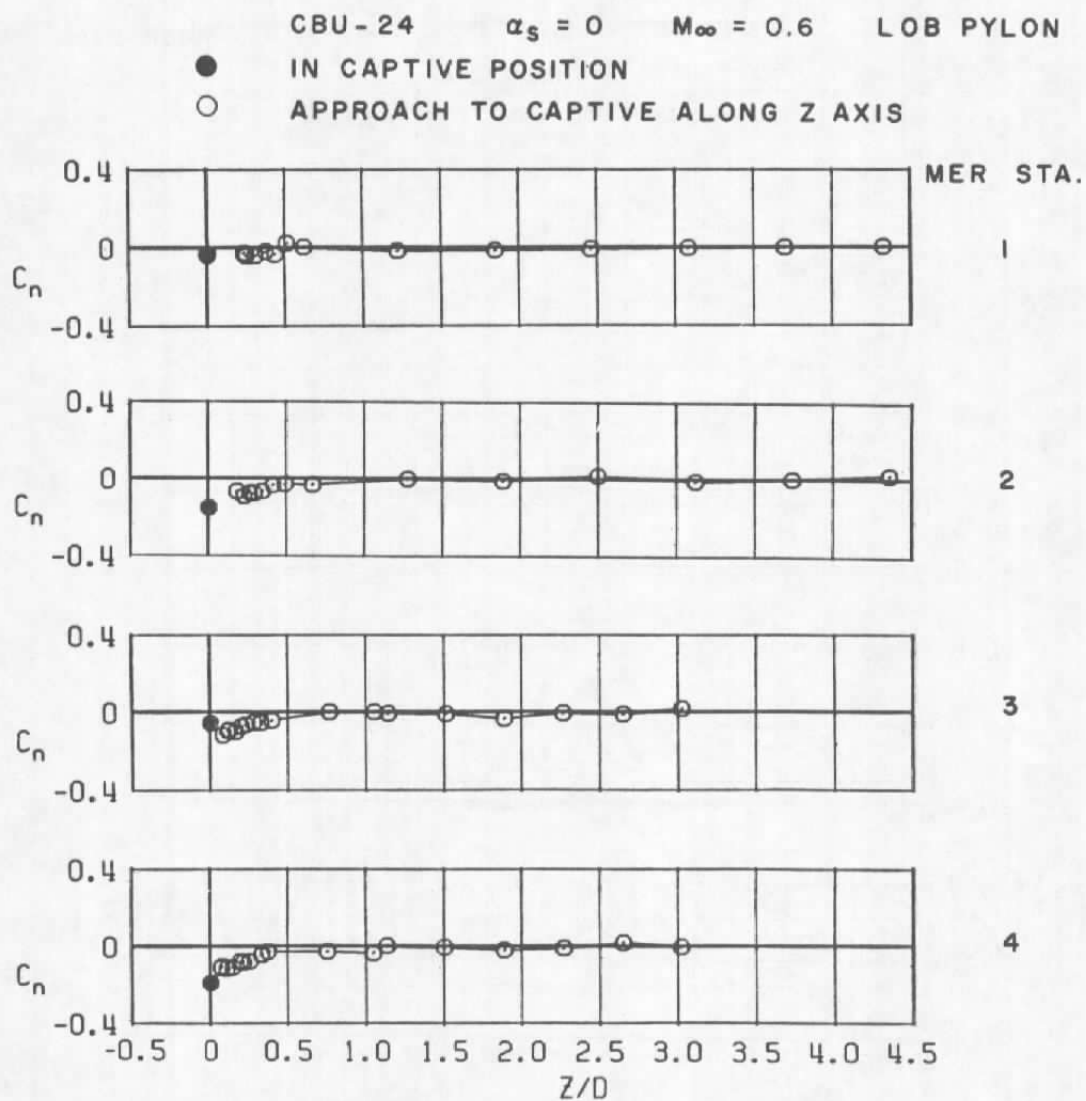
● IN CAPTIVE POSITION  
○ APPROACH TO CAPTIVE ALONG Z AXIS



c.  $M_\infty = 1.1$   
Figure 57. Continued.



d.  $M_\infty = 1.2$   
Figure 57. Concluded.



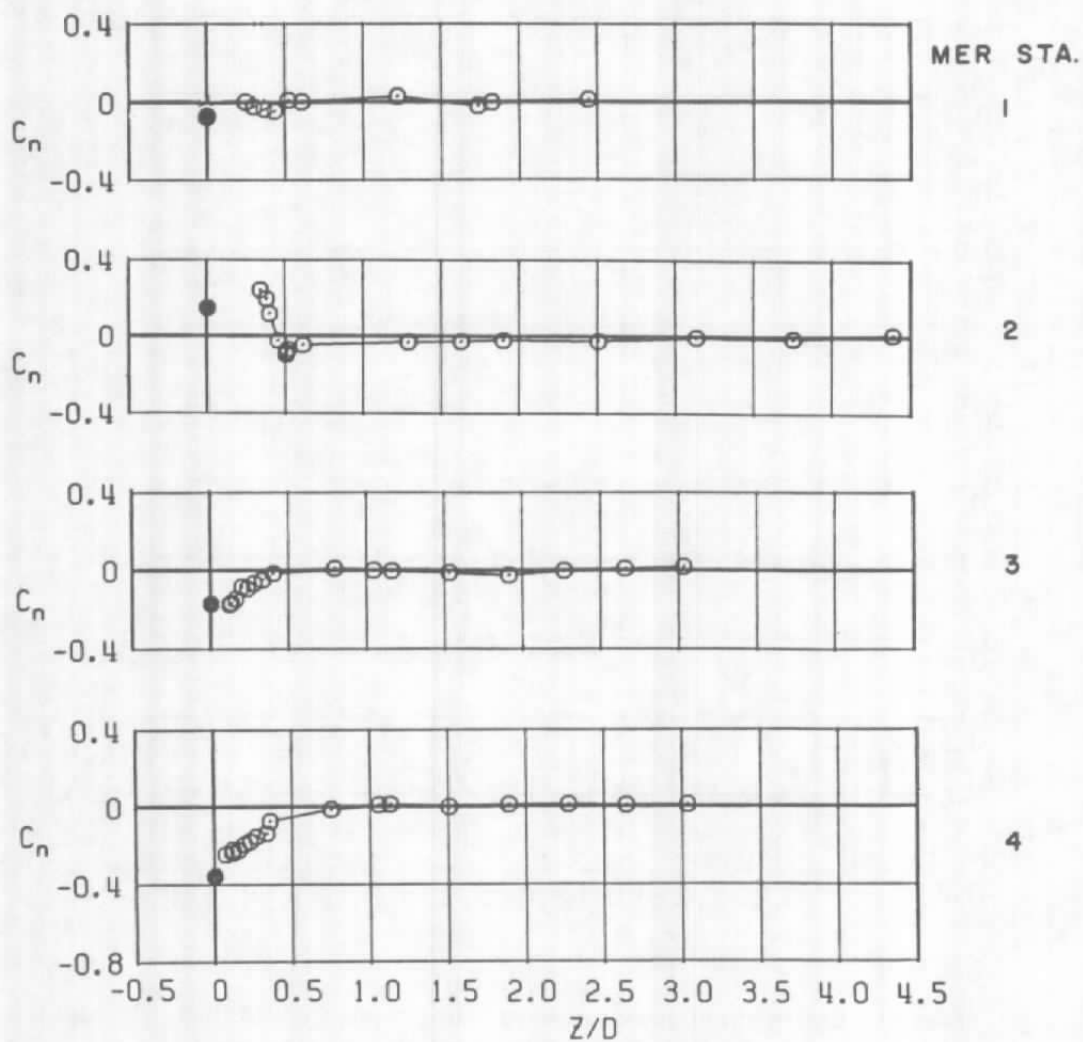
a.  $M_\infty = 0.6$

Figure 58. Coefficient of yawing moment acting on the CBU-24 (SUU-30) store as a function of normal distance between the store and four captive positions on the MER mounted on the LOB pylon.

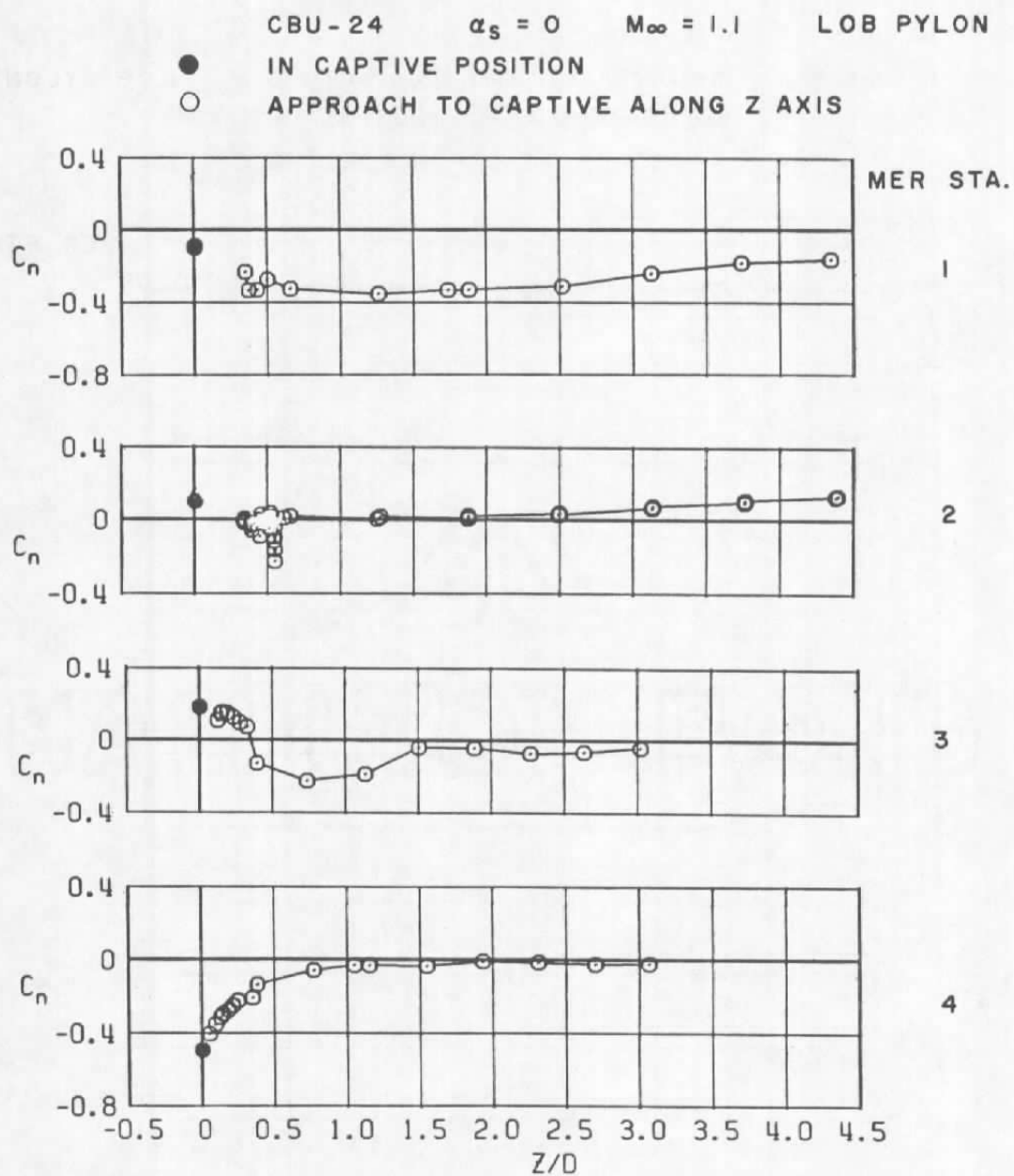
CUB-24       $\alpha_s = 0$        $M_\infty = 0.9$       LOB PYLON

● IN CAPTIVE POSITION

○ APPROACH TO CAPTIVE ALONG Z AXIS



b.  $M_\infty = 0.9$   
Figure 58. Continued.

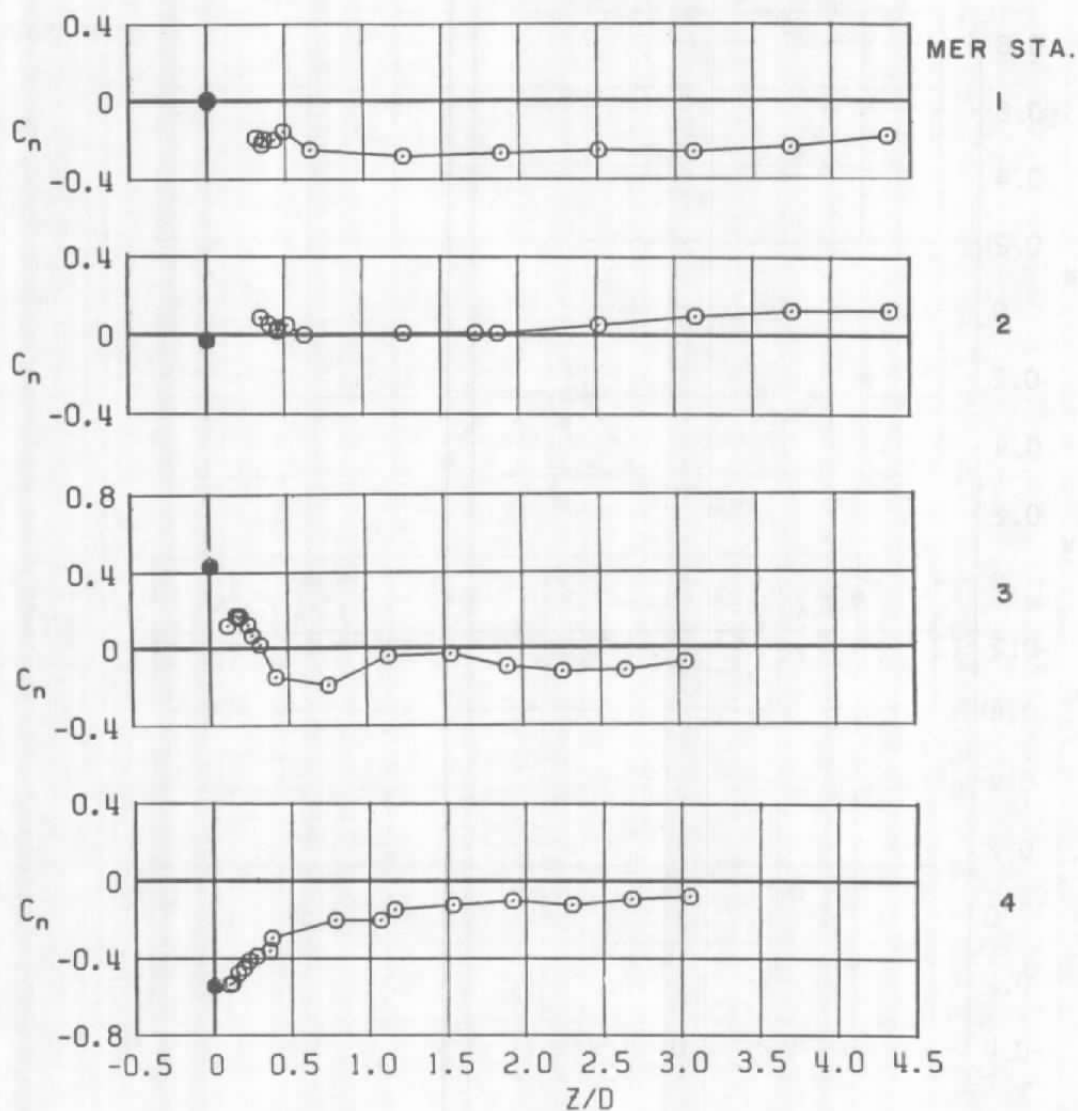


c.  $M_\infty = 1.1$   
 Figure 58. Continued.

CBU-24       $\alpha_s = 0$        $M_\infty = 1.2$       LOB PYLON

● IN CAPTIVE POSITION

○ APPROACH TO CAPTIVE ALONG Z AXIS



d.  $M_\infty = 1.2$   
Figure 58. Concluded.



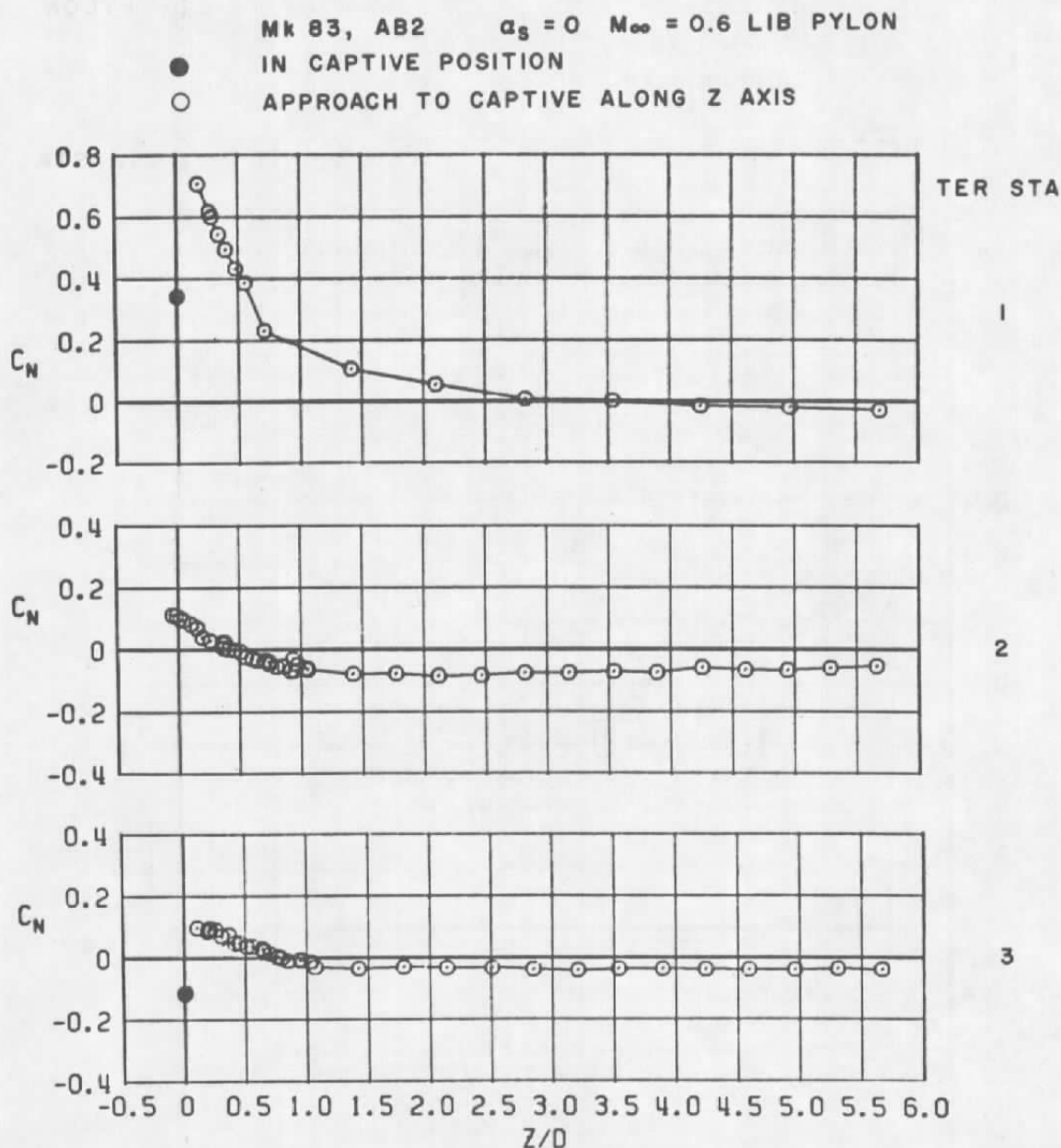
a.  $M_\infty = 0.6$ 

Figure 59. Coefficient of normal force acting on the MK 83 store as a function of normal distance between the store and three captive positions on the TER mounted on the LIB pylon.

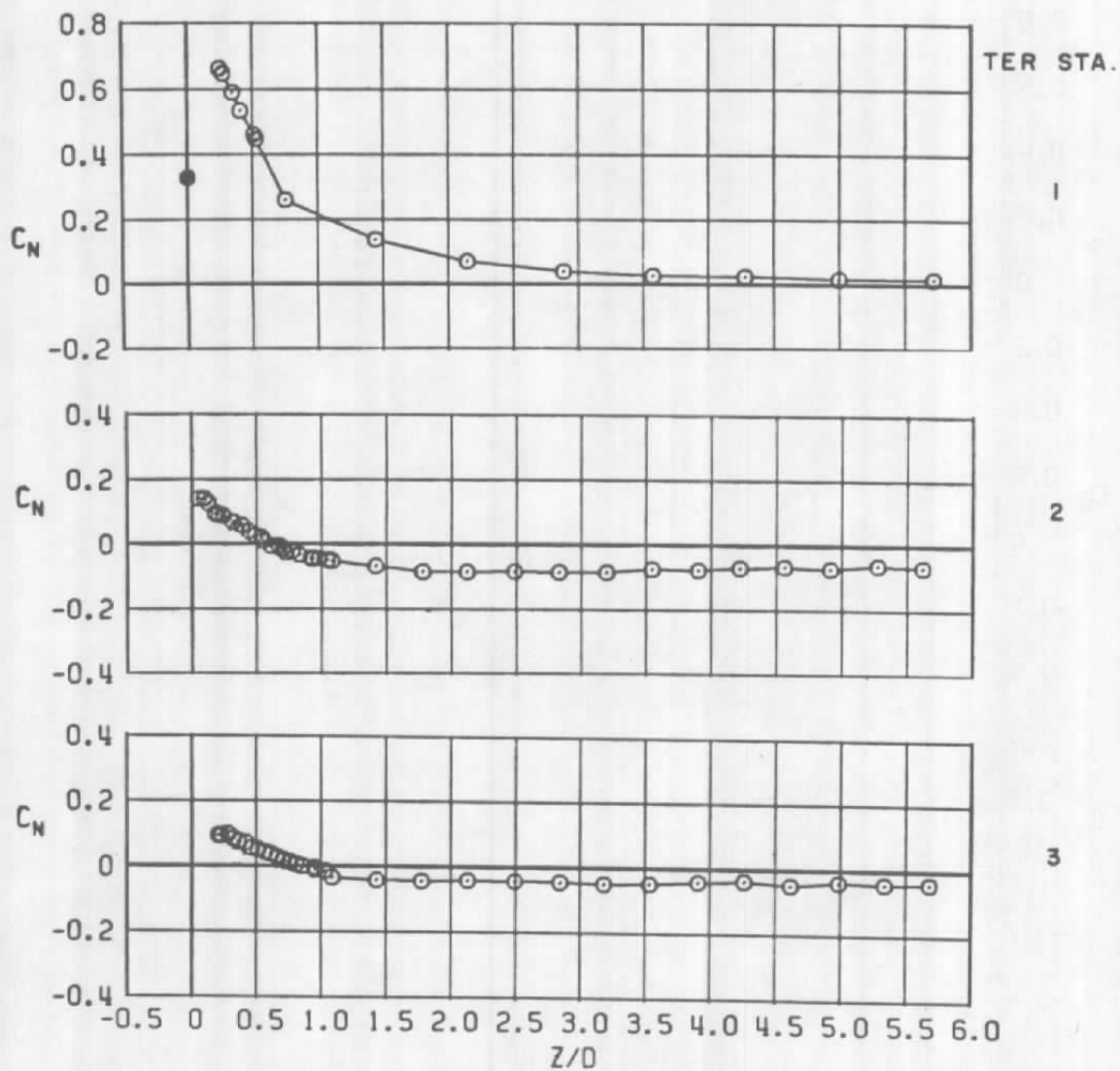
Mk 83, AB2  $\alpha_s = 0$   $M_\infty = 0.8$  LIB PYLON

●

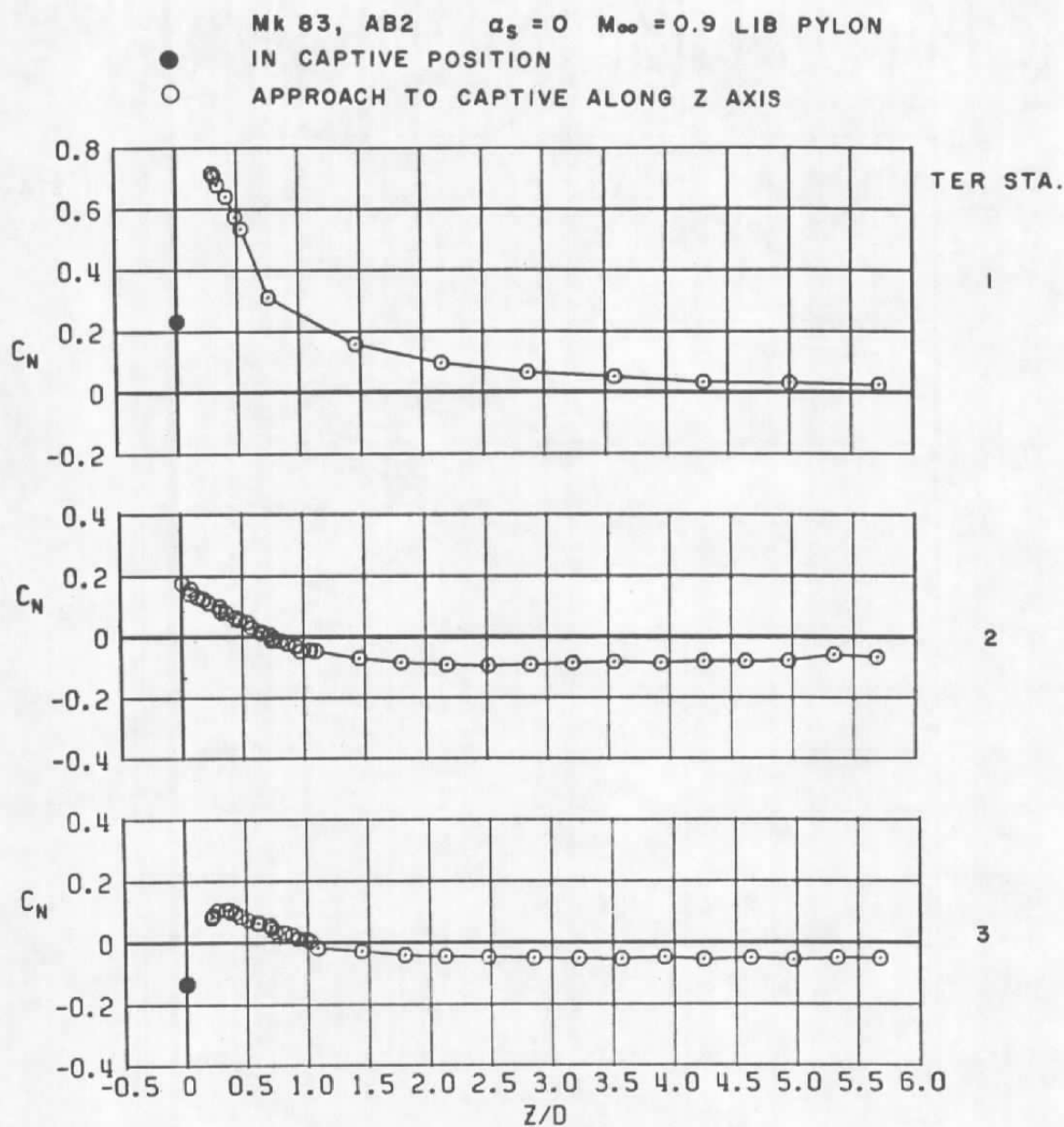
IN CAPTIVE POSITION

○

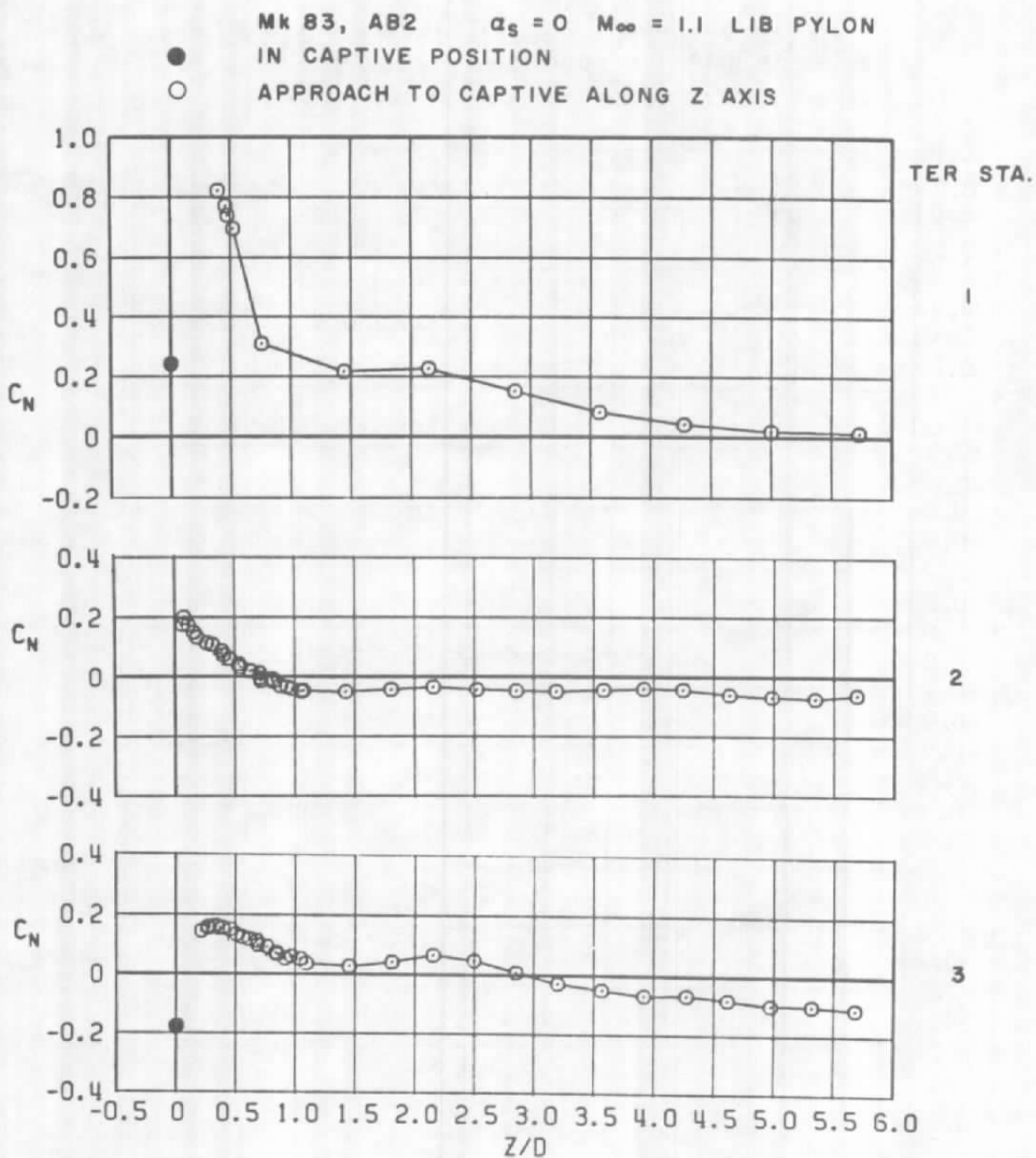
APPROACH TO CAPTIVE ALONG Z AXIS



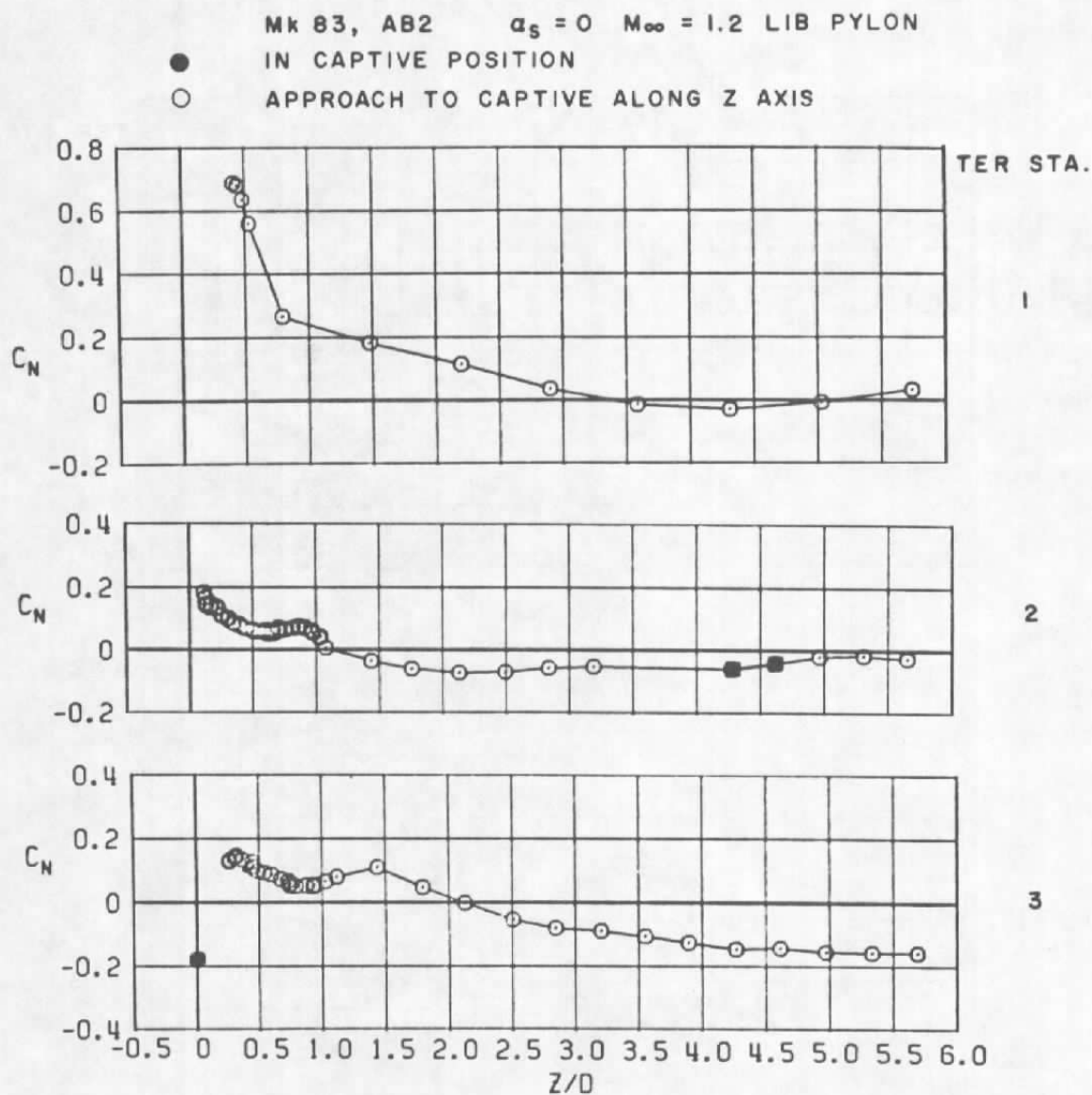
b.  $M_\infty = 0.8$   
Figure 59. Continued.



c.  $M_\infty = 0.9$   
Figure 59. Continued.



d.  $M_\infty = 1.1$   
Figure 59. Continued.



e.  $M_\infty = 1.2$   
Figure 59. Concluded.

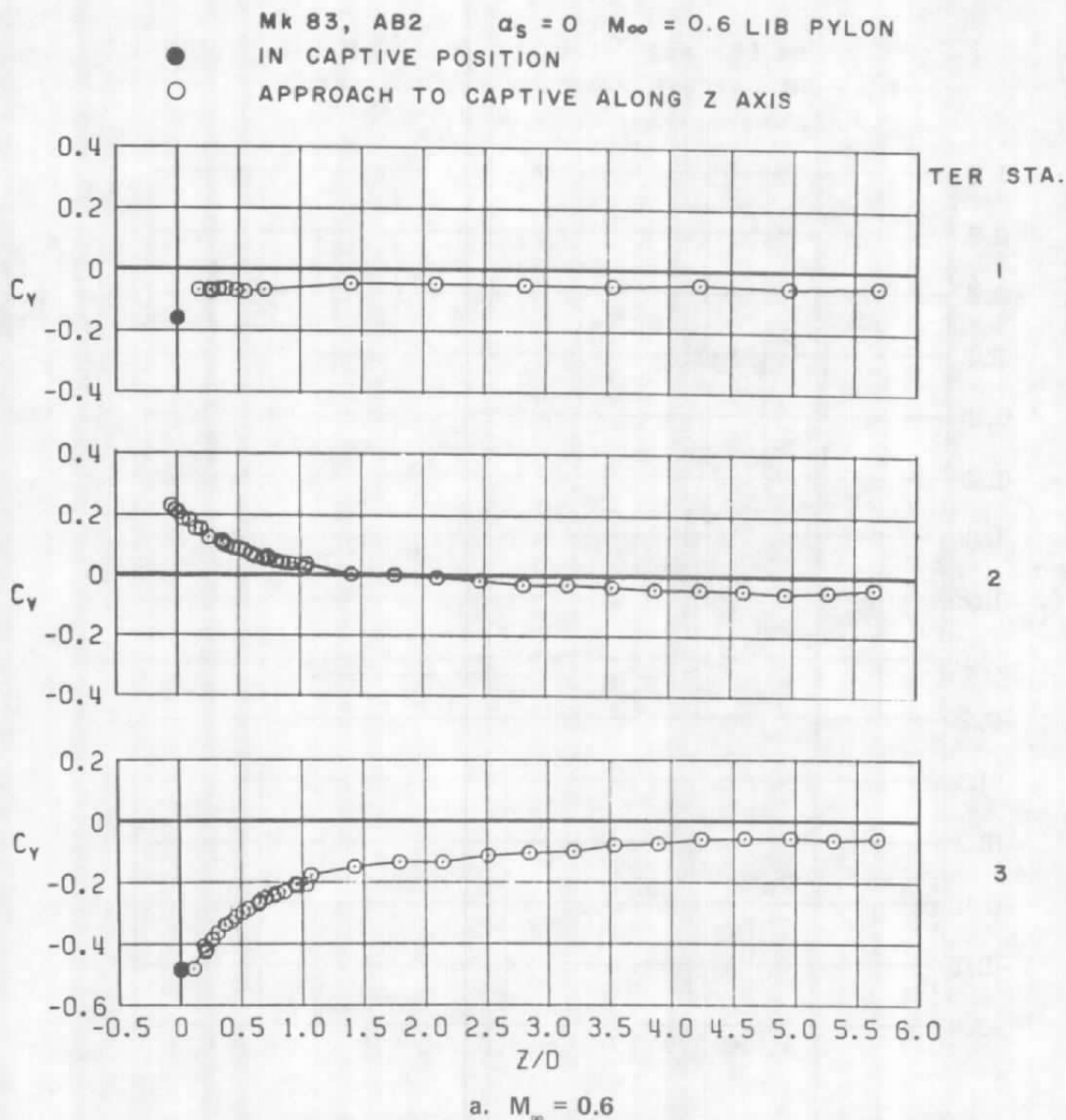
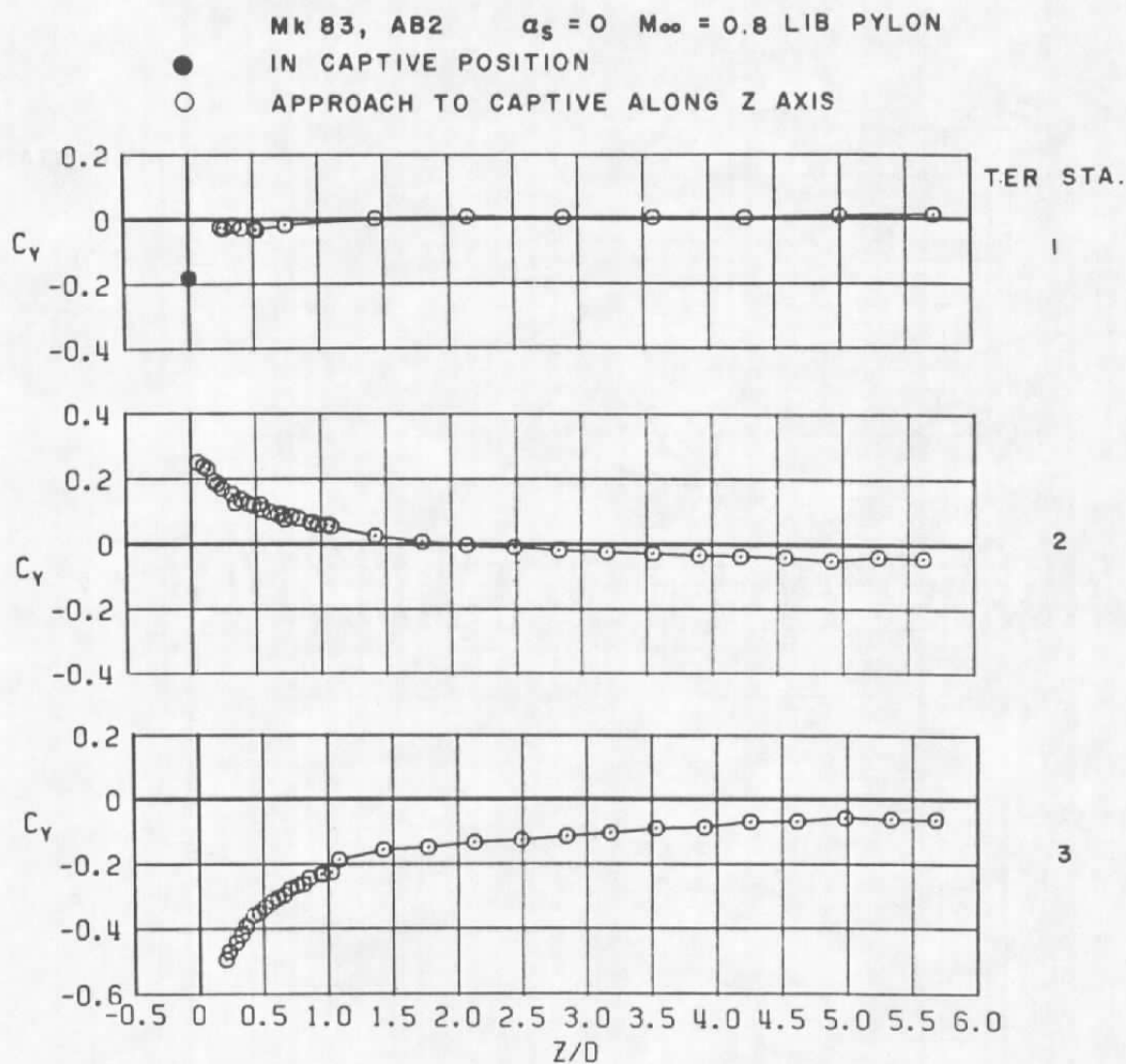


Figure 60. Coefficient of side force acting on the MK 83 store as a function of normal distance between the store and three captive positions on the TER mounted on the LIB pylon.

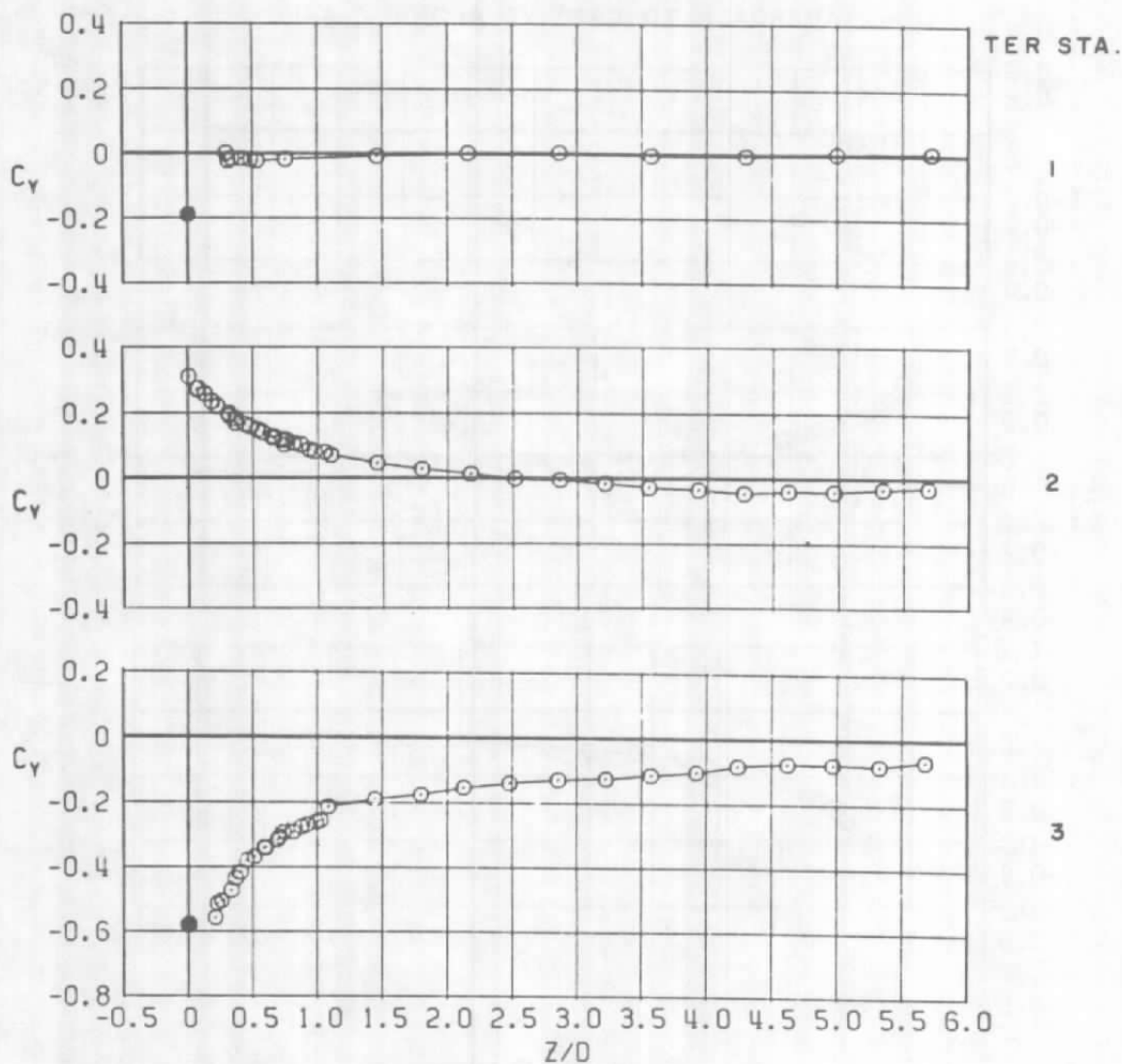


b.  $M_\infty = 0.8$   
Figure 60. Continued.

Mk 83, AB2  $\alpha_s = 0$   $M_\infty = 0.9$  LIB PYLON

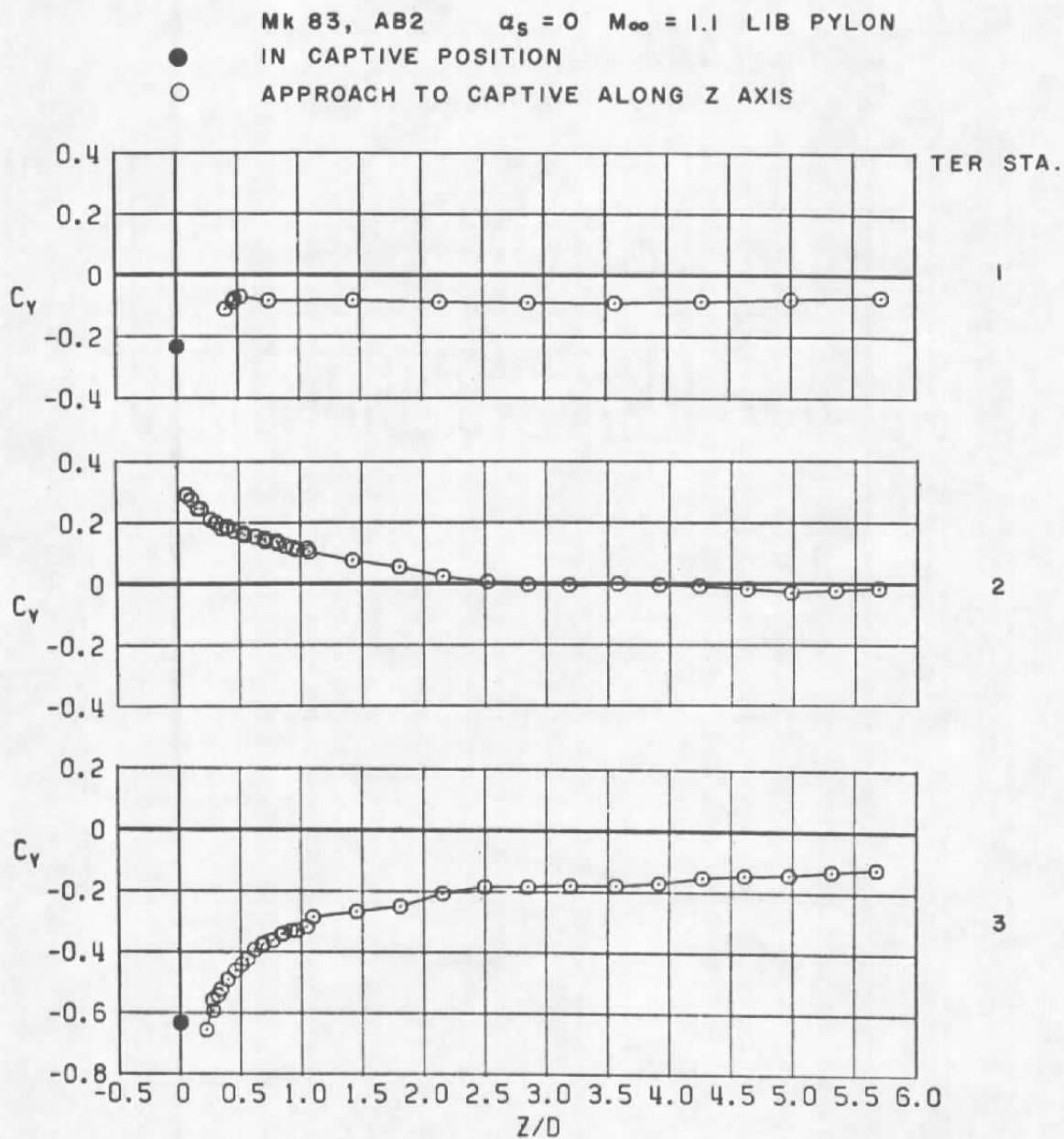
● IN CAPTIVE POSITION

○ APPROACH TO CAPTIVE ALONG Z AXIS



c.  $M_\infty = 0.9$   
Figure 60. Continued.



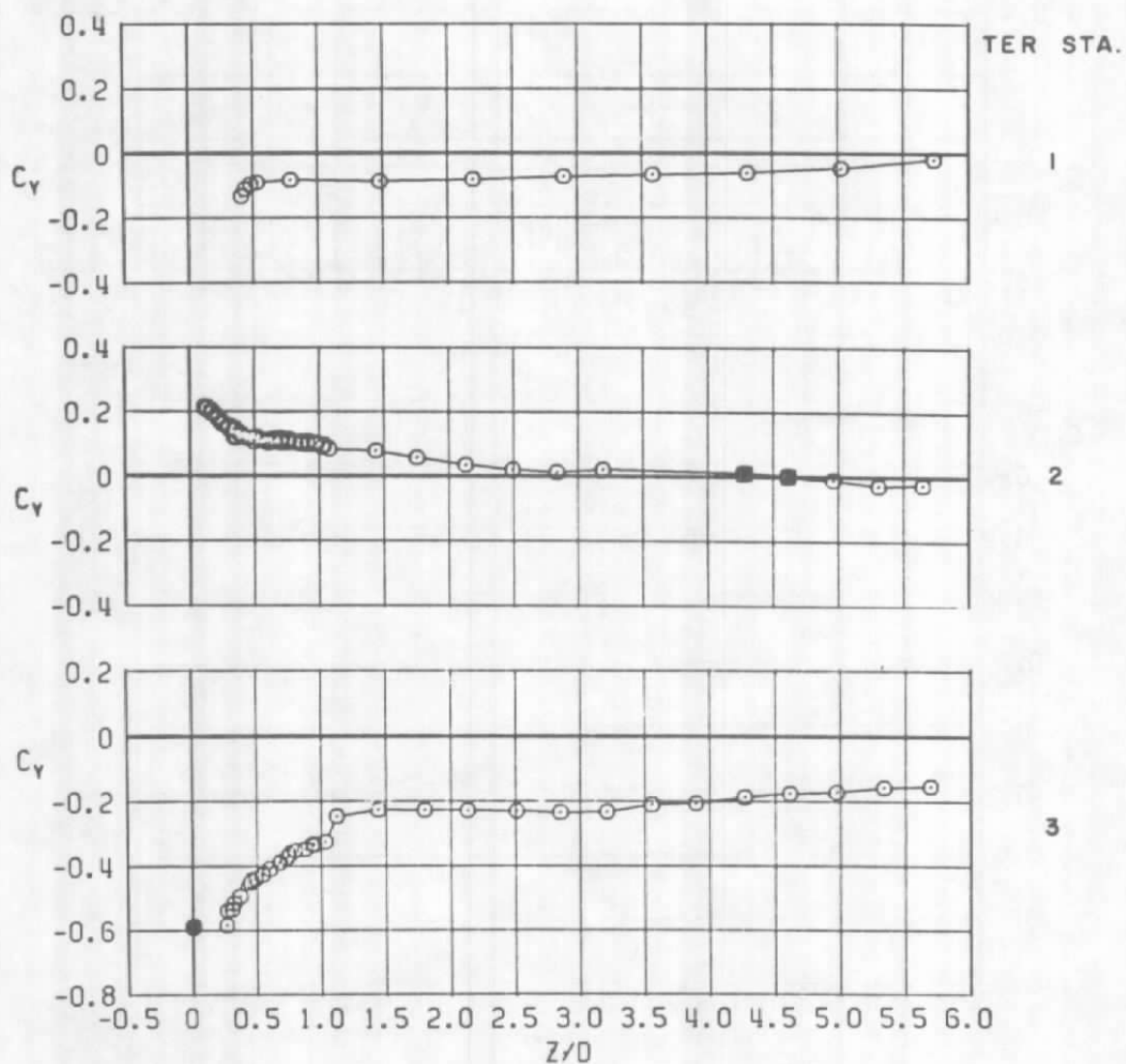


d.  $M_\infty = 1.1$   
Figure 60. Continued.

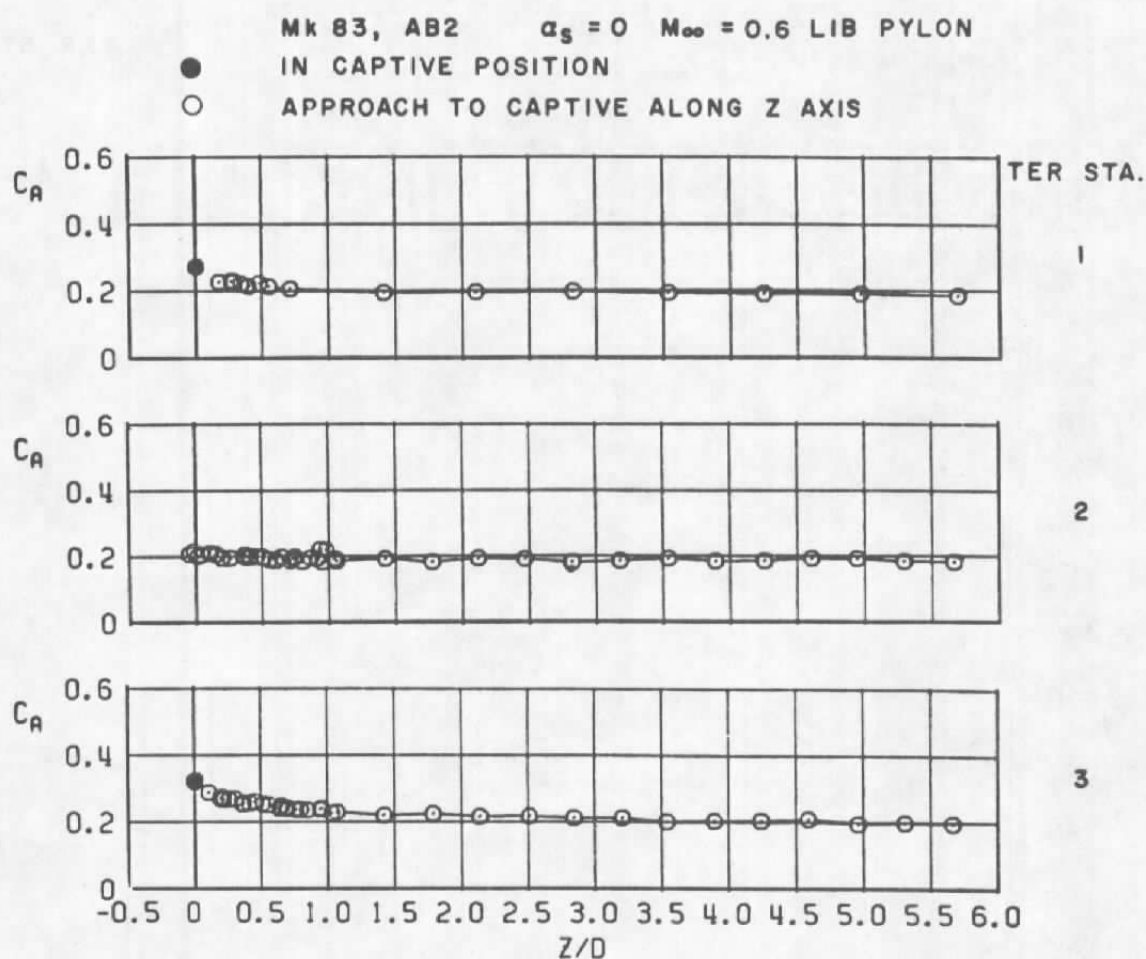
Mk 83, AB2  $\alpha_s = 0$   $M_\infty = 1.2$  LIB PYLON

● IN CAPTIVE POSITION

○ APPROACH TO CAPTIVE ALONG Z AXIS

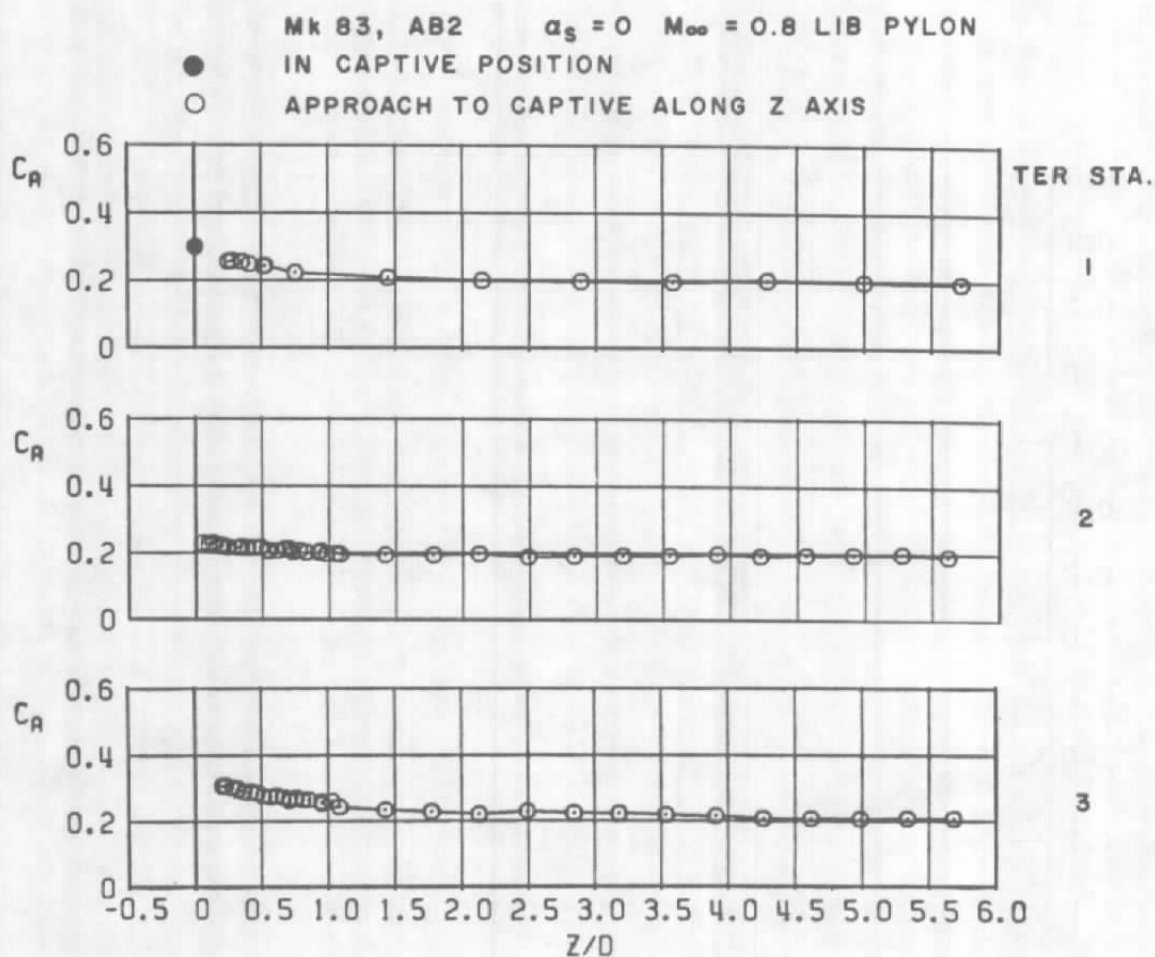


e.  $M_\infty = 1.2$   
Figure 60. Concluded.

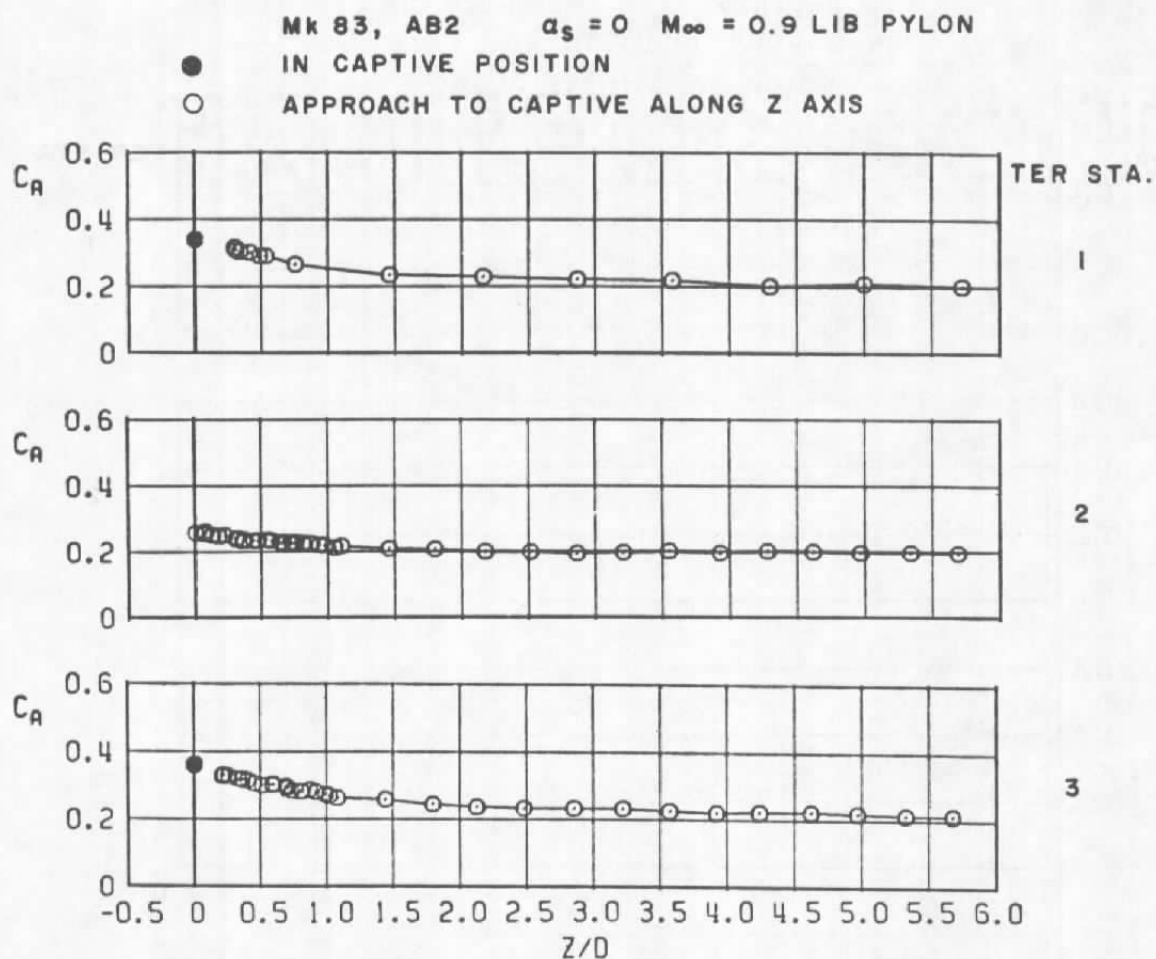


a.  $M_\infty = 0.6$

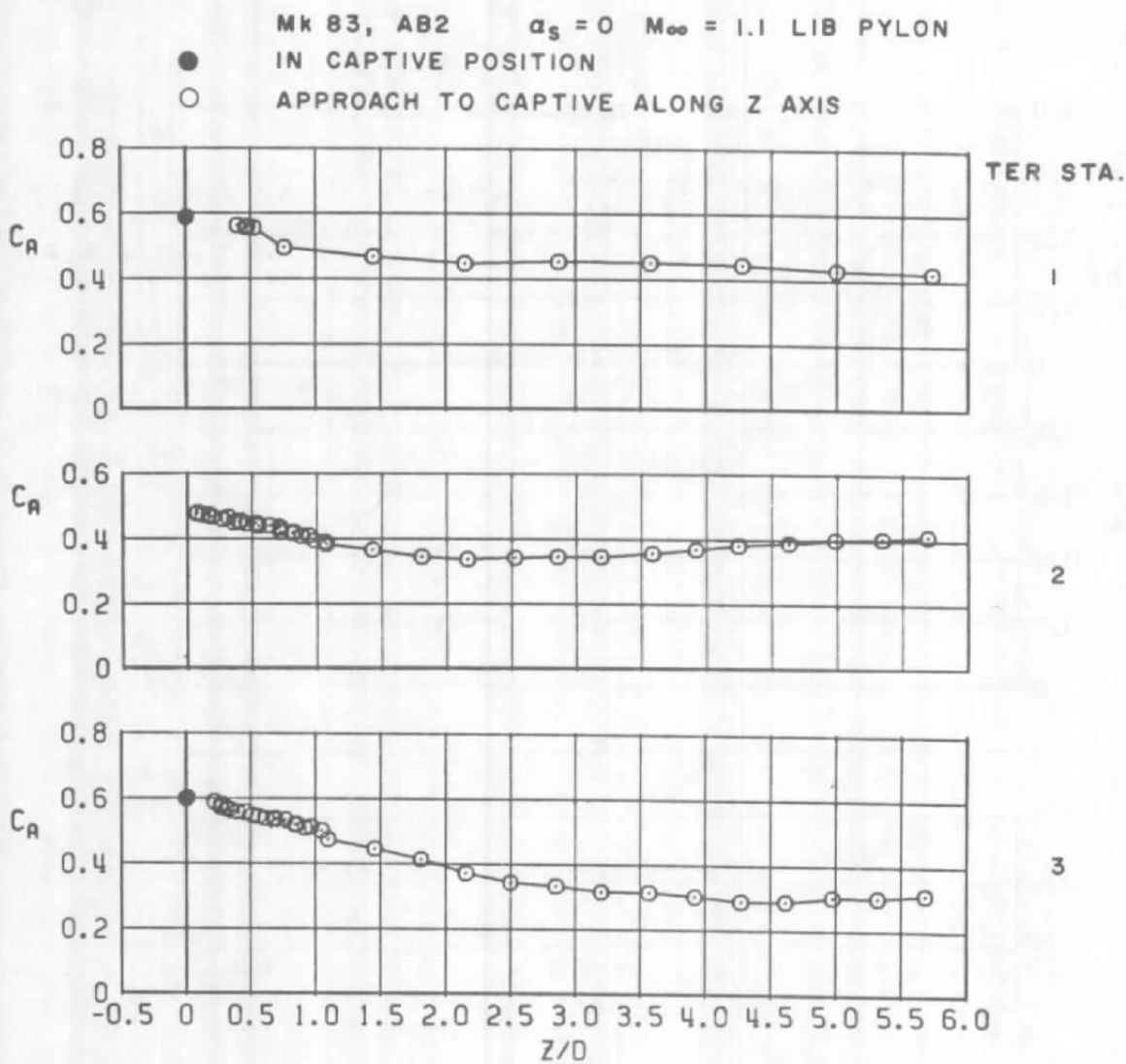
Figure 61. Coefficient of axial force acting on the MK 83 store as a function of normal distance between the store and three captive positions on the TER mounted on the LIB pylon.



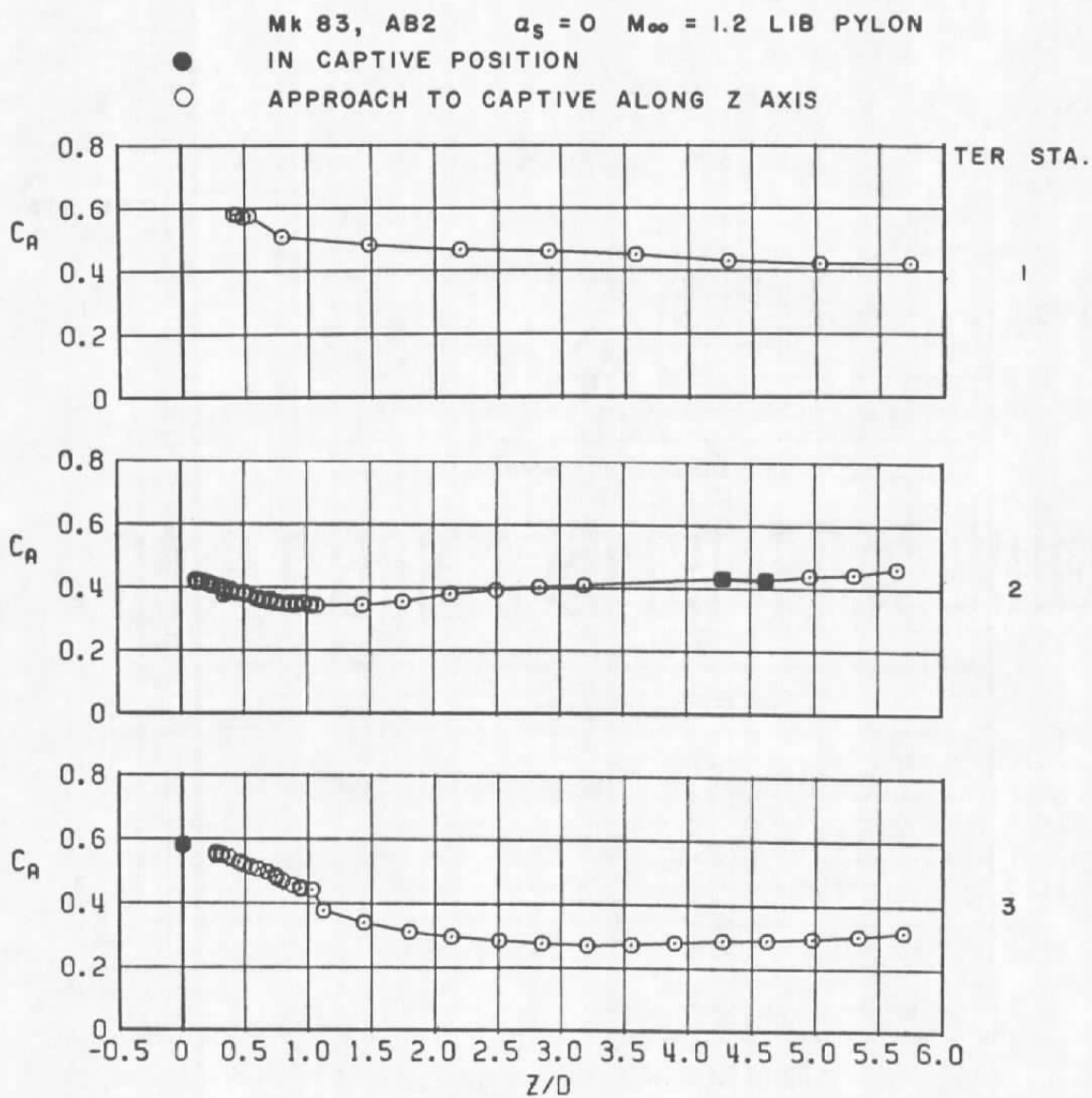
b.  $M_\infty = 0.8$   
Figure 61. Continued.



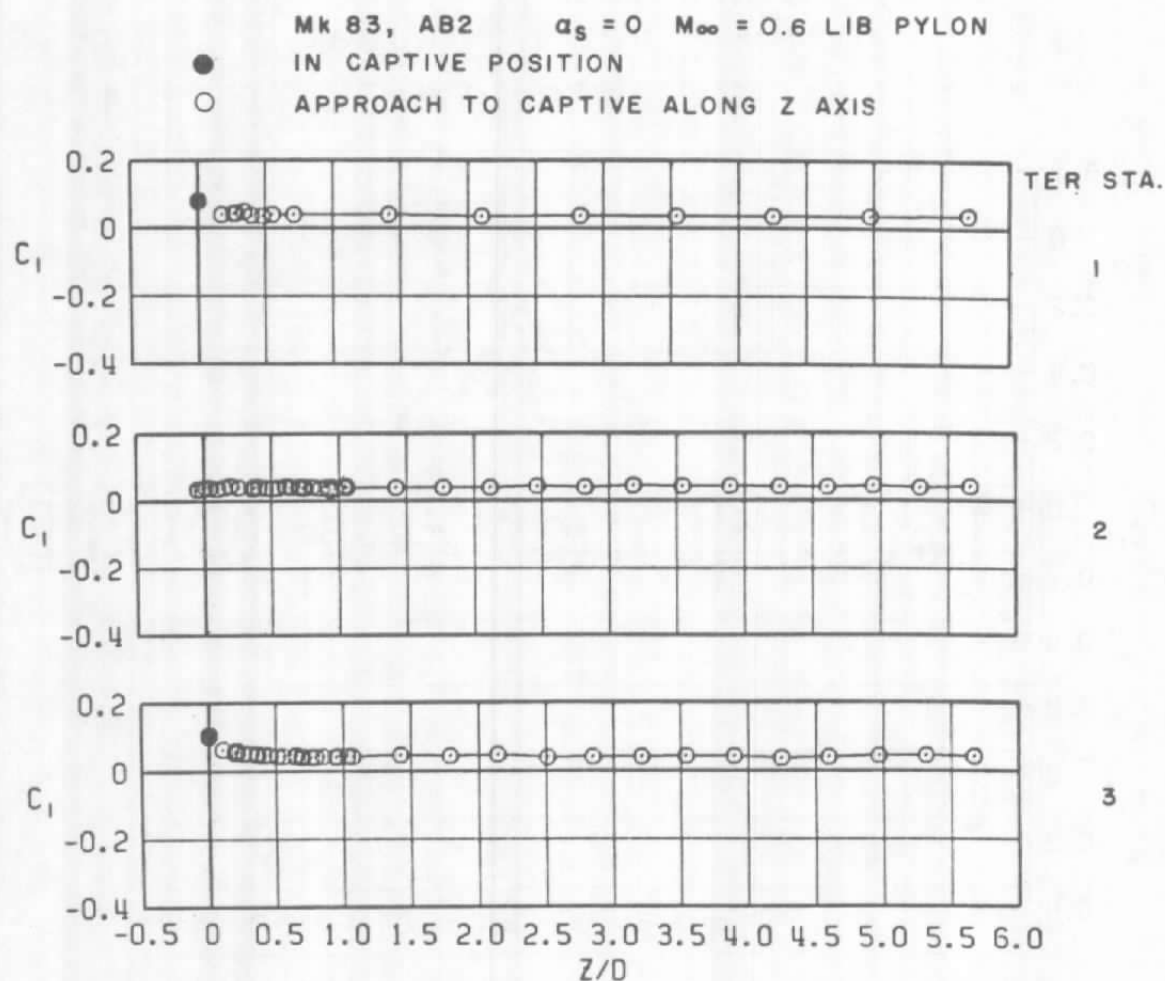
c.  $M_\infty = 0.9$   
Figure 61. Continued.



d.  $M_\infty = 1.1$   
Figure 61. Continued.



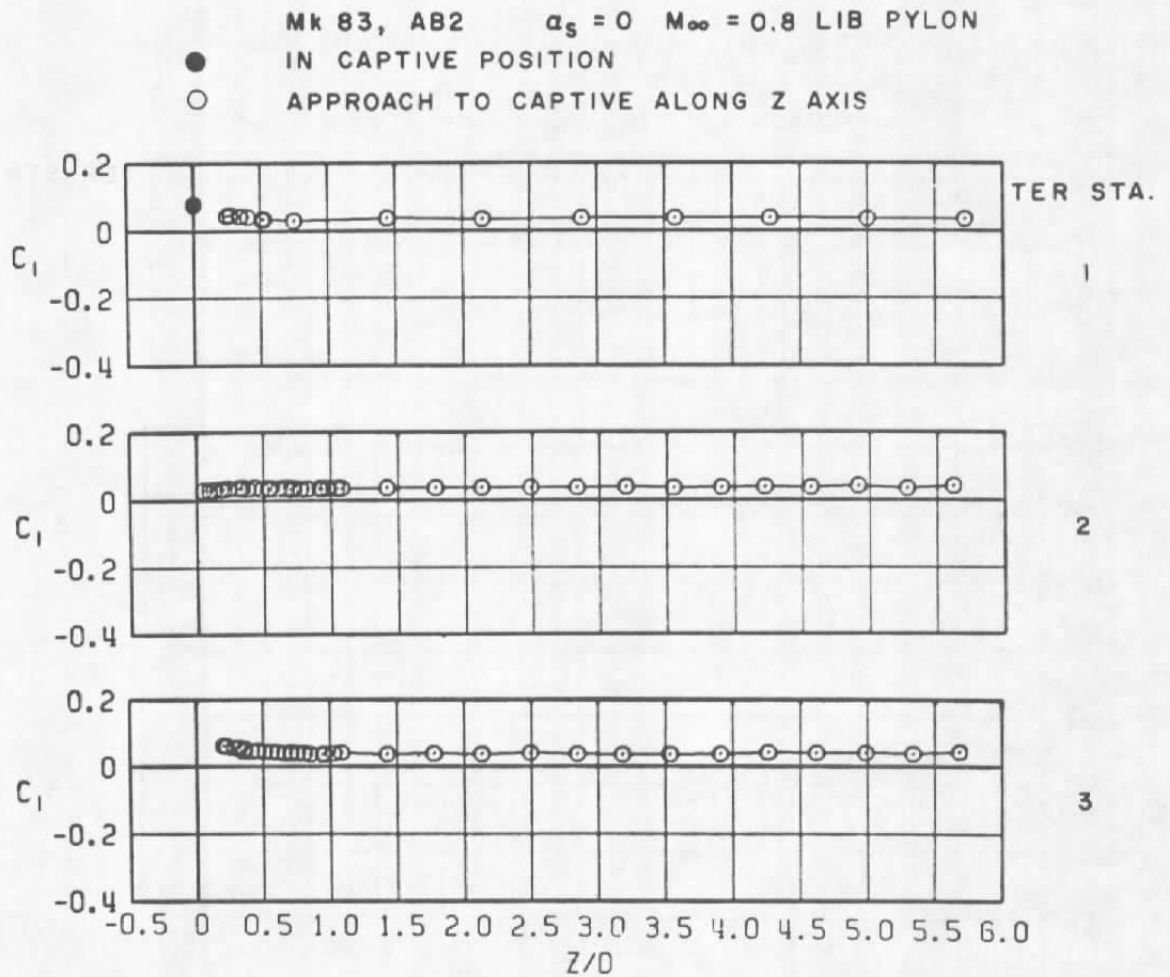
e.  $M_\infty = 1.2$   
Figure 61. Concluded.



a.  $M_\infty = 0.6$

Figure 62. Coefficient of rolling moment acting on the MK 83 store as a function of normal distance between the store and three captive positions on the TER mounted on the LIB pylon.



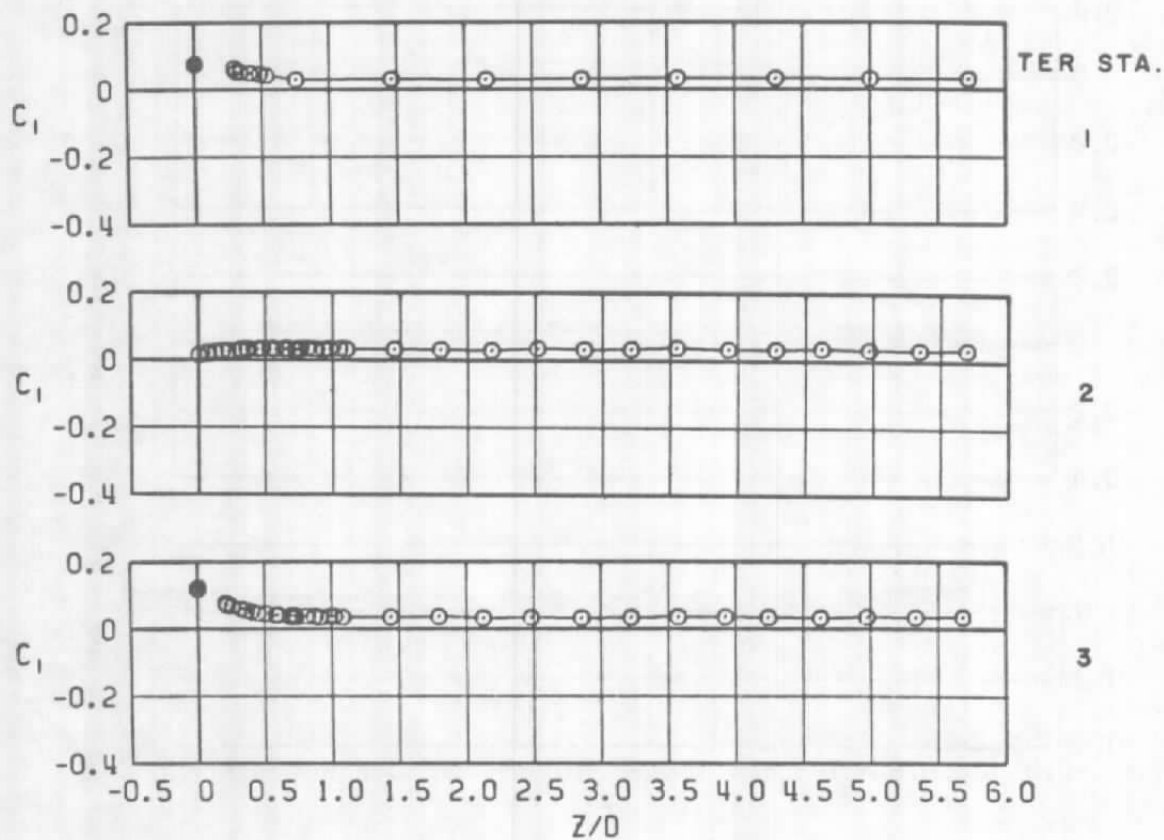


b.  $M_\infty = 0.8$   
Figure 62. Continued.

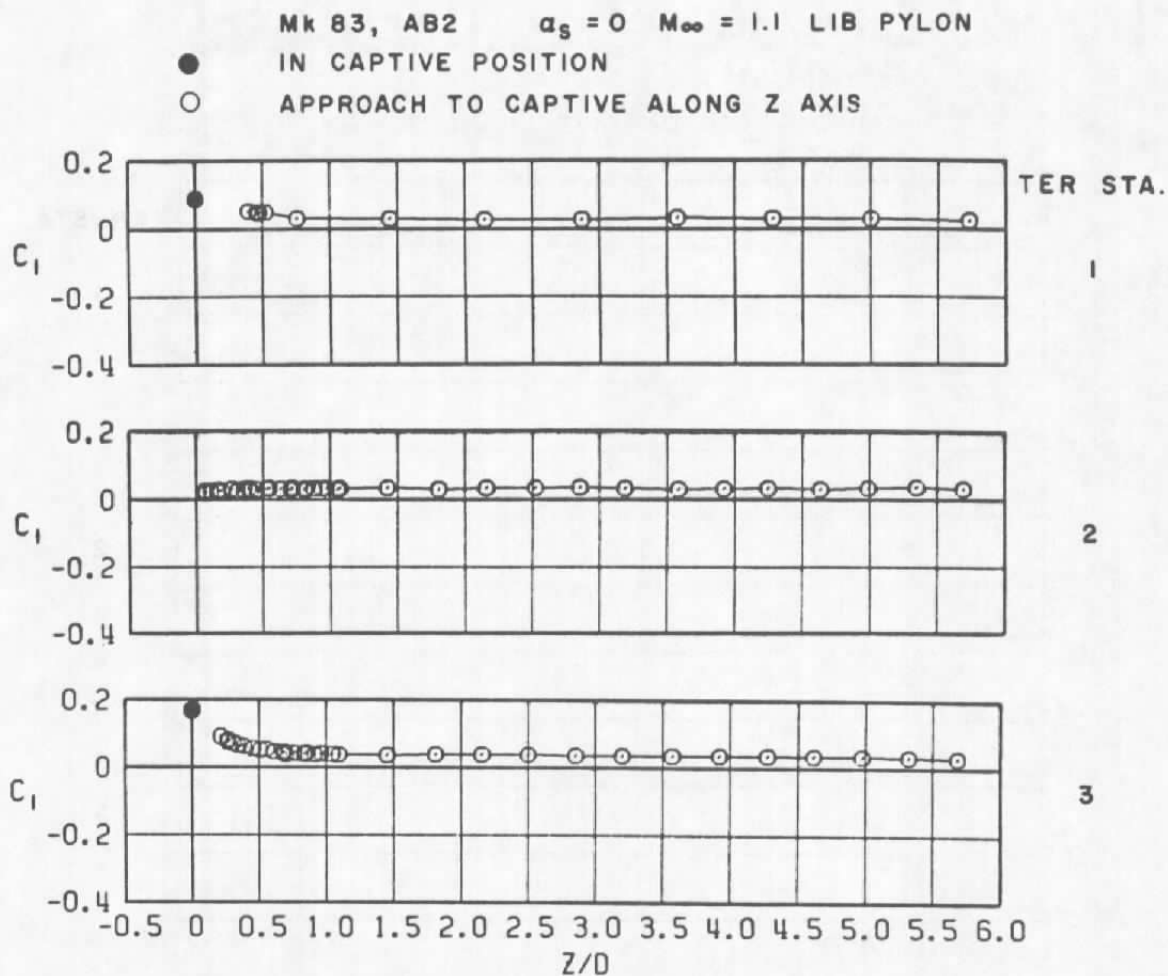
Mk 83, AB2  $\alpha_s = 0$   $M_\infty = 0.9$  LIB PYLON

● IN CAPTIVE POSITION

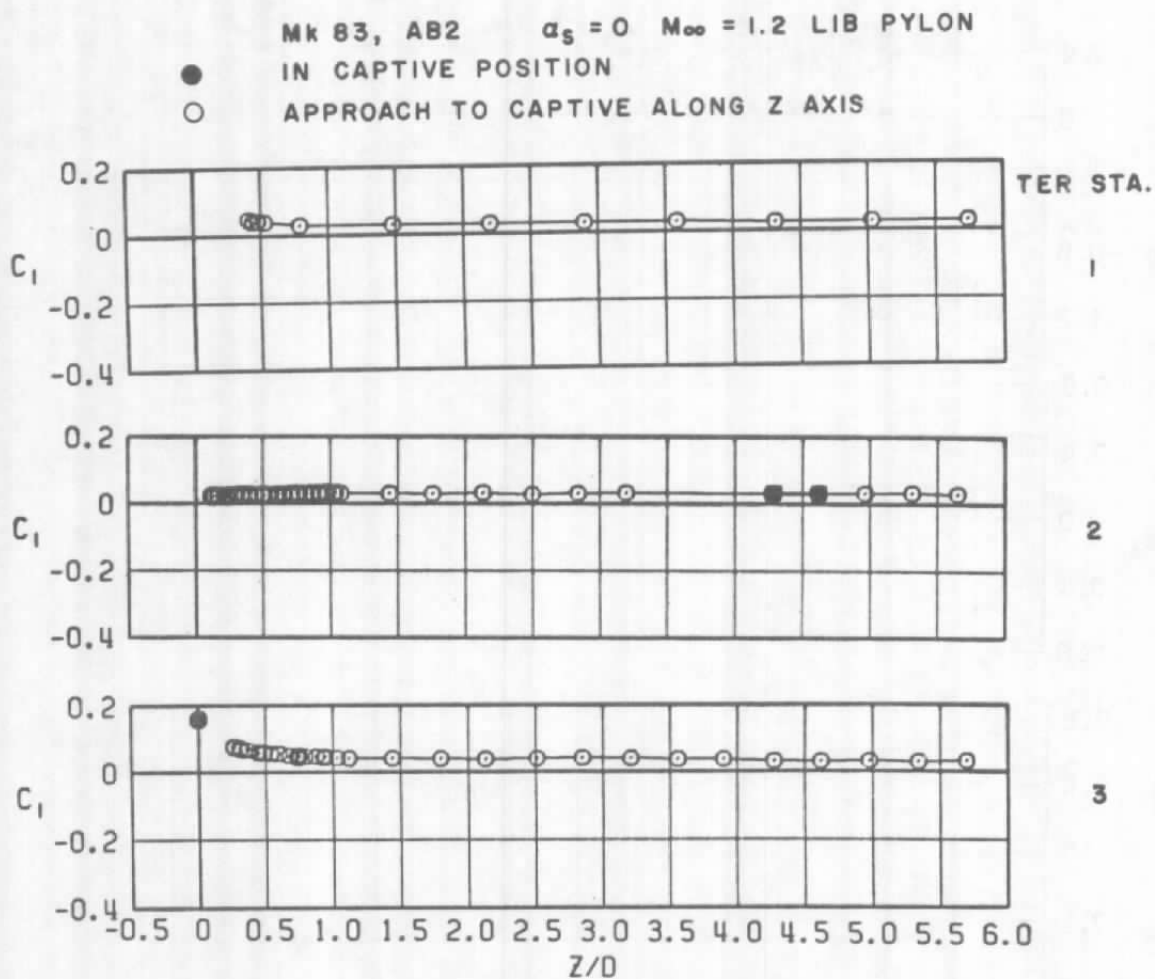
○ APPROACH TO CAPTIVE ALONG Z AXIS



c.  $M_\infty = 0.9$   
Figure 62. Continued.



d.  $M_\infty = 1.1$   
Figure 62. Continued.



e.  $M_\infty = 1.2$   
Figure 62. Concluded.

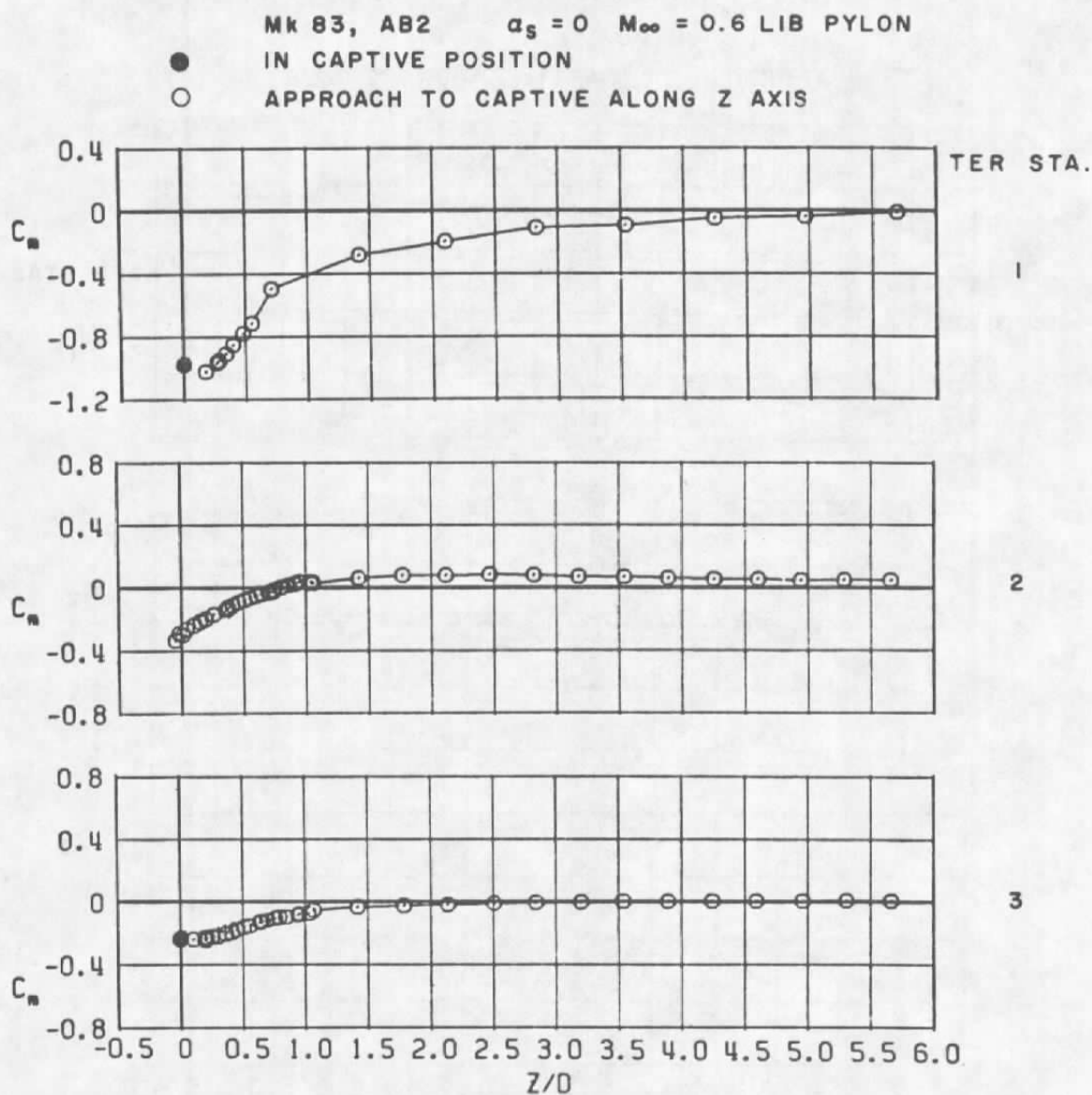
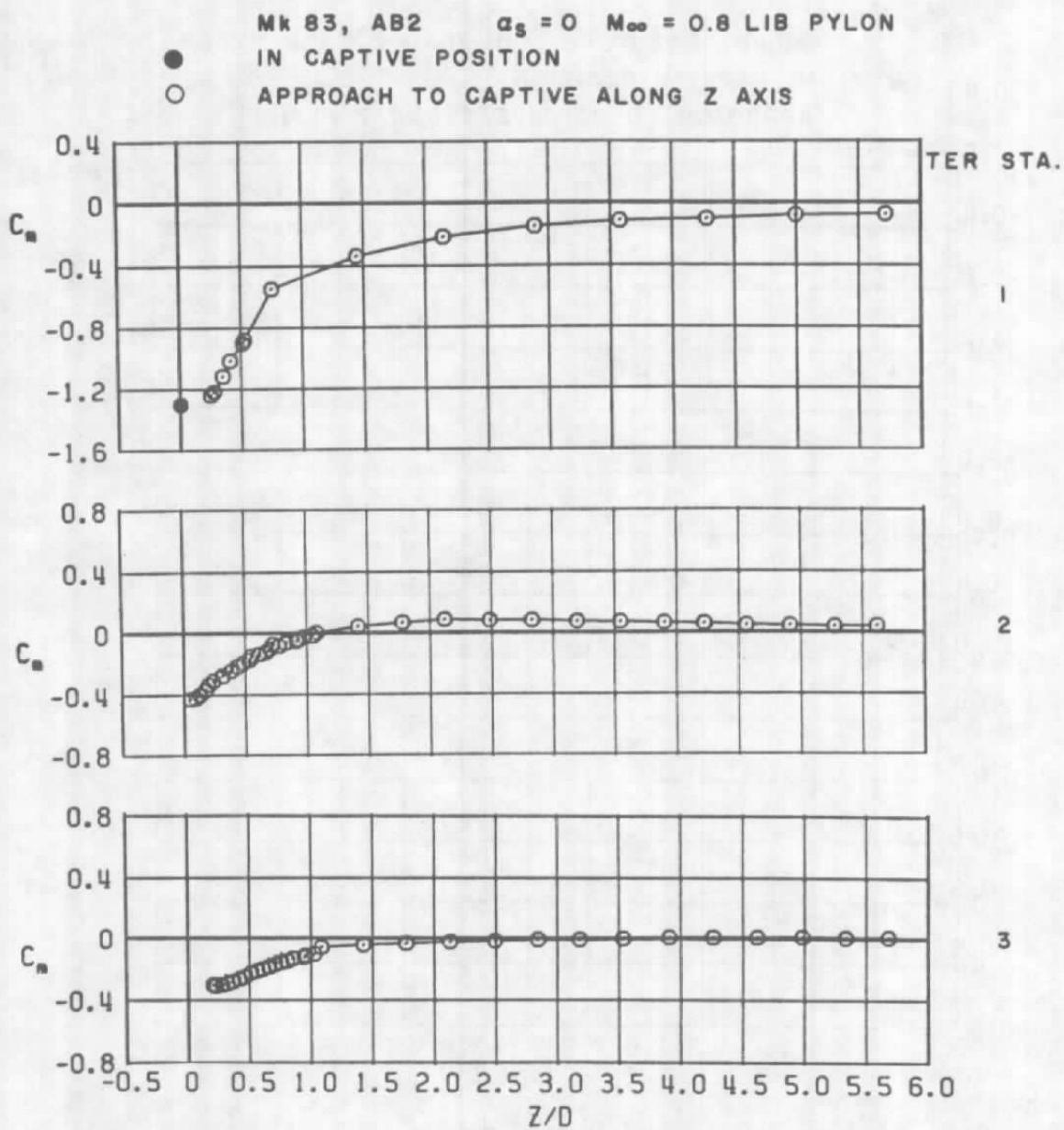
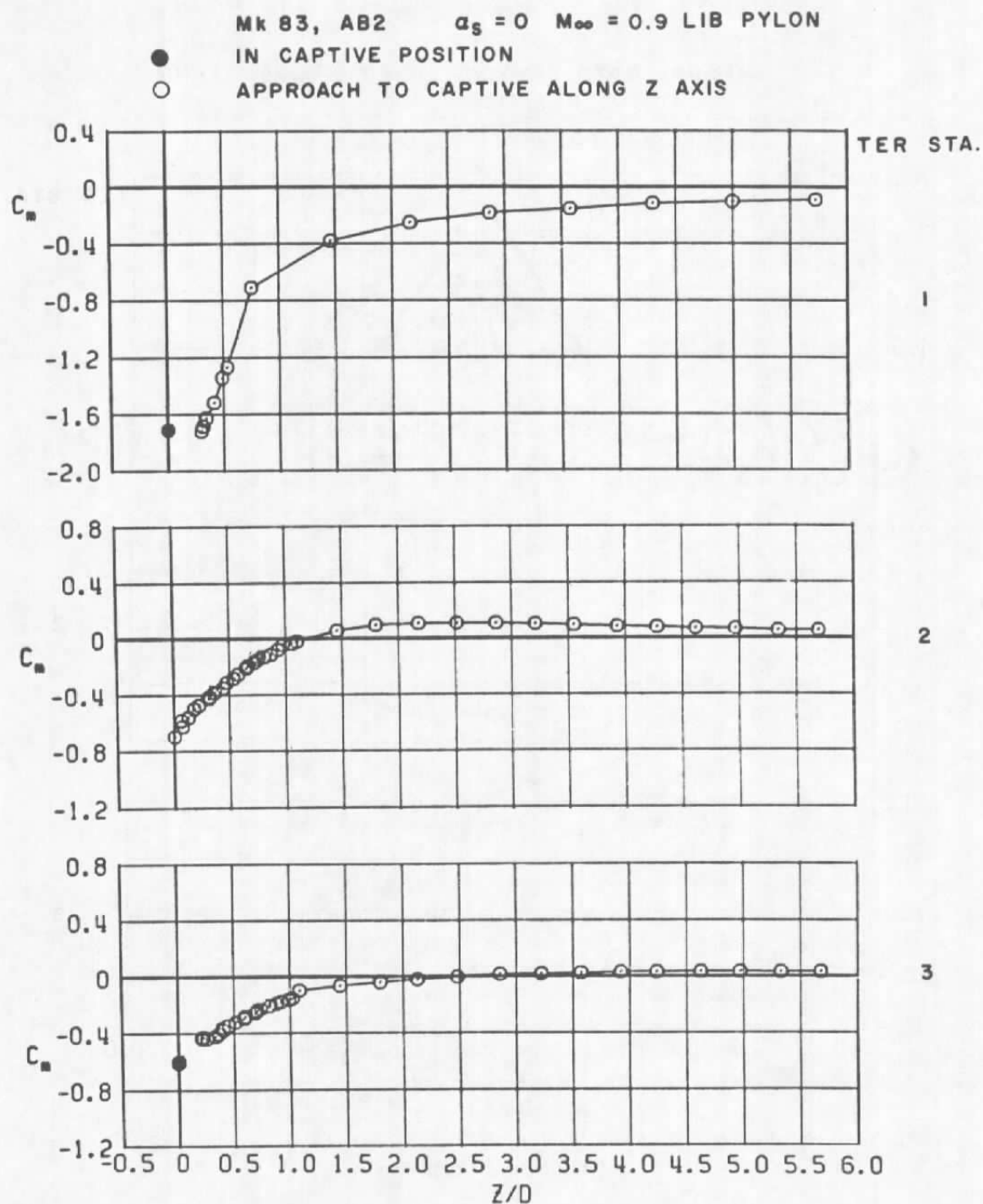
a.  $M_\infty = 0.6$ 

Figure 63. Coefficient of pitching moment acting on the MK 83 store as a function of normal distance between the store and three captive positions on the TER mounted on the LIB pylon.



b.  $M_\infty = 0.8$   
Figure 63. Continued.

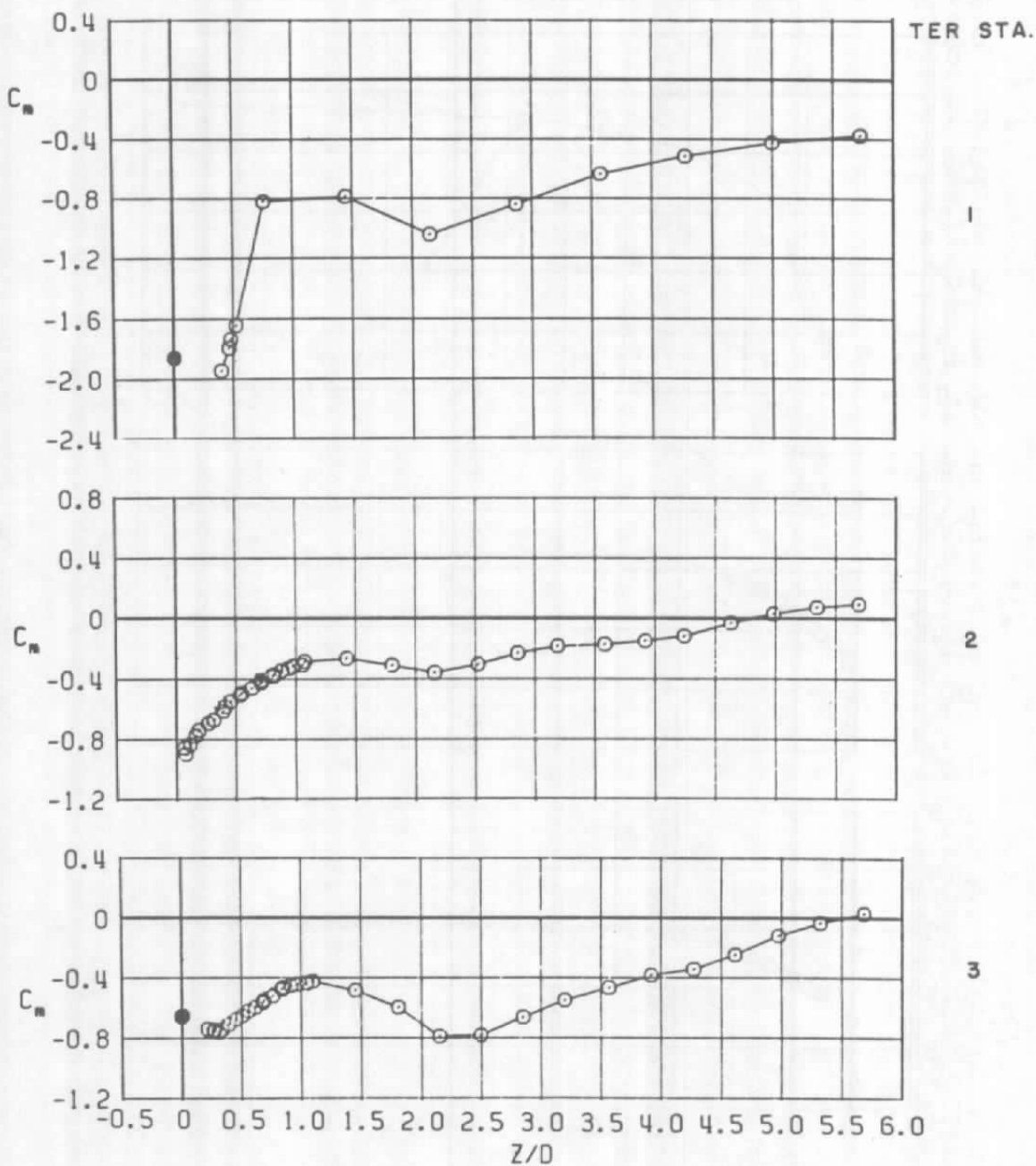


c.  $M_\infty = 0.9$   
Figure 63. Continued.

Mk 83, AB2  $\alpha_s = 0$   $M_\infty = 1.1$  LIB PYLON

● IN CAPTIVE POSITION

○ APPROACH TO CAPTIVE ALONG Z AXIS



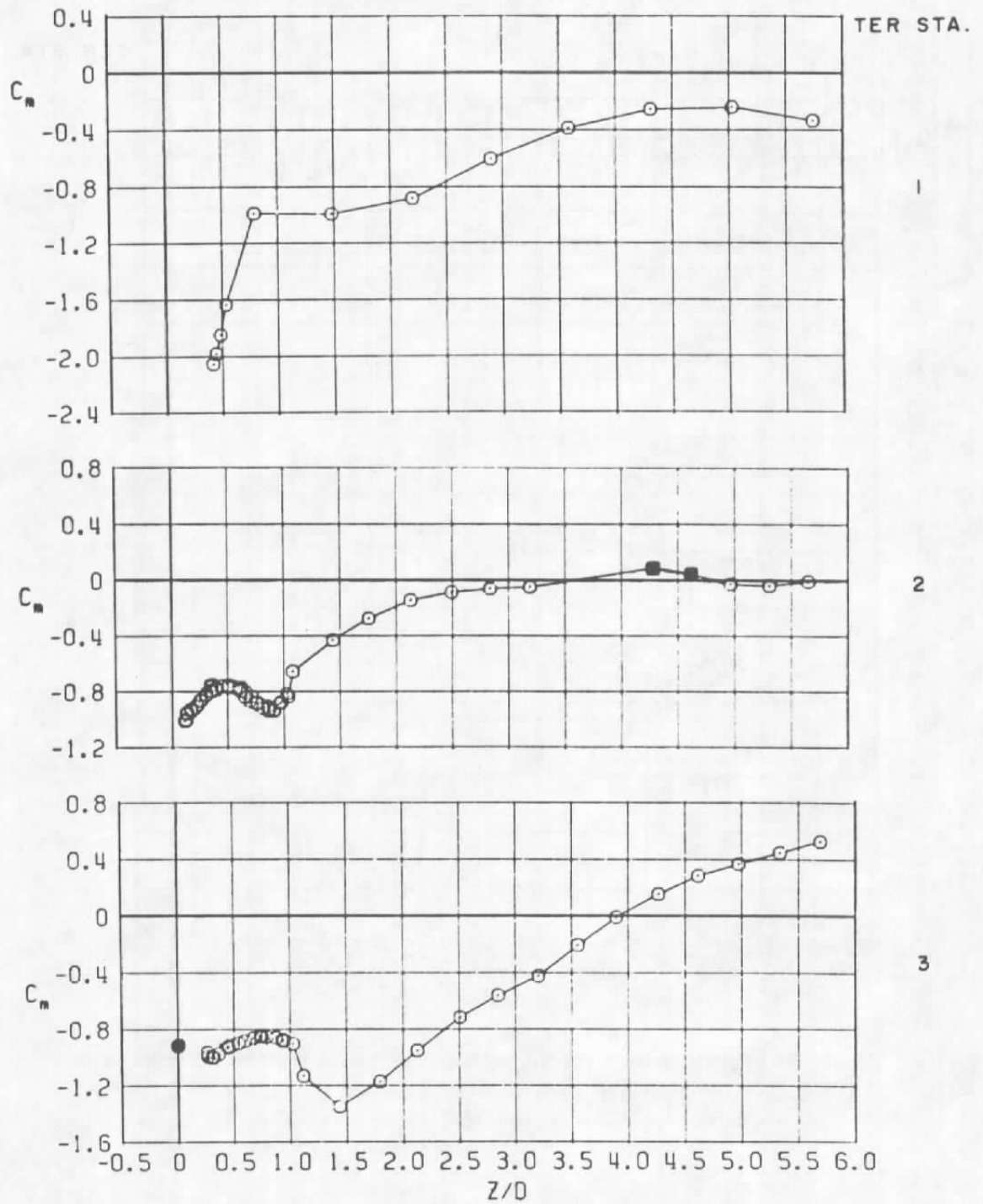
d.  $M_\infty = 1.1$   
Figure 63. Continued.



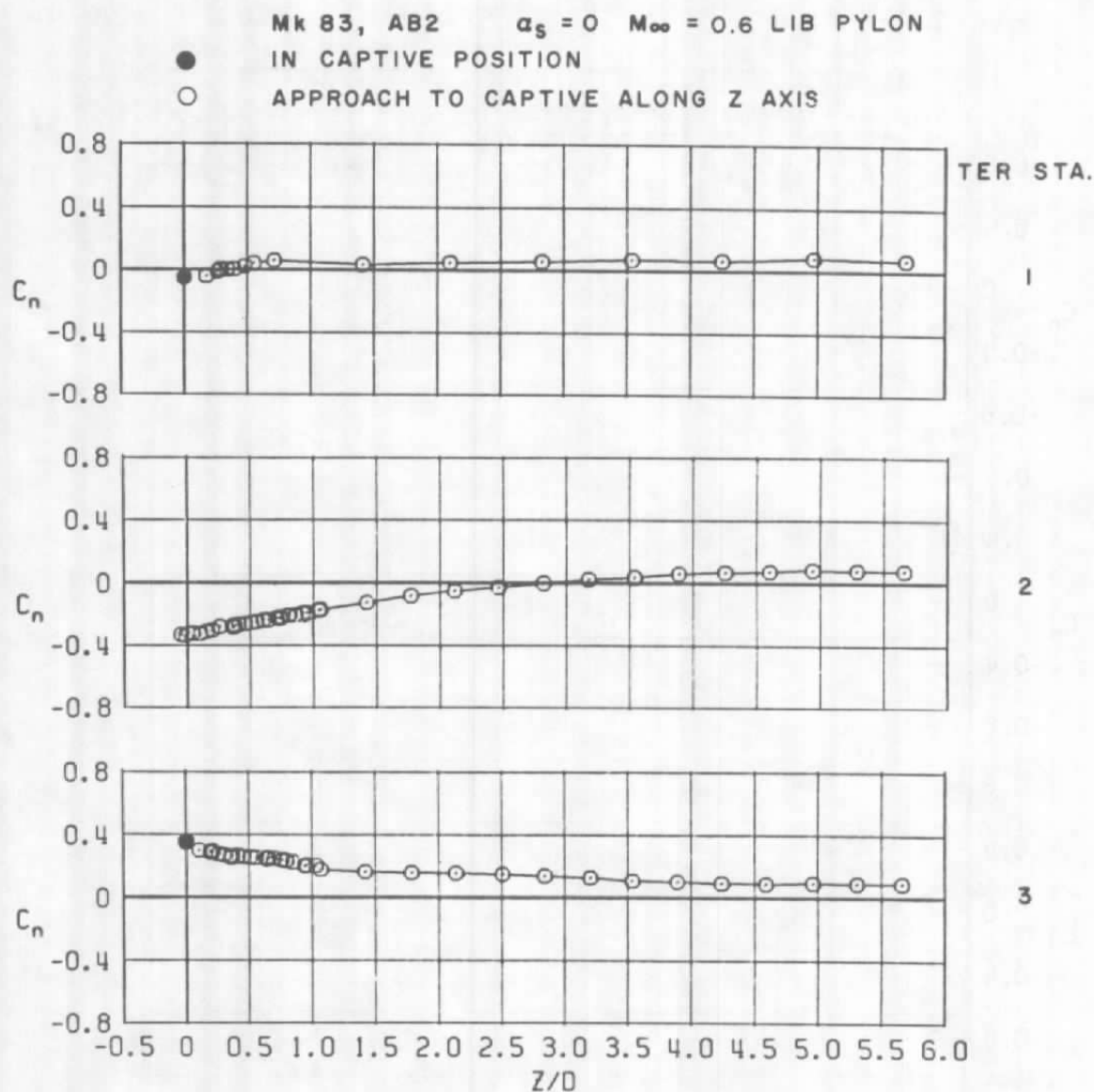
Mk 83, AB2  $\alpha_s = 0$   $M_\infty = 1.2$  LIB PYLON

● IN CAPTIVE POSITION

○ APPROACH TO CAPTIVE ALONG Z AXIS

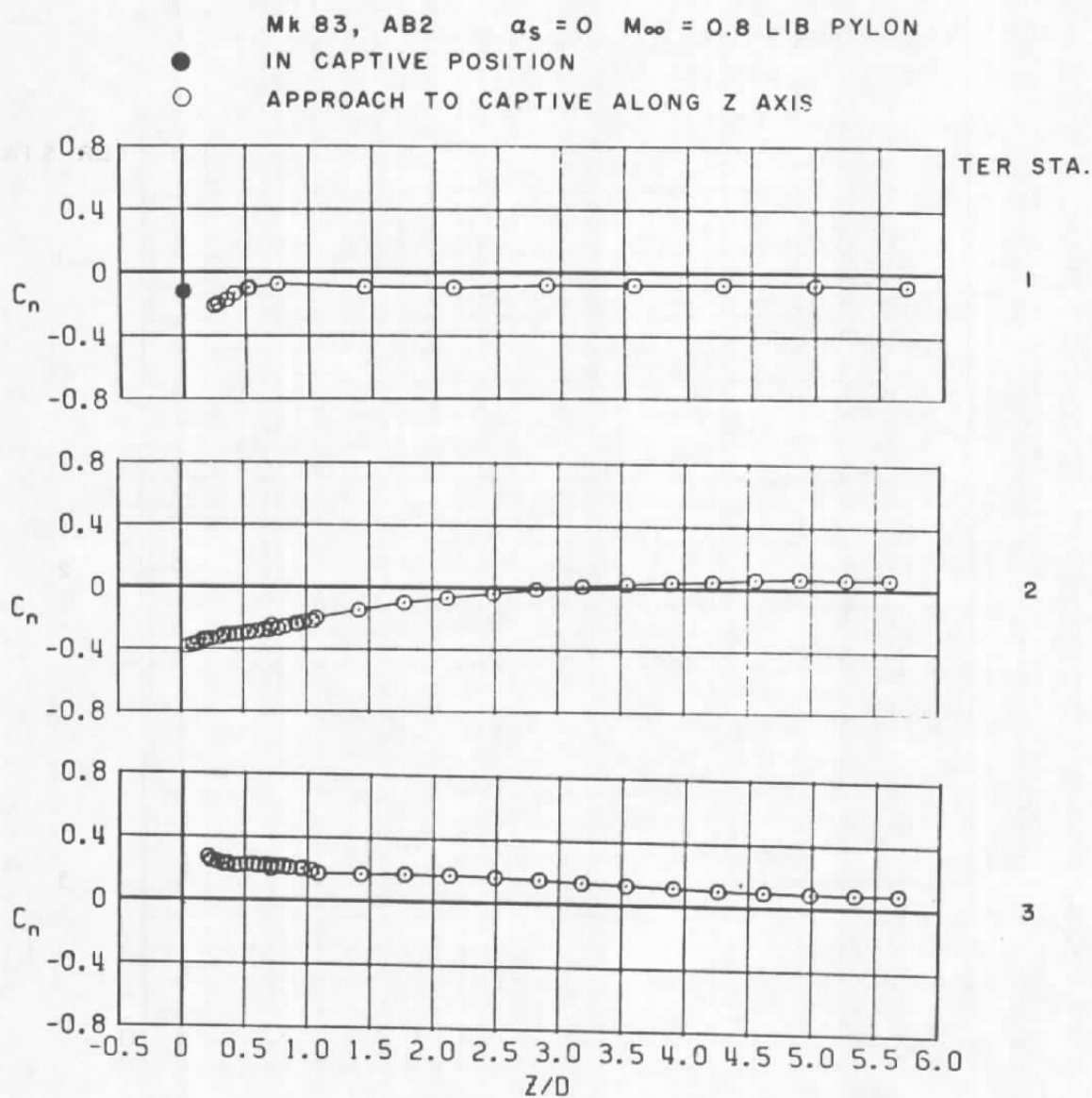


e.  $M_\infty = 1.2$   
Figure 63. Concluded.



a.  $M_\infty = 0.6$

Figure 64. Coefficient of yawing moment acting on the MK 83 store as a function of normal distance between the store and three captive positions on the TER mounted on the LIB pylon.

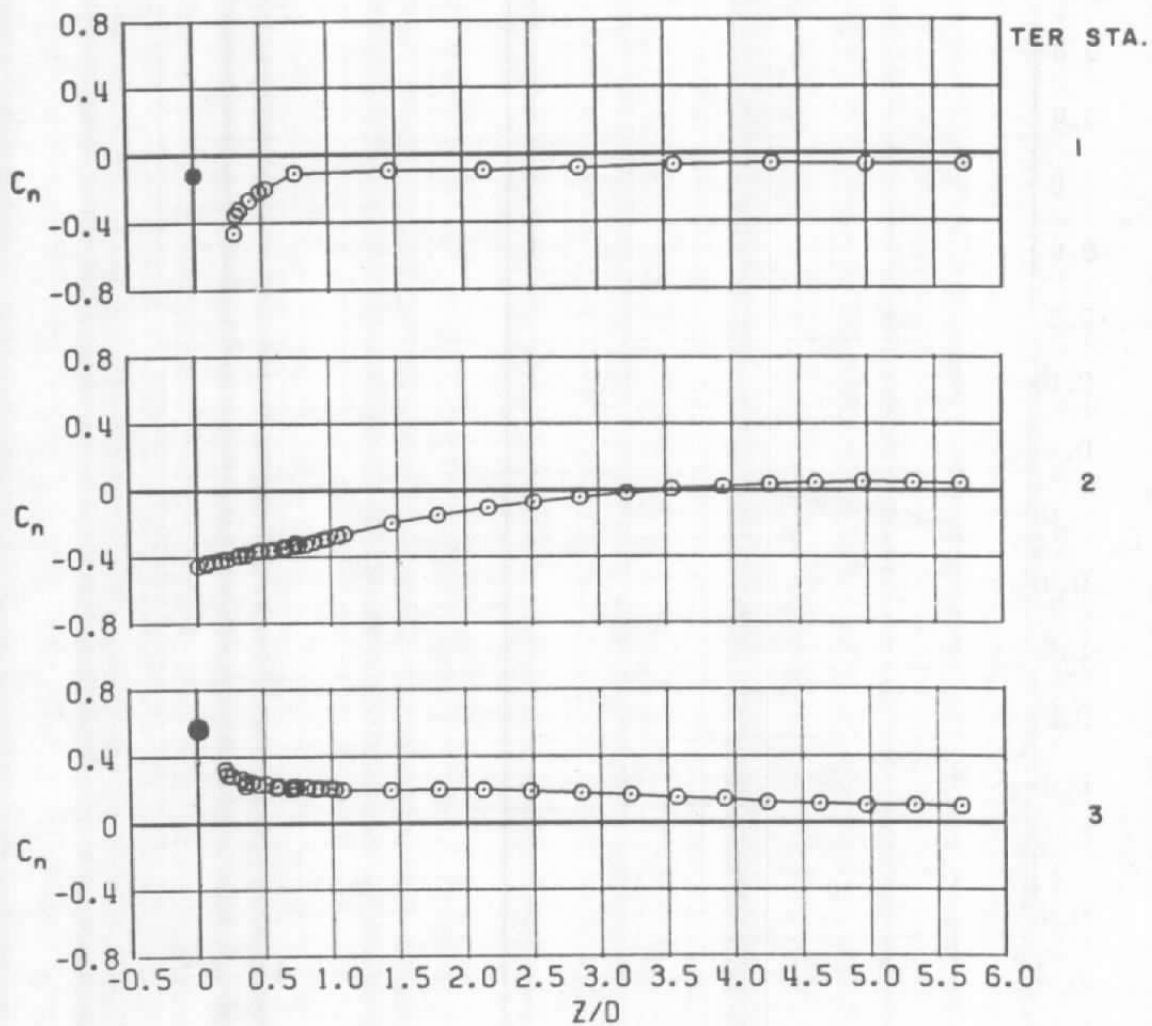


b.  $M_\infty = 0.8$   
Figure 64. Continued.

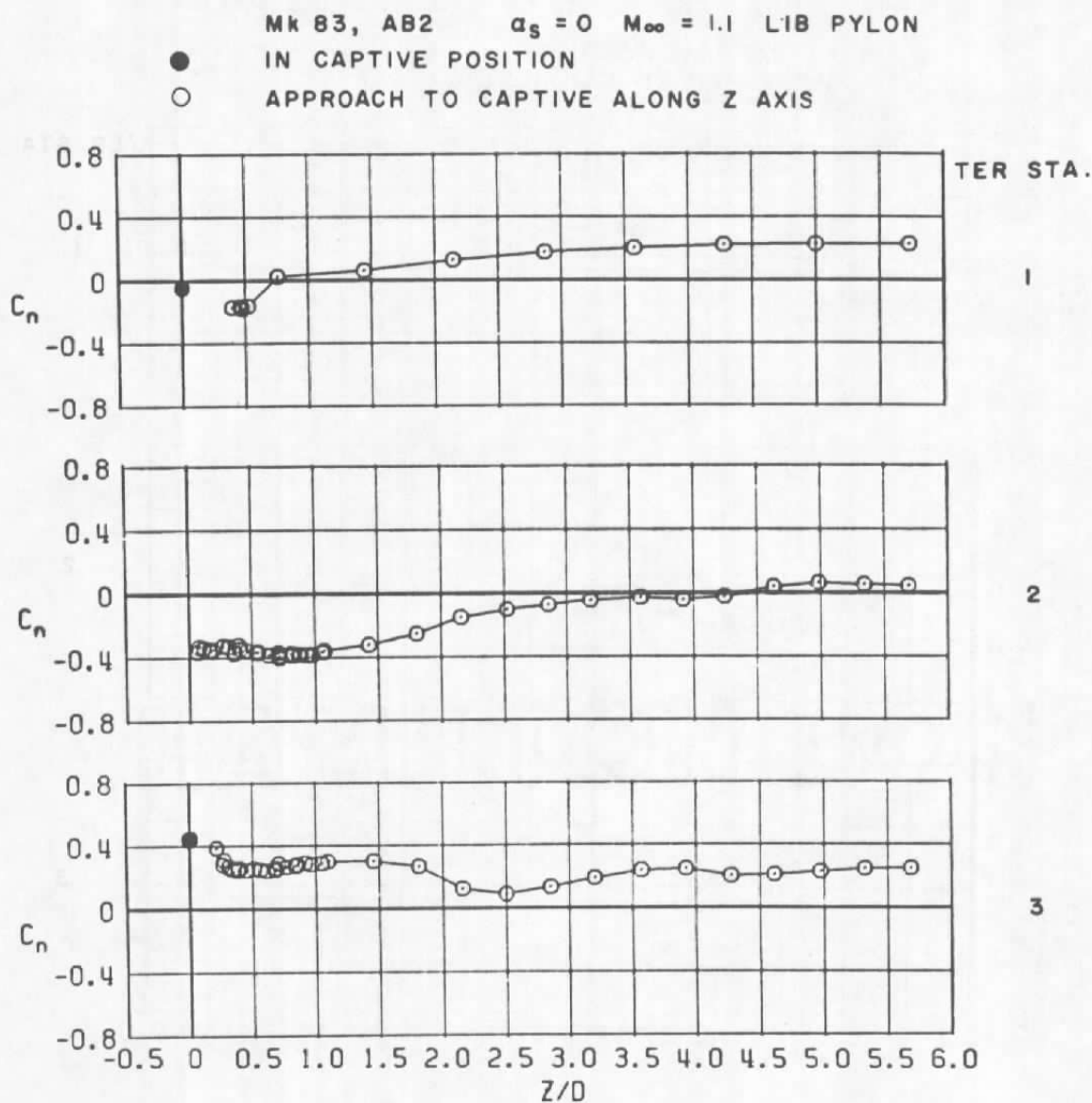
Mk 83, AB2  $\alpha_s = 0$   $M_\infty = 0.9$  LIB PYLON

● IN CAPTIVE POSITION

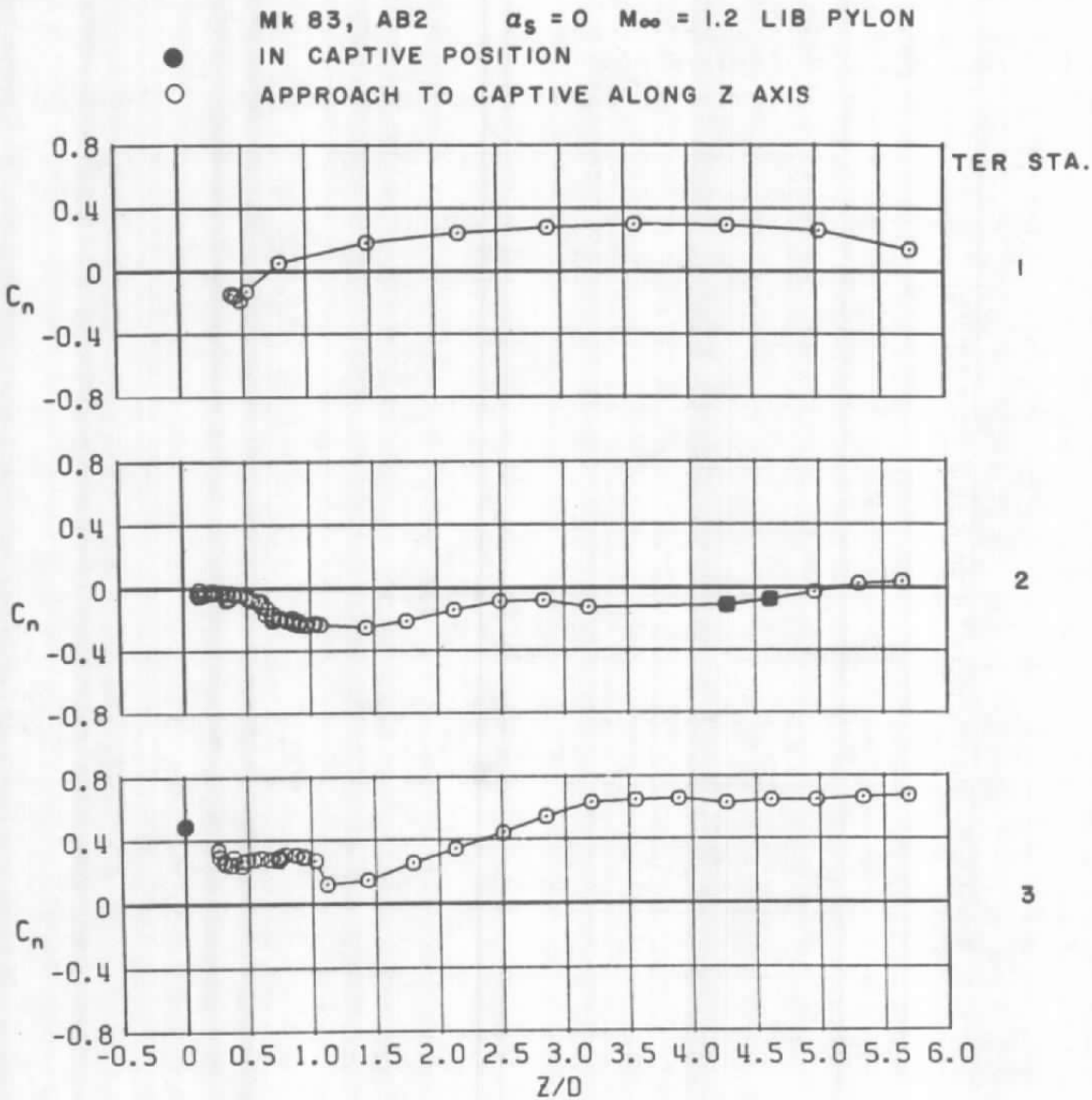
○ APPROACH TO CAPTIVE ALONG Z AXIS



c.  $M_\infty = 0.9$   
Figure 64. Continued.



d.  $M_\infty = 1.1$   
Figure 64. Continued.



e.  $M_\infty = 1.2$   
Figure 64. Concluded.

Table 1. Miscellaneous Dimensions of Store Models

Store	$X_{FL}$ , in.	$X_{CG}$ , in.	D, in.	AB Number	$D_B$ , in.	$D_s$ , in.	$L_s$ , in.	$D_s/D_B$	$L_s/D_B$
Black Crow	4.546*	5.296	1.100	1	1.100	0.40	6.05	0.36	5.50
HSM	3.680*	4.430	0.900	1	0.900	0.40	6.30	0.44	7.00
BLU-1	2.875**	3.215	0.930	1	---	---	---	---	---
				2	0.490	0.40	5.99	0.82	12.22
M-118	2.074**	2.810	1.206	1	0.319	---	---	---	---
				2	0.627	0.40	4.17	0.64	6.65
ASP	1.990**	2.335	0.800	1	0.800	0.25	4.19	0.31	5.24
CBU-24	1.700**	1.933	0.800	1	0.437	0.25	4.01	0.57	9.18
CBU-46	2.615**	2.990	0.780	1	0.150	---	---	---	---
				2	0.330	0.25	3.94	0.76	11.94
MK 83	2.175**	2.525	0.700	1	---	---	---	---	---
				2	0.470	0.25	3.45	0.53	7.34

\* Forward 30-in. Suspension Point

\*\* Forward 14-in. Suspension Point

Table 2. Uncertainty Intervals in Force and Moment Coefficients for Store Models

Store	$M_{\infty}$	$\epsilon(C_N)$	$\epsilon(C_Y)$	$\epsilon(C_A)$	$\epsilon(C_L)$	$\epsilon(C_m)$	$\epsilon(C_n)$
Black Crow	0.6	$\pm 0.023$	$\pm 0.030$	$\pm 0.032$	$\pm 0.029$	$\pm 0.068$	$\pm 0.026$
	0.9	0.017	0.022	0.024	0.022	0.050	0.018
	1.1	0.015	0.020	0.021	0.019	0.044	0.016
	1.2	0.015	0.019	0.020	0.019	0.043	0.015
HSM	0.6	$\pm 0.036$	$\pm 0.047$	$\pm 0.048$	$\pm 0.054$	$\pm 0.126$	$\pm 0.051$
	0.9	0.027	0.034	0.035	0.040	0.093	0.035
	1.1	0.023	0.030	0.031	0.035	0.082	0.031
	1.2	0.023	0.029	0.030	0.034	0.079	0.031
BLU-1	0.6	$\pm 0.033$	$\pm 0.042$	$\pm 0.044$	$\pm 0.049$	$\pm 0.114$	$\pm 0.056$
	0.9	0.024	0.031	0.033	0.036	0.085	0.041
	1.1	0.022	0.027	0.029	0.032	0.075	0.036
	1.2	0.021	0.026	0.028	0.031	0.072	0.035
M-118	0.6	$\pm 0.020$	$\pm 0.026$	$\pm 0.027$	$\pm 0.022$	$\pm 0.052$	$\pm 0.017$
	0.9	0.015	0.019	0.020	0.017	0.038	0.013
	1.1	0.013	0.017	0.017	0.015	0.033	0.011
	1.2	0.012	0.016	0.017	0.014	0.032	0.011
ASP	0.6	$\pm 0.012$	$\pm 0.014$	$\pm 0.024$	$\pm 0.009$	$\pm 0.013$	$\pm 0.016$
	0.9	0.009	0.011	0.019	0.007	0.010	0.012
	1.1	0.008	0.010	0.017	0.006	0.009	0.011
	1.2	0.008	0.009	0.016	0.006	0.008	0.011
CBU-24	0.6	$\pm 0.013$	$\pm 0.015$	$\pm 0.024$	$\pm 0.009$	$\pm 0.017$	$\pm 0.017$
	0.9	0.009	0.011	0.018	0.007	0.011	0.012
	1.1	0.009	0.010	0.016	0.006	0.010	0.011
	1.2	0.009	0.009	0.016	0.006	0.010	0.010
CBU-46	0.6	$\pm 0.012$	$\pm 0.016$	$\pm 0.025$	$\pm 0.010$	$\pm 0.014$	$\pm 0.018$
	0.9	0.009	0.012	0.019	0.007	0.010	0.014
	1.1	0.008	0.010	0.017	0.007	0.010	0.012
	1.2	0.008	0.010	0.016	0.006	0.009	0.011
MK 83	0.6	$\pm 0.022$	$\pm 0.025$	$\pm 0.028$	$\pm 0.022$	$\pm 0.027$	$\pm 0.031$
	0.8	0.018	0.020	0.023	0.018	0.022	0.025
	0.9	0.016	0.018	0.021	0.016	0.020	0.023
	1.1	0.015	0.017	0.019	0.014	0.018	0.020
	1.2	0.014	0.016	0.018	0.014	0.018	0.019



## NOMENCLATURE

AB	Afterbody
BL	Aircraft buttock line, measured from the plane of symmetry, in., model scale
$\bar{C}_L$ , C-L	Centerline
$C_A$	Axial-force coefficient for a store, axial force/ $q_\infty S$
$C_\ell$	Rolling-moment coefficient for a store (referenced to the axis of symmetry of the store), rolling moment/ $q_\infty S D$
$C_m$	Pitching-moment coefficient for a store (referenced to the center of gravity of the store), pitching moment/ $q_\infty S D$
$C_N$	Normal-force coefficient for a store, normal force/ $q_\infty S$
$C_n$	Yawing-moment coefficient for a store (referenced to the center of gravity of the store), yawing moment/ $q_\infty S D$
$C_Y$	Side-force coefficient for a store, side force/ $q_\infty S$
D	Maximum diameter of a store, in., model scale
$D_B$	Diameter of the base of a store, in., model scale
$D_s$	Diameter of a sting, in.
FS	Aircraft fuselage station, in., model scale
LIB	Left inboard
LOB	Left outboard
$L_s$	Length of the constant-diameter portion of a sting, measured from the base of a store to the upstream extent of the variable-diameter portion of the sting, in.
$M_\infty$	Free-stream Mach number
$p_\infty$	Free-stream static pressure, psfa
$p_{t_\infty}$	Free-stream total pressure, psfa
$q_\infty$	Free-stream dynamic pressure, $0.7 p_{t_\infty} M_\infty^2$ , psfa

R	Radius
S	Reference area of a store model, $\frac{\pi D^2}{4(144)}$ , ft <sup>2</sup>
WL	Aircraft waterline, measured from the aircraft horizontal reference plane, in., model scale
X <sub>cg</sub>	Location of the center of gravity of a store, measured along the longitudinal axis of the store from the nose of the store, in., model scale
X <sub>FL</sub>	Location of the forward suspension point of a store, measured along the longitudinal axis of the store from the nose of the store, in., model scale
Z	Distance between a point on the top $\phi$ surface of the body of a store model at any position in the flow field and the location that point occupied in the captive position during wind-off installation activities, measured normal to the lower surface of a pylon or rack station, positive away from the aircraft (see Fig. 13)
Z/D	Nondimensional separation distance of a store model from the captive position
$\alpha_s$	Gravimetric angle of attack for a store model, deg
$\epsilon(C)_x$	Uncertainty interval of a force or moment coefficient

## DESCRIPTION OF AXES

The system of axes referred to as "tunnel axes" is defined in a manner similar to the flight axis system, but with a constant zero roll angle:

- $X_T$  Parallel to the free-stream wind vector (assumed parallel to the longitudinal axis of the test section in the wind tunnel); positive direction is forward looking upstream
- $Y_T$  Perpendicular to the  $X_T$  and  $Z_T$  axes; positive direction is to the right with respect to the aircraft
- $Z_T$  Perpendicular to the free-stream wind vector and parallel to the plane of symmetry of the aircraft at zero roll angle; positive direction is away from the bottom of the aircraft

The "pylon axis" system is defined as follows:

- $X_P$  Parallel to the lower surface of the pylon and parallel to the  $X_T$ - $Z_T$  plane; positive direction is forward looking upstream
- $Y_P$  Perpendicular to the  $X_P$  axis and parallel to the  $X_T$ - $Y_T$  plane; positive direction is to the right with respect to the aircraft
- $Z_P$  Perpendicular to both the  $X_P$  and  $Y_P$  axes; positive direction is away from the lower surface of the pylon